

INFORMATION TO USERS

This manuscript has been reproduced from the microfilm master. UMI films the text directly from the original or copy submitted. Thus, some thesis and dissertation copies are in typewriter face, while others may be from any type of computer printer.

The quality of this reproduction is dependent upon the quality of the copy submitted. Broken or indistinct print, colored or poor quality illustrations and photographs, print bleedthrough, substandard margins, and improper alignment can adversely affect reproduction.

In the unlikely event that the author did not send UMI a complete manuscript and there are missing pages, these will be noted. Also, if unauthorized copyright material had to be removed, a note will indicate the deletion.

Oversize materials (e.g., maps, drawings, charts) are reproduced by sectioning the original, beginning at the upper left-hand corner and continuing from left to right in equal sections with small overlaps.

Photographs included in the original manuscript have been reproduced xerographically in this copy. Higher quality 6" x 9" black and white photographic prints are available for any photographs or illustrations appearing in this copy for an additional charge. Contact UMI directly to order.

**ProQuest Information and Learning
300 North Zeeb Road, Ann Arbor, MI 48106-1346 USA
800-521-0600**

UMI[®]

PERFORMANCE CHARACTERISTICS OF A NOVEL LIQUID-LIQUID CONTACTOR

by

Mohammad Salem El-Ali

Submitted

in partial fulfillment of the requirements
for the degree of

DOCTOR OF PHILOSOPHY

Major Subject: Chemical Engineering

at

DALHOUSIE UNIVERSITY

Halifax, Nova Scotia

August, 2001

© Copyright by Mohammad Salem El-Ali, 2001



**National Library
of Canada**

**Acquisitions and
Bibliographic Services**

**395 Wellington Street
Ottawa ON K1A 0N4
Canada**

**Bibliothèque nationale
du Canada**

**Acquisitions et
services bibliographiques**

**395, rue Wellington
Ottawa ON K1A 0N4
Canada**

Your file Votre référence

Our file Notre référence

The author has granted a non-exclusive licence allowing the National Library of Canada to reproduce, loan, distribute or sell copies of this thesis in microform, paper or electronic formats.

The author retains ownership of the copyright in this thesis. Neither the thesis nor substantial extracts from it may be printed or otherwise reproduced without the author's permission.

L'auteur a accordé une licence non exclusive permettant à la Bibliothèque nationale du Canada de reproduire, prêter, distribuer ou vendre des copies de cette thèse sous la forme de microfiche/film, de reproduction sur papier ou sur format électronique.

L'auteur conserve la propriété du droit d'auteur qui protège cette thèse. Ni la thèse ni des extraits substantiels de celle-ci ne doivent être imprimés ou autrement reproduits sans son autorisation.

0-612-63475-2

Canada

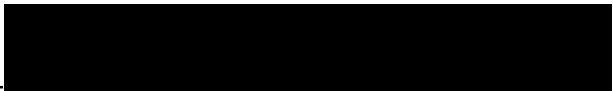
Dalhousie University
Faculty of Engineering

Chemical Engineering/Doctor of Philosophy

The undersigned hereby certify that they have examined, and recommended to the Faculty of Graduate Studies for acceptance, the thesis entitled "Performance Characteristics of a Novel Liquid-Liquid Contactor" by Mohammad Salem El-Ali in partial fulfillment of the requirements for the degree of Doctor of Philosophy.

Date: December 5th/01

Supervisor:



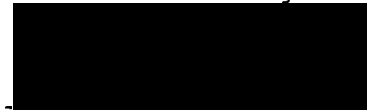
Dr. Adel Al Taweel

External Examiner



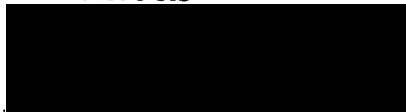
Dr. Malcolm H. I. Baird
McMaster University

Member:



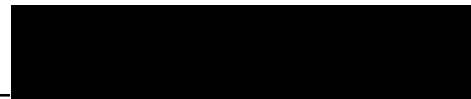
Dr. Mort Fels

Member:



Dr. Feridun Hamdullahpur

Member:



Dr. Hassan Goma

Dalhousie University
Faculty of Engineering

Date: Aug. 24th 2001

AUTHOR: Mohammad Salem El-Ali
TITLE: Performance Characteristics of a Novel Liquid-liquid Contactor
MAJOR SUBJECT: Chemical Engineering
DEGREE: Doctor of Philosophy
CONVOCATION: October, 2001

Permission is herewith granted to Dalhousie University to circulate and to have copied for non-commercial purposes, at its discretion, the above thesis upon the request of individuals or institutions.



Signature of Author

The author reserves other publication rights, and neither the thesis nor extensive extracts from it may be printed or otherwise reproduced without the author's written permission.

The author attests that permission has been obtained for the use of any copyrighted material appearing in this thesis (other than brief excerpts requiring only proper acknowledgement in scholarly writing), and that all such use is clearly acknowledged.

CONTENTS

LIST OF TABLES.....	vii
LIST OF FIGURES.....	viii
NOMENCLATURE.....	xv
ACKNOWLEDGEMENT.....	xix
ABSTRACT.....	xx
Chapter 1 INTRODUCTION	1
Chapter 2 LITERATURE REVIEW	4
2.1 <i>FLOW THROUGH SCREENS</i>	4
2.1.1 Reynolds Numbers.....	5
2.1.2 Pressure Drop across Screens	5
2.1.3 Turbulence Intensity and Turbulence Energy.....	10
2.1.4 Decay of Turbulence Intensity.....	14
2.1.5 Kinetic Energy and Energy Dissipation.....	19
2.1.6 Homogeneous Turbulence.....	20
2.2 <i>DROP BREAKUP AND COALESCENCE</i>	21
2.2.1 Effect of Hydrodynamics.....	24
2.2.2 Effect of System Properties.....	33
2.2.3 Effect of Interfacial Characteristics.....	38
2.2.4 Effect of Electrolytes.....	47
2.3 <i>KINETICS OF DROP BREAKUP AND COALESCENCE</i>	49
2.4 <i>DROP SIZE DISTRIBUTION</i>	52
2.4.1 Effect of Hydrodynamics.....	53
2.4.2 Effect of System Properties.....	64
2.4.3 Effect of Interfacial Characteristics.....	67
Chapter 3 EXPERIMENTAL	69
3.1 <i>EXPERIMENTAL SET UP</i>	69
3.2 <i>INVESTIGATED SYSTEM</i>	74
3.3 <i>EXPERIMENTAL PROCEDURE</i>	77

3.4	<i>ERROR ANALYSIS</i>	78
3.4.1	Drop Size Measurement.....	79
3.4.2	Pressure Drop Measurement.....	81
3.4.3	Continuous Flowrate Measurement.....	81
3.4.4	Energy Dissipation Rate.....	81
3.5	<i>DROP SIZE MEASUREMENT</i>	81
3.5.1	Sample Size.....	81
3.5.2	Reproducibility of Drop Size Measurement.....	83
3.6	<i>DATA TREATMENT</i>	83
3.6.1	Flowrates of Dispersed and Continuous Phases Fraction.....	83
3.6.2	Drop Size Distribution.....	84
3.6.3	Mean Energy Dissipation Rate.....	88
3.6.4	Surface Excess.....	88
Chapter 4	RESULTS AND DISCUSSIONS	90
4.1	<i>FLOW THROUGH SCREENS</i>	90
4.1.1	Single Phase Flow.....	91
4.1.2	Two Phase Flow through Screens.....	101
4.2	<i>FACTORS AFFECTING MEAN DROP SIZE</i>	107
4.2.1	Effect of Superficial Velocity and Energy Dissipation Rate.....	107
4.2.2	Effect of Screen Geometry.....	120
4.2.3	Effect of Number of Elements.....	130
4.2.4	Effect of Dispersed Phase Volume Fraction.....	132
4.2.5	Effect of Interfacial Characteristics.....	136
4.2.6	Correlation of Experimental Data.....	148
4.3	<i>MAXIMUM STABLE DROP SIZE</i>	150
4.4	<i>DROP SIZE DISTRIBUTION</i>	156
4.4.1	Drop Number Density Distribution.....	157
4.4.2	Drop Volume Density Distribution.....	178
4.4.3	Characterization of Drop Size Distributions.....	189

4.5	<i>USING POPULATION BALANCE TO MODEL DROP BREKUP/COALESCENCE</i>	220
4.6	<i>EFFICIENCY OF ENERGY UTILIZATION</i>	228
4.7	<i>COMPARISON WITH OTHER MIXERS</i>	233
Chapter 5	CONCLSIONS AND RECOMMENDATIONS	249
	REFERENCES	254
Appendix A	Drop Number Density Distributions	272
Appendix B	Drop Volume Density Distributions	309
Appendix C	Analytical Solution of Population Balance Equation Presented by Rod and Misk	347
Appendix D	Comparison of Cumulative Drop Density Distributions with Rod and Misk (1982) Model	349

LIST OF TABLES

Table 2.1. Reynolds number used in flow through screens.....	6
Table 2.2: Constants of Turbulence Decay Equation (2-16).....	17
Table 3.1. Characteristics of the woven screens studied	72
Table 3.2. Physical properties of the pure phases at 25 °C.....	77
Table 3.3. Interfacial characteristics of investigated systems.....	77
Table 3.4. Reported sample sizes in the literature.....	82
Table 3.5. Statistical analysis of samples with different drop numbers.....	82
Table 3.6. Reproducibility of drop size measurements.....	83
Table 3.7. Sample of drop size calculation.....	86
Table 3.8. Physical meaning of drop mean diameters.....	88
Table 4.1. Effect of screen open area on the value of b ($\phi = 0.5\%$).....	113
Table 4.2. Dependence of the mean drop diameter on energy dissipation rate in static mixers.....	119
Table 4.3. Dependence of drop size on the Weber number.....	126
Table 4.4. Dependence of the mean drop diameter on the Weber number in static mixers.....	127
Table 4.5. Fitting results of bi-modality testing.....	190
Table 4.6. Results of fitting the experimental data to probability models at different superficial velocities ($\alpha = 41\%$, 9 screens, $L = 10$ mm).....	208
Table 4.7. Results of fitting the experimental data to probability models at different superficial velocities ($\alpha = 33\%$, 9 screens, $L = 10$ mm).....	208
Table 4.8. Results of fitting the experimental data to probability models at different superficial velocities ($\alpha = 27\%$, 9 screens, $L = 10$ mm).....	209
Table 4.9. Results of fitting the experimental data to probability models at different dispersed phase holdups ($\alpha = 41\%$, 9 screens, $L = 10$ mm).....	209
Table 4.10. Results of fitting the experimental data to probability models at different dispersed phase holdups ($\alpha = 27\%$, 9 screens, $L = 10$ mm).....	210
Table 4.11. Results of fitting the experimental data to probability models in presence of surfactant ($\alpha = 27\%$, $U = 0.70$ m/s, 9 screens, $L = 10$ mm).....	210
Table 4.12. Regression analysis of the normalized normal cumulative drop volume density (Bayol oil-water system).....	219

LIST OF FIGURES

Figure 1.1. Effect of the density ratio on the separation a dispersion of two immiscible liquids (Lamella gravity separator of 2.5cm plate spacing).....	2
Figure 2.1 Geometry of the flow behind the grid.....	12
Figure 2.2. The effect of screen geometry on the value of C in Equation (2-19).....	19
Figure 3.1. Schematic diagram of the experimental set up.....	70
Figure 3.2. Schematic diagram of the top view of the imaging chamber.....	73
Figure 3.3. A sample of imaged drops ($\alpha = 27\%$, $\phi = 4\%$, 9 screens, $L = 10$ mm).....	75
Figure 3.4. Microscope calibration curve.....	80
Figure 4.1. Pressure drop in the empty pipe (entrance, exit and frictional losses).....	92
Figure 4.2. Effect of superficial velocity on total pressure drop in the mixer.....	92
Figure 4.3. Effect of the jet Reynolds number on drag coefficient.....	94
Figure 4.4. Evolution of Taylor length scale in grid-generated turbulence ($U = 1.94$ m/s).....	96
Figure 4.5. Turbulence intensity decay behind screens ($U = 1.94$ m/s).....	97
Figure 4.6. Effect of screen open area on energy dissipation rate ($U = 1.94$ m/s).....	99
Figure 4.7. Variation of energy dissipation rate behind screens ($\alpha = 27\%$).....	99
Figure 4.8. Variation of energy dissipation rate behind screens ($\alpha = 33\%$).....	100
Figure 4.9. Variation of energy dissipation rate behind screens ($\alpha = 41\%$).....	100
Figure 4.10. Effect of dispersed phase holdup on pressure drop in the mixer ($U = 0.40$ m/s).....	102
Figure 4.11. Effect of dispersed phase holdup on pressure drop in the mixer ($U = 0.70$ m/s).....	102
Figure 4.12. Change in drag coefficient in presence of the dispersed phase ($\alpha = 27\%$).....	103
Figure 4.13. Change in drag coefficient in presence of the dispersed phase ($\alpha = 33\%$, $\phi = 0.5\%$).....	103
Figure 4.14. Change in drag coefficient in presence of the dispersed phase ($\alpha = 0.41$).....	104
Figure 4.15a. Effect of the superficial velocity on Sauter mean diameter ($\alpha = 27\%$, $\phi = 0.5\%$, 9 screens, $L = 10$ mm).....	109
Figure 4.15b. Effect of the superficial velocity on Sauter mean diameter ($\alpha = 33\%$, $\phi = 0.5\%$, 9 screens, $L = 10$ mm).....	109
Figure 4.15c. Effect of the superficial velocity on Sauter mean diameter ($\alpha = 41\%$, $\phi = 0.5\%$, 9 screens, $L = 10$ mm).....	110
Figure 4.15d. Effect of the superficial velocity on Sauter mean diameter ($\alpha = 27\%$, $\phi = 4\%$, 9 screens, $L = 10$ mm).....	110
Figure 4.15e. Effect of the superficial velocity on Sauter mean diameter ($\alpha = 41\%$, $\phi = 4\%$, 9 screens, $L = 10$ mm).....	111
Figure 4.16. Variation of the Sauter mean diameter with the superficial velocity ($\phi = 0.5\%$, 9 screens, $L = 10$ mm).....	111
Figure 4.17. Variation of the Sauter mean diameter with the superficial velocity	

($\phi = 4\%$, 9 screens, $L = 10\text{mm}$).....	112
Figure 4.18a. Effect of mean energy dissipation rate on the Sauter mean diameter.....	116
Figure 4.18b. Effect of mean energy dissipation rate on the Sauter mean diameter ($\phi = 0.5\%$, 9 screens, $L = 10\text{mm}$).....	117
Figure 4.18c. Effect of mean energy dissipation rate on the Sauter mean diameter ($\phi = 4\%$, 9 screens, $L = 10\text{mm}$).....	117
Figure 4.19. Effect of screen open area on Sauter mean diameter ($\phi = 0.5\%$, 9 screens, $L = 10\text{mm}$).....	121
Figure 4.20. Variation of the Sauter mean diameter with Re_M (9 screens, $L = 10\text{mm}$)	122
Figure 4.21. Variation of the Sauter mean diameter with Re_b (9 screens, $L = 10\text{mm}$)	122
Figure 4.22. Variation of the Sauter mean diameter with Re_{jet} (9 screens, $L = 10\text{mm}$)	123
Figure 4.23. Variation of the Sauter mean diameter with Re_j (9 screens, $L = 10\text{mm}$)	123
Figure 4.24. The variation of Sauter mean diameter with the Weber number ($\phi = 0.5\%$, 9 screens, $L = 10\text{mm}$).....	125
Figure 4-25. The variation of Sauter mean diameter with the Weber number ($\phi = 4\%$, 9 screens, $L = 10\text{mm}$).....	125
Figure 4.26. Variation of the Sauter mean diameter with We_{jet} ($\phi = 0.5\%$, 9 screens, $L = 10\text{mm}$).....	128
Figure 4.27. Variation of the Sauter mean diameter with We_{jet} ($\phi = 4\%$, 9 screens, $L = 10\text{mm}$).....	129
Figure 4.28. Effect of number of mixing elements on the average drop size ($L = 10\text{mm}$)	131
Figure 4.29. Schematic representation of drop breakup/coalescence.....	133
Figure 4.30. The effect of the dispersed phase volume fraction on the Sauter mean diameter ($U = 0.40\text{ m/s}$, $\alpha = 27\%$, 9 screens, $L = 10\text{mm}$).....	134
Figure 4.31. The effect of the dispersed phase volume fraction on the Sauter mean diameter ($U = 0.70\text{ m/s}$, $\alpha = 27\%$, 9 screens, $L = 10\text{mm}$).....	134
Figure 4.32. Schematic diagram of Drop breakup mechanisms.....	135
Figure 4.33. Effect of SAA on the Sauter mean diameter ($U = 0.70\text{ m/s}$, $\alpha = 0.27$, 9 screens, $L = 10\text{mm}$).....	138
Figure 4.34. Effect of SAA on mean drop diameters ($\phi = 0.5\%$, $U = 0.70\text{ m/s}$, $\alpha = 27\%$, 9 screens, $L = 10\text{mm}$).....	139
Figure 4.35. Effect of SAA on mean drop diameters ($\phi = 4\%$, $U = 0.70\text{ m/s}$, $\alpha = 27\%$, 9 screens, $L = 10\text{mm}$).....	139
Figure 4.36. Effect of equilibrium interfacial tension on Sauter mean diameter ($U = 0.70\text{ m/s}$, $\alpha = 27\%$, 9 screens, $L = 10\text{mm}$).....	142
Figure 4.37. Effect of surface excess on the Sauter mean diameter. ($\alpha = 27\%$, $U = 0.70\text{ m/s}$, 9 screens, $L = 10\text{mm}$).....	143
Figure 4.38. Variation of diffusivity with surfactant concentration.....	145

Figure 4.39. The Sauter mean diameter as a function of surfactant diffusivity.....	146
Figure 4.40. Effect of Marangoni number on the Sauter mean diameter ($\alpha = 27\%$, $U = 0.70$ m/s, 9 screens, $L = 10$ mm).....	148
Figure 4.41. Comparison of predicted maximum drop size using Equation (4-21) with experimental values.....	149
Figure 4.42. Comparison of predicted maximum drop size by Equation (4-22) and calculated values from experimental data.....	152
Figure 4.43. Comparison of predicted maximum drop size using Equation (2-26) with experimental values.....	154
Figure 4.44. Effect of number of mixing elements on maximum stable drop size ($\alpha = 27\%$, $U = 0.40$ m/s, $\phi = 2\%$, $L = 10$ mm).....	155
Figure 4.45. Effect of dispersed phase holdup on maximum stable drop size ($\alpha = 27\%$, $U = 0.40$ m/s, 9 screens, $L = 10$ mm).....	156
Figure 4.46. Drop number density distribution ($\alpha = 41\%$, $\phi = 0.5\%$, $U = 0.30$ m/s, 9 screens, $L = 10$ mm).....	160
Figure 4.47. Drop number density distribution ($\alpha = 0.45$, $\phi = 0.5\%$, $U = 0.85$ m/s, 9 screens, $L = 10$ mm).....	160
Figure 4.48. Drop number density distribution ($\alpha = 41\%$, $\phi = 0.5\%$, $U = 1.94$ m/s, 9 screens, $L = 10$ mm).....	161
Figure 4.49. Drop number density distribution ($\alpha = 27\%$, $\phi = 0.5\%$, $U = 0.30$ m/s, 9 screens, $L = 10$ mm).....	161
Figure 4.50. Drop number density distribution ($\alpha = 27\%$, $\phi = 0.5\%$, $U = 0.90$ m/s, 9 screens, $L = 10$ mm).....	162
Figure 4.51. Drop number density distribution ($\alpha = 27\%$, $\phi = 0.5\%$, $U = 1.94$ m/s, 9 screens, $L = \text{cm}$).....	162
Figure 4.52. Drop number density distribution ($\alpha = 33\%$, $\phi = 0.5\%$, $U = 0.30$ m/s, 9 screens, $L = 10$ mm).....	163
Figure 4.53. Drop number density distribution ($\alpha = 33\%$, $\phi = 0.5\%$, $U = 0.85$ m/s, 9 screens, $L = 10$ mm).....	163
Figure 4.54. Drop number density distribution ($\alpha = 0.33$, $\phi = 0.5\%$, $U = 1.94$ m/s, 9 screens, $L = 10$ mm).....	164
Figure 4.55. Drop number density distribution ($\alpha = 27\%$, $\phi = 4\%$, $U = 0.30$ m/s, 9 screens, $L = 10$ mm).....	164
Figure 4.56. Drop number density distribution ($\alpha = 27\%$, $\phi = 4\%$, $U = 0.70$ m/s, 9 screens, $L = 10$ mm).....	165
Figure 4.57. Drop number density distribution ($\alpha = 27\%$, $\phi = 4\%$, $U = 1.55$ m/s, 9 screens, $L = 10$ mm).....	165
Figure 4.58. Drop number density distribution ($\alpha = 41\%$, $\phi = 0.5\%$, $U = 0.40$ m/s, 9 screens, $L = 10$ mm).....	168
Figure 4.59. Drop number density distribution ($\alpha = 41\%$, $\phi = 2\%$, $U = 0.40$ m/s, 9 screens, $L = 10$ mm).....	168
Figure 4.60. Drop number density distribution ($\alpha = 41\%$, $\phi = 4\%$, $U = 0.40$ m/s, 9 screens, $L = 10$ mm).....	169

Figure 4.61. Drop number density distribution ($\alpha = 27\%$, $\phi = 0.5\%$, $U = 0.70$ m/s, 9 screens, $L = 10$ mm).....	169
Figure 4.62. Drop number density distribution ($\alpha = 27\%$, $\phi = 2\%$, $U = 0.70$ m/s, 9 screens, $L = 10$ mm).....	170
Figure 4.63. Drop number density distribution ($\alpha = 27\%$, $\phi = 4\%$, $U = 0.70$ m/s, 9 screens, $L = 10$ mm).....	170
Figure 4.64. Drop number density distribution ($\alpha = 27\%$, $\phi = 2\%$, $U = 0.40$ m/s, 2 screens, $L = 5$ mm).....	172
Figure 4.65. Drop number density distribution ($\alpha = 27\%$, $\phi = 2\%$, $U = 0.40$ m/s, 4 screens, $L = 5$ mm).....	172
Figure 4.66. Drop number density distribution ($\alpha = 27\%$, $\phi = 2\%$, $U = 0.40$ m/s, 9 screens, $L = 5$ mm).....	173
Figure 4.67. Drop number density distribution ($\alpha = 27\%$, $\phi = 0.5\%$, $U = 0.70$ m/s, $c = 0.01$ mole/m ³ , 9 screens, $L = 10$ mm)...	175
Figure 4.68. Drop number density distribution ($\alpha = 27\%$, $\phi = 0.5\%$, $U = 0.70$ m/s, $c = 0.10$ mole/m ³ , 9 screens, $L = 10$ mm)...	175
Figure 4.69. Drop number density distribution ($\alpha = 27\%$, $\phi = 0.5\%$, $U = 0.70$ m/s, $c = 0.30$ mole/m ³ , 9 screens, $L = 10$ cm)...	176
Figure 4.70. Drop number density distribution ($\alpha = 27\%$, $\phi = 4\%$, $U = 0.70$ m/s, $c = 0.01$ mole/m ³ , 9 screens, $L = 10$ mm).....	176
Figure 4.71. Drop number density distribution ($\alpha = 27\%$, $\phi = 4\%$, $U = 0.70$ m/s, $c = 0.10$ mole/m ³ , 9 screens, $L = 10$ mm).....	177
Figure 4.72. Drop number density distribution ($\alpha = 27\%$, $\phi = 4\%$, $U = 0.70$ m/s, $c = 0.30$ mole/m ³ , 9 screens, $L = 10$ mm).....	177
Figure 4.73. Drop volume density distribution ($\alpha = 27\%$, $\phi = 0.5\%$, $U = 0.40$ m/s, 9 screens, $L = 10$ mm).....	180
Figure 4.74. Drop volume density distribution ($\alpha = 27\%$, $\phi = 0.5\%$, $U = 0.97$ m/s, 9 screens, $L = 10$ mm).....	180
Figure 4.75. Drop volume density distribution ($\alpha = 27\%$, $\phi = 0.5\%$, $U = 1.94$ m/s, 9 screens, $L = 10$ mm).....	181
Figure 4.76. Drop volume density distribution ($\alpha = 41\%$, $\phi = 0.5\%$, $U = 0.40$ m/s, 9 screens, $L = 10$ mm).....	182
Figure 4.77. Drop volume density distribution ($\alpha = 41\%$, $\phi = 2\%$, $U = 0.40$ m/s, 9 screens, $L = 10$ mm).....	183
Figure 4.78. Drop volume density distribution ($\alpha = 41\%$, $\phi = 4\%$, $U = 0.40$ m/s, 9 screens, $L = 10$ mm).....	183
Figure 4.79. Drop volume density distribution ($\alpha = 27\%$, $\phi = 2\%$, $U = 0.40$ m/s, 2 screens, $L = 5$ mm).....	184
Figure 4.80. Drop volume density distribution ($\alpha = 27\%$, $\phi = 2\%$, $U = 0.40$ m/s, 4 screens, $L = 5$ mm).....	185
Figure 4.81. Drop volume density distribution ($\alpha = 27\%$, $\phi = 2\%$, $U = 0.40$ m/s, 12 screens, $L = 5$ mm).....	185

Figure 4.82. Drop number density distribution with SAA ($\alpha = 27\%$, $\phi = 4\%$, $U = 0.70$ m/s, $c = 0.01$ mole/m ³ , 9 screens, L = 10 mm).....	187
Figure 4.83. Drop number density distribution with SAA ($\alpha = 27\%$, $\phi = 4\%$, $U = 0.70$ m/s, $c = 0.10$ mole/m ³ , 9 screens, L = 10 mm).....	188
Figure 4.84. Drop number density distribution with SAA ($\alpha = 27\%$, $\phi = 4\%$, $U = 0.70$ m/s, $c = 0.30$ mole/m ³ , 9 screens, L = 10 mm).....	188
Figure 4.85. Cumulative drop number density distribution ($\alpha = 41\%$, $\phi = 0.5\%$, $U = 0.85$ m/s, 9 screens, L = 10 mm).....	190
Figure 4.86. Mean, median and mode in a distribution skewed to the right ($\alpha = 27\%$, $\phi = 0.5\%$, $U = 0.30$ m/s, 9 screens, L = 10 mm).....	191
Figure 4.87. Effect of superficial velocity on skewness ($\alpha = 41\%$, $\phi = 0.5\%$, 9 screens, L = 10 mm).....	193
Figure 4.88. Effect of superficial velocity on skewness ($\alpha = 27\%$, $\phi = 0.5\%$, 9 screens, L = 10 mm).....	193
Figure 4.89. Effect of superficial velocity on skewness ($\alpha = 33\%$, $\phi = 0.5\%$, 9 screens, L = 10 mm).....	194
Figure 4.90. Effect of superficial velocity on skewness ($\alpha = 41\%$, $\phi = 4\%$, 9 screens, L = 10 mm).....	194
Figure 4.91. Effect of superficial velocity on skewness ($\alpha = 27\%$, $\phi = 4\%$, 9 screens, L = 10 mm).....	195
Figure 4.92. Effect of dispersed phase holdup on skewness ($\alpha = 41\%$, $U = 0.40$ m/s, 9 screens, L = 10 mm).....	196
Figure 4.93. Effect of dispersed phase holdup on skewness ($\alpha = 27\%$, $U = 0.40$ m/s, 9 screens, L = 10 mm).....	197
Figure 4.94. Effect of dispersed phase holdup on skewness ($\alpha = 41\%$, $U = 0.70$ m/s, 9 screens, L = 10 mm).....	197
Figure 4.95. Effect of dispersed phase holdup on skewness ($\alpha = 27\%$, $U = 0.70$ m/s, 9 screens, L = 10 mm).....	198
Figure 4.96. Effect of surfactant concentration on skewness ($\alpha = 27\%$, $\phi = 0.5\%$, $U = 0.70$ m/s, 9 screens, L = 10 mm).....	199
Figure 4.97. Effect of the superficial velocity on the normalized variance ($\phi = 0.5\%$, 9 screens, L = 10 mm)	200
Figure 4.98. Effect of the superficial velocity on the normalized variance ($\phi = 4\%$, 9 screens, L = 10 mm).....	201
Figure 4.99. Effect of the Weber number on the normalized variance ($\phi = 0.5\%$, 9 screens, L = 10 mm).....	202
Figure 4.100. Effect of the jet Weber number on the variance (9 screens, L = 10 mm).....	203
Figure 4.101. Effect of the Weber number on the variance in Sulzer mixer.....	203
Figure 4.102. Effect of surfactant concentration on the normalized variance ($\alpha = 27\%$, $U = 0.7$ m/s, 9 screens, L = 10 mm).....	205
Figure 4.103. Effect of equilibrium interfacial tension on the normalized variance ($\alpha = 27\%$, $U = 0.70$ m/s, 9 screens, L = 10 mm).....	205

Figure 4.104. Effect of surface excess on the normalized variance ($\alpha = 27\%$, $U = 0.70$ m/s, 9 screens, $L = 10$ mm).....	206
Figure 4.105. Variation of the normalized variance with surfactant diffusivity ($\alpha = 27\%$, $U = 0.7$ m/s, 9 screens, $L = 10$ mm).....	206
Figure 4.106. Variation of the normalized variance with Marangoni number ($\alpha = 27\%$, $U = 0.70$ m/s, 9 screens, $L = 10$ mm).....	207
Figure 4.107. Self-similarity of the cumulative volume drop size distributions ($\alpha = 27\%$, $\phi = 0.5\%$, 9 screens, $L = 10$ mm).....	212
Figure 4.108. Self-similarity of the cumulative drop volume distributions ($\alpha = 27\%$, $\phi = 4\%$, 9 screens, $L = 10$ mm).....	213
Figure 4.109. Self-similarity of the cumulative drop volume distributions ($\alpha = 33\%$, $\phi = 0.5\%$, 9 screens, $L = 10$ mm).....	213
Figure 4.110. Self-similarity of the cumulative drop volume distributions ($\alpha = 41\%$, $\phi = 0.5\%$, 9 screens, $L = 10$ mm).....	214
Figure 4.111. Self-similarity of the cumulative drop volume distributions ($\alpha = 41\%$, $\phi = 4\%$, 9 screens, $L = 10$ mm).....	214
Figure 4.112. Self-similarity of the cumulative drop volume distributions at different dispersed phase holdups ($\alpha = 27\%$, $U = 0.40$ m/s, 9 screens, $L = 10$ mm).....	215
Figure 4.113. Self-similarity of the cumulative drop volume distributions at different dispersed phase holdups ($\alpha = 27\%$, $U = 0.70$ m/s, 9 screens, $L = 10$ mm).....	215
Figure 4.114. Self-similarity of the cumulative drop volume distributions at different dispersed phase holdups ($\alpha = 41\%$, $U = 0.40$ m/s, 9 screens, $L = 10$ mm).....	216
Figure 4.115. Self-similarity of the cumulative drop volume distributions at different dispersed phase holdups ($\alpha = 41\%$, $U = 0.70$ m/s, 9 screens, $L = 10$ mm).....	216
Figure 4.116. Self-similarity of the cumulative drop volume distributions with SAA ($\alpha = 27\%$, $U = 0.70$ m/s, 9 screens, $L = 10$ mm).....	217
Figure 4.117. Self-similarity of the cumulative drop volume distributions for all experiments (9 screens, $L = 10$ mm).....	218
Figure 4.118. Comparison of results with the analytical solution of the population balance equation ($\phi = 2\%$, $U = 0.40$ m/s, 9 screens, $L = 10$ mm).....	224

Figure 4.119. Cumulative drop number density distribution ($\alpha = 27\%$, $\phi = 4\%$, $U = 0.70$ m/s, 9 screens, $L = 10$ mm).....	226
Figure 4.120. Cumulative drop number density distribution ($\alpha = 27\%$, $\phi = 1\%$, $U = 0.70$ m/s, 9 screens, $L = 10$ mm).....	226
Figure 4.121. Cumulative drop volume density distribution ($\alpha = 41\%$, $\phi = 4\%$, $U = 0.97$ m/s, 9 screens, $L = 10$ mm).....	227
Figure 4.122. Cumulative drop volume density distribution ($\alpha = 27\%$, $\phi = 4\%$, $U = 0.70$ m/s, 9 screens, $L = 10$ mm).....	227
Figure 4.123. Efficiency of energy utilization at various velocities ($\phi = 0.5\%$, 9 screens, $L = 10$ mm).....	229
Figure 4.124. Effect of superficial velocity on efficiency of energy utilization ($\alpha = 27\%$, $\phi = 4\%$, 9 screens, $L = 10$ mm).....	229
Figure 4.125. Effect of dispersed phase holdup on efficiency of energy utilization ($\alpha = 27\%$, $U = 0.70$ m/s, 9 screens, $L = 10$ mm).....	231
Figure 4.126. Effect of number of screens on efficiency of energy utilization ($\alpha = 27\%$, $\phi = 2\%$, $U=0.40$ m/s, $L_m = 5$ mm).....	232
Figure 4.127. Comparison of predicted efficiency by Equation (4-47) and calculated values from experimental data.....	233
Figure 4.128. Variation of the interfacial area with mean energy dissipation rate (9screens, $L = 10$ mm).....	236
Figure 4.129. Variation of the interfacial area with energy utilization (9 screens, $L = 10$ mm).....	237
Figure 4.130. Comparison with MAT on basis of energy dissipation rate.....	239
Figure 4.131. Comparison with MAT based on energy utilization.....	241
Figure 4.132. Comparison with other static mixers based on mean energy dissipation rate.....	244
Figure 4.133. Comparison with other static mixers based on energy dissipated per unit mass of processed liquid.....	246

NOMENCLATURE

<i>A</i>	Interfacial area.	[m ²]
<i>A_c</i>	cross-sectional area	[m ²]
<i>A_h</i>	Hamaker-London constant	[J]
<i>A_o</i>	Screen open area	[m ²]
<i>A_t</i>	Total cross-sectional area of screen	[m ²]
<i>b</i>	Wire diameter	[m]
<i>B</i>	Dimensionless empirical constant.	[-]
<i>c</i>	Concentration of surfactant.	[mole/m ³]
<i>C_{coe.}</i>	Contraction coefficient of jet.	[-]
<i>C_c</i>	Critical surfactant concentration	[mole/m ³]
<i>C_s</i>	Surfactant concentration in the bulk	[mole/m ³]
<i>C₀</i>	Bulk concentration of the surfactant.	[mole/m ³]
<i>D</i>	Surfactant diffusivity.	[m ² /s]
<i>d</i>	Drop diameter.	[μm]
<i>d_{jet}</i>	Jet diameter	[m]
<i>D₀</i>	Orifice diameter.	[m]
<i>D</i>	Pipe or vessel diameter.	[m]
<i>d_m</i>	Average drop diameter.	[μm]
<i>d_{max.}</i>	Maximum stable drop diameter.	[μm]
<i>d₀</i>	Sauter mean diameter of an inviscid drop.	[μm]
<i>d₁₀</i>	Number-length mean or arithmetic mean.	[μm]
<i>d₃₂</i>	Sauter mean diameter.	[μm]
<i>d₄₃</i>	Volume mean.	[μm]
<i>d₅₀</i>	Drop diameter at 50% volume of drops smaller than <i>d₅₀</i> .	[μm]
<i>d₉₅</i>	Drop diameter at 95% volume of drops smaller than <i>d₉₅</i> .	[μm]
<i>E</i>	Mean energy dissipated per unit mass of processed liquid	[J/Kg]

E_G	Gibbs elasticity.	[mN/m]
g	Gravity.	[m/s ²]
h	Liquid film thickness.	[μ m]
h_c	Critical film thickness	[mm]
K	Compressibility of the surface film.	[-]
L	Distance between two consecutive screens	[mm]
L_f	Mixer length.	[m]
L_j	Jet coalescence length	[μ m]
M	Mesh size.	[m]
Ma	Marangoni number	[-]
N	Impeller speed.	[rpm]
$N\%$	Drop number density	[-]
$N\nu_i$	Viscosity group.	[Pa.s m Kg ^{-0.5} N ^{-0.5}]
n_a, n_l	Refractive indices for air and liquid respectively	[-]
n	Sample size.	[-]
n_i	Number of drops in an interval.	[-]
P	Static pressure	[N/m ²]
ΔP	Pressure drop.	[N/m ²]
Q	Volumetric flow rate	[m ³ /s]
R	Gas constant	[JK ⁻¹ mol ⁻¹]
Re	Reynolds number.	[-]
Re_b	Wire Reynolds' number	[-]
Re_M	Mesh Reynolds number	[-]
Re_j	Jet Reynolds number	[-]
Re_{j-b}	Jet-wire Reynolds number	[-]
S_{ac}	Actual distance	[m]
S_{ap}	Apparent distance	[m]
S_c	Critical surface coverage.	[-]

rpm	Revolution per minute.	[m ⁻¹]
<i>T</i>	Absolute temperature.	[°K]
<i>T_{dr}</i>	Drainage time	[s]
<i>T_{min}</i>	Minimum time to reach equilibrium.	[s]
<i>U</i>	Superficial velocity,.	[ms ⁻¹]
<i>U_j</i>	Liquid velocity in the jet	[ms ⁻¹]
<i>u_{rms.}</i>	Root mean square velocity.	[ms ⁻¹]
<i>u_{rms0}</i>	Root mean square velocity in single phase flow	[ms ⁻¹]
<i>We</i>	Weber number, $\frac{\rho U^2 D}{\sigma}$	[-]
<i>We_c</i>	Critical drop Weber number.	[-]
<i>We_D</i>	Drop Weber number.	[-]
<i>We_{jet}</i>	Jet Weber number, $\frac{\rho U^2 D}{\alpha^2 \sigma}$	[-]
<i>X</i>	Distance down the screen.	[m]
\bar{X}	Mean of the normalized normal drop size distribution	[-]
\bar{X}_{lg}	Mean of the normalized lognormal drop size distribution	[-]
Greek Letters		
α	Fractional open area of screen.	[-]
$\beta(p,q)$	Parameter of daughter drop size distribution.	[m ⁻¹]
ϵ	Energy dissipation rate.	[W/Kg]
η	Kolmogoroff eddy size.	[μ m]
Γ	Surface excess of surfactant.	[Mole/m ²]
λ	Coalescence efficiency.	[s ⁻¹]
λ_T	Taylor length scale	[μ m]
ρ_c	Density of continuous phase.	[Kg/m ³]
ρ_d	Density of dispersed phase.	[Kg/m ³]

$\Delta\rho$	Density difference.	[Kg/m ³]
μ_c	Viscosity of the continuous phase.	[Pa.s]
μ_d	Viscosity of dispersed phase.	[Pa.s]
ν	Kinematic viscosity.	[m ² /s]
σ	Interfacial tension.	[N/m]
σ_{\min}	Interfacial tension at high surfactant concentrations.	[N/m]
σ_{0SAA}	Surfactant free interfacial tension.	[N/m]
$\sigma_{\text{dyn.}}$	Dynamic interfacial tension.	[N/m]
$\sigma_{\text{eq.}}$	Equilibrium interfacial tension.	[N/m]
$\sigma_{\text{st.}}$	Static interfacial tension	[N/m]
v	Drop volume.	[μm^3]
ϕ	Dispersed phase hold up.	[-]
x	Dimensionless drop diameter.	[-]
Ψ	Drag coefficient	[-]

ACKNOWLEDGEMENT

The author expresses his deep appreciation to his research supervisor, Dr A. M. Al Taweel for his criticisms and encouragement throughout the course of this work. The author is also grateful to the members of his thesis guiding committee: Dr. M. Fels, Dr. F. Hamdullahpur and Dr. H. Gomaa for their interest and helpful comments.

The work of the technical support staff at the Chemical Engineering Department is gratefully acknowledged, Mr. R. Dube, Mr. J. Kozel and B. Liekens. The financial support provided by the Environmental Science and Technology Alliance of Canada and the University of Dalhousie is greatly appreciated.

Special thanks are expressed to Miss Mona Al-Mosawi and to the author's family and friends for their constant support and understanding during his years of university study.

ABSTRACT

This thesis investigates the performance characteristics of a novel liquid-liquid contactor that employs woven screens as static mixing elements. The drag coefficient for single-phase flow was determined and compared to data reported in the literature. This showed that there is a relatively large discrepancy between the experimental data and the reported correlations, particularly for high fractional screen open area. Introduction of the dispersed phase to the main flow causes the drag coefficient to deviate slightly from its original value. The highest turbulence intensities and energy dissipation rates were found to occur immediately behind the screen and falls sharply with increasing downstream distance.

At 0.5% holdup, d_{32} was found to decrease logarithmically with the increasing superficial velocity with an exponent value of -1.15 to -1.40 . Much lower dependence was obtained at 4% holdup. It was also found to vary exponentially with the energy dissipation rate with an exponent value of -0.42 and -0.26 at 0.5% and 4% holdups respectively. d_{32} was found to decrease with the increasing dispersed phase holdup, a result proposes that screen wires exert a cutting action on drops. Under fully developed turbulent conditions, the average drop size was found to correlate with the jet Weber number with an exponent value of -0.75 and -0.34 at 0.5% and 4% holdups respectively. The mean drop size was found to decrease with increasing surfactant concentration and to correlate using the equilibrium interfacial tension, the Marangoni number and surface excess.

d_{32} generated in this static mixer was satisfactorily correlated by,

$$d_{32} = 0.302 \text{Re}_{jet}^{1.38} \text{We}_{jet}^{-1.05} \phi^{-0.084} \left(\frac{b}{M} \right)^{0.349}$$

while the maximum stable drop size achievable in this contactor was well correlated by,

$$d_{\max} = 1.66 \sigma^{0.6} \epsilon^{-0.53} \rho^{-0.6}$$

The variance of the resultant drop size distributions decreases with the increasing superficial velocity, the Weber number and the jet Weber number. It was also found to vary with the jet Weber number exponentially with an exponent value of -3.74 under fully developed turbulent flow conditions. No single distribution could fit the normalized drop number density distributions. Cumulative drop volume density distributions were found to exhibit self-similarity and to be well represented by the normal distribution. For a p value of zero, the Rod and Misk (1982) model can predict the average equilibrium drop size well. It was also found to predict reasonably well the generated cumulative drop size distributions.

The efficiency of energy utilization achievable in this contactor was satisfactorily correlated by,

$$\eta = 107.15 \phi^{1.40} U^{-0.38} \alpha^{1.11}$$

Screen mixing elements were found capable of generating much higher interfacial areas when compared with other static mixers and mechanically agitated tanks.

Chapter 1

INTRODUCTION

Liquid-liquid dispersion operations are encountered in a wide range of chemical processes and industries such as petroleum, food, pharmaceutical, emulsion polymerization, liquid-liquid extraction, distillation, etc., in which mass and heat transfer processes are of prime importance.

Since, the mass transfer coefficient in immiscible liquid systems is not strongly affected by the hydrodynamic factors (Brodkey and Hershey, 1988), one can only increase the mass transfer rate by maximizing the available interfacial area of contact between the phases (dispersing one phase in the form of fine drops that have large specific interfacial area). Therefore, the objective of liquid-liquid mixing operations is to increase the interfacial area of contact between the two phases in order to promote mass and heat transfer rates and chemical reactions. Although, the maximization of the interfacial area can be easily accomplished by increasing the energy input to the mixing equipment, this could be very problematic. Improper use of very high-energy input results in the formation of very fine droplets rendering the subsequent separation of the two dispersed phases a very difficult task, especially when the density ratio of the two phases is close to unity. Figure 1.1 shows the effect of drop size on the separability of the two phases at various density ratios. The data in Figure 1.1 have been calculated using Stokes law assuming lamella gravity separator of 2.5cm plate spacing.

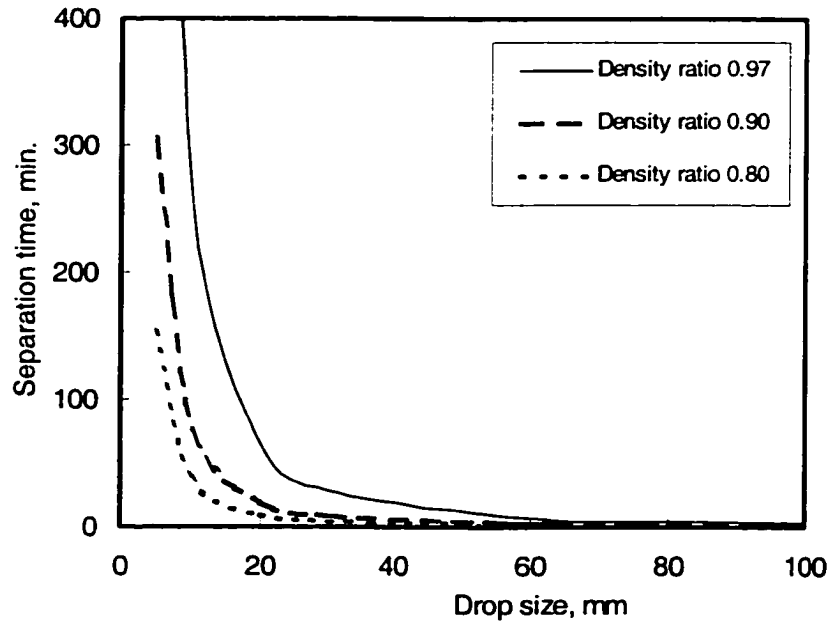


Figure 1.1. Effect of drop size and density ratio on the time needed to separation the constituents of an immiscible liquid dispersion (Lamella gravity separator of 2.5cm plate spacing).

The mixing of two immiscible liquids results in dispersions, in which simultaneous drop breakup and coalescence occurs continuously. Depending on the prevalent hydrodynamic conditions in the mixer, a steady state drop size distribution is obtained, when a state of dynamic equilibrium is attained between the breakup and coalescence processes. The resultant drop size distribution is affected by several factors such as the physical properties of the two phases, system hydrodynamics (e.g., average energy dissipation rate, local energy dissipation rate, dispersed phase hold-up) the type and geometry of mixing elements, and the vessel (e.g., impeller diameter-to-vessel diameter ratio) (Kubie and Gardner, 1977; Calabrese et al., 1986; Chatzi et al, 1991; Rincon-Rubio et al., 1994; Chatzi and Kiparissides, 1995, 1997; Lo et al., 1998; Seidshazileh, 1999).

Mechanically agitated tanks, and in-line mechanical mixers, are the equipment most commonly used to generate large interfacial areas between immiscible liquids. In such equipment, unfortunately, because of the large spatial variation in energy dissipation

rate and the uncontrolled recirculation pattern, a wide and complex drop size distribution is produced at high-dispersed phase concentrations. In addition, the results obtained in mechanically agitated tanks are difficult to scale up. They also proved to be relatively difficult to design and are associated with higher power consumption (Cutter, 1966; Merchuk et al., 1980; Zhou and Kresta, 1997).

In the last three decades, static mixer technology became an essential part of the chemical industry. These mixers are available in different types and configurations and can be used for single and multi-phase mixing as well as for laminar, transitional and turbulent mixing. Static mixers use motionless mixing elements, installed in a pipe, to direct or obstruct the fluid flow in order to achieve effective mixing.

Static mixers offer a wide variety of advantages over the mechanically agitated tanks; the most important advantages are (Myers et al, 1997):

- Mechanical stability and absence of moving parts.
- Almost no maintenance requirements.
Suitability for limited spaces and easiness of incorporation in existing processes.
- Available in a wide variety of construction materials.
- Power requirements for pumping only.
- Narrow residence time distribution.
- Cost effective.

This proposed research project is aimed at developing a static mixer that can be used to generate small and narrowly sized dispersions and can thus be used to intensify heat and mass transfer operations for immiscible liquid systems.

Chapter 2

LITERATURE REVIEW

In this chapter, previous work pertaining to flow through screens is first reviewed, followed by a discussion of the factors affecting liquid-liquid dispersions produced in various mixing equipment. The topics covered in the second part have been subdivided into three sections in order to facilitate understanding of the effect different parameters have on the average drop size and drop size distribution. In the first and the second sections, drop breakup and coalescence are reviewed whereas the factors affecting drop size distributions in liquid-liquid systems are discussed in the third section.

2.1 FLOW THROUGH SCREENS

In this section, the literature dealing with fluid flow through screens is reviewed. This includes pressure drop across screens, turbulence intensity and its decay rate, as well as the structure of turbulence in the flow behind screens (e.g. turbulence scale, homogeneity, and isotropy).

Screens are usually characterized by their mesh number, mesh size, M ; bar size, b ; and the fractional open area, α . The mesh number is the number of openings in a lineal inch measured from the center of one wire to a point one inch distant. Mesh size is the measured distance between adjacent parallel wires. The turbulence structure generated downstream of the screen is controlled by the upstream superficial velocity as well as by these parameters. For example, Davies (1972) reported that the bar size, b , has a strong influence on the size of eddies behind the screen. Small b/m ratios thus generate small

eddies which tend to decay more rapidly than the larger ones. Therefore, screen geometric parameters are usually utilized as characteristic lengths in the dimensionless numbers used to characterize fluid flow through screens.

2.1.1 Reynolds Numbers

The Reynolds number represents the ratio of momentum to viscous forces. However, several Reynolds number definitions can be used to describe flow through screens (Table 2.1).

Although there is still disagreement over which Reynolds number should be used to characterize flow behind screens, the mesh Reynolds number, Re_M , appears to be the most commonly used one. However, if one considers the effect of screen geometry on grid-generated turbulence, the screen-wire, Re_b and jet Reynolds numbers, Re_{jet} , seem to be the more proper numbers. The effect of screen geometry, represented by the macroscopic jet Reynolds number, on the transient mean drop will be discussed later. In addition to the above Reynolds numbers, several length scale Reynolds numbers can be defined but are less frequently used.

2.1.2 Pressure Drop across Screens

Pressure drop across screens can be treated in a fashion similar to that of flow through orifices (Chen and Liu, 1991; Liu et al., 1993, Zhang and Chen, 1996) where the drag coefficient is a function of Reynolds number. On the other hand flow across screens can be analyzed in an approach similar to flow past submerged objects using one of several drag coefficient expressions proposed by several authors (Gad-El_Hak and Corrsin, 1974; Ehrhardt, 1983; Groth and Johansson, 1988). The first approach is used in the present study due to its flexibility and because it facilitates comparison with the available experimental data.

Table 2.1. Reynolds number used in flow through screens.

NAME	Characteristic length	Expression
Wire Reynolds' number Re_b	Wire diameter	$\frac{\rho b U}{\mu}$
Mesh Reynolds number Re_M	Opening width	$\frac{\rho M U}{\mu}$
Individual jet Reynolds number Re_j	Jet diameter	$\frac{\rho}{\mu \alpha} \frac{2(M-b)U}{\sqrt{\pi}}$
Jet Reynolds number Re_{jet}	Wire diameter	$\frac{\rho D(U/\alpha)}{\mu}$

The flow through screens/grids can be dealt with as a closely-packed set of jets that approach each other as they move downstream, finally coalescing into what may be considered an essentially uniform flow. Consequently, the flow through screens may be subdivided into three regions (Baines and Peterson, 1951):

- the region of the free stream well ahead of the screen;
- the region at which the jets emerging from the openings are fully contracted but still essentially non-diffused or non-coalesced;
- the region of the free stream well behind the screen.

Laws and Livesey (1978) suggested that the turbulence structure downstream of a screen is affected by a combination of the three distinct turbulence profiles. The first one is due to the upstream turbulence, the second one is caused by screen-generated turbulence and the third one is shear-generated turbulence created by non-uniformity in the generated time-mean profile as it decays. The interaction between those three turbulence profiles makes it difficult to accurately predict flow past screens.

A combination of the energy and momentum equations for the upstream to the downstream of a screen can be written as (Baines and Peterson, 1951):

$$P_1 + \frac{\rho}{2}(U_1^2 - U_2^2) = P_3 - \rho U_3(U_2 - U_3) \quad (2-1)$$

where U_1 and U_3 equal the mean velocity in the free stream, U_2 is the velocity in the contracted jets, and ΔP is the pressure drop across the screen ($P_1 - P_3$). The equation of continuity can be written in terms of the open area, A_0 , and total area, A_t , as:

$$C_0 A_0 U_2 = A_t U \quad (2-2)$$

Since the open area fraction $\alpha = A_0/A_t$, the continuity equation can be re-written as

$$\frac{U_2}{U} = \frac{1}{C_{coe} \alpha} \quad (2-3)$$

where C_{coe} is the coefficient of contraction of the jets.

Neglecting the resistance along the pipe walls (relative to the losses across the screen), the Bernoulli equation can be written as

$$\frac{\Delta P}{0.5 \rho U^2} = \left[\frac{1}{C_{oe.c} \alpha} - 1 \right]^2 \quad (2-4)$$

Both viscous and inertial forces cause pressure drop through the screens. The viscous resistance usually dominates in the laminar flow region, where pressure drop is caused by viscous drag (e.g. skin friction at the surface of the screen wires). As the flow velocity increases, the effects of the viscous forces become relatively unimportant and the total inertial pressure losses result mainly from the turbulent vortexes and pressure drop caused by sudden contraction and enlargement around the wires of the screen.

The drag coefficient (or pressure drop coefficient), which expresses the magnitude of the screen pressure drop, is defined by:

$$\psi = \frac{\Delta P}{0.5 \rho U^2} \quad (2-5)$$

The drag coefficient (or the pressure drop coefficient) represents the ratio of the pressure drop to the dynamic pressure of the bulk flow and is an important parameter that describes the hydrodynamics of flow through the screens. As is the case with many other geometries, its value can be influenced by external parameters. For example, Nakagawa (1985) suggested that the transition from laminar to turbulent flow in the region upstream from the screen might play an important role in the experimentally observed fluctuations

in screen drag coefficient. According to his observation, when the upstream flow to the grid is laminar the fluctuations are greater whereas when the upstream flow is turbulent they diminish.

The magnitude of the drag coefficient of screens is a function of the percentage open area of screens, the Reynolds number Re_b , and the Mach number. For incompressible flow, it is a function of the open area fraction ratio and the grid Reynolds number (Laws and Livesey, 1978; Ehrhardt, 1983; Groth and Johansson, 1988). The variation of $\Psi=f(\alpha, Re_b)$ will predict a reduction in ψ with increasing Re_b until the critical value of $Re_b > 250$ is exceeded (Laws and Livesey, 1978). After that point, the drag coefficient becomes a function of percentage open area only. Groth and Johansson (1988) reported that the function $f(Re_b)$ reached a constant value at high Re_b values, but increases quite dramatically as Reynolds numbers decrease below 100. For the higher Reynolds number, $Re_b > 100$, the Groth and Johansson's value of $f(Re_b)$ approaches 0.45 while Pinker and Herbert (1967) and Reynolds (1969) report a final value of $f(Re_b) \approx 0.52$.

In general, the drag coefficient can be written as the product of two functional groups:

$$\psi = f(Re_b) \cdot f(\alpha) \quad (2-6)$$

Several attempts have been made to relate the drag coefficient with screen open area. The expression proposed by Pinker and Herbert (1967), Laws and Livesey (1978), and later adopted by Groth and Johansson (1988) is as follows:

$$\psi = f(Re_b) \frac{1-\alpha^2}{\alpha} \quad (2-6a)$$

The above relationship is believed to be valid for $0.32 < \alpha < 0.64$.

Ehrhardt (1983) proposed the following relationship that correlates data covering more than 100 different types of wire mesh and different fluids such as water, petroleum and air:

$$\psi \propto \frac{1-\alpha}{\alpha^2} \quad (2-7)$$

Then he used by the above relationship to develop a general expression for the drag coefficient, which is applicable for $0 < Re_b < 1000$ and $0.25 < \alpha < 0.68$,

$$\psi \frac{\alpha^2}{1-\alpha} = 0.72 + \frac{49}{Re_b/\alpha} \quad (2-7a)$$

Gad-El-Hak and Corrsin (1974) developed another expression by combining Bernoulli's equation with the continuity equation. Some simplifying assumptions introduced by them include: thin boundary layers which separate at the "throat" of the contraction of the opening channel, and neglecting viscous and body forces. Sudden expansion flow was also assumed. The following expression (which is valid for the range $10^3 < Re_b < 10^5$) was obtained:

$$\psi \propto \left(\frac{1-\alpha}{\alpha} \right)^2 \quad (2-8)$$

It must be borne in mind that variations in grid dimensions could lead to significant effects on the pressure losses, particularly in the case of fine-mesh screens. Nakagawa (1985) reported that the drag coefficient varies with the mesh Reynolds number up to a value of $Re_M \approx 500$, beyond which the drag coefficient becomes virtually independent of Re_M . Since $Re_b = (1 - \sqrt{\alpha})Re_M$, the corresponding critical value of Re_b would vary between 52.8 and 276 as the solidity $(1-\alpha)$ ranges from 0.2 to 0.8.

Recently, Chen (1996) investigated the pressure drop caused by single-flow (water) through screens and correlated his experimental data in a fashion similar to that proposed by Ehrhardt (1983). He obtained the following expression for the drag coefficient:

$$\psi \frac{\alpha^2}{1-\alpha} = \frac{21.72}{(Re_b/\alpha)^{0.46}} \quad (2-9)$$

Chabra and Richardson (1985) suggested that the flow through a screen could be presented in a fashion similar to that used for flow through beds of particles. They suggested the use of the jet velocity ($U_j = U/\alpha$) as a correlating parameter. The drag coefficient thus becomes:

$$\psi = \frac{2\Delta P}{\rho(U/\alpha)^2} \frac{1}{(1-\alpha)} \quad (2-10)$$

The factor $(1-\alpha)$ was introduced in order to take the effect of solidity into account on the drag coefficient. Considering the shape of the screen elements, it was suggested (Baines and Peterson, 1951) that such parameters are of secondary importance in all cases, because they only influence the energy loss and not the general distribution of velocity and turbulence.

2.1.3 Turbulence Intensity and Turbulence Energy

Although grids are extensively used to generate isotropic turbulence in flows, the grid-generated turbulence is anisotropic in the region close to the grid. The ratio of turbulence intensity in different spatial co-ordinate directions is commonly used to show the deviation from isotropy in the case of three-dimensional flows. However, in the case of screens this reduces to a two-dimensional situation due to the presence of axial symmetry (Gad-El-Hak and Corrsin, 1974; Groth and Johansson, 1988). By testing grids with open area of 0.56 and 0.66 in a wind tunnel, Comte-Bellot and Corrsin (1966) showed that the ratio of the turbulence intensities in the stream direction to the normal ones could be as high as 1.25. This was later confirmed by Walker (1986) who obtained turbulence intensity ratios as high as 1.3.

As shown by most of experimental investigations (Uberoi and Wallis, 1967; Gad-El-Hak and Corrsin, 1974; Groth and Johansson, 1988), grid-generated turbulence very closely approaches perfect isotropy downstream from the region of grid turbulence establishment. Groth and Johansson (1988) showed that the turbulence becomes almost isotropic at a distance of about 20 mesh widths downstream of the screen. As a result, the equations of motion and the resulting correlations may be greatly simplified. The lateral scales of turbulence on the y - and z - coordinates may thus be assumed to be equal, and equal to one half the longitudinal scales L_x (Groth and Johansson, 1988). Turbulence intensity decreases and the turbulence length scale increases with increasing distance downstream from the screen. Gad-El-Hak and Corrsin (1974) suggested that the velocity

distribution behind a screen is simple with a one-dimensional mean flow and closely approximates plug flow. However, the profile can be quite complicated even in the case of low to moderate wire size Reynolds numbers with solidity below the unstable range ($1-\alpha < 48\%$). Laws and Livesey (1978) and Villermaux et al. (1991) suggested that the wakes generated by the individual bars become turbulent in the region adjacent to the grid, that they spread individually and interact in some complicated manner. The wakes eventually merge, resulting in nearly homogeneous turbulence at a large number of mesh lengths.

A more appropriate way is to consider flow through screens as a number of jets, which are independently formed and then gradually spread and coalesce with neighboring jets at a certain distance downstream from screen (Villermaux et al., 1991). The energy of the mean flow is thus converted into turbulent energy by eddies generated in the dead zones adjacent to the jets where intense shear is encountered (Figure 2.1). These eddies start to decay due to their eddy-eddy interaction and their energy is converted into heat. Any expression for the decay of turbulence intensity should, therefore, reflect the influence of the coalescence length which is shown in Figure 2.1. Meanwhile, the initial jets formed behind the screen should reflect the pattern of the screen openings. These jets oscillate and expand with increasing distance from the screen and eventually coalesce with adjacent ones when the equivalent diameter of each jet reaches the wire mesh size M . For grid-generated turbulence, Villermaux et al. (1991) found that the jet coalescence length, L_j , could be best expressed by the following relation for $Re_j < 3000$:

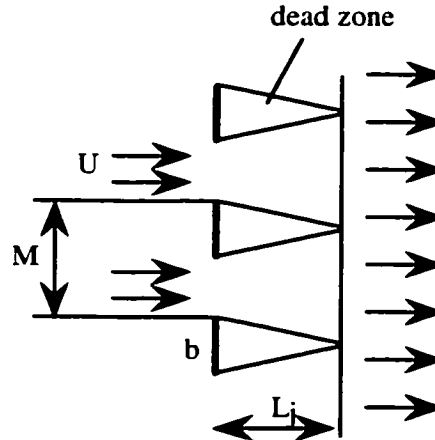


Figure 2.1 Geometry of the flow behind the grid.

M --mesh size, b --bar size, L_j -- jet coalescence length , U --mean velocity

Redrawn from Villermaux et al. (1991)

$$\frac{L_j}{M} = \frac{10^4}{Re_j} \quad (2-11)$$

where $M' = M/\sqrt{2}$ for square weave screen and $M' = M/\sqrt{3}$ for triangular weave grid. The corresponding jet Reynolds number was defined by:

$$Re_j = \frac{(U/\alpha)(M-b)\rho}{\mu} \quad (2-12)$$

Because the above correlations were obtained using very low grid porosities ($\alpha = 0.08$ and 0.13 , and M/d_{jet} varying between 2.54 and 3.47), they concluded that the influence of b becomes minimal and there is little need to use b -in addition to M' - to obtain good correlations. However, Davies (1972) suggested that the size of the energy-containing eddies generated by the grid will be largely determined by the geometry of the grid, i.e., by the ratio b/M . He further suggested that the bar size b has a strong influence on the size of the eddies shed behind each bar, and that the small eddies formed behind small wires decay more rapidly than do larger eddies. As first predicted by von Kármán's theory, it is the bar size b rather than the mesh size M , which is the significant reference length in the region of isotropic turbulence decay (Baines and Peterson, 1951).

However, Baines and Peterson (1951) emphasized that the influence of the screen geometry on the intensity extends only to a relatively short distance down stream.

Tests conducted on grids by Villermaux et al. (1991) show that L_j/M approaches the value of 4 under conditions of $Re_{jet} > 3000$. This means that L_j is approximately $2.8M$ for the above mentioned conditions. Furthermore, the correlation of their jet coalescence length can be significantly improved (maximum of 22% additional reduction in relative error) by using $(M' - d_{jet})$ instead of M . Since $M' - d_{jet} = b$, it may be possible to conclude that in the transition flow region, coalescence of jet is decided by jet Reynolds number as well as b ; while at $Re_{jet} > 3000$ the merging length only depends on the bar size b . This suggest that the magnitude of grid turbulence depends on the Reynolds number computed on the basis of the diameter of the screen wire.

As discussed above, the flow within the merging length L_j is dominated by the individual oscillating jets. After merging, the oscillations are indistinct because of the intense small scale turbulence. However, the frequency of oscillation still dominate the spectrum (Villermaux et al., 1991) and the turbulence intensity is higher than that before the jets are merged. According to the Taylor hypothesis, the oscillations' periodicity corresponds to a streamwise length-scale about twice the connection length L_j (typically 10 times the grid mesh). Villermaux et al. (1991) suggested that this phenomenon is very different from the ordinary grid turbulence generated using low solidity screens, where the length scale is of the order of the grid mesh. These large-scale instabilities could bear some relationship to recent conjectures on inverse energy cascade in three-dimensional turbulence (Shtilman and Sivashinsky, 1986; Yakhot and Pelz, 1987). Indeed, different classes of spatially-periodic flows have been found to be linearly unstable to large-scale perturbations. In grid-generated turbulence, the relaxation toward isotropy probably happens before significant inverse energy cascade can occur. However, Villermaux et al. (1991) suggested that this might not be so in the more anisotropic turbulence produced by large-solidity grids.

2.1.4 Decay of Turbulence Intensity

The decay of turbulence intensity in the flow behind grids and screens is of fundamental importance to a wide range of fields and can be dealt with as a one-dimensional problem. As soon as the fluid passes through the screen, vortex trails form immediately downstream, but after a relatively short distance, a homogeneously radial profile and quasi-isotropic turbulence flow with low intensity is formed (Bourne and Lips, 1991). Once the variation in mean velocity has been diminished by turbulent diffusion, more and more of its initial stock of energy is transferred to and dissipated in the smallest eddies by viscous flow (Reynolds, 1974; Davies, 1972).

In order to relate experimentally-generated grid turbulence to the homogeneous model, should be used (Reynolds, 1974). Taylor's hypothesis states that the statistical properties measured at a fixed point (past which slowly decaying turbulence is carried by a uniform flow) are identical to those which would be found by averaging over a large volume of homogeneous turbulence. The most important assumption that needs to be emphasized here is that grid-generated turbulence is generally treated as isotropic turbulence although it is, more precisely speaking, quasi-isotropic.

Using the K-H equation to describe isotropic turbulence, Von Karman and Howarth (1961) were able to derive the following expression for the decay of turbulence intensity along the downstream distance:

$$\frac{U}{u_{rms}} = \frac{5}{MA^2} X + Const. \quad (2-13)$$

It should be borne in mind that Equation (2-13) is only valid under the assumption of isotropic turbulence. Various semi-empirical correlations have been proposed for describing the decay of grid-turbulence when departure from the isotropic conditions assumed.

Taylor (1935) was the first to propose generating turbulent flow with a regular honeycomb or grid hoping to generate the simplest form of turbulence in the laboratory, which would approximate isotropic turbulence. He assumed that large scale turbulence is

constant in size and developed a theory for turbulence decay, which could predict the decay of his data:

$$\left(\frac{U}{u_{rms}}\right)^2 = \left(\frac{X}{M}\right)^2 \quad (2-14)$$

Where u_{rms} is the root mean square fluctuating velocity in the stream. Later Taylor's results were found to be incorrect when measurements became available for larger x/M values. Corrsin(1963) proposed a modified decay law, which later was confirmed by Comte-Bellot and Corrsin (1966):

$$\left(\frac{U}{u_{rms}}\right)^2 = \left(\frac{X - X_0}{M}\right)^n \quad (2-15)$$

where n varies between 1.28 and 1.35. Subsequently, most investigators (Uberoi, 1963; Comte-Bellot and Corrsin, 1966; Uberoi and Wallis, 1967; Davies, 1972; Yeh and van Atta, 1973; Gad-El-Hak and Corrsin, 1974; Alcaraz et al., 1981; Britter et al., 1983; Stapountzis et al., 1986; Nakamura et al., 1987; Groth and Johansson, 1988; Bourne and Lips, 1991; Lance and Bataille, 1991;) started to use a slightly modified expression for the description of the decay of turbulence intensity behind screens. It is given by:

$$\left(\frac{U}{u_{rms}}\right)^2 = C \left(\frac{X - X_0}{M}\right)^n \quad (2-16)$$

where C and n are constants. This can be expressed using relative turbulence intensity as:

$$\left(\frac{u_{rms}}{U}\right)^2 = \frac{1}{C} \left(\frac{X - X_0}{M}\right)^{-n} \quad (2-17)$$

The virtual origin of the decay laws based on (X_0/M) is the hypothetical axial position where u_{rms} is infinite. The resulting values of the constants C , n and (X_0/M) , are listed in Table 2.2. The widely scattered values of those parameters developed in previous studies (Bennani et al., 1985; Britter et al., 1983; Stapountzis et al., 1986; Comte-Bellot and Corrsin, 1963; Gad-El-Hak and Corrsin, 1974; Sreenivasan et al., 1980; Groth and Johansson, 1988; Nakamura et al., 1987; Uberoi and Wallis, 1969; Uberoi and Wallis, 1967; Alcaraz et al., 1981; Bourne and Lips, 1991; Davies, 1972; Yeh and van Atta,

1973; Lance and Bataille, 1991; Wahrhaft and Lumley, 1978) could have been caused by incomplete accounting for all the factors influencing the decay of turbulence behind screens. For example, the major drawback of Equation (2-17) is that the characteristic length scale used was mesh size M whereas one can expect that the decay of turbulence is decided by both mesh size and the distance downstream from the screen. As can be seen from Table 2.2 there exists no common agreement on the value of virtual origin as well as the constant C .

The turbulence decay (Equation (2-16)) is based on experimental data which were obtained using screens with limited porosities ($0.56 < \alpha < 0.71$). Hence, in a manner similar to that investigated in relation to the jet coalescence length (Section 2.1.3) the constants in the decay equation are expected to depend not only on the mesh size, but also on the geometry of the screen. This is in agreement with the suggestions made by Baines and Peterson (1951), Uberoi and Wallis (1967) and Davies (1972). Whereas Kolmogoroff predicted that $n = 10/7$ (i.e. $n = 1.43$) if the existence of the Loitsiansky invariant is assumed (Uberoi and Wallis, 1967). A listing of the various proposed correlations (Table 2.2) indicates that the experimental value of the exponent n varies between 1.00 to 1.67. The value of exponent n may thus be considered as an empirical parameter the value of which varies between 1 and 1.67. In this work, the approach proposed by Groth and Johansson (1988) will be used because it covers a wider range of α and fits the data obtained by several previous investigators rather well. Their correlation uses the point of maximum energy dissipation (rather than infinite relative turbulence intensity) as virtual origin for energy decay length.

Table 2.2: Constants of Turbulence Decay Equation (2-16).

α	$Re_M \times 10^{-4}$	x_0/M	n	C	Researcher
0.56	0.85 1.70 2.60		1.30 1.28 1.35	20.0 23.0 17.0	Corrsin (1942)
0.66	0.55 1.10		1.13 1.25	70.0 48.0	Batchelor and Townsend (1948)
0.56	2.40		1.37	8.5	Baines and Peterson (1951)
0.66	3.30		1.35	10.0	Tsuji and Hama (1953)
0.66	242.00		1.00	71.0	Kistler and Vrebalovich (1961)
0.56	2.90		1.20	24.0	Uberoi (1963)
0.87 0.81 0.75 0.71 0.69 0.62	1.18 1.15 0.82 2.64 0.61 1.82		1.67 1.52 1.43 1.14 1.34 1.43	--- --- --- --- --- ---	Harris (1965)
0.66 0.56 0.69	1.70 3.40 6.80 13.50 3.40 6.80 3.40 6.80		1.29 1.27 1.25 1.15 1.24 1.26 1.32 1.33	19.0 20.0 22.0 29.0 35.0 34.0 7.1 7.9	Comte-Bellot and Corrsin (1966)
0.63	4.83 5.72 6.26		1.32 1.32 1.30	13.2 14.1 14.8	Gad-El-Hak and Corrsin (1974)
		3 2.5	1.28 1.14	23 62	Walker (1986)
0.64	0.148-0.297	3	1.45	17.7	Nakamura et al. (1987)
0.56- 0.71	0.0056-0.84	6 0.8 0	1 1.32 1.34	25.2	Groth and Johansson (1988)

Based on recent data obtained using Laser Doppler Anemometer, Lance and Bataille (1991) adopted a different approach to correlating turbulence decay and obtained the following correlation:

$$\left(\frac{U}{u_{rms}}\right)^2 = 48^2 \left(\frac{X}{M}\right)^{2.32} \quad (2-18)$$

This equation is similar to Taylor's original approach (Equation (2-14)) and is applicable for $X/M > 25$ and $Re_M > 5000$.

Most researchers investigated screens with limited range of porosities ($\alpha = 0.56 - 0.7$) and used the mesh size and mesh Reynolds numbers to characterize grid-generated turbulence. Such approach may thus be considered as a simplified way of dealing with the mesh geometrical parameters (b , M and α). Due to the limited range of screen open area studied, the significance of different bar size relative to the mesh size is quite small. The errors rising from this approach became clear when the above approach was applied to the screens used in the present study ($\alpha = 0.27$ to 0.41 and $b = 0.62$ to 0.508 mm) where the turbulence intensity of a screen with $\alpha = 0.41$ was predicted to be higher than that of a screen with $\alpha = 0.33$.

The geometry of a wire cloth screen can be characterized by only two parameters, namely b and M . Using the ratio b/M , Bourne and Lips (1991) suggested the following empirical correlation to calculate the constant C :

$$C = \frac{106(1 - b/M)^4}{(b/M)(2 - b/M)} \quad (2-19)$$

The effect of screen geometry on the value of the parameter C is shown in Figure 2.2. When b/M is small (which corresponds to high open area) the value of C is large; this, correspondingly, results in smaller turbulence intensity (Equation (2-17)). Although this corresponds with phenomenological predictions, Equation (2-19) should be cautiously used at very large b/M values since it approaches the value of $C = 0$ (i.e. no turbulence intensity) for the case of $b/M = 1$ which represents open pipe flow.

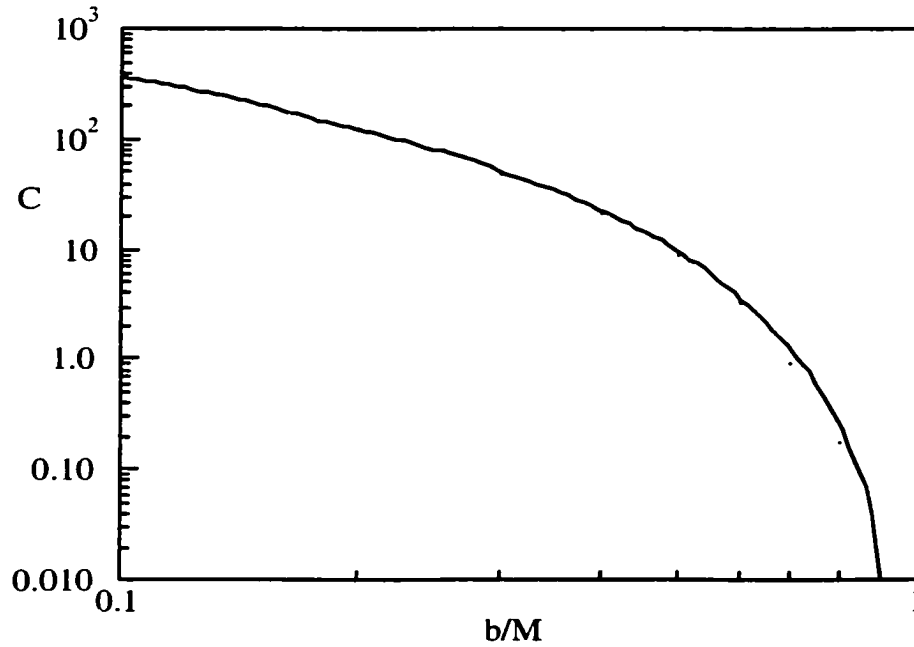


Figure 2.2. The effect of screen geometry on the value of C in Equation (2-19) (Chen, 1996).

2.1.5 Kinetic Energy and Energy Dissipation

Energy dissipation per unit mass in isotropic turbulent flows is the most commonly evaluated parameter. It can be expressed as (White, 1974):

$$\varepsilon = \nu \left(\frac{\partial u_i}{\partial x_j} + \frac{\partial u_j}{\partial x_i} \right) \frac{\partial u_i}{\partial x_j} \quad j=1, 2, 3 \quad (2-20)$$

In isotropic homogeneous turbulence, the energy dissipation rate can be expressed as (White 1974):

$$\varepsilon = -15\nu u_{rms}^2 \left(\frac{\partial^2 f}{\partial r^2} \right)_{r=0} = 30\nu \frac{u_{rms}^2}{\lambda_T^2} \quad (2-21)$$

As can be seen from Equation (2-21), in isotropic turbulence, energy dissipation rate is proportional to the square of turbulence intensity and inversely proportional to the square of Taylor length scale. This implies that the higher the turbulence intensity, the higher the energy dissipation rate. On the other hand, the smaller the size of vortex generated by turbulence, or the greater the number of smaller eddies generated, the smaller is the Taylor's micro-length scale and hence more turbulent energy is being dissipated.

Lance and Bataille (1991) studied air/water flow in grid-generated turbulent flows, and found that the turbulent kinetic energy increases strongly with increasing dispersed phase holdup, ϕ . They observed the existence of two distinct regimes: the first one corresponds to low value of ϕ (where hydrodynamic interactions between individual jets are negligible) and the second one corresponds to higher α values. At higher porosities, the bubbles transfer a greater amount of kinetic energy to the liquid due to their mutual interactions. The Reynolds stress tensor shows that the quasi-isotropy is not altered. At low enough values of ϕ , the difference between the turbulent kinetic energy in the liquid phase and the energy associated with the grid-generated turbulence seems to be approximately equal to the intensity of the pseudo-turbulence (i.e., the fluctuating energy under non-turbulent conditions).

2.1.6 Homogeneous Turbulence

Screens or grids are widely used for the generation of quasi-isotropic turbulence (Hinze, 1975). Baines and Petterson (1951) reported that the fractional open area should be low enough in order to obtain homogeneous turbulence. It was found that the optimum screen open area for generating quasi-isotropic turbulence to be 0.56 for circular rods (Comte-Bellot and Corrsin, 1966).

Screen-generated turbulence becomes statistically homogeneous across the flow after traveling downstream a few mesh sizes. Hinze (1975) suggested that after a distance of about 10-20 mesh sizes the vortex trails formed immediately downstream from the grid evolved to a radially homogeneous turbulence. This low intensity and nearly isotropic turbulence then decays gradually into what can be considered as essentially a one-dimensional problem.

For a screen open area larger than 0.54, several investigators observed that the uniformity of the mean velocity profile dramatically breaks down behind the grid (Corrsin, 1944; Baines and Peterson, 1951). Baines and Peterson (1951) observed that when a grid with a solidity ratio equal to 0.75 was used, the resulting flow pattern (i.e.,

Lateral non-uniformity) remains fairly steady in time, and such flow pattern is maintained over large-scales compared to the grid mesh.

In homogeneous turbulence, the vortices shrink from 12η to 1η during a lifetime τ_{vor} given by (Villermaux et al., 1991):

$$\tau_{vor} = 12 \left(\frac{v}{\varepsilon} \right)^{1/2} \quad (2-22)$$

where η is the Kolmogoroff velocity microscale, which is expressed as:

$$\eta = \left(\frac{v^3}{\varepsilon} \right)^{1/4} \quad (2-23)$$

Villermaux et al. (1991) observed that for low open area screens the flow homogeneity breaks down at some distance downstream from the screen. They could not verify whether this is due to successive jet coalescence or not as conjectured by Baines and Peterson (1951). However, they reported that the mean velocity is fairly uniform at the location where initial merging of the jets takes place while non-uniformities start to appear at values of X/M greater than 50.

2.2 DROP BREAKUP AND COALESCENCE

Dispersion and coalescence processes occur simultaneously in two-phase liquid turbulent flows until, as time progresses, a local dynamic equilibrium is reached. Under such conditions, the rates of dispersion and coalescence processes will be equal, therefore resulting in no further change in drop size and drop size distribution. There are many factors that affect drop breakup and coalescence such as the turbulent energy dissipation rate, the physical properties of both phases (the continuous and dispersed phases) and their relative concentrations.

In this section a brief review of the literature dealing with drop breakup and coalescence processes will be conducted. Particular emphasis will be placed on the effect of the dispersed phase volume fraction, energy dissipation rate and the interfacial characteristics on the two processes.

Drop Breakup

Turbulent flows are characterized by the formation of eddies moving randomly within the main flow. Eddies of all sizes exhibit kinetic energy as rotational motion and dissipate energy by viscous shear. The largest eddies (i.e. eddies of a scale comparable to the scales of the main flow) are the most effective in extracting energy from the main flow via the Reynolds stresses. These eddies lose their energy by transferring it to smaller eddies which in turn transfer this energy to smaller ones and so on to the smallest eddies. These smallest eddies have a finite scale, at these scales the liquid motion is characterized by very high shear and hence energy dissipation rates.

Generally speaking, the dispersion or breakage process can be defined as the reduction of the length scale of the dispersed phase blobs upon the mixing of two immiscible liquids. A drop suspended in a continuous phase undergoes breakage, if the disruptive forces exceed the stabilizing forces due to surface tension and dispersed phase viscosity. This explicitly means that the drop breakage is an energy consuming process. This energy may come from the forces associated with fluctuating turbulent eddies, fluid shearing forces and the kinetic energy of the drops themselves (Hinze, 1955).

In regards to droplet breakup, two types of turbulent eddies are distinguished, those larger than or of similar scale to the drop size are only responsible for drop transportation while eddies smaller than drop size cause drop breakage. Therefore, an important parameter in the breakage process is the Kolmogoroff eddy size (i.e., length scale), l_k , which is approximately given by Equation (2-23). Based on Kolmogoroff eddy size, two mechanisms of droplet breakup can be distinguished. These are the inertial-dominated breakup (or turbulent flow breakup) and viscous shear breakup (e.g., laminar flow breakup) (Hinze, 1955). The turbulent flow breakup mechanism will only be considered due to the turbulent nature of the two-phase flow used in the present investigation.

Drop Breakup in Turbulent Flow

Hinze (1955) developed a theory discussing drop breakage in turbulent flow according to which drop breakage occurs as a result of the dynamic pressure fluctuations created by turbulent eddies that bombard the drop surface. For the drop break up to occur, the forces associated with these turbulent eddies should overcome the counteracting surface tension forces. The ratio of the disruptive turbulent energy to the resistive surface energy; is known as the droplet Weber Number, which can be defined as:

$$We_D = C \frac{(\rho_c \varepsilon^{2/3} d^{5/3})}{16\sigma} \quad (2-24)$$

Where C is the constant in the energy function $E(K)$ derived by Kolomogorov for the estimation of the energy associated with turbulent eddies of wave number larger less than $1/d$, where d is the drop diameter. Therefore, according to the Kolmogorov-Hinze model droplet breakup occurs when the drop Weber number exceeds a certain critical value. Gas bubbles in liquids are more deformed than liquid drops due to the large density difference. To account for that Levich (1962) modified the critical Weber number for that effect and Equation (2-24) becomes:

$$d = \left(\frac{We_c}{2} \right)^{0.6} \left(\frac{\sigma}{\rho_c} \right)^{0.6} \left(\frac{\rho_c}{\rho_d} \right)^{0.2} \varepsilon^{-0.4} \quad (2-25)$$

where We_c is the critical Weber number and ρ_d is the dispersed phase density.

Drop Coalescence

Coalescence is a common phenomenon in liquid-liquid dispersions. Coalescence, which is the opposite of drop breakup, results in the formation of a larger drop from two or more drops. The coalesced drops lose their identities and form a single homogeneous drop. For coalescence to occur the drops should approach close enough to each other and the liquid film between them must drain out until a critical thickness is reached which is followed by film rupture. Tsouris and Tavlarides (1994) reported a critical film thickness of about 500 \AA . This means that the drops must collide and be held together for sufficient time to allow for the drainage process to take place. Two important parameters should therefore

be considered when the drop coalescence is discussed; these are the contact and coalescence times. The contact time is defined as the duration of contact between two drops upon collision. The coalescence time is defined as the time taken for the draining of the continuous phase film present between the two drops before a critical thickness is reached, which upon its rupture, coalescence takes place. The contact time is a function of the diameter of the two colliding droplets and the intensity of mixing, while the coalescence time is a function of the diameter of the two droplets, the viscosity and density of the continuous phase and the intensity of mixing. The film drainage is the rate-limiting step in the coalescence process which can also be affected by such factors as the surface or interfacial tension and its gradient (i.e. Marangoni-Gibbs effect), viscosities of both phases, surface viscosities, presence of surfactants or charged species, dispersion forces, film size, droplet sizes and dispersed phase fraction (Davies, 1992; Wright and Ramkrishna, 1994).

High levels of turbulence result in violent collisions and eventually insufficient time for film drainage. As drop size decreases, the adhesive forces, which are responsible for holding the cluster of droplets together, become greater than the turbulent energy associated with the smaller scale fluctuations. In such a situation, keeping the droplets apart becomes impossible and they coalesce.

To sum up, whether drops contact and/or coalesce is strongly influenced by several factors such as the hydrodynamic resistance to near-contact, attraction and repulsion forces, turbulence intensity, presence of surfactants.

2.2.1 Effect of Hydrodynamics

Kolmogorov (1949) and Hinze (1955) studied the dynamics of liquid-liquid dispersions in isotropic turbulent flows and outlined the conditions for the domination of the viscous or inertial forces. Subsequent investigations by other researchers dealt with the dynamics of breakup/coalescence process, were based on the assumption of isotropic turbulence, and were aimed at testing the validity of Kolmogoroff-Hinze's model.

Energy Dissipation Rate

Energy dissipation rate is a major factor affecting the drop breakup/coalescence in turbulent liquid-liquid systems (Olamoto et al, 1981; Davies, 1985). Kolmogorov (1949) and Hinze (1955) proposed the following equation for the maximum stable drop size, d_{max} , in isotropic turbulent flows:

$$d_{max} \propto \sigma^{0.6} \varepsilon^{-0.4} \rho_c^{-0.6} \quad (2-26)$$

Where σ is the equilibrium interfacial tension of the system, ρ is the density of the continuous phase and ε is the turbulent energy dissipation rate per unit mass. The proportionality constant must be determined from experimental data. In the development of the above expression two important assumptions were made. First, the viscosity of the dispersed phase is so small that its resistance to drop breakup can be neglected. Second, the drop size falls in the inertial subrange of the turbulence, which means that the dispersive stress is inertial and not viscous. Hinze (1955) interpreted experimental data taken by Clay (1940) in a couette flow field and obtained a value of 0.725 for the constant C when d_{max} was taken as d_{95} .

Several investigators (Chen and Middleman, 1967; Brown and Pitt, 1972; Middleman, 1974; McManamey, 1979) assumed that d_{32} is directly related to d_{max} . It therefore follows that the Sauter mean diameter can be related to the energy dissipation per unit mass by:

$$d_{32} \propto \varepsilon^{-0.4} \quad (2-27)$$

In the case of isotropic turbulence, the superficial velocity can be related to the energy dissipation rate per unit mass by (Tavlarides and Stamatoudis, 1981; Baldyga and Bourne, 1994):

$$U^2 \propto \varepsilon^{2/3} \quad (2-28)$$

Substituting Equation (2-27) into Equation (2-28) yields:

$$d_{32} \propto U^{-1.2} \quad (2-29)$$

The validity of Equations (2-27) and (2-29) has been studied by several investigators who used various liquid-liquid contacting devices and low holdup dispersions (Sleicher, 1962; Collins and Knudsen, 1970; Kubie and Gardner; Karabelas,

1978; Tavlarides and Stamatoudis, 1981; Lee et al., 1983; Hass, 1987; Clark, 1988, Pacek et al, 1998). The variation of the Sauter mean diameter with energy dissipation rate in mechanically agitated tanks, MAT, equipped with different impeller types yielded exponent values varying between -0.4 to -0.8. The difference between these values and that reported by Hinze is attributed to the departure from the isotropic flow conditions assumed in the derivation of Kolomogrov-Hinze model (Molag et al, 1980; Pacek et al., 1998). Large spatial variation in the local energy dissipation rates, and the uncontrolled recirculation between regions of high and low energy dissipation rates, are the main contributors to the to non-uniform hydrodynamic conditions.

Nishikawa et al. (1987) investigated liquid dispersions in an agitated vessel and obtained different correlations for the Sauter mean diameter in the breakup-dominated and coalescence dominated regions:

$$d_{32} \propto \left(\frac{\sigma}{\rho_c} \right)^{\frac{3}{5}} \varepsilon^{-\frac{2}{5}} \quad (2-30)$$

$$d_{32} \propto \varepsilon^{-1/4} \quad (2-31)$$

Howarth (1967) proposed that a sudden reduction in the impeller speed results in a higher new steady-state value of the mean drop size. Under such transitional conditions the drop coalescence is dominant. This was verified experimentally and it was found that the coalescence frequency is strongly dependent on the impeller speed as shown in Equation (2-33):

$$\lambda = N^{1.90-2.25} \quad (2-32)$$

or since $\varepsilon \propto N^3$ (Pacek et al., 1998), therefore Equation (2-32) can be rewritten as:

$$\lambda \propto \varepsilon^{0.63-0.75} \quad (2-33)$$

Equation (2-33) shows that as the energy dissipation rate increases the drop coalescence frequency increases, which in turn results in a faster rate of drop size increase. Later, Park and Blair (1975) studied drop coalescence and they found that coalescence takes place in a very short time after drop collision and its probability increases as the collision

energy increases. However, Ross et al. (1978) reported that previous works in liquid-liquid dispersion suggest that the overall coalescence rate decreases with the rotation rate. Static or motionless mixers are relatively simple devices, in which mixing elements are placed in the line through which the liquid is pumped. As mentioned in chapter 1, static mixers provide good means for liquid-liquid mixing for enhancing heat and mass transfer processes as well as for producing dispersions. Even though there still limited information available concerning their ability of dispersing one liquid phase into another. In this section an intensive review of the literature dealing with the effect of energy dissipation rate and superficial velocity on dispersion in static mixers is conducted.

Middleman was unsuccessful in applying Kolomogrov-Hinze model to the case of dispersions generated in a Kenics mixer with several immiscible liquid pairs. He found that the mean drop size decreases linearly with the energy dissipation rate with a slope of -0.7 . A similar study was conducted by Chen and Libby (1978) using a Kenics mixer with oil-in-water systems and they obtained a slope value of -0.75 . Liquid-liquid data collected by Matsumura et al. (1981) using a Hi-mixer static mixer and viscous liquids showed that the Sauter mean diameter decreases exponentially with the energy dissipation rate with an exponent value varies from -0.45 to -0.60 depending on the viscosity ratios of the phases. Al Taweel and Walker (1983) investigated 1% kerosene-in-water dispersions using inline-Lightnin static mixer. The Sauter mean drop diameter was found to be dependent on the energy dissipation rate with an exponent value of -0.63 . Walker (1984) extended this study to 4-fold higher values of energy dissipation rate and obtained the same exponent value. El-Hamouz et al. (1994) investigated kerosene/water dispersions produced in a static mixer using inline-Lightnin mixing elements. Their experimental data showed that the Sauter mean diameter showed an exponential dependence on the energy dissipation rate with an exponent value of -0.49 to -0.60 . Al-Taweel and Chen (1996) investigated the dispersion of kerosene in water using woven screens as static mixing elements. They found that the spatial mean equilibrium drop diameter and the rate of energy dissipation could be correlated by the following equation:

$$d_{32\infty} = \varepsilon^{-0.6} \quad (2-34)$$

The discrepancy between the experimental values reported above and theoretical results was attributed mainly to the departure from the homogeneous isotropic turbulence assumed in the derivation of Kolomogrov-Hinze model.

Haas (1987) investigated turbulent dispersion of aqueous solutions in organic liquids using three types of dispersion devices: small-diameter tube and a Kenics static mixer. His results showed good agreement with the Kolomogrov-Hinze model (exponent value of -0.40). Streiff et al. (1997) investigated liquid-liquid dispersions (cyclohexane-in-water and decaline-in-water) using different types of Sulzer mixers (SMX, SMXL, SMV). Their results showed that the normalized drop size data over the whole range of Reynolds numbers (20 to 150000) gives -0.40 for the exponent of the energy dissipation rate as predicted by the Kolomogrov-Hinze model.

Sleicher (1962) studied the dispersion of various organics in water using superficial velocities of 0.56 to 2.4 m/s in an open pipe of 0.035 m diameter and 6.7 m long. His results showed a stronger dependence on velocity (proportional to $U^{-2.5}$) than that predicted by the Kolomogrov-Hinze model. On the other hand, Kubie and Gardener (1977) reported lower dependence of the obtained average drop size on the superficial velocities in pipe flow. Their correlation is based on dispersions of water/isoamyl alcohol and water/n-butyl acetate at velocities of 0.4 to 6.0 m/s using an open pipe of 0.017m diameter and 4 m long. Karabelas (1978) dispersed transformer oil mixtures in water at velocities of 1.2 to 3.0 m/s using a 20 m long pipe 0.0504 m in diameter and found that the drop size is proportional to $U^{1.2}$ which is in accordance with the theoretical value. He attributed the deviation of Sleicher's results from the theoretical one to the inadequacy of the pipe length, which did not allow the dispersion to reach equilibrium conditions.

Walker (1984) produced a result for 1% kerosene/ water system using in-line Lightnin static mixer giving an exponent value of -1.95 for the dependence of drop size on the superficial velocity, which is somewhat higher than the value predicted by the Kolmogoroff-Hinze's model. He also found that the average drop sizes generated by woven screens vary, nearly in proportion with the square of the fluid velocity in the turbulent jets formed by the screens. Walker's results are based on data collected from

kerosene-water dispersions using a 0.0254 m diameter pipe loop using inline-Lightnin and woven screens as static mixing elements. Later, Chen (1996) proposed a correlation for the average drop size generated by woven screens that showed a stronger dependence on the superficial velocity than the theoretical values. The exponent value ranges from 1.77 to 2.10 depending on the hydrodynamic conditions and the physical properties of the system examined. This model is based on data obtained from dispersion of four different petroleum products in tap water using a 0.0254 m pipe loop containing woven screens as static mixing elements. He attributed the deviation of his results from the predicted ones to the departure from the homogeneous, isotropic turbulence structure assumed in the development of Kolomogrov-Hinze model.

Angeli and Hewitt (2000) investigated oil-water dispersions in pipes using dispersed phase volume fractions from 3.4 to 9%. They found that both the maximum and the Sauter mean diameters to depend on the -1.8 power of the continuous phase velocity. They attributed this discrepancy to the assumptions used in the development of the Kolomogrov-Hinze model, that simplify the turbulent field, accepting an average critical Weber number throughout and do not take into account its modifications resulting from the presence of the dispersed phase drops.

Recently, Simmons and Azzopardi (2001) studied a two-phase mixture of kerosene and aqueous potassium carbonate solution in steel and plastic pipes. They found the maximum drop size data at low dispersed phase holdups (1.2 to 3.3 % vol.) follow the Kolomogrov-Hinze model whereas the high concentrations (6 to 42% vol.) data were found to deviate from the theoretical predictions. They attributed the deviation at high dispersed phase holdups to the significant drop coalescence taking place.

Dispersed Phase Volume Fraction

The dispersed phase volume fraction (the holdup) is defined as the volumetric concentration of the dispersed phase in the dispersion. It is believed that the dispersed phase hold-up affects the dispersion process by influencing turbulence structure within the dispersion, which in turn affects both drop breakup and coalescence efficiencies (Brown and Pitt, 1972; Ross et al., 1978; Schott and Yuu, 1978). The variation in the

dispersed phase volume fraction ultimately will be reflected onto the generated drop size and drop size distribution as well as the interfacial area. In the following paragraphs, the effect of the holdup on energy dissipation rate and the average drop size will be discussed while its influence on drop size distribution will be reviewed in sections 4.4.1 and 4.4.2.

Generally speaking as the dispersed-phase volume fraction increases, both the average drop size and the interfacial area increase while the drop size distribution becomes broader (Scott et al., 1958; Ross et al., 1978; Kumar et al., 1991; Chen and Al Taweel, 1996). This phenomenon becomes more pronounced at lower energy dissipation rates as reported by Vergoff et al. (1978) who observed that at an impeller speed of 160 rpm and a holdup of 0.20 the drops formed are about four times larger than those formed at 0.05 holdup. As the holdup increases, larger drops are formed mainly as a result of the enhanced drop coalescence due to the increase in the probability of drop collision (Doulah, 1975; Tavlarides and Stamatoudis, 1981). However, it has been suggested that higher concentrations of the dispersed phase dampens turbulence intensity, which results in lower breakup rates (Ross et al., 1978; Schott and Yuu, 1978). This phenomenon becomes more pronounced at lower energy dissipation rates as reported by Vergoff et al. (1978) who observed that at an impeller speed of 160 rpm and a holdup of 0.20 the drops formed are about four times larger than those formed at 0.05 holdup.

It is important to take into account the ability of the dispersed phase to modulate or dampen the continuous phase turbulence. Several investigators therefore studied the effect of the dispersed phase volume fraction on the energy dissipation rate in the mixer, which in turn affects the drop size generated as seen in the last section. Doulah (1975) proposed the following correlation to account for the effect of dispersed phase hold-up on the energy dissipation rate:

$$\varepsilon \propto (1 + 2.5\phi)^{-3} \quad (2-35)$$

Coulaloglou and Tavlarides (1976) used an approach similar to that of Doulah (1975) to explain the effect of increasing dispersed phase on the energy dissipation rate in mechanically-agitated tanks:

$$\varepsilon \propto (1 + \phi)^{-3} \quad (2-36)$$

Later, Calabrese et al (1986) proposed the following expression, which relates the local energy dissipation rate to the holdup and takes into account the density difference between the two phases, for very dilute dispersions in stirred tank contactors:

$$\hat{\varepsilon} = \hat{\varepsilon}_{\sigma=0} \left(\frac{\rho_d}{\rho_c} \right)^3 (1 + 5\phi)^{-3} \quad (2-37)$$

Several attempts were made to correlate coalescence frequency to dispersed phase concentration in liquid-liquid dispersions from the equilibrium drop size distributions generated in stirred vessels at different turbulence intensities (Howarth, 1967; Mlynek and Resnick, 1972; Coualoglou and Tavlarides, 1977; Das et al., 1987). It was found that the coalescence frequency is proportional to ϕ^n where n varies from 0.5 to 1.0.

The literature reviewed dealing with liquid-liquid dispersions in mechanically-agitated tanks, pipes and static mixers shows that the effect of the dispersed phase volume fraction on the Sauter mean diameter has received more attention in the last three decades. Several investigators correlated the Sauter mean diameter to dispersed phase hold-up. Scott et al. (1958) found that the mean drop size varies with dispersed phase volume fraction as shown in Equation (2-38) for dispersions of kerosene-in-water using a single orifice meter:

$$\frac{d_{32}}{D_0} \propto \phi^{0.874} \quad (2-38)$$

Later McDonough et al. (1960) extended this work to other liquid-liquid systems and obtained a slightly different correlation. In pipe flow, Sleicher (1962) found that low holdups have little influence on the pipe turbulence and hence the drop breakup. Based on that he assumed that drop coalescence can be neglected at dispersed phase volume fractions less than 0.5%. In Kenics mixer, Middleman (1974) observed that the Sauter mean diameter increases with the holdup at low Reynolds numbers while the increase at high Reynolds numbers is insignificant. He concluded that at the discussed holdups (i.e., 0.5% to 1%) the drop breakup is dominating and therefore the drop size is determined by only the factors that affect the breakage process. In other words, once the drop is formed, it may undergo further breakage by the interaction with higher energy eddies neglecting

the possibility of drop coalescence. This suggestion is somewhat in accordance with earlier ones made by Sleicher (1962). In pipe mixers using woven screens as static mixing elements, Al Taweel and Chen (1996) observed a net increase in the value of the Sauter mean diameter as the holdup increases from 0.5% to 4%. They also observed, at a dispersed phase volume fraction as low as 0.5%, a consistent increase in the drop size as the drops move away from the high-energy dissipation rate region indicating that drop coalescence is taking place. These findings contradict the assumptions made earlier by Sleicher (1962) and Middleman (1974) that the drop size is only determined by factors affecting drop breakup. These assumptions, which ignore the possibility of drop coalescence, can not be applied in the case of stirred tanks where coalescence or dispersion may be neglected only under non-equilibrium conditions. At equilibrium the coalescence and breakup rates are equal. Therefore it was recognized that the effect of dispersed phase holdup should be taken into account even in low-coalescing systems. Lee et al. (1983) correlated the Sauter mean diameter to the holdup as follows:

$$\frac{d_{32}}{D} \propto (1 + C\phi) \quad (2-39)$$

The value of C ranges from 1.8 to 9 as reported by Tavlarides and Stamatoudis (1981).

Later, the limitations encountered by assuming a linear relationship between the average drop size and the dispersed phase holdup was recognized. For example Lagisetty et al. (1986) proposed the following correlation for batch stirred tank reactors:

$$\frac{d_{32}}{D} \propto (1 + C\phi)^{1/2} \quad (2-40)$$

Similarly, a more complicated non-linear correlation, which is only applicable to holdups less than or equal to 0.34, was proposed for the case of mechanically agitated tanks (Calabrese et al., 1986; Wang and Calabrese, 1986):

$$\frac{d_{32}}{D} \propto (1 + 3\phi) \left[1 + 4.42(1 - 2.5)V_i \left(\frac{d_{32}}{L} \right)^{1/3} \right]^{0.60} \quad (2-41)$$

Depending on the region in mechanically agitated tanks, Nishikawa et al. (1987) obtained the following two correlations for the Sauter mean diameter as a function of the dispersed phase concentration:

$$d_{32} \propto (1 + 2.5\phi^{2/3}) \quad (2-42)$$

$$d_{32} \propto (1 + 3.5\phi^{3/4}) \quad (2-43)$$

The first one refers to the coalescence-dominated zone while the second is applicable to the breakup-dominated region. They also suggested that there is a critical energy dissipation rate at which the transition of the domination from breakup to coalescence takes place.

Later Cohen (1991) reported a similar correlation to that obtained by Lee et al. (1980) (Equation 2-40). Kumar et al. (1991) reported that the value of the maximum stable drop size increases with the dispersed phase hold-up.

2.2.2 Effect of System Properties

As pointed out earlier, the physical properties of the two phases are among the factors that affect drop breakup and coalescence rates. Since in the current investigation only a single liquid-liquid system is considered, the effect of the viscosity of both the dispersed and continuous phases as well as their densities on the dispersion process is briefly discussed.

Dispersed Phase Viscosity and Viscosity Ratio (μ_d/μ_c)

As the dispersed phase viscosity increases, the liquid flow or circulation inside the drop becomes more retarded due to the higher resisting viscous forces and the drops tend to be more rigid (Hinze, 1955, Wang and Calabrese, 1986; Calabrese et al., 1986). Several investigators also reported that the viscosities of both phases, (μ_c and μ_d), have a marked influence on both mean drop size and drop size distribution (Shinnar, 1961; Arai et al. 1977, Calabrese et al. 1986, Wang and Calabrese. 1986). Church and Shinnar (1961) pointed out that very large values of the viscosity ratio ($\mu_d/\mu_c > 200$) can be employed to

stabilize mechanically agitated dispersions. Arai et al (1977) reported that the maximum drop size increases with dispersed phase viscosity.

To account for the effect of the dispersed phase viscosity on drop breakup, Hinze (1955) introduced a viscosity group that is defined as:

$$N_{vi} = \frac{\mu_d}{(\rho d \sigma_d)^{1/2}} \quad (2-44)$$

Equation (2-44) shows the importance of the dispersed phase viscosity at low values of density and interfacial tension of the dispersed phase. The critical drop Weber number was, therefore, modified as follows:

$$We_c = C[1 + \varphi(N_{vi})] \quad (2-45)$$

The function φ becomes zero as N_{vi} goes to zero. C is constant, which depends on the flow conditions. Therefore as the dispersed phase viscosity increases the critical Weber number becomes larger, which in turn will show up in the resultant mean drop size and maximum stable drop size, as well as the drop size distribution. He also showed that the maximum stable drop diameter varies with the proposed viscosity group as follows:

$$\frac{d_{max}}{D} \propto We^{-0.6} [1 + \varphi(N_{vi})]^{0.60} \quad (2-46)$$

In order to apply Hinze's model for predicting the effect of dispersed phase viscosity on the maximum stable drop size in stirred tanks, Arai et al (1977) had to redefine the viscosity group as follows:

$$N_{vi} = \frac{(\mu_d \varepsilon^{1/3} d_{max}^{1/3})}{\sigma} \quad (2-47)$$

and obtained the following correlation:

$$\frac{(d_{max})_{N_{vi}}}{(d_{max})_{N_{vi} \rightarrow 0}} = [1 + f(N_{vi})]^{0.6} \quad (2-48)$$

where $(d_{max})_{N_{vi}}$ and $(d_{max})_{N_{vi} \rightarrow 0}$ represent the maximum drop size at N_{vi} and $N_{vi} \rightarrow 0$ respectively.

Calabrese et al. (1986) suggested another viscosity group, which is expressed as follows:

$$N_{vi} = \left(\frac{\rho_d}{\rho_c} \right)^{1/2} \frac{(\mu_d \varepsilon^{1/3} d_{32}^{1/3})}{\sigma} \quad (2-49)$$

and they used it to correlate the Sauter mean diameter of their data as well as those reported by Chen and Middleman (1967). They found that the Sauter mean diameter varies with the proposed viscosity group as follows:

$$\frac{d_{32}}{d_{320}} \propto (1 + CN_{vi})^{3/5} \quad (2-50)$$

Wang and Calabrese (1986) used the same viscosity group (Equation (2-50)) to develop a correlation for the Sauter mean diameter in baffled batch stirred vessels:

$$\frac{d_{32}}{L} \propto (1 + 1.35N_{vi}^{3/4})^{3/5} \quad (2-51)$$

In a Kenics mixer the following expression was found to apply for dilute dispersions (Berkman and Calabrese, 1988):

$$\frac{d_{32}}{D} \propto \left(1 + 1.38N_{vi} \left(\frac{d_{32}}{D} \right)^{1/3} \right)^{3/5} \quad (2-52)$$

where

$$N_{vi} = \left(\frac{\mu_d U}{\sigma} \right) \left(\frac{\rho_c}{\rho_d} \right)^{1/2} \quad (2-53)$$

Equation (2-53) implies that near the inviscid limit, the Sauter mean diameter increases slowly with the dispersed phase viscosity but more rapidly at higher viscosities. It was shown that in the limit of $(N_{vi}) \rightarrow \infty$ (the viscous forces become much greater than the surface force), d_{32} varies with the viscosity as follows (Calabrese et al., 1986; Wang and Calabrese, 1986):

$$\frac{d_{32}}{L} \propto \mu_d \quad (2-54)$$

They also observed that the ratio d_{32}/d_{max} decreases slightly as the dispersed phase viscosity increases. On the other hand it was observed that, in oil-water dispersions, the

Sauter mean diameter is independent of the viscosity at low viscosities but increases when the viscosity of the dispersed phase exceeds 150-200 mPa.s (Otake et al, 1987). Nishikawa et al. (1987) investigated the effect of the viscosity ratio on the mean drop diameter in stirred tanks and proposed the following two correlations for the variation of the Sauter mean diameter with the viscosity ratio for drop breakup- and drop coalescence-dominated regions respectively:

$$d_{32} \propto \left(\frac{\mu_d}{\mu_c} \right)^{1/5} \quad (2-55)$$

$$d_{32} \propto \left(\frac{\mu_d}{\mu_c} \right)^{1/8} \quad (2-56)$$

Although, an increase in the dispersed phase viscosity is expected to increase the resistance to drop breakup, the results of the dispersion of different petroleum products using woven screens showed that smaller Sauter mean diameters were obtained with increasing viscosity (Chen, 1996). This anomaly was attributed to the possibility of presence of high concentrations of impurities in the heavier and the more viscous oils. It was also suggested that the resulting change in interfacial characteristics may overshadow the influence exerted by the increasing dispersed phase viscosity.

The minimum time required to reach steady-state conditions was found to be influenced by the viscosity ratio as shown by the following correlation (Hong and Lee, 1983):

$$T_{min} \propto (\mu_d / \mu_c) \quad (2-57)$$

Effect of Continuous Phase Viscosity

Analogously, the continuous phase viscosity is expected to have a profound effect on the mean drop diameter as well as the drop size distribution. As the continuous phase viscosity increases, the resistance to flow increases and thus the viscous shear increases, favoring drop breakup to a certain point, after which drop breakup becomes virtually impossible, as with drop breakup in shear flows (Karam and Bellinger, 1968).

Middleman (1974) studied liquid dispersions in a Kenics mixer and correlated the Sauter mean diameter to continuous phase viscosity by the following relation:

$$\frac{d_{32}}{D} \propto \mu_c^{-0.1} \quad (2-58)$$

Stamatoudis and Tavlarides (1981) studied the effect of μ_c on the drop breakup. They obtained the following correlation for drop breakup rate as a function of μ_c :

$$\log r_b \propto \mu_c^m \quad (2-59)$$

Where m is the slope of the plot of impeller power vs. impeller Reynolds number on a log scale. Stamatoudis and Tavlarides (1985) studied liquid dispersions in agitated tanks and found that the steady state was reached in less than one and a half hours for $\mu_c < 12$ cp compared with 3 to 8 hours for $\mu_c > 50$ cp. They proposed that at low μ_c , the turbulent eddies are dominant in the dispersion but as μ_c increases, the turbulent eddies diminish and shear forces become more significant. They also showed that the logarithm of the Sauter mean diameter varies linearly with the impeller speed depending on the continuous-phase viscosity. At the beginning, the slope increases until it reaches maximum and then starts to decrease with increasing continuous-phase viscosity. Furthermore, they observed that there are two modes for the variation of the Sauter mean diameter with the increasing continuous phase viscosity depending on the impeller speed. These modes are:

- At impeller rotational speeds below 325 rpm, d_{32} increases initially with μ_c , reaches a maximum, and then decreases.
- At impeller speeds above 325 rpm, d_{32} changes slightly as the viscosity varies between 3.0 and 223.1 cp. On the other hand, a small decrease is observed in the range between 20 and 40 cp.

Density Difference

As mentioned before, drops must be brought together via colliding with each other prior to coalescence. This collision may result from turbulence, Brownian motion, buoyancy or

laminar shear. In case of droplets smaller than the micro-scale of turbulence, collision is caused by one of either of the two mechanisms, the buoyancy or laminar shear. This is determined by the density difference between the dispersed and continuous phases (Elsayed and Al Taweel, 1994). The buoyancy force is a function of density difference. As the density difference increases, the drop rising velocity increases, which may increase the coalescence efficiency by promoting more effective drop collisions.

The density difference plays a more important role in gas-liquid contacting than in liquid-liquid systems due to the large density difference between the phases. For that reason, this effect is very rarely investigated in liquid-liquid dispersions. Howarth (1967) reported that the density difference might affect the drop coalescence frequency. Chen et al. (1984) observed that the coalescence time increases as the density difference increases. Muralidhar and Ramkrishna (1986) pointed out that when a large density difference exists between the phases, the inertia of the dispersed phase may become significant even at small separating distances promoting drop coalescence efficiency as a result of the enhanced drop collision.

2.2.3 Effect of Interfacial Characteristics

Interfacial characteristics play an important role in liquid-liquid dispersions since they strongly affect both drop breakup and coalescence processes, which in turn affect the drop size generated. Interfacial characteristics affect the surface forces, which are very important in keeping the droplets intact. Interfacial characteristics include static and dynamic interfacial tension, diffusivity, interfacial tension gradient, surface elasticity, etc.

Equilibrium Interfacial Tension and the Presence of Surface Active Materials

As pointed out earlier, the Weber number represents the ratio of the disruptive inertial forces to the stabilizing interfacial forces. Therefore, decreasing the interfacial tension is expected to enhance drop breakage and vice versa. The effect of the interfacial characteristics on the drop size distribution will be discussed in detail in the coming sections.

Hinze (1955) reported that the maximum stable drop size in an isotropic turbulent two-phase flow varies with the interfacial tension as shown in Equation (2-60):

$$d_{\max} \propto \sigma^{0.6} \quad (2-60)$$

Equation (2-60) is usually written in terms of the Weber number as follows:

$$d_{\max} \propto We^{-0.6} \quad (2-61)$$

This correlation was validated by several investigators for turbulent flows in mechanically agitated tanks, pipes and static mixers (Sleicher, 1962; Chen and Middleman, 1967, Coualoglou and Tavlarides, 1976; Brown and Pitt, 1974; Karabelas, 1978; Al Taweel and Walker, 1983; Hong and Lee, 1983; Calabrese et al., 1986; Nishikawa et al., 1987; Berkman and Calabrese, 1988; Al Taweel and Chen, 1996). The occasional deviation in the exponent value from the theoretical one was attributed to the departure from isotropic flow conditions assumed in the derivation of Hinze's model. Table 4.4 (page 132) shows the different exponents reported in the literature.

The surface tension exponent values reported for the static mixers (where the conditions are essentially those of plug flow) differ significantly from those reported for mechanically agitated tanks, in which drops move in uncontrolled manner between regions with wide variation in energy dissipation rate (Molag et al., 1980, Nishikawa et al., 1987; Konno and Saito, 1987). For example, Konno and Saito obtained an exponent value of -0.93 for very low dispersed phase viscosity. They attributed this large deviation from the theoretical value to the fact that drop breakup in mechanically agitated tanks takes place in the vicinity of the impeller tip where the flow is highly anisotropic. Tavlarides and Stamatoudis (1981) reported the following expressions relating the maximum stable drop size and the interfacial tension in laminar and transition ranges for non-deformable and deformable drops respectively:

$$d_{\max} \propto \sigma \quad (2-62)$$

$$d_{\max} \propto \sigma^{0.5} \quad (2-63)$$

Kourio et al. (1994) investigated the effect of the interfacial tension on drop coalescence in three different liquid systems, namely, water/MIBK, water/toluene and

water/hexane. They reported a reduction in the film drainage time as the interfacial tension increases and attributed this phenomenon to the stiffening of the drop interface, which eventually decreases the drop tendency to deform and increases its internal stress. Such conditions encourage the flow of the liquid present in the film and, hence, enhance film drainage.

In all of the previously mentioned studies, the interfacial tension was altered by using different organic compounds in the dispersion. Special precautions were taken to ensure that the materials used are free from contaminants and that the equipment are clean. Under such conditions, the interfacial tension has a singular value that is not affected by the rate at which new interfaces are generated. On the other hand, the situation is very different in the case of contaminated systems where the presence of even very small traces of tertiary compounds is known to significantly alter the dynamic interfacial characteristics and shifts the dispersion/coalescence processes towards the formation of finer drops.

Drop breakage/coalescence is a dynamic process that results in stretching the interface so rapidly that the surfactants and other chemical contaminants present in the system may not have the opportunity to diffuse and be adsorbed onto the interface in sufficient concentrations to maintain equilibrium conditions. As a result, the interfacial tension is expected to deviate from its equilibrium value with the deviation being a function of the factors affecting the surfactant diffusion/adsorption rate (surfactant diffusivity, concentration difference, temperature etc.). Unfortunately, the effect of interfacial characteristics on drop breakup/dispersion processes received little attention particularly in the industrially important turbulent flows.

A study of the breakage process in a stirred dispersions of styrene-water system with Teepol as surfactant showed that the presence of surfactant affects the drop breakage via both reduction of interfacial tension and development of an interfacial gradient across the drop. This leads to an additional stress, which, when combined with the turbulence stress results in drop breakage. For low viscosity liquids, this effect depends on the difference between dynamic and static interfacial tension, it increases as the difference

increases. For viscous liquids, this effect becomes smaller and eventually vanishes at very high viscosity (Koshy et al., 1988).

The importance of using appropriate interfacial characteristics in the case of impure systems has been highlighted by Lucassen-Reynders and Kuipers (1992) who found that the Sauter mean diameter does not correlate well with the equilibrium interfacial tension in the case of sunflower seed oil-in-water system which contained triacylglycerol as a surfactant. They suggested that there are other interfacial characteristics that play an important role in determining the drop size in the dispersions. They proposed that as surfactant concentration increases, the interfacial viscosity of the drop rises to such high levels that the viscosity ratio becomes unfavorable for breakup. The effect of varying impeller speed on the Sauter mean diameter was investigated by Chatzi and Kiparissides (1994 and 1995) for a highly concentrated dispersion of n-butylchloride in water in which poly vinyl alcohol acted as a surfactant. The relationship was found to depict a minimum at intermediate rotational speeds. The decrease in drop sizes with increasing impeller speed was attributed to a higher breakage frequency. However, as the interfacial area increases due to the presence of a huge number of small drops in the dispersion, the effectiveness of the surfactant starts to diminish, resulting in coalescence and therefore to an increase in drop size.

In the case of very-low holdup dispersions containing hydroxypropyl methylcellulose, Borwankar et al., (1986) reported that above a certain value of interfacial surfactant concentration, the dispersion became non-coalescing. This was explained on the basis that the adsorption of surfactant molecules onto the drop surface reduces the coalescence efficiency to the point that at a high enough interfacial concentration coalescence will be completely brought to a halt.

Davies (1992) reported that coalescence of drops could be retarded to a large extent by the presence of electrical charges and surfactants, even at very small concentrations. The presence of substantial droplet charges can considerably retard coalescence between drops in agitated organic-in-water dispersions. The adsorbed OH^- anions onto the organic-water interface provide a substantial degree of stabilization for

the dispersions. Large and small droplets were found to be affected to different degrees by the charge (Tobin and Ramkrishna, 1992).

Several investigators accounted for the effect of surface-active substances by virtue of their ability to influence film drainage (which is the rate determining step in drop coalescence). For example, Sagert and Quin (1978), and Muralidhar and Ramkrishna (1986) adopted the following relationship between interfacial tension and drainage time:

$$T_{dr} \propto \sigma^{-2} \quad (2-64)$$

This is in agreement with the findings of Peru and Lorenz (1989) who observed that the coalescence time increases sharply with the addition of small surfactant concentrations but becomes less sensitive at higher concentrations.

Seidshazileh (1999) investigated the effect of Triton surfactants on Bayol oil-water dispersion prepared in a tank agitated by a Rushton-type impeller. He found that the Sauter mean diameter correlates reasonably well with the equilibrium interfacial tension with the value of the surface tension exponent varying from 0.47 to 0.93 depending on how close to equilibrium the experimental conditions were. This dependency on mixing time is in agreement with the findings of Berkman and Calabrese (1988) who discussed liquid-liquid dispersions in a Kenics mixer. On the other hand, he found a rather poor correlation between the coalescence rate (determined at the initial stages of a step down in agitation intensity) and the equilibrium interfacial tension. It, however, correlated very well with surfactant diffusivity, a parameter derived from dynamic surface tension measurement. He suggested that the coalescence process is highly controlled by surfactant diffusion of the surface-active species.

Effect of the Gibbs Surface Excess

The direct determination of the concentration of the surfactant adsorbed per unit area of fluid-fluid interface is a very difficult task due to the difficulty of isolating the interfacial phase from the bulk phase. Instead, the concentration of the surfactant is computed indirectly from surface tension measurements. A plot of the interfacial tension versus the

concentration of the surfactant in the bulk solution is usually used to describe the adsorption at fluid interfaces. Hence, from that plot, the amount of the surfactant per unit area of the interface or the surface excess can be computed by the application of the Gibbs adsorption equation.

The adsorption of surfactant molecules at the interface results in an expanding force acting normally to the interfacial tension, which hence will be reduced. This follows from the general Gibbs adsorption isotherm, which for a dilute binary system containing non-ionic surface active agent is expressed as (Stewart et al., 1996):

$$\Gamma_s = -\left(\frac{1}{RT}\right)\left(\frac{d\sigma}{d \ln C_s}\right) \quad (2-65)$$

Whereas for a dilute solution containing completely dissociated ionic surface active agent the adsorption isotherm becomes:

$$\Gamma_s = -\left(\frac{1}{2RT}\right)\left(\frac{d\sigma}{d \ln C_s}\right) \quad (2-66)$$

where Γ_s is the surface excess of the surfactant, C_s is the surfactant bulk concentration and σ is the interfacial tension. This equation is only valid for dilute surfactant solutions and for slight surface curvatures where the adsorbed molecules form a monolayer. The surface excess, which relates the change of the interfacial tension with the surfactant concentration, is a measure of the degree of surface coverage by the solute molecules.

Borwankar et al. (1986) investigated the stability of very dilute dispersions and observed that above a critical concentration of the surfactant (hydroxypropyl methylcellulose), the dispersion becomes almost stabilized. They measured the Sauter mean diameter at 500 and 100 rpm at different concentrations of the surfactant and they observed that at low surfactant concentration, the Sauter mean diameter increases following the reduction of the rotation rate, which indicates the occurrence of drop coalescence. When the surfactant concentration exceeds 0.05% by weight the drop size decreases very slightly. This was attributed to the reduction in coalescence efficiency, which becomes close to zero as the Gibbs surface excess exceeds a certain value, due to the adsorption of surfactant molecules on the drop surface. This was confirmed by using

incident light interferometric to investigate the film thinning, which revealed that the film was stable. For any particular surface active compound, the critical surface coverage (S_c), which corresponds to the critical surfactant concentration, can be expressed as follows:

$$S_c = \frac{(1-\phi)d_{33}}{\phi} C_c \quad (2-67)$$

where C_c is the critical surfactant concentration.

Cheng (1994) found that the interfacial area in mechanically agitated tanks with stator is better correlated using the Gibbs surface excess rather than the equilibrium interfacial tension. This may suggest that the Gibbs surface excess affect the coalescence time. Ramadan (1996) reported similar observations in the case of coalescence-controlled operations in two-phase sparger.

Effect of Gibbs Elasticity and Gibbs-Marangoni Effect

The onset of surface deformation and film drainage results in the formation of concentration gradients along the interface. This in turn produces strong interfacial forces that retard coalescence. Such phenomenon is usually referred to as the Marangoni effect and is related to Gibbs excess energy. Perez De Ortiz (1992) found that the Marangoni effect might influence both drop breakup and coalescence. He explained that in very thin films (i.e. the intervening liquid films), the interfacial flow induced by the variation in interfacial tension is large enough to change the film thickness. In the section of the film where the thickness is minimal, the solute concentration increases faster than in the adjacent sections leading to local drop in interfacial tension. The interfacial driven flow may be strong enough to breakup the film thus promoting coalescence.

For liquid-liquid systems containing a surfactant that is soluble in the continuous phase and under dynamic conditions, it is believed that hindering of drop coalescence is due to the Gibbs-Marangoni effect (Walstra, 1993). When two drops suspended in a system containing a surfactant approach each other, they tend to gain more surfactant molecules during their movement but the amount of the adsorbed molecules will be minimal at the interfaces of the thinnest part of the intervening liquid film. This will result in the establishment of interfacial gradients, which will be highest at the thinnest

part of the film. This in turn will make the surfactant molecules move towards regions of low surface excess. In addition, the liquid will move along the interface in the direction of the low interfacial tension regions (i.e., the Marangoni effect), driving the drops away from each other and preventing them from coalescing (Walstra, 1993).

Chen and Lee (1999) reported that as two drops approach each other, the liquid in the intervening film tend to flow outwardly causing the drop interface to stretch. In the case of the presence of surface-active materials, the interfacial tension in the zone between the two coalescing drops becomes higher as a result of the interface stretching. The surfactant molecules will be swept under the influence of the surface convection to the rest of the drop interfaces where they tend to accumulate and lower the interfacial tension. Eventually, interfacial gradients are developed and hence a net force on the interface exerting Marangoni stress, which increases the drag resistance to film drainage preventing drop coalescence. They reported that the critical film thickness could be expressed as follows:

$$\frac{QRk^2}{\sigma} = \frac{2}{kh_c} - (kh_c)^2 \quad (2-68)$$

$$Q = \frac{2c}{RT} \left(\frac{d\sigma}{dc} \right)^2 \quad (2-69)$$

$$k = \left(\frac{12\pi\sigma}{A_h R} \right)^{1/3} \quad (2-70)$$

It was found that the most dominant stage of film drainage is determined by the right hand side of Equation (2-68). Chen and Lee (1999) also defined a parameter M that can be used as an indicator of the likelihood of coalescence of two drops and is expressed as follows:

$$M \equiv C \left(\frac{R}{\sigma} \right)^{1/3} \left(\frac{d\sigma}{dc} \right)^2 \quad (2-71)$$

Equation (2-71) implies that M is proportional to QRk^2/σ . As the magnitude of M increases, the coalescence becomes more difficult. For water- CCl_4 system containing the surfactant sodium lauryl sulfate, the value of M increases with the increasing surfactant

concentration or in other words the drop coalescence becomes more difficult as the surfactant concentration increases. At high surfactant concentration, the added stability to the dispersion becomes insignificant compared with the increase in surfactant concentration.

Diffusivity

Drop coalescence as well as the interface stretching is a dynamic process and so rapid, that the surfactants and other chemical contaminants, which might be present in the system, may not have the opportunity to diffuse and be adsorbed onto the interface in sufficient concentrations and very short time. As a result, the interfacial tension is expected to deviate from its equilibrium value. The surfactant diffusivity is therefore a crucial factor in drop breakup/coalescence and should be taken into account when liquid-liquid dispersions are investigated. The surfactant diffusivity depends on several factors such as the molecular weight of the surface-active species, bulk concentration, molecular length, etc. (Xue, 1999).

Clift et al. (1978) reported that surfactants having lower surface diffusion coefficients are more effective in prevention of drop/bubble coalescence due to their higher efficiency in suppressing fluid circulation within the drop/bubble as a result of the increased formation of interfacial gradients.

Krawczyk et al. (1991) studied drop coalescence and the interfacial phenomena in crude oil emulsions containing oil-soluble demulsifiers and found that the most important factors determining the demulsifier efficiency are high interfacial activity and high diffusion/adsorption rate.

Al Taweel et al. (1995) proposed a parameter known as the effective diffusivity, which is determined by using dynamic surface tension measurements. This parameter accounts for both the interfacial rheology (i.e., the interfacial pressure and diffusivity) and surface-active materials under dynamic conditions of changing surfaces during bubble/drop coalescence. Kim et al. (1996) reported that, surfactant diffusivity is inversely proportional to the square of the molecular weight. This means that small molecules diffuse very rapidly to the drop/bubble interface, which in turn implies that

under dynamic conditions the interfacial concentration of smaller surfactant molecules might be relatively higher than that under equilibrium conditions. Hence, the diffusivity determined over a short duration is expected to be higher than that over a long duration of time. Due to their high diffusivity, molecules of an efficient demulsifier rapidly become adsorbed onto the interface thereby decreasing the interfacial tension as well as interfacial viscosity and virtually promoting film drainage, or in other words decreasing the drainage time.

Seidshazileh (1999) attempted to correlate drop coalescence rate to dynamic interfacial characteristics, including the diffusivity of surfactant. Excellent correlation was found to exist between drop coalescence rate and the surfactant diffusivity determined from data obtained by using the drop-volume-technique. This result suggests that the coalescence process is controlled by the surfactant diffusivity to a great extent. On the other hand, the surfactant diffusivity determined from data obtained by the maximum-drop-pressure technique could not correlate the drop coalescence rate. This could have possibly have been caused by the fact that the time scale of diffusion for the surfactant molecules may be large compared to the surface aging in the maximum-drop-pressure technique. Furthermore, this technique is prone to additional errors due to the residual surfactant, which might be present from the preceding drop.

2.2.4 Effect of Electrolyte Concentration and Charge

It is a well-known fact that droplets in aqueous media acquire a surface charge due to the adsorption of ions present in the solution. The presence of electrolytes is thus expected to influence the surface charge of drops, which in turn affects the coalescence process. Several researchers reported that the addition of salts to gas-liquid or liquid-liquid dispersions could appreciably decrease the drop/bubble size with the effect being more pronounced in the case of gas/liquid systems. It is believed that the presence of salts suppresses the coalescence process by hindering the drainage of the intervening liquid film. At sufficiently high salt concentration, the fluid-fluid interface becomes immobilized as a result of the formation of interfacial gradients (Marrucci, 1969; Zlokarnik, 1985; Jamialahmadi and Muller-Steinhagen, 1990)).

Zlokarnik (1985) attributed the decrease in bubble size, in the presence of inorganic salts in aqueous media, to the reduction in coalescence frequency rather than to bubble breakup. This is an anticipated result because the presence of salts result in very low, or negative, Gibbs surface excess. Accordingly, it is suggested that the decrease in mean bubble size results mainly from a reduction in the coalescence frequency. Similarly, Kato et al. (1991) observed that the coalescence of oil drops is slower than that of similarly sized water drops. This was mainly due to the accumulation of charge on the droplets formed in the former case.

Later, Kumar et al. (1991) suggested that oil drops acquire a negative charge upon dispersion of oil in water. Tests on a purified soybean oil-water system, containing sodium chloride showed that the interfacial tension does not change upon the addition of surface active compounds such as stearic acid, oleic acid and linoleic acid. On the other hand, interfacial tension is significantly reduced in the presence of the ricinoleic acid, a difference which was attributed to the hydroxyl group being closer to the double bond (between C-9 and C-10). Davies (1992), also, reported that coalescence could be retarded to a large extent by the presence of electrical charges and surfactants, even at very small concentrations. It is believed that the presence of substantial droplet charges can considerably retard coalescence between drops in agitated organic-in-water dispersions. The adsorbed OH^- anions onto the organic-water interface provide a substantial degree of stabilization for the dispersions. Large and small droplets were affected to different extent by the charge (Tobin and Ramkrishna, 1992).

In liquid dispersions, the surface charges are surrounded by ions of opposite charge, which leads to the formation of an electric double layer creating an electrical potential difference between the dispersed and the continuous phases (Stein, 1995). Therefore, as the charged drops become close to each other, the film between drops will be very saturated with the counter-ions and depleted in co-ions. This establishes a concentration gradient between the drops and the regions away in the continuous phase and eventually resulting in osmotic pressure, which is a repulsive force, proportional to the double layer length between the particles and those regions. Increasing the ionic

strength of the continuous phase is expected to result in a thinner double layer and thus less repulsive force between the charged drops. In other words, the drop coalescence is expected to decrease as the ionic strength increases.

Chen et al. (1998) studied the effect of NaCl concentration and polarity on the coalescence of MIBK drops in an aqueous phase and found that coalescence time increases as the sodium chloride concentration increases. In addition, they found that the coalescence time of aqueous drops decreases with increasing NaCl concentration when the continuous phase is a polar organic liquid (e.g., *n*-butyl acetate). It was observed that those effects are relatively less pronounced in electrolytes of higher valency. They suggested that in the case of liquid dispersions of polar organics, the coalescence time of aqueous drops generally decreases as the electrolyte content increases; while that of the organic drops increases. In addition, they found that the higher the valency of the electrolyte, the more significant is the impact on coalescence rates of organic drops while the effect is less pronounced in the case of the coalescence rate of the aqueous drops. They also observed that in the case of non-polar liquids (e.g. *n*-heptane) the type, valency and concentration of the salt does not influence the coalescence time of the aqueous drops. Acidic and basic electrolytes were found to have similar influence to salts. For example, addition of sodium hydroxide or hydrochloric acid increases the coalescence rate of aqueous drops in polar organics and vice versa for organic drops in aqueous medium. They attributed their findings to the difference between mutual solubilities of the polar and non-polar organics in water. In the case of polar compounds in contact with water, the two phases form binary solutions and hence the addition of salts may alter the intermolecular forces and ultimately the composition of the two phases through preferential association in liquid phases affecting drop coalescence rate.

2.3 KINETICS OF DROP BREAKUP AND COALESCENCE

The study of the kinetics of drop breakup/coalescence processes in liquid-liquid systems is of great importance since they control mass and heat transfer rates, and eventually chemical reaction rates and their selectivity. The literature shows that there has been only

limited number of investigations that addressed drop breakup/coalescence from a kinetic point of view.

Most of drop breakup/coalescence models were obtained from studies involving batch operations, using mechanically agitated tanks (Hong and Lee, 1983; Stamatoudis and Tavlarides, 1985; Skelland and Kanel, 1992; Zhou and Kresta, 1997). As mentioned earlier, mechanically agitated tanks are characterized by extremely complex hydrodynamic conditions. This usually results in large spatial variations in energy dissipation rate ($10 < \varepsilon_{\max}/\varepsilon_{\min} < 200$ (Cutter, 1966)), which means that the dispersed phase continuously circulates between regions of high and low energy dissipation rates. In addition, the residence time in the high-energy dissipation region and the dispersion dynamics are not well defined. Generally speaking after a sudden increase in mixing speed (from $\frac{1}{2}$ to $3\frac{1}{2}$ hours), drop size was found to decrease with time. Equilibrium drop size is approached as time increases to infinity. This behavior is often misinterpreted as representing the temporal variation of drop size, a situation that contradicts the observation that drop breakage/coalescence in non-viscous systems can take place in microseconds. Furthermore, most of the existing models deal with breakage- or coalescence-dominated situation, which is not valid assumption as well. In fact breakup and coalescence processes occur simultaneously within a given liquid dispersion.

Hong and Lee (1983) investigated the change in Sauter mean diameter with time in liquid dispersions after a sudden increase in rotation rate and until the equilibrium was re-established. It was observed that the Sauter mean diameter initially decreases exponentially and then asymptotically as the equilibrium conditions are approached. Furthermore, they found that near equilibrium, their data could be well-correlated by the following equation:

$$\frac{D_{32}}{D_{32\infty}} = 1 + \alpha^\beta \quad (2-73)$$

Where β is about -0.7 and α is a function of the physical properties of the system and the mixing conditions. Later, Hong and Lee (1985) used another correlation to describe

the variation of drop size with time due to breakup in turbulent stirred tanks. This correlation is as follows:

$$\frac{d_{32} - d_{32\infty}}{d_{32\infty}} = \alpha(Nt)^\beta \quad (2-74)$$

Where α was found to be a function of the physical properties of the system and the mixing conditions, as before, N is the impeller speed and t the residence time. They also found that β is about -0.7 . Skelland and Kanel (1992) also found that the same correlation well describes the variation of the Sauter mean diameter with time in mechanically agitated tanks (in the case of chlorobenzene-in-water system containing the surfactant TritonX100). The parameter β was correlated to the interfacial tension as follows:

$$\beta = -0.28 \frac{\sigma - \sigma_{\min}}{\sigma_{0.5AA} - \sigma_{\min}} - 0.66 \quad (2-75)$$

where the value of β varies between -0.6 and -1.0 . On the other hand, Wright and Ramkrishna (1994) suggested that after a sudden reduction in rotation rate the average drop volume is directly proportional to time^{0.5}.

Recently, Seidshazileh (1999) proposed a modified form of equation (2-73) in attempt to correlate the variation of the Sauter mean diameter with time following a step decrease in impeller speed. For organics-water dispersions containing different surfactants from the TritonX series, the proposed expression is:

$$d_{32} = d_{320}(t+1)^b \quad (2-76)$$

where d_{320} is the Sauter mean diameter at $t = 0$ and b is constant, which depends on the system's hydrodynamics and the interfacial characteristics as well as the type of surfactant. However, the experimental data were found to fit the proposed equation only in the case of in highly. Further, he assumed a homogeneous mono-dispersed system and substituted equation (2-77) in an expression for coalescence frequency, which Howarth (1967) obtained, as follows:

$$\text{Coalescence rate} = \left. \frac{d(d_{32})}{dt} \right|_{t=0} \frac{1}{d_{320}} \frac{1}{2 - 2^{\frac{2}{3}}} \quad (2-77)$$

This expression represents the variation of the Sauter mean diameter with time normalized by the initial Sauter mean diameter. Therefore, the proposed coalescence rate becomes:

$$\text{Coalescence rate} = \frac{b}{2 - 2^{\frac{2}{3}}} \quad (2-78)$$

He found that estimates of coalescence rates, their standard deviation and the corresponding correlation coefficients of different highly coalescing organic-water systems are significant at the 99% confidence level. He also found that the coalescence rate decreases with increasing surfactant concentration.

2.4 DROP SIZE DISTRIBUTION

In the following sections the drop size distributions generated in the most commonly used mixers in chemical industries (mechanically agitated tanks and static mixers) are reviewed. Even though static mixers offer a better alternative to agitated tanks, most of the existing literature on liquid-liquid dispersions deals with stirred vessels. The effect of energy dissipation rate, dispersed phase volume fraction and interfacial characteristics on the drop size distributions generated in both types of mixers is discussed in detail.

Mechanically agitated tanks are characterized by large spatial variation in energy dissipation rates and highly non-uniform flow characteristics as well as a broad residence time distributions, all of which will be reflected on the uniformity and broadness of the drop size distribution generated. On the other hand, nearly plug flow conditions are encountered in static mixers resulting in relatively more uniform and controlled hydrodynamic conditions prevailing throughout the mixer. Static mixers are also characterized by narrow residence time distribution.

Lack of information on the effect of interfacial characteristics and system properties on the dispersion characteristics in static mixers can be overcome by referring to literature dealing with these aspects in mechanically agitated tanks.

A lot of research has been carried out to characterize drop size distributions of various dispersions and several models have been proposed. Two main types of drop size

distributions were reported, normal and log-normal. Because of improvements in methods of drop size measurement several other distributions have been reported such as Gamma , Schwartz-Bezemer, etc.

2.4.1 Effect of Hydrodynamics

Energy Dissipation Rate

One of the major parameters, which strongly influence liquid-liquid dispersion processes, is the turbulent energy dissipation rate in mixing vessels, which increases with increasing impeller speed. In mechanically agitated tanks, the impeller speed was found to have a strong effect on drop size distributions (Ward and Knudsen, 1967; Sprow, 1967a and 1967b; Hong and Lee, 1983; Laso et al., 1987; Chatzi et al., 1991 Zhou and Kresta, 1997; Pacek et al., 1998). For static mixers, the energy dissipation rate could be expressed in terms of flow rate or flow velocity and the pressure drop across the mixer (Equation 3-2). Since both of them increase with increasing flow velocity, the energy dissipation rate increases with flow velocity.

Under turbulent flow conditions, the fluctuating motion in the continuous phase, or in other words the turbulent energy, is considered to be the main cause of drop breakage (Hinze, 1955). The rate at which turbulent energy is dissipated greatly affects both breakage frequency as well as drop coalescence frequency and efficiency. It is therefore expected that as the dissipation rate varies, the drop size distribution generated will be accordingly affected depending on the magnitude of that variation.

Sprow (1967a) studied the variation of the drop size distribution with location in tanks agitated by a turbine mixer. The studied system was methyl isobutyl ketone-in-salt water with dispersed phase volume fraction of 0.25. A rotation rate of about 100 rpm was used. He found that drop size, as well as drop size distribution, is strongly dependent on the location in the tank. The smallest drop sizes occurred close to the impeller tip, while the largest drop sizes occurred away from the impeller. This was attributed to the differences in local energy dissipation rates between the two locations. Furthermore, to justify the spatial variation in drop size distribution, Sprow (1967a) proposed that drop

coalescence is dominant at the remote location whereas drop breakup is dominant near the impeller tip where the highest-energy dissipation takes place. As drops move away from the tip of the impeller along their circulation path, turbulence intensity tends to decrease promoting drop coalescence. For this to occur, the coalescence rate should be high enough in comparison with the circulation time. In addition, high holdup tends to enhance drop coalescence via increasing the drop density.

In a later study, which supported his previous findings, Sprow (1967b) reported that the drop size distributions at various impeller speeds and in the vicinity of a turbine impeller for a dilute iso-octane/water dispersion were well approximated by the Schwartz-Bezemer equation. He also reported that the maximum drop size decreases linearly with increasing impeller speed. This means that as the impeller speed increases the turbulence intensity increases promoting drop breakup. In other words, higher energy dissipation rates generate smaller drop sizes. On the contrary, Mlynek and Reshnik (1972) concluded that the drop size is virtually not influenced by location in the vessel after their work on liquid-liquid dispersion using agitated tank equipped with a six-blade impeller. Hold-ups of 0.025 to 0.34 and various rotational speeds (140-450 rpm) were used. This is probably due to the small volume of the vessel used (i.e., 29 cm diameter and liquid depth of 29 cm) which may have ensured dispersion homogeneity and did not allow long enough circulation time for drop coalescence to occur. In addition, although the coalescence rate increased with increasing dispersed phase hold-up, it was not relatively high enough in order to be dominant even away from the impeller region. Based on the above results, it can be concluded that the drop size distribution is expected to be independent of location in small-agitated tanks with low tank diameter-to-impeller diameter ratio.

Collins and Knudsen (1970) examined the dispersive action of pipelines by monitoring the drop size distribution obtained upon injection of different organic liquids in a pipe with turbulent water flow. The drop size distributions obtained can be considered as the sum of two individual ones. The first drop size distribution was generated by the injection process itself and reflects the nozzle characteristics whereas

the second drop size distribution was generated by the drop breakage under the action of turbulence. Drop deformation and drop break up seemed to be most effective in the close vicinity of the pipe wall rather than in the turbulent region away from the pipe wall. This suggests that the shear breakup mechanism is more effective than the turbulent one. For holdups of 0.6%, the results obtained showed that only 5% of the produced drops had diameters more than 230 μm , the predicted maximum stable drop size using a formula developed by Sleicher.

Coulaloglou and Tavlarides (1976) measured the drop size distributions in the circulation region away from the impeller and in the impeller vicinity respectively for aqueous dispersions of kerosene and dichlorobenzene. The dispersed phase hold-up ranged from 0.025 to 0.15, impeller speeds of 190-310 rpm and a nominal residence time of 10 minutes were used. The results revealed small differences between the drop size distributions in the two regions. They attributed the observed relative uniformity of dispersion to the low coalescence frequency of drops, which ranged from 0.148 to 1.12 min^{-1} compared to the circulation frequency of 35-60 min^{-1} . They also proposed the use of the ratio of the coalescence frequency to the circulation frequency as a criterion for the prediction of the uniformity of dispersion. The smaller this ratio the more homogeneous is the dispersion. The preceding argument is in favor of the findings of Sprow (1967a) who adopted a similar hypothesis to explain his results.

In another approach for the investigation of the effect of energy dissipation rate on the drop size distribution, Brown and Pitt (1972) studied the dispersion of kerosene-in-water with hold ups of 0.05 to 0.2 in a mechanically agitated tank at different impeller speeds (250, 300, 350 and 400 rpm). A normal drop size distribution was obtained when the results were plotted as cumulative volume fraction against drop diameter, which has been normalized by the Sauter mean diameter. The drop size distribution was well correlated by:

$$F_v\left(\frac{d}{d_{32}}\right) = \frac{1}{0.2\pi^{0.5}} \exp\left[-12.5\left(\frac{d}{d_{32}} - 1.07\right)^2\right] \quad (2-79)$$

It was found that the impeller speed has no effect on the drop size distribution. They attributed this finding to the dampening effect imparted by the hold-up on the turbulence, and not by drop coalescence. They explained that the drop size distribution shows a sharp truncation of the maximum drop size indicating that the system is a non-coalescing one. In addition, if the system were a coalescing one, a step change in agitation rate would have resulted in a new steady value of the Sauter mean diameter being achieved in a short time. The drop size volume distribution was found to be normal but depicted bimodality at moderate dispersed phase holdups. It was proposed that one of the modes corresponds to the smaller daughter drops produced upon break up while the other one corresponds to the largest stable drop sizes.

Middleman (1974) reported that the friction factor in Kenics mixer was found to decrease as the pitch (i.e., Le/D) of the mixer increases. The variation of drop size with the number of mixing elements at constant Weber number shows that steady state drop size distribution is obtained after about eight elements. A plot of the mean drop size against the superficial velocity at different pitch values showed that the drop size is inversely proportional to the velocity at the same pitch while larger drop sizes are produced as the pitch increases. The drop size distributions generated can be correlated by a normal distribution around the Sauter mean diameter:

$$f\left(\frac{d}{d_{32}}\right) = \frac{1}{0.25(2\pi)^{0.5}} \exp\left[-9\left(\frac{d}{d_{32}} - 1\right)^2\right] \quad (2-80)$$

Kubie and Gardner (1977) studied the drop size distributions for isoamyl alcohol and n-butyl acetate in water, and water in isoamyl alcohol and n-butyl acetate. The dispersed phase was injected in a horizontal tube where the continuous phase was flowing. The drop size distributions were found to be strongly dependent on the superficial velocity and widened as the superficial velocity increased.

The dispersions of water in kerosene and transformer oil were investigated at various flow velocities using a 5.04 cm inside diameter pipe loop with 32-m straight testing section (Karabelas, 1978). In both cases (Organic-in-water and water-in organic)

the drop size distribution could be well correlated by either an upper limit log-probability function, or the Rosin-Rammler type of equation, which is written as follows:

$$V = \exp\left[-2.996\left(\frac{d}{d_{95}}\right)^n\right] \quad (2-81)$$

where V is the volumetric fraction of droplets with diameter greater than d , n is the slope of the log plot and d_{95} is the droplet diameter corresponding to 95% volume of droplets smaller than d_{95} . The upper limit log-probability function is represented by:

$$V = \frac{1}{2}[1 - \operatorname{erf}(\delta z)] \quad (2-82)$$

where

$$z = \ln\left[\frac{ad}{d - d_{\max}}\right] \quad (2-83)$$

and

$$a = \frac{d_{\max} - d_{50}}{d_{50}} \quad (2-84)$$

The calculated fit parameters obtained at different flow rates were found to be almost constant which indicates that whereas the value of d_{95} changes with velocity, the velocity does not affect the shape of the distribution (Karabelas, 1978).

Molag et al. (1980) investigated the equilibrium drop size distribution obtained in a mechanically agitated tank for a benzene/carbon tetrachloride-in-water dispersion with dispersed phase holdup of 4.2%. Baffled and unbaffled vessels as well as different types of agitators were used. After equilibrium conditions were reached, hexamethyldiamine was added to the continuous phase to stabilize the droplets and a sample of the coated drops was withdrawn and photographed in order to determine their sizes. The normalized drop size distributions were found to follow the normal (Gaussian) distribution with the standard deviation not being strongly influenced by the stirrer type or its speed. Very slight changes in drop size distribution were observed at lower speeds. This suggests that insignificant drop coalescence occur in regions of low energy dissipation rates away from the impeller. Slightly broader distributions were obtained when inclined blade stirrer and

baffled vessels were used. It was also found that the largest drop size generated is about twice of the Sauter mean diameter. They suggested that this corresponds to the maximum stable drop size (i.e. $d_{max.} = 2 d_{32}$). In a single-pass vessel, the drop size distribution deviated from the normal distribution with the standard deviation becoming slightly lower than that in batch agitated tanks. This was attributed to the drop breakup process being far from equilibrium. For example, in the case of the turbine impeller the average drop size was found to be still much bigger (i.e., 2-3 times larger) than the equilibrium size. Therefore, they proposed that drop breakup process never reaches equilibrium due to the insufficient residence time in the impeller region. Based on the preceding reasons, they suggested that newly produced droplets are not randomly distributed.

Sembira et al (1986) investigated the dispersion of kerosene in water using a SMV-4 Sulzer motionless mixer. Two sets of static mixing elements, stainless steel SS316 and Teflon coated stainless steel. The drop size distributions generated were found to be normal and the variance of the distribution decreased with the increasing velocity. The drop size distribution generated can be approximated by:

$$f\left(\frac{d}{d_{32}}\right) = \frac{1}{0.17\pi^{1/2}} \exp\left[-19\left(\frac{d}{d_{32}} - 1\right)^2\right] \quad (2-85)$$

At low velocities, a bimodal distribution was observed which seemed to be comprised of two superimposed distributions, the first represents the large drops while the second represents the smaller drops. This was attributed to the formation of non-homogeneous turbulent flow field at low velocities. It was observed that the higher superficial velocity the narrower the distribution becomes. Significantly large difference in the performance of the Teflon coated and stainless steel SS316 mixers was observed. This was attributed to the possibility that the surface of the mixing elements plays an important role in drop breakup and coalescence processes.

Haas (1987) examined three types of contacting equipment for the dispersion of aqueous solutions in organic liquids. These are small-diameter tubes, a Kenics mixer and an annular disperser with Couette flow. The three devices generate homogeneous and nearly isotropic turbulence. The drop size distribution in the three types of mixers was

correlated by a log normal distribution. The standard deviation ranged from 1.21 to 1.50, the values 1.28 to 1.35 being the most typical. The most uniform dispersion had a standard deviation of 1.28 (an equilibrium size spectrum in homogeneous turbulence). The static mixers gave the best uniformity whereas the open tube gave the least, with a standard deviation of 1.3 to 1.4. For the three mixers, the average diameter of aqueous drops in trichloroethylene and 2-ethyl-1-hexanol was correlated empirically in terms of Reynolds number. In the three cases, the average drop diameter is directly proportional to $Re^{-0.2}$. Consequently, as the Reynolds number increases, the drop size distribution is expected to shift towards smaller drop sizes.

Berkman and Calabrese (1988) investigated the dispersion of viscous liquid by turbulent flow in a Kenics mixer. Silicon oil, paraffin oil and *p*-xylene of different viscosities were used as the dispersed phase. The distributions generated were found to be normally distributed in volume and widen with decreasing Reynolds number.

Rincon-Rubio et al. (1994) studied the effect of phase flow rate and agitation rate on the dispersion of six organic-water systems, at three locations along the axis of a Wirtz Π agitated column. The results show that as the agitation rate increases, the drop size distribution shifts to smaller drop sizes, and become narrower and more symmetric about the mean. In addition, it was observed that the large drops continuously disappear as the agitation rate increases. On the other hand, the flow rates of both phases had an insignificant effect on the shape of the drop size distribution. At a given agitation rate, no significant variation in both the Sauter mean diameter and the drop size distribution was observed along the column height. For all systems, it was observed that the Sauter mean diameter sharply decreases as the agitation rate increases, while it increased as the flow rate of both phases increased. The effect of the velocity of the continuous phase was more pronounced at high interfacial tensions and low density ratios (i.e. ρ_d/ρ_c). The drop size distributions were well correlated by the Gamma function.

Good knowledge and understanding of the factors affecting the time required to reach steady state conditions and eventually equilibrium drop size distribution, is very important in designing and sizing of liquid-liquid contacting equipment. In Kenics mixer,

it was found that steady state drop size distribution is obtained after eight elements. As mentioned before, the drop size distribution generated was normal around the Sauter mean diameter. Hong and Lee (1983) studied the effect of agitation rate on the dispersion of two immiscible systems (5 cSt Dow Corning fluid-in-water and ethyl acetate-in-water) in agitated tanks equipped with six-bladed flat turbines. They found that at low impeller speeds (216 rpm), the equilibrium drop size distribution follows normal distribution compared to log-normal distribution at higher impeller speed (565 rpm). On the other hand, at intermediate agitation rates the drop size distribution follows normal distribution in most cases. They also found that at a given agitation rate, the distribution becomes progressively narrower and the average drop size becomes smaller as dispersion time progresses from 1 to 30 minutes. Meanwhile, the drop size distribution changed from multi-modal to bimodal then to normal distribution. The results show that the minimum time required for reaching steady state drop size distribution decreases sharply with increasing agitation rate and can be correlated by the following expression:

$$T_{\min} \propto N^{\gamma} \quad (2-86)$$

Where $\gamma = -6$ and -1 for ethyl acetate-water system and 5cSt Dow Corning fluid (dimethyl siloxanes)-water system respectively. The difference in γ was attributed to differences in the physical properties of the two systems, which in turn affect the rates at which the coalescence/break up mechanisms proceed.

Chatzi et al. (1991) investigated the influence of impeller speed on the transient drop size distribution for 1% holdup of styrene dispersed in water containing poly vinyl alcohol as a stabilizing agent. They observed that bimodal distributions are attained after a very short time of mixing. As the agitation time increases the drop sizes become smaller and both peaks shifted towards smaller drop sizes without significantly altering the shape of the drop size distribution. Similarly, as the agitation rate increases the drop size shifts towards smaller values whereas the shape of the distributions remains unchanged. Laso et al. (1987), who observed similar bimodal drop size distributions attributed that to neglecting the very small drops from counting during the process of determining the drop size distribution.

Zhou and Kresta (1997) investigated the effect of energy dissipation rate on the drop size distributions in liquid-liquid dispersion of very low hold up (0.03%) using mechanically agitated tanks at different rotational speeds. A phase Doppler particle analyzer was used for measurement of drop size. Measurements were made at locations near the impeller and in the bulk of the agitated mixture. The following observations can be drawn from the generated drop size distributions:

- At relatively low agitation rates (e.g., $N = 11.3 \text{ s}^{-1}$), the drop size distribution can be considered to consist of two distinct parts. The first part, which is characterized by a high peak, corresponds to small drop sizes and can be correlated by a normal distribution. The second part corresponds to larger drop sizes and has a lower peak in addition to a long tail;
- As the agitation rate increases (e.g., $N = 13.3 \text{ s}^{-1}$) the second peak becomes more pronounced and the resulting bimodal distribution can be considered to consist of two normal distributions, each one having its own mean drop size and standard deviation. The formation of a second peak was attributed to breakage of the largest drops by the increased turbulence intensity;
- As the agitation rate increases further, the second peak gradually disappears until the entire distribution shifts to mono-modal one that is broader and skewed to the right. This has been attributed to the observation that the turbulence intensity becomes more and more enhanced with increasing rotation rate, which causes further breakage of the largest drops causing the second peak to diminish;
- At sufficiently high rotational speeds (e.g., $N = 22.7 \text{ s}^{-1}$), the distribution shifts to a more symmetric and mono-modal one that can be approximately correlated by a normal distribution. They suggest that the small droplets disappear due to drop coalescence while the concentration of the large drops decreases due to enhanced drop breakage. The increased rotation rate increases circulation rate and hence the turbulence intensity, thereby enhancing both drop breakup and coalescence at the same time. This is in accordance with the

findings of Howarth (1967) that coalescence frequency in liquid dispersions is strongly influenced by the impeller speed (i.e., $\lambda \propto N^{1.9-2.25}$).

Pacek et al. (1998) investigated liquid dispersion in an agitated vessel where rotational speeds of 180, 330 and 480 rpm were used, all of which seemed to give uniform dispersions. The systems investigated were chlorobenzene-in-water and chlorobenzene-in-0.1 M NaCl solution. The generated normalized cumulative volume drop size distributions were found to be well-correlated by log-normal distribution. On the other hand, the drop number density distributions showed that none of the tested distributions, namely, the Schwartz-Bezemer, normal and log-normal distributions, could correlate the data well. This apparent contradiction stems from the ability of the probability density function to depict detailed variations in the data, a feature that the cumulative distribution does not possess. They also observed that at low impeller speeds, the generated drop size distributions for all chlorobenzene-water systems exhibit bi-modality, a result that is similar to those reported by Zhou (1997) and Chatzi et al. (1991). This bi-modality gradually decreased with increasing impeller speed until it completely vanishes at sufficiently high speeds.

In summary, the literature reviewed indicates that as the energy dissipation rate increases, more symmetrical and narrower distributions are generated in both mixer types. In mechanically agitated tanks, the generated drop size distribution varies with the location in the tank due to the existence of two regions of very high and low energy dissipation rates.

Dispersed Phase Volume Fraction

The dispersed phase holdup (or the dispersed phase volume fraction) can affect the homogeneity of dispersion via either imparting a damping effect on the generated turbulence or/and promoting the coalescence efficiency by increasing the drops density (Brown and Pitt, 1970).

Brown and Pitt (1972) obtained a bi-modal drop size distribution for kerosene-water system using an agitated tank. They found that size distribution is influenced by the

dispersed phase hold-up. As the dispersed volume fraction increases, the mode, which corresponds to the small drop size fraction, shifts to larger drop sizes. Meanwhile the mode that corresponds to high drop size fraction shifts to smaller drop sizes without significantly altering the distribution shape. As stated before, this was attributed to the damping effect imposed by the increased holdup on turbulence intensity and not due to the enhancement of drop coalescence.

Wang and Calabrese (1986) reported that drop size distributions for low and moderate dispersed phase-viscosity systems are normally distributed in volume. They found that as the dispersed phase viscosity increases, the number of smallest drops increases while their size decreases. They also correlated the drop size distribution for dispersed phase viscosity less than or equal 0.5 Pa.s, after normalizing it with the experimental Sauter mean diameter, using the following expression:

$$F_v\left(\frac{d}{d_{32}}\right) = 0.5 \left[1 + \operatorname{erf} \left(\frac{\frac{d}{d_{32}} - 1.07}{0.24(2)^{0.5}} \right) \right] \quad (2-87)$$

They combined the above equation with a similar correlation obtained, for drop size distribution of low dispersed phase viscosity in agitated tanks, by Chen and Middleman (1967) giving a more generalized correlation for drop size distribution, which is expressed as follows:

$$F_v\left(\frac{d}{d_{32}}\right) = 0.5 \left[1 + \operatorname{erf} \left(\frac{\frac{d}{d_{32}} - 1.07}{0.23(2)^{0.5}} \right) \right] \quad (2-88)$$

The above correlation applies to very small hold ups in the limit of $\phi \rightarrow 0$. It was suggested that as the dispersed phase hold-up increases, the equilibrium drop size distribution could be influenced by the following mechanisms. First, with increasing hold up the drops become closer to each other, a situation that leads to a reduction in the turbulent energy available for drop breakage due to changes made to the small-scale structure of the continuous phase (turbulence modulation). Second, higher hold ups

increase the probability of drop collision and eventually the possibility of drop coalescence. They proposed that in both cases drops of larger diameters will be formed shifting the distribution mode to larger sizes without altering the shape of the distribution. Pacek et al (1998) studied liquid-liquid dispersions of hold ups of 0.005 to 0.05 using stirred vessels. They observed that for hold-up values less than 0.05 and at low impeller speeds the number distribution shows strong bi-modality. The bigger peak, which corresponds to drops of small diameters, almost disappears as the hold up increases to 0.1. This result is in disagreement with the findings of Brown and Pitt (1972) and the predictions made by Wang and Calabrese (1986).

2.4.2 Effect of System Properties

Dispersed phase viscosity

In addition to surface forces, the drop viscous forces tend to resist breakup by turbulent forces and thus keeping droplets intact. The dispersed-phase viscosity is thus expected to influence the equilibrium drop size distribution by affecting the balance between droplet breakup and coalescence. The limited studies, which addressed this topic revealed a profound influence imparted on equilibrium drop size distribution by the dispersed phase viscosity.

Using a mechanically agitated tank, Calabrese et al (1986) studied the effect of the dispersed phase viscosity on equilibrium mean drop size and drop size distribution of aqueous dispersions of different grades of silicon oil. They found that at a constant agitation rate and constant surface tension, the equilibrium drop size distribution widens considerably with increasing dispersed phase viscosity. The number of largest drops tends to decrease; meanwhile their size increases. On the other hand, smallest drops behave differently, their number increases while their size decreases. At a viscosity range of 0.1 to 0.5 Pa.s the drop size number distribution is normal and a relatively small difference between the number median and the Sauter mean diameter is observed. This difference increases as the dispersed phase viscosity increases. The distribution shifts to log-normal at viscosities of 5 to 10 Pa.s and the difference between the number median

and the Sauter mean diameters becomes comparatively high. They also observed that the drop breakup becomes more difficult as the viscosity increases and the drop becomes stretched rather than burst resulting in wider distributions. Due to the lack of experimental observations for systems of dispersed phase viscosities equal or more than unity, they proposed that the existence of large numbers of small drops indicates different breakup mechanism from that for systems of lower dispersed phase viscosities. Further, they suggested that the drop breakup is only limited to the vicinity of the impeller and is more erosive in nature, which leads to the production of numerous numbers of small drops. The distribution at intermediate viscosities could not be represented by any of the existing distributions. They suggested that large drops exist because they do not stay long enough in the highly turbulent region near the impeller to breakup. As reported earlier, Chen and Middleman (1967) studied the dispersion of 1-5% volume fraction of different organics dispersed in water using six-blade turbine impellers at different rotational rates. They found that the drop size distribution is correlated by the following normal distribution function:

$$F_v\left(\frac{d}{d_{32}}\right) = \frac{1}{0.23\pi^{0.5}} \exp\left[-9.2\left(\frac{d}{d_{32}} - 1.06\right)^2\right] \quad (2-89)$$

They also observed that the standard deviation of the distribution, which has a value of 0.23, is independent of the viscosity of the dispersed phase for all systems.

For three different dispersers (small-diameter tube, Kenics mixer and Couette device), Haas (1987) found that the equilibrium average diameter of aqueous drops in trichloroethylene and 2-ethyl-1-hexanol increases with increasing dispersed phase viscosity meanwhile the drop size distribution becomes wider.

A study of dilute dispersions of several oils in water using a Kenics static mixer showed that the drop size distribution widens as the dispersed phase-viscosity increases. Low dispersed phase viscosity resulted in a finite but small overlap between the two distributions. The initial distribution and the overlap widened very rapidly with increasing viscosity. For example, for highly viscous paraffin, an initial bimodal distribution was obtained, which had many small satellite drops. Also, studies on silicon

oil and paraffin oil revealed that at constant Reynolds number and constant interfacial tension, the distribution widened with increasing dispersed phase viscosity. This result is in agreement with the findings of Calabrese et al. (1986) for the dispersion of silicon oils of different grades in agitated tanks. A similar argument to that proposed by Calabrese et al (1986) was adopted to explain this behavior. The drop size distributions are found to follow the normal distribution after normalization with d_{32} (Berkman and Calabrese, 1988).

Density Difference

High values of density difference between the dispersed and continuous phases can greatly influence the drop size distribution. At high values of density difference, the buoyancy force can exceed the drag force, a situation which enhances the segregation tendency of dispersion.

Chen and Middleman (1967) studied the dispersion of 1-5% volume fraction of different organics dispersed in water using six-blade turbine impellers. The investigated impeller speeds ranged from 80 to 1000 rpm, which gave Reynolds numbers from 1.2×10^4 to 10.4×10^4 . They reported that the standard deviation (a measure of the homogeneity of the dispersion) of the drop size distribution for all the studied systems is independent of the dispersed phase density.

Rincon-Rubio et al. (1994) reported that the density difference between two liquid phases has no consistent effect on drop size distribution when two immiscible liquids were dispersed using a Wirz II agitated column. On the contrary, Seidshazileh (1999) observed that the drop size distribution for Bayol oil, which has a specific gravity of 0.78, dispersed in water using a stirred vessel shifts to smaller drop sizes as the rotation speed was reduced from 500 to 250 rpm. He proposed that at low rotation rates the large drops tend to segregate in the upper part of the tank leaving the smaller drops at the base of the tank due to large density difference between the two phases. In other words, reducing the rotation rate enhances drop coalescence causing the size of the drops to increase and eventually increasing the buoyancy force exerted on the drops, which together with large density difference lead to drop segregation at the top.

2.4.3 Effect of Interfacial Characteristics

The limited investigations dealing with the role of interfacial characteristics in liquid-liquid dispersion proved that they strongly affect drop coalescence and breakage processes, which in turn affect the evolved drop size distribution. Interfacial characteristics affect the surface forces which are very important in keeping the droplets intact. Interfacial characteristics include static and dynamic interfacial tension, diffusivity, interfacial tension gradient, surface elasticity, etc.

The study of silicon oil-in water dispersion showed that under conditions of constant agitation, the relative effect of interfacial tension on equilibrium drop size and drop size distribution decreased as the dispersed-phase viscosity increased. It was suggested that at low values of interfacial tension, the surface resistance to breakage became very small compared with viscous resistance at dispersed-phase viscosity approximately of 1 Pa.s. At low to moderate values of dispersed-phase viscosity (0.001-0.5 Pa.s.), the equilibrium drop sizes were correlated by normal distribution, whereas at high viscosity, in systems with high interfacial tension, deviations from normal distribution were observed. Drop size distributions were broadened with increasing interfacial tension, dispersed-phase viscosity, and decreasing impeller speed. This behavior was attributed to exceeding the stabilizing forces (i.e., due to surface tension and dispersed viscosity) the disruptive or turbulent forces, which increase the relative resistance to drop breakage.

In styrene-in-water system containing poly vinyl alcohol as a surface-active agent, a bimodal drop size distribution was obtained. The drop size distribution broadened and the two modes shifted towards smaller drop diameters upon the reduction of the interfacial tension from a value of 22.9 dyn/cm to 3.8 dyn/cm. This was an expected result, since both processes the drop coalescence and breakage are very much influenced by the drop surface energy, which in turn depends on the interfacial tension. The decrease in interfacial tension decreases the resistance to drop breakage (Chatzi et al., 1991). On the contrary, Rincon-Rubio et al (1994) found that at low interfacial tension and a given agitation rate, narrower and more uniform drop size distribution about the mean were

obtained. As the interfacial tension of cyclohexane- and butanol-water systems (the organic is the dispersed phase) was reduced from 4.1 to 1.8 mN/m, both the drop size and the standard deviation decreased.

The generated drop size distributions for 50% n-butyl chloride-in-water dispersion containing poly vinyl alcohol as a surfactant (stabilizer) and using an agitated vessel broadened towards smaller sizes as the agitation rate increased from 400 to 550 rpm at high PVA concentration (1g/L). Meanwhile it remained the same at impeller speeds more than 550 rpm. At 400 rpm, as the PVA concentration increased the drop sizes distribution shifted towards smaller drop sizes. This shows that the drop breakage becomes dominant even at low agitation rates in presence of high PVA concentration (Chatzi and Kiparissides, 1995).

Seidshazileh (1999) studied the effect of mixing time required to reach equilibrium for Bayol oil/Water system containing Triton X100 as a surfactant using a stirred vessel. He found that as mixing time increases, the peaks, in both volume and number density distributions shift to smaller drop sizes without altering the shape of the distribution. It was suggested that longer mixing time enhances drop breakage resulting in the formation of smaller drops as time increases. It was also concluded that the presence of surfactant in liquid-liquid dispersions may delay equilibrium conditions indefinitely.

Chapter 3

EXPERIMENTAL

In this chapter, the experimental set up used in this work is presented, which is then followed by the investigated liquid-liquid system and a description of the experimental procedure. An error analysis is also conducted and the repeatability of drop size measurement is validated. Finally, the data treatment methods adopted in this research are discussed.

3.1 EXPERIMENTAL SET UP

The process of dispersion in screen-type static mixers was investigated using a 25.4 mm pipe loop shown in Figure 3.1. The continuous phase (aqueous solution of sodium chloride) is drawn from a 460-litre pressurized stainless steel tank using a Procon (Procon Prod., Model 104C330F12XX) centrifugal pump. The pressurized tank is used to maintain a pressure of at least 20 psi at the pump inlet in order to prevent cavitation and the formation of bubbles that could interfere with the measurements in the flow visualization section. The flow rate of the continuous phase, which can be adjusted via a control valve on a by-pass line, is measured by a flow sensor (Cole-Parmer, Model P-32919-70, maximum capacity of 21 liters/minute), which is connected to a digital display (Cole-Parmer, Model P-32919-00), with an accuracy of $\pm 1\%$ of the reading. The dispersed phase (Bayol oil) is pumped from a 60-liter pressurized steel vessel (Motomaster, Model GA970). A rotameter (Cole-Parmer, Model FM044-40C) is used to adjust and monitor the flow rate of the dispersed phase.

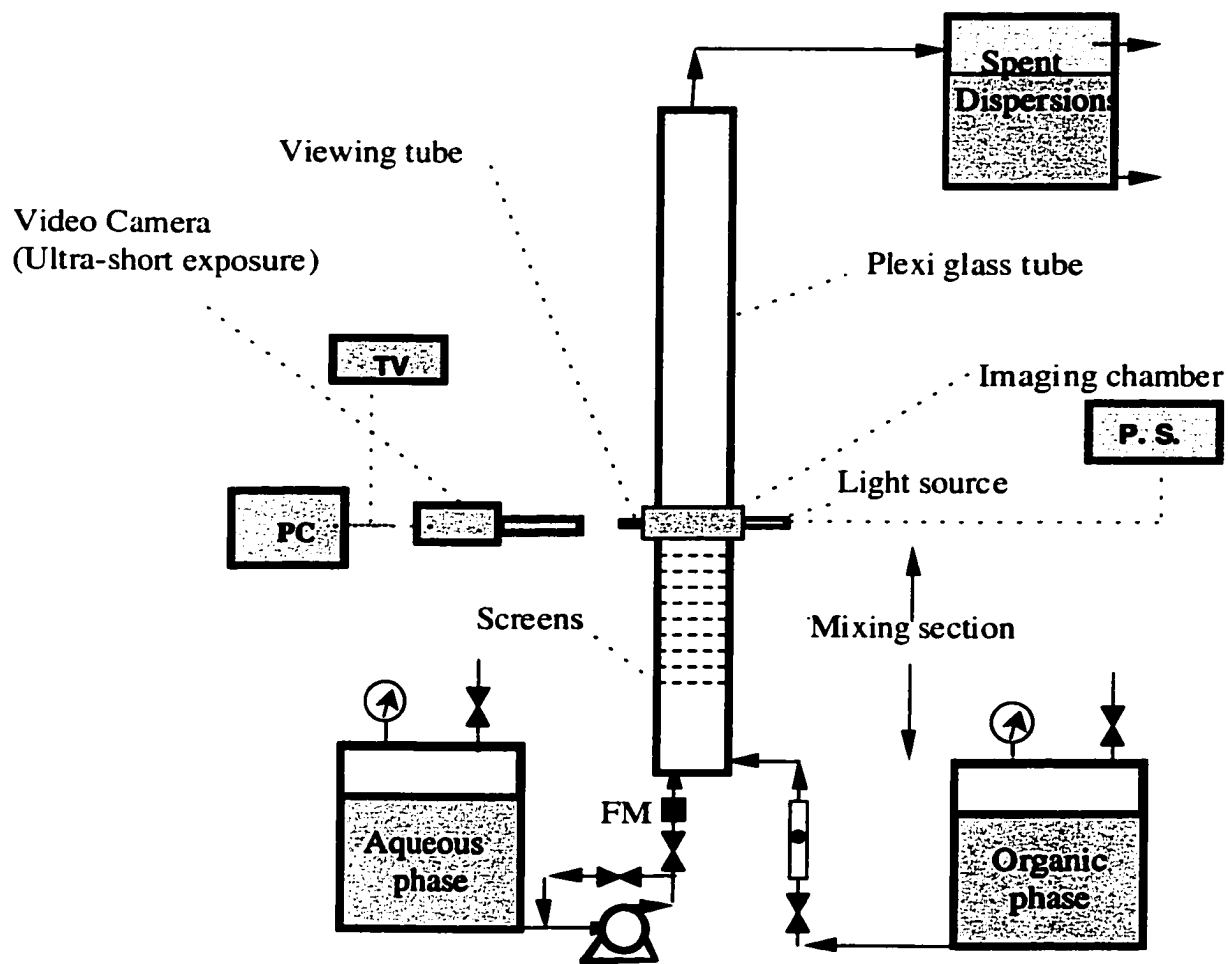


Figure 3.1. Schematic diagram of the experimental setup

The continuous and dispersed phases are introduced to a vertical mixing section where dispersion takes place. A vertical arrangement was selected to avoid the onset of phase concentration non-uniformity due to the action of gravity. The dispersed phase is fed into the continuous phase pipe flow using four evenly distributed capillary tubes (ID = 0.76mm) to achieve efficient initial mixing of the phases.

The mixing section consists of a stainless steel pipe 130 mm long, which incorporates a set of stainless steel static mixing elements made from woven screens of different characteristics (see Table. 3.1). A set of brass rings 25.4mm inside diameter and a height of 10 and 5 mm were used to adjust the distance between the consecutive screens. In some experiments, brass rings with ID's of 21.50 and 15.24 mm were used in order to obtain higher superficial velocities. A differential pressure transmitter (Omega, Model PX273-030DI) is used to measure the pressure drop across the mixing section. The signal generated by the sensor is fed to a digital pressure display (Omega Model DP3002-E).

The spent dispersions are collected in a 1153-liter polyethylene tank where they are left for at least 24 hours to separate before the water layer is decanted.

An image analysis technique is used for measuring the sizes of the drops present in the dispersion. It consists of:

- An adjustable intensity light source to provide the necessary lighting for imaging the dispersion at the very short exposure times necessary to freeze the images of the moving drops. The light source is a 150W/115V fiber optic illuminator (Dolan Jenner Model PL-800, Edmund Scientific Co.) equipped with a liquid light guide, which exhibits excellent UV transmission properties.
- A flow-through drop imaging arrangement made of PVC (Figure 3.2). The inner diameter is 25.4 mm in order to minimize flow disturbances. Two 5-mm brass tubes equipped with optical windows on the wet side are introduced from opposite sides of the PVC imaging chamber vertical to the direction of the two-phase flow. The distance between the two tubes is adjusted to provide a gap of 3 mm. The end of the light guide is inserted in the end of one brass

tube while the opposite tube is used for viewing the drops passing through the gap.

Table 3.1. Characteristics of the woven screens investigated.

No.	Wire Size (mm)	Open Area (%)	Mesh Size (mm)	b/M
1	0.508	27	0.55	0.92
2	0.15	33	0.21	0.71
3	0.305	41	0.54	0.56

- An adjustable microscope (VZM Model 450, Edmund Scientific Co) is capable of achieving a maximum magnification of 180X. Depending on the magnification an adjustable field view that varies from 1.4-7 mm drop images of size 7 μm to 1400 μm can be captured. A C-mount is added to the microscope to provide very fine focusing.
- Drop images were recorded using a FlashCam 335 NG 0027 video camera (PCO Co., U.S.A.) which is equipped with a high sensitivity CCD-video chip (2/3" chip, 640 x 380 pixels) capable of obtaining good images within very short exposure times (1 to 1000 μs ; 2 μs were used) needed in order to freeze the images of rapidly moving drops.

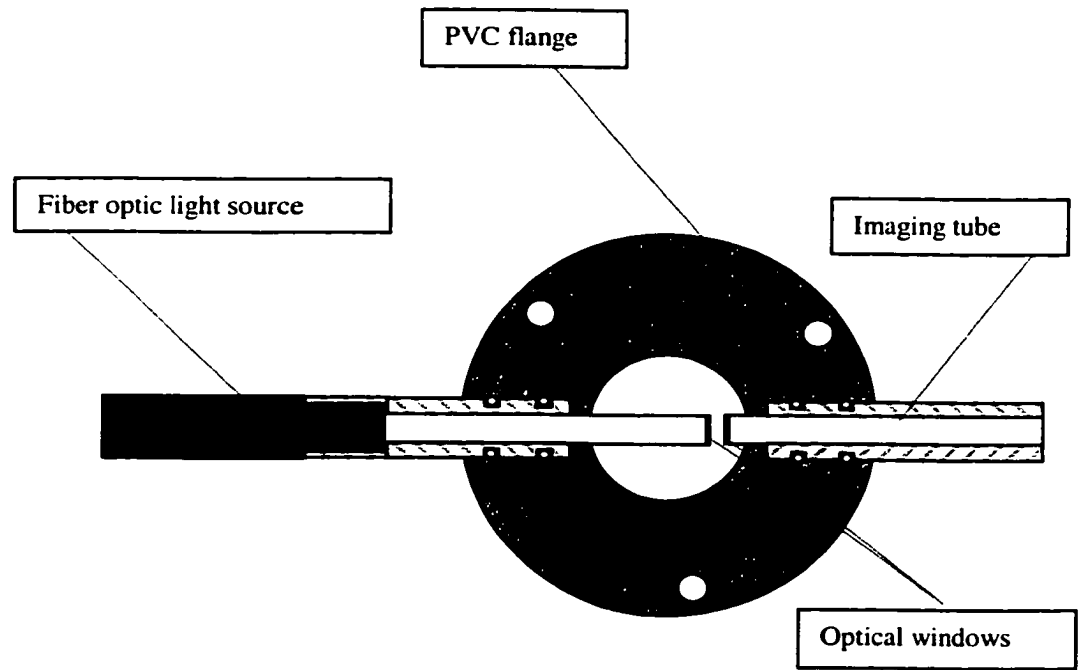


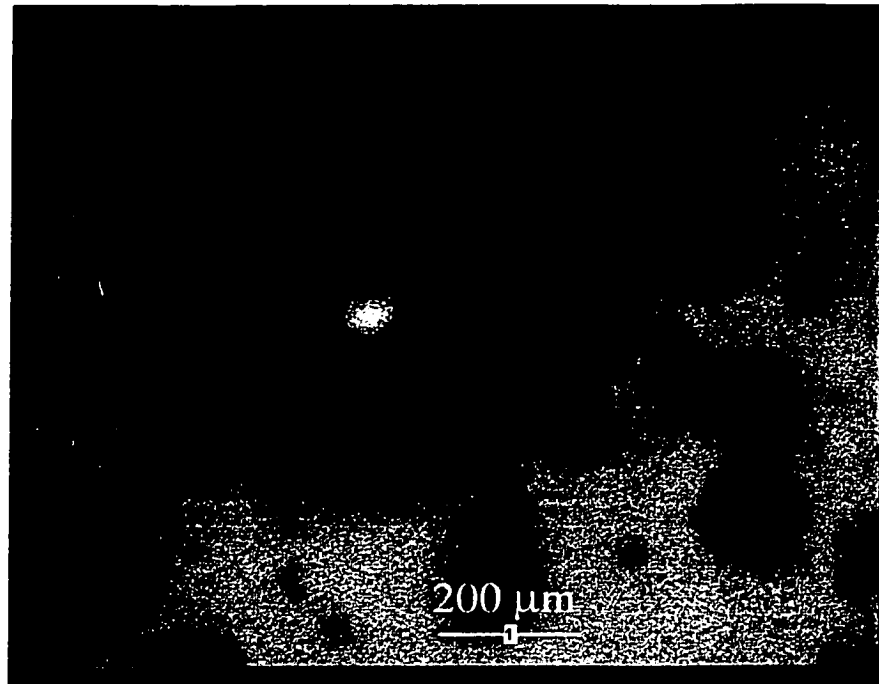
Figure 3.2. Schematic diagram of the imaging chamber.

- Frame grabber, PC, monitor (13" TV, JVC Model C-13910) and semi-automated image analysis software. The frame grabber (CX100 LINUX-based software) was used manually to grab frames of the captured images directly from the camera. The grabbed frames were saved as BIN files on the computer hard drive. Then the BIN files were converted to BMP files to be readable by the Scion image software. Images grabbed directly from the camera (no pre-recording on a video tape) exhibit better resolution and picture quality. A total of more than 9000 image frames were grabbed, in which the number of drops varied from 2 drops in case of low dispersed phase holdup dispersions to more than 100 drops in dispersions of 4% holdup. Figure 3.3 shows a sample of the grabbed images. The monitor was used for purposes of focusing and visual monitoring of the dispersion process while frames grabbing was taking place.
- Scion image Windows based semi-automated image analysis software (produced by the National Institutes of Health, Ohio, U.S.A) was used to measure the drop sizes. The software has image enhancement capabilities. It provides filters for smoothing, sharpening, finding edges and reducing noise in images. The measurement of drop size was done manually. The drop was outlined using a circular selection tool and then the perimeter was measured from which the drop diameter was calculated. Images in focus were only measured.

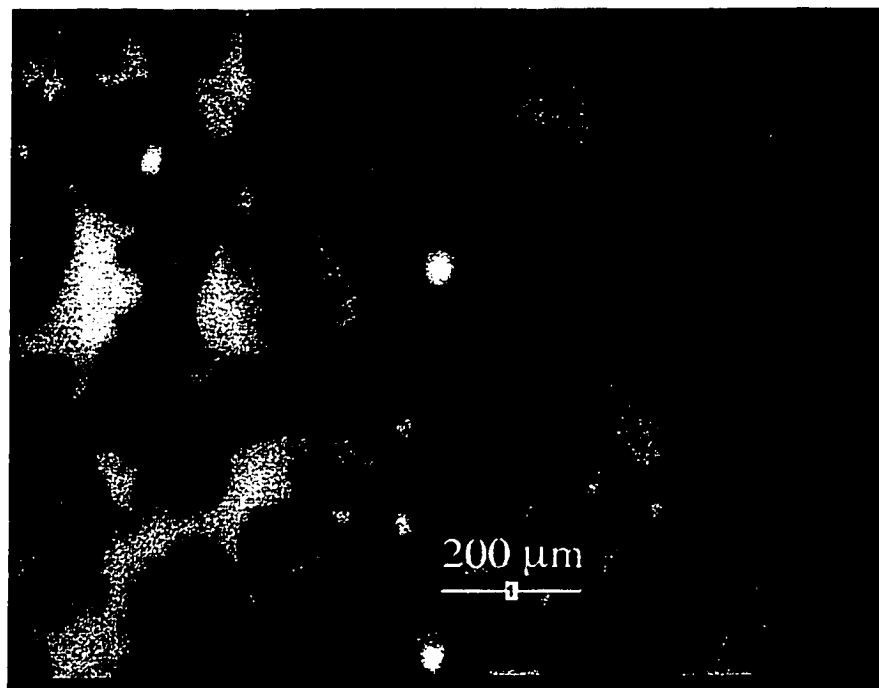
3.2 INVESTIGATED SYSTEM

In deciding on the liquid-liquid system to be studied, the following factors were taken into account:

- The dispersion characteristics of the system should have already been investigated using a mechanically agitated tank in order to provide a good basis for comparison.



0.3 m/s



0.7 m/s

Figure 3.3. A sample of imaged drops ($\alpha = 27\%$, $\phi = 4\%$, 9 screens, $L = 10$ mm).

- The static and dynamic interfacial characteristics of the system should have also been studied and well analyzed in order to determine their relative significance to the dispersion process.

Recently, the interfacial characteristics of the following system were studied by Xue (1999),

- Bayol oil (dispersed phase).
- Water containing 500 ppm of sodium chloride (continuous phase) in order to compensate for the uncontrolled variation in tap water.
- Interfacial characteristics were modified by adding trace quantities of TritonX100 (0.01 to 0.3 mole/m³) to the continuous phase.

Seidshazileh (1999) studied the dispersion characteristics of this system using a stirred tank; his results can be used as a basis for comparing the performance of the screen-type static mixers with those of MAT. Table 3.2 shows the physical properties of the pure phases. The properties of water were taken from “The CRC Chemical and Physical Handbook (1991)” and those for Bayol oil from the supplier. Table 3.3 shows the equilibrium interfacial tension of the investigated system containing different concentrations of Triton X100 surfactant (Xue, 1999). The effect of the presence of sodium chloride on the interfacial tension is very small and was neglected.

Bayol oil (supplied by Esso) is a colorless mineral oil used as a plasticizer for rubber products used in food packaging, as a drawing or forming oil for the manufacture of food containers from sheet metal or foil, as a light lubricant for food-processing machines, etc.

Triton X100 (supplied by Sigma Co.) is a non-ionic surface active agent that exhibits an HLB (i.e., hydrophile-lypophile balance) of about 18. This ensures its solubility in the aqueous phase. It has a molecular weight of 625 kg/kmole and a density of 1065 kg/m³. The use of a non-ionic surfactant ensures the avoidance of formation of electrical charges on the drops, which can strongly interfere with drop coalescence. Triton X-series surfactants are essentially composed of alkylaryl polyether alcohols

produced by the reaction of octylphenol with ethylene oxide forming a polyoxyethylene chain. The subscript "X" represents the average number of ethylene oxide units.

Table 3.2. Physical properties of the pure phases at 25 °C.

Phase	Density (kg/m ³)	Viscosity (cP)
Water	997	1.0
Bayol Oil	792	2.26

Table 3.3. Interfacial characteristics of investigated system.

Triton X100 concentration (mole/m ³)	σ (mN/m)	Γ_s mole/m ²	D m ² /s	Ma/L
0	19.00			
0.01	11.00	1.5×10^{-4}	4.43×10^{-10}	4.43×10^9
0.05	6.00	2.2×10^{-4}	6.50×10^{-10}	6.50×10^9
0.10	4.78	2.6×10^{-4}	1.15×10^{-10}	1.15×10^{10}
0.20	2.56	2.9×10^{-4}	3.20×10^{-12}	3.20×10^{10}
0.30	2.10	3.1×10^{-4}	2.30×10^{-12}	2.30×10^{10}

The Marangoni number, Ma , is defined in Equation (4-17).

3.3 EXPERIMENTAL PROCEDURE

All tests were carried out using water containing 500 ppm of sodium chloride as the continuous phase and Bayol oil as the dispersed phase. The sodium chloride solutions were prepared in a 450-liter agitated polyethylene tank then transferred to the continuous phase tank.

To determine the conditions at the point of entry to the static mixers, dispersion tests were conducted in the absence of screens (i.e. open pipe) at velocities of 0.70, 0.85, 0.97, 1.80 and 1.94 m/s at dispersed phase holdup of 0.5%.

Three sets of experimental runs were completed using screen open areas of 41, 33 and 27%. For each set of screens, oil-in-water dispersions were produced under different

conditions of superficial velocity and dispersed phase volume fraction. The studied superficial velocities ranged from 0.30 to 1.94 m/s. The superficial velocity was varied by adjusting the continuous phase flowrate. This results in pipe Reynolds numbers of 7000 to 50000, wire Reynolds numbers of 91 to 982, mesh Reynolds numbers of 160-1063, individual jet Reynolds numbers of 61 to 1290, jet Reynolds numbers of 18000 to 109000, Weber numbers of 119 to 3010, jet Weber numbers of 713 to 41285 and mean energy dissipation rates of 5.65 to 1315.87 W/Kg depending on the screen characteristics. The investigated dispersed phase volume fractions were 0.5, 1, 2, 3 and 4%. At a given velocity, the holdup was varied by adjusting the flowrates of the water and oil phases in order to obtain the desired volumetric ratio. Solutions of 0.01, 0.05, 0.10, 0.20 and 0.30 mole/m³ of TritonX100 in the continuous phase were prepared in a 450-liter agitated polyethylene tank. The solutions were stirred for at least three hours to ensure the complete dissolution of the surfactant before they were pumped to the aqueous phase tank. A set of 27% open area screens was used to generate dispersions in the presence of the S.A.A at a velocity of 0.7 m/s and dispersed phase holdups of 0.5 and 4%. In all the above experiments a distance of 10 mm between the consecutive screens was used.

In order to investigate the effect of the residence time in the mixer on the dispersion, screen sets of 2, 3, 4, 9, 12 and 15 were tested using 2% holdup dispersions, a superficial velocity of 0.40 m/s and a distance of 5 mm between every two consecutive screens.

Drop images were captured and then grabbed after five minutes following startup of any experiment in order to allow the dispersion to equilibrate and to ensure that steady state conditions were achieved. In all runs the magnification was kept constant at 180X except for the open pipe runs, in which lower magnifications were used (i.e. 1.5X).

3.4 ERROR ANALYSIS

There are some potential sources of error, which could have been encountered in this investigation. These sources of error stem from: drop size measurements, pressure drop and flowrate readings.

3.4.1 Drop Size Measurement

The drop size measurements conducted in this investigation are subjected to the following sources of errors: errors in magnification, errors resulting from drop movement, errors resulting from the limited resolution of the video camera, and errors stemming from the refractive index of the continuous phase.

Magnification

The microscope was calibrated after adding the C-mount using an “Objective Micrometer” supplied by Fischer Scientific. The calibration curve is shown in Figure 3.4. At a magnification of 180X, the microscope has a depth of field of 1 mm and a field distance of 96.9 mm. The microscope length is 160 mm and the C-mount is 85 mm long. A constant magnification of 180X was used throughout this research except for the open pipe experiments, in which lower magnifications were used. When the magnification is 180X, a difference of 1 mm in the location of the drop within the depth of field results in a maximum magnification error of $\pm 0.28\%$.

Drop Movement

Assuming no slip velocities between the phases, it is estimated that the movement of a 350 μm drop size is expected to generate an error of 0.51 % at the maximum superficial velocity and an exposure time of 2 μs . This increases to 6.00% for a drop size of 30 μm . These errors reduce to 0.22% and 2.60% respectively at minimum superficial velocity.

The Video Camera

This type of error results from the accuracy of the video camera itself, which is about ± 0.5 pixel. For example a drop of diameter of 30 μm is expected to have an error of $\pm 4.06\%$ compared to $\pm 0.35\%$ for a drop 350 μm in diameter.

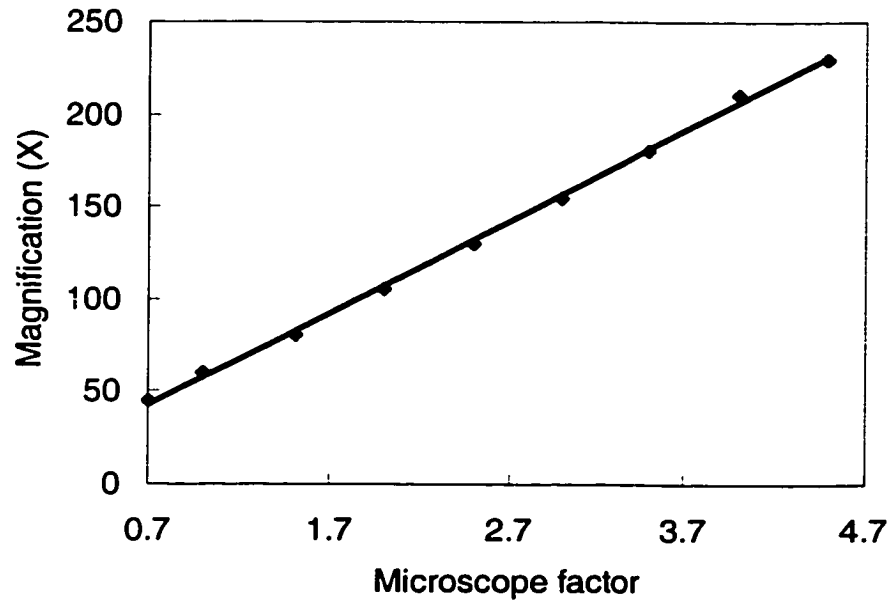


Figure 3.4. Microscope calibration curve.

Refractive Index of the Continuous Phase

Another important source of error is due to the refractive index effect of the continuous phase. Sears and Zemansky (1960) correlated the apparent distance, S_{ap} , to the actual one S_{ac} , of an object immersed in a fluid of refractive index, n_l , as follows:

$$S_{ap} = S_{ac} \left(\frac{n_a}{n_l} \right) \quad (3-1)$$

where the subscripts a and l refer to air and liquid respectively. Since the refractive indices of water and air are 1.33 and 1.00 respectively and the farthest point in the imaging area is about 3 mm from the imaging tube, the apparent distance for a drop suspended in water is about 2.25 mm. So, the expected error in drop size measurement will be less than 0.28%.

3.4.2 Pressure Drop Measurement

As stated earlier, the pressure transducer produces an error of $\pm 1\%$ of the reading.

3.4.3 Continuous Flow Rate Measurement

The flow rate sensor produces an error $\pm 1\%$ of full scale (21.5 liters/min.), which is ± 0.22 liters/min. The measured flow rates ranged from 9.07 to 21.3 liters/min. thus yielding an error of $\pm 2.4\%$ and $\pm 1\%$ respectively.

3.4.4 Energy Dissipation Rate

The volumetric average energy dissipation rate in the mixer can be expressed as follows:

$$\varepsilon = \frac{U\Delta P}{\rho_c L_m} \quad (3-2)$$

where $U = Q/A_c$. As shown in Equation (3-2), the calculated energy dissipation rates are subjected to errors rising from errors associated with pressure and flowrate measurements, which generate errors of $\pm 1\%$ of the reading and $\pm 1\%$ of full scale respectively. For example, when 27% open area screens are used as static mixing elements, at maximum superficial velocity (i.e., 1.94 m/s), the generated error in the calculated energy dissipation rate in the mixing section is about $\pm 0.74\%$ compared to $\pm 1.18\%$ at minimum superficial velocity and the same holdup. The nominal and the actual dissipation rates were calculated and the resulting error was determined (Holman, 1978, p. 43).

3.5 DROP SIZE MEASUREMENT

3.5.1 Sample Size

It is widely acknowledged that the larger the sample size the better it represents the population that it is taken from. In most of liquid-liquid dispersion studies the sample size ranges from 300-1400 drops (Sleicher, 1962; Collins and Knudsen, 1970; Kubie and Gardener, 1977; Wang and Calabrese, 1986, Calabrese et al., 1986, Tobin et al., 1990;

Pacek et al, 1994; Brook and Richmond, 1994; Ni et al., 1998; Pacek et al., 1998; Seidshazileh, 1999). Table 3.4 shows the minimum number of drops used per experimental run in most recent studies.

In order to determine the minimum number of drops needed to ensure good representation of the population it is taken from, a sample was withdrawn from a dispersion produced using 12 screens of 27% open area, at distance of 5 mm between consecutive screens, holdup of 2% and a velocity of 0.40 m/s. Table 3.5 shows the number length means for the sample calculated with 95% confidence interval as well as the their standard deviations. It clearly shows that a sample size of about 600 drops yields a very good representation of the population. However, more than 1000 drops were measured in each experimental run in order to ensure an excellent representation of the populations studied.

Table 3.4. Reported sample sizes in the literature

Researcher	Number of drops
Tobin et al. (1990)	1000
Pacek et al. (1994)	800
Brook and Richmond (1994)	300
Ni et al. (1998)	400
Pacek et al. (1998)	600
Seidshazileh (1999)	1400

Table 3.5. Statistical analysis of samples with different drop numbers.

Sample	Number of drops	Arithmetic mean (μm)	Standard deviation (μm)
1	606	167 ± 7	90.4
2	1000	166 ± 6	90.5
3	1211	167 ± 5	89.6

3.5.2 Reproducibility of Drop Size Measurements

In order to ensure that the experimental technique used in this investigation yields reproducible results, the characteristics of Bayol oil-in-water dispersions (generated using of 0.5 % dispersed phase holdup, nine screens of 27% open area, superficial velocity of 1.55 m/s, and a sample size of more than 1000 drops) were replicated 9 times. The results obtained are displayed in Table 3.6 from which it is clear that the resultant standard error in the different mean drop diameters varies from ± 1.5 to ± 1.9 % depending on the type of the mean.

Table 3.6. Reproducibility of drop size measurements

Run	d_{10} (mm)	d_{20} (mm)	d_{30} (mm)	d_{32} (mm)	d_{43} (mm)
1	0.0422	0.0450	0.0478	0.0541	0.0604
2	0.0380	0.0406	0.0433	0.0494	0.0560
3	0.0425	0.0455	0.0486	0.0553	0.0619
4	0.0445	0.0473	0.0500	0.0560	0.0619
5	0.0395	0.0423	0.0452	0.0515	0.0578
6	0.0444	0.0478	0.0511	0.0584	0.0649
7	0.0424	0.0453	0.0482	0.0547	0.0613
8	0.0441	0.0470	0.0499	0.0560	0.0618
9	0.0432	0.0462	0.0494	0.0566	0.0642
mean	0.0423	0.0452	0.0482	0.0547	0.0611
s.d (mm)	0.0022	0.0024	0.0025	0.0028	0.0027
s.e (mm)	0.0007	0.0008	0.0008	0.0009	0.0009

3.6 DATA TREATMENT

In the following sections the methods used for calculating drop size distributions and their different parameters as well as the drop mean diameters, energy dissipation rate, the surface excess and the surfactant diffusivity are reviewed.

3.6.1 Flowrates of Dispersed and Continuous Phases

$$\text{Total flow rate (dispersed and continuous phases)} \quad Q = UA_c \quad (3-3)$$

where U is the superficial velocity and A is the pipe cross-sectional area.

$$\text{Dispersed phase flow rate} = \frac{\text{volume fraction of dispersed phase} \times Q}{100} \quad (3-4)$$

$$\text{Continuous phase flow rate} = Q - \text{dispersed phase flow rate} \quad (3-5)$$

3.6.2 Drop Size Distribution

Calculation of Drop Size Distribution

The distributive number-density, volume-density, and cumulative volume distributions were generated from the drop size data generated under different experimental conditions. In order to generate those drop size distributions, the measured drop sizes for each experiment were grouped into n classes of width (d). The mean diameter of each class was calculated and it was given to all drops within the class (Orr, 1983). The drop number-density and volume-density were then computed as follows,

The drop number density ($N\%$) for the i^{th} interval is given by:

$$N\% = \frac{n_i}{n_{\text{total}}} \times 100 \quad (3-6)$$

The drop volume density ($V\%$) is given by:

$$V\% = \frac{n_i d_i^3}{\sum_{j=1}^{j=n} n_j d_j^3} \quad (3-7)$$

The cumulative drop volume density ($C.V\%$) is given by:

$$C.V\% = \frac{\sum_{j=1}^{j=i} n_j d_j^3}{\sum_{j=1}^{j=n} n_j d_j^3} \times 100 \quad (3-8)$$

The computed densities were plotted against the drop size in order to obtain the drop size distribution curve. Drop number density distributions emphasize the contribution of the small drops while drop volume density distributions are strongly

influenced by the fraction of the large drops present in the dispersion. A sample of drop size distribution calculation is shown in Table 3.7. Because of the large number of points (typically 1000 points) and the large number of classes used (30 Classes) the errors arising from the use of class intervals are minimal.

The standard deviation and the mean of each set of data (i.e. sample) were computed using the following expressions (Kennedy and Neville, 1986):

$$d_{10} = \frac{1}{n} \sum_{i=1}^n d_i \quad (3-9)$$

$$s = \sqrt{\frac{\sum_{i=1}^n (d_i - \bar{d})^2}{n-1}} \quad (3-10)$$

The skewness of the sample distributions was computed using the following equation:

$$Skewness = \frac{E[(X - \mu)^3]}{(\sigma^2)^{3/2}} \quad (3-11)$$

Drop Size Distribution Fitting

An attempt was made to mathematically quantify the drop size distributions generated. This included fitting the number density distributions generated for each experiment to 30 theoretical probability distributions using ExpertFit software (Averill M. Law and Associates, U.S.A.). The test statistic used for testing the statistical significance was the Andersen-Darling test. The computed test statistic was compared with the critical values provided by the same software at the 95% level of significance. If the test statistics were lower than the critical value at the chosen level of significance, the fit was accepted.

Attempts were also made to fit the resulting cumulative drop volume density to the theoretical normal and log-normal distributions using linear regression. The standard deviation and the mean of the distribution were determined at the 95% confidence level. This had to be undertaken separately since the ExpertFit software allows for fitting of number density distributions only whereas most commonly reported distributions are those based on cumulative volume. The normalized cumulative normal and log-normal

volume distributions are given by Equations (3-12) and (3-13) respectively ((Tavlarides and Stamatoudis, 1981; Wang and Calabrese, 1986):

Table 3.7. Sample of drop size distribution calculation
(Bayol oil-water, $\phi = 0.5\%$ $U = 0.40$ m/s, $\alpha = 41\%$, 9 screens, $L = 10$ mm)

Interval	Frequency	Mid-interval	N%	V%	C.V%
0.11-0.15	13	0.131	0.90	0.00	0.00
0.15-0.20	52	0.176	3.60	0.04	0.04
0.20-0.24	138	0.221	9.56	0.21	0.25
0.24-0.29	186	0.266	12.89	0.49	0.75
0.29-0.33	140	0.311	9.70	0.59	1.34
0.33-0.38	66	0.356	4.57	0.42	1.76
0.38-0.42	99	0.401	6.86	0.90	2.66
0.42-0.47	71	0.446	4.92	0.89	3.54
0.47-0.51	36	0.491	2.49	0.60	4.14
0.51-0.56	35	0.536	2.43	0.76	4.90
0.56-0.60	39	0.581	2.70	1.08	5.98
0.60-0.65	28	0.626	1.94	0.97	6.95
0.65-0.69	16	0.671	1.11	0.68	7.63
0.69-0.74	38	0.716	2.63	1.97	9.60
0.74-0.78	34	0.761	2.36	2.11	11.71
0.78-0.83	37	0.806	2.56	2.73	14.45
0.83-0.87	30	0.851	2.08	2.61	17.05
0.87-0.92	37	0.896	2.56	3.76	20.81
0.92-0.96	45	0.941	3.12	5.29	26.10
0.96-1.01	38	0.986	2.63	5.14	31.24
1.01-1.05	34	1.031	2.36	5.26	36.50
1.05-1.10	28	1.076	1.94	4.92	41.42
1.10-1.14	51	1.121	3.53	10.14	51.57
1.14-1.19	32	1.166	2.22	7.16	58.73
1.19-1.23	20	1.211	1.39	5.01	63.74
1.23-1.28	24	1.256	1.66	6.71	70.45
1.28-1.32	20	1.301	1.39	6.22	76.67
1.32-1.37	22	1.346	1.52	7.57	84.25
1.37-1.41	10	1.391	0.69	3.80	88.05
1.41-1.46	8	1.436	0.55	3.34	91.39
1.46-1.50	4	1.481	0.28	1.83	93.23
1.50-1.55	2	1.526	0.14	1.00	94.23
1.55-1.59	6	1.571	0.42	3.28	97.51
1.59-1.64	2	1.616	0.14	1.19	98.71
1.64-1.68	2	1.661	0.14	1.29	100.00
Total	1443 drops		100	100	

Plotting the cumulative drop volume distribution on normal probability paper gives a straight line if the data are normally distributed. Likewise if the data are log-normally distributed, plotting them on a log-normal probability paper produces a straight

$$f_v(X) = 0.5 \left[1 + \operatorname{erf} \left(\frac{X - \bar{X}}{\sigma \sqrt{2}} \right) \right] \quad (3-12)$$

$$f_v(X) = 0.5 \left[1 + \operatorname{erf} \left(\frac{\log(X / \bar{X}_{lg})}{\log \sigma_{lg} \sqrt{2}} \right) \right] \quad (3-13)$$

line. In both cases, the mean corresponds to cumulative volume density of 50% and the standard deviation extends from 50 to 84% or 16 to 50% cumulative volume densities.

Deviations from these theoretical distributions (such as the presence of bi-modality, the broadness, skewness and existence of long tails) were qualitatively examined at different hydrodynamic conditions and different surfactant concentrations. In addition, the standard deviation and the mean for each distribution were determined.

Calculation of the Mean Diameters

There are different types of mean diameters, which could be used as a criterion for the characterization of liquid-liquid dispersions. The mean diameters provide a one-value representation of a liquid-liquid system by focusing on particular parameters from among those of number, length and volume. The use of drop means diameters provide means of reducing a large set of data to an easily handled one. They, also, provide a suitable correlation parameter. For example, for comparison of mass transfer rates in two emulsions, an obvious choice will be the use of a mean diameter involving the generated interfacial area as the compared parameter. The most commonly used drop mean diameters (d_{10} , d_{20} , d_{30} , d_{32} and d_{43}) in characterization of liquid-liquid dispersions were computed using Equation (3-14):

$$d_{pq} = \left[\frac{\sum_{all} n_i \cdot d_i^p}{\sum_{all} n_i \cdot d_i^q} \right]^{\frac{1}{p-q}} \quad (3-14)$$

Table 3.8 explains the physical meaning of the computed mean diameters.

Table 3.8. Physical meaning of drop mean diameters.

Mean diameter	Description
d_{10}	Number-length mean (arithmetic mean)
d_{20}	Number-surface mean (diameter of average surface)
d_{30}	Number-volume mean (diameter of average volume)
d_{32}	Surface-volume mean (Sauter mean diameter)
d_{43}	Volume (or weight)-mean.

The magnitude of the number length mean (i.e., d_{10}) is strongly affected by the density of the smallest drops in the generated dispersion. As the moment increases the contribution of the larger drops into the mean diameter becomes bigger. A similar trend is observed with drop size distributions and this emphasizes the need for taking into account the average drop sizes of low and high moments at the same time when the characteristics of a given dispersion are investigated.

3.6.3 Mean Energy Dissipation Rate

For pipe flow, the volumetric average rate of energy dissipation per unit time and unit mass of the flowing mixture can be expressed as:

$$\varepsilon = \frac{U\Delta P}{\rho_c L_m} \quad (3-2)$$

where U is the superficial velocity, ΔP is the pressure drop across the mixer, ρ_c is the continuous phase density and L_m is the length of the mixer.

3.6.4 Surface excess

The value of the surface excess or the equilibrium interfacial concentration was calculated using the Gibbs isotherm given in Equation (2-65). The derivative of the

equilibrium interfacial tension with respect to the surfactant concentration in the bulk liquid for the liquid-liquid system investigated was computed using the following expression (Xue, 1999):

$$\frac{\partial \sigma}{\partial C_s} = -9.28 - 1.22 \ln(C_s) \quad (3-15)$$

Chapter 4

RESULTS AND DISCUSSIONS

This chapter consists of seven sections. Section 4.1 addresses the hydrodynamics of single and two-phase flow through screens. Topics such as pressure drop, turbulence intensity and length scales, as well as the energy dissipation rates generated by screens under single and two-phase flow conditions were discussed. Section 4.2 focuses on the factors affecting dispersion/coalescence processes in the screen-type static mixers (i.e. Superficial velocity, screen geometry, number of screens, dispersed phase volume fraction and interfacial characteristics). Section 4.3 investigates the maximum drop sizes generated. Section 4.4 addresses the factors affecting drop size distributions in the dispersion generated by the static mixer. An attempt to interpret the results obtained (mean drop sizes and drop size distribution) using the analytical population balance solution developed by Rod and Misk (1982) is undertaken in section 4.5. Finally the efficiency of energy utilization by the studied mixer is evaluated, which is then followed by a performance comparison with other static mixers and mechanically agitated tanks in sections 4.6 and 4.7 respectively.

4.1 FLOW THROUGH SCREENS

As mentioned before, this section focuses on single and two phase flows through screens. Topics of pressure drop, drag coefficient, turbulence intensity and energy dissipation rates generated by the investigated screens are discussed.

4.1.1 Single Phase Flow

In this section the effect of the superficial velocity of single phase flow (i.e., continuous phase only) on the pressure drop across mixing elements, and the drag coefficient, is investigated. The decay of turbulence intensity and energy dissipation rate behind the screens are also studied.

Pressure Drop across the Empty Pipe

The total pressure drop across the mixer results from the frictional losses associated with fluid flow through the pipe, the drag caused by screens, and the entrance/exit losses caused by the sudden changes in flow area.

Figure 4.1 shows pressure drop in an empty pipe (i.e. caused by the combined effect of the frictional losses as well as entrance and exit effects). As can be seen, the measured values are somewhat higher than the ones calculated using the Moody diagram (in which the measured roughness is 14 μm). The roughness of soldering of the pressure taps as well as the noise on the pressure transducer signal may have caused this difference.

The pressure losses due to entrance effect, wall friction and exit effects were found to be much less than that of the measured total pressure drop across the mixing elements (a maximum of 20%). The pressure losses due to the presence of screens were therefore calculated by subtracting the previously-mentioned losses from the overall pressure drop data obtained in the presence of screens.

Pressure Drop across Screens

Figure 4.2 shows the effect of the continuous phase velocity on the pressure drop across nine screens placed 10 mm apart. As shown, the pressure drop across the mixer increases

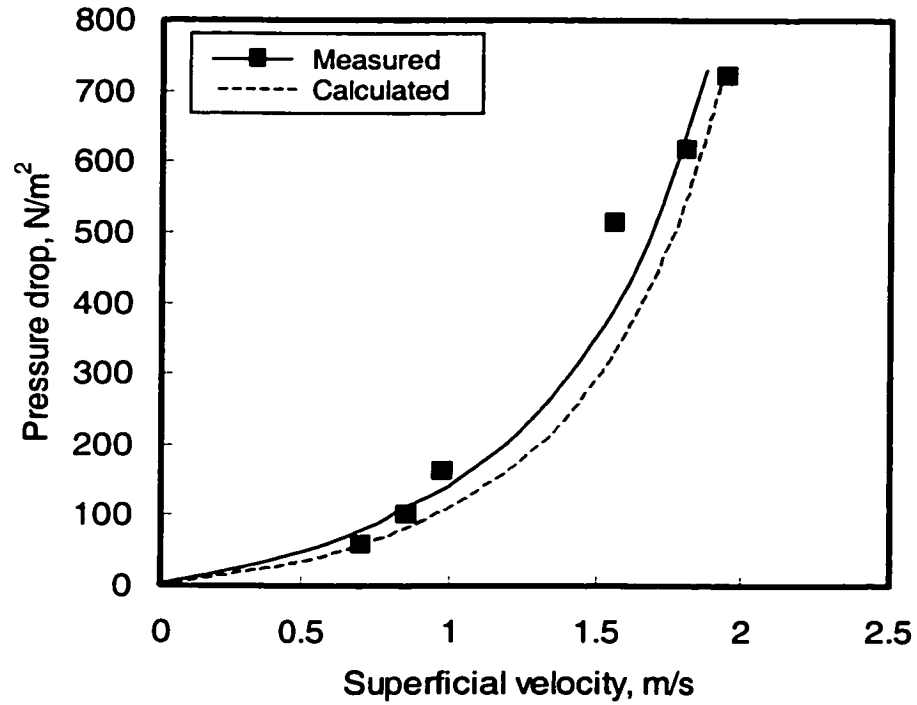


Figure 4.1. Pressure drop in the empty pipe (entrance, exit and frictional losses).

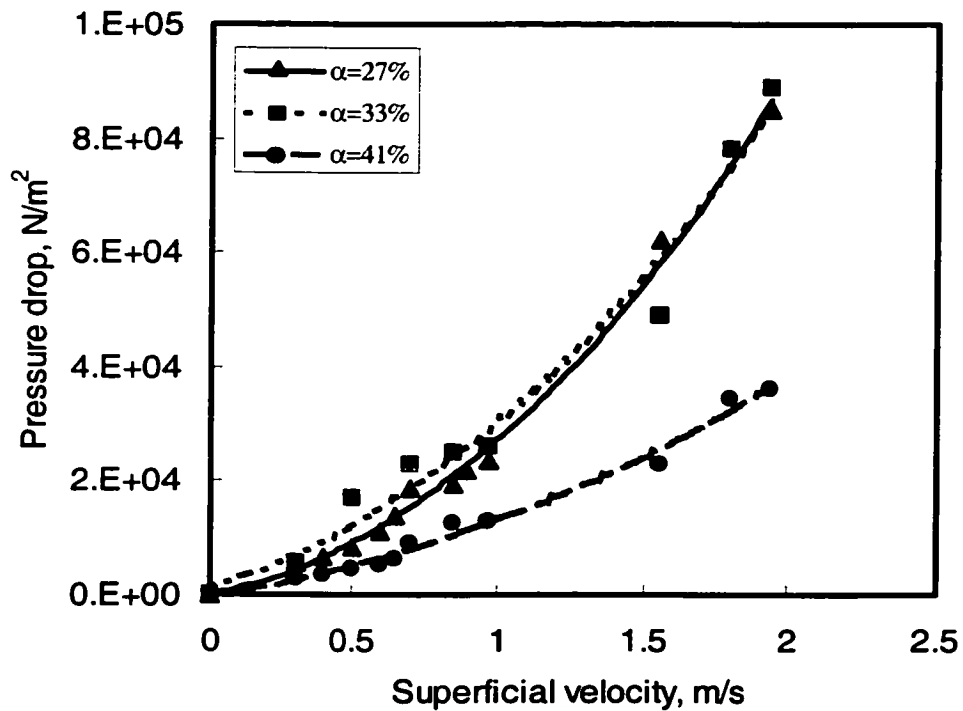


Figure 4.2. Effect of superficial velocity on total pressure drop in the mixer.

monotonically with the superficial velocity. This increase is more pronounced at lower screen porosities due to the greater flow obstruction caused.

Figure 4.3 shows the resulting drag coefficients as a function of the jet Reynolds number as well as the predicted values obtained using the correlations of Ehrhardt (1983), Groth and Johansson (1988) and Chen (1996) (Equations 2-6, 2-7, and 2-9). As expected, the drag coefficient of the screens, ψ , was found to decrease with increasing superficial velocity; however, the values predicted by Ehrhardt (1983) and the Groth and Johansson (1988) correlations are significantly smaller than those experimentally observed; the variation is most pronounced at higher screen porosities (i.e. $\alpha = 0.33$ and 0.41). The predicted values can not be correlated using the jet Reynolds number. Part of this deviation may have been caused by the fact that their correlations were mostly based on data obtained using bigger screen porosities and screen elements that are not necessarily circular or woven. The fact that they used conduits with diameters much larger than 50 mm (as compared to 25.4 mm used in the present study) is expected to play a minor role since the pressure losses due to entrance effects and wall friction have been accounted for. Consequently, the correlation proposed by Chen (1996), who used similar pipe diameter and screen system, yields a much better correlation of the experimental data. This insignificant difference may have been caused by errors in pressure drop measurement (pressure manometer was used). However the experimentally observed dependency on Re_j in the present study can be described by:

$$\psi = 2.20 Re_j^{-0.61} \quad (4-1)$$

with a good degree of confidence ($R = 0.941$).

Taylor Microscale

The transverse length scale, L_T , can be considered the largest length scale in grid-generated turbulence; whereas the Taylor microscale, λ_T , can be taken to represent the length scale of the small eddies (Dickey and Mellor, 1980). The Taylor length scale is often called as dissipation length scale, due to its dependence on the rate of dissipation of turbulent kinetic energy.

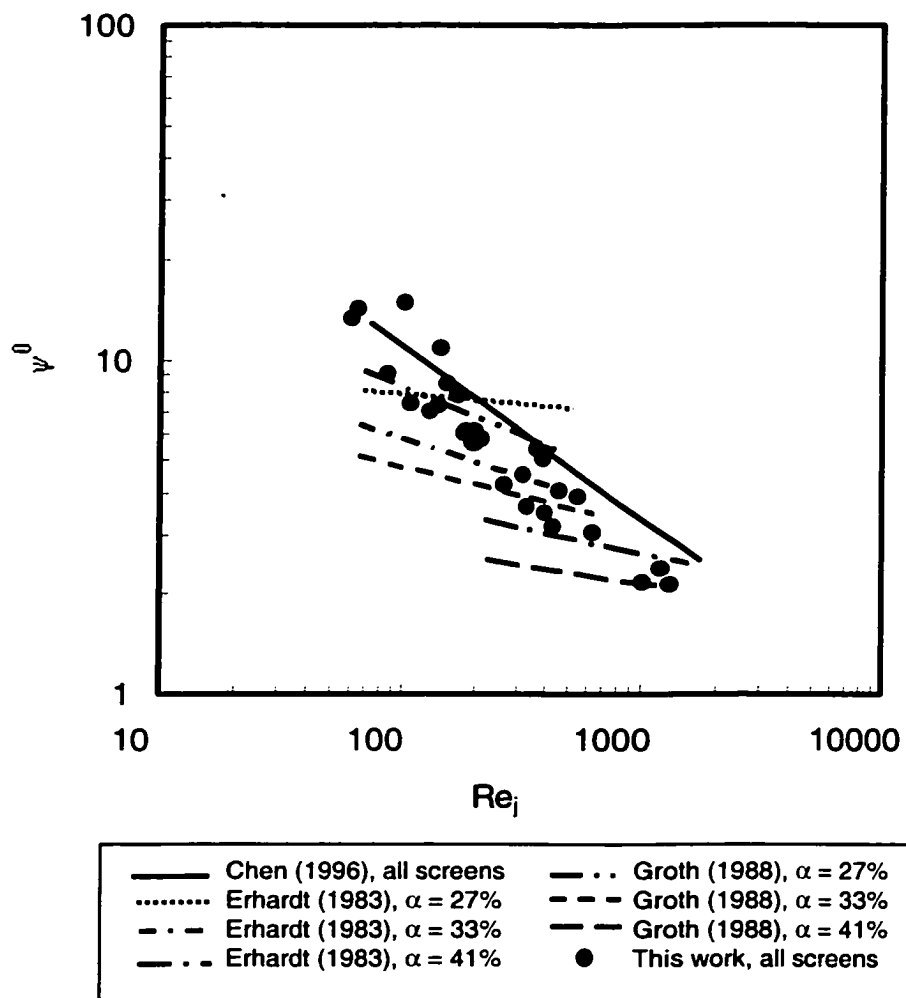


Figure 4.3. Effect of the jet Reynolds number on drag coefficient.

The Taylor length scale can be calculated by:

$$\frac{\lambda_T}{M} = C_T \sqrt{\frac{v}{Mu_{rms}}} \quad (4-2)$$

The parameter C_T varies between 1.95 and 2.20 and was considered as constant has a value of 2.

Figure 4.4 shows the variation of the Taylor length scale with the distance downstream of the screen-type static mixing elements investigated. It clearly shows that in the first 2 mm, there is slight difference among the Taylor length scales generated by the screens. As the downstream distance increases, the screens of 33% open area ($M = 0.21$ mm) generate smaller length scales whereas the 41% and 27% screens ($M = 0.54$ and 0.55 mm respectively) produce almost the same size of length scales. As predicted by Equation (4-2), the Taylor length scale is strongly influenced by the mesh size. On the contrary, Chen (1996) found that the larger Taylor length scales are associated with higher open area screens. This disagreement may be attributed to the difference in screen structures and constants used to calculate the stream root mean square fluctuating velocity in the present study.

Turbulence Intensity and Energy Dissipation Rates Behind Screens

In addition to the superficial velocity of the fluid, the geometry of the screens used (e.g., wire size, mesh size and screen open area or open area) plays an important role in determining the turbulence structure generated behind screens. The scale of the energy containing eddies generated by grids is influenced by the size of the wires used. For example, Davies (1972) argued that the size of eddies shed behind grid wires is dependent on the wire size. Smaller ratios of b/M were found to produce smaller eddy sizes, which decay more rapidly than the larger eddies. The wire size was also found to determine the merging length of the adjacent jets.

The range of screens fractional open area used in this investigation ($\alpha = 0.27$ -0.41) is much smaller than those reported in the literature dealing with turbulence structure behind screens (see Table 3.1). Furthermore, the jet Reynolds numbers

encountered in this investigation (Re_j varied from 62-1063) are much smaller than those reported by most investigators of turbulence behind screens except for Groth and Johansson (1988) who investigated a similar range of jet Reynolds numbers. Therefore, in the absence of further information, Equation (2-16) was used to estimate turbulence intensity dissipation rates behind screens and its variation with axial distance from the screen. The values of constants reported by Groth and Johansson (1988) (i.e., $X_0/M = 0.8$, $n = 1.32$, $C = 25.2$) were used for estimating the turbulence intensity and energy dissipation rates in this study.

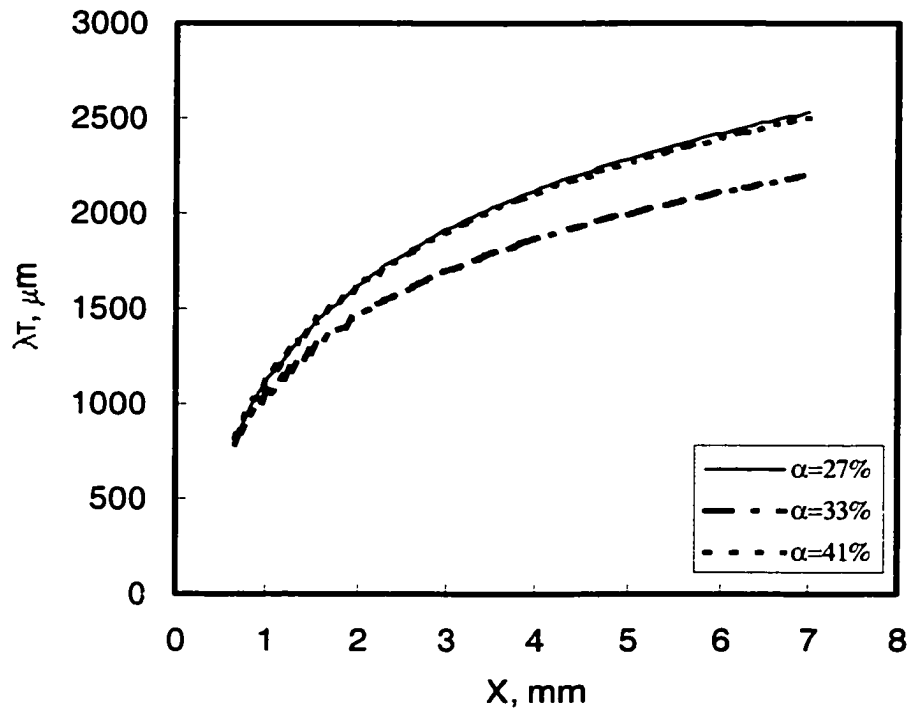


Figure 4.4. Calculated Taylor length scale in grid-generated turbulence ($U = 1.94$ m/s).

The effect of screen characteristics on the predicted spatial variation of turbulence intensity for the case of $U = 1.94$ m/s is shown in Figure 4.5. It clearly shows that the highest turbulence intensities occur immediately behind the screen and fall sharply with increasing downstream distance from the screen; they continue to decrease but at a much lower rate as the downstream distance increases further. This decay is less pronounced in the case of the 33% open area screen, which has the lowest mesh size. As can be seen from Equation (2-16) the turbulence characteristics are strongly influenced by the screen mesh size. The larger the mesh size, the higher the peak value of turbulence intensity and the faster the decay takes place. Chen (1996) found that the rate of decay of turbulence intensity is strongly affected by screen open area and increases with decreasing screen open area. Also, higher peak values of turbulence intensity are achieved with smaller fraction open areas.

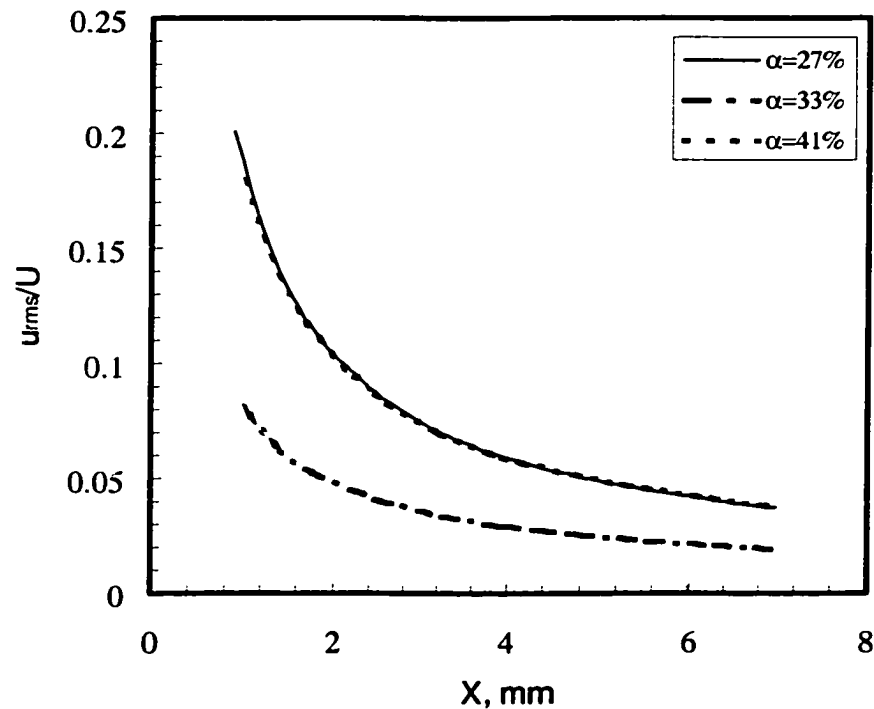


Figure 4.5. Calculated turbulence intensity decay behind screens ($U = 1.94$ m/s).

The spatial variation in the turbulent energy dissipation rate behind the screens was calculated using Equations (4-2) and (2-21) and the results obtained are plotted as a function of the downstream distance of screens (Figures 4.6 to 4.9). Figure 4.6 shows that the energy dissipation rate behind screens undergoes a dramatic change and continues to decrease as the downstream distance increases but at a much lower rate. Up to an 8-fold reduction (in case of 27% open area screen) within a very short distance (e.g. as small as 2 mm) was observed. Meanwhile up to a 150-fold reduction in energy dissipation rate was obtained at 5 mm downstream of screen compared to 50-fold variation reported by Chen (1996) for the same screen.

Figures 4.7 to 4.9 show the effect of superficial velocity on the spatial variation of the energy dissipation rate as a function of downstream distance of screens. As can be clearly seen from those figures the peak energy dissipation value, as well as the decay rate, was found to increase dramatically as the superficial velocity increases. The ratio of the maximum to minimum energy dissipation rates obtained is 155 to 1, 255 to 10 and 1320 to 15 for screens of fractional open area of 27%, 33% and 41% respectively at maximum superficial velocity.

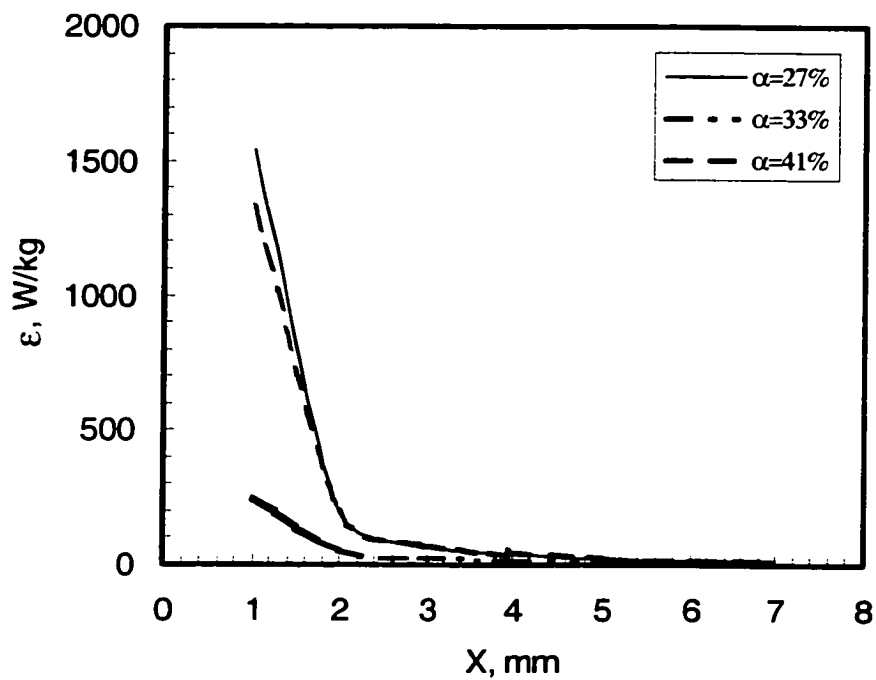


Figure 4.6. Effect of screen open area on calculated energy dissipation rate ($U = 1.94$ m/s).

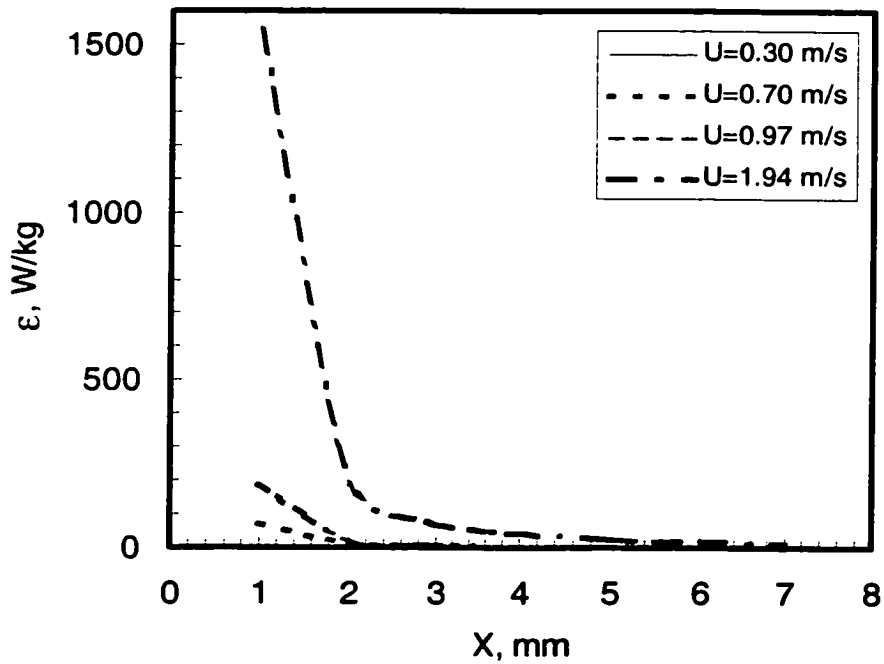


Figure 4.7. Variation of calculated energy dissipation rate behind screens ($\alpha = 27\%$).

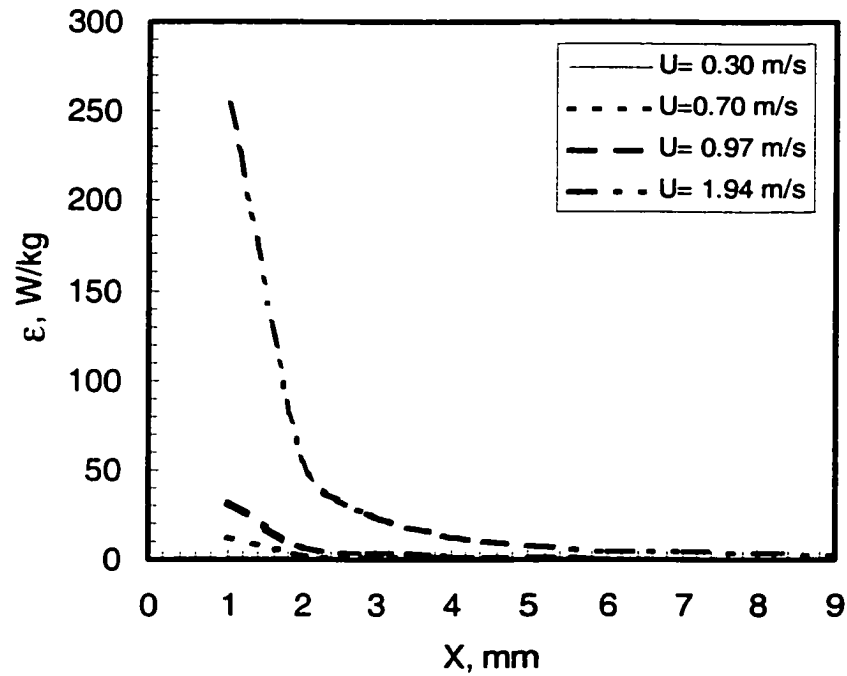


Figure 4.8. Variation of calculated energy dissipation rate behind screens ($\alpha = 33\%$).

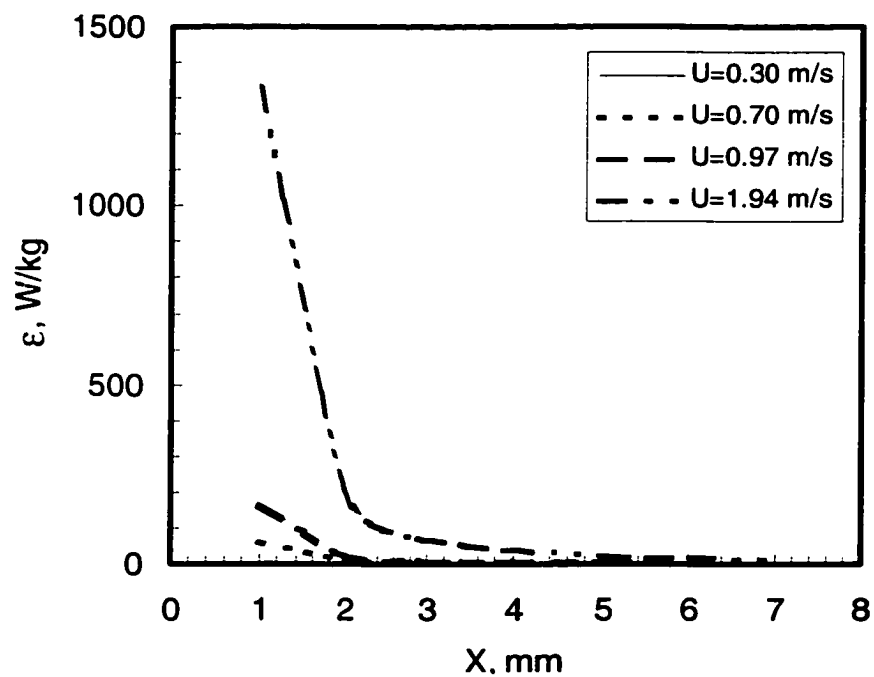


Figure 4.9. Variation of calculated energy dissipation rate behind screens ($\alpha = 41\%$).

4.1.2 Two-Phase Flow through Screens

Several investigators (Brown and Pitt, 1972; Al Taweel and Landau, 1977; Tavlarides and Stamatoudis, 1981; Calabrese et al., 1986; Gore and Crow, 1989; Yarin and Hetsroni, 1994; Elghobashi, 1994; Kenning and Crow, 1997; Crowe, 2000; Ahmad and Elghobashi, 2000) suggested that the presence of immiscible dispersed phase entities in a turbulently flowing liquid phase alters their turbulence structure and, consequently, the local turbulent energy dissipation rate. For example, the injection of small concentrations of fine droplets into a free turbulent gas jet was found to attenuate turbulence intensity selectively in the high frequency range, reduce turbulent energy dissipation rate, and jet spread rate. However, the general impact of the presence of dispersed phase entities on the turbulent structure of the continuous phase is rather complex with the possibility of either reducing or enhancing the turbulence intensity being a function of the size and concentration of the dispersed phase entities and the relative density between the phases (Ahmad and Elghobashi, 2000). The effect of introducing the dispersed phase (i.e. Bayol oil) on the drag coefficient of screens flow will, therefore, only be briefly discussed here.

Contrary to the observations obtained by Walker (1984), in which the drag across the in-Line Lightnin mixing elements was found to decrease in the presence of the dispersed phase. The presence of dispersed phase did not result in any systematic discernable variation in the pressure drop as shown in Figures 4.10 and 4.11. This difference suggests that the presence of the dispersed phase has an insignificant effect on the turbulence structure of the continuous phase, or it could be the result of the interaction between several variables the net effect of which cancel each other. A better understanding of the effect that the dispersed phase has on two-phase flow across screens may be obtained by investigating the effect of dispersed phase holdup on the drag coefficient. This comparison is shown in Figures 4.12 to 4.14.

Generally speaking, the drag coefficients obtained in presence of very small quantities of the dispersed phase are not significantly different from those of single-phase flow. This is in line with the conclusions reported by Al Taweel and Landau (1977) that the effect of dispersed phase in liquid flows is relatively small unless the diameter to

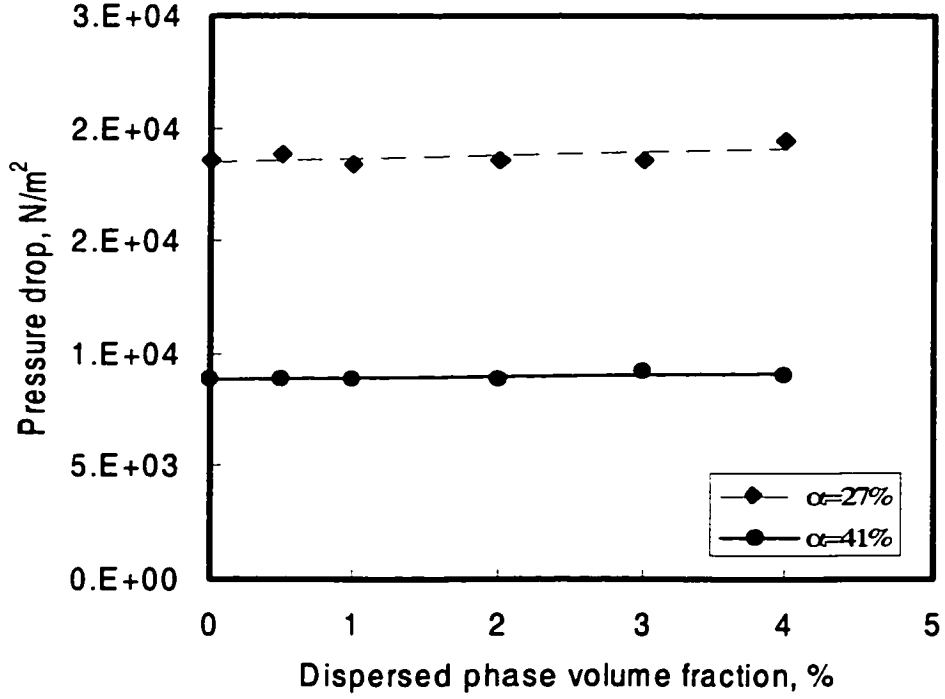


Figure 4.11. Effect of dispersed phase holdup on pressure drop in the mixer ($U = 0.70$ m/s).

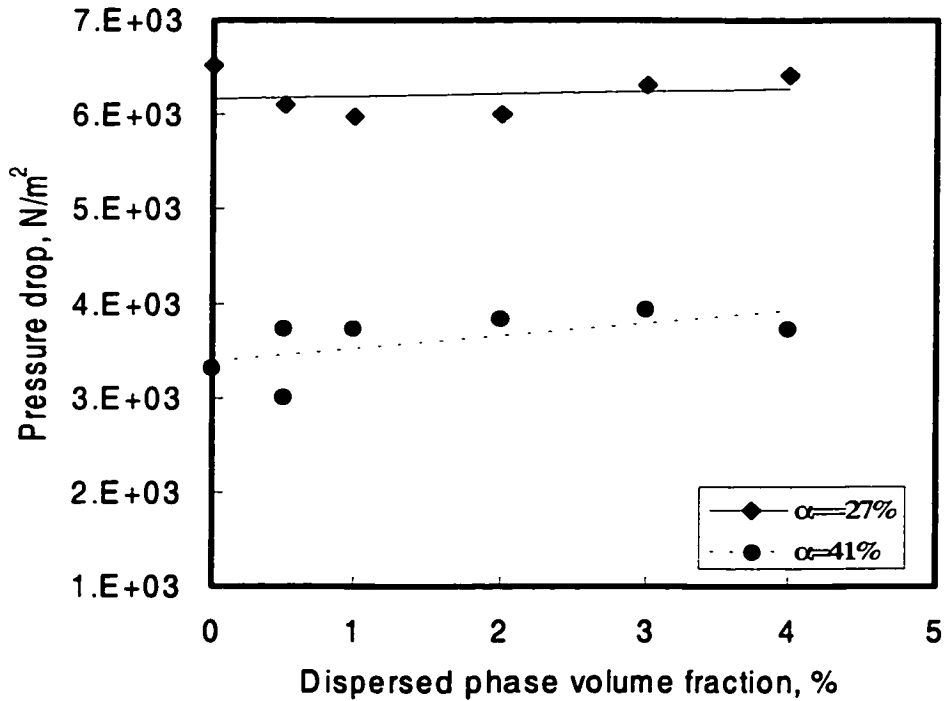


Figure 4.10. Effect of dispersed phase holdup on pressure drop in the mixer ($U = 0.40$ m/s).

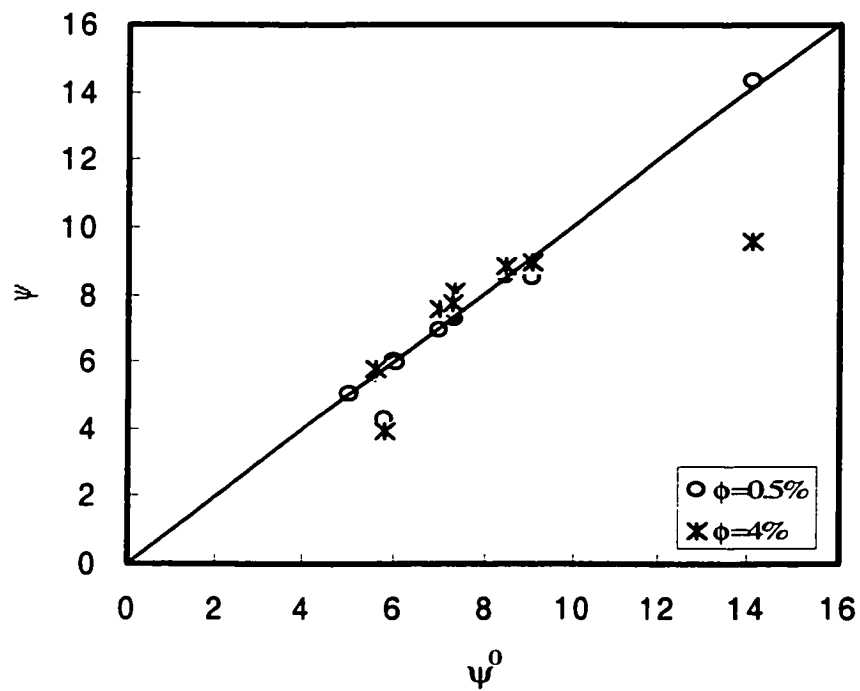


Figure 4.12. Change in drag coefficient in presence of the dispersed phase ($\alpha = 0.27$).

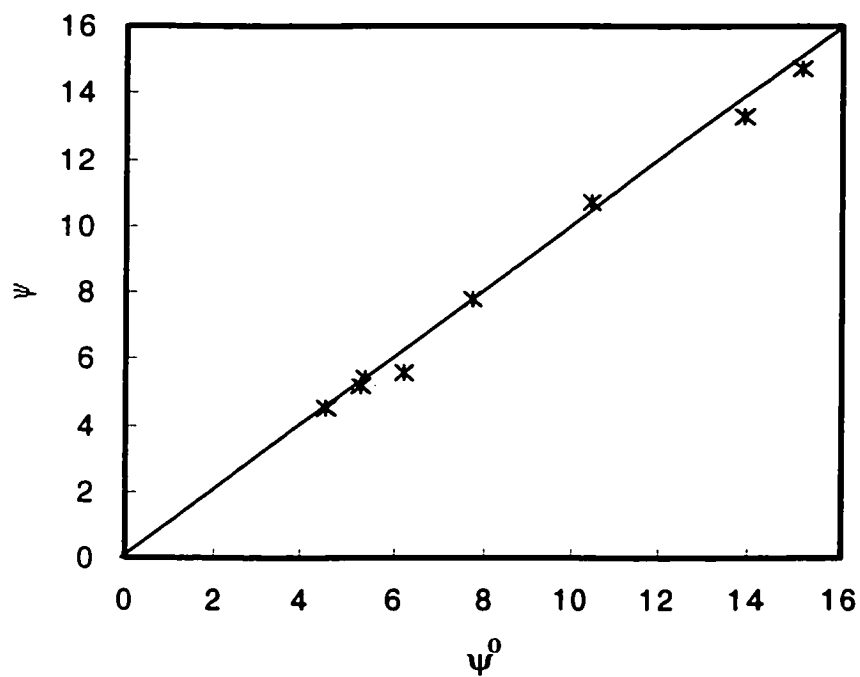


Figure 4.13. Change in drag coefficient in presence of the dispersed phase ($\alpha = 0.33$, $\phi = 0.5\%$).

aspect ratio are large enough (e.g. Fibers and long crystals) to significantly modulate the turbulence. The relatively higher drag coefficients obtained at higher dispersed phase holdups and low superficial velocities can thus not have been caused by the extraction of the energy consumed in drop breakup from the continuous phase turbulent energy, which causes minor reduction in the energy containing region of the turbulent spectrum but a significant reduction in the high frequency region responsible for turbulent energy dissipation within the continuous phase (eddy-eddy interaction). Such mechanisms are mostly associated with the fluctuating and steady slip velocities between the phases and the resulting interference with Kolmogorov's concept of spectral energy transfer (Yuan and Michaelides, 1992). Similarly Lance and Bataille (1991) observed that grid-generated turbulence isotropy is not altered by the injection of air bubbles. It can thus be concluded that the occasional deviation in the drag coefficients, which is more frequent in the case of the 41% open area screen, does not result from changes in turbulent flow regimes.

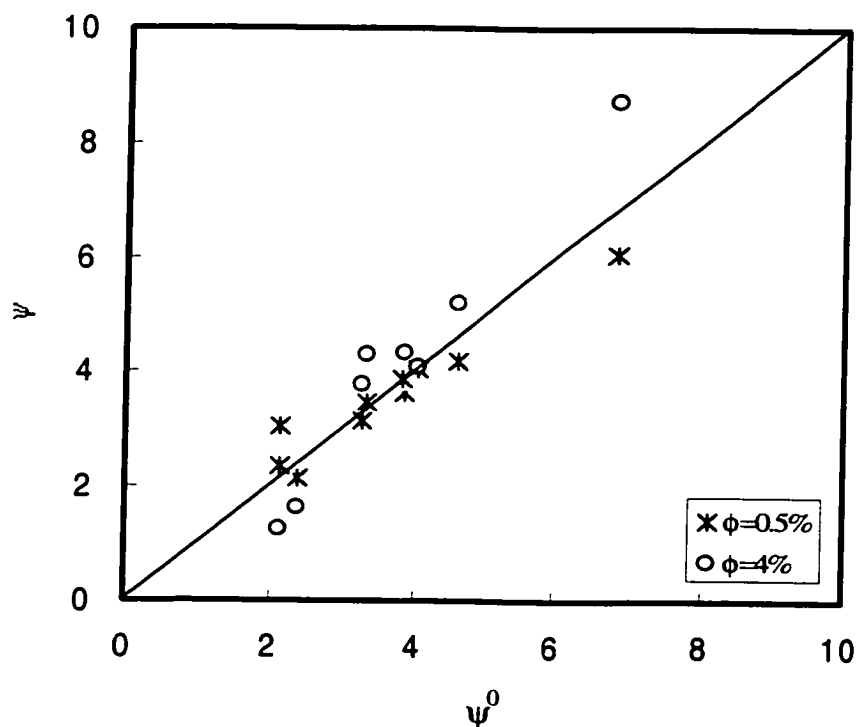


Figure 4.14. Change in drag coefficient in presence of the dispersed phase ($\alpha = 0.41$).

Figure 4.14 shows that in the case of 41% open area screen the drag coefficients are significantly elevated at high dispersed phase holdup. This agrees with Chen's (1996) findings. Walker (1984) observed a similar phenomenon in the case of screens, which he attributed to the possible attachment of drops to screens at lower superficial velocities. Ehrhardt (1983) who found that bubbles adhering to screen wires could increase the drag coefficient up to 40% particularly at low superficial velocities reported similar observation.

The concept of turbulence modulation has been extensively used to explain the tendency of the average drop size to increase with increasing dispersed phase holdup. Doulah (1975) developed a theory for the increase of drop size, in the absence of coalescence, due to change in turbulence intensity in the continuous phase. He also related the turbulence intensity in the dispersion to the change in the dispersion viscosity using Einstein's equation. Following the approach adopted by Laats and Frishman (1974) for the case of gas jet flow, Tavlarides and Stamatoudis (1981) empirically correlated the turbulence modulating effect encountered in this case by the following expression:

$$\frac{u_{rms}}{u_{rms0}} = \frac{1+0.2\phi}{1+\phi} \quad (4-3)$$

This expression predicts a reduction in turbulent energy dissipation rate due to eddy-eddy interaction in the gaseous phase, an observation that is in line with the analyses of Al Taweel and Landau (1977) as well as that of Ahmad and Elghobashi (2000). However, as mentioned before, no direct observation of turbulence modulation has been reported in the case of liquid dispersions unless the ratio of the particle diameter to the turbulence length scale $[d/l_e]$ is smaller than 0.001 (Gore and Crowe, 1989; Crowe, 2000). In the present investigations the value of the d/l_e was usually higher than 0.1, the critical point beyond which turbulence enhancement was observed in solid laden flows.

Calabrese et al. (1986) used an approach similar to that of Doulah (1975) to explain the effect of increasing dispersed phase holdup on the average drop size in mechanically agitated tanks. They also re-interpreted the data obtained by Brown and Pitt

(1970) and found that their data, as well as those of Brown and Pitt (1970), can be correlated by:

$$d_{32} \propto (1 + 3\phi) \quad (4-4)$$

The above mentioned observations are usually obtained under steady-state conditions, in which an equilibrium between drop breakage and coalescence exists. The use of the turbulence modulating approach to explain the variations in drop size overlooks the fact that:

- No direct experimental verification of the phenomenon has been reported in the case of liquid flows, except in the case of suspensions of fibers and elongated crystalline matter where the associated phenomenon of drag reduction has been reported (Nsom, 1994).
- Furthermore, as will be shown in section 4.6, the amount of energy extracted to form finer dispersions is a very small fraction of the total energy dissipated due to flow through the screens. Substantial lowering of the former is therefore expected to result in insignificant reduction of the total energy dissipated.

All these factors suggest that the reported increase in drop size at high dispersed phase holdups can not be attributed to presumed reduction in turbulent energy dissipation. It could, however, be caused by the change in turbulence scales resulting from increasing dispersion viscosity (Doulah, 1975), or due to the enhanced coalescence probability.

The results obtained in this investigation can thus not be used to explain the behavior of two-phase flow through screens. Turbulence modulation is expected to result in a small reduction in the pressure drop due to the dampening of eddy-eddy interaction in the continuous phase. On the other hand, the blockage of a small fraction of the area available for flow due to the temporary blockage of drops to the screens is expected to significantly enhance the pressure drop due to the increase of kinetic energy in the micro jets.

4.2 FACTORS AFFECTING MEAN DROP SIZE

When two immiscible liquids are mixed, a dispersion is formed in which drop breakup and coalescence simultaneously take place. The drop size distribution thus rapidly changes from its initial value until, eventually, a local dynamic equilibrium is established for which the mean drop size depends on the physical properties of the dispersed liquids and the hydrodynamic conditions encountered in the mixer. The hydrodynamic conditions include the intensity and scale of turbulence and energy dissipation rate, which depends on the flow velocity. Furthermore, turbulence intermittence, which leads to fluctuations in energy dissipation rate around a mean value, is considered to be a very important factor affecting the value of the mean drop size (Baladyga and Bourne, 1993; Baladyga and Podgorska, 1998).

The present work focuses upon the effect of energy dissipation rate, residence time, mixing element geometry, dispersed phase holdup, and the interfacial characteristics of the system on the mean drop size generated by screen-element static mixers.

4.2.1 Effect of Superficial Velocity and Energy Dissipation Rate

Effect of Superficial Velocity

As stated earlier in the literature review, the superficial velocity is one of the major factors, which governs liquid-liquid dispersion processes. The superficial velocity or the velocity of the bulk phase in flowing systems was found explicitly to affect the maximum stable drop size and the drop mean diameters (Sleicher, 1962; Kubie and Gardener, 1977; Karabelas, 1978; Al Taweel and Chen, 1996). In the case of static mixers, the superficial velocity affects both the local rate of energy dissipation, ϵ , as well the residence time of the fluid elements within the region of high local energy dissipation rate.

The effect of superficial velocity on the Sauter mean diameter, at dispersed phase holdups of 0.5% and 4%, is shown in Figures 4.15a to 4.15e. In all cases, the Sauter mean diameter was found to decrease with increasing superficial velocity; with this tendency being most pronounced at low dispersed phase holdup. This behavior can be explained by

the fact that as the superficial velocity increases the energy dissipation rate in the system increases, which in turn promotes the competing drop breakup and coalescence processes. However, it appears that the effect of energy dissipation rate on the drop breakup is much greater than that on the coalescence process, resulting in enhancing the net breakage rate with increasing energy dissipation rate (Tavlarides and Stamatoudis, 1981; Laso et al., 1987; Kanel, 1990). That, in turn, results in the formation of finer drop sizes.

The results presented in Figures 15a to 15e suggest that the Sauter mean drop diameter is an exponential function of the superficial velocity. This is tested in Figures 4.16 and 4.17. It is evident from Figure 4.16 that the data obtained using a dispersion holdup of 0.5% can best be represented by two separate regions. The first corresponds to two simultaneously drop breakup mechanisms (drop cutting by screen wires and turbulent breakup) region while the second corresponds mainly to turbulent drop breakup. The mean drop size in the two drop breakup mechanisms region (superficial velocities below 0.7 m/s) was found to depict a lower sensitivity to the superficial velocity than that in the turbulent breakup zone. This indicates that the proposed drop cutting action becomes insignificant at higher superficial velocities. The results also suggest that the turbulent drop mechanism produces relatively smaller drop sizes.

Attempts were made to correlate the data depicted in Figures 4.16. First, the data for the 41% open area screen were fitted as two separate straight lines, where deviation from linearity occurs, then all points were fitted as one straight line. The sums of squares of errors obtained (0.2015 and 0.0256 for all points and as two regions respectively) were compared with each other and there was a significant difference between the two approaches, at a significance level of 95% using the F-test. The data generated using low holdup (0.5%) dispersions will therefore be dealt with as two set of data, the first corresponding to the two drop breakup mechanism zone while the second corresponds to the turbulent breakup region, which dominates at superficial velocities greater than 0.70 m/s.

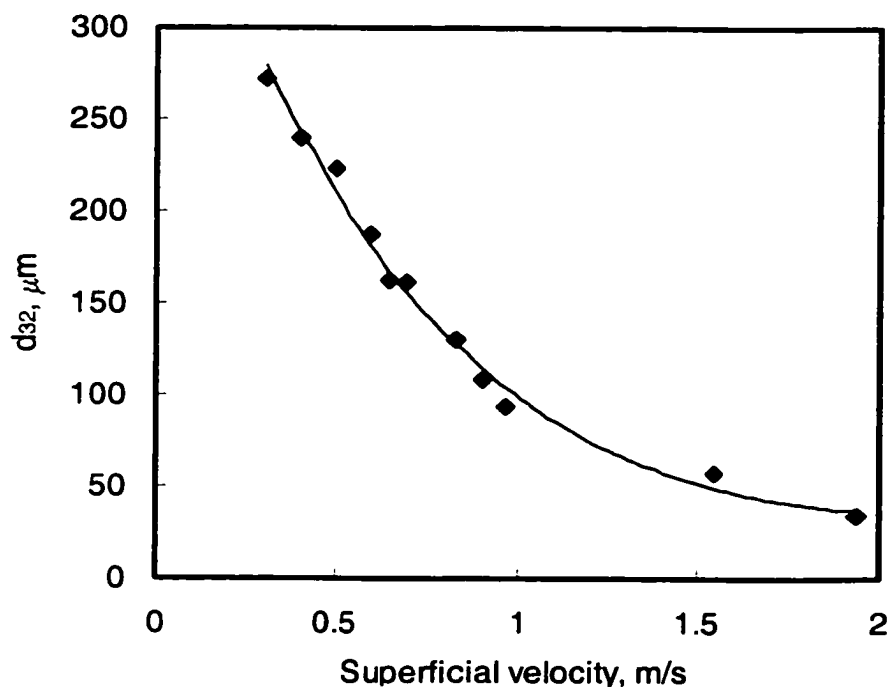


Figure 4.15a. Effect of the superficial velocity on Sauter mean diameter ($\alpha = 27\%$, $\phi = 0.5\%$, 9 screens, $L = 10$ mm).

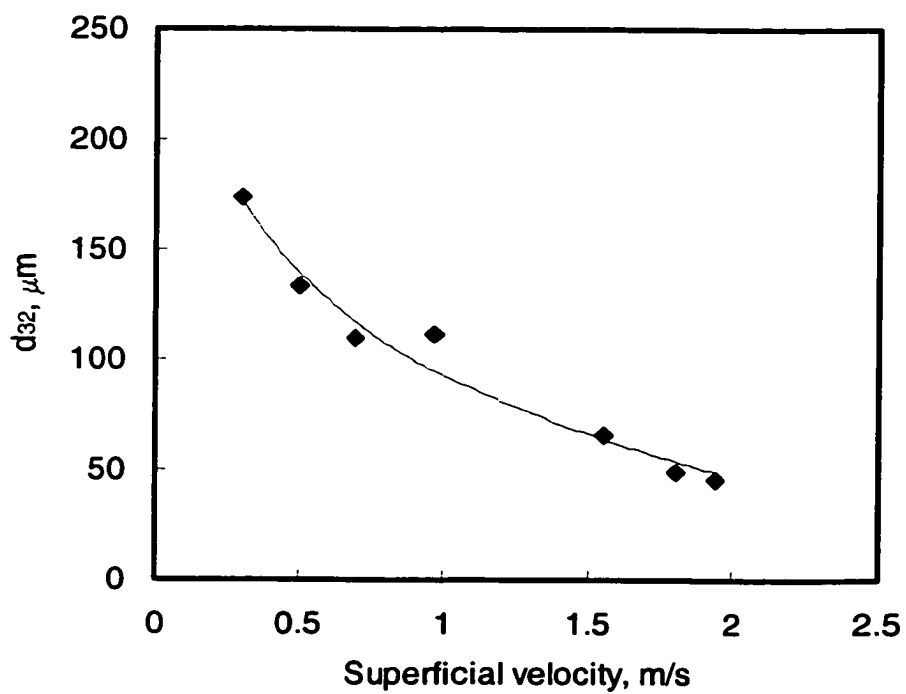


Figure 4.15b. Effect of the superficial velocity on Sauter mean diameter ($\alpha = 33\%$, $\phi = 0.5\%$, 9 screens, $L = 10$ mm).

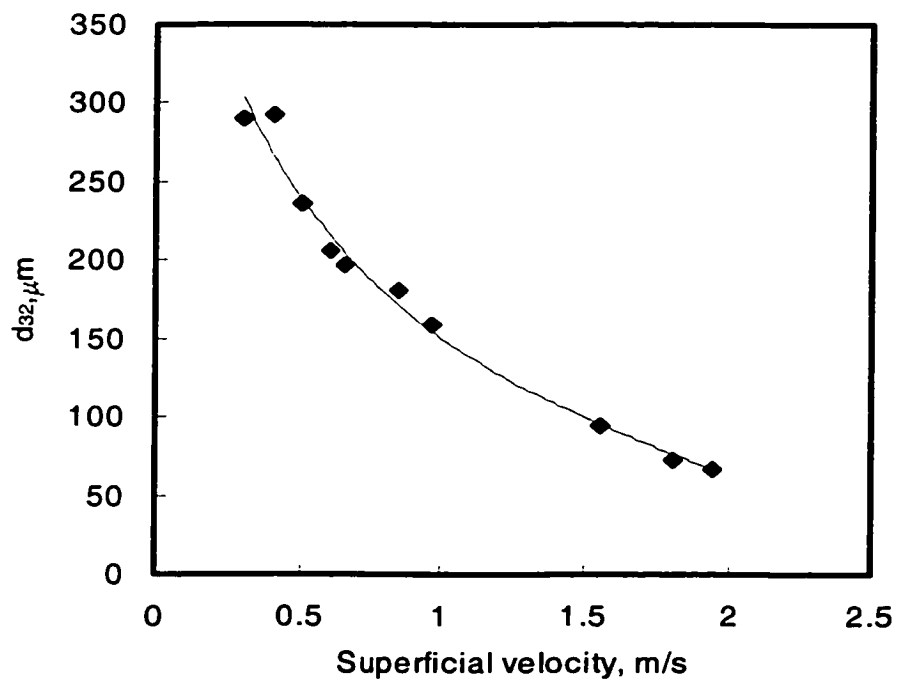


Figure 4.15c. Effect of the superficial velocity on Sauter mean diameter ($\alpha = 41\%$, $\phi = 0.5\%$, 9 screens, $L = 10$ mm).

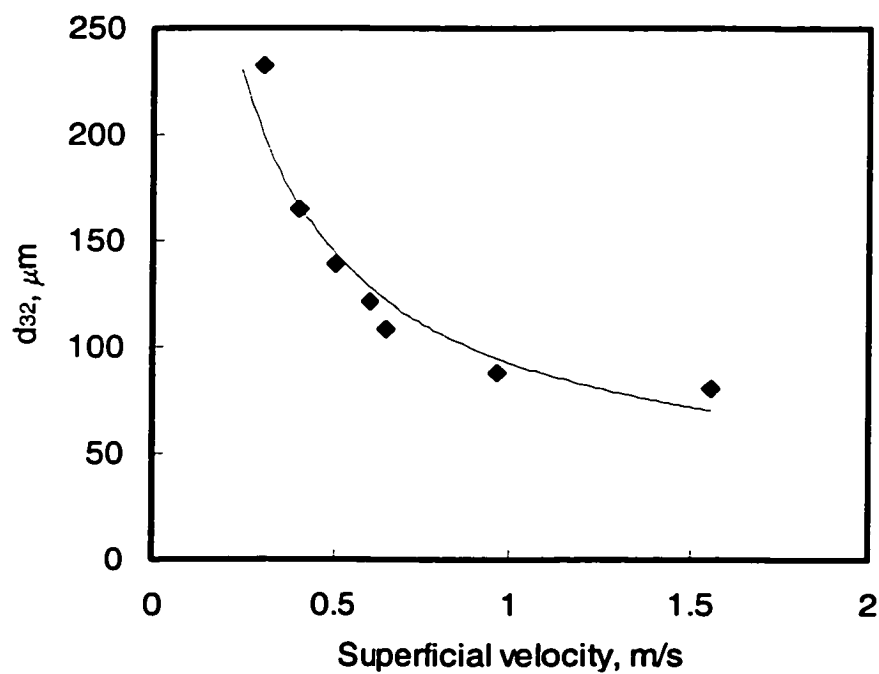


Figure 4.15d. Effect of the superficial velocity on Sauter mean diameter ($\alpha = 27\%$, $\phi = 4\%$, 9 screens, $L = 10$ mm).

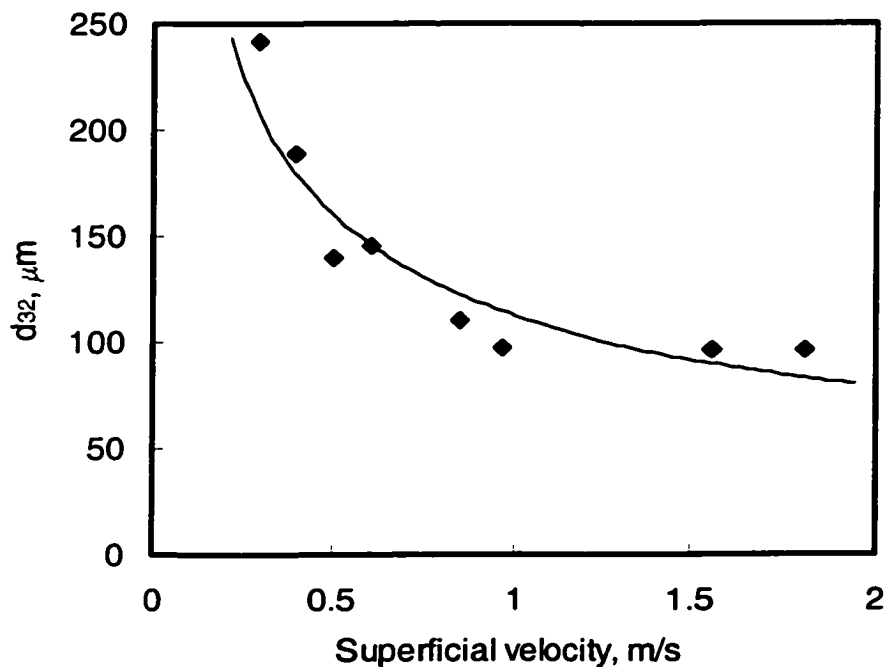


Figure 4.15e. Effect of the superficial velocity on Sauter mean diameter ($\alpha = 41\%$, $\phi = 4\%$, 9 screens, $L = 10$ mm).

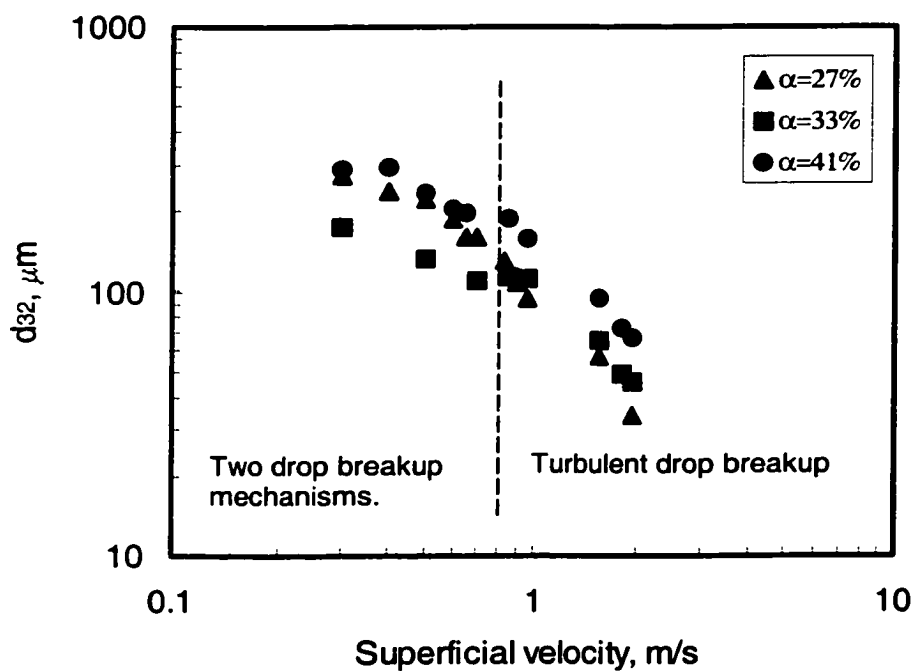


Figure 4.16. Variation of the Sauter mean diameter with the superficial velocity ($\phi = 0.5\%$, 9 screens, $L = 10$ mm).

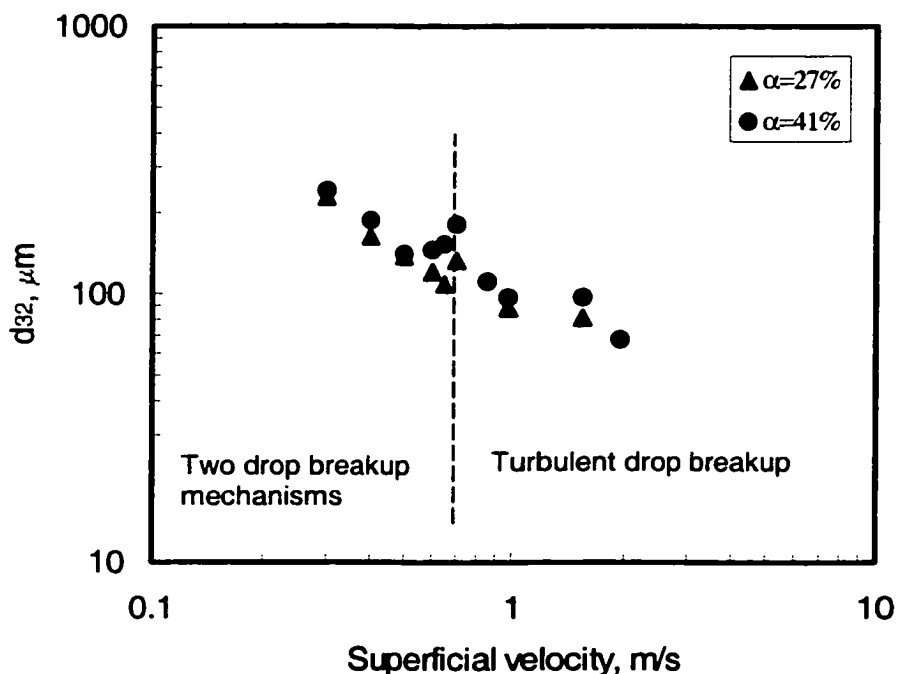


Figure 4.17. Variation of the Sauter mean diameter with the superficial velocity ($\phi = 4\%$, 9 screens, $L = 10$ mm).

As shown in section 3.3, the values of the pipe Reynolds number range from 7,000 to 50,000 as the superficial velocity is increased from 0.3 to 1.94 m/s. This suggests that most experiments were conducted under fully turbulent pipe flow regime with the exception of those done at very low velocities, which are in the transition pipe flow range. On the other hand, the individual jet Reynolds numbers were found to vary between 61 and 1290 depending on the superficial velocity and screen characteristics. These figures are well in excess of the critical values needed for the development of turbulent jet flows (McKenzie and Wall, 1968; Marsters, 1969; Cheremisinoff, 1986). The observation of two regions in the relationship between d_{32} and the superficial velocity can thus be attributed only to the presence of two simultaneous drop breakup mechanisms.

At high superficial velocities (≥ 0.70 m/s) which corresponds to the region of turbulent breakup mechanism, the Sauter mean drop diameter obtained at low dispersed phase holdup ($\phi = 0.5\%$) was found to vary with the superficial velocity as follows:

$$d_{32} = cU^b \quad (4-5)$$

where b was found to vary from -1.15 to -1.40 depending on the screen open area (Table 4.1) The non-systematic variation in the value of b may be attributed to the screen structures, which in turn results in different turbulence intensities and energy dissipation rates as discussed in section 4.1.1. The values of the exponent b obtained in the present investigation are very close to that predicted by the Kolomogrov-Hinze model ($b = -1.20$). This result is also close to the exponent values obtained by Karabelas (1978) for liquid-liquid dispersions in turbulent pipe flows and Hass (1987), who studied liquid-liquid dispersions in a Kenics mixer. The above results are also in agreement with those reported by Kurban et al. (1995) and Simmons and Azzopardi (2001) for pipe flows.

Table 4.1. Effect of screen open area on the value of b ($\phi = 0.5\%$).

Screen open area (%)	c	b	R
27	1.8	-1.40	0.993
33	2.0	-1.15	0.989
41	2.2	-1.23	0.998

Walker (1984) produced a result for 1% kerosene-water system using in-line Lightnin static mixer giving a value of the exponent b (-1.95) significantly different from that obtained in this study. This difference may have been mainly caused by the relatively non-uniform and non-isotropic flow generated by in-line Lightnin static mixing elements compared to uniform and isotropic flow conditions in case of screen-type mixing elements. He also found that the average drop size generated by woven screens varies, nearly in proportion with the square of the fluid velocity in the turbulent jets formed by the screens. Later, Chen (1996) proposed a correlation for the average drop size generated by woven screens that showed a stronger dependence on the superficial velocity than that obtained in the present investigation. The exponent b ranges from 1.77 to 2.10 depending on the hydrodynamic conditions and the physical properties of the system examined. Both higher values reported by Walker (1984) and Chen (1996) for the screen-type mixing elements can be attributed to the use of a light attenuation method for

the measurement of the interfacial area generated, from which the Sauter mean diameter is determined. Light attenuation methods are highly sensitive to the ultrafine drops, whereas the photographic method used in the present investigation can be biased to the larger drops.

The data obtained at a dispersed phase holdup of 4% (Figure 4.17) do not show a pronounced break at $U = 0.7$ m/s as is the case for 0.5% holdup. The effect of screen open area, α , is less pronounced and the dependence of the average drop diameter on the superficial velocity is lower. The data shown in Figure 4.17 were fitted to straight line in a similar fashion to that used in Figure 4.16. It was found that there is a significant difference between the two approaches (sum of square errors of 0.767 and 0.178 were obtained for all the data points and as two regions respectively). Therefore, the value of the exponent b corresponding to the turbulent breakup region, for the 27% and 41% open area screens is -0.59 ($R = 0.892$) and -0.74 ($R = 0.871$) respectively. Mathematically:

$$d_{32} = 2.00U^{-0.59} \quad (4-6)$$

$$d_{32} = 2.06U^{-0.74} \quad (4-7)$$

for 27 and 41% open area screens respectively.

The fact that these values are smaller than those predicted from the Kolmogorov-Hinze model (-1.20), and the results obtained at lower concentrations, may be attributed to the turbulence modulation effect (Al Taweel and Landau, 1977; Elghobashi and Abou-Arab, 1983, Ahmed and Elghobashi, 2000) that increases with increasing dispersed phase holdup, or alternatively to the presence of two drop dispersion mechanisms (namely turbulent breakup and drop cutting by screen wires) that are differently influenced by the dispersed phase holdup. As will be shown in section 4.2.3, drop dispersion by the cutting mechanism plays an increasingly important role at higher dispersed phase holdups whereas, as shown in section 4.1.2, turbulence modulation is predicted to play a relatively a minor role in the case of liquid-liquid dispersions. The results obtained can not be compared with those of other investigators, who studied dispersion in static mixers, since most of the investigations were conducted using low holdup dispersions (i.e., $\leq 1\%$).

The presence of more than a one-drop dispersion mechanism has been used by Sembira et al. (1986) to explain their results. They observed that the values of the Sauter mean diameter generated by a Sulzer mixer using SS316 and Teflon-coated internals are nearly similar at high velocities, while at low velocities the Teflon-coated elements give larger mean drop diameters. Consequently, they suggested the coexistence of two drop-breakup mechanisms, the first depends on the turbulent shearing forces and predominates at high velocities while the other mechanism predominates at low velocities and is associated with the shear at the surface of the mixing element. This suggestion agrees well with the CFD analysis recently undertaken by Streiff et al. (1997) who studied the flow conditions in Sulzer mixers in which the intersecting flow channels are formed by corrugated plates, crossing bars, or crossing tubes. They found that the distribution of local energy dissipation between two layers in a Sulzer SMV corrugated plate mixer, at turbulent flow conditions with relatively low Reynolds numbers, is concentrated in a relatively thin layer at the crossing points of the sheets with very low dissipation rates near the solid liquid boundary.

Effect of energy dissipation rate

The local turbulent energy dissipation rate is the most important factor in both dispersion and coalescence processes. Although the screen element static mixers generate very high average energy dissipation rates (Section 4.1.1), about 95% of that energy is dissipated in a very small volume immediately after the screen, thus creating a region of very high local turbulent energy dissipation rates. For example, up to a 8-fold variation in local energy dissipation rates was observed within a very short distance (i.e. 2 mm) downstream of the screen. Drop breakup is therefore expected to dominate in the high-energy dissipation region close to the screen while coalescence becomes significant further downstream where low turbulent energy dissipation rates prevail. For simplicity, the local energy dissipation is often assumed uniform throughout the mixer and assumed equal to the volumetric average rate, which can be computed from the macroscopic flow variables.

The variation of the Sauter mean drop diameter with the average energy dissipation rate is illustrated in Figures 4.18a to 4.18c for the screens tested. As can be seen from Figure 4.18a, the average drop size varies exponentially with the energy dissipation rate. Generally speaking, smaller average drop diameters were obtained at larger average energy dissipation rates. These results suggest that although higher energy dissipation rate results in increasing both drop breakup and coalescence rates, the effect on the former is larger to the extent that a net breakage rate is achieved with increasing energy dissipation rate. Tavlarides and Stamatoudis (1981) and Kanel (1990) also found similar trends. As can be clearly seen from Figure 4.18b, all the mean drop size data, corresponding to 0.5% holdup and turbulent breakup, can be represented by a straight line with a slope of -0.42 ($R = 0.964$):

$$d_{32} = 2.98\epsilon^{-0.42} \quad (4-8)$$

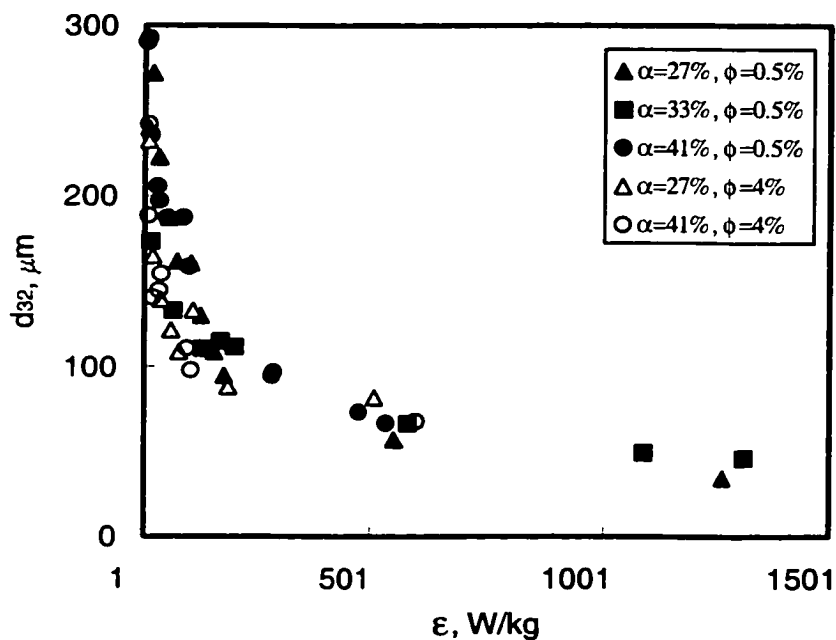


Figure 4.18a. Effect of mean energy dissipation rate on the Sauter mean diameter (9 screens, $L = 10$ mm).

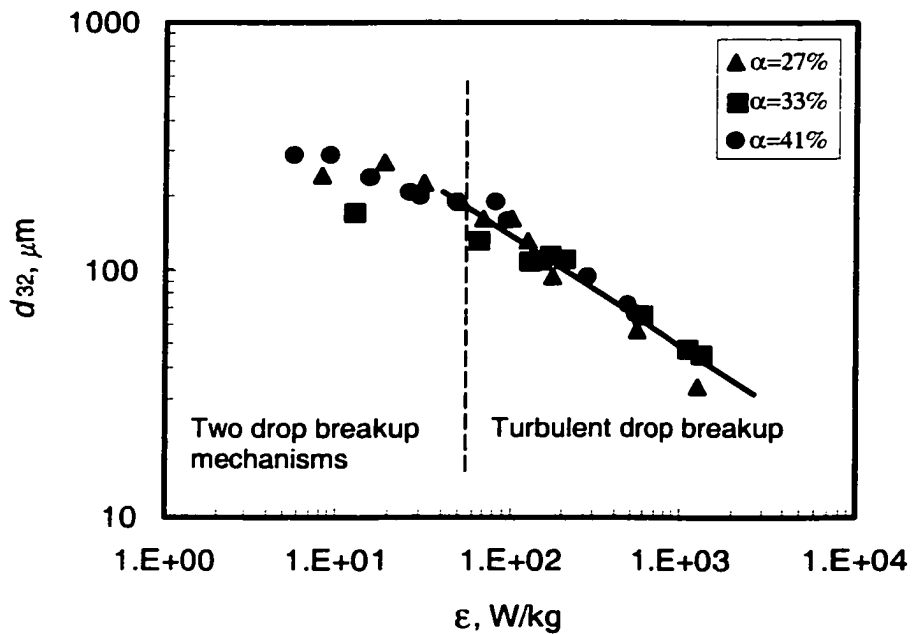


Figure 4.18b. Effect of mean energy dissipation rate on the Sauter mean diameter ($\phi = 0.5\%$, 9 screens, $L = 10 \text{ mm}$).

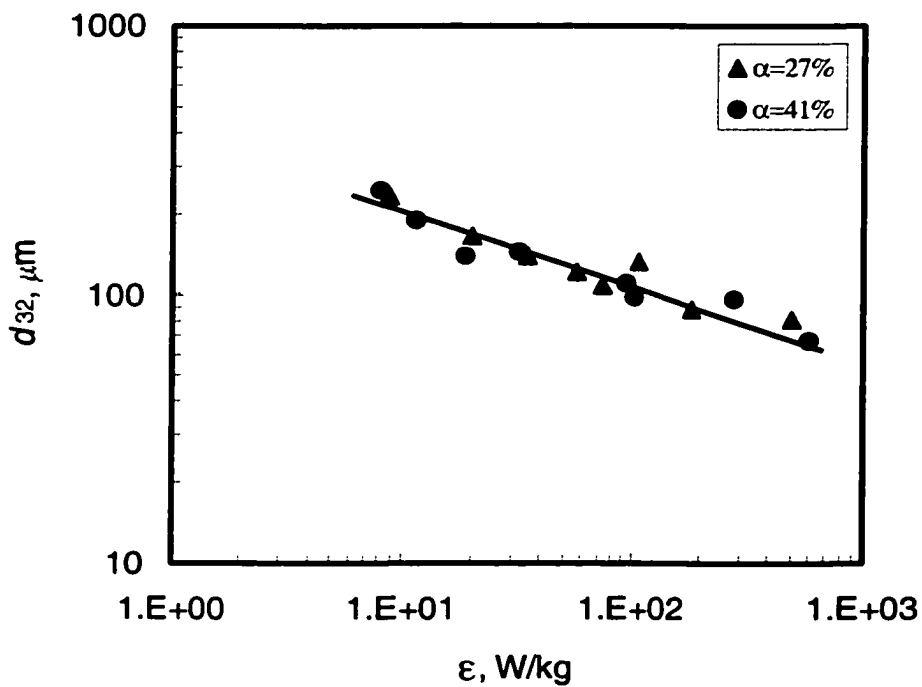


Figure 4.18c. Effect of mean energy dissipation rate on the Sauter mean diameter ($\phi = 4\%$, 9 screens, $L = 10 \text{ mm}$).

This compares very well with the exponent value of -0.40 predicted by the Kolmogorov-Hinze model. However, the data tend to segregate, depending on geometry of the screen used, at average energy dissipation rates lower than 70 W/kg . This change in behavior does not appear in the case of $\phi = 4\%$ (Figure 4.18c) where all the data can be represented by a single line ($R = 0.954$), given by:

$$d_{32} = 2.55\epsilon^{-0.26} \quad (4-9)$$

The deviation of this value from the theoretical prediction may be attributed to the existence of two drop breakup mechanisms, namely, cutting by screen wires and turbulent breakup. Turbulence modulation may play a minor role in this difference. This discrepancy can not be attributed to departure of turbulence structure from isotropic conditions since the hydrodynamic conditions downstream from screens can be considered as being the closest experimental equivalent to an isotropic turbulence. Furthermore, the Kolmogorov scale of turbulence is significantly smaller than the drop sizes obtained in this study for all the superficial velocities investigated. The ratio of d_{32}/l_k for the 27, 33 and 41% open area screens ranges from 6.8 to 12.6, 9.2 to 10.2 and 9.4 to 14.5 respectively. This implies that the scale of drop sizes measured in this investigation would fall in the inertial subrange of turbulence where the Kolmogorov-Hinze model is assumed to be valid. It is therefore expected that the existence of the two aforementioned mechanisms of drop breakup (drop cutting by the wires of the screens and turbulent drop dispersion) may have played a crucial role in this difference. It appears that drop disintegration by the cutting mechanism plays a more important role at higher dispersed phase holdups, particularly at low average energy dissipation rates, where the second mechanism is expected to play a less prominent role.

In mechanically agitated tanks the exponent relating the mean drop size to the average energy dissipation rate, n , varies from -0.25 to -0.80 (Molag et al., 1980; Nishikawa et al., 1987; Pacek et al.; 1998). The deviation from the theoretically predicted value of -0.4 is generally attributed to the complex hydrodynamics prevalent in such mixing devices and the fact that the two-phase liquid recirculating stream do not entirely flow through the high energy dissipation region.

The results obtained in this investigation also differ from those reported by other workers who studied various static mixers as shown in Table 4.2. Al Taweel and Chen (1996) attributed the difference between their experimental value n and the theoretical one to the departure of the flow in the high energy dissipation rate region (i.e., the high velocity jets formed behind the screens) from the ideal conditions assumed in the derivation of the homogeneous, isotropic drop breakup theory. The exponents shown in Equations (4-6) and (4-7) are close to those reported by Streiff et al. (1997) who investigated the dependence of the maximum drop size on the energy dissipation rate in various types of Sulzer mixers and they found that the exponent value varies from - 0.28 to -0.33.

Table 4.2. Dependence of the mean drop diameter on energy dissipation rate in static mixers

Reference	Mixer	Dispersion	Exponent
Middleman (1974)	Kenics	Different organics in water	- 0.70
Matsamura et al. (1981)	Hi-Mixer	Water-in-different organics	- 0.45 to - 0.67
Al Taweel and Walker (1983)	Lightnin	Kerosene-in-water	- 0.63
El-Hamouz et al (1994)	Lightnin	Kerosene-in-water	- 0.49 to -0.60
Al Taweel and Chen (1996)	Screens	Petroleum oils-in-water	- 0.61 to - 0.79
Streiff et al. (1997)	Sulzer	Different organics in water	- 0.28 to - 0.33

Table 4.2 shows that all n values reported by the previous investigators are much higher than those predicted by the Hinze-Kolmogoroff theory, or that experimentally found in this investigation under low dispersed-phase holdup ($\phi = 0.5\%$) and turbulent drop breakup conditions. This difference can most probably be explained by the fact that although the hydrodynamic conditions in static mixers are much more uniform than those encountered in MAT, they can still be very non-uniform at different locations in the pipes

cross section. This difficulty is not encountered in the case of screen-type elements where the flow is virtually uniform across the cross section. The difference between the present study and the results of Walker (1984) and Al Taweel and Chen (1996) is most probably due to the use of two significantly different drop size measurement techniques.

4.2.2 Effect of Screen Geometry

As mentioned earlier, three sets of screens with open areas of 0.27, 0.33 and 0.41 were used in the generation of Bayol oil-in-water dispersions. Screens with lower open area are expected produce higher velocity jets and hence higher local energy dissipation rates in the regions immediately downstream from the screens. Consequently, finer dispersions are expected to be formed as the screen open area is decreased.

The variation of the Sauter mean diameter with screen open area is depicted in Figure 4.19. At very high superficial velocities ($U = 0.97$ and 1.94 m/s), where the turbulent drop dispersion mechanism prevails, the Sauter mean diameter was found to increase linearly with the increasing screen open area. This suggests that under highly turbulent jet flow conditions ($U \geq 0.70$ m/s) the percentage open area in the screen and not its geometrical configuration plays a significant role in the overall dispersion process. These results are in accordance with findings of Chen (1996). On the other hand, the Sauter mean diameter shows a distinct dip in the case of screen having a fractional area of 33% indicating that the lowest mean drop size is obtained using screens with small mesh sizes (i.e. $174 \mu\text{m}$). It can therefore be concluded that the importance of the drop cutting action gains more relative importance at lower superficial velocities.

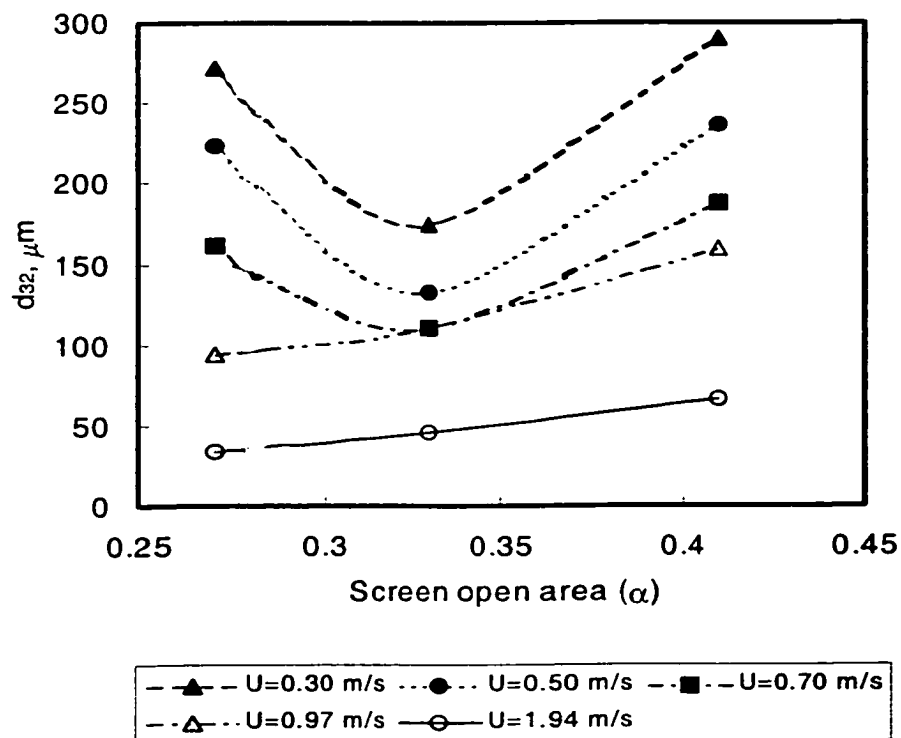


Figure 4.19. Effect of screen open area on Sauter mean diameter ($\phi = 0.5\%$, 9 screens, $L = 10$ mm).

Attempts were made to account for the influence of screen geometry (i.e. mesh size, wire size and percent open area) on drop breakup. Therefore the variations of the average drop diameter with Re_M , Re_b , Re_{jet} and Re_j were plotted in Figures 4.20 to 4.23 respectively. In the case of Re_M , and Re_b , the data tended to segregate according to screen open area, but in the case of Re_{jet} , the data tended to converge to a straight line at high Reynolds numbers (particularly in the case of 0.5% dispersed phase holdup).

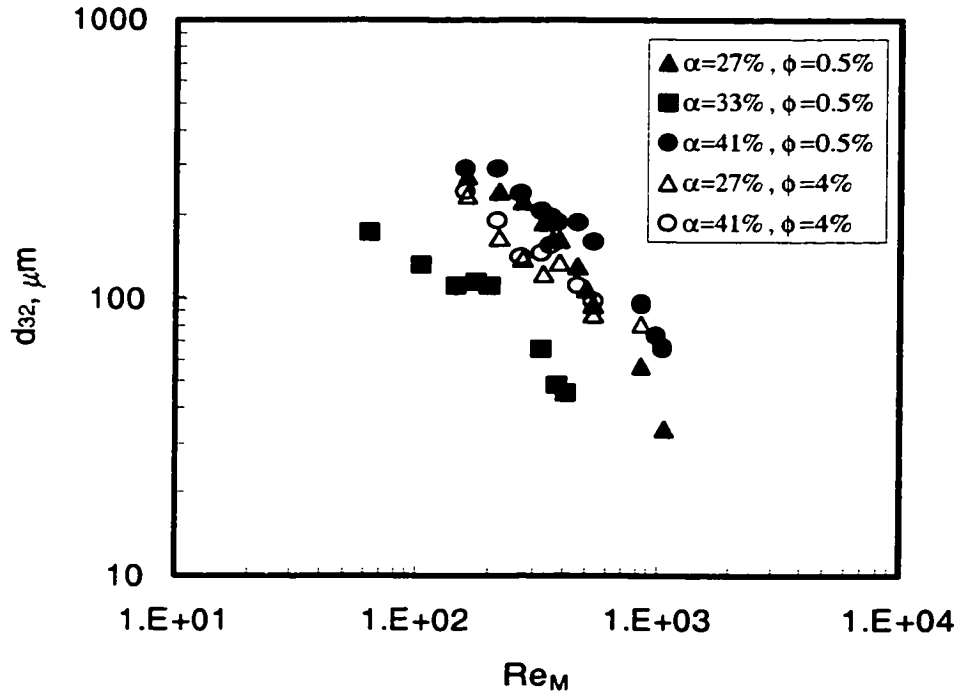


Figure 4.20. Variation of the Sauter mean diameter with Re_M , (9 screens, $L = 10$ mm).

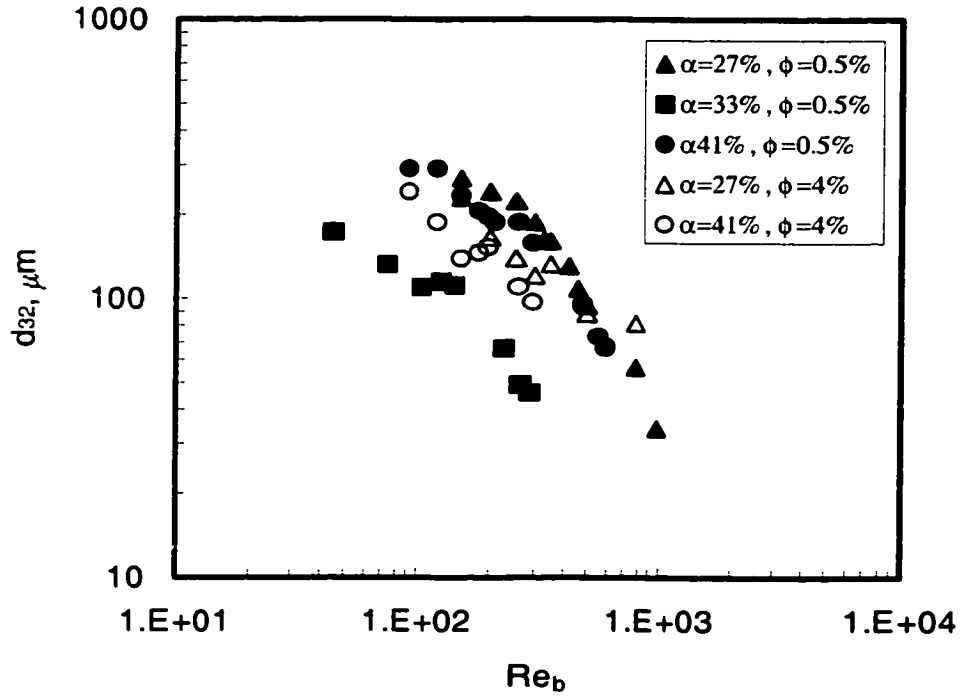


Figure 4.21. Variation of the Sauter mean diameter with Re_b , (9 screens, $L = 10$ mm).

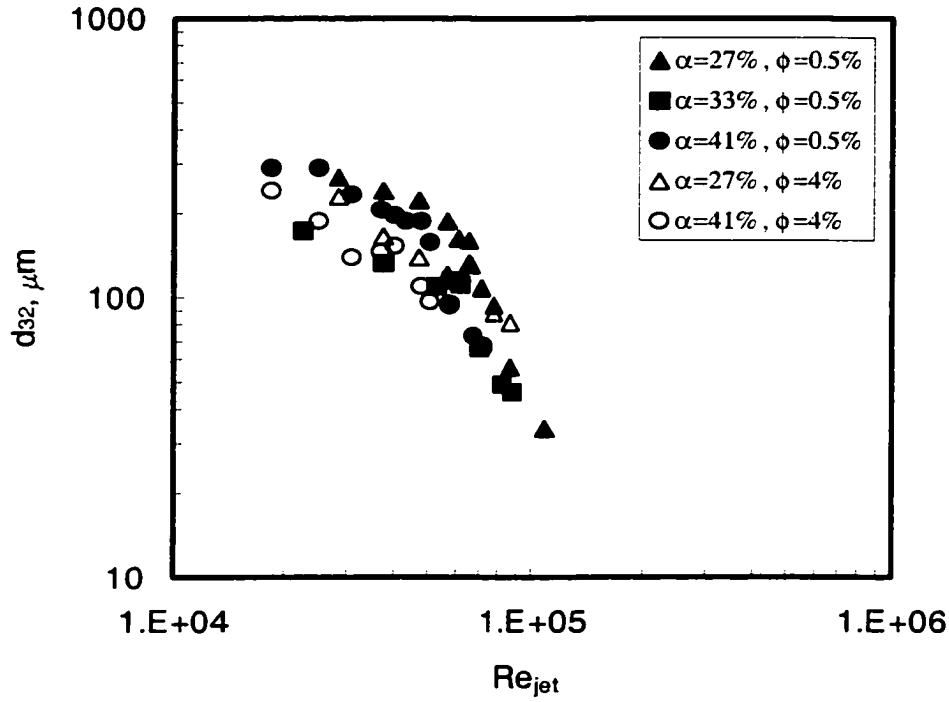


Figure 4.22. Variation of the Sauter mean diameter with Re_{jet} (9 screens, $L = 10$ mm)

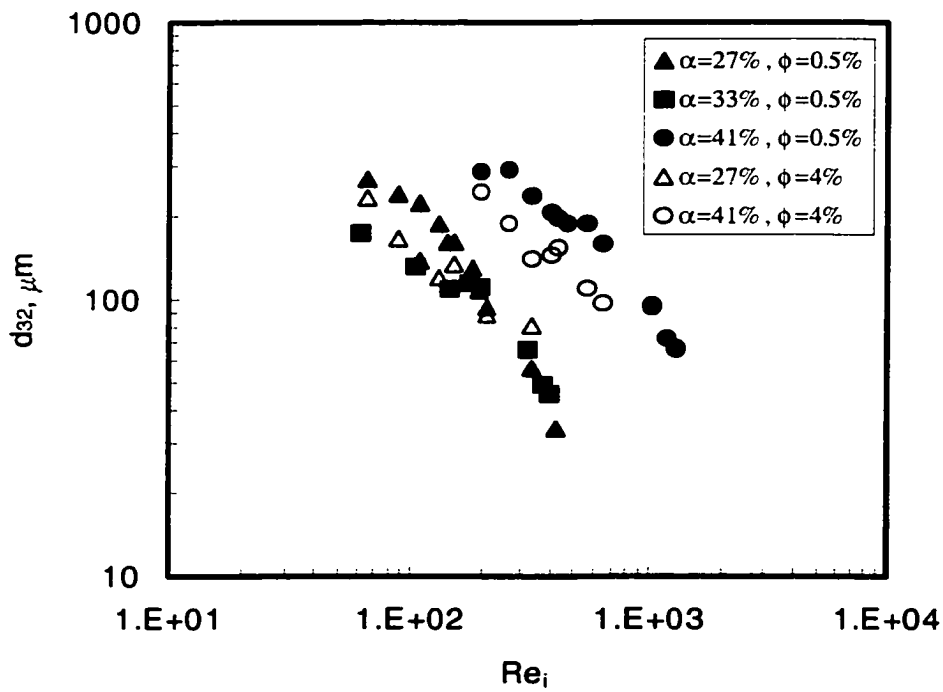


Figure 4.23. Variation of the Sauter mean diameter with Re_i (9 screens, $L = 10$ mm)

From Figures 4.20 to 4.23, it is evident that none of the Reynolds numbers investigated can be used singularly to satisfactorily correlate the drop dispersion in screen mixing elements except at jet Reynolds numbers higher than those investigated in this work. The significance of screen geometry in drop breakup suggests that cutting action (caused by the flow across the screen lattice) plays an important role except at very highly turbulent conditions where the turbulent drop breakup (which takes place in liquid jets behind the screens) dominates and the impact of the cutting action becomes relatively insignificant.

The above results are in line with those obtained by Chen (1996) who found that the liquid-liquid dispersion in two-phase flow through screens is affected by the screen geometry. He further suggested that the screen open area is a major factor in the dispersion process and to a lesser extent the mesh size and the wire diameter. On the other hand, Walker (1984) found that drop breakup is not significantly affected by screen geometry, a result, which contradicts the findings of the present investigation.

The possibility of correlating the average drop size using the Weber number was investigated (Figures 4.24 and 4.25). In a fashion similar to Figures 4.16, the mean drop size data of 0.5% holdup can be split into two distinct groups depending on the drop breakup mechanism regions (Figure 4.24). The data also show tendency to segregate according to screen open area and the dependency on Weber number is higher in the case of the turbulent drop breakup region ($We \geq 700$). This confirms the significant effect of screen geometry on the dispersion process at low dispersed phase holdups. This dependence disappears at higher holdups for the reasons discussed in the previous paragraphs (Figure 4.25).

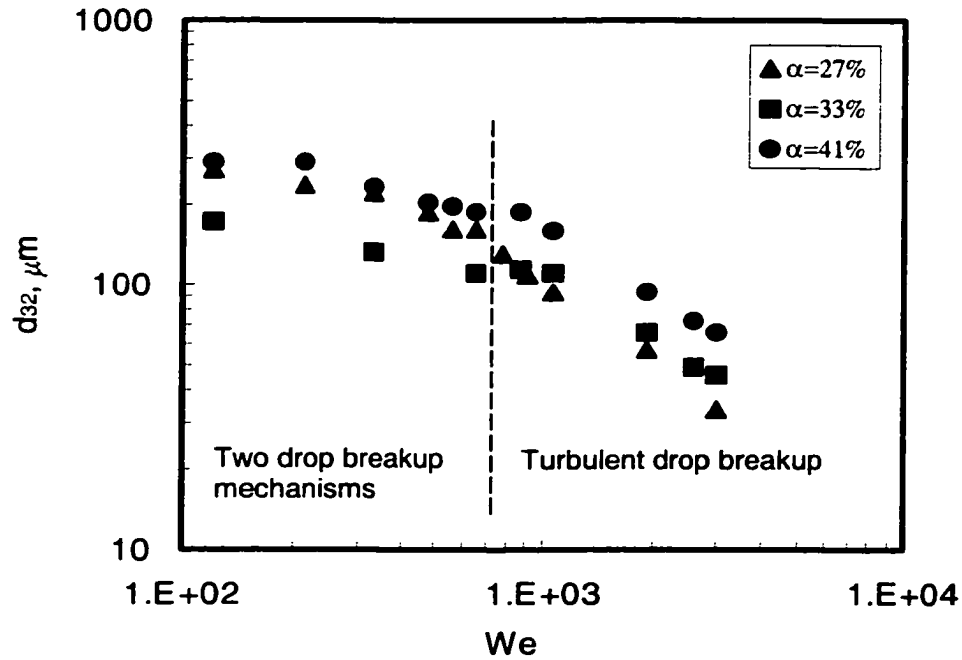


Figure 4.24. The variation of Sauter mean diameter with the Weber number ($\phi = 0.5\%$, 9 screens, $L = 10$ mm).

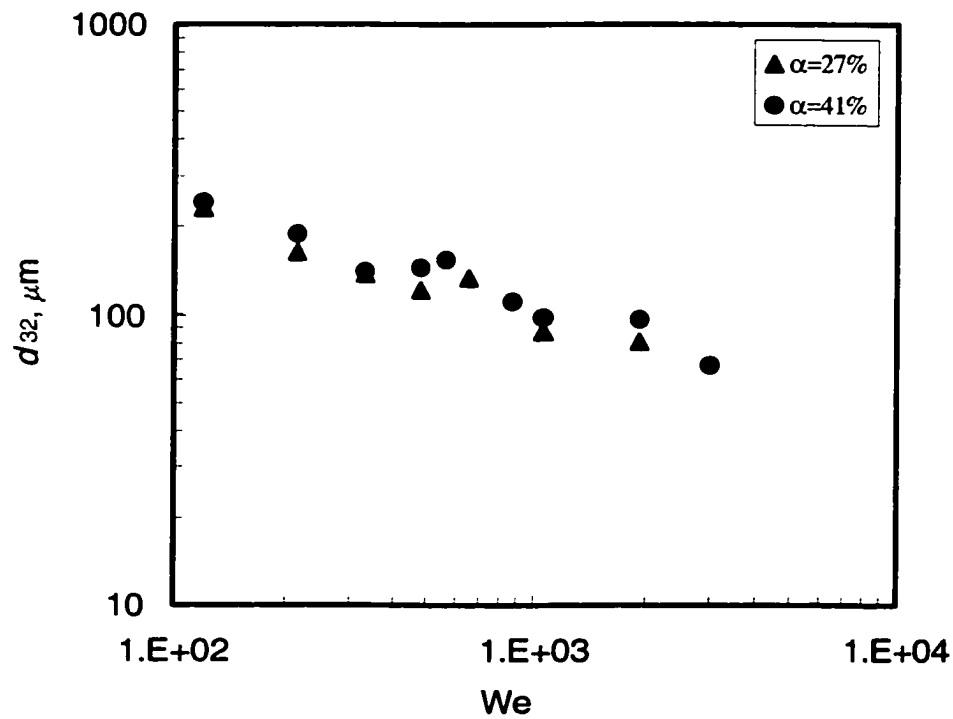


Figure 4.25. The variation of Sauter mean diameter with the Weber number ($\phi = 4\%$, 9 screens, $L = 10$ mm).

Table 4.3. Dependence of drop size on the Weber number

Screen open area	Constant	$\phi = 0.5\%$	R	Constant	$\phi = 4\%$	R
0.27	4.79	$We^{-0.88}$	0.996	3.11	$We^{-0.37}$	0.970
0.33	3.97	$We^{-0.66}$	0.964	NA	NA	NA
0.41	4.10	$We^{-0.65}$	0.970	3.08	$We^{-0.34}$	0.956

For Weber numbers greater than 700 (corresponding to superficial velocities larger than or equal 0.70m/s), the Sauter mean diameter was found to depend on the Weber number with an exponent value that varies between -0.34 and -0.88 depending on the percentage open area and dispersed phase holdup (Table 4.3). This compares reasonably well with the results of previous investigators who studied liquid-liquid dispersion in static mixers (Table 4.4).

Since turbulent drop breakup mainly occurs in the micro jets generated behind the screens (Al Taweel and Chen, 1996; Walker and Al Taweel, 2001), the inertial forces causing drop breakup are expected to be strongly dependent on the liquid velocity in the jets rather than on the superficial velocity in the open pipe. Consequently, it is more realistic to correlate the dispersion process to the jet Weber number, which reflects the influence of the velocity of the fluid in the jets generated behind the screen. Such behavior is depicted in Figure 4.26 where the data obtained at jet Weber numbers lower than 7000 exhibit lower dependency on We_{jet} . The smaller drops obtained in the case of screen of 33% open area are due to the larger role played by cutting action mechanism in the case of this screen, which has a mesh size that is much smaller than the other two. At low dispersed phase holdups and higher Weber numbers, where turbulent drop breakup dominates, the data from the different screens converge to a single straight line given by ($R = 0.933$):

$$d_{32} = 5.05We_{jet}^{-0.75} \quad (4-10)$$

It can thus be concluded that at sufficiently high jet velocities the drop breakup process in screen-elements is controlled by the inertial forces in the micro-jets. Similar

conclusions were made by Al Taweel and Chen (1996), and Al Taweel and Walker (2001).

Table 4.4. Dependence of the mean drop diameter on Weber number in static mixers

Reference	Mixer	Dispersion	Dependence
Middleman (1974)	Kenics	Anisole, Benzene, Cyclohexane, Toluene-in-water	$We^{-0.6}$
		Benzyl alcohol, Oleic acid-in-water	$We^{-0.40}$
Chen and Libby (1978)	Kenics	Kerosene, Mineral oil-in-water	$We^{-0.75}$
Streiff (1977)	Sulzer	Benzene, Toluene, Cyclohexane, Kerosene-in-water	$We^{-0.50}$
Schott and Yuu (1978)	Ross LLPD	Hexane-in-water	$We^{-0.90}$
	Ross LPD	Hexane, Heptane, Petroleum ether-in-water	$We^{-0.62}$
Matsamura et al. (1981)	Hi-Mixer	Water-in-paraffin	$We^{-(0.50-0.67)}$
Al Taweel and Walker (1983)	Lightnin	Kerosene-in-water	$We^{-0.87}$
Walker (1984)	Screens	Kerosene-in-water	$We_{jet}^{-(0.95-1)}$
Sembira et al (1986)	Sulzer	Kerosene-in-water	$We^{-0.50}$
Berkman and Calabrese (1988)	Kenics	p-xylene-in-water	$We^{-0.6}$
El-Hamouz et al (1994)	Lightnin	Kerosene-in-water	$We^{-(0.71-0.83)}$
Al Taweel and Chen (1996)	Screens	Petroleum oils-in-water	$We_{jet}^{-0.89}$
Present study (2001)	Screens	Bayol oil-in-water	$We_{jet}^{-0.75}$

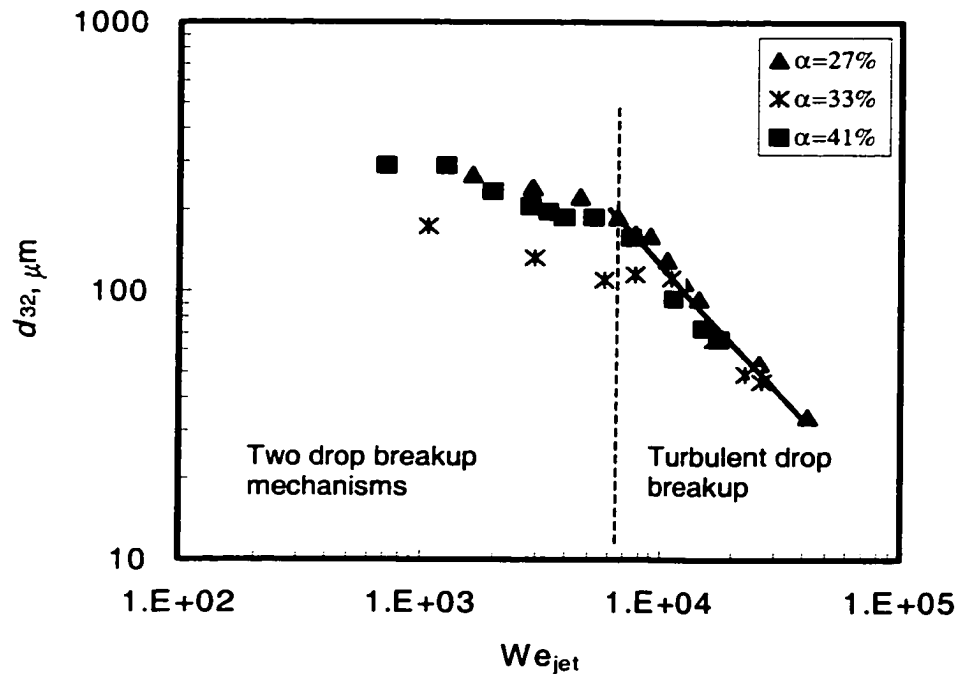


Figure 4.26. Variation of the Sauter mean diameter with We_{jet} ($\phi = 0.5\%$, 9 screens, $L = 10$ mm).

The value of the exponent in Equation (4-10) is somewhat in agreement with that reported by Al Taweel and Walker (1983) for dispersions of 1% kerosene-in-water generated using in-line Lightnin static mixers, and Al Taweel and Chen (1996) for dispersions of 1% petroleum oil-in-water using woven screens. Furthermore, this exponent is in agreement with most of the findings of other investigators who similarly reported exponent values lower than that predicted by the Kolmogorov-Hinze model (exponent = -0.6). However, it is important to keep in mind that with the exception of Streiff's (1977) data, all the early studies (from 1974-1980) were conducted at low superficial velocities where turbulent conditions may have not been fully developed, a factor that makes the total dependence of drop breakup on the inertial forces questionable.

The results obtained at $\phi = 4\%$ (Figure 4.27) are well correlated over the whole Weber number range by the following expression ($R = 0.932$):

$$d_{32} = 3.36We_{jet}^{-0.34} \quad (4-11)$$

The very low exponent value in Equation (4-11) is caused by the larger role played by the drop cutting mechanism in the case of higher dispersed phase holdups.

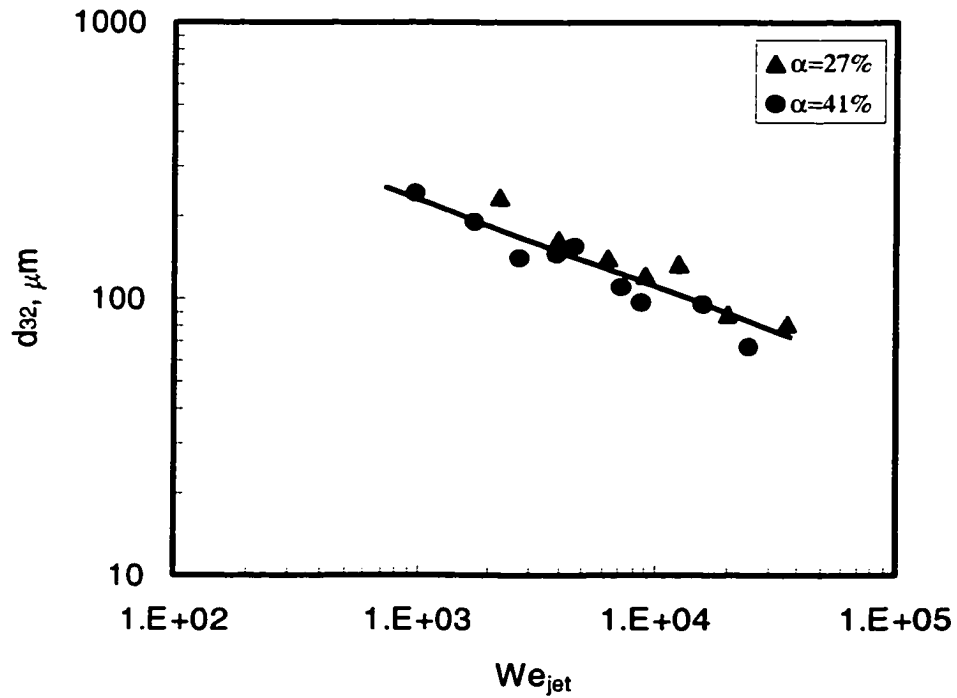


Figure 4.27. Variation of the Sauter mean diameter with We_{jet} ($\phi = 4\%$, 9 screens, $L = 10$ mm).

4.2.3 Effect of Number of Elements

The residence time, θ , in screen-type static mixers can be calculated from the following,

$$\theta = \frac{L_m}{U} \quad (4-12)$$

where L_m is the mixer length and U is the superficial velocity. Equation (4-12) is derived on the assumption that axial back mixing in this device is negligible, a situation which is based on the observation that fully-developed turbulent pipe flow exhibits relatively little axial mixing and that the presence of screens will significantly reduce this axial mixing. At any particular superficial velocity, higher residence times will be achieved by using longer static mixers. This, in turn, results in drops remaining for longer periods in the high-energy dissipation region where they will undergo further breakage.

Figure 4.28 shows the variation of the Sauter mean diameter with the number of mixing elements from which it is clear that the average drop size rapidly changes with increasing number of elements, with the effect being more pronounced in the initial stages. An equilibrium average drop size appears to be approached at large screen numbers (9 in the case of $U = 0.4$ m/s and $\alpha = 0.27$). This equilibrium average drop size represents the conditions under which a state of dynamic equilibrium exists between drop breakup and coalescence processes and is not affected by increasing the residence time (i.e. mixer length). On the other hand, the value of the equilibrium drop size, as well as the rate at which it is approached is expected to be strongly dependent on the energy dissipation rate (which is affected by the superficial velocity and the screen characteristics). This behavior is in agreement with the observations reported by Middleman (1974), Chen and Libby (1978), Al Taweel and Walker (1983), Walker (1984), Al Taweel and Chen (1996) and Chen (1996). Contrary to the present findings, Schott and Yuu (1978) reported some preliminary results indicating that the average drop size might increase with increasing residence time; however, this inconsistency may be partially attributed to some inaccuracy in the photographic method used to determine drop sizes.

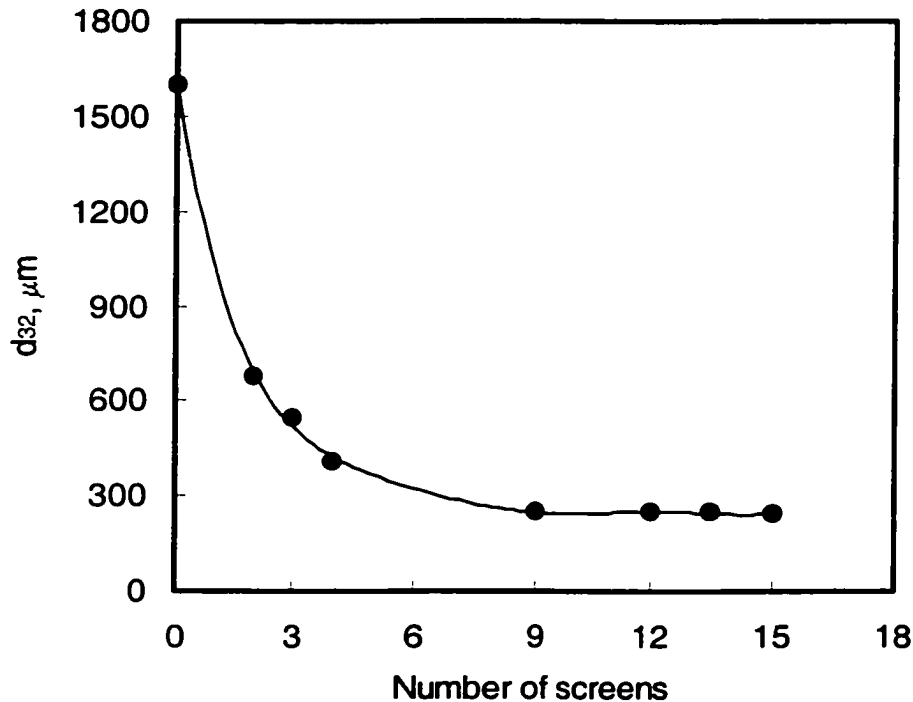


Figure 4.28. Effect of number of mixing element on the average drop size
 $(\alpha = 27\%, \phi = 2\%, U = 0.40 \text{ m/s}, L = 0.5 \text{ cm})$

Similar observations were reported in the case of batch mechanically-agitated tanks (Hong and Lee, 1983; Chatzi et al., 1991; Skelland and Kanel, 1992; Lo et al., 1998; Pacek et al., 1999, Seidshazileh, 1999) but it is important to mention that the situation in MAT is complicated by its complex hydrodynamic conditions and the flow pattern circulating between regions of high and low energy dissipation rates. Consequently, whereas equilibrium is achieved within a fraction of a second in the present investigation, it can take several hours to approach equilibrium in the case of MAT.

The tested velocities in the present investigation range from 0.30 to 1.94 m/s and the number of screens used in the rest of the experimental runs is 9, therefore it is believed that the equilibrium drop size is very closely approached in all tests.

Walker (1984) results approached equilibrium after 4 screens. He found that the equilibrium average drop size is strongly dependent on the superficial velocity as well as the screen open area. Also, the rate at which the equilibrium is achieved was found to be

slowest at low superficial velocities. Low open area screens showed a continuation of drop breakup with increasing distance down the screen, whereas the ones of higher open area show an increase in drop size with increasing distance between the screens, which was attributed to the occurrence of drop coalescence. This became less dominant as the equilibrium size was approached. This relatively lower number of screens required to approach equilibrium drop size may be attributed to the higher superficial velocities used as well as to the fact that the dispersed phase used in Walker's study (kerosene) is less viscous than the dispersed phase used in the present study (i.e. Bayol oil). Chen (1996) used screens of 27% open area (with a distance of 1 cm between the screens) to disperse different petroleum products in water and approached equilibrium drop size after the sixth element. The difference between Chen's results and those obtained in the present study can be mainly attributed to the significantly different drop size measuring techniques and the different superficial velocities used in both studies. However, the present results are very close to those reported by Walker (1984) and Chen (1996) if the difference in the superficial velocity is taken into account. Walker (1984) used a superficial velocity of at least 0.70 m/s, whereas Chen (1996) used minimum superficial velocity of 0.65 m/s compared to 0.40 m/s in the present investigation.

4.2.4 Effect of Dispersed Phase Volume Fraction

At any particular experimental condition, the mean drop size is determined by two simultaneous and counteracting competing processes, namely: drop breakup and coalescence (Figure 4.29). While drop breakup can be promoted by increasing the turbulence intensity, the drop coalescence can be enhanced by increasing turbulence intensity as well as by increasing the volume fraction of the dispersed. An increase in the dispersed phase holdup results in increasing the drop population density, which in turn, promotes collision frequency. An increase in the dispersed phase holdup, or the drop population density, is thus expected to shift the equilibrium towards the left-hand side resulting in the formation of larger drop sizes. On the other hand, the presence of the dispersed phase drops is claimed to influence the turbulence structure in the continuous phase (Ahmad and El-Ghobashi, 2000). Several investigators suspected that turbulence

modulation is the cause of a reduced drag coefficient at high velocities and could be partially responsible for turbulence dampening (Sleicher, 1962; Doulah, 1975; Tavlarides and Stamatoudis, 1981). This phenomenon may adversely affect the breakage rate.

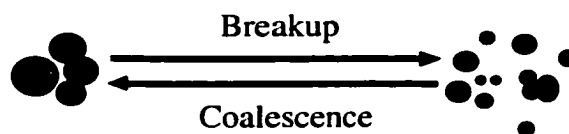


Figure 4.29. Schematic representation of drop breakup/coalescence.

The effect of varying dispersed phase holdup on the Sauter mean diameter is shown in Figures 4.30 and 4.31 for superficial velocities of 0.40 and 0.70 m/s. Generally speaking, the Sauter mean diameter was found to decrease with increasing dispersed phase holdup with this effect being more pronounced at the lower superficial velocity of 0.40 m/s. This behavior is most probably caused by the presence of two drop-dispersion mechanisms (namely turbulent drop breakup and drop cutting by screen wires) that are differently influenced by the superficial velocity and the dispersed phase holdup. Figure 4.32 shows a schematic illustration of the two breakup mechanisms. The turbulent drop breakup is influenced by the turbulence intensity in the micro-jets formed by the screen elements which, in turn, is mainly influenced by the jet velocity ($U_{jet} = U/\alpha$). The predominance of this mechanism under highly-turbulent conditions (large superficial velocities and low open area fractions) is the reason why a single equation was able to correlate all the data meeting such requirements (Equation (4-10)). Those hydrodynamic conditions also met most of the assumptions included in the Kolmogorov-Hinze model, a fact that explains why the experimentally determined exponent is equal to that theoretically predicted. On the other hand, drop breakup due to the cutting action of the screen's wires is expected to play a more significant role when very fine mesh screens are used for the purpose of dispersing immiscible liquids. The existence of this mechanism can easily be understood when the drops are larger than the mesh size but it continues to play a role even when the average drop size is smaller than the mesh size. This is caused

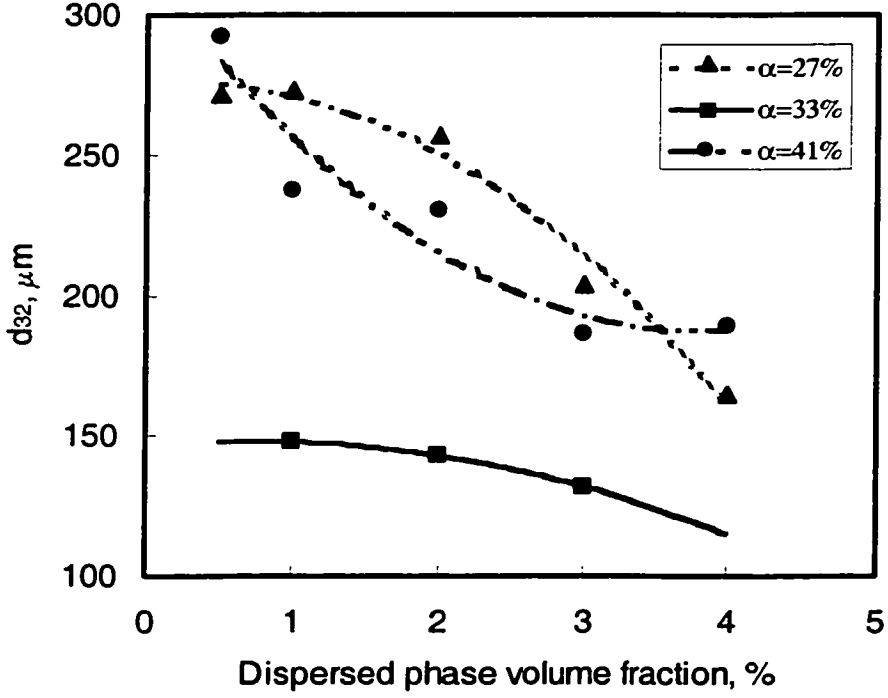


Figure 4.30. The effect of the dispersed phase volume fraction on the Sauter mean diameter ($U = 0.40$ m/s, 9 screens, $L = 10$ mm).

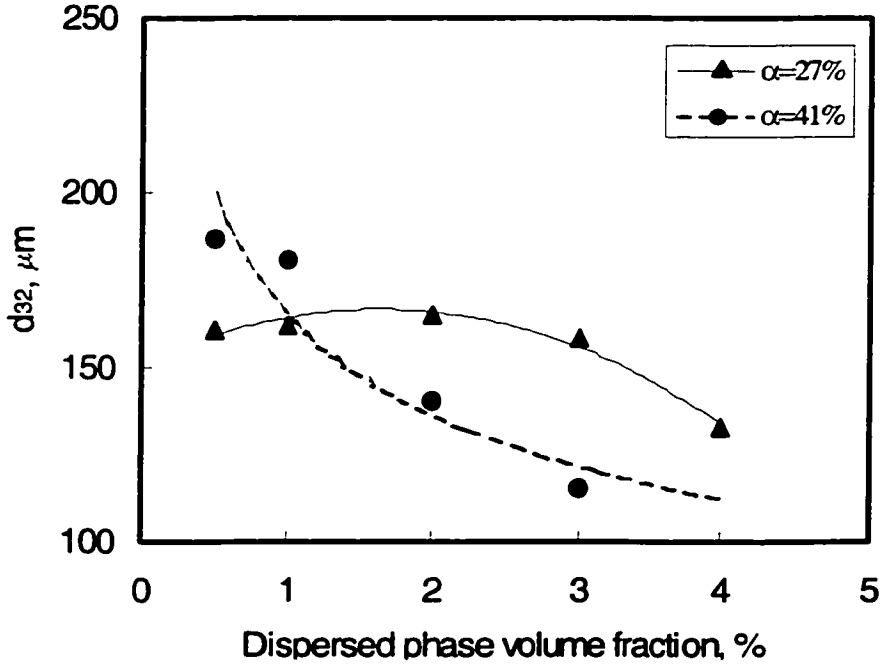


Figure 4.31. The effect of the dispersed phase volume fraction on the Sauter mean diameter ($U = 0.70$ m/s, 9 screens, $L = 10$ mm).

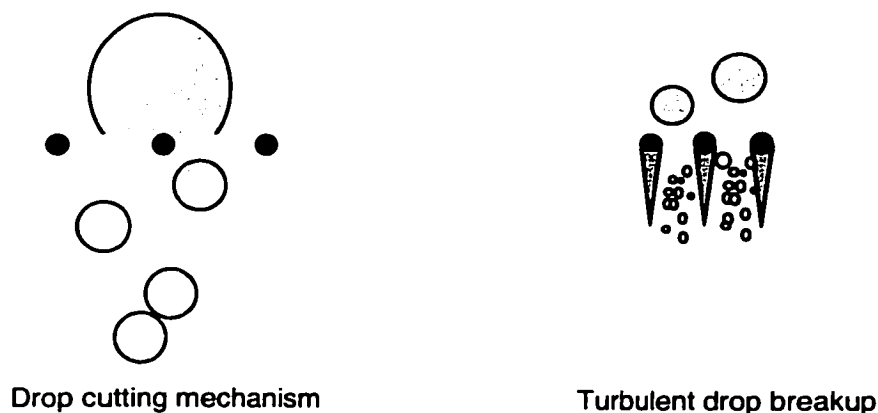


Figure 4.32. Schematic diagram of Drop breakup mechanisms.

by the presence of a significant fraction of the dispersed phase volume in the form of drops that are larger than the mean (typically up to two-fold the mean size) which will be more selectively broken down to smaller entities. The other factor that plays a role in the drop cutting mechanism is the probability of drops hitting the wires of the screen elements in a fashion that will cause them to disintegrate. This is somewhat analogous to the concept of target hitting efficiency extensively used in particulate collector design. Some of the experimental results obtained in this investigation (section 4.4.1) confirm the role of drop cutting mechanism. The effect of dispersed phase holdup on the average drop size suggest that that drop disintegration by the cutting mechanism plays a more important role at higher dispersed phase holdups, particularly at low average energy dissipation rates where the turbulent breakage mechanism is expected to play a less prominent role. This may be due to enhancement in the target hitting efficiency, and/or a reduction of the ability to deform and pass through the screen without breaking, that is achieved due to the presence of adjacent drops. These results are similar to those of Sreenivasulu et al. (1997) who attributed drop breakup in pulsed columns to turbulence due to pulsing, disintegration on collision with the perforated plates and the wall, and to the breakup while drops pass through the perforated plates.

Unfortunately, this topic has not been investigated and there are no independent studies of this phenomenon; however, the prevalence of the drop cutting mechanism at low superficial velocities is expected to be the reason why the exponent of the energy dissipation rate (Equation (4-9)) is much smaller in the case of higher holdups.

All previous investigations of drop dispersion in MAT and static mixers (with the exception of Walker, 1984; Al Taweel and Chen, 1996; and Chen, 1996) dealt with hydrodynamic conditions where drop breakup is dominated by turbulent and/or laminar shear action and the drop cutting mechanism does not exist (Scott et al., 1958; McDonough et al., 1960; Coulaloglou and Tavlarides 1976; Ross et al., 1978; Middleman, 1974; Al Taweel and Walker, 1983; Kumar et al., 1991; El-Hamouz et al., 1994; Streiff et al., 1997; Paceck et al., 1999). Hence, the effect of dispersed phase holdup observed in this investigation is in disagreement with all previously reported theoretical and experimental investigations, which indicate that the mean drop size increases with increasing dispersed phase holdup.

4.2.5 Effect of Interfacial Characteristics

In dispersion processes two types of forces compete—the disruptive or turbulent forces which cause drop breakup, and the interfacial and viscous forces that tend to restore the drop to its original shape. There is, therefore, a general agreement that the interfacial tension affects both drop breakup and coalescence in liquid-liquid systems (Tavlarides and Stamatoudis, 1981, Chatzi et al., 1991; Chatzi and Kiparissides, 1995). In accordance with the Kolmogorov-Hinze model, it is generally believed that low interfacial tensions facilitates drop breakup and shift the dynamic equilibrium towards the formation of finer drops. This concept was experimentally proven in the case of pure uncontaminated systems (Calabrese et al., 1986; Hass, 1987, Rincon-Rubio et al., 1994).

Several concepts have been proposed to explain the impact SAA (surface active agent) have on turbulent drop breakage and coalescence process (Koshy et al., 1988; Peru and Lorenz, 1989; Walstra, 1993; Janssen et al., 1994, Seidshazileh, 1999). Unfortunately, there is very little agreement between these theories, and experimental

results can not be fully relied upon mainly because of the complex hydrodynamics encountered in the most commonly used mixing device, namely MAT, and the difficulty of accurately determining the more advanced dynamic interfacial characteristics. There is, however, a consensus that SAA have two main roles to play: they lower interfacial tension thereby facilitating droplet breakup; and they hinder coalescence. The relative significance of those two roles depends on the interaction between the physico-chemical properties of the system and the hydrodynamics encountered in the mixer.

In this section, an attempt is made to correlate the average drop size (Sauter mean diameter) to the static and dynamic interfacial characteristics of the liquid-liquid system studied. Static interfacial characteristics include the surfactant concentration, equilibrium interfacial tension, and Gibbs surface excess; while the dynamic interfacial characteristics are the surfactant diffusivity and Marangoni number.

Figures 4.33 to 4.35 show the effect of surfactant concentration in the aqueous continuous phase on the mean drop sizes generated at holdups of 0.5% and 4%. As shown in Figure 4.33, the mean drop size was found to decrease with increasing surfactant concentration with the effect being more pronounced at very low SAA concentrations and in the case of lower dispersed phase holdups. The mean diameters obtained at higher dispersed-phase holdup ($\phi = 4\%$) are smaller than those obtained at lower holdups ($\phi = 0.5\%$) suggesting that drop breakage by the cutting mechanism plays a significant role even in the presence of SAA.

The results obtained at $\phi = 0.5\%$ are most probably breakup dominated due to the low holdups used. At low dispersed phase holdup the drop size varies by a factor of more than one and a half over the surfactant concentrations range investigated. This result indicates that in low coalescing systems the surfactant reduces the resistance to drop breakup probably by means of reducing the interfacial tension leading to the formation of smaller drop sizes. The reduced impact of the presence of surfactant at high dispersed phase concentrations suggests that drop coalescence plays an important role under those conditions due to the much higher drop population density (about one order of magnitude). On the other hand, the fact that two curves approach each other at higher

SAA concentrations ($\geq 0.20 \text{ mole/m}^3$) indicates that the role of coalescence is virtually eliminated.

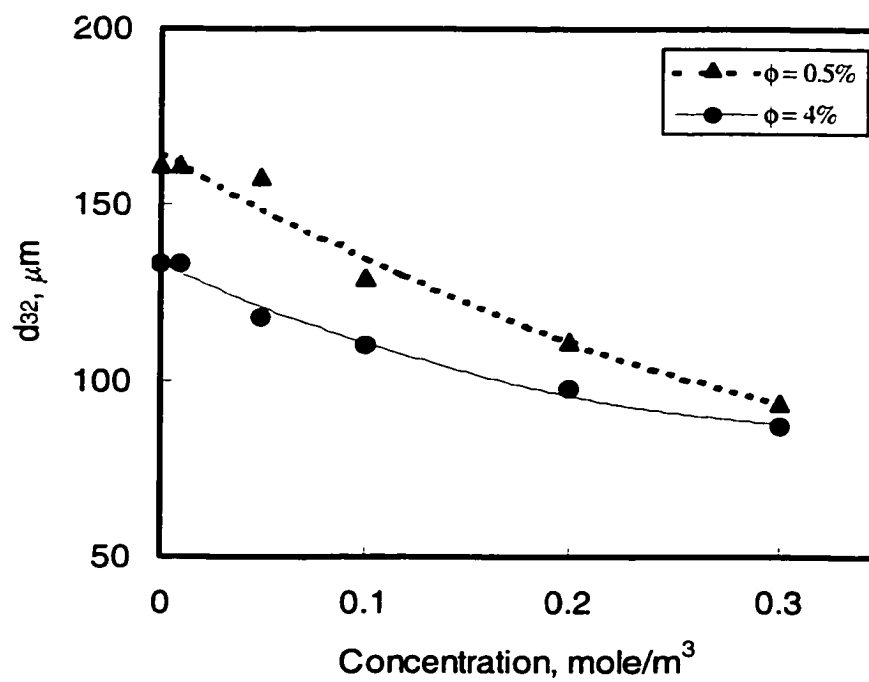


Figure 4.33. Effect of SAA on the Sauter mean diameter ($\alpha = 27\%$, $U = 0.70 \text{ m/s}$, 9 screens, $L = 10 \text{ mm}$).

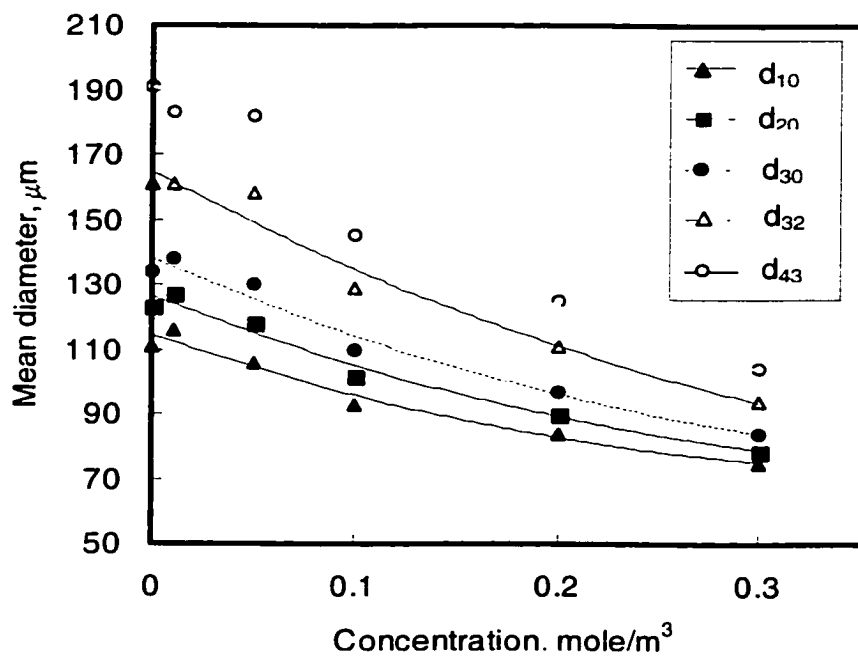


Figure 4.34. Effect of SAA on mean drop diameters ($\alpha = 27\%$, $\phi = 0.5\%$, $U = 0.70$ m/s, 9 screens, $L = 10$ mm).

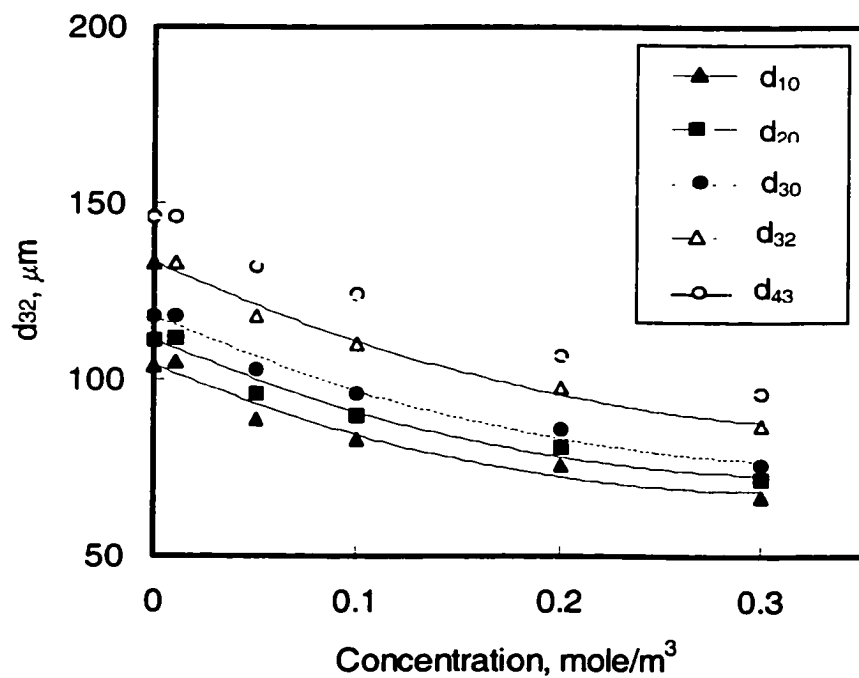


Figure 4.35. Effect of SAA on mean drop diameters ($\alpha = 27\%$, $\phi = 4\%$, $U = 0.70$ m/s, 9 screens, $L = 10$ mm).

As can be seen from Figures 4.34 and 4.35, all drop size means decrease with increasing surfactant concentration with the effect being most pronounced at low concentrations and low dispersed phase holdups. However, the influence of surfactant is most pronounced in the case of d_{43} and it decreases at lower moments with the number mean (i.e. d_{10}) being the least affected. Mean drop sizes calculated using higher moments are strongly influenced by the presence of the larger drops while mean diameters calculated using lower moments are sensitive to the presence of the smaller drops. This suggests that the presence of surfactants preferentially facilitate the breakage of larger drops into smaller entities without the excessive formation of fine drops at the surfactant concentrations investigated. The drop number density generated in the presence of the surfactant confirms the above suggestion (section 4.4.1). At much higher concentrations of the same surfactant very fine emulsions were formed as reported by Pal (1987).

The above mentioned results are in agreement with those reported in the literature (Peru and Lorenz, 1989; Walstra, 1993; Rincon-Rubio et al., 1994; Chatzi and Kiparissides, 1995; Nakache, 1995; Seidshazileh, 1999). Peru and Lorenz (1989) observed that, upon the addition of small amounts of surfactant, the coalescence time increases considerably followed by a gradual decrease in coalescence time as the concentration increased further. Walstra (1993) found that the volume surface average diameter undergoes a sharp decrease as the concentration of a non-ionic surfactant increases until a concentration value is reached beyond which no further change in drop size is produced. Rincon-Rubio et al (1994) observed a decrease in drop volume-surface average diameters for six different organic-water systems in a Wirz- Π agitated column upon the reduction of interfacial tension. Chatzi and Kiparissides (1995) observed that at the same impeller speed, the mean drop diameter decreases with increasing surfactant concentration. Nakache (1995) found that the interface drainage time of heptane drop approaching a water surface increases with the surfactant concentration. Seidshazileh (1999) found that the coalescence rate decreases as the concentration of surfactant increases (i.e., Triton X100). He also reported that the mean drop diameters (d_{30} , d_{32} and

d_{43}) progressively decrease with the concentration of surfactants TritonX100 and TritonX165 dissolved in different organic-water systems.

The results of the present study appear to be in contradiction with the findings of Stewart et al. (1996) who reported an increase in the value d_{32} in the presence of small additive (demulsifier) quantities. The interfacial tension between kerosene and water was found to decrease with increasing additive concentration but no information concerning the effect of the additive on the interfacial charge were provided. It is therefore postulated that the addition of small quantities of the DE5010 demulsifier results in neutralizing the negative charge commonly present on most commercial hydrocarbon dispersions, thereby facilitating coalescence and the shifting the dynamic equilibrium depicted in Figure 4.29 towards the formation of larger drops.

The effect of equilibrium interfacial tension on the Sauter mean diameter is depicted in Figure 4.36, which clearly shows that the data correlates well with the equilibrium interfacial tension at 0.5 and 4% holdups, respectively as follows:

$$d_{32} = 1.94\sigma^{0.24} \quad (R = 0.902) \quad (4-13)$$

$$d_{32} = 1.90\sigma^{0.19} \quad (R = 0.958) \quad (4-14)$$

However, the exponents obtained for both holdups (0.24 and 0.19 respectively) do not agree with the Kolmogorov-Hinze model of drop breakup in turbulent flows (exponent 0.60). This discrepancy is most probably caused by the significant role played by the drop cutting mechanism which appears to be less sensitive to variations in the equilibrium interfacial tension, at the relatively low superficial velocities used in these tests ($U = 0.70$ m/s). This assumption is in agreement with the observation that a lower exponent was obtained in the case of the 4% holdup dispersions where the contribution of the drop cutting action is more significant. These exponents also do not agree with those obtained earlier in the present study, which are based on the Weber numbers as discussed in section 4.2.2. This difference suggests that the surfactant affects the dispersion process differently from that of the interfacial tension of the pure system.

The above mentioned results disagree with the results obtained by Seidshazileh (1999) using the same system where the surface tension exponent was found to vary from

0.4 to 0.93 depending on the extent to which equilibrium conditions were approached. The present findings also contradict those of Lucassen-Reynders and Kuijpers (1992) who found that the average drop size could not be correlated with the equilibrium interfacial tension in oil-water system containing triacylglycerol surfactant. It should, however, be remembered that the use of static interfacial tension to describe the complex phenomenon taking place in the presence of surface active agents is an oversimplification of the situation.

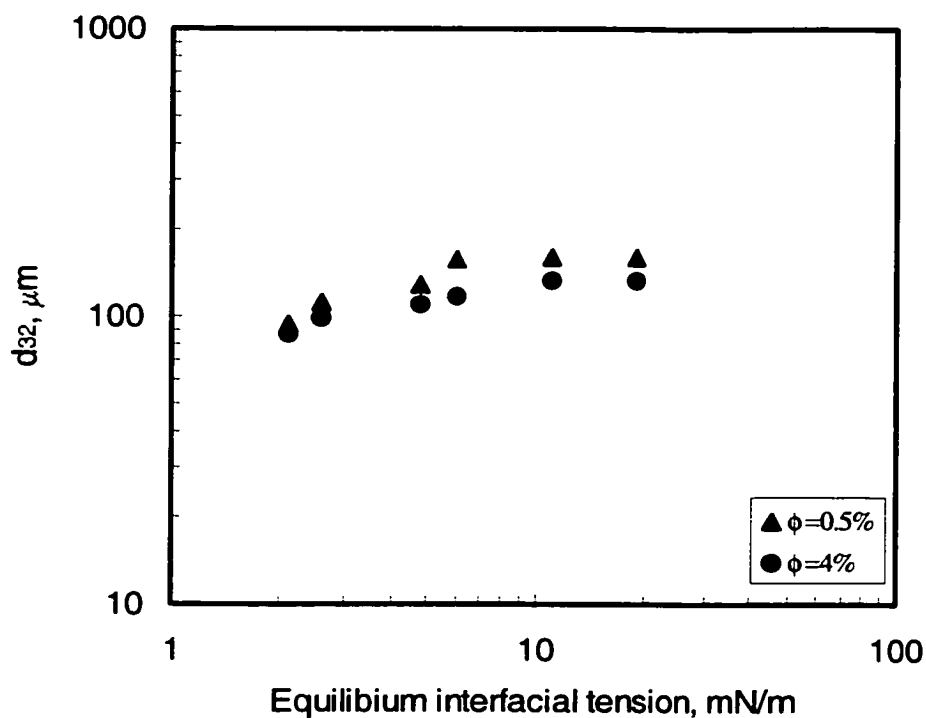


Figure 4.36. Effect of equilibrium interfacial tension on Sauter mean diameter ($\alpha = 27\%$, $U = 0.70$ m/s, 9 screens, $L = 10$ mm).

As previously mentioned, the exclusive use of equilibrium interfacial tension has been questioned by many investigators and the use of surfactant surface excess, or interfacial concentration, has been proposed as a means to account for the elasticity of the interfacial film and its ability to resist deformation. An attempt was therefore made to account for the effect of the surfactant surface excess, or interfacial concentration, on the

Sauter mean diameter and the results are shown in Figure 4.37. The results obtained show that the Sauter mean diameter can be correlated very well with the surface excess. Figure 4.37 also shows that the mean drop size decreases monotonically with the increasing surface excess. This is in agreement with the results of Al Taweel and Cheng (1995) who found that the interfacial area, which is inversely related to d_{32} , in MAT with a stator is better correlated using the Gibbs surface excess. Equations (4-15) and (4-16) show the expressions relating d_{32} with the surface excess for 0.5 and 4% holdup dispersions respectively:

$$d_{32} = -407768\Gamma_s + 231.3 \quad (R = 0.914) \quad (4-15)$$

$$d_{32} = -265743\Gamma_s + 174.8 \quad (R = 0.977) \quad (4-16)$$

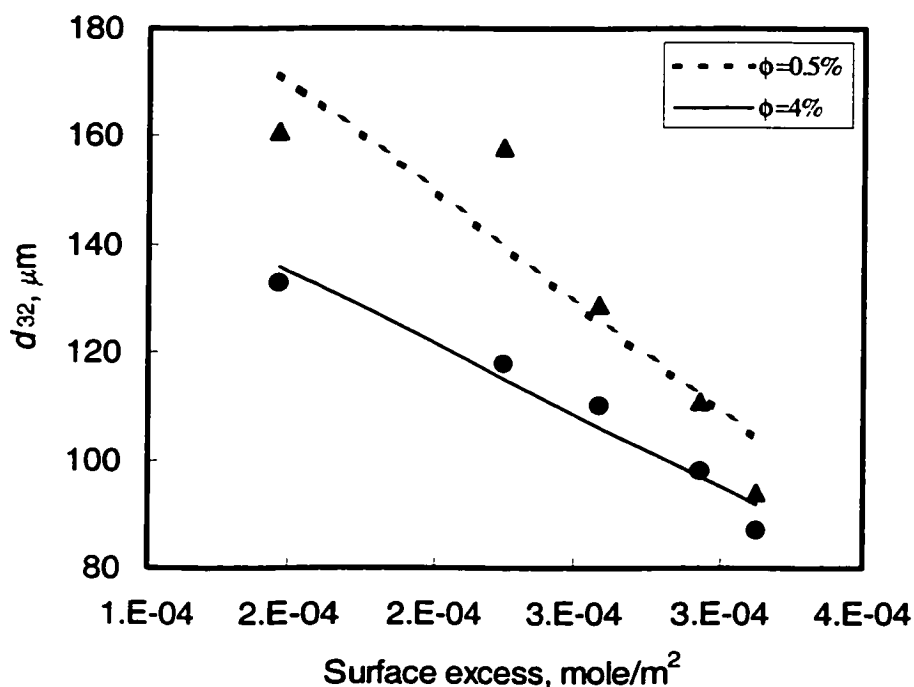


Figure 4.37. Effect of surface excess on the Sauter mean diameter.
($\alpha = 27\%$, $U = 0.70$ m/s, 9 screens, $L = 10$ mm)

Drop breakup/coalescence involves dynamic interface stretching which is so rapid that surfactants and other chemical contaminants that might be present in the system, may

not have the opportunity to be fully adsorbed onto the interface within the very short times associated with those processes (on the order of 1 ms). This causes the interfacial tension to deviate from its equilibrium value and the surfactant to diffuse to the interface. Consequently the surfactant diffusivity is expected to play a more crucial role in drop breakup/coalescence and should therefore be taken into account when liquid-liquid dispersions are investigated. The SAA diffusivity was found to depend on several factors such as the molecular weight of the surface-active species, molecular length, temperature, etc (Xue, 1999). The importance of diffusivity was recognized by Clift et al. (1978) who reported that SAA having lower surface diffusion coefficients are more effective in prevention of drop coalescence due to their higher efficiency in suppressing fluid circulation within the drop. As the amount of the adsorbed surfactant molecules on the interface decreases, the fluid circulation becomes slower due to the increased interfacial tension gradients. The importance of diffusivity in drop coalescence has been identified by Krawczyk (1991) who studied the interrelationship between drop coalescence and interfacial phenomena in crude oil emulsions containing oil-soluble demulsifiers. They found that the most important factors determining the demulsifier efficiency are high interfacial activity and high diffusion/adsorption rates. Walstra (1993) reported similar results.

The effect of surfactant concentration on the diffusivity of Triton X 100 in the system investigated was determined by Xue (1999) and the results obtained are plotted in Figure 4.38. The diffusivity was found to increase very sharply with increasing surfactant concentration reaching a maximum value possibly due to the resultant increase in concentration gradient. As the concentration increases further, the diffusivity falls very sharply and then it levels out. Xue (1999) attributed this phenomenon to the partitioning of the surfactant monomers between the interface and a growing number of micelles in the bulk of the solution as a result of increasing surfactant concentration. Significant error in the value of diffusivity may thus be encountered at high surfactant concentration.

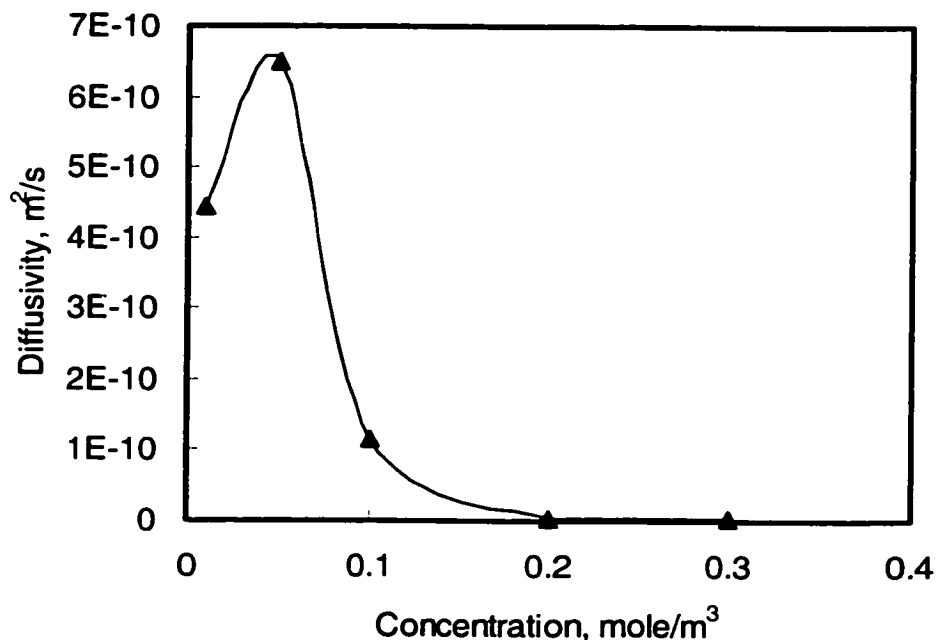


Figure 4.38. Effect of surfactant concentration on diffusivity

An attempt was made to correlate average drop size (Sauter mean diameter) to the surfactant diffusivity at different concentrations and the results obtained are shown in Figure 4.39. It clearly shows that the Sauter mean diameter increases with increasing surfactant diffusivity up to a point where further increase in surfactant diffusivity results in a slight reduction in the Sauter mean diameter particularly at high holdup. This behavior can be attributed to the following factors affecting the rate of transfer of surfactant molecules from the bulk of the liquid to the fresh interfaces generated as a result of the drop deformation under the action of turbulent shear:

- At high surfactant concentrations, very low diffusivities are encountered (Xue, 1999) leading to inadequate diffusion of the surfactant molecules from the bulk to be adsorbed onto the interface. Regions of different interfacial tension are thus formed leading to the establishment of interfacial gradients, which result in the development of a force that tend to resist or counteract any further expansion or contraction of the drop surface. This phenomenon is known as the Gibbs-Marangoni effect giving a finite elasticity to the interface known as

the Gibbs elasticity (Walstra, 1996). This eventually makes the drops more stabilized and less susceptible to breakup; hence, larger average drop sizes are formed upon stretching of a droplet interface.

- At intermediate surfactant concentrations and low surface renewal rates, the diffusion rates are probably adequate to keep the interfacial tension near its equilibrium value, which prevents the formation of interfacial gradients or the reduction of the interfacial tension; thus leading to an insignificant variation in the size of drops generated.
- At low surfactant concentrations (high diffusivities) the surfactant molecules will rapidly diffuse to the newly-formed interface where they get adsorbed and reduce the interfacial tension, hence promoting drop breakup. It was also found that the Marangoni elasticity decreases with increasing surfactant diffusivity (Xue, 1999), thus, making the drops more prone to breakup.

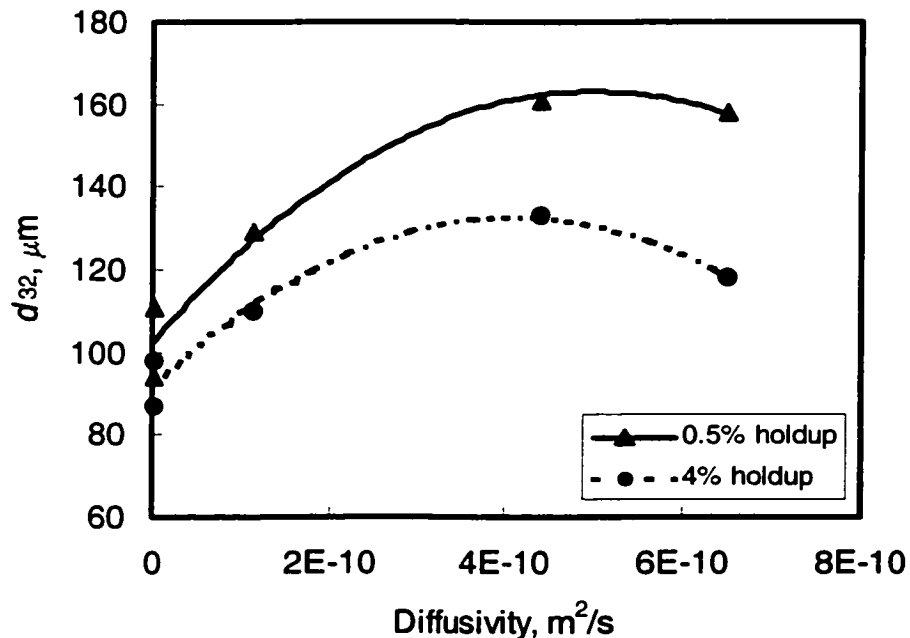


Figure 4.39. The Sauter mean diameter as a function of surfactant diffusivity ($\alpha = 27\%$, $U = 0.7$ m/s, 9 screens, $L = 10$ mm).

The Marangoni number is used extensively in interphase mass transfer, which is often accompanied by cellular convection at the interface induced by surface tension gradients that result from solute concentration gradients or temperature gradients (Choi et al., 1998; Kang and Choi, 2000). The Marangoni number is thus expected to provide an appropriate means for correlating the mean drop size in liquid-liquid dispersions since it combines several interfacial characteristics, which affect the drop deformation and breakup.

The Marangoni number, Ma , is given by,

$$Ma = \frac{\frac{\partial \sigma}{\partial c} \Delta c L_f}{\mu D} \quad (4-17)$$

where Δc is the concentration difference of the surfactant between the bulk phase and the interface, D is the surfactant diffusivity, σ is the interfacial tension, c is the surfactant concentration and L_f is the fluid layer thickness.

The Marangoni number is thus expected to provide an appropriate means for correlating the mean drop size in liquid-liquid dispersions since it combines several interfacial characteristics, which affect the drop deformation and breakup.

Figure 4.40 shows the variation of the Sauter mean diameter with the Marangoni number from which it is clear that the Marangoni number provides an excellent means for correlating the effect of surfactant concentration on the average drop size in breakage dominated turbulent flows. However, further testing using different surfactants is needed to confirm the universal suitability of this parameter. As can be seen from Figure 4.40, the average drop size decreases monotonically with the increasing Marangoni number with the effect being more pronounced at lower dispersed phase holdups. Equations (4-18) and (4-19) show the expressions obtained for 0.5 and 4% holdups respectively:

$$d_{32} = -8 \times 10^{-10} \frac{Ma}{L_f} + 164.1 \quad (R = 0.969) \quad (4-18)$$

$$d_{32} = -5 \times 10^{-10} \frac{Ma}{L_f} + 128.7 \quad (R = 0.923) \quad (4-19)$$

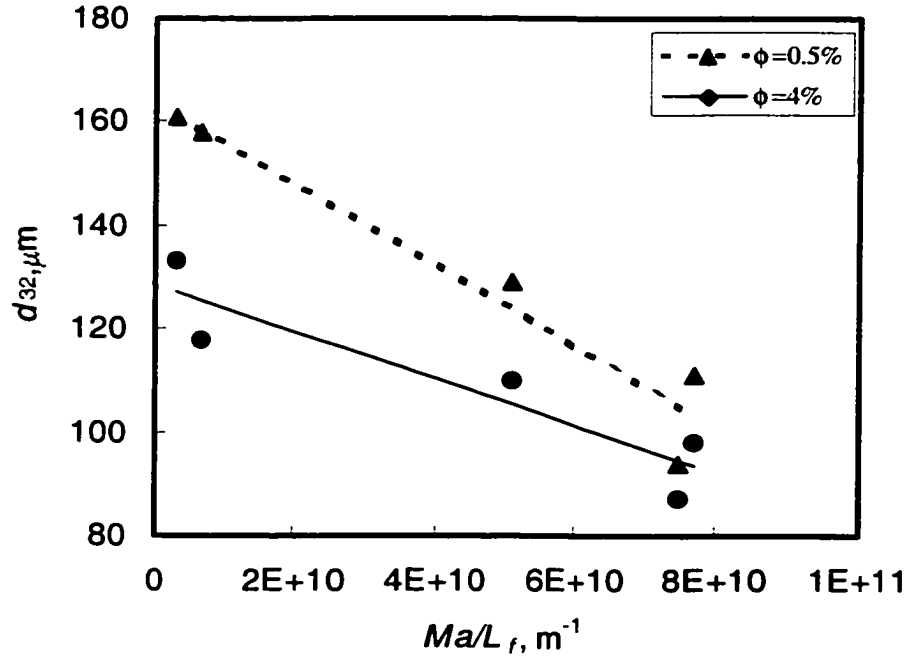


Figure 4.40. Effect of Marangoni number on the Sauter mean diameter ($\alpha = 27\%$, $U = 0.70$ m/s, 9 screens, $L = 10$ mm).

4.2.6 Correlation of Experimental data

The results obtained under the different experimental conditions investigated (in absence of the surfactant) indicate that the equilibrium average drop size is affected by U , ϕ , b , M and σ . The values of μ_d , μ_c , ρ_d , ρ_c did not change due to the fact that only one liquid-liquid system was used in the present investigation. The average drop size data obtained under equilibrium conditions were correlated using the following dimensionless groups:

$$d_{32} = c \text{Re}_{jet}^a \text{We}_{jet}^b \phi^d \left(\frac{b}{M} \right)^e \quad (4-20)$$

Stepwise regression was performed on 67 data points using Minitab software and the values of a , b , c , d and e were found to be 1.38, -1.05, -0.084, 0.349 and 0.302 respectively with a correlation coefficient of 0.903. Equation (4-20) therefore becomes,

$$d_{32} = 0.302 \text{Re}_{jet}^{1.38} \text{We}_{jet}^{-1.05} \phi^{-0.084} \left(\frac{b}{M} \right)^{0.349} \quad (4-21)$$

As can be seen from Equation (4-21), the jet Reynolds number was found to be a significant factor for the range of the experimental conditions investigated. The dependence of the equilibrium drop size on the jet Weber number is higher than that found in section 4.2.2. This difference is due to the fact that all data were correlated regardless of the flow regime or the dispersed phase holdup. Also, the effect of dispersed phase concentration is contrary to that reported in the literature due to the existence of two drop breakup mechanisms as reported in section 4.2.4. Figure 4.41 shows a comparison between the drop sizes predicted by Equation (4-21) and the experimental values. As shown this correlation tends to underestimate the Sauter mean diameter at high drop sizes and should thus be used mainly in the range of the experimental conditions investigated. However, the correlation was found to fit the data quite satisfactorily.

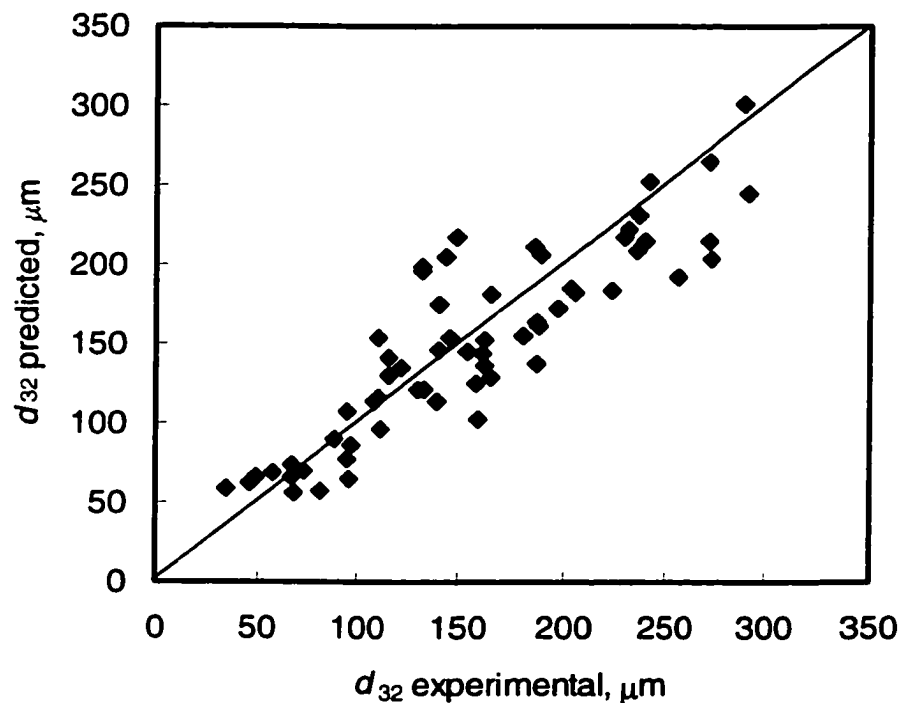


Figure 4.41. Comparison of predicted average drop size by Equation (4-21) and calculated values from experimental data.

4-3 MAXIMUM STABLE DROP SIZE

Although the Kolmogorov-Hinze model discussed the maximum stable drop size present in a liquid-liquid dispersion, very few investigations addressed this issue. Most studies (Middleman, 1974; Al Taweel and Walker, 1983; Al Taweel and Chen, 1996, Pacek et al., 1999) focused on the Sauter mean diameter, which is related to d_{max} in a fashion that is not yet clearly established. The maximum stable drop size, d_{max} , is determined by the balance between the disruptive turbulent forces, which tend to cause drop deformation and breakup, and the interfacial tension and viscous forces which tend to keep the drop intact.

The data obtained in this investigation were correlated using a form similar to that Hinze (1955) derived. The value of d_{max} for any particular experimental condition is very difficult to determine since the drop size distribution theoretically extends to infinitely large drops, the probability of which is zero. In order to achieve relatively consistent results, the value of d_{max} was taken to be equal to d_{95} , which represents the drop size below which 95% of the dispersed phase exists in the form drops with d less than or equal d_{95} . This approach is similar to that adopted by Hinze (1955) Sleicher (1962) and Karabelas (1978) in their analysis of drop dispersion.

The Kolmogorov-Hinze model and variations thereof, are commonly used to predict the maximum stable drop size that can exist in a turbulent flow. Its simplest form is given as,

$$d_{max} = C \sigma^{0.6} \epsilon^{-0.4} \rho_c^{-0.6} \quad (2-26)$$

Where σ is the equilibrium interfacial tension of the system, ρ_c is the density of the continuous phase and ϵ is the turbulent energy dissipation rate per unit mass. Hinze, in his analysis of drop dispersion in Couette flow field, obtained a value of 0.725 for the constant C .

Most of the experimental data obtained in this investigation were obtained using a single two-phase system in which the local energy dissipation rate was altered but the physical properties were not. In only 10 experiments were the interfacial characteristics changed through the addition of the surfactant Triton X100. These two factors will

therefore be treated separately in order to minimize statistical interference. In a fashion similar to that used in most MAT studies (Calabrese et al., 1986; Pacek et al., 1999, Seidshazileh, 1999), the average value of ε was calculated using the whole volume of the static mixer (Equation (3-2)). However, this approach was criticized in recent time as being non-representative of hydrodynamics in the region where most of the drop breakup takes place (McManamey, 1979; Davies, 1985; Pacek et al., 1999). Consequently, a similar approach was adopted in this situation based on the knowledge that more than 95% of the energy dissipation takes place in the first 2 mm downstream from the screen (section 4.1.1). The value of ε_{\max} is thus five times larger than the volumetric average ε .

Using Minitab 13 statistical software, the experimental data obtained at low dispersed-phase holdups (i.e., $\phi = 0.5\%$), high velocities (e.g., ≥ 0.70 m/s) and 9 mixing elements (18 points where turbulent dispersion dominates) were found to correlate well (see Figure 4.42) with Equation 2.26 yielding the following expressions for the maximum drop size based on the entire mixer volume and small volume behind the screen (2 mm) (only the energy dissipation exponent was varied; the other theoretically derived exponents were consequently assumed to apply) ($R = 0.955$ and 0.956 respectively),

$$d_{\max} = 1.66\sigma^{0.6} \varepsilon^{-0.53} \rho_c^{-0.6} \quad (4-22)$$

and

$$d_{\max} = 4.68\sigma^{0.6} \varepsilon_{\max}^{-0.53} \rho_c^{-0.6} \quad (4-23)$$

The values of the energy dissipation exponent and constant C obtained in both correlations are significantly different from that predicted by the Kolmogorov-Hinze model (exponent of -0.40). This difference may have been caused mainly by the existence of two drop breakup mechanisms (drop cutting action and turbulent breakup). It is more likely that the larger drops undergo cutting or breakup by screen wires and to a lesser extent by turbulence. The above result is also in contradiction with other results reported in the literature. Sleicher (1962) reported that d_{\max} is proportional to the -0.83 power of energy dissipation rate, ε . Kubie and Gardener (1977) compared their results for the maximum drop size versus values calculated from Equation (2-26) and found an

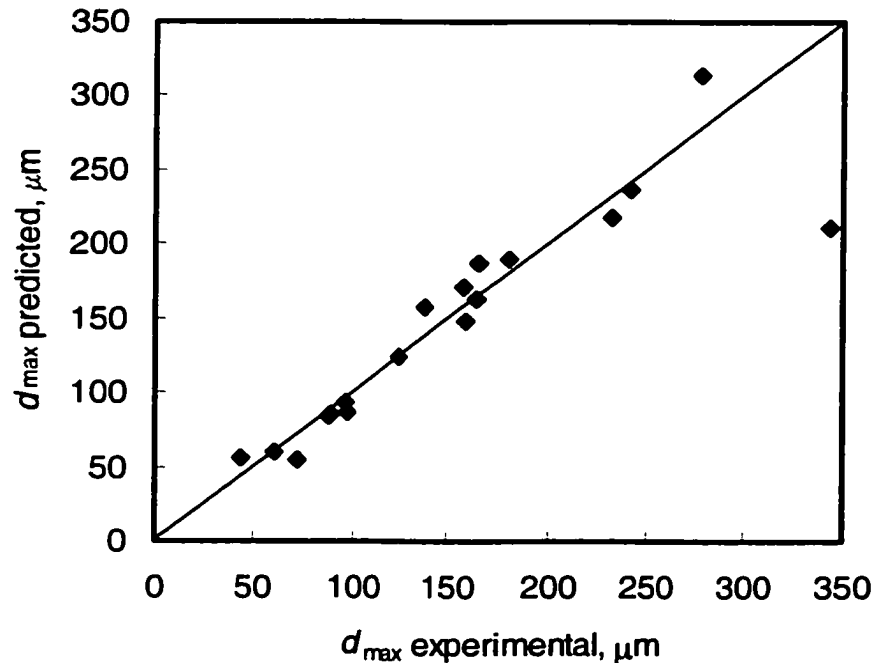


Figure 4.42. Comparison of predicted maximum drop size using Equation (4-22) with experimental values.

excellent agreement between the experimental and predicted values, concluding that there was no reason to alter the constant obtained by Hinze (1955). Similarly, Karabelas (1978) found out that Equation (2-26) could fit his experimental data of liquid-liquid dispersions. Hass (1987) obtained a value of 1.2 for the constant C . Angeli and Hewitt (2000) found that experimental data of low holdup liquid-liquid dispersions from a steel pipe show good agreement with the predictions of Kolomogrov-Hinze model. Recently, Simmons and Azzopardi (2001) also showed that low concentration data produced from a plastic pipe agree with Kolomogrov-Hinze model.

The values of the energy dissipation rate exponent obtained in case of d_{max} (-0.53) and d_{32} (-0.42) under conditions of turbulent breakup using 0.5% holdup dispersions are significantly different from each other. This difference may be attributed to the fact that larger drops are relatively more vulnerable to breakup and d_{32} is not very sensitive to the presence of the larger drops. The above findings thus raise a question about the validity of the recommendation made by McManamey (1979) that the maximum drop size and

the Sauter mean diameter are related to each other, and thus, the maximum drop diameter can be replaced by the Sauter mean diameter, which is much easier to determine experimentally, in Equation (2-26). Although, the above mentioned approach was accepted by many investigators (Collins and Knudsen, 1970; Kubie and Gardner, 1977; Karabelas, 1978; Molag et al., 1980; Tavlarides and Stamatoudis, 1981; Lee et al., 1983; Borwankar, 1986; Hass, 1987; Clark, 1988, Berkman and Calabrese, 1988; Al Taweel and Chen, 1996; Pacek et al., 1999). In the case of mechanically agitated tanks, values of the exponent b varying between -0.40 to -0.80 were recently reported by Pacek et al. (1999). Different impellers yield different b values. It was suggested that low-power number impellers might cause drop breakup by mechanisms different from those found with high power number impellers.

In order to determine the dependence of d_{\max} on equilibrium interfacial tension, a linear regression was performed on the experimental data obtained in presence of surfactant at low dispersed-phase holdups (i.e., 0.5%), superficial velocity of 0.70 m/s and 9 mixing elements. Only the exponent of the interfacial tension was varied, the energy dissipation exponent determined in Equation (4-22) was assumed to apply. An exponent value of 0.37 ($R = 0.956$) was obtained, which is different from the theoretical value of 0.6. As mentioned in section 4.2, this difference may be attributed to the preferential facilitation of the larger drops breakup by the surfactant as suggested in section 4.2.5.

The measured maximum drop diameters obtained in the present work were compared with the Kolmogorov-Hinze model (Equation (2-26)) under conditions of turbulent drop breakup and low dispersed phase holdup ($\phi = 0.5\%$). The result of this comparison is depicted in Figure 4.43. It can be seen that at low energy dissipation rates the Kolmogorov-Hinze model underpredicts the experimental values. This difference diminishes as the energy dissipation rate increases until a good agreement is achieved between the predicted and measured values at high energy dissipation rates. The significant difference between the measured and predicted values at lower energy dissipation rates may be attributed to the existence of two drop breakup mechanisms.

Meanwhile the agreement between the experimental and the predicted diameters at higher energy dissipation rates indicates that the turbulent drop breakup dominates under such conditions and the drop cutting action diminishes.

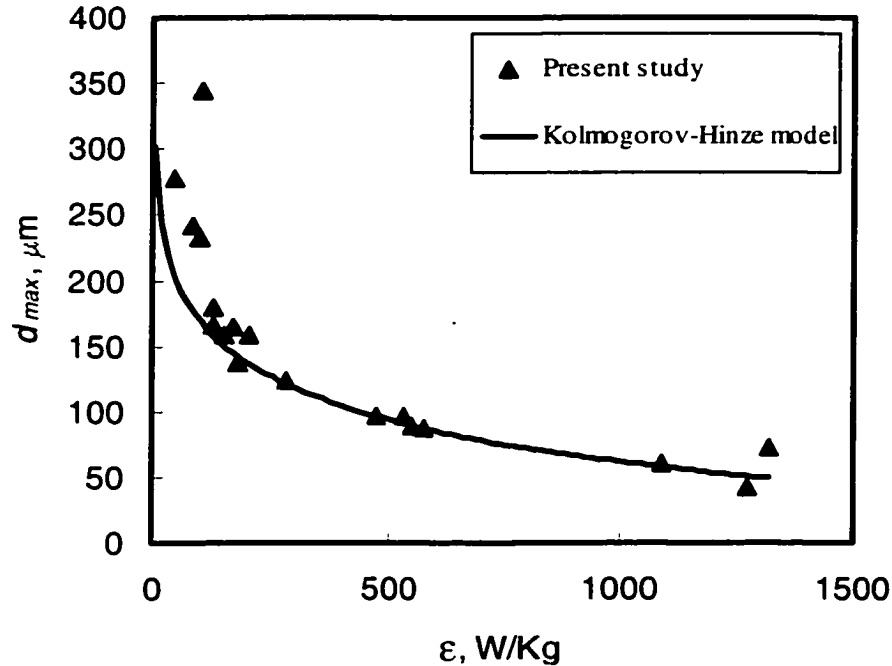


Figure 4.43. Comparison of predicted maximum drop size using Equation (2-26) with experimental values.

The effect of varying the number of screen elements on the value of d_{max} is shown in Figure 4.44. It clearly shows that the maximum drop sizes observed at low number of screens are larger than those predicted by Equation (4-22), with the difference decreasing as the number of mixing elements increases until they become almost equal after 15 screens. Equation (4-22) implies that drops whose size is larger than d_{max} will instantaneously disintegrate into smaller units; however the results shown in Figure 4.44 clearly show that the kinetics of drop breakup play a major role. This is an experimental proof that not all large drops passing through a region of high-energy dissipation rates will undergo breakage to a size smaller than that of d_{max} unless given enough residence time in that region. The concept of drop breakage efficiency has been proposed by

several investigators (Tavlarides and Stamatoudis, 1981; Laso et al., 1987; Skelland and Kanel., 1990) as a means for explaining deviations from theoretical predictions, these results of the present study may be the first direct experimental evidence of the existence of such a phenomenon. A preferential breakage of large drops takes place with increasing

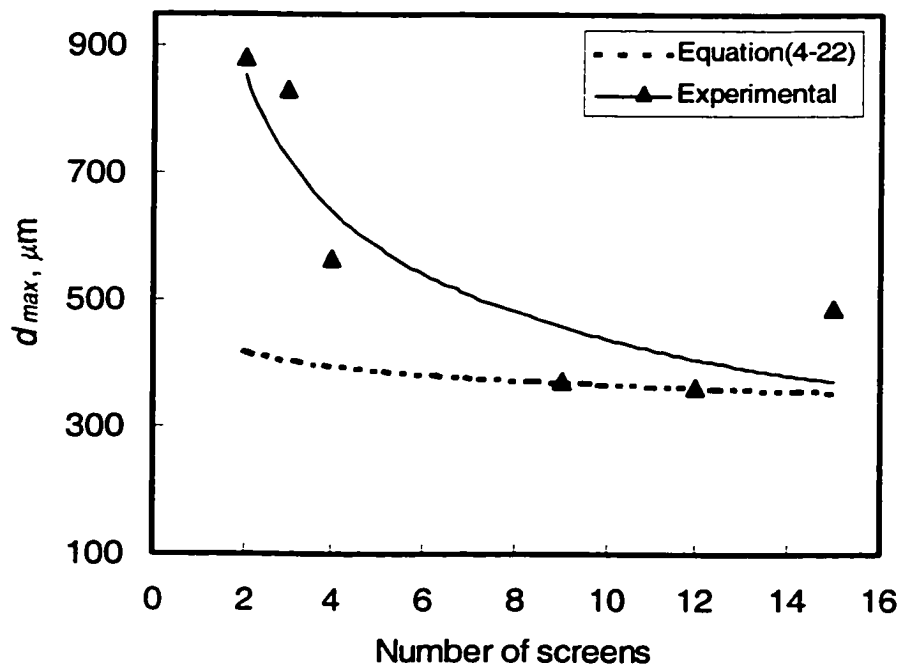


Figure 4.44. Effect of number of mixing elements on maximum stable drop size ($\alpha = 27\%$, $U = 0.40$ m/s, $\phi = 2\%$, $L = 5$ mm)

residence time, with the consequent reduction in the value of d_{max} . Taking deviations from the theoretical value of d_{max} as an indicator, drop breakup efficiency was found to increase with increasing residence time. In their analysis of liquid-liquid dispersions in a Kenics mixer Berkman and Calabrese (1988) suggested that drops slightly larger than d_{max} may not have sufficient time to break, which is in accordance with the present results.

The effect of dispersed phase holdup on d_{max} is presented in Figure 4.45. The results obtained clearly show that there is initially a large difference between the experimentally obtained maximum drop size and those predicted by Equation (4-22). As the dispersed phase concentration increases this difference lessens sharply, yielding a maximum drop size even smaller than the predicted value at a dispersed phase holdup of 3%. This is mainly caused by the prevalence of the drop cutting mechanism at the low superficial velocity used and at high dispersed phase holdups. These findings also suggest that the drop cutting mechanism is very efficient in utilizing the flow energy as is the turbulent breakage mechanism, particularly at high dispersed-phase holdups.

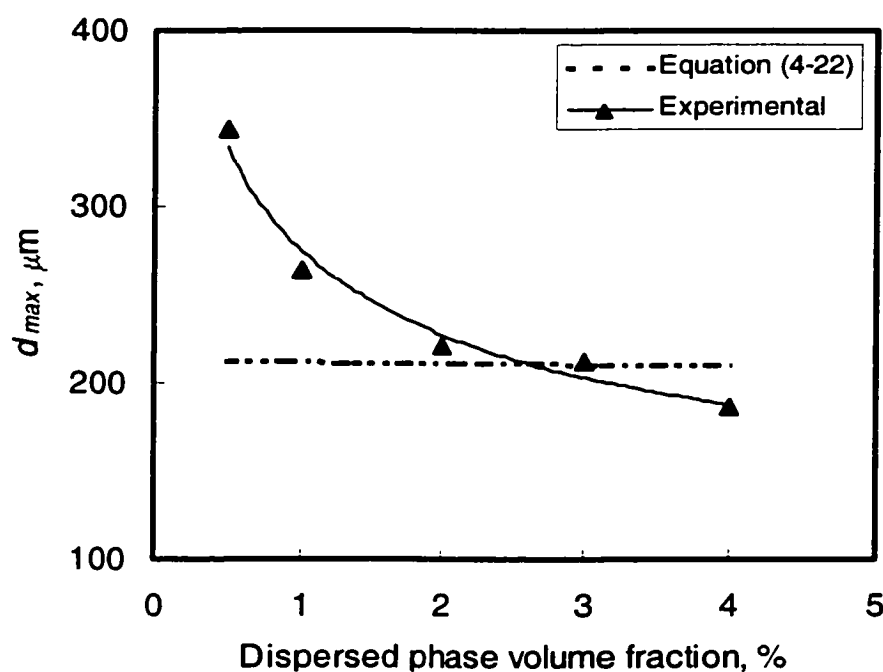


Figure 4.45. Effect of dispersed phase holdup on maximum stable drop size ($\alpha = 27\%$, $U = 0.70$ m/s, 9 screens, $L = 10$ mm)

4.4 DROP SIZE DISTRIBUTION

The mean drop diameters can not be used as the sole criterion to characterize liquid-liquid dispersions due to the fact that different dispersions might have equal mean diameters but significantly different drop size distributions. It is therefore necessary to

use both the mean drop diameters and the drop size distribution in order to fully characterize liquid-liquid dispersions. In the following sections, the drop size distributions (number density and volume density) generated by the screen-element static mixer are presented. The effect of the unit configuration (i.e., number of screens and screen open area), flow velocity, and dispersed phase volume fraction on the dispersion process is discussed. The effect of the system's static and dynamic interfacial characteristics is also analyzed.

4.4.1 Drop Number Density Distribution

Effect of the Superficial Velocity

Knowledge concerning how drop size distribution and how it is affected by turbulence characteristics is of prime importance in the attempt to understand the fundamentals of dispersion processes and their implications to various industrial operations. In this investigation, Bayol oil-in-water systems (having a dispersed phase holdup of 0.5% and 4%) were dispersed using nine consecutive woven screens placed 10 mm apart. In the case of 0.5% holdup, screens with 27, 33, and 41% open area, were used whereas screens with 27 and 41% were used in the case of 4% holdup. The effect of superficial flow velocity (which affects the local energy dissipation rate) and dispersed phase holdup on the normalized (d/d_{32}) drop size distributions is shown in Figures A1 to A47 in Appendix A but a few examples are given in Figures 4.46 to 4.57. Non-normalized data is available in the attached file.

The normalized drop number density distributions generated by the different screens tested varies with the superficial velocity in the following fashion:

At low holdups (i.e., 0.5%) and a velocity of 0.3 m/s, screens with 41 and 27% open area generate bimodal distributions skewed to the right (Figures 4.46 and 4.49). This bi-modality is more pronounced in case of screens with 41% open area. This is probably due to the lower jet velocities produced in the case of the 41% screen, which is expected to result in lower turbulent breakage rates. As the velocity is increased, the large drops are preferentially broken by the enhanced turbulence intensity resulting in

shrinking of the large diameter peak. As the velocity increases further, the larger drops undergo more breakage and the second peak becomes more pronounced and shifted towards smaller drop sizes. Then the superficial velocity reaches a value at which the small drops undergo coalescence while the large diameter side undergoes breakage due to the enhanced turbulence intensity. As a result, both sides shrink and a uni-modal and relatively narrower distribution is produced (Figures 4.47, 4.48, 4.50 and 4.51). In case of screens with 33% open area (mesh size 0.21 mm), the drop size distribution generated at superficial velocity of 0.3 m/s exhibits bi-modality but less pronounced than that showed by both 41% and 27% open area screens (with mesh sizes 0.55 and 0.54 mm respectively). This difference may mainly be attributed to the significant contribution of the drop cutting into the dispersion process as a result of the lower mesh size. As shown in Figures 4.52 to 4.54, the drop size distribution varies in a similar fashion to that shown by the 41% and 27% open area screens as the velocity increases.

At a high holdup (i.e., 4%) and a velocity of 0.3 m/s, the drop size distribution generated by screens with 41 and 27% open area has a high peak on the small diameter side and a long tail on the large drops side (skewed to the right) (Figure 4.55). Similarly, as in low holdup dispersions, as the velocity increases (Figures 4.56 and 4.57) the large drops are broken by the enhanced cutting action, which dominates at higher holdups and to a lesser extent by turbulence, while the smaller drops coalesce due to the increased drop collision frequency. The peak therefore shifts to smaller drop values. As the velocity increases further, both processes (i.e. the drop breakup and coalescence) are enhanced; the larger drops undergo more breakage while the smaller ones coalesce. This results in further shifting of the peak to slightly lower drop sizes with relatively narrower drop size distribution being formed.

The low holdup findings of the present study are in agreement with those previously reported by other investigators. For example, Middleman (1974) observed bi-modality in dilute dispersions in a Kenics static mixer while Ward and Knudsen (1967) observed double-peaked drop size distributions for dispersions flowing through pipes. Bi-modality was also encountered in most investigations conducted using MAT (Chen and

Middleman 1967; Hong and Lee, 1983; Laso et al., 1987). Chatzi et al. (1991) obtained bi-modal distributions and they reported that increasing the impeller speed results in shifting both peaks to smaller drop diameters, which is in disagreement with the results of the present study where the bimodality disappeared at high superficial velocities. They suggested that higher turbulence intensities are more effective in drop breakup. Zhou and Kresta (1997) investigated the formation of liquid dispersions at very low holdup ($\phi = 0.03\%$) in stirred tanks and reported the formation of bi-modal distributions that are skewed to the right at low rotational speeds. As the rotational speed was increased, the bimodality gradually disappeared and, eventually, the distributions changed to uni-modal ones at very high speeds. Similarly, Pacek et al. (1998) observed the formation of bi-modal drop number density distributions at low impeller speeds and low dispersed phase holdup ($\phi = 1\%$). This bi-modality lessens as, both, the rotational speed and dispersed phase concentration increase and the distribution becomes uni-modal at high speeds and high holdups, which is in agreement with the present findings.

The results obtained for the 4% holdup dispersions in the present investigation are in agreement with the findings of Pacek et al. (1998) who did not observe bi-modality in drop size distributions at high holdups. On the other hand, the present results contradict other investigations reported in the literature. For example, Brown and Pitt (1972) observed bi-modality in the distributions of a high holdup ($\phi = 0.20$) kerosene-water dispersion stirred by Rushton turbines. They reported that the rotational speed has no effect on the generated distribution. Nishikawa et al (1987) reported that the drop number distribution in liquid-liquid dispersions in agitated vessels ($\phi = 0.005$ to 0.3) could be represented by a combination of two normal distributions. The generation of bi-modal drop size distributions in mechanically agitated tanks may be attributed to the relatively complex hydrodynamics prevalent in such mixing devices and the fact that the two-phase liquid recirculating streams do not entirely flow through the high energy dissipation region.

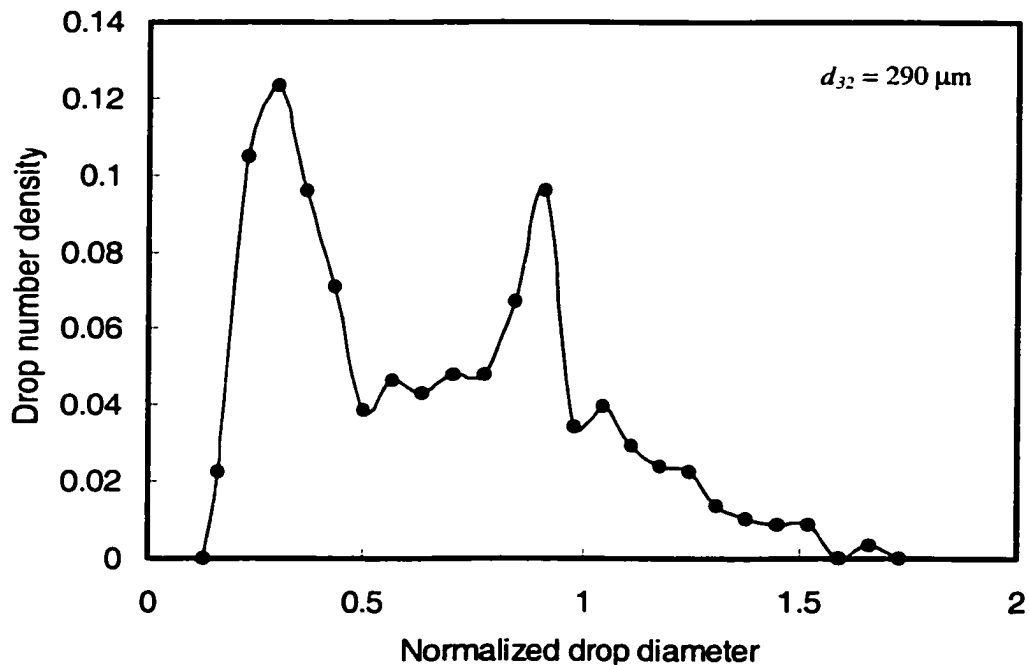


Figure 4.46. Drop number density distribution
 ($\alpha = 41\%$, $\phi = 0.5\%$, $U = 0.30$ m/s, 9 screens, $L = 10$ mm).

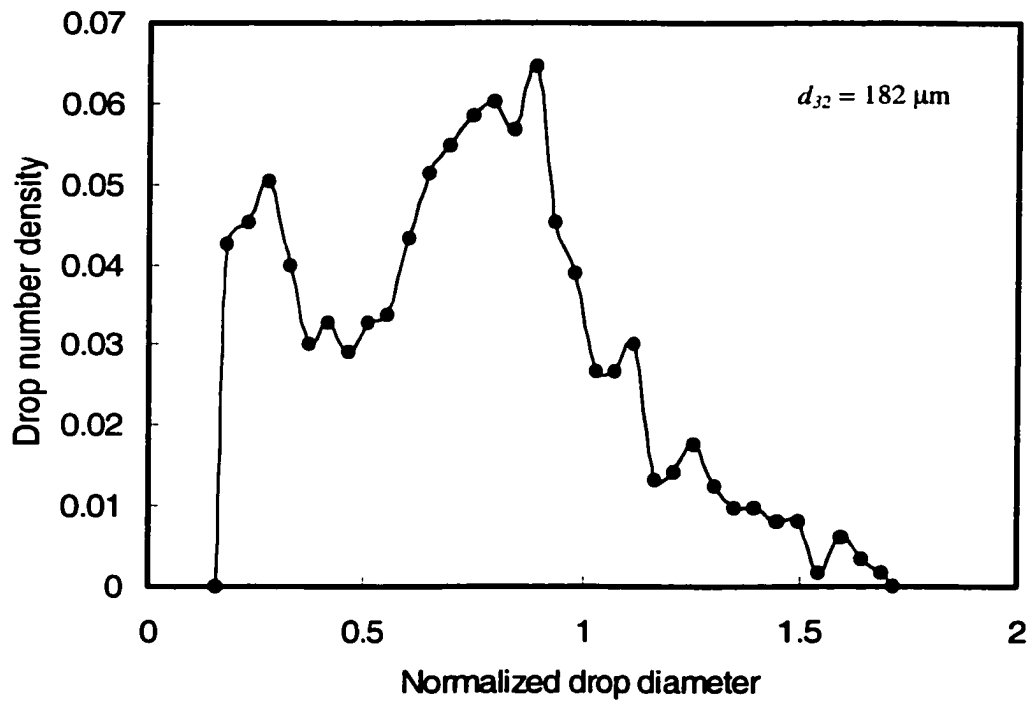


Figure 4.47. Drop number density distribution
 ($\alpha = 41\%$, $\phi = 0.5\%$, $U = 0.85$ m/s, 9 screens, $L = 10$ mm).

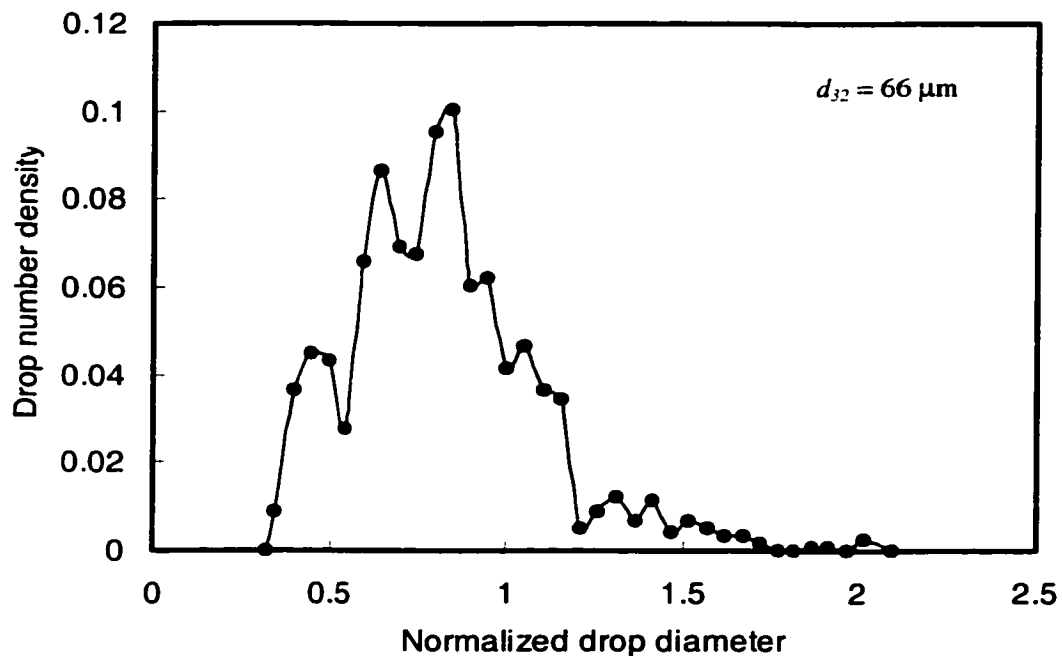


Figure 4.48. Drop number density distribution ($\alpha = 41\%$, $\phi = 0.5\%$, $U = 1.94 \text{ m/s}$, 9 screens, $L = 10 \text{ mm}$).

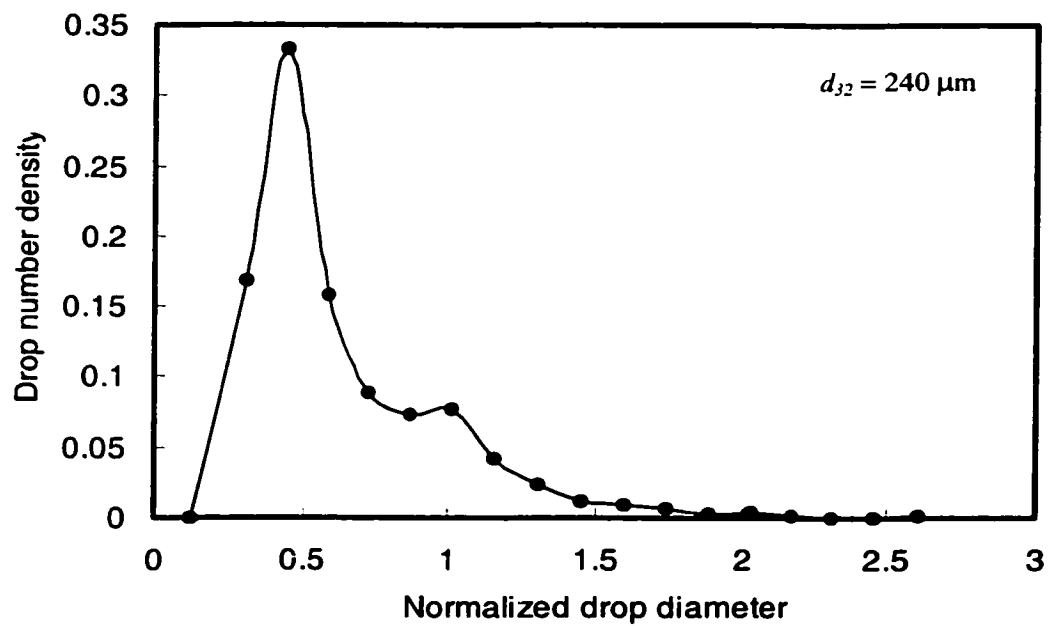


Figure 4.49. Drop number density distribution ($\alpha = 27\%$, $\phi = 0.5\%$, $U = 0.30 \text{ m/s}$, 9 screens, $L = 10 \text{ mm}$).

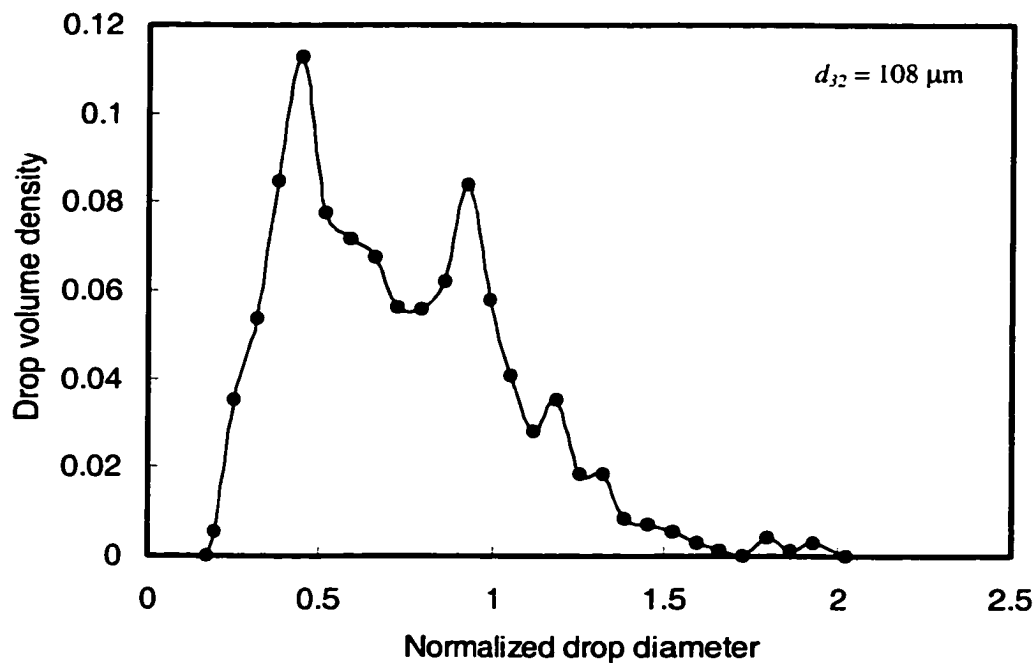


Figure 4.50. Drop number density distribution
 ($\alpha = 27\%$, $\phi = 0.5\%$, $U = 0.90$ m/s, 9 screens, $L = 10$ mm).

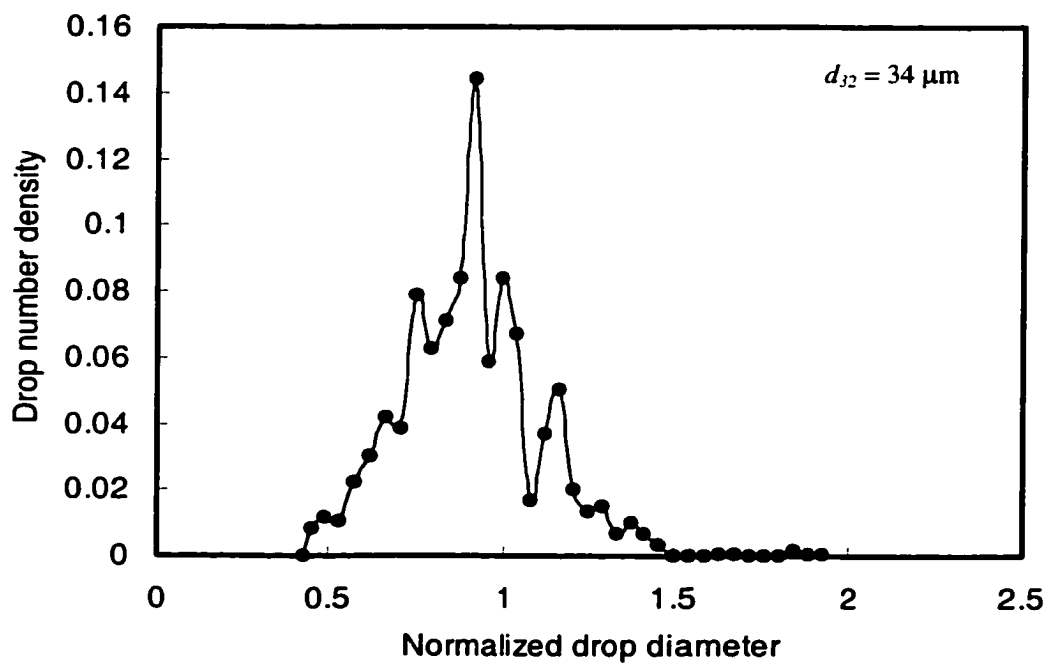


Figure 4.51. Drop number density distribution
 ($\alpha = 27\%$, $\phi = 0.5\%$, $U = 1.94$ m/s, 9 screens, $L = 10$ mm).

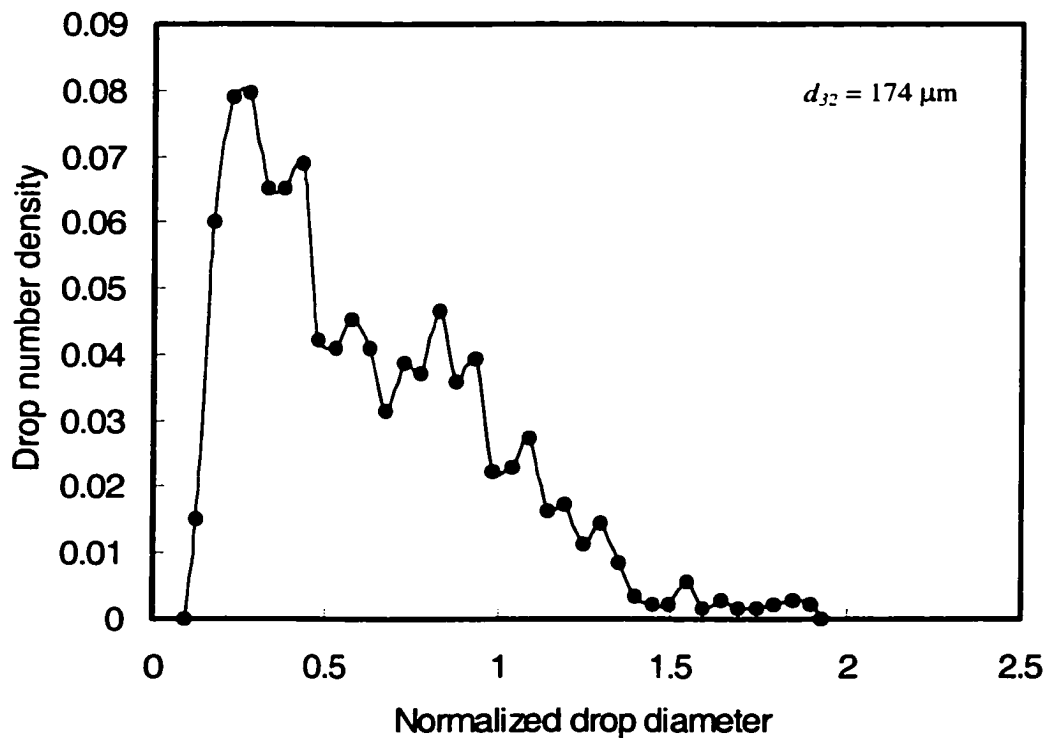


Figure 4.52. Drop number density distribution
 ($\alpha = 33\%$, $\phi = 0.5\%$, $U = 0.30$ m/s, 9 screens, $L = 10$ mm).

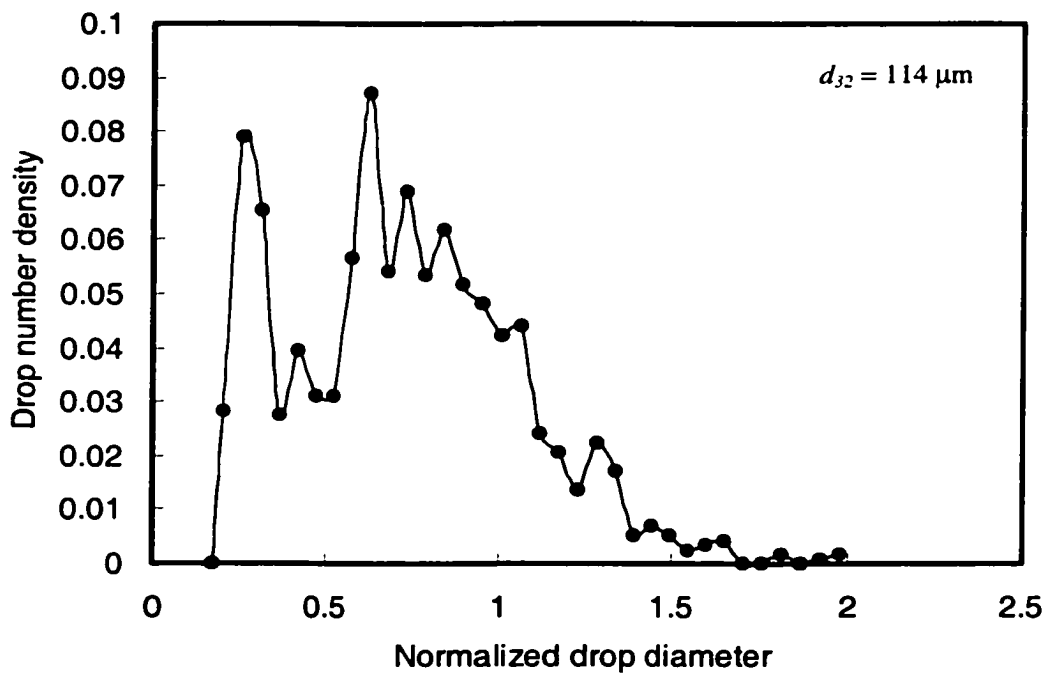


Figure 4.53. Drop number density distribution
 ($\alpha = 33\%$, $\phi = 0.5\%$, $U = 0.85$ m/s, 9 screens, $L = 10$ mm).

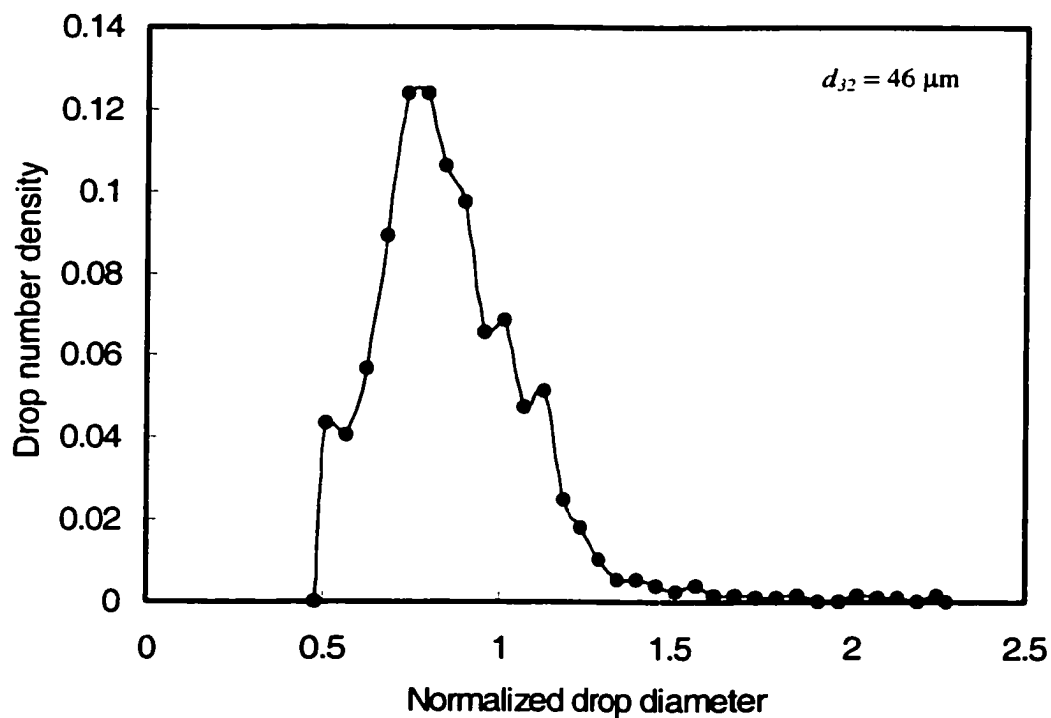


Figure 4.54. Drop number density distribution
 ($\alpha = 33\%$, $\phi = 0.5\%$, $U = 1.94 \text{ m/s}$, 9 screens, $L = 10 \text{ mm}$).

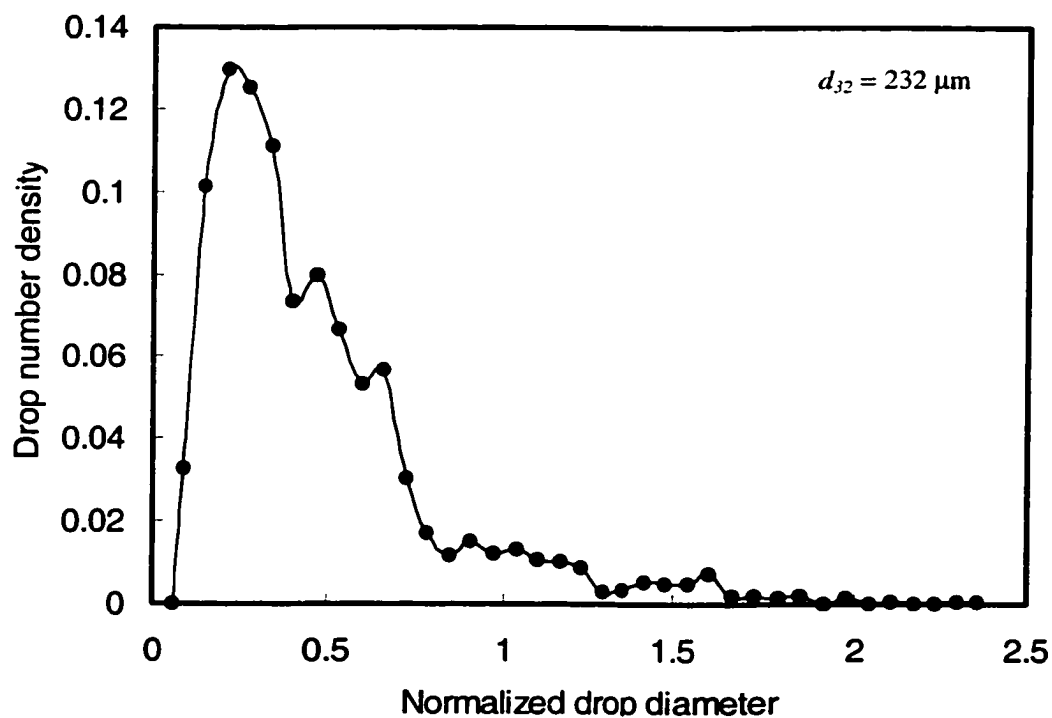


Figure 4.55. Drop number density distribution
 ($\alpha = 27\%$, $\phi = 4\%$, $U = 0.30 \text{ m/s}$, 9 screens, $L = 10 \text{ mm}$).

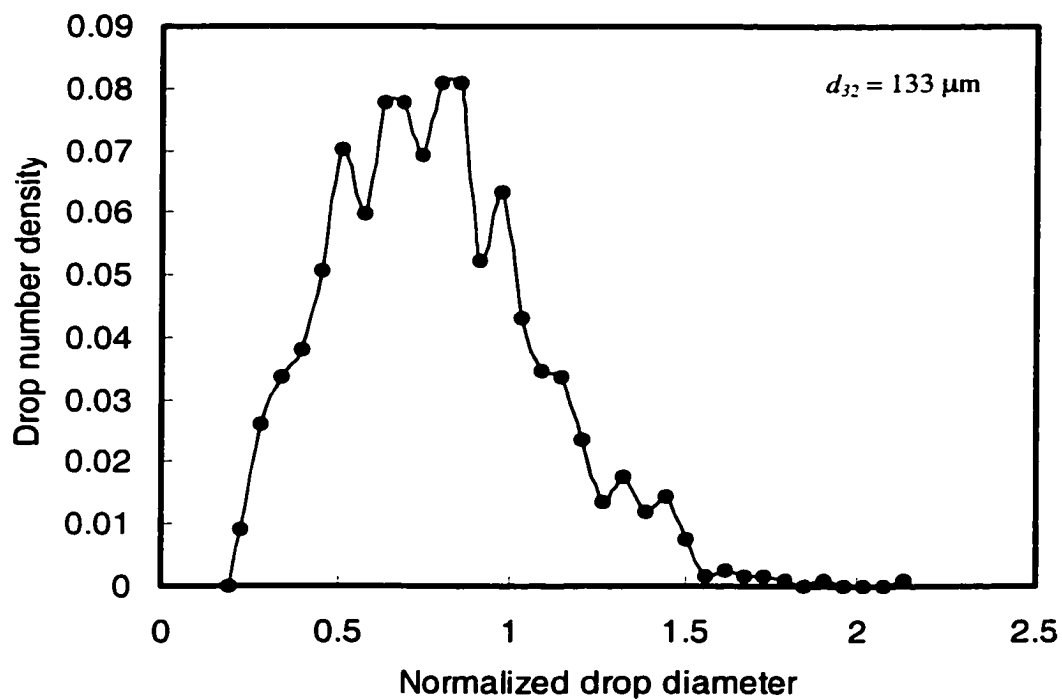


Figure 4.56. Drop number density distribution
 ($\alpha = 27\%$, $\phi = 4\%$, $U = 0.70 \text{ m/s}$, 9 screens, $L = 10 \text{ mm}$).

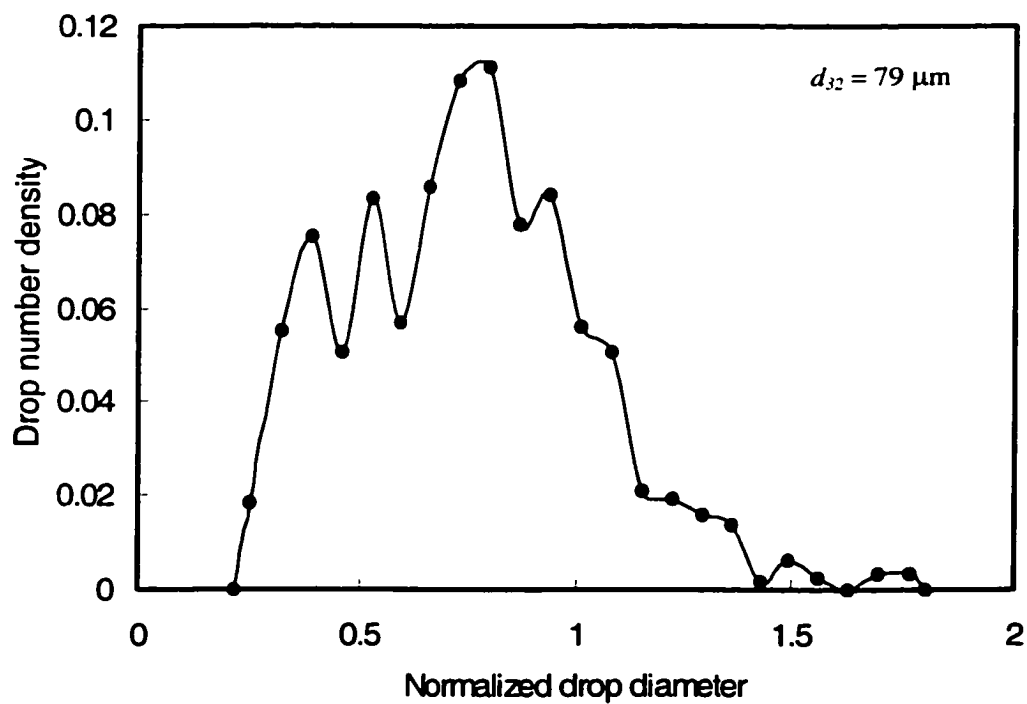


Figure 4.57. Drop number density distribution
 ($\alpha = 27\%$, $\phi = 4\%$, $U = 1.55 \text{ m/s}$, 9 screens, $L = 10 \text{ mm}$).

Effect of the Dispersed Phase Volume Fraction (Holdup)

The dispersed phase holdup is one of the major factors affecting drop breakage/coalescence and, eventually, the equilibrium drop size distribution. As the holdup increases, the density of the drops in the continuous phase increases thereby promoting drop collision frequency, which, in turn, increases turbulent coalescence rate. However, as mentioned in section 4.2.4, the drop cutting action, which appears to play a relatively major role in the case of screen-type static mixing elements, appears to play a role that increases in significance with increasing dispersed phase holdup. Figures A48 to A59 in Appendix A show the variation of the number density distribution with the dispersed phase holdup.

Figures 4.58 to 4.63 show the drop size distribution at different holdups using 41 and 27% open area screens. At a superficial velocity of 0.40 m/s and holdup of 0.5%, the 41% open area screens generate bi-modal skewed to the right drop size distributions characterized with a high peak on the smaller diameter side and a relatively much smaller peak corresponding to larger drop size (Figures 4.58). As the holdup increases, the smaller peak shrinks gradually with the increasing dispersed phase concentration as a result of the proposed drop cutting action until a uni-modal distribution skewed to the right with relatively long tail is formed at high holdups. The peak on the smaller drop size does not change position significantly but it becomes higher as a result of the breakage of the larger drops. The 27% open area screen shows similar behavior.

Similarly, at a superficial velocity of 0.7 m/s and low holdup, the 27% open area screens generate distributions that are skewed to the right and exhibit bimodality. The bimodality is more pronounced in the case of 41% open area screen (Figure 4.61), possibly due to the relatively lower jet velocities (U/α) produced. This bimodality is also more pronounced than that at 0.40 m/s and lessens as the holdup increases due to the drop cutting of the larger drops, which is expected to become more significant at higher dispersed phase holdups (Figures 4.62 and 4.63). At the same time the peak on the small diameter side shrinks gradually due to the increased coalescence of the smaller drops with the increased holdup while the second peak grows bigger continually but does not

change its position significantly. At a superficial velocity of 0.70 m/s, the higher turbulence intensities obtained promote drop collision and hence drop coalescence. This eventually leads to the generation of a relatively narrower uni-modal distribution at high holdups. Dispersions generated by the 41% open area screen at 0.70 m/s varies in a similar fashion with the increased dispersed phase holdup.

The above results are in agreement with Pacek et al. (1998) who observed the disappearance of bi-modality in liquid-liquid dispersions as the dispersed phase concentration increases, On the contrary, Brown and Pitt (1972) observed the persistence of bi-modality at high holdup dispersions stirred by Rushton turbines with increasing impeller speed. They suggested that the system is a non-coalescing one and that the breakup process occurs in an orderly manner removing small random sized elements from drops, which are approaching the maximum stable size. Nishikawa et al. (1987), similarly reported the presence of bi-modality in drop number distributions in mechanically agitated vessels at low and high dispersed phase holdups ($\phi = 0.5\%$ to 30%). However, the bimodal drop size distributions reported by Collins and Knudsen (1970) upon the injection of different organics into tap water flowing through a pipe ($\phi = 0.6$ to 10%), is attributed to the presence of two drop breakage mechanisms each generating a separate drop size distribution. One of the distributions was generated by the injection nozzle while the other resulted from turbulent drop breakup in the pipe. This situation is very similar to that encountered in this investigation.

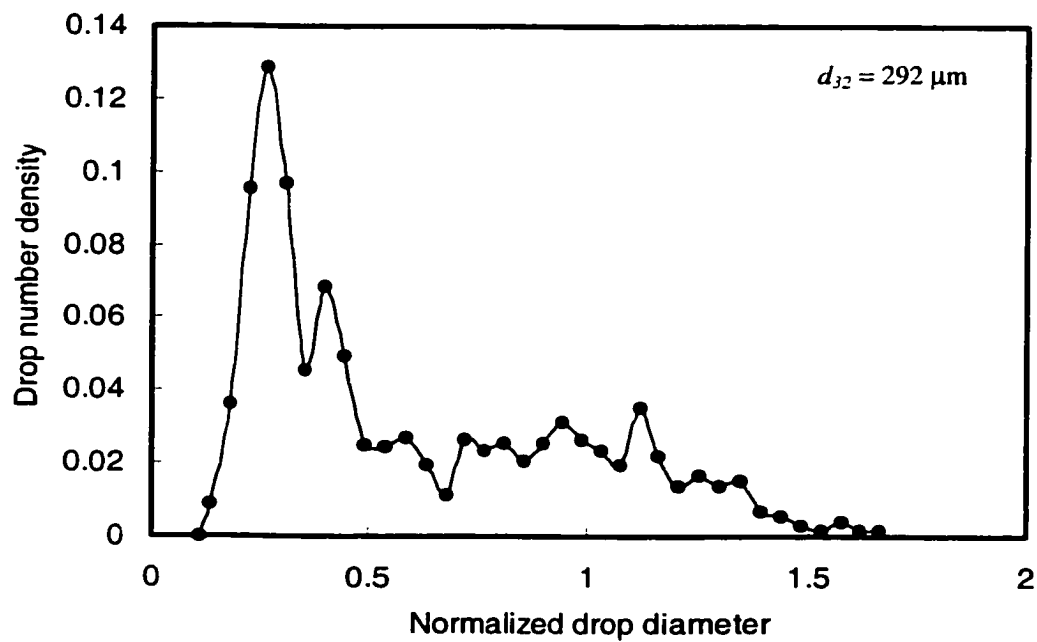


Figure 4.58. Drop number density distribution
 ($\alpha = 41\%$, $\phi = 0.5\%$, $U = 0.40 \text{ m/s}$, 9 screens, $L = 10 \text{ mm}$).

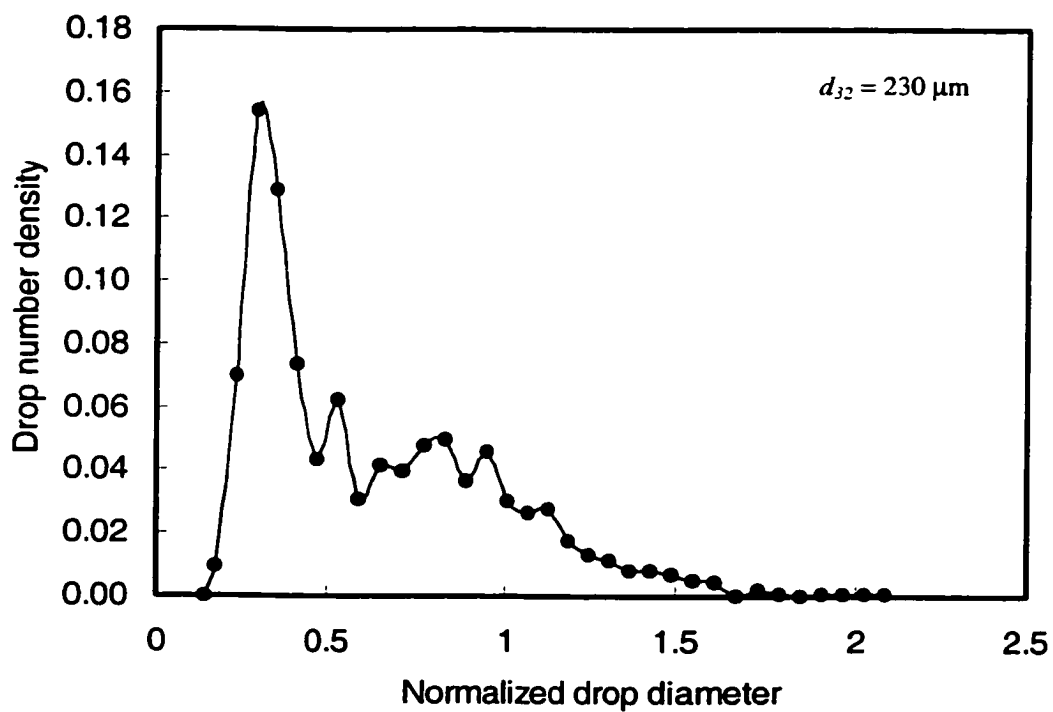


Figure 4.59. Drop number density distribution
 ($\alpha = 41\%$, $\phi = 2\%$, $U = 0.40 \text{ m/s}$, 9 screens, $L = 10 \text{ mm}$).

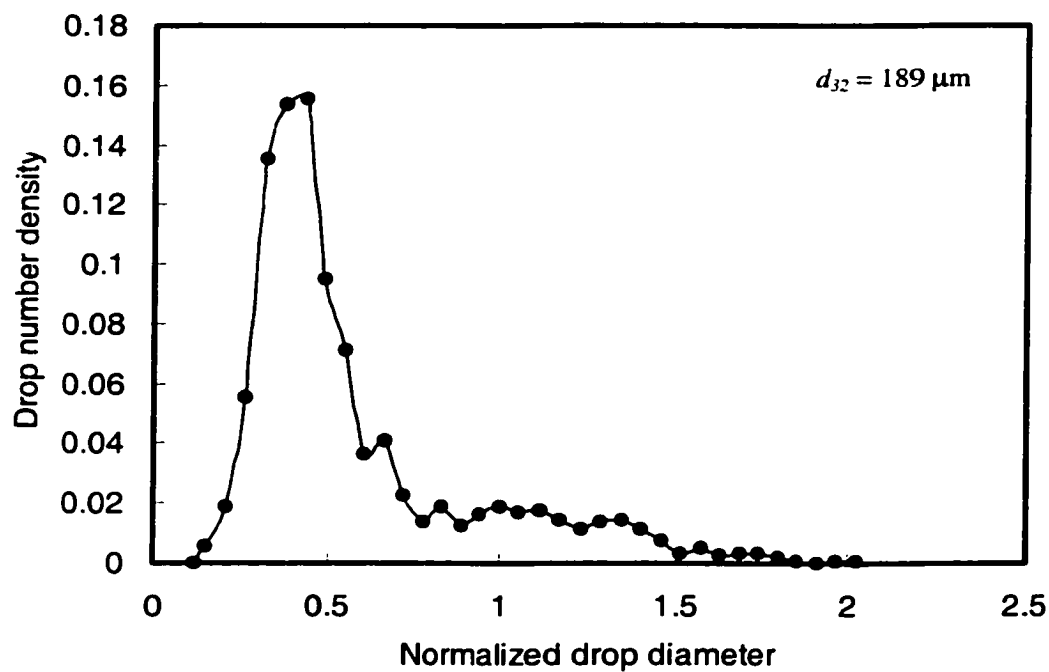


Figure 4.60. Drop number density distribution
 ($\alpha = 41\%$, $\phi = 4\%$, $U = 0.40$ m/s, 9 screens, $L = 10$ mm).

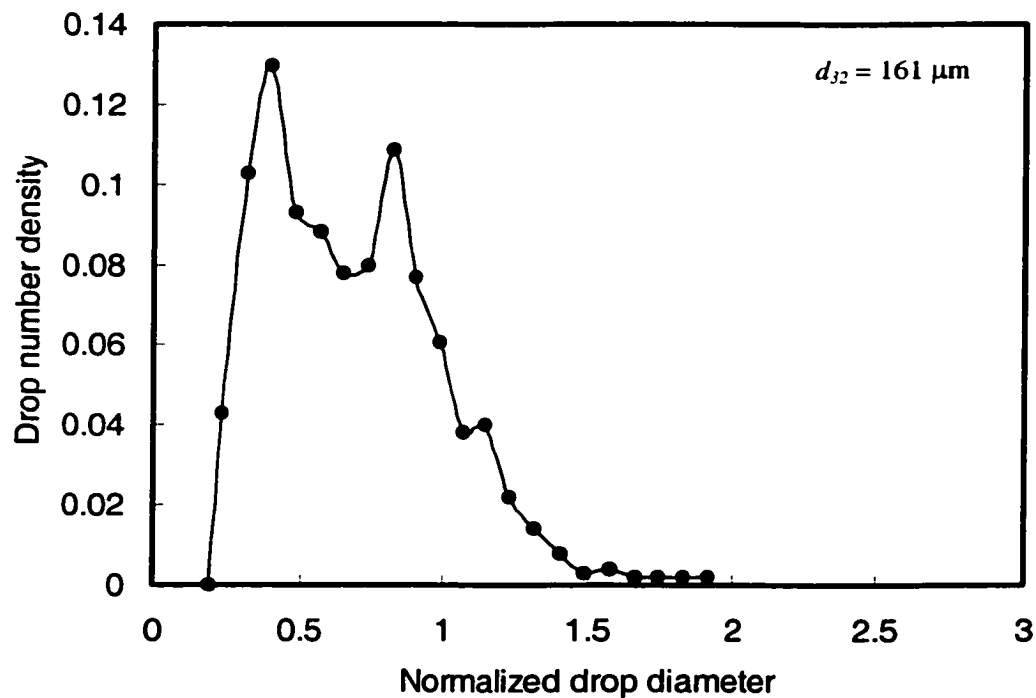


Figure 4.61. Drop number density distribution
 ($\alpha = 27\%$, $\phi = 0.5\%$, $U = 0.70$ m/s, 9 screens, $L = 10$ mm).

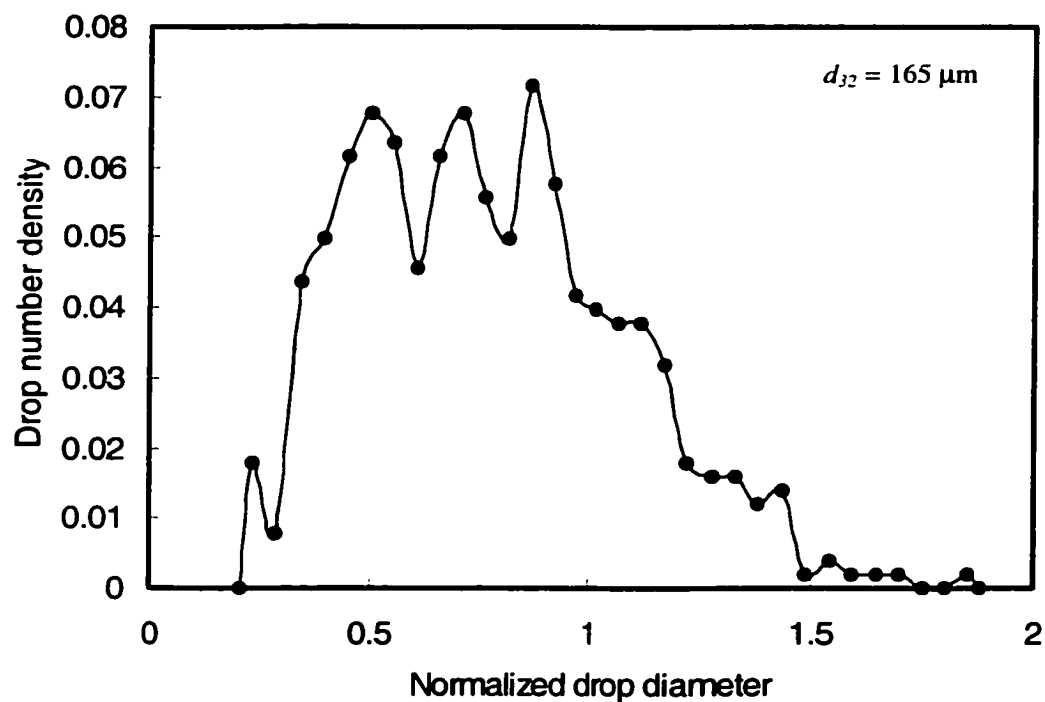


Figure 4.62. Drop number density distribution
 ($\alpha = 27\%$, $\phi = 2\%$, $U = 0.70 \text{ m/s}$, 9 screens, $L = 10 \text{ mm}$).

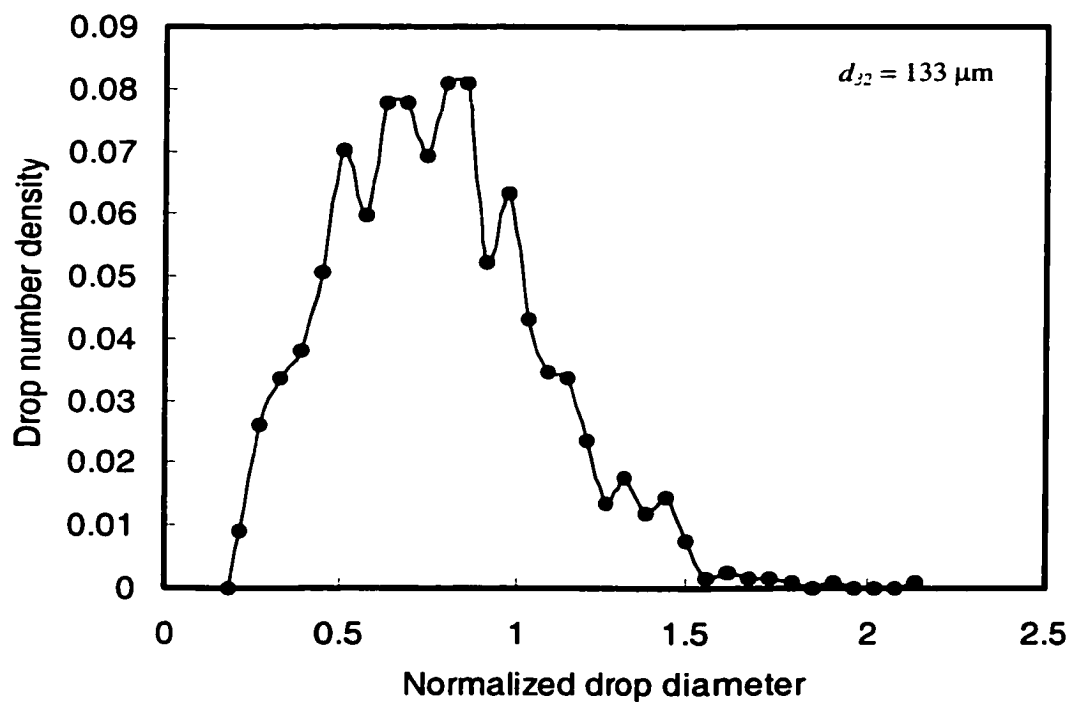


Figure 4.63. Drop number density distribution
 ($\alpha = 27\%$, $\phi = 4\%$, $U = 0.70 \text{ m/s}$, 9 screens, $L = 10 \text{ mm}$).

Effect of Number of Elements

As mentioned earlier in section 4.2.3 the number of mixing elements (i.e. residence time) plays an important role in the dispersion process. Drops remaining for longer periods in the high-energy dissipation region are more vulnerable to breakup. Figures A60 to A65 in Appendix A show the variation of the drop number density distribution with the number of mixing elements.

As shown in Figures 4.64 to 4.66, the drop size distribution changes drastically with increasing number of screens with this effect is more pronounced at low number of elements. It is clearly shown that a preferential breakage of large drops takes place with increasing number of mixing elements (residence time) until an equilibrium drop size distribution is achieved after 9 screens, which is in accordance with the effect of residence time on the average drop size (section 4.2.3). A unimodal distribution skewed to the right was obtained. These results reveal that not all large drops passing through screens or a region of high-energy dissipation rates undergo breakage unless given enough residence time in the mixer, which is in accordance with earlier findings (section 4.3) that drop breakup efficiency increases with increasing residence time. Since the turbulent drop breakup mechanism is insignificant under non-fully developed turbulent conditions and relatively high dispersed phase holdups ($U = 0.4$ m/s, $\phi = 2\%$), the results also suggest that the cutting action mechanism dominate under those conditions. Turbulent breakup may still take place in the jets (velocity of jet = U/α) formed behind the screens.

The above mentioned results are in agreement with the tendency of achieving more uniform drop size distributions with increasing energy dissipation rate in pipe flow as reported by Kubie and Gardener (1977) and Karabelas (1978). This also is in agreement with the findings of Streiff et al., (1997) in static mixers and those of Hong and Lee (1983) and Seidshazileh (1999) in stirred tanks, which all indicate obtaining of narrower drop size distributions as equilibrium conditions are approached.

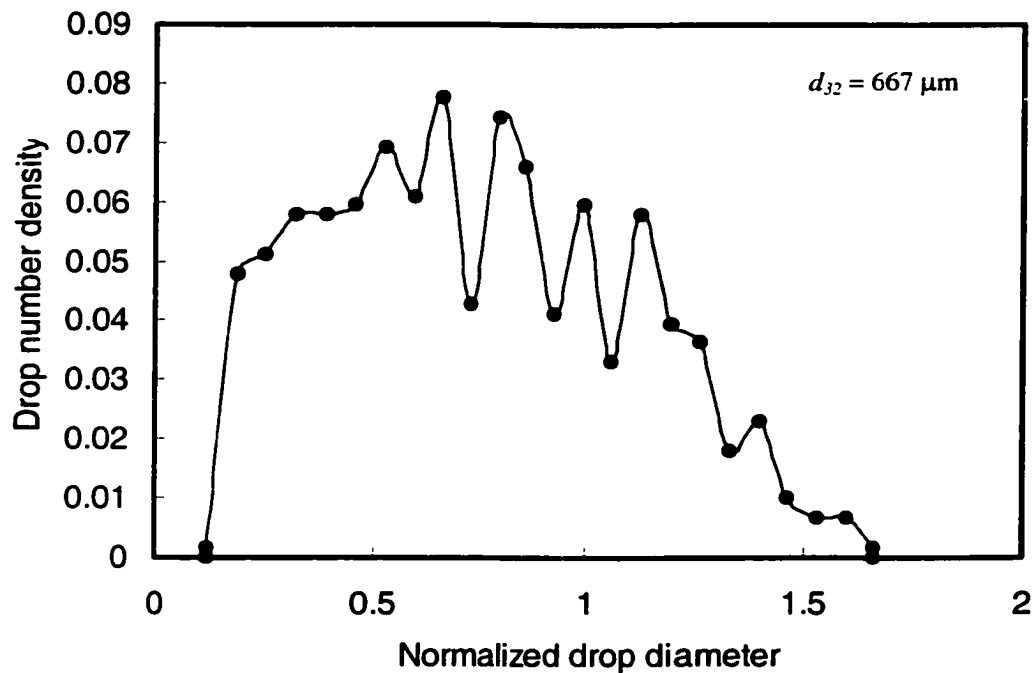


Figure 4.64. Drop number density distribution
 ($\alpha = 27\%$, $\phi = 2\%$, $U = 0.40 \text{ m/s}$, 2 screens, $L = 5 \text{ mm}$).

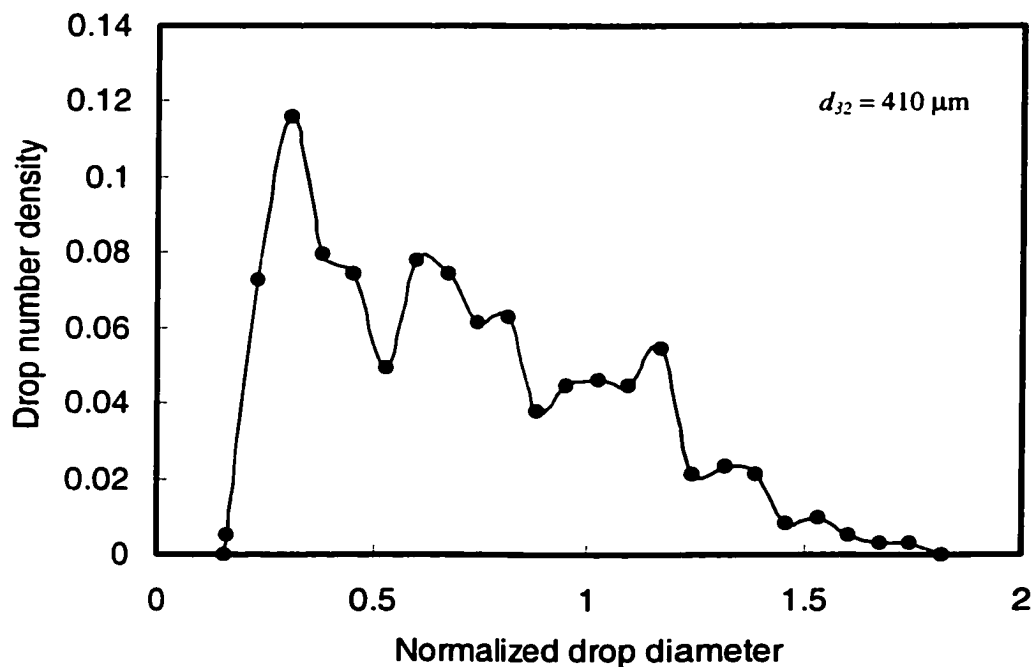


Figure 4.65. Drop number density distribution
 ($\alpha = 27\%$, $\phi = 2\%$, $U = 0.40 \text{ m/s}$, 4 screens, $L = 5 \text{ mm}$).

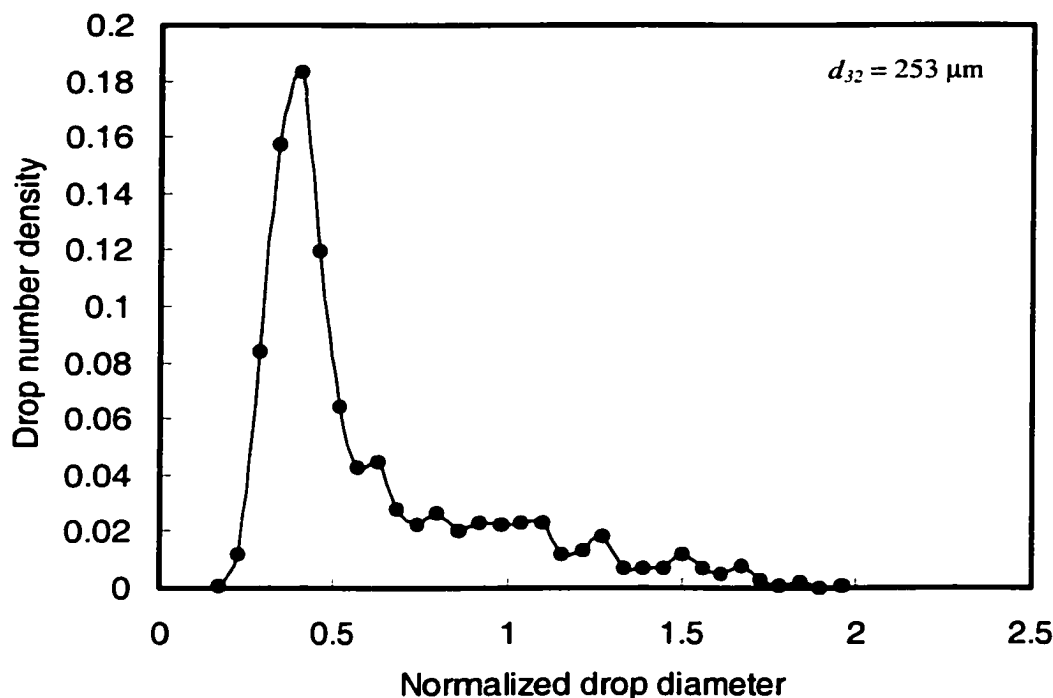


Figure 4.66. Drop number density distribution
 ($\alpha = 27\%$, $\phi = 2\%$, $U = 0.40$ m/s, 9 screens, $L = 5$ mm).

Effect of Surfactant

The presence of surface-active materials in liquid-liquid systems strongly influences the dispersion process; hence the drop size distribution, which is determined by the relative contributions of drop breakup and coalescence, is expected to be affected by the interfacial characteristics of the system as well. In this section, the effect of surfactant concentration (Triton X100) on the drop size distribution is discussed using the normalized drop number density distributions (Figures A66 to A75).

Compared to the shape of the drop size distributions obtained in the absence of surfactants (Figure 4.49), the presence of very small surfactant concentrations ($c = 0.01$ mole/m³) insignificantly alters the normalized distribution at low holdups (Figure 4.67). This suggests that although the presence of surfactants significantly affects both drop breakup and coalescence (through reduction of the interfacial tension and coalescence retardation), the relative influence on both appears to be equal at low concentrations. On the other hand, the peaks of the unimodal skewed normalized distributions were found to

move towards the center upon further increase in surfactant concentration (Figures 4.68 and 4.69). The normalized distribution at high surfactant concentrations are based on a much smaller mean drop diameter. These changes are caused by the preferential breakage of the larger drop size, thereby shifting the distribution towards smaller diameters and resulting in a relatively more symmetrical distribution. Since the drop cutting mechanism is insignificant at low holdups (section 4.2.4) these results suggest that the presence of surfactant facilitates the turbulent drop breakup to a greater extent. This confirmed by the results obtained at high holdups ($\phi = 4\%$) where the presence of surfactants was found to result in insignificant change in the shape of drop size distribution (Figures 4.70 to 4.72). The results obtained in this investigation are in line with those reported by various investigators (Wang and Calabrese, 1986; Lee et al., 1987; Rincon-Rubio et al., 1994; Seidshazileh, 1999). who found that the drop size distribution becomes narrower and more uniform as the interfacial tension is reduced.

Chatzi et al (1991) and Chatzi and Kiparissides (1995) obtained bi-modal distributions in the case of styrene-in-water dispersions containing poly vinyl alcohol as a stabilizer. This bimodal distribution was found to persist at various additive concentration and agitation intensities and is most probably caused by the interaction between coalescence retardation and the complex hydrodynamics present in MAT. However, Seidshazileh (1999) observed no bimodality in the number density distributions in the presence of different types of Triton surfactants. This anomaly may have been caused by less sensitive drop size measuring technique used in the latter investigation.

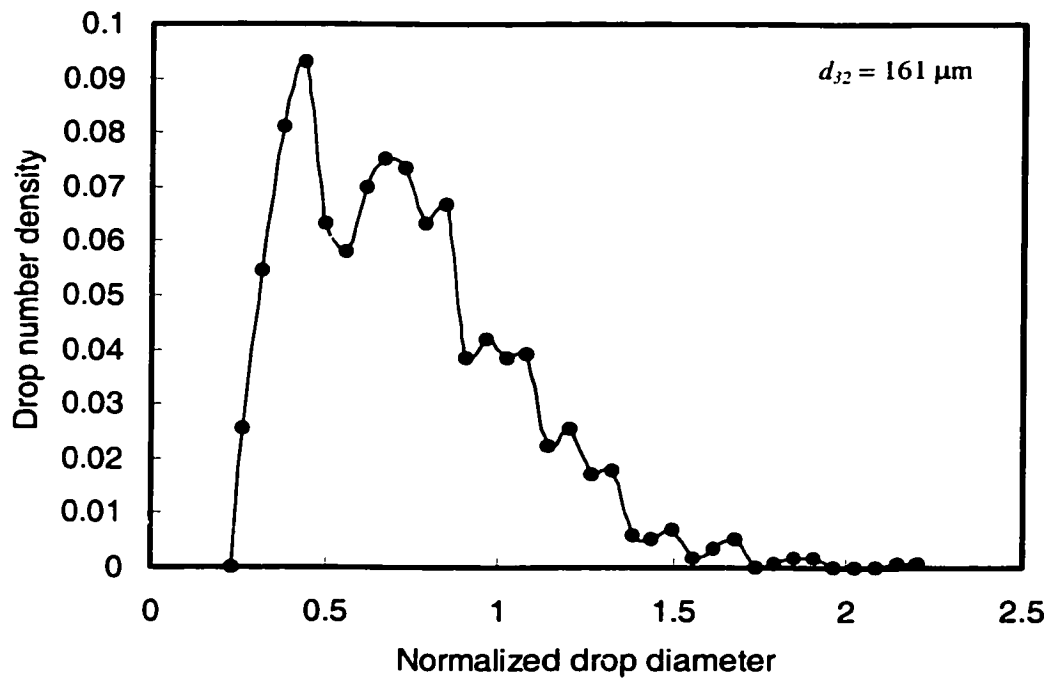


Figure 4.67. Drop number density distribution with SAA
 ($\alpha = 27\%$, $\phi = 0.5\%$, $U = 0.70 \text{ m/s}$, $c = 0.01 \text{ mole/m}^3$, 9 screens, $L = 10 \text{ mm}$)

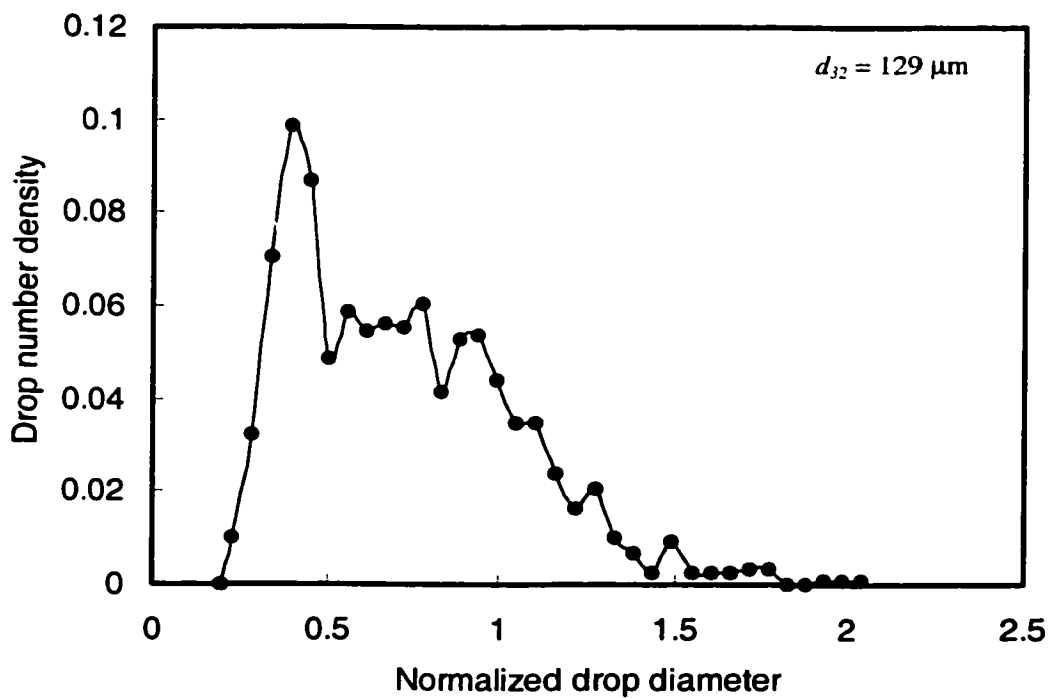


Figure 4.68. Drop number density distribution with SAA
 ($\alpha = 27\%$, $\phi = 0.5\%$, $U = 0.70 \text{ m/s}$, $c = 0.10 \text{ mole/m}^3$, 9 screens, $L = 10 \text{ mm}$).

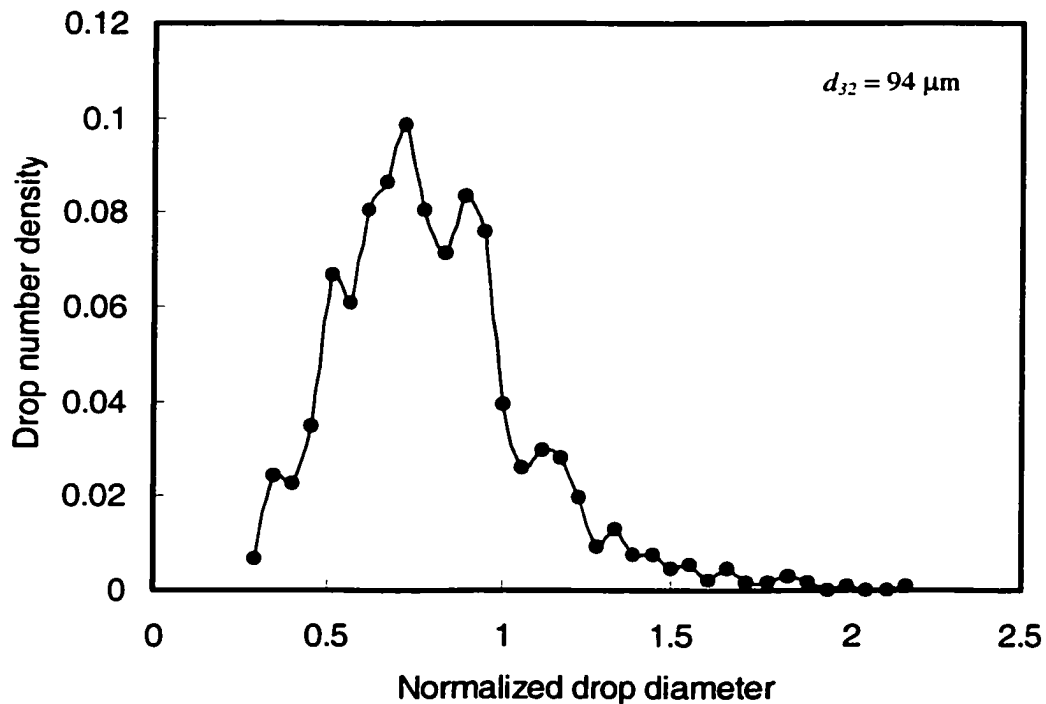


Figure 4.69. Drop number density distribution with SAA ($\alpha = 27\%$, $\phi = 0.5\%$, $U = 0.70$ m/s, $c = 0.30$ mole/m³, 9 screens, $L = 10$ mm).

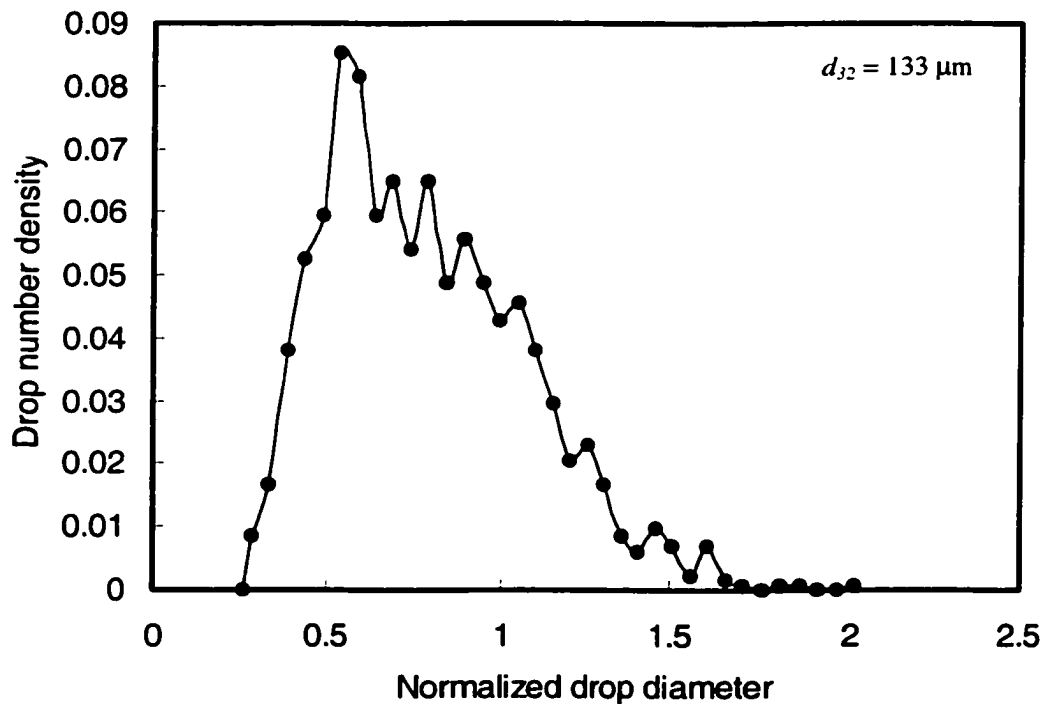


Figure 4.70. Drop number density distribution with SAA ($\alpha = 27\%$, $\phi = 4\%$, $U = 0.70$ m/s, $c = 0.01$ mole/m³, 9 screens, $L = 10$ mm).

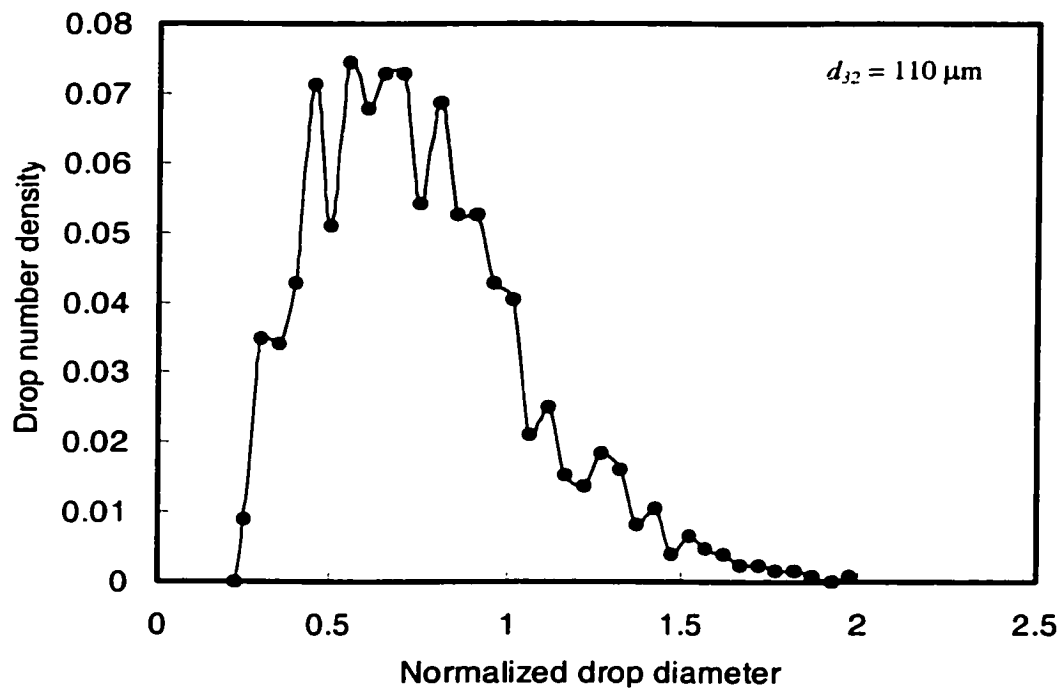


Figure 4.71. Drop number density distribution with SAA ($\alpha = 27\%$, $\phi = 4\%$, $U = 0.70 \text{ m/s}$, $c = 0.10 \text{ mole/m}^3$, 9 screens, $L = 10 \text{ mm}$).

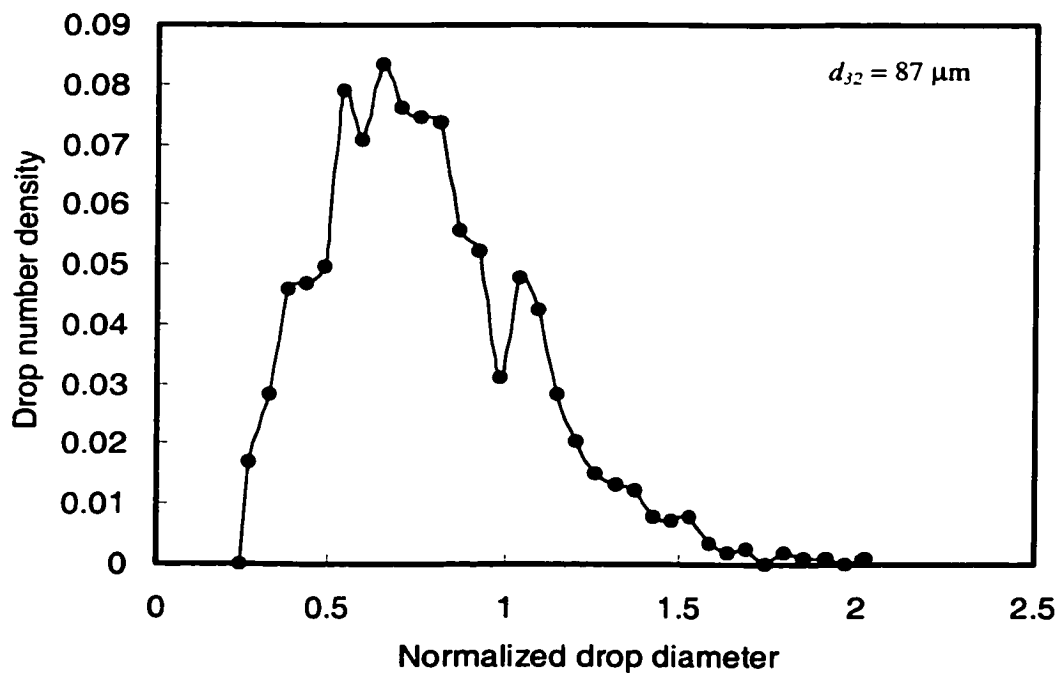


Figure 4.72. Drop number density distribution with SAA ($\alpha = 27\%$, $\phi = 4\%$, $U = 0.70 \text{ m/s}$, $c = 0.30 \text{ mole/m}^3$, 9 screens, $L = 10 \text{ mm}$).

4.4.2 Drop Volume Density Distribution

In contrary to the number density distribution, the volume density distribution gives a better idea about the contribution of the larger drops into the generated drop size distribution. Therefore, expressing the generated spectra of drop sizes in liquid-liquid dispersions as volume density distributions provides a more appropriate tool for understanding the ease of separation of the dispersed phase, inter-phase mass transfer, and hence chemical reaction rates and reaction selectivity.

The literature shows that very few investigators reported their experimental data as drop volume density distributions. Also, the researchers who discussed drop volume density distributions, most of them reported their results as cumulative volume density distributions. Pacek et al. (1998) attributed that to the ability of the cumulative distributions to smooth out detailed variations, which usually appear when the experimental data are plotted as density distributions.

In this section, the generated experimental data will be presented in the form of drop volume density distributions. The variation of the resultant distributions with the investigated parameters will be discussed briefly to avoid too much repetition. In general, as seen in Appendix B, the generated drop volume density distributions often show bimodality but to a lesser extent than that in number density distributions and they are skewed to the left towards the smaller drop sizes. Similarly, Chen and Middleman (1967) observed bi-modality in volume density distributions generated upon the dispersion of kerosene in water using a Kenics static mixer. Also Laso et al. (1987) and Seidshazileh (1999) observed bi-modality in liquid-liquid dispersions in stirred tanks following a step decrease in impeller speed. It was suggested that the existence of bimodality might be associated with transient conditions, which may be due to either changes in hydrodynamic conditions and/ or interfacial characteristics. (Tavlarides and Stamatoudis, 1981; Pacek et al., 1998; Seidshazileh, 1999).

Effect of Superficial Velocity

Figures B1 to B47 in Appendix B show the variation of the normalized drop volume density distribution with the superficial velocity for the tested screens. At low superficial velocities, a unimodal skewed to the left drop size distribution is generated (Figure 4.73). As the superficial velocity increases (Figures 4.73 and 4.74) the peak shifts to lower normalized drop sizes while larger drop size side shrinks gradually due to breakup of the larger drops and the simultaneous coalescence of the smaller drops as they move further into regions of the lower energy dissipation rates downstream of the screens. Finally, at sufficiently high superficial velocity, relatively narrower and more symmetrical unimodal distribution is generated.

The three tested screens show similar behavior except that drop cutting action is more pronounced in case of the 33% open area screen, which has a lower mesh size than the other two tested screens, particularly at lower superficial velocities as indicated by the more efficient removal of the larger drops. The same trends were shown at both holdups ($\phi = 0.5$ and 4%) tested at different superficial velocities with a difference that drop cutting action is dominating at the higher holdup as indicated by the more breakup the larger drops undergo.

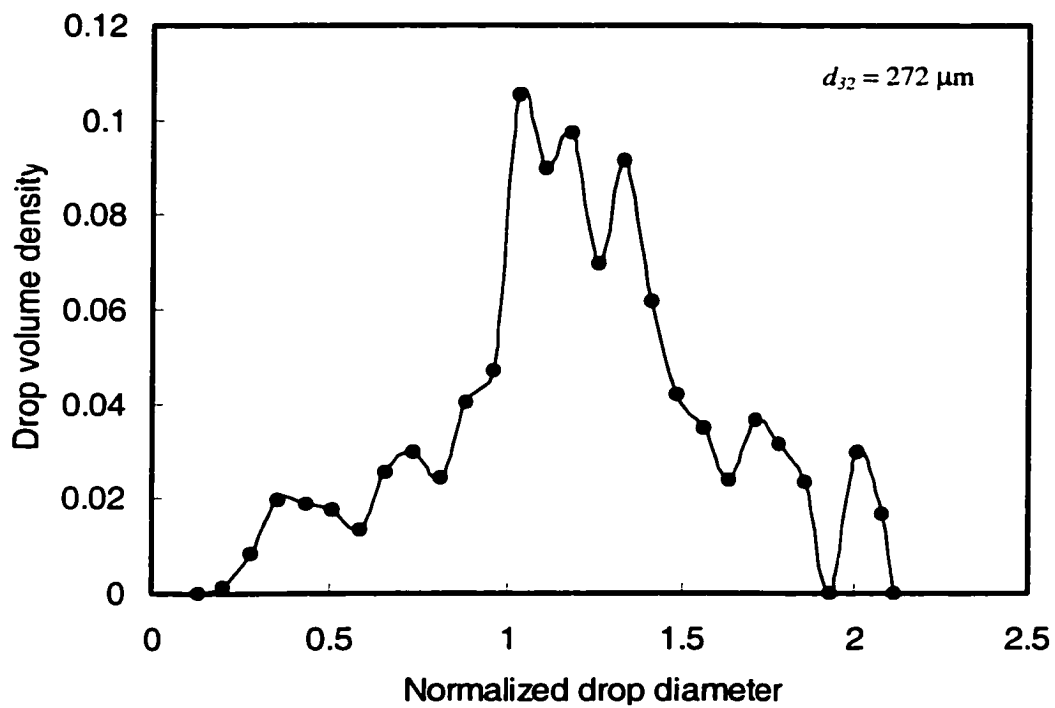


Figure 4.73. Drop volume density distribution
 ($\alpha = 27\%$, $\phi = 0.5\%$, $U = 0.40 \text{ m/s}$, 9 screens, $L = 10 \text{ mm}$).

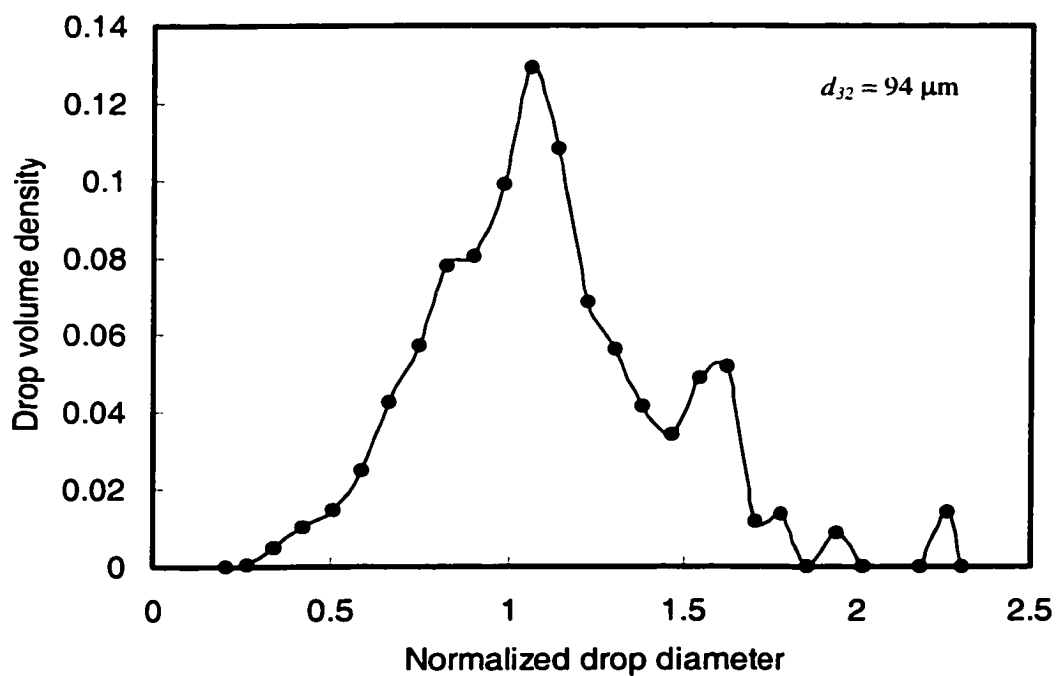


Figure 4.74. Drop volume density distribution
 ($\alpha = 27\%$, $\phi = 0.5\%$, $U = 0.97 \text{ m/s}$, 9 screens, $L = 10 \text{ mm}$).

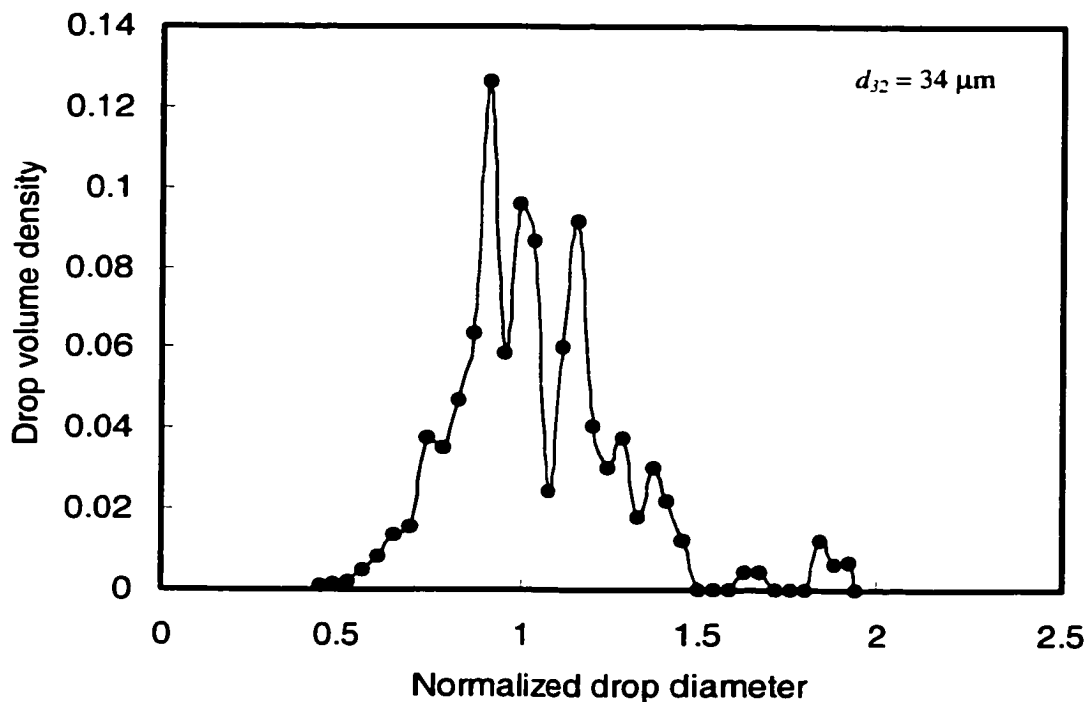


Figure 4.75. Drop volume density distribution
($\alpha = 27\%$, $\phi = 0.5\%$, $U = 1.94 \text{ m/s}$, 9 screens, $L = 10 \text{ mm}$).

Effect of Dispersed Phase Volume Fraction

The influence of the dispersed phase concentration on the generated drop volume density distributions using 41 and 27% open area screens and superficial velocities of 0.40 and 0.70 m/s is shown in Figures B48 to B59.

At low holdup ($\phi = 0.5\%$) unimodal distribution, which is skewed to the left, is formed (Figure 4.76). As the holdup increases (Figures 4.77 and 4.78) the peak shifts to smaller drop sizes as a result of breakup of the larger drops, most probably by the cutting action, as indicated by the continuous removal of the larger drops (their volume density almost does not increase with the increasing holdup). Furthermore, as the holdup increases the density of the smaller drops increases suggesting that the breakage mechanism (drop cutting), at high holdups results in the production of very large number of drops which are much smaller than the mother drop. These results are clear evidence

that the liquid-liquid dispersion investigated is breakup dominated even at high holdups. The drop size distribution varies with the increasing holdup in a similar fashion at both velocities (0.40 and 0.70 m/s) tested suggesting that the drop cutting mechanism is the dominant one under these conditions. Both tested screens (41 and 27% open area) show similar behavior.

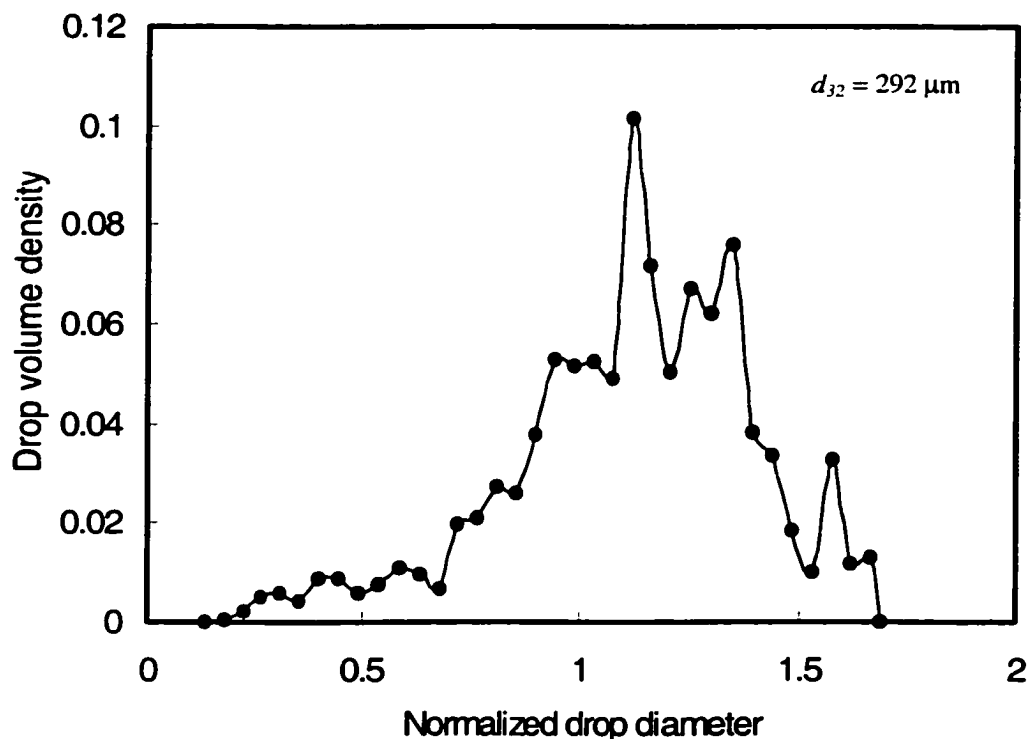


Figure 4.76. Drop volume density distribution
($\alpha = 41\%$, $\phi = 0.5\%$, $U = 0.40$ m/s, 9 screens, $L = 10$ mm).

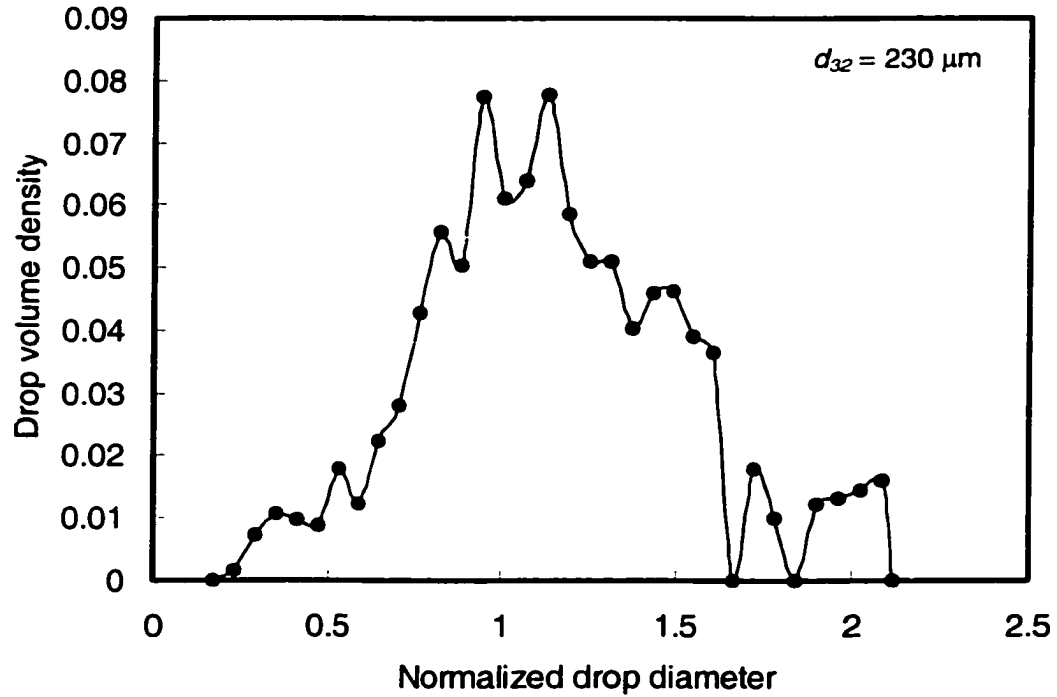


Figure 4.77. Drop volume density distribution
($\alpha = 41\%$, $\phi = 2\%$, $U = 0.40 \text{ m/s}$, 9 screens, $L = 10 \text{ mm}$).

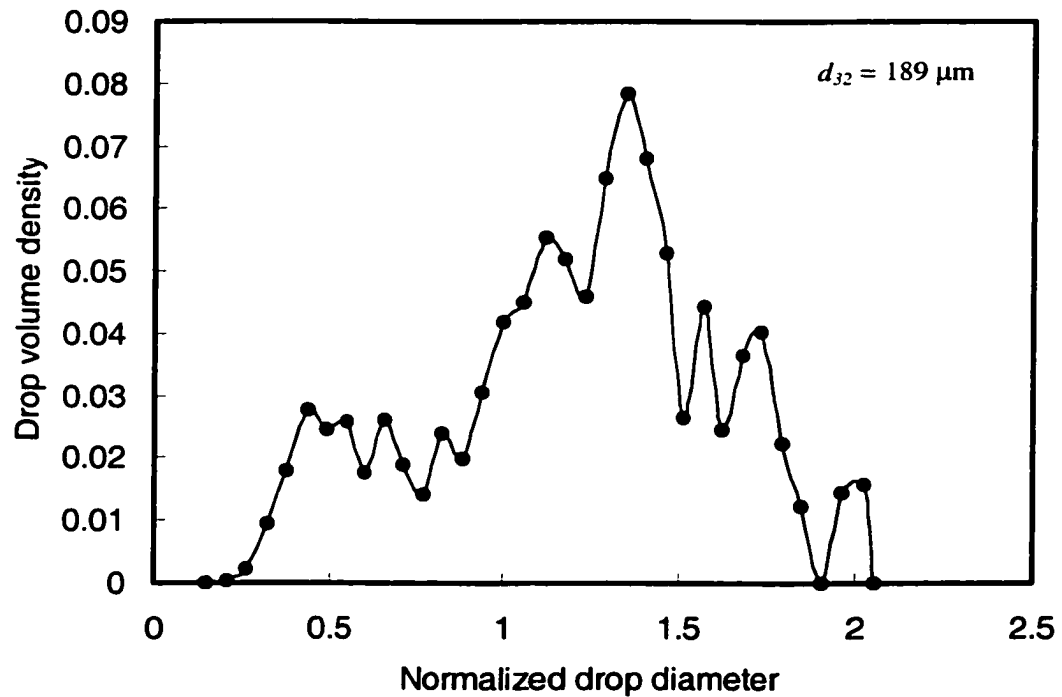


Figure 4.78. Drop volume density distribution
($\alpha = 41\%$, $\phi = 4\%$, $U = 0.40 \text{ m/s}$, 9 screens, $L = 10 \text{ mm}$).

Effect of Number of Elements

Figures B60 to B65 show the effect of the number of screens (i.e., the static mixing elements) on the generated drop volume distribution at holdup of 2% and velocity of 0.40 m/s. When two mixing elements are used, unimodal distribution, which is skewed to the left, is formed (Figure 4.79). As the number of elements increases (Figure 4.80) the larger drop size shrinks and the volume density of the smaller drops increases as a result of breakage of the larger drops and the peak shifts to smaller drop size. Further increase in number of screens results in more breakage of the larger drops until equilibrium are reached after the ninth element and the distribution becomes more uniform and relatively narrower (Figure 4.81). Again, these results emphasize the importance of residence time in liquid-liquid mixing operations, which is expected to have a strong effect on drop breakage efficiency.

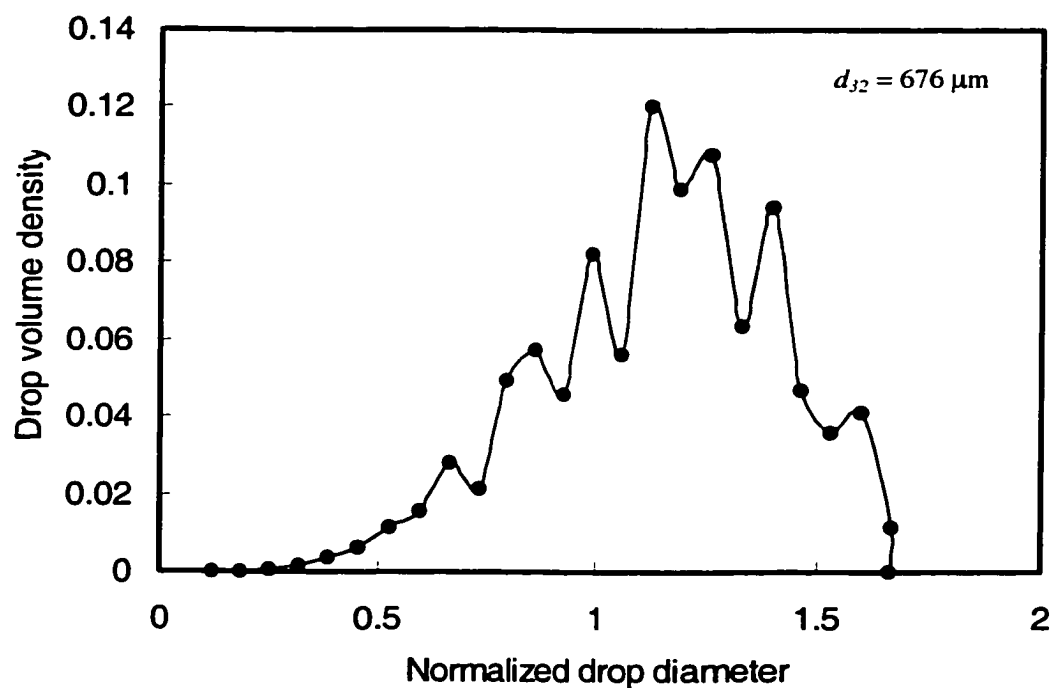


Figure 4.79. Drop volume density distribution
 ($\alpha = 27\%$, $\phi = 2\%$, $U = 0.40$ m/s, 2 screens, $L = 5$ mm).

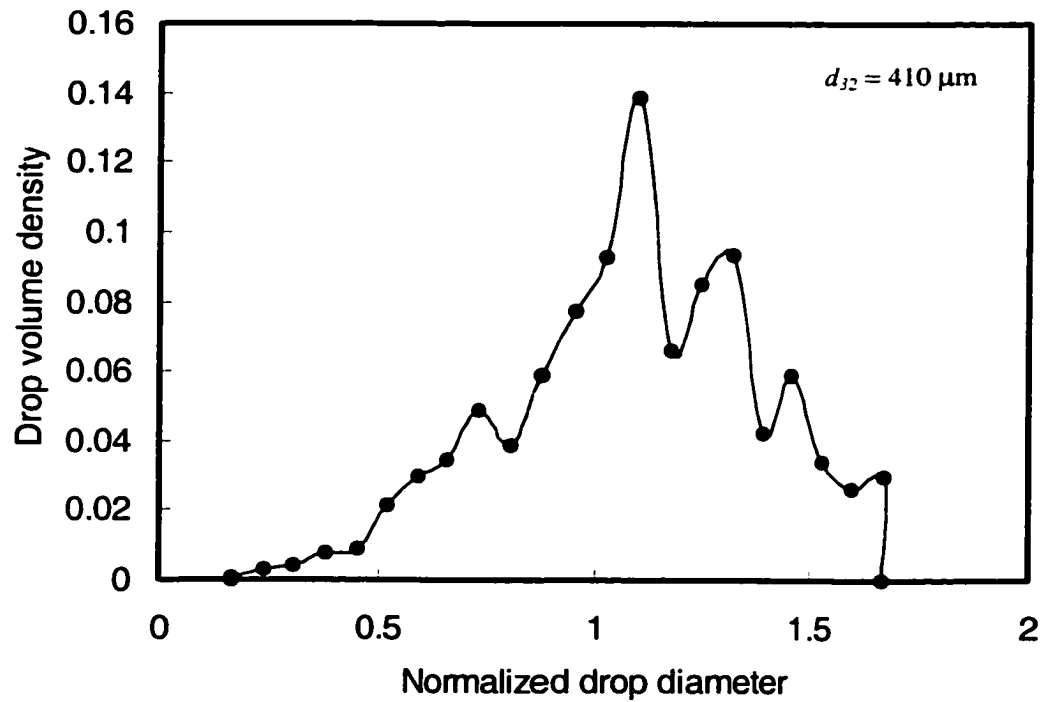


Figure 4.80. Drop volume density distribution
 ($\alpha = 27\%$, $\phi = 2\%$, $U = 0.40$ m/s, 4 screens, $L = 5$ mm).

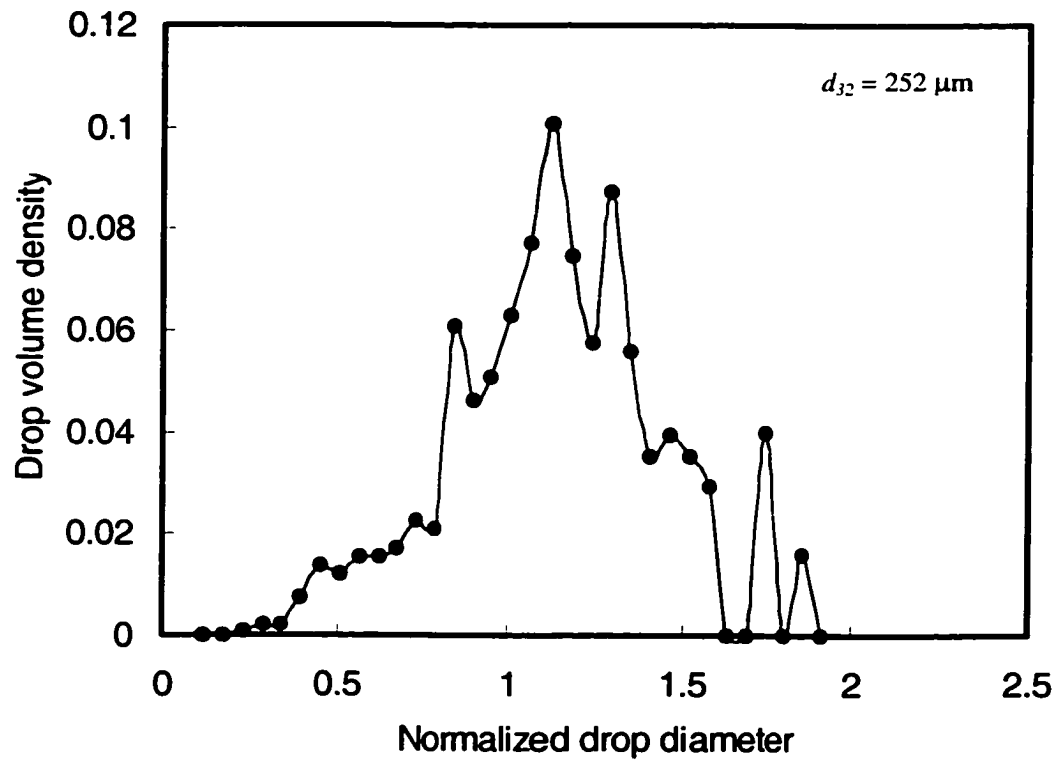


Figure 4.81. Drop volume density distribution
 ($\alpha = 27\%$, $\phi = 2\%$, $U = 0.40$ m/s, 12 screens, $L = 5$ mm).

Effect of Presence of Surfactant

Figures B66 to B75 show the variation of drop volume distribution as a function of the concentration of surfactant Triton X100 at velocity of 0.7 m/s and holdups of 0.5 and 4% using 27% open area screen.

At low surfactant concentration a unimodal and relatively symmetrical distribution is formed (Figure 4.82). Similarly, as observed in the drop number density distributions, the distribution in presence of very small surfactant concentrations ($c = 0.01$ mole/m³) (Figure 4.63, insignificantly differs from that obtained under the same conditions but in absence of surfactant). As the surfactant concentration increases, the shape of the distribution, which is based on a much smaller mean drop diameter, changes insignificantly while the peak shifts to smaller drop sizes. (Figure 4.83 and 4.84). This is less pronounced at low holdup ($\phi = 0.5\%$). This behavior is due to the preferential breakage of the larger drop size, without the formation of excessive fine drops thereby shifting the distribution towards smaller diameters (not normalized). These results are in line with those found in drop number density distributions, which suggest that the presence of surfactant facilitates the turbulent drop breakup to a greater extent. Meanwhile, surfactant presence was found to result in insignificant change in the shape of drop size distribution at high holdups ($\phi = 4\%$) under which drop cutting action dominates suggesting that the presence of surfactant does not enhance drop cutting action.

The above results contradict those obtained by Chatzi et al. (1991) and Seidshazileh (1999), who observed bi-modal volume distributions in surfactant containing dispersions in stirred tanks. Seidshazileh (1999) attributed that to the coalescence retardation caused by the presence of the surfactant. Later, Chatzi and Kiparissides (1995) obtained uni-modal steady-state drop volume density distributions in high holdup dispersions containing PVA at different agitation rates. It was found that at low surfactant concentration the peak shifts to smaller drop sizes as the agitation rate increases. They also found that as PVA concentration increases the drop size distribution

shifts to lower drop diameters, which is in accordance with the present results. This indicated that the drop breakup was the predominant mechanism that determined the development of the drop size distribution. At low surfactant concentration and high agitation rates the coalescence became significant leading to wider distributions and shorter peaks.

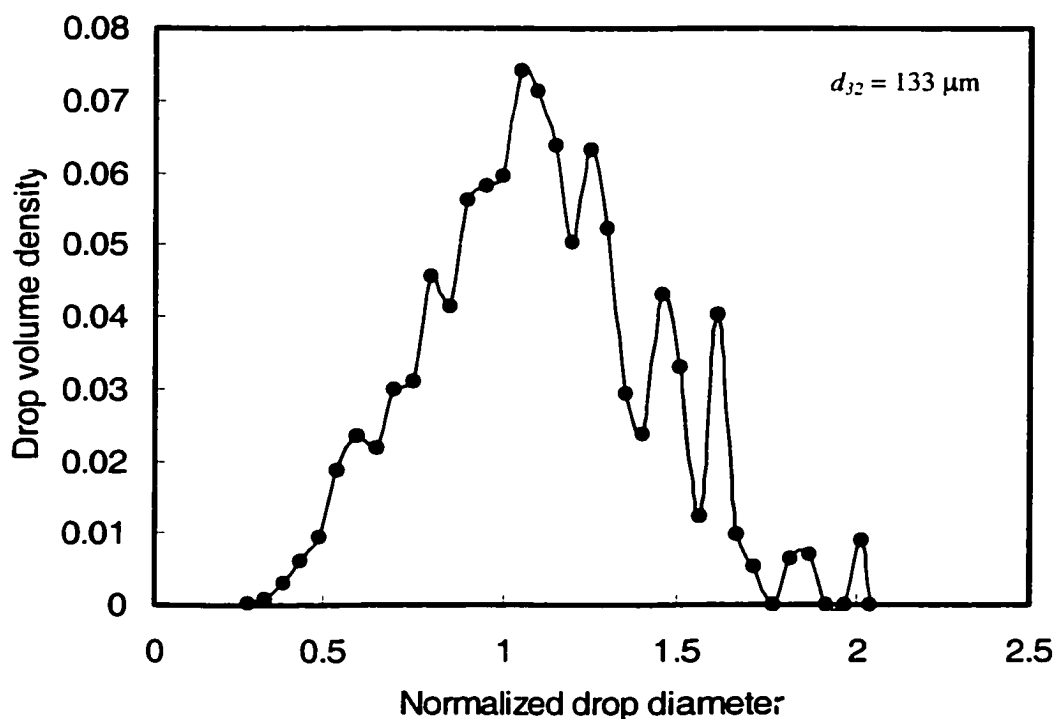


Figure 4.82. Drop number density distribution with SAA ($\alpha = 27\%$, $\phi = 4\%$, $U = 0.70$ m/s, $c = 0.01$ mole/m³, 9 screens, $L = 10$ mm).

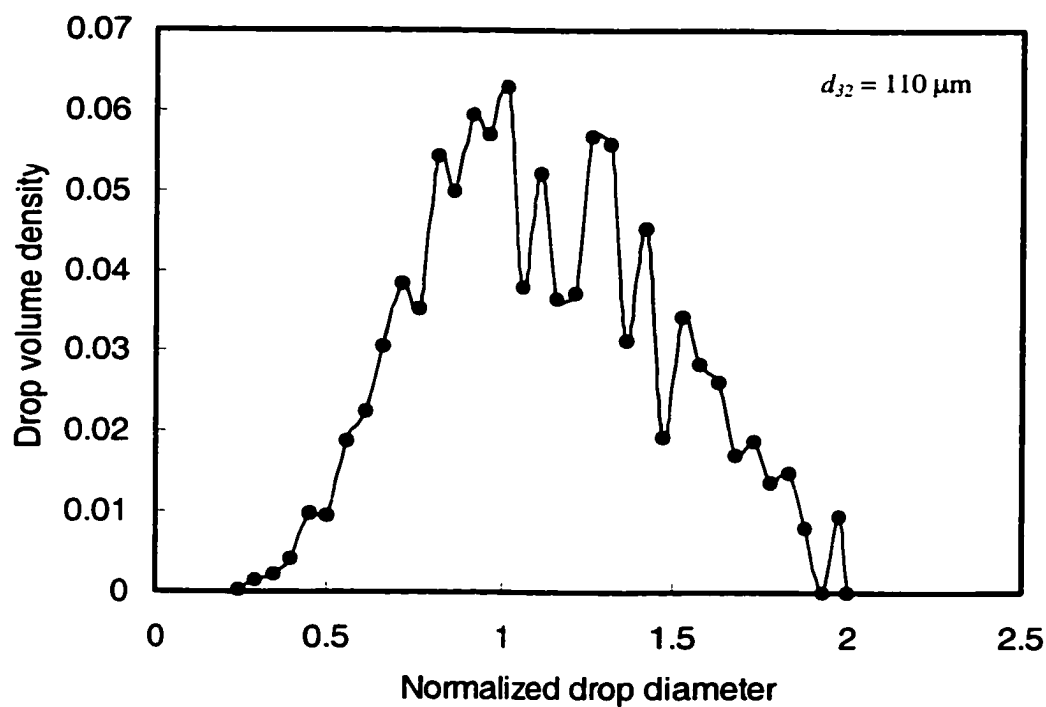


Figure 4.83. Drop number density distribution with SAA ($\alpha = 27\%$, $\phi = 4\%$, $U = 0.70$ m/s, $c = 0.10$ mole/m³, 9 screens, $L = 10$ mm).

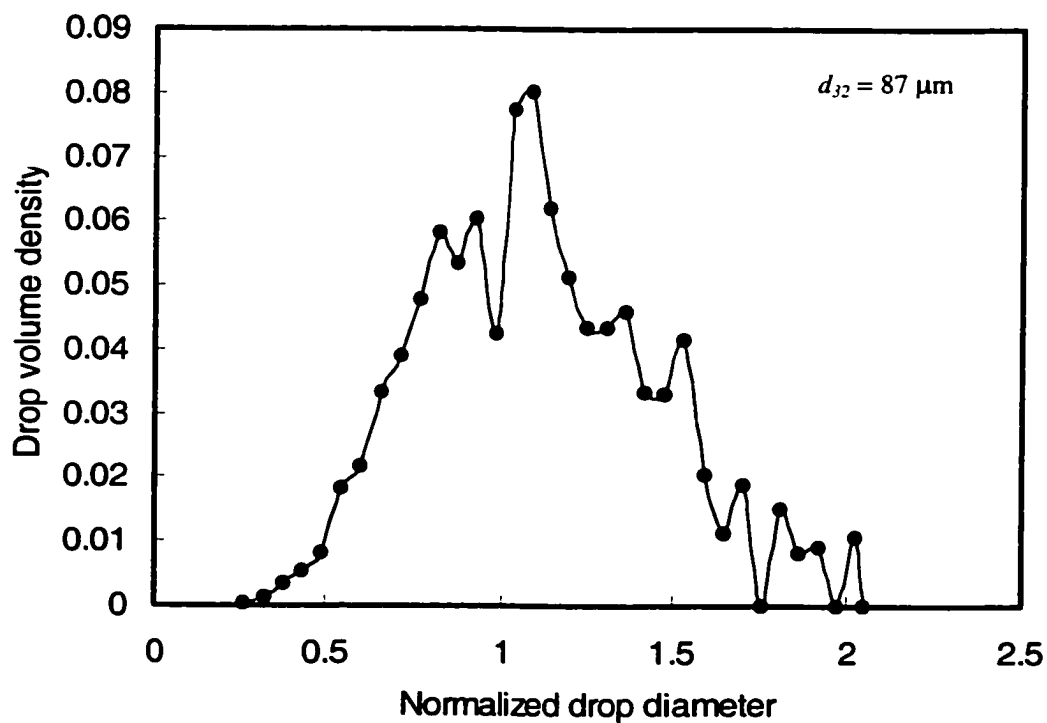


Figure 4.84. Drop number density distribution with SAA ($\alpha = 27\%$, $\phi = 4\%$, $U = 0.70$ m/s, $c = 0.30$ mole/m³, 9 screens, $L = 10$ mm).

4.4.3 Characterization of Drop Size Distributions

There are two methods for the characterization of a set of data or distributions; central tendency and dispersion. Central tendency is described by the different averages while dispersion deals with the scatter of data around those means. The different averages were discussed in section 4.2. In this section the following parameters were used to describe the drop size distributions generated under the experimental conditions investigated:

Modality

The mode is defined as the value of the observation that occurs most frequently. The mode therefore represents the highest peak in a frequency distribution. Some distributions have more than one mode particularly in liquid-liquid dispersion data where bi-modal distributions are often encountered (Chen and Middleman, 1967; Tavlarides and Stamatoudis, 1981; Chatzi et al., 1991; Nishikawa et al., 1991; Pacek et al., 1998).

As shown in Appendices A and B, both drop number and drop volume density distributions often exhibit clear bi-modality but this is less pronounced in the later. On the other hand, plotting the distributions in cumulative density form smoothens errors rising from drop size measurements, which can also hide subtle variations. It will be seen in later sections that the cumulative drop volume distributions show self-similarity and can be represented reasonably well by normal distribution. Plotting normally distributed cumulative density distributions on a normal probability paper produces a straight line (Figure 4.85). Therefore, to test for the existence of bi-modality, the cumulative distribution is fitted to normal distribution. First, the two parts of the curve where deviation from linearity occurs are fitted separately and then all the data points are fitted as one curve. The correlation coefficients obtained were compared with each other. If no significant difference was found then the distribution was considered as uni-modal distribution or simply stated the system can be represented by a single distribution.

The number and volume density distributions depicted in Figures A7 and B40 respectively, which show high degree of bimodality, were tested. Table 4.5 shows the fitting results for the cumulative drop number and volume distributions tested:

Table 4.5. Fitting results of bi-modality testing.

	R	
	Number density	Volume density
Single distribution	0.998	0.990
Two distributions	0.986	0.980

Clearly, as can be seen from Table 4.5 the correlation coefficients obtained using a single distribution for both number and volume density distributions are not significantly different from those obtained using two distributions at the 95% confidence level. Consequently, it can be concluded that all drop size distributions generated can be considered uni-modal.

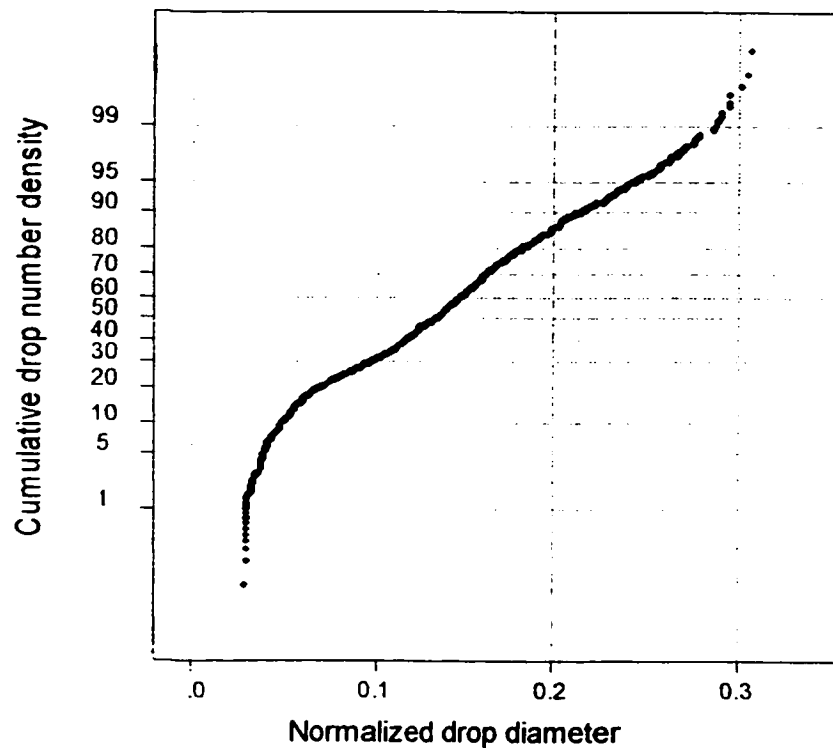


Figure 4.85. Cumulative drop number density distribution ($\alpha = 41\%$, $\phi = 0.5\%$, $U = 0.85$ m/s, 9 screens, $L = 10$ mm)

Skewness

The sample skewness is a measure of the symmetry of the distribution that generated the data (Kennedy and Neville, 1986). Distributions that have a longer "right tail" than "left tail" such as the exponential, gamma, and log-normal have a positive skewness and are said to be skewed to the right. Conversely, a distribution with a longer left tail such as the extreme value type A has a negative skewness and is said to be skewed to the left. Therefore, for a symmetrical distribution, the skewness is zero, and the three parameters; mean, median and mode coincide. In case these parameters do not coincide the distribution is said to be skewed. Several investigators reported skewed drop size distributions in liquid-liquid dispersions (Sprow, 1967a; Chatzi et al., 1991; Zhou and Kresta, 1997; Pacek et al., 1998). Figure 4.86 shows a drop size distribution that is skewed to the right.

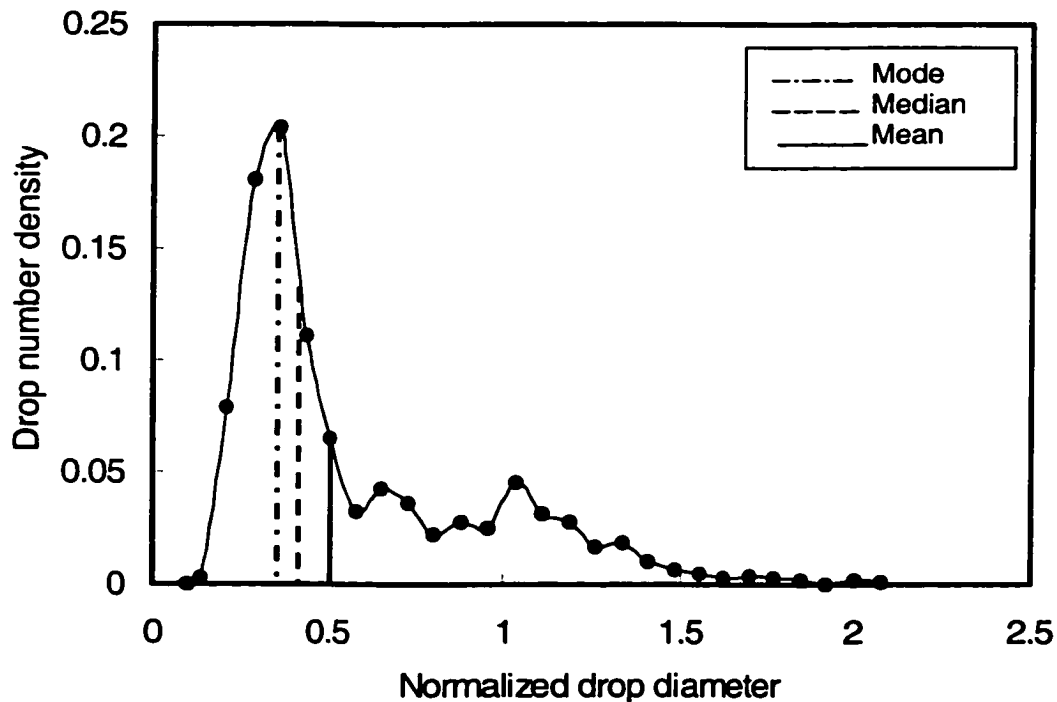


Figure 4.86. Mean, median and mode in skewed distribution ($\alpha = 27\%$, $\phi = 0.5\%$, $U = 0.30$ m/s, 9 screens, $L = 10$ mm).

Equation (3-11) was used to compute the skewness of the drop number density distributions generated under the different experimental conditions investigated.

Figures 4.87 to 4.91 show the effect of the superficial velocity on skewness of the drop size distributions generated using screens with different percentage open areas. The skewness of the resultant drop size distributions was found to decrease with increasing superficial velocity reaching a minimum value beyond which it increases again as the velocity is further increased. As the velocity increases the turbulence intensity is enhanced resulting in more breakage of the larger drops and thus shorter tails, which contribute mostly to the sample skewness. It should be mentioned that the 4-fold reduction in skewness observed as the velocity is increased to 0.70 m/s (Figure 4.91) since d_{32} simultaneously undergoes about 2-fold reduction over the same velocity range.

As shown in Figures A1 to A47 in Appendix A, at low velocities the distributions are characterized with long tail on the larger drop side, Figures A1 to A47 also show that as the superficial velocity increases the tail continuously shrinks as a result of the increased drop breakup due to the enhanced turbulence intensity. The position of the peak remains unaltered while it becomes higher. At intermediate velocities (i.e., 0.85-1.55) the mode shifts to smaller drop sizes. This is due to the breakage of the larger drops as a result of the enhanced turbulence intensity, which leads to further decrease of the skewness. As the velocity increases further, the larger drops undergo more breakup and a new tail is formed causing the skewness to rise again. At high holdup ($\phi = 4\%$) the skewness varies with the superficial velocity in a similar fashion to that observed at low holdup ($\phi = 0.5\%$).

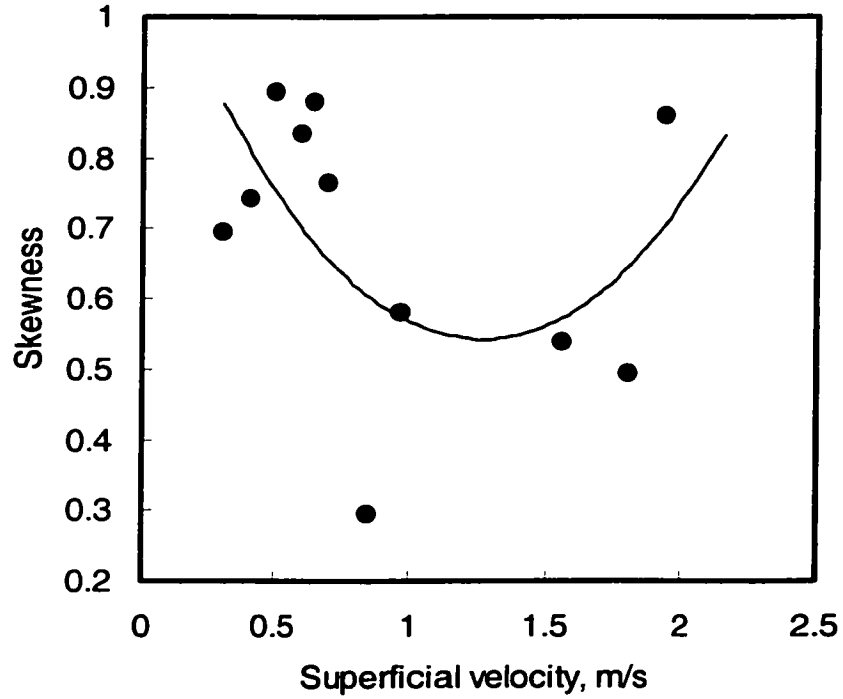


Figure 4.87. Effect of superficial velocity on skewness
 ($\alpha = 41\%$, $\phi = 0.5\%$, 9 screens, $L = 10$ mm)

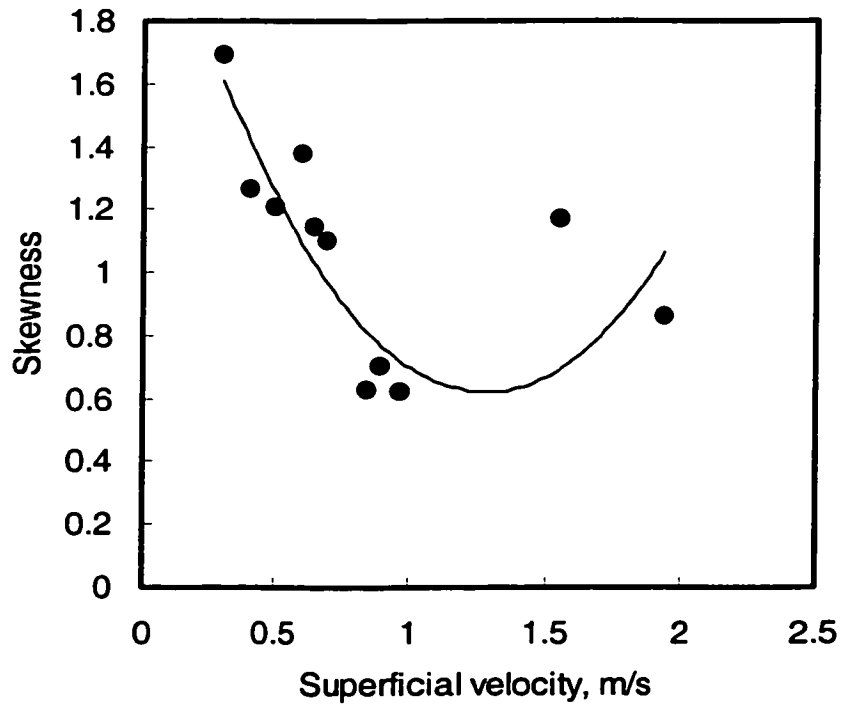


Figure 4.88. Effect of superficial velocity on skewness
 ($\alpha = 27\%$, $\phi = 0.5\%$, 9 screens, $L = 10$ mm)

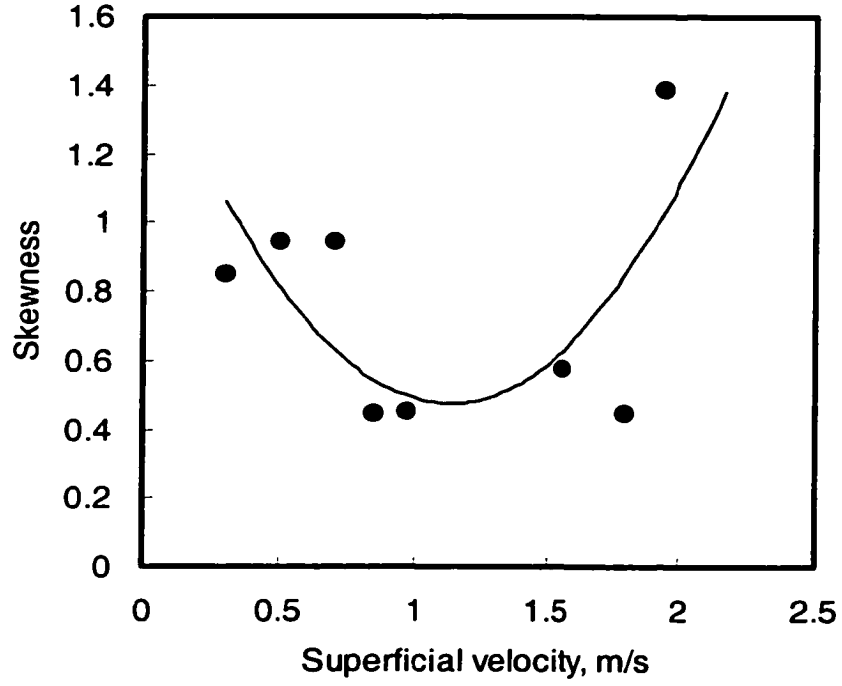


Figure 4.89. Effect of superficial velocity on skewness ($\alpha = 33\%$, $\phi = 0.5\%$, 9 screens, $L = 10$ mm)

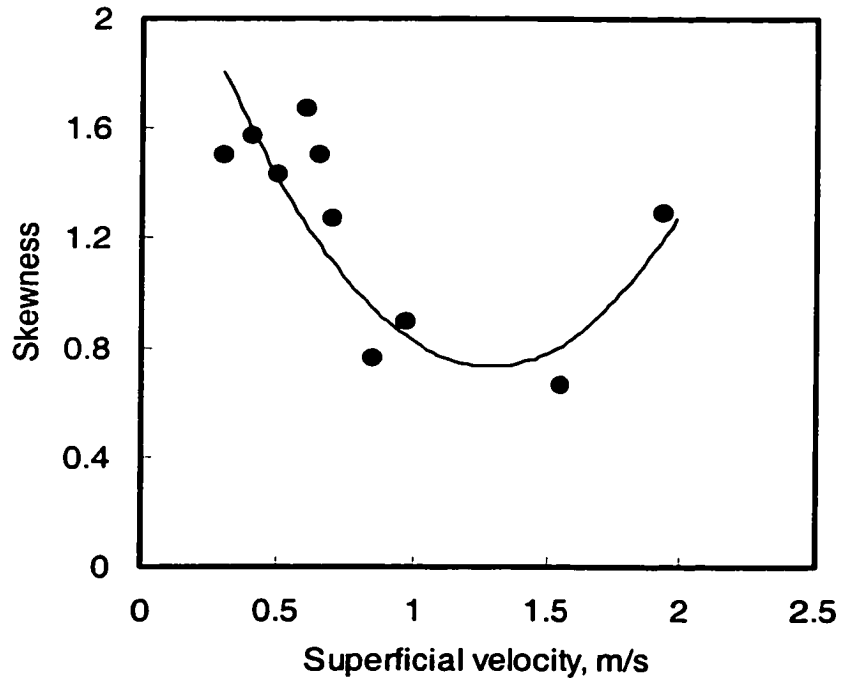


Figure 4.90. Effect of superficial velocity on skewness ($\alpha = 41\%$, $\phi = 4\%$, 9 screens, $L = 10$ mm)

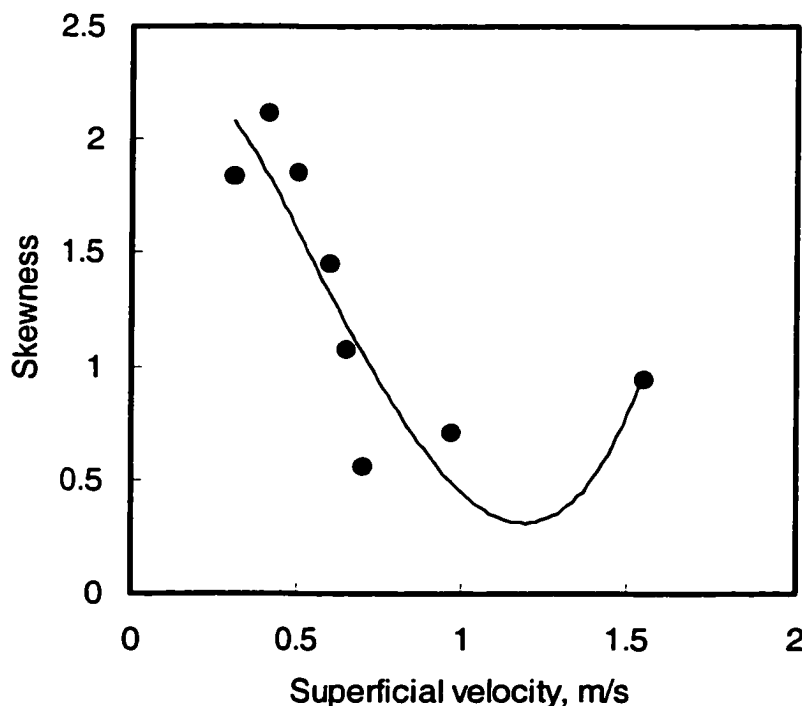


Figure 4.91. Effect of superficial velocity on skewness
($\alpha = 27\%$, $\phi = 4\%$, 9 screens, $L = 10$ mm)

Figures 4.92 to 4.95 show the variation of skewness with the dispersed phase holdup. Clearly, as can be seen from Figures 4.92 and 4.93 at a superficial velocity of 0.40 m/s, the skewness was found to increase monotonically with the increasing dispersed phase holdup. Figures A2, A48 to A50, A13, A30, A54 to A56 and A40 in Appendix A show that at a dispersed phase holdup of 0.5%, the generated drop size distribution is bi-modal and characterized by a high peak on the smaller diameter side and relatively much smaller peak corresponding to larger drop size. As the dispersed phase holdup increases, the smaller peak shrinks gradually due to the proposed drop cutting action as a result of breakup of the larger drops leaving long tail of the unbroken drops, which is another evidence of the validity of the concept of breakage efficiency proposed in section 4.3. This causes the skewness to increase monotonically.

On the contrary, at superficial velocity of 0.70 m/s the skewness was found to decrease as the dispersed phase holdup increases until a minimum value is reached. After

this, an increase in skewness is observed as the dispersed phase holdup increases further. This is less pronounced in the case of 41% open area screen. Figures A6, A51 to A53, A34, A57 to A59 and A45 in Appendix A, show that at a velocity of 0.7 m/s and low dispersed phase holdup, bi-modal distributions were obtained. The peak on the small diameter side shrinks gradually due to the increased coalescence of the smaller drops. Meanwhile the mode at the larger drop side becomes higher due to the enhancement of cutting of the larger drops as the dispersed phase holdup increases and thus shifts to lower drop sizes resulting in lower values of skewness. At dispersed phase holdups higher than 3%, the mode shifts to lower drop sizes probably due to the increased drop cutting action leaving behind a tail of the larger drops and thus resulting in higher skewness values.

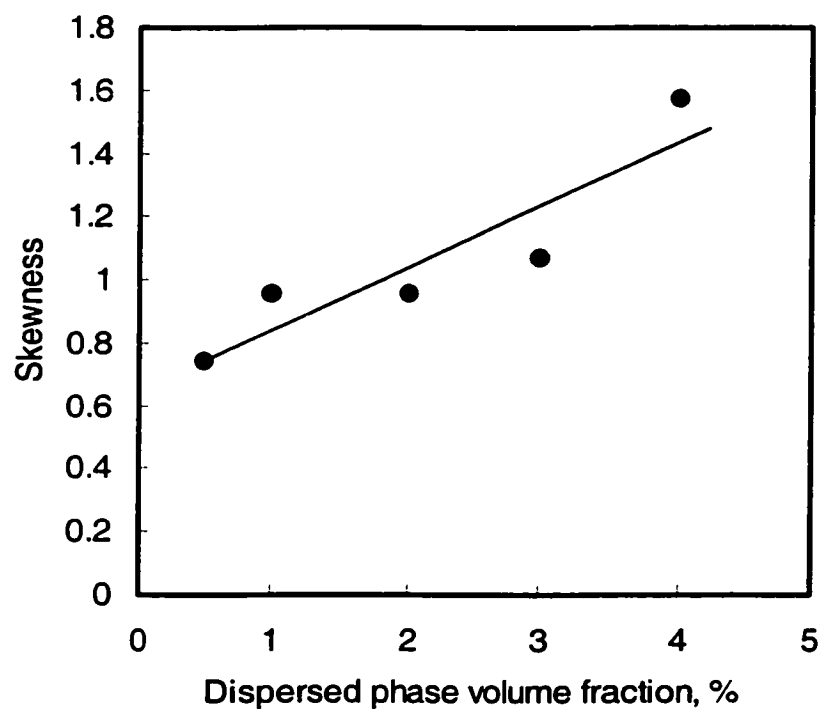


Figure 4.92. Effect of dispersed phase holdup on skewness
($\alpha = 41\%$, $U = 0.40$ m/s, 9 screens, $L = 10$ mm)

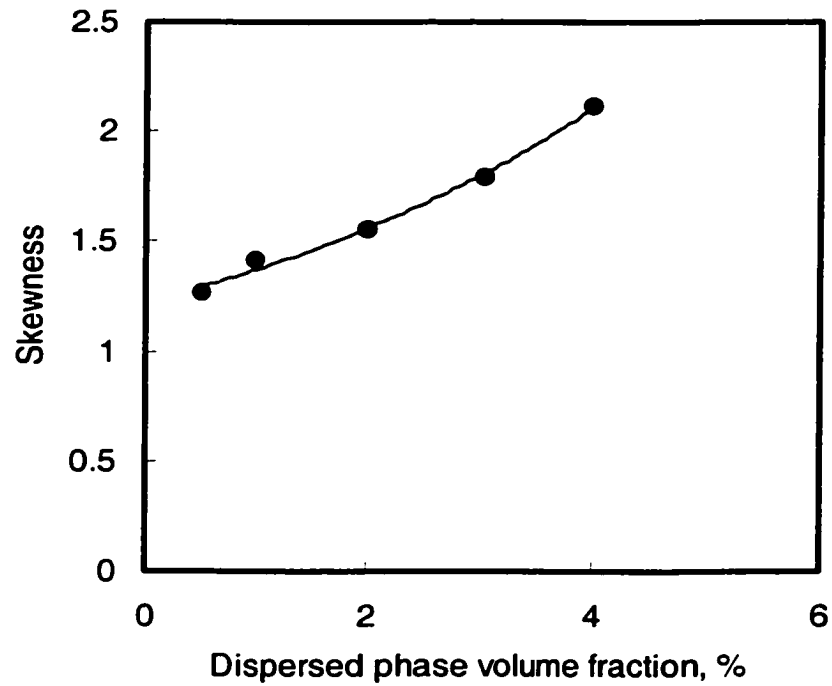


Figure 4.93. Effect of dispersed phase holdup on skewness
 ($\alpha = 27\%$, $U = 0.40$ m/s, 9 screens, $L = 10$ mm)

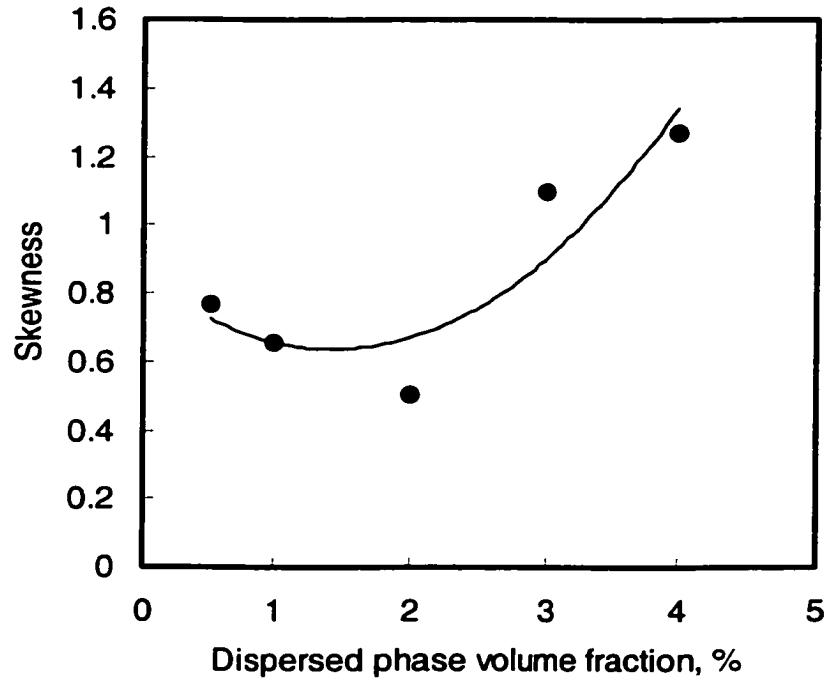


Figure 4.94. Effect of dispersed phase holdup on skewness
 ($\alpha = 41\%$, $U = 0.70$ m/s, 9 screens, $L = 10$ mm)

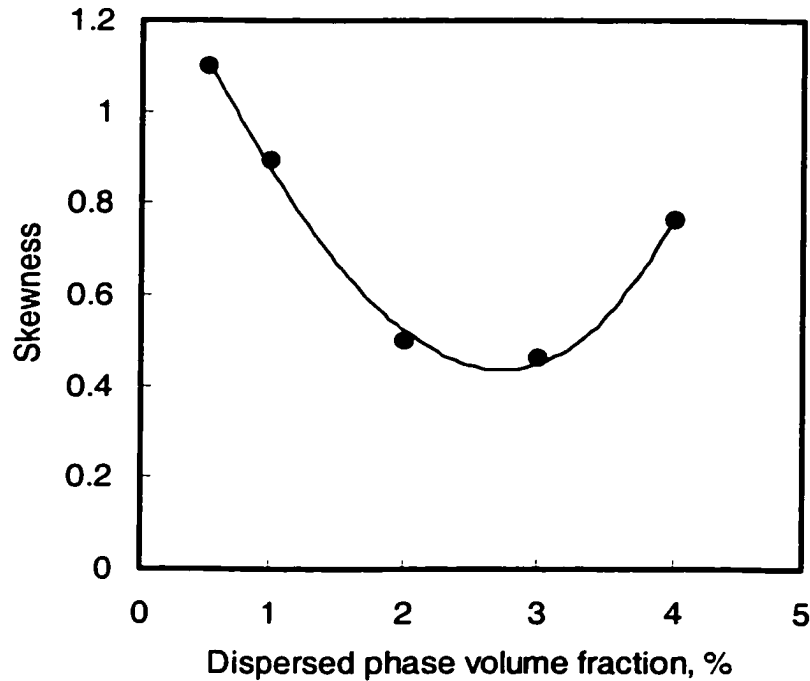


Figure 4.95. Effect of dispersed phase holdup on skewness
 ($\alpha = 27\%$, $U = 0.70$ m/s, 9 screens, $L = 10$ mm)

Figure 4.96 shows the variation of the skewness of the generated drop size distributions with surfactant concentration. Clearly, the skewness was found to decrease with increasing surfactant concentration reaching a minimum value before it begins to increase with further increase in the concentration of the surfactant. Figures A66 to A70 show that upon increasing surfactant concentration the larger drops in the tail undergo breakup as indicated by the formation of a small peak corresponding to the larger drop side and thus yielding lower values of skewness. At concentrations higher than 0.1 mole/m³ the larger drops undergo further breakage causing the small peak to shift to lower drop sizes until it merges with the higher peak leaving a long tail of larger drop behind thus increasing the skewness.

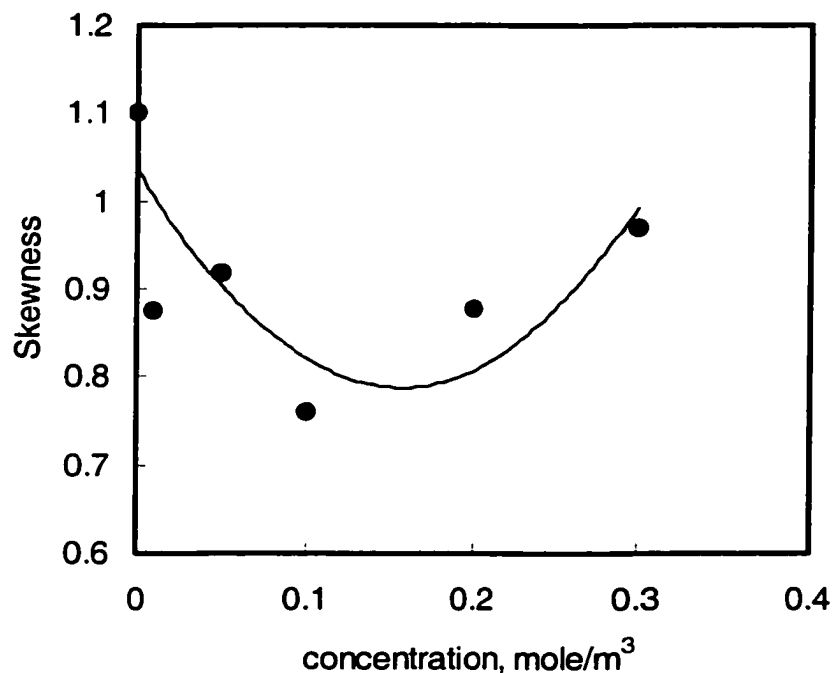


Figure 4.96. Effect of surfactant concentration on skewness ($\alpha = 27\%$, $\phi = 0.5\%$, $U = 0.70$ m/s, 9 screens, $L = 10$ mm)

Variance

The variance, which is the square of the standard deviation, is a measure of the scatter of the data around the mean of the distribution and is computed by Equation (3-10). In this section, the effects of the different experimental conditions tested on the normalized variance are investigated.

Figures 4.97 and 4.98 show the variation of the normalized variance of the generated drop size distributions with the superficial velocity for the tested screens at dispersed phase holdups of 0.5% and 4%. Clearly, for all tested screens and at both dispersed phase concentrations, the variance was found to decrease with the increasing superficial velocity but this is more pronounced at lower holdups. The lower slope showed at low velocities (< 0.7 m/s) might indicate that initially as the velocity increases, the coalescence of the smaller drops becomes more significant, while the breakup frequency of the larger drops increases. At higher velocities, a continuous decrease in the variance is observed, which indicates that drop breakup predominates. It can be

concluded that, generally, the higher the superficial velocity the narrower the drop size distribution is. The scatter of data at higher dispersed phase holdups may have been caused by errors in drop size measurement due to resolution limitations associated with photographic method used. Similar findings were reported by Luhnig and Sawistowski (1971) for liquid-liquid dispersions in stirred tanks. They found that the higher the agitation rates the lower the variance of the drop size distribution. Later, Sembira et al (1986) reported similar results for kerosene-water dispersions using a Sulzer static mixer. Recently, Zhou and Kresta (1997) observed similar behavior of the standard deviation (i.e., the square root of the variance) with increasing rotation rates in stirred tanks using different types of impellers.

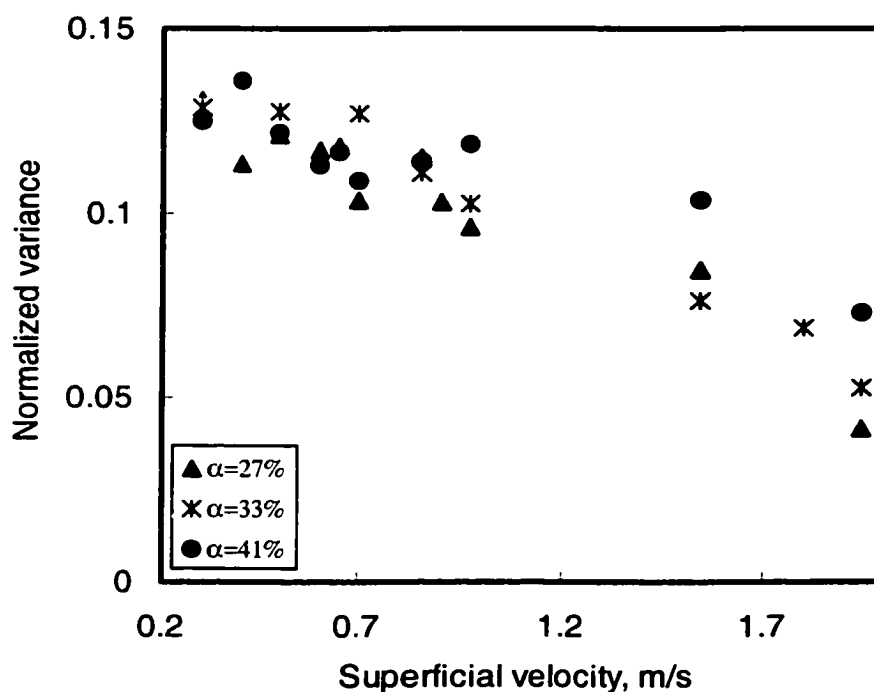


Figure 4.97. Effect of the superficial velocity on the normalized variance ($\phi = 0.5\%$, 9 screens, $L = 10$ mm)

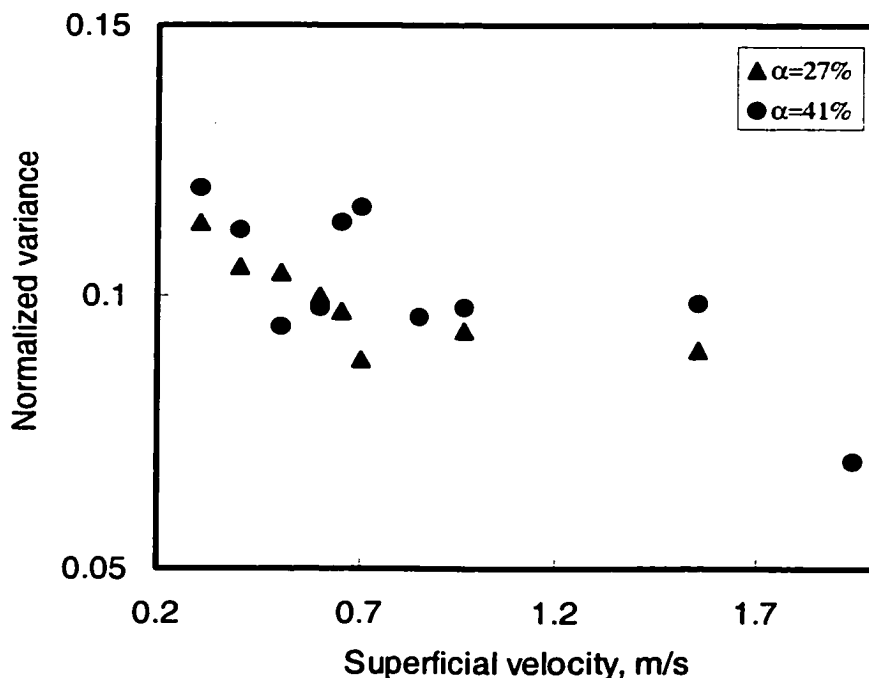


Figure 4.98. Effect of the superficial velocity on the normalized variance ($\phi = 4\%$, 9 screens, $L = 10$ mm).

A more realistic approach is to examine the variation of the variance with the Weber number, which is the ratio of the disruptive inertial turbulent forces to the resistive interfacial forces. This is depicted in Figure 4.99. It is clearly shown that the variance undergoes insignificant decrease in the non-fully developed turbulent region (low We number) while it decreases sharply in the fully developed turbulent zone with the increasing Weber number. It can also be seen that the data segregate according to the screen open area.

Since the kinetic energy of the micro jets generated behind screens is the most important factor in the drop breakup process, an attempt was made to plot the absolute variance as a function of the jet Weber number as shown in Figure 4.100. Figure 4.100 shows that at fully developed turbulent conditions (i.e., $U > 0.70$ m/s) the variance decreases drastically with the increasing jet Weber number and the data fall on the same straight line for the different screens tested suggesting that the data can be successfully

correlated using this method. It was found that for the fully developed turbulent region the variance varies with the jet Weber number as follows ($R = 0.966$):

$$\sigma^2 \propto We_{jet}^{-3.74} \quad (4-24)$$

In order to verify the possibility of correlating the variance with the Weber number, the data for kerosene-water system from Sulzer mixer reported by Sembira et al. (1986) are reproduced and the variance is re-plotted as a function of the Weber number. As shown in Figure 4.101, the variance decreases in a similar fashion to that found in this work but with a slightly higher slope value (-3.83, $R = 0.984$). This insignificant difference in the slope value may be attributed to the low viscosity of the dispersed phase (i.e., kerosene) studied by Sembira et al (1984) compared to that used in the present study and to the different techniques used for drop size measurement. However, this analysis confirms the possibility of correlating the variance of generated drop size distributions in mixing processes to the Weber number.

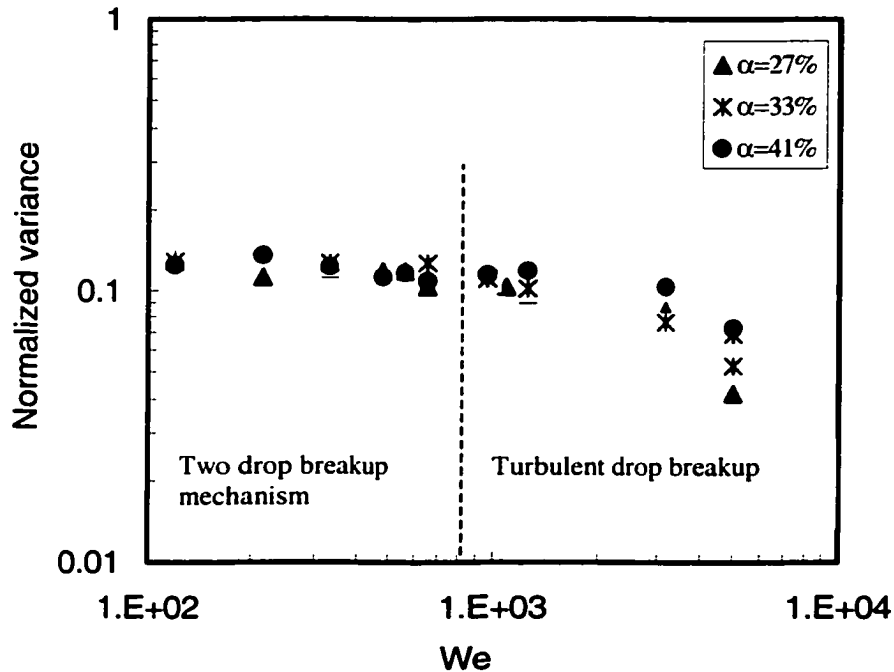


Figure 4.99. Effect of the Weber number on the normalized variance ($\phi = 0.5\%$, 9 screens, $L = 10$ mm).

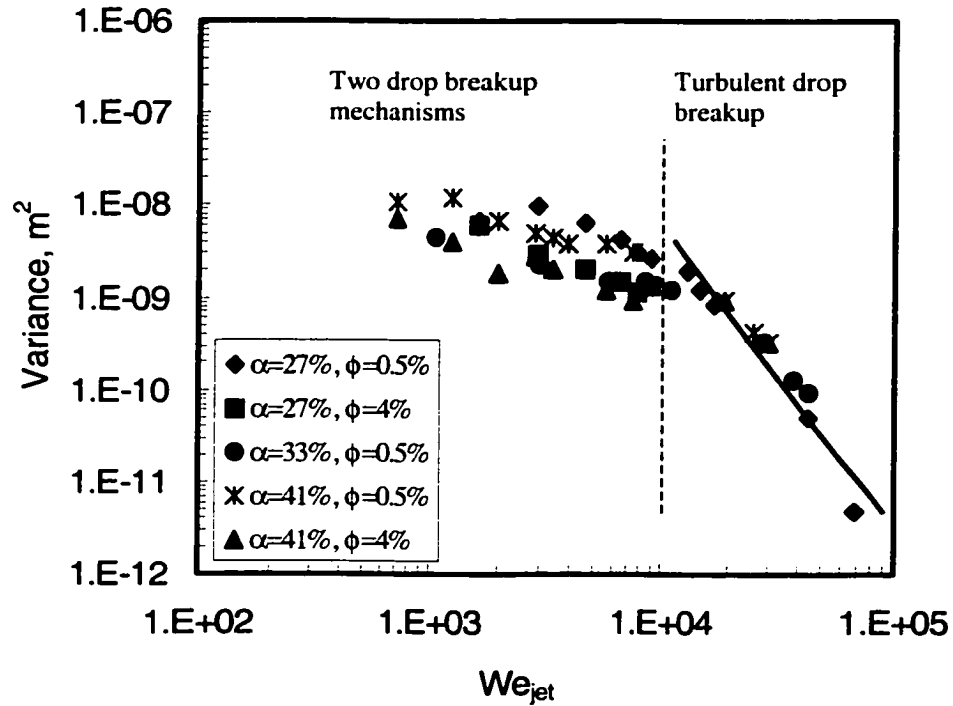


Figure 4.100. Effect of the jet Weber number on the variance (9 screens, $L = 10$ mm).

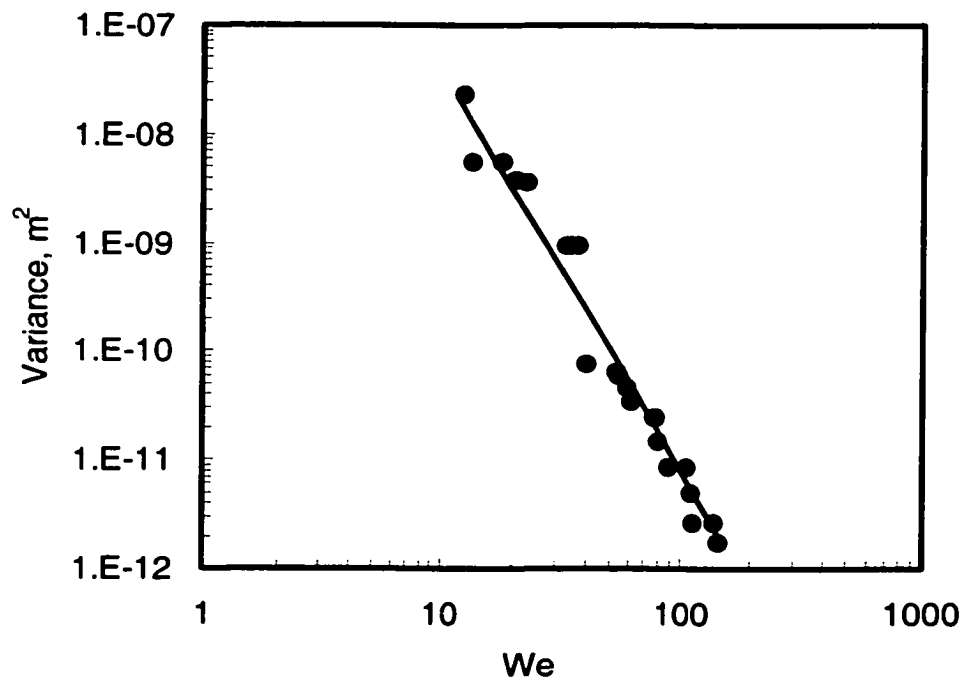


Figure 4.101. Effect of the Weber number on the variance in Sulzer mixer (Sembira et al., 1986).

Figure 4.102 shows the normalized variance as a function of surfactant concentration. Initially the normalized variance does not change significantly upon the addition of surfactant, which is then followed by a sharp decrease as the surfactant concentration increases. This is more pronounced at lower dispersed phase holdups. At low surfactant concentrations, probably there is insufficient surfactant molecules in the system to facilitate drop breakup, which leads to insignificant change in the values of the variance. As the surfactant concentration increases further the variance starts to decrease due to the preferential breakup of the larger drops, which is most probably caused by lowering the interfacial tension. This decrease is less pronounced in the coalescing system (high holdups) where the higher densities of the smaller drops cause the ability of the surfactant to retard drop coalescence diminishes gradually as resulting in the flat portion of the curve. At both holdups, at higher concentrations, the surfactant becomes more effective in promoting drop breakup and coalescence retardation as indicated by the steady decrease of the variance. As the surfactant concentration increases, the Marangoni elasticity decreases (Xue, 1999) and hence the resistance to drop breakup decreases.

Attempts were made to correlate the normalized variance to the different interfacial characteristics, namely equilibrium interfacial tension, surface excess, surfactant diffusivity and the Marangoni number. As can be seen from Figures 4.103 to 4.106, none of the characteristics can provide a reasonable correlation of the variance of the drop size distributions generated.

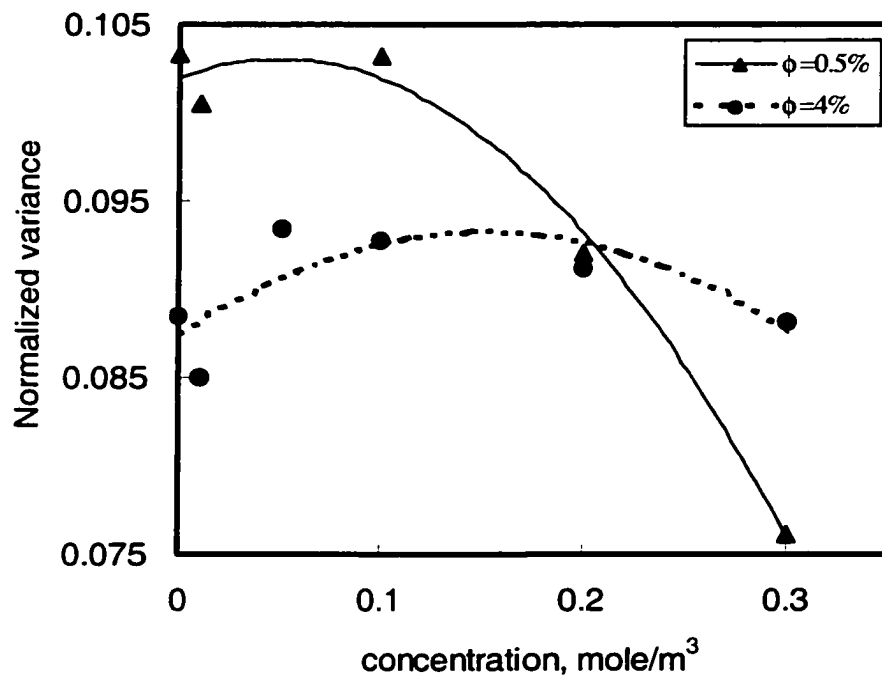


Figure 4.102. Effect of surfactant concentration on the normalized variance ($\alpha = 27\%$, $U = 0.70$ m/s, 9 screens, $L = 10$ mm).

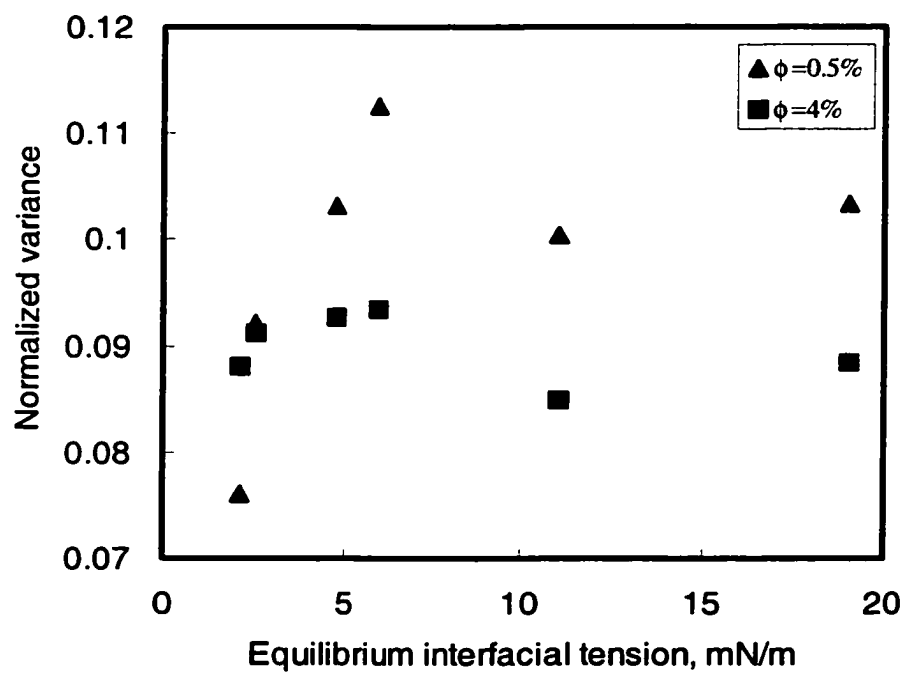


Figure 4.103. Effect of equilibrium interfacial tension on the normalized variance ($\alpha = 27\%$, $U = 0.70$ m/s, 9 screens, $L = 10$ mm)

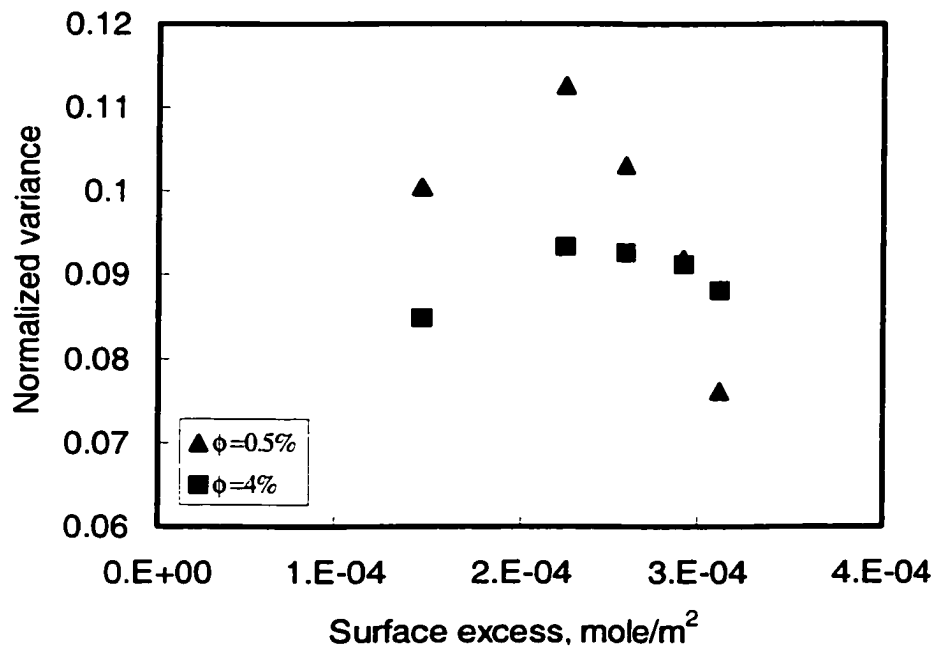


Figure 4.104. Effect of surface excess on the normalized variance ($\alpha = 27\%$, $U = 0.70$ m/s, 9 screens, $L = 10$ mm).

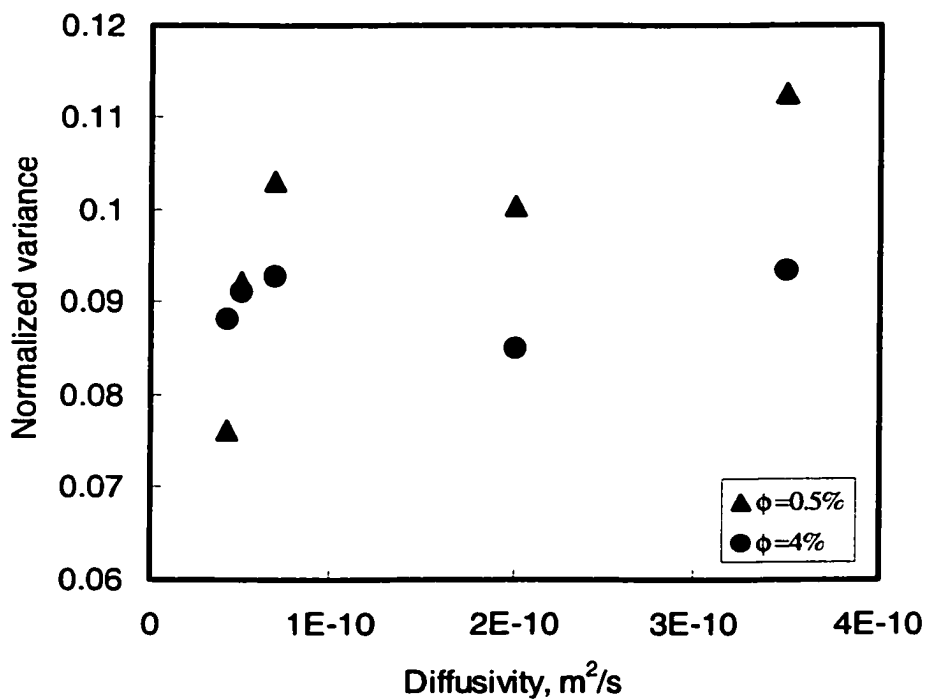


Figure 4.105. Variation of the normalized variance with surfactant diffusivity ($\alpha = 0.27$, $U = 0.70$ m/s, 9 screens, $L = 10$ mm).

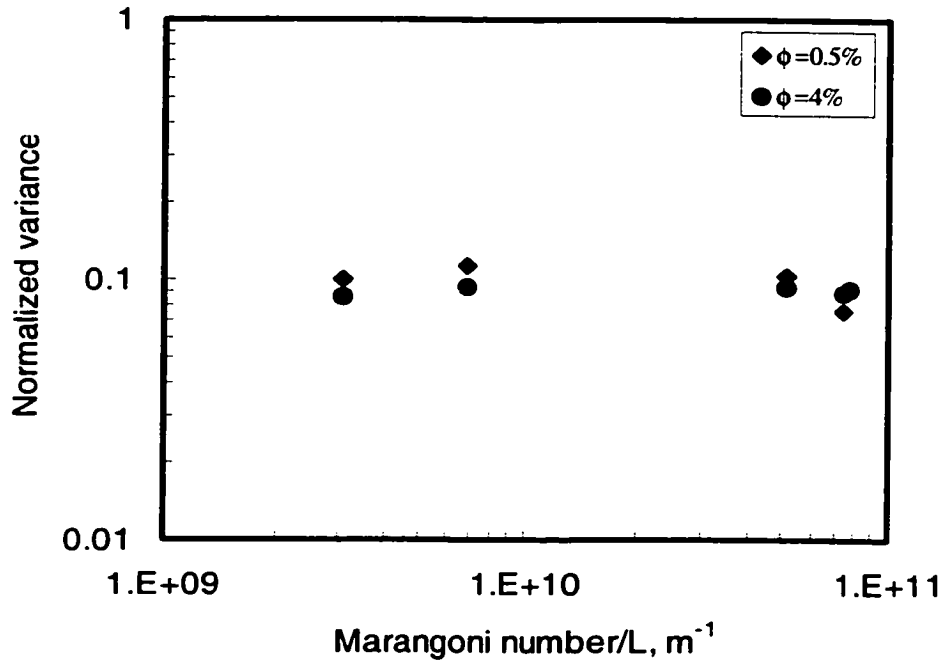


Figure 4.106. Variation of the normalized variance with Marangoni number ($\alpha = 27\%$, $U = 0.70$ m/s, 9 screens, $L = 10$ mm).

Fitting to Theoretical Probability Distributions

The literature shows that, there is no single theoretical probability distribution or empirical model, which can be used to fit the experimental data obtained from liquid-liquid dispersion processes successfully. Therefore, different distribution models were reported under different experimental conditions. Furthermore, due to difficulties in the measurement of drop size in high holdup dispersions, most of the reported studies have been limited to holdups less than 1% (Bae and Tavlarides, 1989). In this research dispersed phase holdups as high as 4% were used.

The uni-modal normalized number density data generated under the different experimental conditions investigated were fitted to the best known theoretical probability distributions using the software X-fit at a level of significance of 95% and the results found are shown in Tables 4.6 to 4.11,

1. Effect of Superficial Velocity

Table 4.6. Results of fitting the experimental data to probability models at different superficial velocities ($\alpha = 41\%$, 9 screens, $L = 10\text{mm}$).

velocity (m/s)	$\phi = 0.5\%$	$\phi = 4\%$
0.85		Johnson SB Random Walk Weibull
0.90		Weibull
0.97		Weibull
1.55		Johnson SB Weibull
1.80	Weibull	
1.94	None	Pearson Type 6 Random Walk

Table 4.7. Results of fitting the experimental data to probability models at different superficial velocities ($\alpha = 33\%$, 9 screens, $L = 10\text{mm}$).

Velocity (m/s)	$\phi = 0.5\%$
0.85	None
0.97	None
1.55	Rayleigh Weibull
1.80	Inverse Gaussian Johnson SB Random Walk Weibull
1.94	Inverse Gaussian Pearson Type 6

Table 4.8. Results of fitting the experimental data to probability models superficial at different velocities ($\alpha = 27\%$, 9 screens, $L = 10\text{mm}$).

velocity (m/s)	$\phi = 0.5\%$	$\phi = 4\%$
0.30	None	Log-logistic Log-normal Pearson Type 6 Random Walk
0.40	None	Log-logistic Pearson Type 6
0.50	None	Log-logistic Pearson Type 6
0.60	None	Log-logistic Pearson Type 6
0.65	None	Inverse Gaussian Log-normal Pearson Type 6
0.70	None	Rayleigh
0.85	Weibull	
0.90	Weibull	
0.97	Weibull	Weibull

2. Effect of Dispersed Phase Holdup

Table 4.9. Results of fitting the experimental data to probability models at different dispersed phase holdups ($\alpha = 41\%$, 9 screens, $L = 10\text{ mm}$).

Holdup (%)	$U = 0.40\text{ m/s}$	$U = 0.70\text{ m/s}$
0.5	None	NA
1	None	NA
2	None	None
3	None	Gamma Johnson SB Pearson type 5
4	None	Gamma Weibull

Table 4.10. Results of fitting the experimental data to probability models at different dispersed phase holdups ($\alpha = 27\%$, 9 screens, $L = 10\text{mm}$).

Holdup (%)	$U = 0.40$ m/s	$U = 0.70$ m/s
0.5	None	None
1	None	Weibull
2	None	Rayleigh Weibull
3	Log-normal E Pearson type 6	None
4	Log-logistic	Rayleigh Weibull

3. Effect of Surfactant

Table 4.11. Results of fitting the experimental data to probability models in presence of surfactant ($\alpha = 27\%$, $U = 0.70$ m/s, 9 screens, $L = 10\text{mm}$)

Surfactant concentration (mole/m ³)	$\phi = 0.5\%$	$\phi = 4\%$
0.01	Weibull (E)	Weibull
0.05	None	Johnson Sb Pearson type 6 Random walk Weibull
0.10	None	Gamma Johnson SB Pearson type 6 Weibull
0.20	Johnson SB Pearson type 6 Weibull	None
0.30	Pearson type 6	Gamma Johnson SB Pearson type 6 Weibull

Tables 4.6 to 4.11 show that in general there is no single probability model that can describe the drop size distributions generated under the different experimental conditions investigated. The Weibull probability model was found to be the most

common model that provides a fit to the experimental data at a significance level of 95%. Attempts were made to fit 92 sets of experimental data with different models. In 21 of such cases, the Weibull probability model gave a fit with the experimental data while the Pearson Type 6 gave a fit in 13 cases.

The results of the experimental data fitting also show that the generated drop size distributions obtained from liquid-liquid dispersions can not be represented by normal and log-normal models the most frequently reported in the literature (Chen and Middleman, 1967; Swartz and Kessler, 1970; Brown and Pitt, 1972; Duffy and Kadlec, 1974; Middleman, 1974; Molag et al, 1980; Hong and Lee, 1983; Wang and Calabrese, 1986; Sembira et al., 1986; Berkman and Clabrese, 1988; Chen et al., 1998; Seidshazileh, 1999). In 92 fitting cases, only in three incidents were the generated drop size distribution described by log-normal at 95% significance level, whereas the normal distribution did not fit even at 75% significance level. These results raise a question about the comprehensiveness of the fitting procedures adopted in the previous investigations and therefore more rigorous statistical fitting procedures are needed.

Self-Similarity

Several investigators reported that the normalized cumulative drop volume density distributions of liquid-liquid dispersions exhibit self-similarity (Sprow, 1967; Chen and Middleman, 1967; Tobin et al., 1990; Wright and Ramkrishna, 1994; Pacek et al., 1998, Seidshazileh, 1999) and therefore can be represented by a single model.

The obtained drop sizes were normalized with respect to the Sauter mean diameter; the cumulative drop volume distributions as a function of the normalized drop size were then plotted as shown in Figures 4.107 to 4.116. As can be seen, the cumulative drop volume distributions show reasonable self-similarity. However, as shown in Figures 4.108 and 4.111 to 4.115, a significant deviation from self-similarity is observed at higher dispersed phase holdups. This inconsistency may have been caused by the existence of two drop breakup mechanisms, namely turbulent breakup and drop cutting action, which is expected to become more significant at higher holdups. Also, as the dispersed phase holdup increased, some of the smaller drops may have been overlooked due to resolution

limitations associated with the photographic method used. On the other hand, as shown in Figure 4.116, it was found that the presence of the surfactant results in highly self-similar cumulative drop volume distributions. This is probably because the surfactant preferentially facilitates the larger drops breakup and thus leading to the formation of unimodal and relatively symmetrical drop size distributions, which show more similarity as seen earlier.

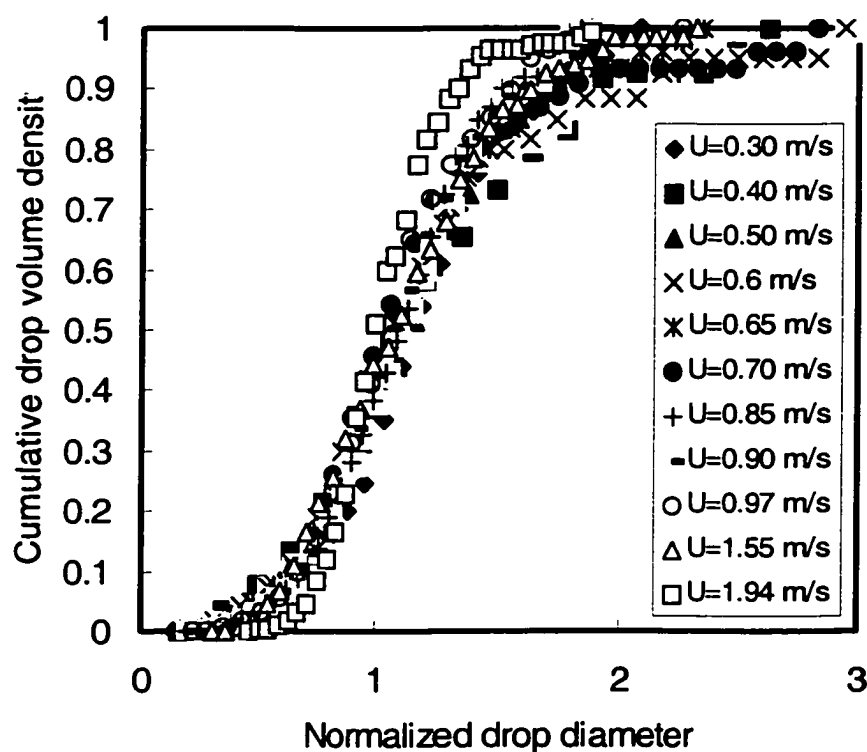


Figure 4.107. Self-similarity of the cumulative volume drop size distributions ($\alpha = 27\%$, $\phi = 0.5\%$, 9 screens, $L = 10\text{mm}$).

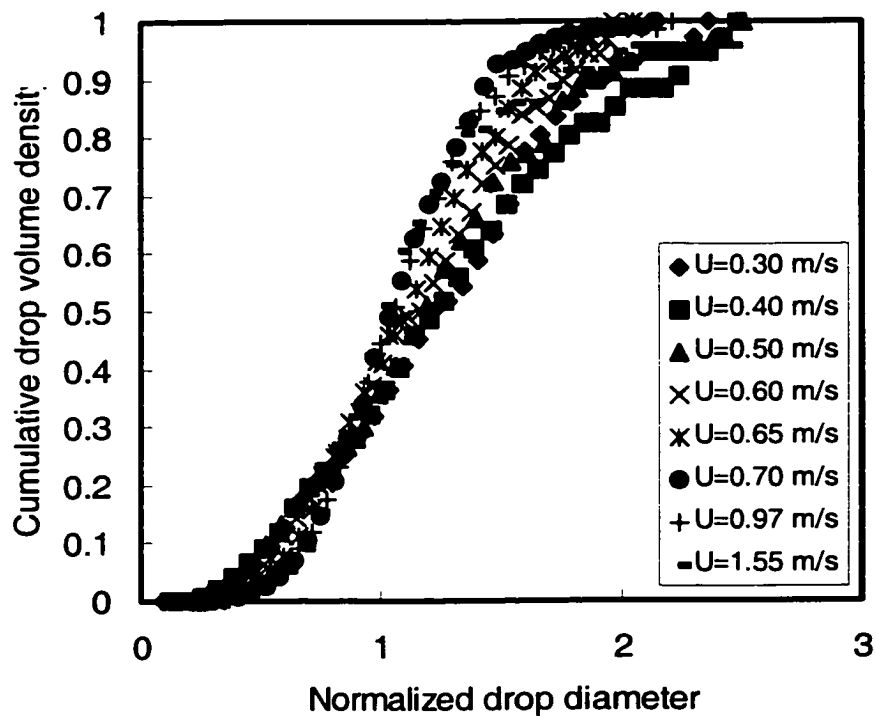


Figure 4.108. Self-similarity of the cumulative drop volume distributions ($\alpha = 27\%$, $\phi = 4\%$, 9 screens, $L = 10$ mm).

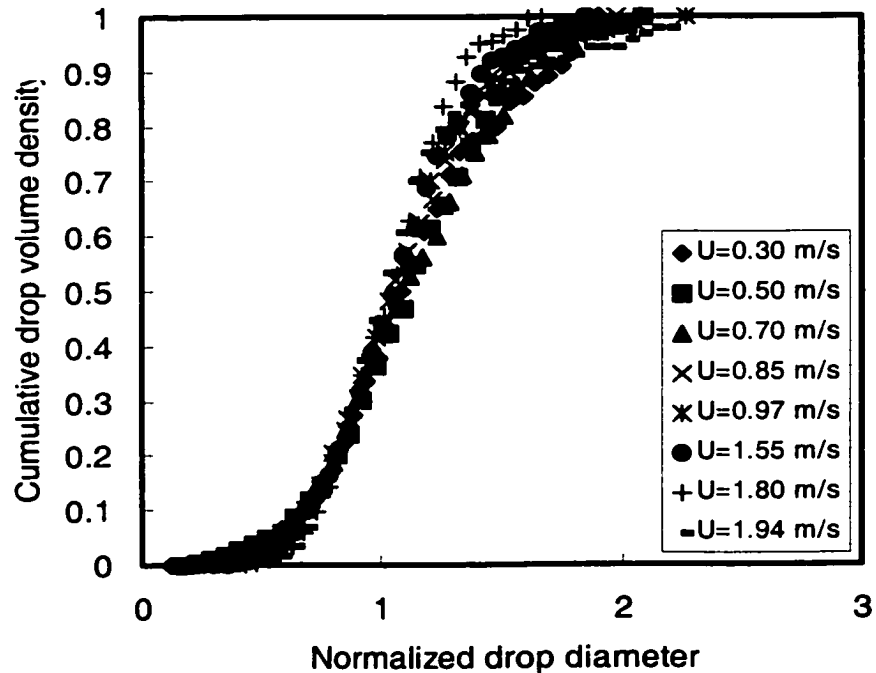


Figure 4.109. Self-similarity of the cumulative drop volume distributions ($\alpha = 33\%$, $\phi = 0.5\%$, 9 screens, $L = 10$ mm).

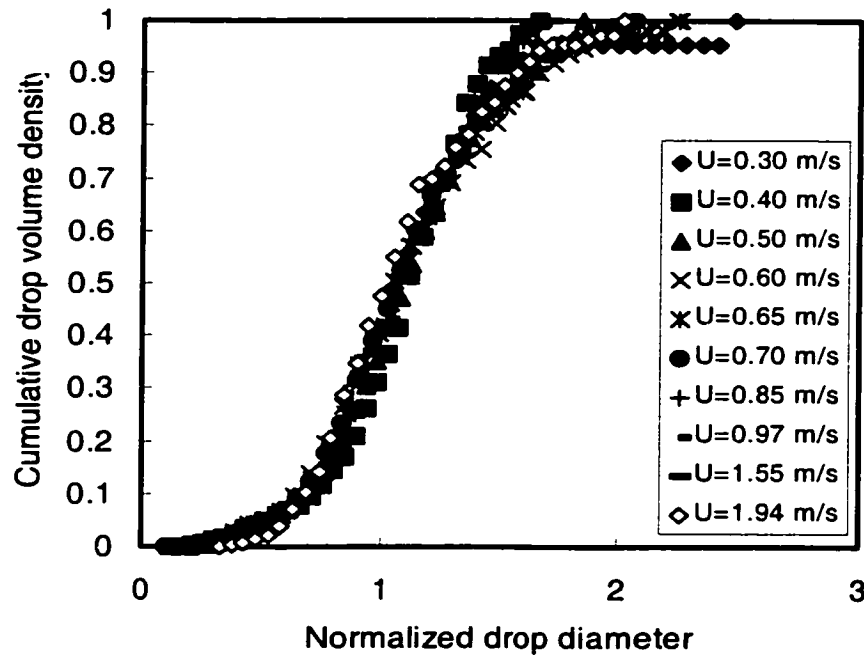


Figure 4.110. Self-similarity of the cumulative drop volume distributions ($\alpha = 41\%$, $\phi = 0.5\%$, 9 screens, $L = 10$ mm).

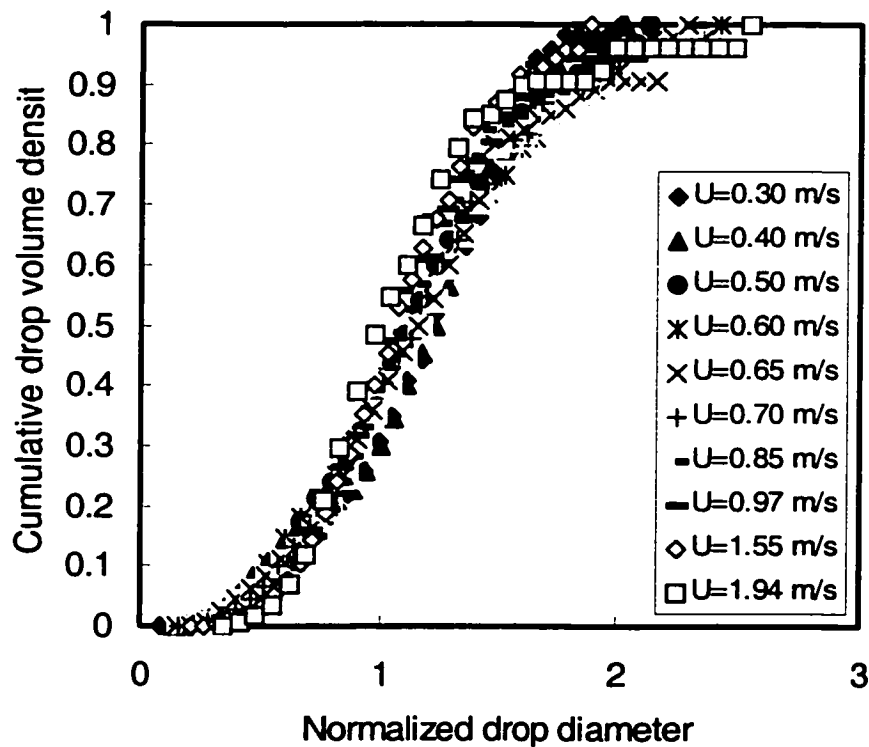


Figure 4.111. Self-similarity of the cumulative drop volume distributions ($\alpha = 41\%$, $\phi = 4\%$, 9 screens, $L = 10$ mm).

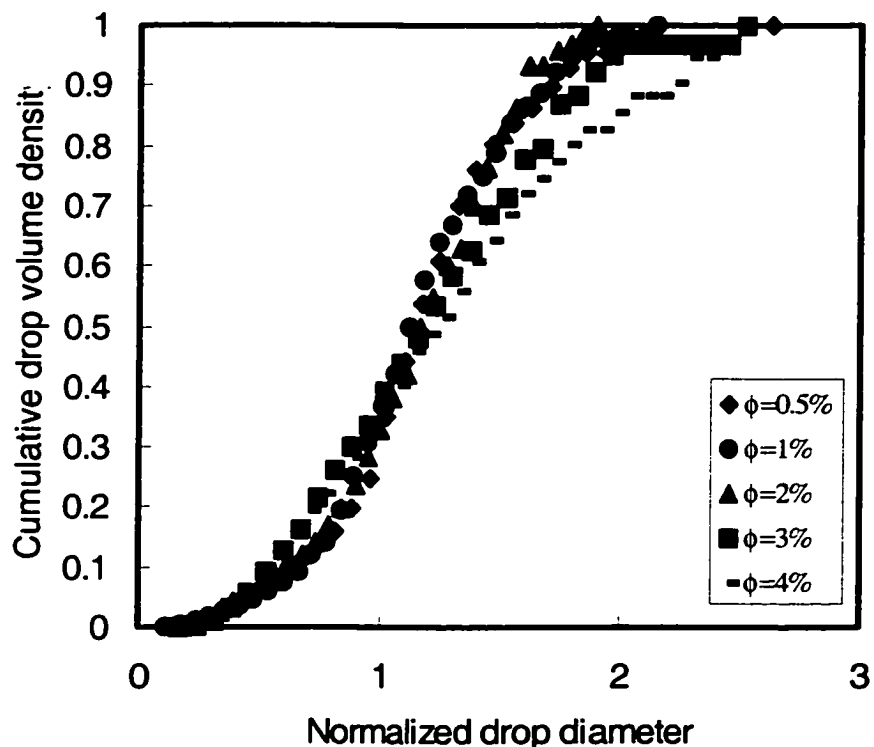


Figure 4.112. Self-similarity of the cumulative drop volume distributions at different dispersed phase holdups ($\alpha = 27\%$, $U = 0.40$ m/s, 9 screens, $L = 10$ mm).

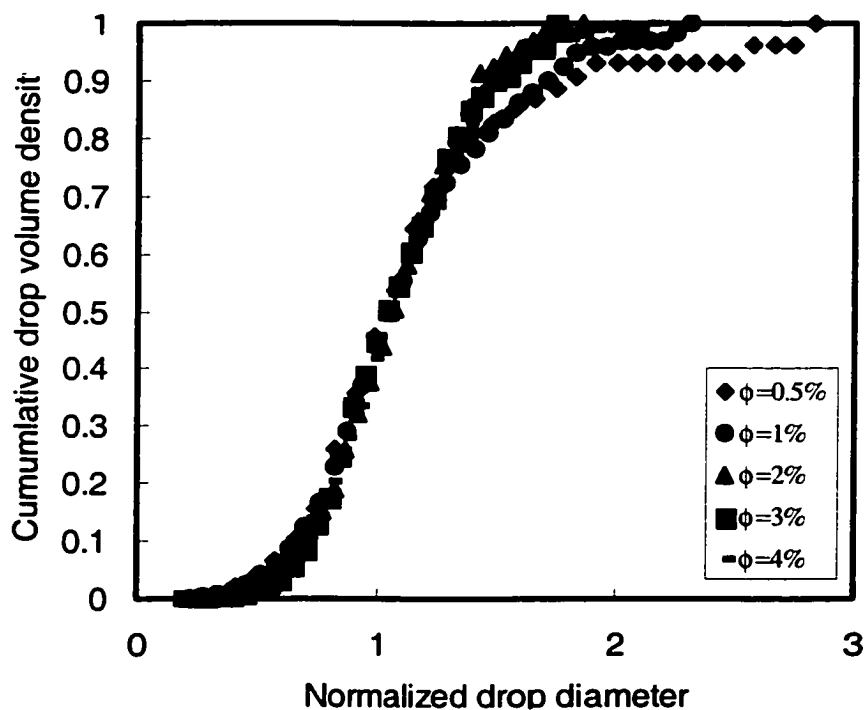


Figure 4.113. Self-similarity of the cumulative drop volume distributions at different dispersed phase holdups ($\alpha = 27\%$, $U = 0.70$ m/s, 9 screens, $L = 10$ mm).

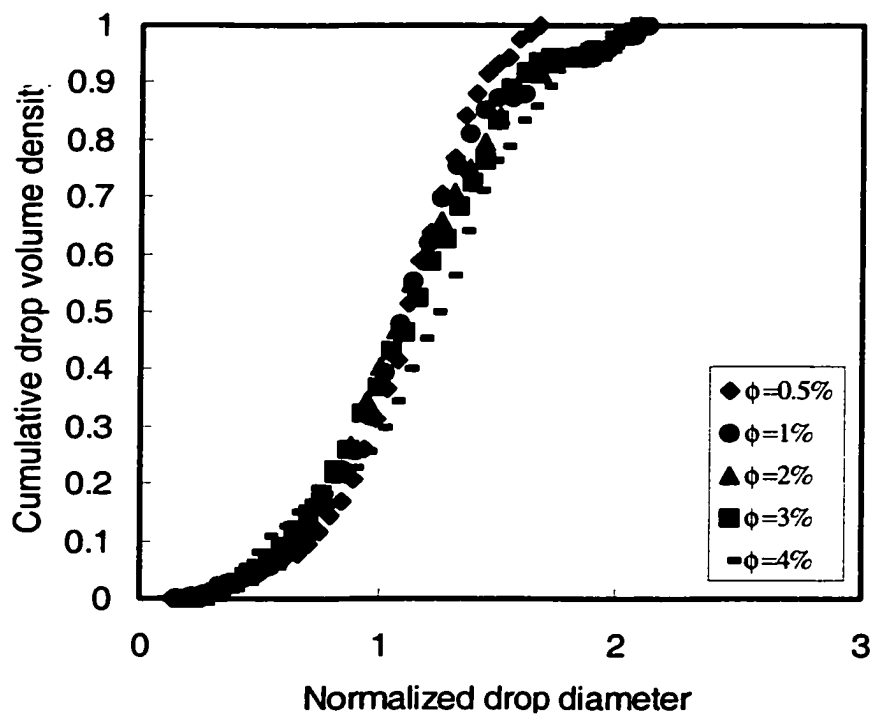


Figure 4.114. Self-similarity of the cumulative drop volume distributions at different dispersed phase holdups ($\alpha = 41\%$, $U = 0.40$ m/s, 9 screens, $L = 10$ mm).

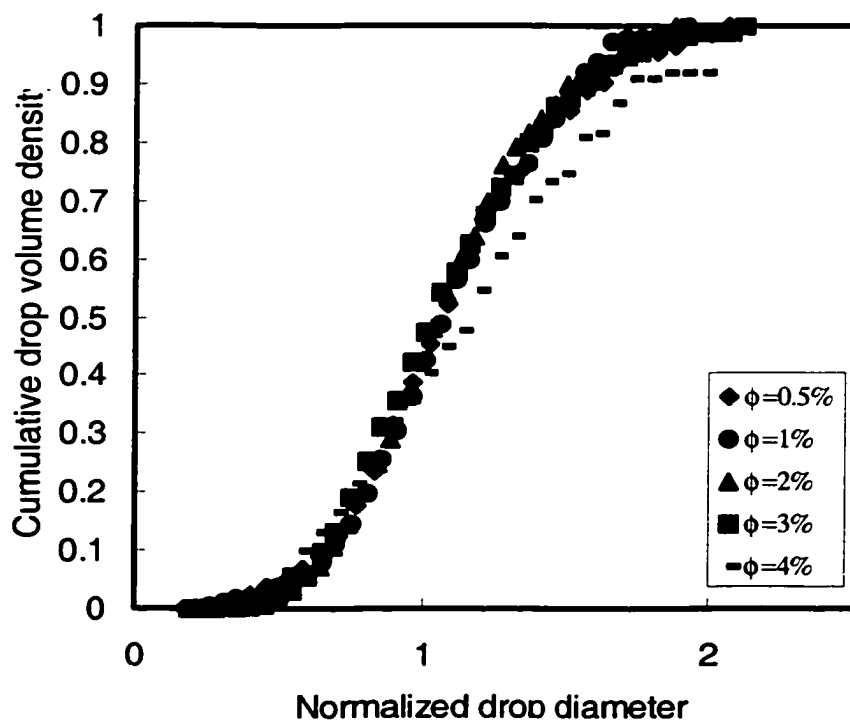


Figure 4.115. Self-similarity of the cumulative drop volume distributions at different dispersed phase holdups ($\alpha = 41\%$, $U = 0.70$ m/s, 9 screens, $L = 10$ mm).

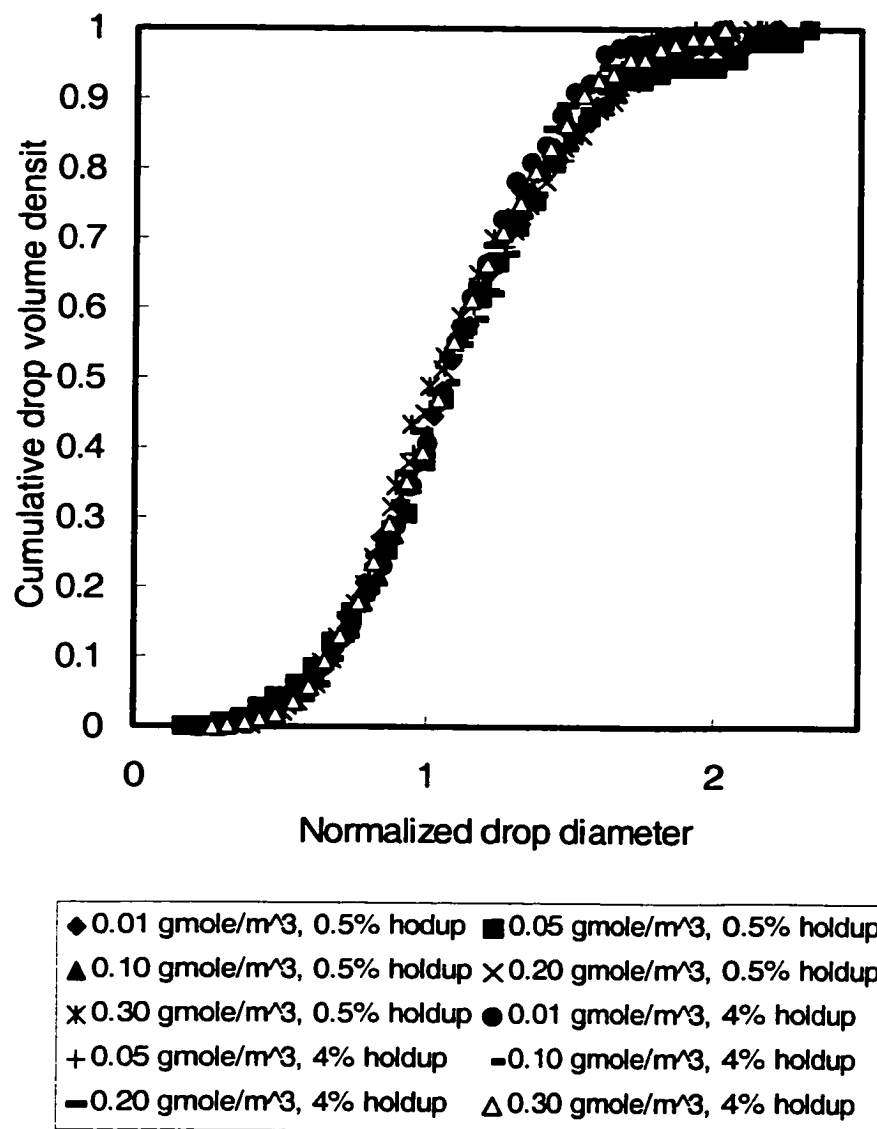


Figure 4.116. Self-similarity of the cumulative drop volume distributions
With SAA ($\alpha = 27\%$, $U = 0.70$ m/s, 9 screens, $L = 10$ mm).

Figure 4.117 shows the cumulative drop volume distribution as a function of the normalized drop diameter for all the obtained experimental data. The normalized distributions were compared with normal and log-normal probability functions, the most commonly reported models in the literature. The normalized cumulative normal and log-normal volume distributions are given by Equations (3-12) and (3-13) respectively.

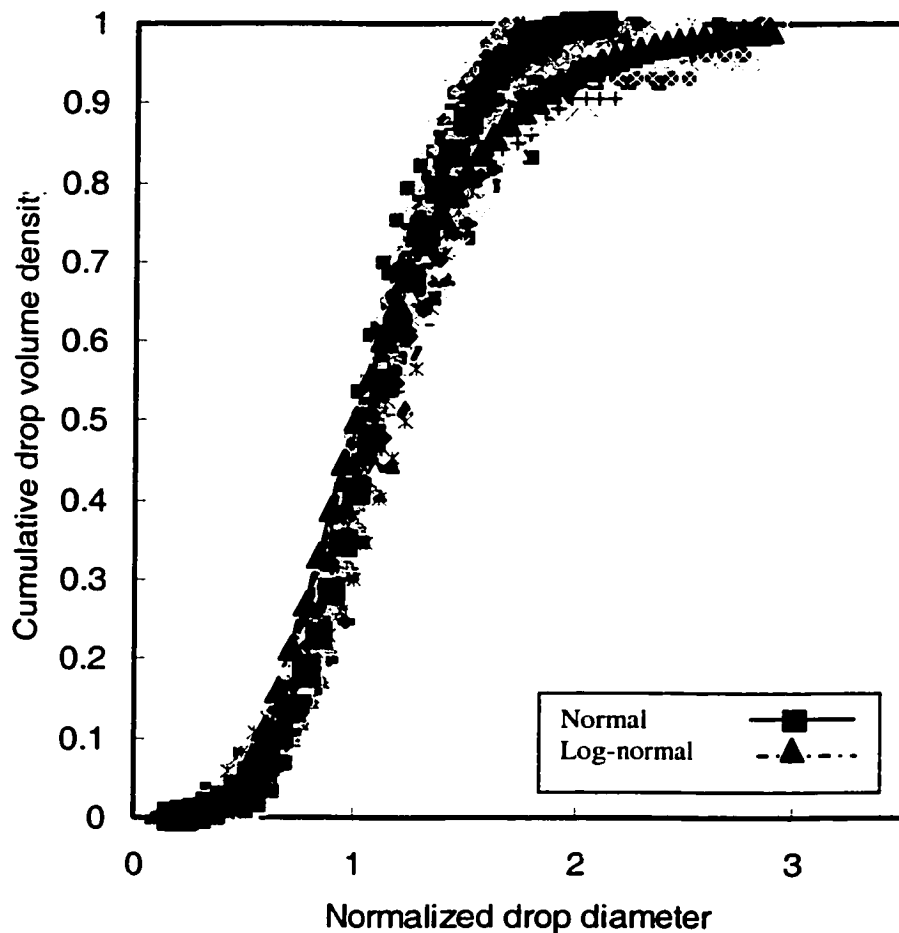


Figure 4.117. Self-similarity of the cumulative drop volume distributions for all experiments (9 screens, $L = 10$ mm).

The coefficients of the distributions were determined by linear regression (using Minitab 13). For the normal distribution $\bar{X} = 1.12$ and $\sigma = 0.30$ with a regression coefficient of 0.917 were obtained. For the cumulative log-normal distribution $\bar{X}_{lg} = 1.01$ and $\sigma = 1.72$ with a regression coefficient of 0.85 were found. These results are in

agreement with several investigators who reported that the cumulative drop volume distributions are normally distributed around the Sauter mean diameter (Seidshazileh, 1999; Pacek et al., 1998; Berkman and Calabrese, 1988; Wang and Calabrese, 1986; Chen and Middleman, 1967). Table 4.12 shows the results obtained for the case of the cumulative normal distribution compared with those reported by other investigators.

Table 4.12. Regression analysis of the normalized normal cumulative drop volume density (Bayol oil-water system)

	Present study	Seidshazileh (1999)	Pacek et al. (1998)	Berkman and Calabrese (1988)	Wang and Calabrese (1986)	Chen and Middleman (1967)
R	0.958	0.967	0.995	NA	NA	NA
Mean	1.12	1.28	0.98	1.12	1.07	1.06
s.d.	0.30	0.43	0.26	0.31	0.24	0.23

Table 4.12 shows that the mean and standard deviation found in this work are in full agreement with that reported by Berkman and Calabrese (1988) but higher than that obtained by Pacek et al. (1998), Berkman and Calabrese (1988) Wang and Calabrese (1986) and Chen and Middleman (1967). These lower results may be attributed to ignoring the larger drops during the process of drop size measurement as indicated by the normalized drop sizes reported in these studies. Pacek et al. (1998) reported a maximum normalized drop size of about 2.1, Wang and Calabrese (1986) reported a value of 1.7 and Chen and Middleman (1967) a value of 1.6 as opposed to a value as high as 3 in this study. Meanwhile, Seidshazileh (1999) who considered a similar range of drop sizes to that in this study and obtained higher values of mean and standard deviation than in this work. Furthermore, the existence of more than one breakup mechanism, namely turbulent breakup and drop cutting action, which is expected to become more significant at higher holdups and lower velocities may have played a role in this as well.

4.5 USING POPULATION BALANCE APPROACH TO MODEL DROP BREAKUP/COALESCENCE

The population balance approach is employed for the description of drop dynamics in various flow fields. A significant advantage of the method is that it provides a vehicle for including detailed analysis of breakage and coalescence processes in terms of the physical parameters and conditions of operation. Solving the resulting population balance equations enable prediction of temporal drop size distributions, which in turn, may be employed to describe in more detail the hydrodynamics and mass transfer rates in the given system. The general population balance is given by a relatively complicated differential equation. To model the drop interactions, either Monte Carlo techniques are applied or the population balance equations are solved numerically. Although the Monte Carlo methods are extremely flexible, powerful and free of convergence problems, they require so much computer time rendering them impractical. The numerical methods are also simple and flexible but present considerable computational difficulties and also consume much computer time (Elsayed and Al Taweel, 1994).

Only one analytical solution was reported in the literature by Rod and Misk (1982) who applied it to a step change in the operation of a batch dispersion system. This approach was recently found to be suitable to model drop breakup/coalescence in flow systems (Chen, 1996). However, the validity of this attempt suffered from the absence of drop size distribution data with which the theoretical predictions can be compared.

The objective of this section is to assess the suitability of using a modified form of the analytical population balance solution developed by Rod and Misk (1982) to describe drop breakup/coalescence to the case of static mixers. A comparison between the predicted and experimental results (temporal variation in Sauter mean diameter and drop size distributions) obtained under the different conditions investigated is presented.

Theoretical Background

Using the population balance approach, the variation of concentration of drops of diameter d with time can be written as follows (Rod and Misk, 1982),

$$\frac{\partial [N(t)f(d,t)]}{\partial t} = B_b(d,t) - D_b(d,t) + B_c(d,t) - D_c(d,t) \quad (4-25)$$

where the rates of drop birth and death by breakup are given by,

$$B_b = 2N(t) \int_0^{\infty} \beta(d,d')g(d')f(d',t) d(d') \quad (4-26)$$

$$D_b(d,t) = N(t)g(d)f(d',t) \quad (4-27)$$

and the rates of drop birth and death by coalescence are given by,

$$B_c(d,t) = \frac{[N(t)]^2}{2} = \int_0^d h[(d^3 - d'^3)^{1/3}, d] \frac{d^2 f[(d^3 - d'^3)^{1/3}, t]}{(d^3 - d'^3)^{2/3}} f(d',t) d(d') \quad (4-28)$$

$$D_c(d,t) = [N(t)]^2 f(d,t) \int_0^{\infty} h(d,d')f(d',t) d(d') \quad (4-29)$$

Where $g(d)$ denotes breakup intensity of drops of diameter d , $\beta(d, d')$ the conditional probability density of the formation of a daughter drop of diameter d by breakup of a drop of diameter d' , and $h(d, d')$ coalescence intensity of drops of diameters d and d' given by the product of the relative collision frequency and the coalescence efficiency. Once the g , β , h and $f(d, 0)$ (i.e. the initial distribution) are known, the generation of the drop size distribution, the instantaneous drop breakup and coalescence frequencies and the steady-state values of those parameters can be found.

Rod and Misek (1982) expressed the functions characterizing the processes of drop breakup and coalescence as follows:

$$g(d) = K_d d^{3(p+1)} \quad (4-30)$$

$$\beta(d, d') = \frac{3d^2}{d'^3} \quad (4-31)$$

$$h(d, d') = K_c (d^3 + d'^3)^p \quad (4-32)$$

where K_c and K_d are the coalescence and breakup coefficients respectively and p is an exponent that ranges from -1 to 1 depending on the mechanism. For any exponent value of more than -1 Rod and Hancil (1981) proved that the solution of the population balance

leads to the steady-state drop number and volume density distributions, which are expressed by,:

$$f(d) = \frac{3d^2}{d_{32}^3} \exp\left[-\left(\frac{d}{d_{32}}\right)^3\right] \quad (4-33)$$

$$\phi(d) = \frac{3d^5}{d_{32}^6} \exp\left[-\left(\frac{d}{d_{32}}\right)^3\right] \quad (4-34)$$

The variation of the Sauter mean diameter with time can thus be described by,

$$\frac{\partial d_{32}}{\partial t} = \frac{\Gamma(p+2)}{3} K_d d_{32}^{3p-2} (d_{32\infty}^6 - d_{32}^6) \quad (4-35)$$

Solving the differential equation using the boundary condition,

$$d_{32}(t)|_{t=0} = d_{320} \quad (4-36)$$

and $p = 0$ gives

$$d_{32}(t) = d_{32\infty} \left[\frac{1 + A \exp(-2K_d d_{32\infty}^3 t)}{1 - A(-2K_d d_{32\infty}^3 t)} \right]^{1/3} \quad (4-37)$$

where

$$A = \frac{d_{320}^3 - d_{32\infty}^3}{d_{320}^3 + d_{32\infty}^3} \quad (4-38)$$

Equation (4-37) is a modification of Equation (49) presented by Rod and Misk (1982)

Similarly for $p = 1$

$$d_{32}(t) = \left[(d_{320}^6 - d_{32\infty}^6) \exp(-2K_d t) + d_{32\infty}^6 \right]^{1/6} \quad (4-39)$$

and for $p = -1$

$$d_{32}(t) = d_{32\infty} \left[\frac{\exp(-4K_d d_{32\infty}^6 t)}{\exp(-4K_d d_{32\infty}^6 t) - 1 \left(\frac{d_{32\infty}}{d_{320}} \right)^6} \right]^{1/6} \quad (4-40)$$

Detailed solution of the above mentioned equations is given in Appendix C.

The results obtained using Bayol oil-water dispersions of 2% holdups, and different number of screens (to analyze the effect of residence time in the region of high energy dissipation) were compared with the three analytical solutions for the Sauter mean diameter as depicted in Figure 4.118. The drop breakup coefficient, K_d , was computed for the different p values by applying Equations (4-37), (4-38) and (4-40) to the experimental results obtained at a residence time of 0.08 seconds yielding,

$$K_d = 51.21 \quad (p = -1)$$

$$K_d = 1.77 \times 10^{11} \quad (p = 0)$$

$$K_d = -6.5 \times 10^{20} \quad (p = 1)$$

As shown in Figure 4.118, the model proposed by Rod and Misek (1982) fits the experimental data reasonably well for a p value of 0. From Figure 4.118, it is clear that the model proposed by Rod and Misek (1982) for a p value somewhere between 0 and 1 can provide a good fit of the experimental data. In order to obtain an analytical solution, the value of p was assumed 0 since it fits the data reasonably well.

Based on the assumption of binary breakup and binary coalescence, for $p = 0$ the functions characterizing breakup and coalescence processes take the following forms:

$$g(d) = K_d d^3 \quad (4-41)$$

$$\beta(d, d') = \frac{3d^2}{d'^3} \quad (4-42)$$

$$h(d, d') = K_c \quad (4-43)$$

Equation (4-41) therefore predicts that breakup frequency depends only on the average drop size. On the other hand, Equation (4-43) predicts that drop coalescence occurs at constant rate or simply stated coalescence frequency is independent of drop size. These predictions are not in full agreement with the drop breakup/coalescence theory discussed in section 2.2, but they are in agreement with Chen's (1996) findings for the case of dispersions of different petroleum products in water.

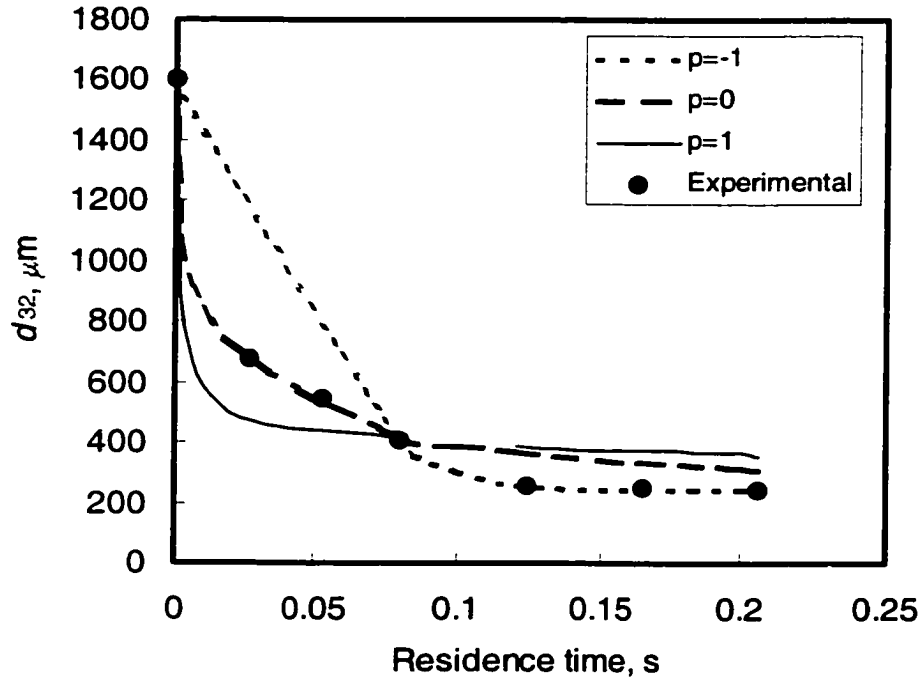


Figure 4.118. Comparison of results with the analytical solution of the population balance equation ($\alpha = 27\%$, $\phi = 2\%$, $U = 0.40$ m/s, 9 screens, $L = 10$ mm)

In analogy with the kinetics of a reversible chemical reaction under equilibrium conditions, Walker (1984) developed the following expression to describe the variation of the average drop size with time:

$$\frac{d(d_{32})}{dt} = K(d_{32} - d_{32}^{\infty})^n \quad (4-44)$$

where the driving force for drop breakage $(d_{32} - d_{32}^{\infty})^n$ becomes equal to zero when the equilibrium drop size is reached. He found that a value of $n = 2$ fits his experimental data for Lightnin in-liner static mixers reasonably well with insignificant deviation for low superficial velocities. This corresponds to a p value of $-1/3$. Meanwhile Chen (1996) found that the best fits for his experimental data were obtained using n values varying between 1.1 and 1.7, which corresponds to p values of $-1.9/3$ and $-1.3/3$. The difference between the above p values and that obtained in the present study may be attributed to the fact that both researchers used a light attenuation method for the measurement of the interfacial area from which the average drop size was computed. This method is very

sensitive to the presence of fine droplets, which do not play as important a role in the image analysis technique used in the present investigation. Furthermore, the expression developed by both researchers represent the overall rate of change in drop size, which is comprised of drop breakup and coalescence rates whereas the p value found in this study perfectly fits the data in a breakage dominated region as shown in Figure 4.118. The physical properties of the systems investigated in the above studies may have played a role in this difference as well.

The cumulative drop size distributions obtained under different experimental conditions were compared with the drop number and drop volume density distributions developed by Rod and Misk (1982). The predicted drop size distributions were computed using Equations (4-33) and (4-34) and the experimentally determined Sauter mean diameters. Samples of the results obtained are shown in Figures 4.119 to 4.122 while the rest of the comparisons are shown in Figures D1 to D65 in Appendix D. These findings clearly show that Rod and Misk model provides a reasonably good fit to the cumulative drop number and volume distributions generated under the different experimental conditions investigated but a better fit is obtained in the case of cumulative drop volume distributions.

The relatively poor fit observed in the case of cumulative drop number density distributions may be attributed to tendency of the model to underestimate breakage particularly in the fine drop range. On the other hand, drop volume density distributions were found to yield better fitting results (Figures 4.121 and 4.122) because they are more strongly influenced by the fraction of the large drops present in the dispersion.

From the above findings it can be concluded that the modified Rod and Misk (1982) model can be successfully used to describe drop breakup/coalescence taking place in relatively homogeneous turbulent flows similar to those encountered in the present study.

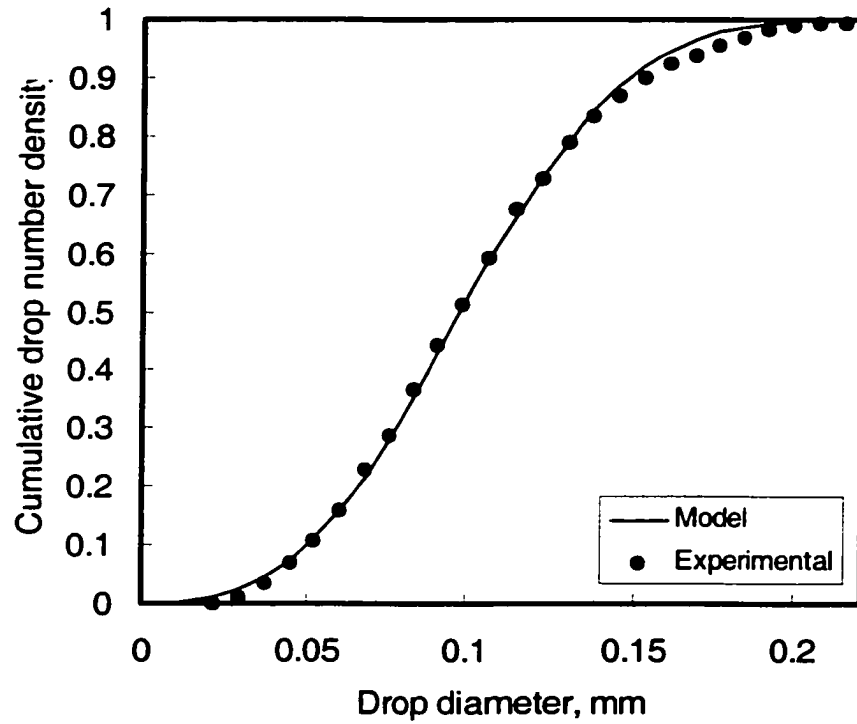


Figure 4.119. Cumulative drop number density distribution ($\alpha = 27\%$, $\phi = 4\%$, $U = 0.70$ m/s, 9 screens, $L = 10$ mm)

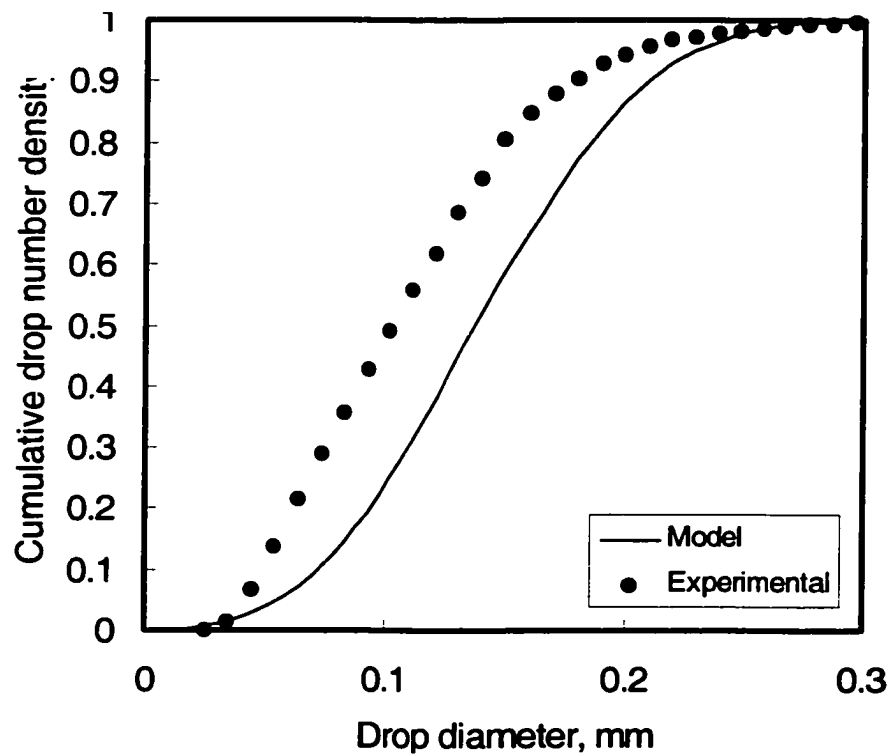


Figure 4.120. Cumulative drop number density distribution ($\alpha = 27\%$, $\phi = 1\%$, $U = 0.70$ m/s, 9 screens, $L = 10$ mm)

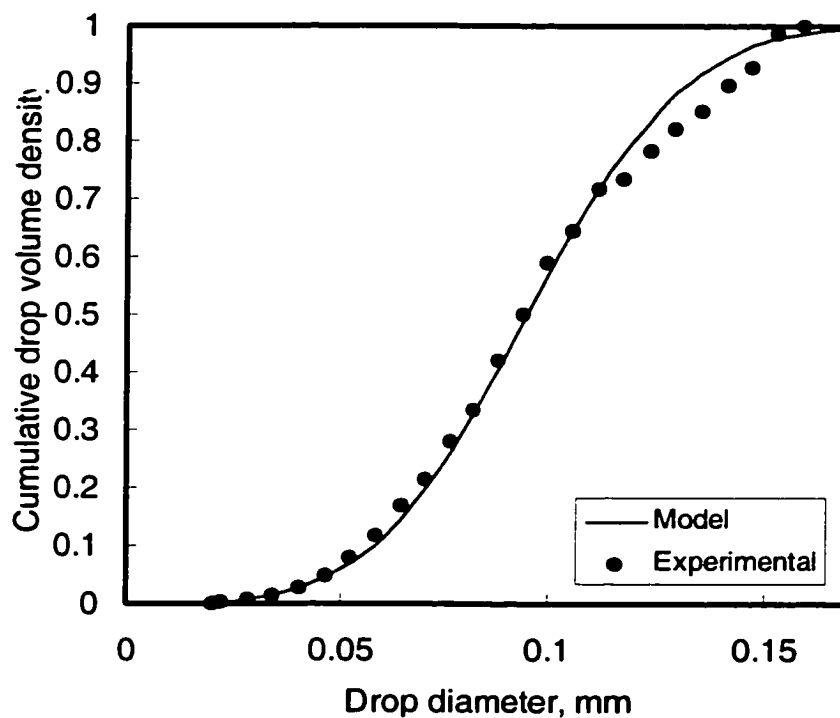


Figure 4.121. Cumulative drop volume density distribution
($\alpha = 41\%$, $\phi = 4\%$, $U = 0.97$ m/s, 9 screens, $L = 10$ mm)

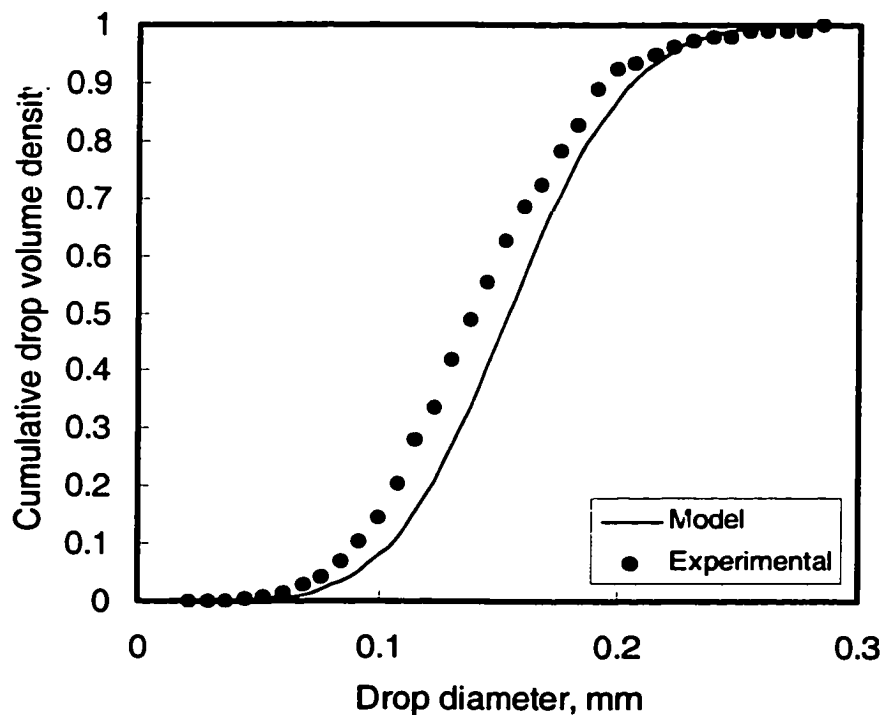


Figure 4.122. Cumulative drop volume density distribution
($\alpha = 27\%$, $\phi = 4\%$, $U = 0.70$ m/s, 9 screens, $L = 10$ mm)

4.6 EFFICIENCY OF ENERGY UTILIZATION

Al Taweel and Walker (1983) proposed the use of the ratio of free energy of the newly generated surface to the mechanical energy expended to generate it, as an indicator of the efficiency of energy utilization by the mixer. Thus,

$$\eta = \frac{6\phi\sigma}{\rho E} \left(\frac{1}{d_{32}} - \frac{1}{d_{320}} \right) \times 100 \quad (4-45)$$

This concept provides a better understanding of the effectiveness of energy utilization to generate and maintain the interfacial area between the phases. Due to the large difference between the inlet and outlet diameters (5- to 8- folds at 0.5% dispersed phase holdup using screens of 41% open area) the term $1/d_{320}$ is generally much smaller than $1/d_{32}$ and can thus be neglected in comparison to the latter. This is particularly true at high dispersed phase holdups.

Figures 4.123 and 4.124 show the effect of superficial velocity on energy utilization efficiency at dispersed phase holdups of 0.5% and 4% respectively. As can be seen from both figures, the energy utilization efficiency was found to decrease with increasing superficial velocity. Also, at both dispersed-phase holdups the slope of each curve decreases with increasing superficial velocity and this being more pronounced at 4% dispersed phase concentration. The results obtained at 0.5% holdup show that the energy utilized in generating the interfacial area between the two phases is extremely low compared with energy dissipated in the mixer. These low efficiencies may be mainly attributed to the low drop population density. Also, as can be seen from Figure 4.123, screens of higher open area show relatively better energy utilization. This may be attributed to the incompatibility of the eddy sizes generated by the lower open area screen. The eddy sizes generated might be much smaller than that required to cause drop breakup. These findings indicate that an increase in the specific energy input to the mixer does not result in commensurate increase in the net breakage of drops. This is in contradiction with the concept of focusing energy dissipation in small volumes in order to maximize local energy dissipation rates and hence enhance drop breakup rates. This contradiction may be attributed to the following:

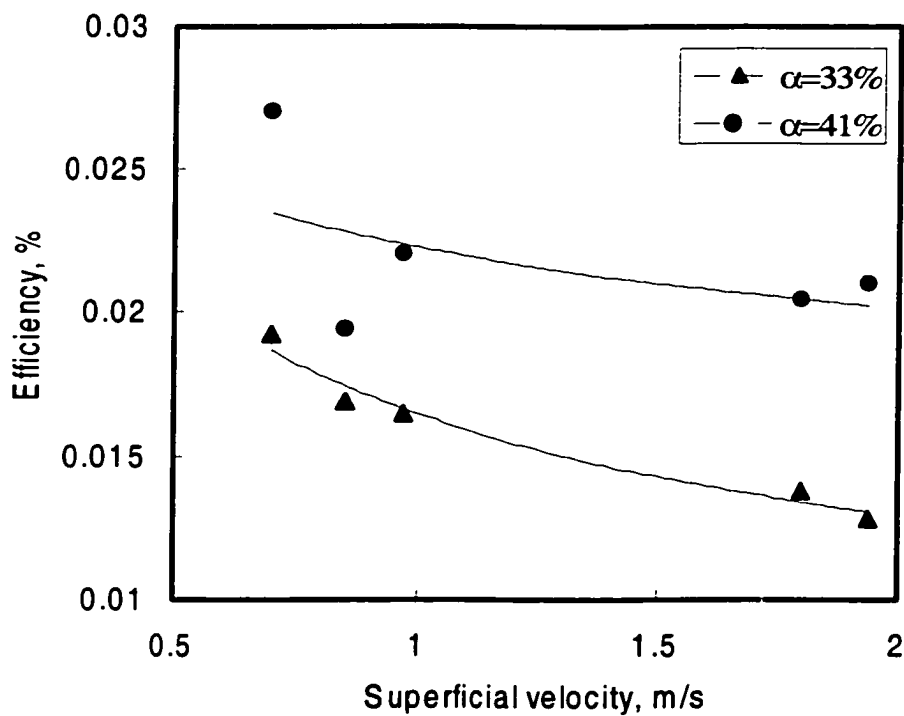


Figure 4.123. Efficiency of energy utilization at various velocities ($\phi = 0.5\%$, 9 screens, $L = 10$ mm).

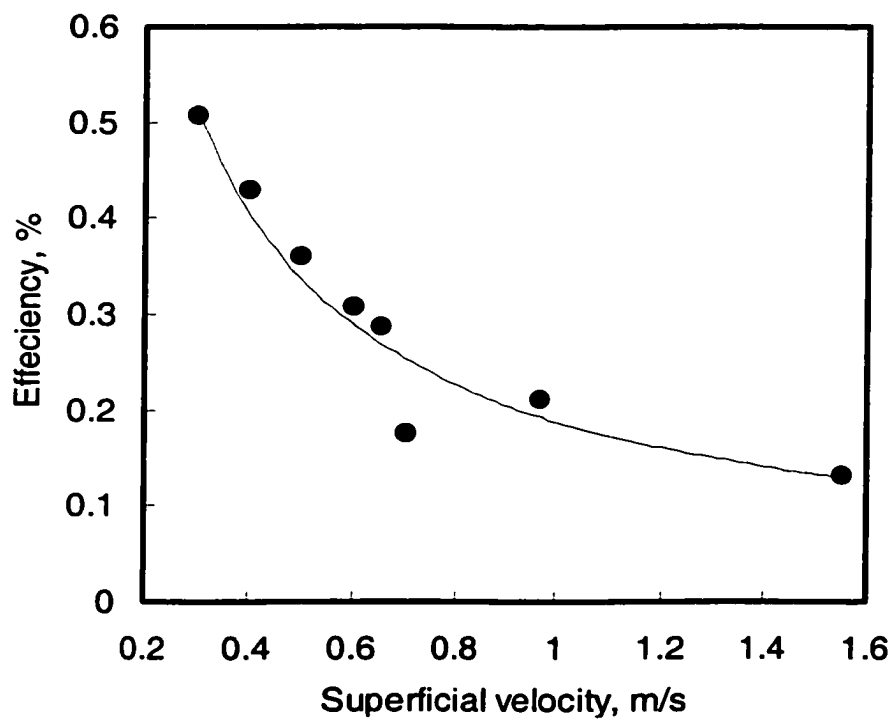


Figure 4.124. Effect of superficial velocity on efficiency of energy utilization ($\alpha = 27\%$, $\phi = 4\%$, 9 screens, $L = 10$ mm)

- Low dispersed phase holdups used, which in turn results in low drop population densities and hence lower interfacial areas. At low holdups the probability of eddy-drop interaction lessens, and consequently decrease in drop breakup frequency results as the drop population density decreases at lower dispersed phase concentrations.
- Short retention times. This means that at higher superficial velocities the drops remain for shorter times in the high energy dissipation rate region. Simply stated, the drops are exposed for shorter times for turbulent eddies, which cause drop breakup resulting in a decrease in breakage efficiency.
- Although the concept of energy dissipation rates being focused in small volumes; where coalescence rate is fast (i.e., in pure systems), is not very energy efficient. In the presence of surface-active agents, it can be very advantageous where drop coalescence can be retarded as seen in section 4.2.

The above findings are in agreement with observations reported by Al Taweel and Walker (1983), and El-Hamouz (1994), who observed that the energy utilization efficiency in in-line Lightning static mixers decreases with increasing superficial velocity. Later, Chen (1996) observed similar behavior in screens, which he attributed, in addition to the shorter residence times at higher velocities, to the inefficient utilization of the continuous phase turbulent energy due to the incompatibility of turbulence scale. He proposed that the turbulence scale is much smaller than that required for drop breakup to occur. Consequently, he suggested the use of screens of progressively smaller open area in order to attain optimum energy utilization.

The effect of increasing dispersed phase holdup on the energy utilization efficiency is illustrated in Figure 4.125 which clearly shows that the efficiency of energy utilization increases with increasing dispersed phase concentration. This can be attributed to the enhanced probability of eddy-drop interaction, and the consequent increase in drop breakage rate that occurs as the drop population density increases as a result of increasing dispersed phase holdup. The nearly linear relationship between the two suggests that

coalescence plays a very limited role under the hydrodynamic and interfacial conditions encountered in this set of experiments.

Figure 4.126 shows the variation of the efficiency of energy utilization with number of screen elements in the static mixer. Initially, the efficiency was found to increase with the number of elements until the fourth screen and then it remains practically constant up to 9 elements, after which it underwent a sharp fall and continues to decrease as the number of screens elements is further increased. This behavior can be explained by the fact that drop size is progressively reduced with increasing number of elements and equilibrium conditions are essentially achieved using 9 elements (Figure 4.27 in section 4.2.3), further increase in the number of elements merely serves to maintain the dispersion at equilibrium conditions in the regions where they are present. The spacing between the elements present in the mixer, downstream from the point where equilibrium conditions are achieved, should therefore be optimized to maintain the desired average

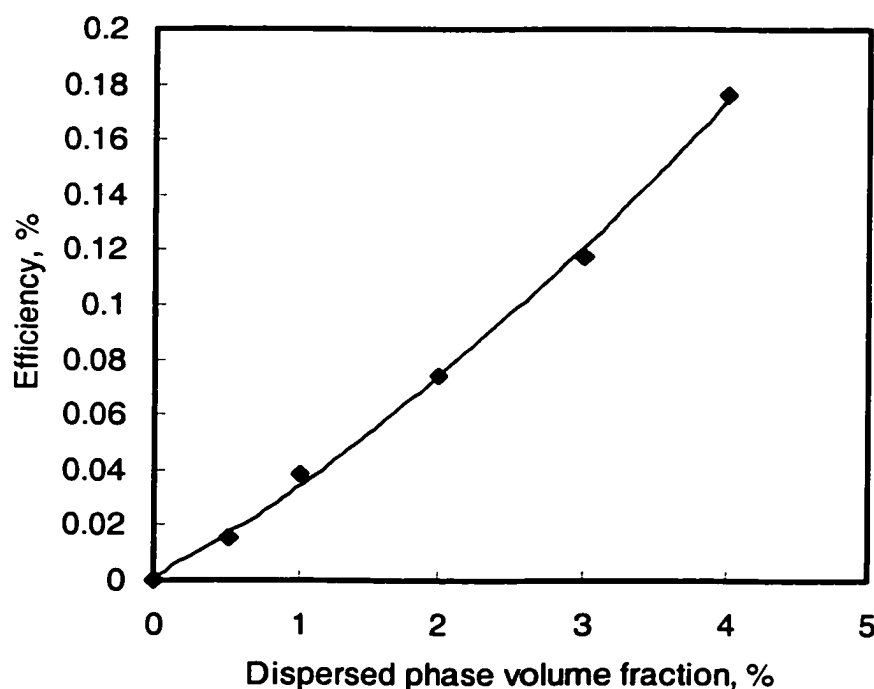


Figure 4.125. Effect of dispersed phase holdup on efficiency of energy utilization ($\alpha = 27\%$, $U = 0.70$ m/s, 9 screens, $L = 10$ mm)

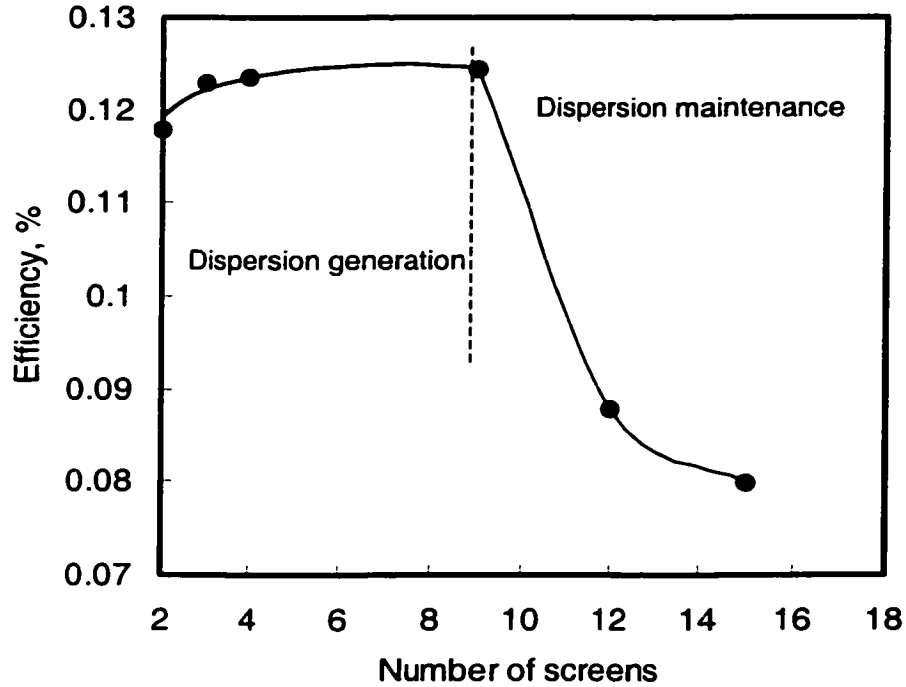


Figure 4.126. Effect of number of screens on efficiency of energy utilization ($\alpha = 27\%$, $\phi = 2\%$, $U=0.40$ m/s., $L = 5$ mm)

drop size without excessive turbulent energy dissipation. This is expected to be a strong function of the drop coalescence rate, hence of the interfacial characteristics, with bigger spacing being desirable in the presence of materials that retard drop coalescence rates. This result emphasizes the need for maintaining a certain residence time in order to achieve the desired drop size.

The efficiency obtained from the experimental data indicates that it depends on ϕ , U and α . Therefore the efficiency of energy utilization (η) can be correlated using the following formula:

$$\eta = c\phi^a U^b \alpha^d \quad (4-46)$$

The values of a , b and c were determined by stepwise regression using Minitab 13 software with a correlation coefficient of 0.989 and hence Equation (4-46) becomes,

$$\eta = 107.15\phi^{1.40} U^{-0.38} \alpha^{1.11} \quad (4-47)$$

Figure 4.127 shows that the above correlation can fit the experimental data very well.

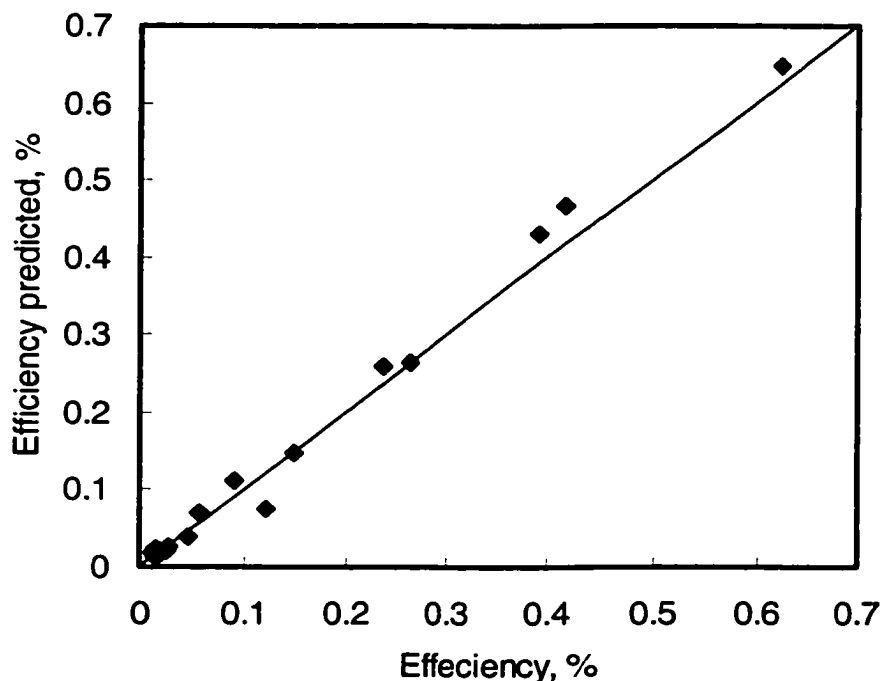


Figure 4.127. Comparison of predicted efficiency by Equation (4-47) and calculated values from experimental data.

4.7 COMPARISON WITH OTHER MIXERS.

Different criteria have been proposed for expressing the energy input to a liquid-liquid contactor. The first approach considers the overall amount of energy supplied to the mixer per unit time. This term represents the power input to, electric motors which drive agitating devices in case of stirred tanks and liquid pumps in case of pipe flow. Such power input, P , is usually related to the overall mixer volume, V , and thus the power consumption per unit volume, P/V , is often used to characterize the energy demands of the respective mixer types.

The second approach focuses on the rate of energy dissipated per unit time and unit mass in the region where mixing takes place. The entire volume of the contactor is often considered if the mixing intensity is taken essentially to be uniform throughout the mixer's volume. For pipe flow, the volumetric average rate of energy dissipation per unit time and unit mass of the flowing mixture can thus be expressed as,

$$\varepsilon = \frac{U\Delta P}{\rho_c L} \quad (3-48)$$

The local energy dissipation rate, which is often assumed to be uniform and equal to the volumetric average rate, is of prime importance when considering the mechanisms of drop breakup and coalescence, and mixing equipment design.

The third approach applies only to the case of continuously flowing systems. This approach, which has been proposed by Koglin et al. (1981) and Al Taweel and Walker (1983), focuses on the energy dissipated in processing a unit mass of the flowing mixture. For a fluid passing through a static mixer, the residence time is given by:

$$\theta = \frac{L}{U} \quad (4-49)$$

Hence, the total energy dissipated per unit mass pumped through the mixer may be calculated as follows,

$$E = \theta\varepsilon \quad (4-50)$$

Substituting Equations (4-48) and (4-49) gives,

$$E = \frac{\Delta P}{\rho_c} \quad (4-51)$$

This approach addresses the concerns of the mixing equipment users rather than those of the equipment designers. It also has the advantage of allowing for the comparison of the performance of contacting equipment with significantly different retention times.

In the present study, the second and the third approaches will be used as basis for evaluating the performance of the static mixer investigated and for comparing it with other mixing devices.

As pointed out earlier, the main objective of any liquid-liquid dispersion operation is to increase the area of contact between the two phases; thereby promoting mass and heat transfer rates, which are of prime importance in the chemical process industries. It is however important to consider the subsequent phase-separation stage which can be adversely affected by the formation of excessively fine drops. Assuming that the various mixing devices generate essentially similar drop size distributions (which has been shown, in section 4.4.3 not to be the case), the users of mixing devices will therefore be

primarily concerned about the power required to process a given mass of feed (while maintaining the same interfacial area of contact) when evaluating the performance of various contactors.

Figure 4.128 shows the effect of the mean energy dissipation rate in the mixer on the interfacial area generated. The experimental results obtained show that for all screen designs tested, the interfacial area generated increases with increasing ϵ values. Although this is true in both holdups tested, the effect is more pronounced at higher dispersed phase holdups ($\phi = 4\%$), a fact which can be attributed to the higher efficiency of energy utilization achieved at higher drop population densities. The data also clearly show that screen design does not play a significant role (no segregation tendency with screen open area) suggesting that screens of different solidity produce the same interfacial area for the same amount of energy expenditure. Deviation from linearity at high energy expenditure rates may be attributed to drop coalescence of the smaller drops, which is expected to be more significant at higher energy dissipation rates particularly at high dispersed phase holdups. As the energy dissipation rate (i.e., superficial velocity) increases, the collision frequency increases and hence the coalescence frequency also increases (Prince and Blanch, 1990). The scatter of the experimental data at high holdups may have been caused by inaccuracies in drop size measurements due to limitations in the imaging field and sample size. Similar findings were reported by Walker (1984) for dispersions of kerosene in water using screens of different open area and different In-liner configurations.

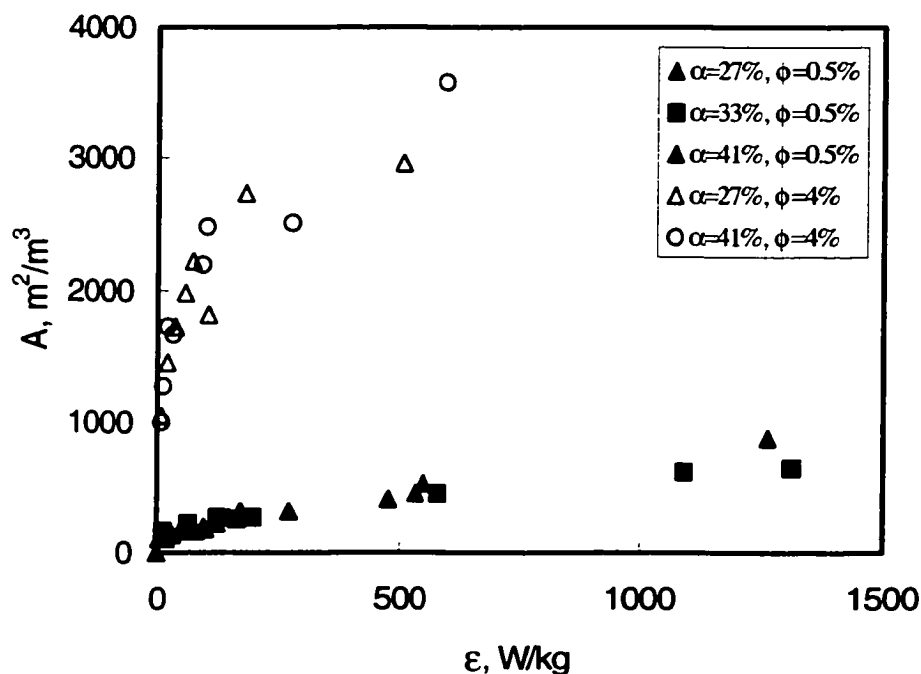


Figure 4.128. Variation of the interfacial area with mean energy dissipation rate (9 screens, $L = 10$ mm).

As can be seen from Figure 4.128, the interfacial areas generated at high holdup are much higher than those expected from a proportional increase in dispersed phase holdup. For example, a mean energy dissipation rate of 250 W/kg produces an interfacial area of approximately $265 \text{ m}^2/\text{m}^3$ when 0.5% dispersed phase holdup is used whereas it is $2900 \text{ m}^2/\text{m}^3$ in the case of $\phi = 4\%$ (i.e. more than the $2100 \text{ m}^2/\text{m}^3$ expected from an 8-fold increase in dispersed phase holdup). This large difference may be attributed to the proposed drop cutting mechanism, which is expected to be more prevalent at high-dispersed phase volume fractions. This, in turn, suggests that drop cutting is a more energetically efficient mechanism resulting in the generation of finer drop sizes and hence higher interfacial areas.

Figure 4.129 shows the variation of the interfacial area, A , in the disperser with the energy expenditure per unit mass of the mixture, E , flowing through the mixer. As can be seen, the experimental data are grouped according to the dispersed phase holdup in a fashion similar to that observed in Figure 4.128. Also, the interfacial areas produced

at high holdups are greater than those attributed to a simple increase in ϕ . This can be attributed to the existence of two drop breakup mechanisms, drop cutting action and turbulent breakup. First, drops undergo cutting action by screen wires, which is then followed by turbulent drop breakup resulting in finer dispersions.

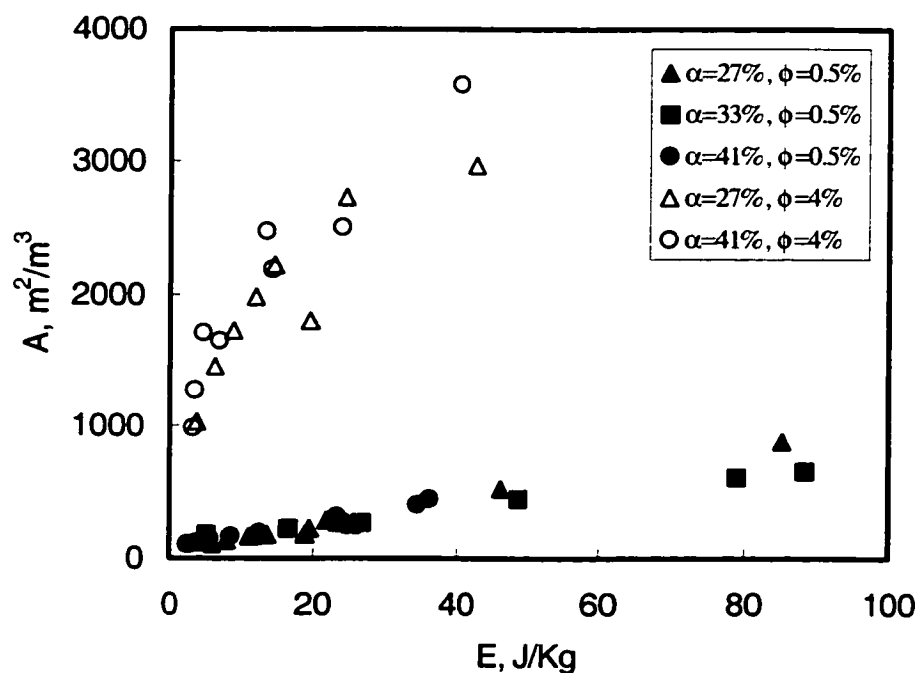


Figure 4.129. Variation of the interfacial area with energy utilization (9 screens, $L = 10$ mm).

In the following sections, the performance of the screen-element static mixer is compared with the performance data reported by other investigators. First, a comparison with continuously flowing mechanically agitated tanks equipped with Rushton type impeller, the most commonly used mixer in industry, is conducted. This is followed by a comparison with the performance of static mixers that exhibit relatively similar hydrodynamic conditions and flow characteristics to the mixer investigated.

Most of the information dealing with the dispersion characteristics of mechanically agitated tanks is based on experimental investigations carried out in batch

mode where equilibrium conditions are approached after very long times, typically ranging from 60 to 180 minutes (Chatzi et al., 1991; Tobin and Ramkrishna, 1992; Seidshazileh, 1999). This does not facilitate the comparison with the continuous flow conditions encountered in the present investigation. Therefore, the comparison is based on data obtained from continuously flowing mechanically agitated tanks.

Figure 4.130 shows a comparison of the performance of the screen-element static mixer with mechanically agitated tanks on the basis of the volumetric average energy dissipation rate. Whereas mechanically agitated tanks require relatively low ϵ values (0.2 – 8 w/kg), static mixers need much higher values of ϵ (10 – 2,000 w/kg in the case of screen elements). These high values are low relative to those encountered in the case of other static mixer designs (Kenics, Lightnin). Under similar conditions of energy dissipation rate and dispersed phase volume fraction, the interfacial area generated using mechanically agitated tanks is at least twice that obtained in the investigated mixer. However, this simple comparison can be misleading since it is known that MAT exhibit very large spatial variation in local energy dissipation rates (Cheng, 1994; Zhou and Kresta, 1997; Torrez and Andre, 1998). Two regions of low and high-energy dissipation rates do therefore coexist in stirred tanks with local energy dissipation ratios as high as 200 being observed (Villermaux, 1988). Drop breakup dominates in the small high-energy region close to the impeller, whereas coalescence dominates in the low energy region prevalent in the rest of the tank's volume. Sampling in stirred tanks is often performed at a point close to the impeller (Pacek et al., 1998; Seidshazileh, 1999), which is not necessarily representative of the conditions throughout the tank unless special precautions are taken. A comparison on the basis of ϵ that is computed using the whole volume of the tank is therefore misleading since the actual value causing the drop dispersion may be up to two orders of magnitude larger. This has been clearly demonstrated by Cutter (1966) and Sprow (1967a) and more recently by (Torrez and Andre, 1998).

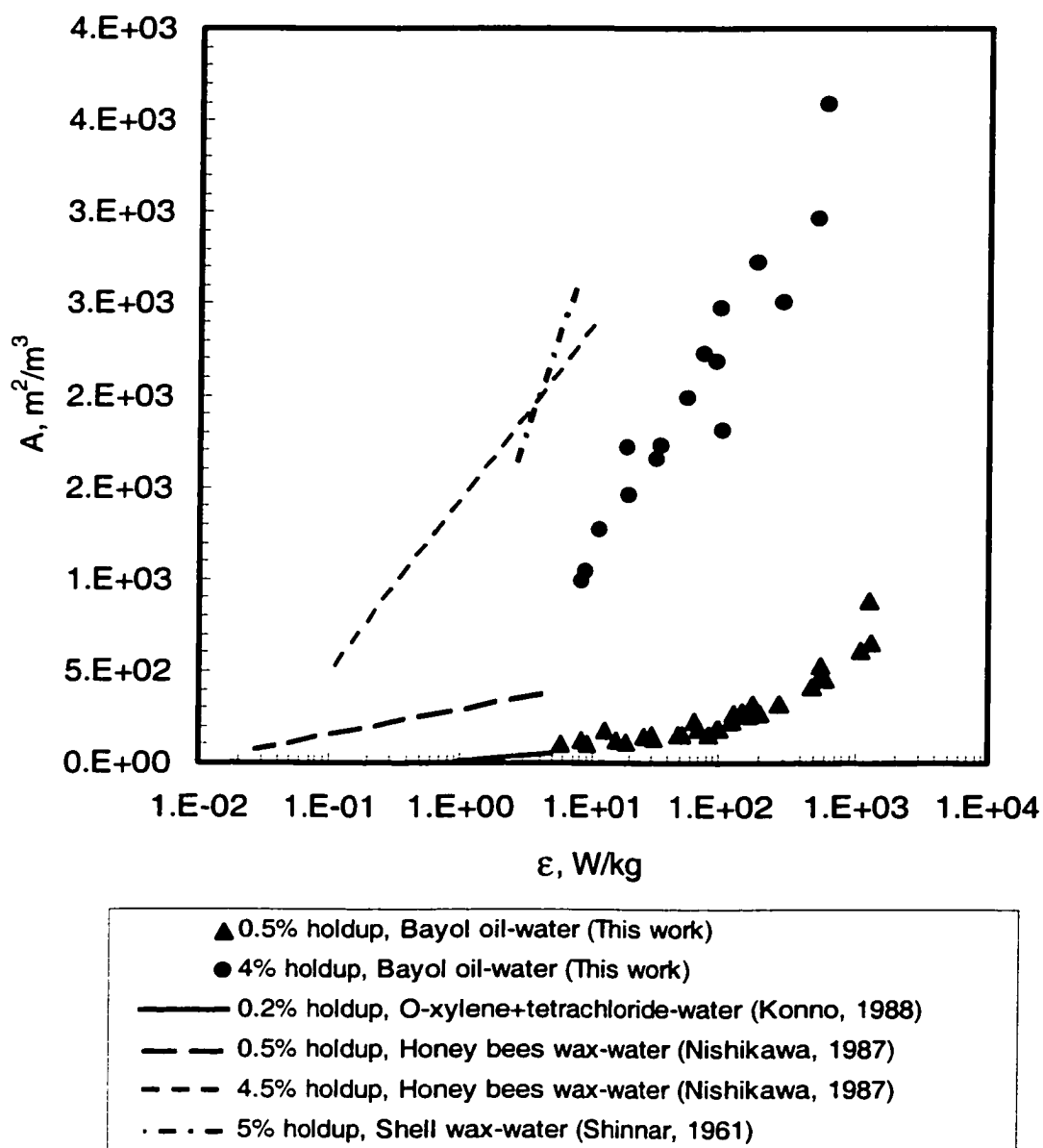


Figure 4.130. Comparison with MAT on basis of energy dissipation rate.

On the other hand, static mixers exhibit much more spatially uniform energy dissipation rates. For example, Streiff (1997) simulated the distribution of local energy dissipation rate in a Sulzer SMV static mixer and found that at higher Reynolds numbers a much more uniform distribution of energy dissipation and turbulent isotropic conditions

are achieved in most parts of the mixer volume. As shown in sections 2.1.3 and 4.1.1, screens generate a turbulent structure that is uniform across the cross section of the pipe and varies only along the axial direction. Screens have also the ability to concentrate energy utilization in very small volumes resulting in very high values of energy dissipation rates.

Figure 4.131 shows a comparison between the present mixer and mechanically agitated tanks based on the energy expenditure per unit mass processed, E . Although the residence time for liquid dispersions in continuously operated mechanically agitated tanks usually varies from 2 to 10 minutes, a value of 2 minutes was used in this comparison in order to be on the conservative side. Although this makes the beneficial features of screen mixing elements less pronounced where residence times of less than a second are encountered.

As can be seen from Figure 4.131, the screen-type static mixing elements are capable of generating interfacial areas at least five times higher than those generated by stirred tanks equipped with Rushton type impellers (under the same conditions of energy expenditure and dispersed phase volume fractions). In addition to the small residence time assumed, this comparison does not take into account the significant difference in dispersed phase viscosity. Whereas lower-viscosity dispersed phases were used by previous investigators (Shell wax 700 of 22.5 centistoke and Honey beeswax of 17.5 centistokes), the Bayol oil used in this investigation has a viscosity of 285 centistoke. According to Calabrese et al. (1986) $d_{32} \propto \mu_d^{3/8}$, therefore this 16-fold difference in dispersed phase viscosity would increase the relative effectiveness of the screen-element static mixers by an additional factor of about 3.

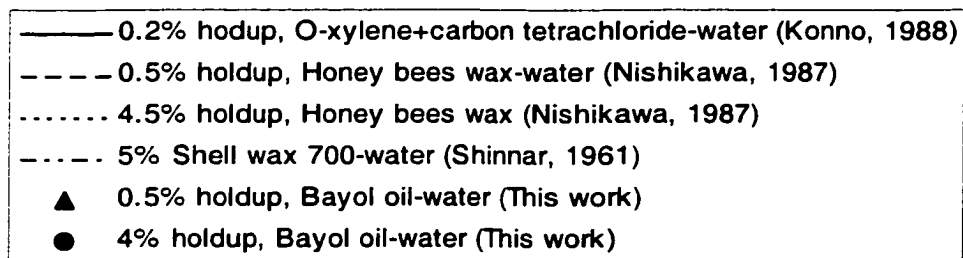
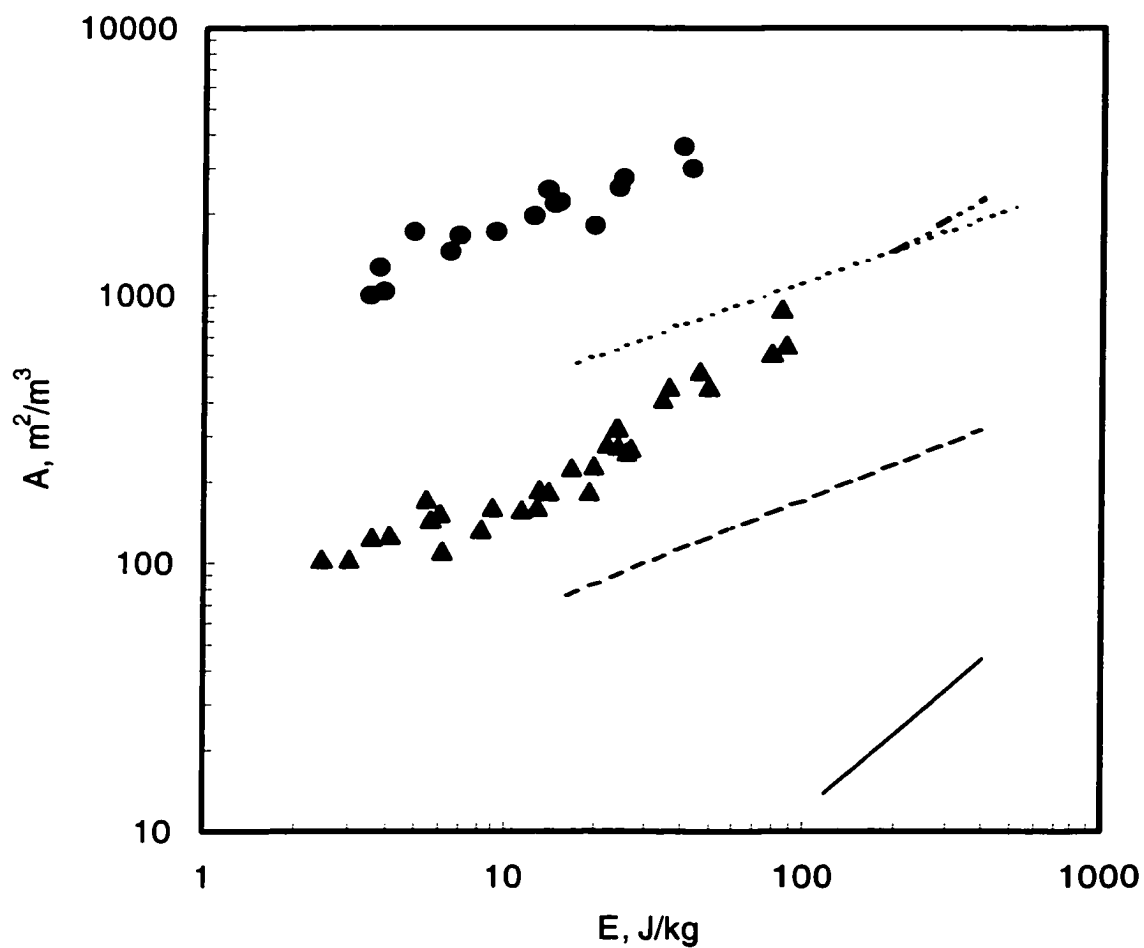


Figure 4.131. Comparison with MAT based on energy utilization.

The above mentioned findings suggest that screen mixing elements can better utilize the mechanical energy input to the mixer. This is most probably caused by the following features of the screen-element static mixers:

- Fluid elements being forced to pass through a uniform turbulent flow region. Neither bypassing nor recirculation between zones of high and low energy dissipation rates occurs. Also very narrow residence time distribution characterizes such mixers. Therefore narrow and controllable drop size distributions, which can be altered to meet varying process conditions, without interrupting the operation may be generated.
- The presence of the cutting action dispersion mechanism playing a more significant role in the initial dispersion stages and at high dispersed phase concentrations.
- A more effective turbulent breakage mechanism that stems from their ability to concentrate turbulent energy dissipation in a small volume of the mixer's volume. For example, Bourne and Lipps (1991) and Villermaux et al. (1991) reported that the maximum energy dissipation rate occurs in the non-isotropic jets immediately behind the wire screen. As shown in section 4.1, up to 95% of the turbulent energy dissipation is focused in less than 2 mm downstream from the screen's center. The dispersion/coalescence equilibrium is thus shifted towards the formation of finer dispersions in those high energy regions.
- In the case of the heavy oil/water system, dispersions with average drop size varying between 290 and 34 mm were achieved using $\Delta P < 15$ psi. Smaller drop sizes can be easily obtained by adding more energy.
- Drop number density distributions of a normalized variance as low as 0.05 can be achieved. In addition to the many operating and maintenance advantages, this feature is of particular significance under conditions requiring good control on drop size and its distribution.

- The time needed to reach dynamic equilibrium is of the order of seconds as compared to hours in the case of MAT. It can thus be used for process control purposes.
- The results obtained can be easily scaled up from small-scale data.

As shown in section 4.3, the passage of a two-phase system through a small region of high energy dissipation rate does not automatically guarantee that all drops larger than the maximum stable size will be broken. This deviation from the thermodynamic, or equilibrium, concept of maximum stable drop size introduced by Hinze and Kolmogorov can be attributed to the important role played by the kinetics of drop breakage that can dominate at very short residence times. The passage of the two-phase flow through successive screens placed at equal and short distances apart promotes drop breakup and keeps drop coalescence rate minimal, resulting in the generation of higher interfacial areas.

Figure 4.132 shows a comparison between the screen-element mixer and other types of static mixers (based on the mean turbulent energy dissipation rate). The screen-type static mixing elements are capable of generating higher interfacial areas than the Kenics and the in-line Lightnin static mixers at similar mean energy dissipation rates and dispersed phase concentrations. For example, at identical mean energy dissipation rates, the results obtained in this investigation at a holdup of 4% are 5-fold larger than those reported by Streiff (1977) who used a Sulzer mixer (Type SMV) for dispersing of different liquid-liquid systems but at a dispersed phase concentrations of 3%. At holdup of 0.5%, the screen static mixing elements can generate an area of contact 2-fold larger than those generated by the Kenics mixer. These large differences can be partially attributed to the higher holdups used in the present study.

Al Taweel and Walker (1983) and Walker (1984) investigated the dispersive characteristics of in-line Lightnin static mixing elements using kerosene at holdups of 1-2%. They used light attenuation method to measure the interfacial area. A similar investigation was conducted by El-Hamouz (1994) who used a modified Malvern 2600 laser diffraction instrument to measure drop size distribution and hence the interfacial

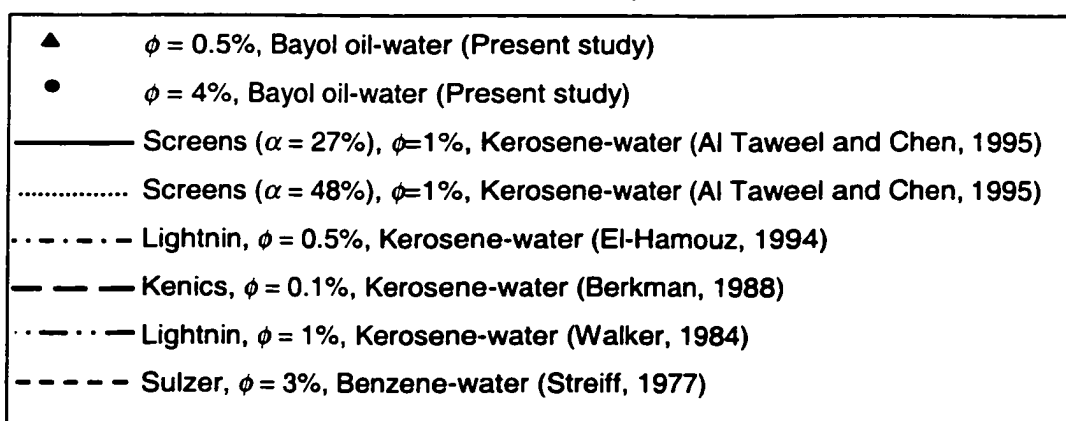
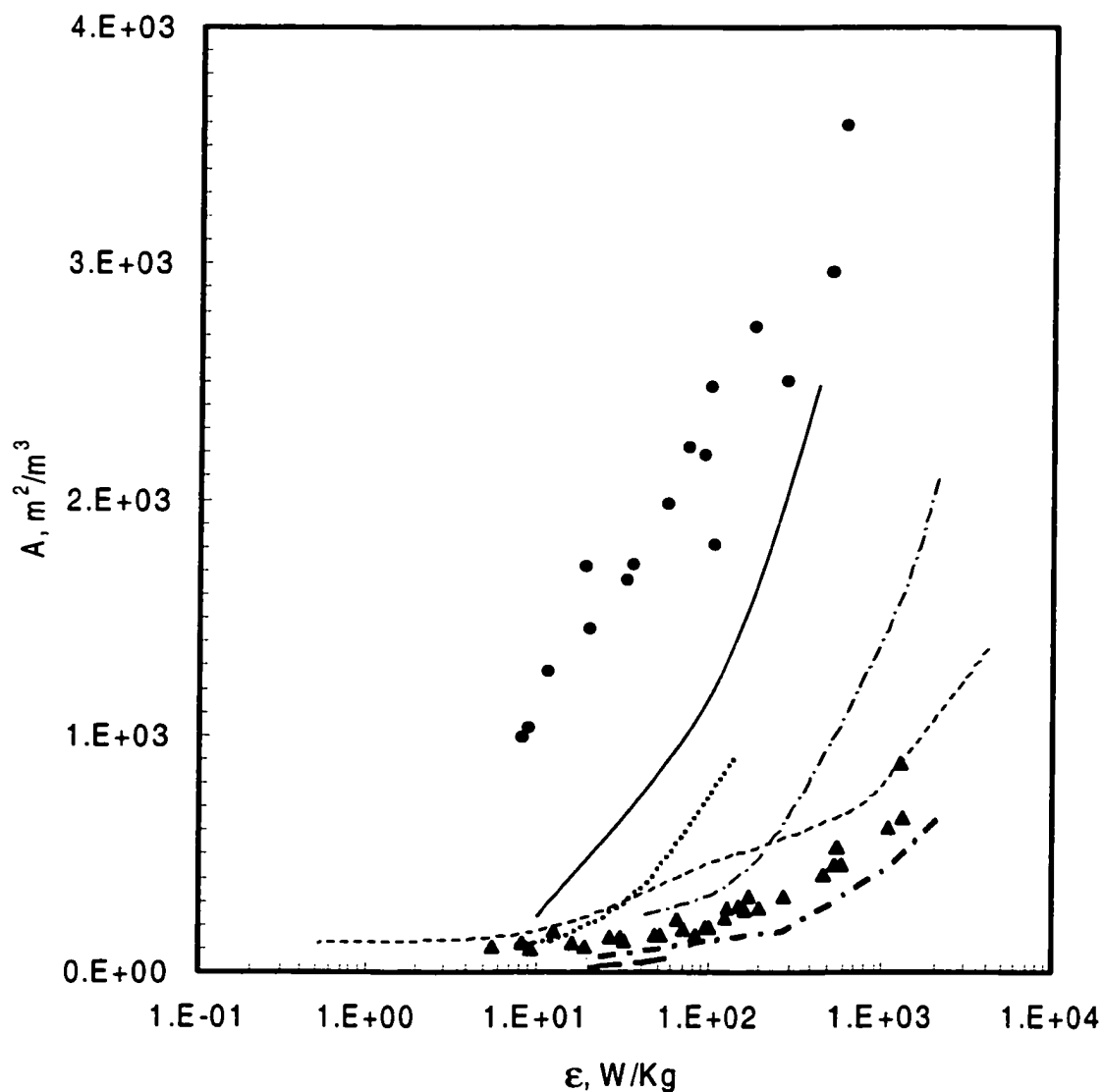


Figure 4.132. Comparison with other static mixers based on mean energy dissipation rate

area of contact. As can be seen from Figure 4.131 the results obtained by Walker and Al Taweel (1983) and Walker (1984) are about twice higher than that reported by El-Hamouz et al. (1994) at the same energy expenditure. This difference can be mainly attributed to the higher holdup used by Walker (1984). Inaccuracies associated with the techniques used for the measurement of the interfacial area may also have played a role in this difference. On the other hand, the interfacial areas obtained by Al Taweel and Walker (1983), and Walker (1984) were found to be about twice that obtained by the mixer using 0.5% dispersed phase holdup. The results obtained by Al Taweel and Chen (1995) using woven screens elements are also 15-fold higher than those obtained in the present investigation under similar mean energy dissipation rates.

Although part of the discrepancy can be attributed to the larger holdups used ($\phi = 1-2\%$ versus 0.5% in the present one), other factors are expected to play a role. For example, the lower dispersed phase viscosity (1.16 Poise in the case of kerosene, compared to 2.26 poise in the case of Bayol oil) is expected to produce drops that are about 20% smaller according to the correlation reported by Calabrese et al. (1986). The accuracy of pressure drop measurements (obtained using a water-on-mercury manometer) may also have introduced more significant errors. However, the largest source of discrepancy is expected to stem from their use of a light attenuation technique to measure the interfacial area. This method is known to be particularly sensitive to the presence of ultrafine droplets, which can bias the results because of their extremely high interfacial area yet very small volumetric contribution (Kassireddy and Al Taweel, 1990).

Figure 4.133 shows a comparison between the screen-element mixer and other types of static mixers (based on the energy expenditure per unit mass per unit mass of processed liquid). The screen-type static mixing elements are capable of generating higher interfacial areas than the Kenics, the in-line Lightnin static, and Sulzer mixers at similar mean energy dissipation rates and dispersed phase holdups. For example, at identical mean energy dissipation rates, the results obtained in this investigation at a holdup of 4% are at least 15-fold larger than those reported by Streiff (1977) who used a Sulzer mixer

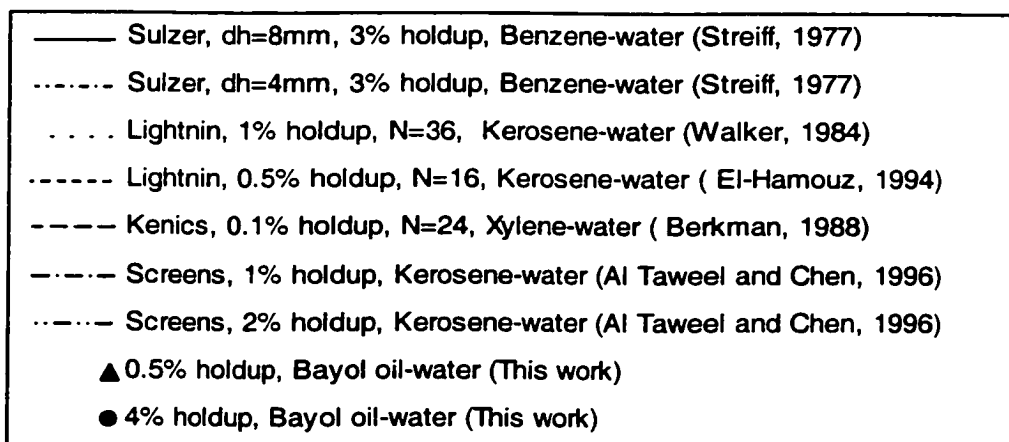
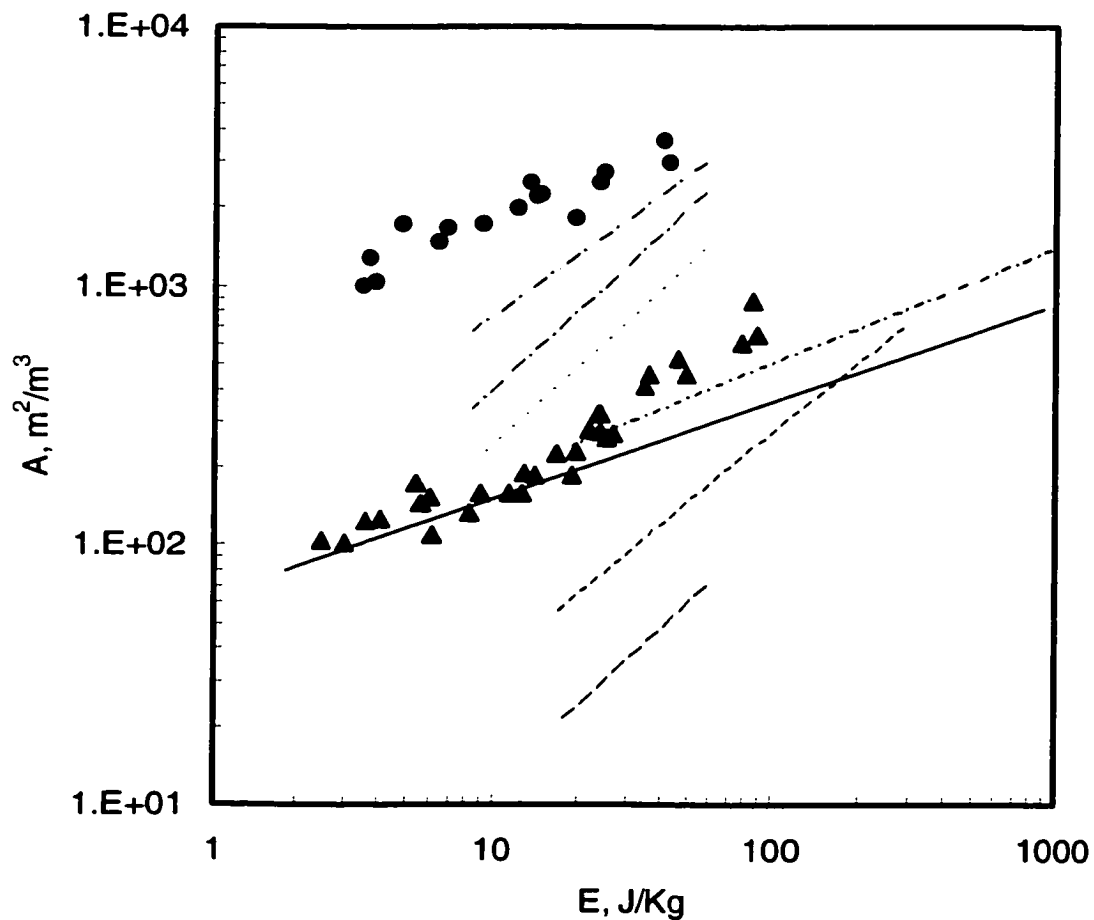


Figure 4.133. Comparison with other static mixers based on energy dissipated per unit mass of processed liquid.

(Type SMV) for dispersing different liquid-liquid systems, but at dispersed phase concentrations of 3%. At a holdup of 0.5%, the results obtained are 2-fold larger than those reported by El-Hamouz et al. (1994) who used in-line Lightnin static mixer to disperse 0.5% kerosene in water. At a 0.5% dispersed phase concentration, the screen static mixing elements can also generate interfacial areas 13-fold larger than that obtained using a Kenics mixer. These large differences can be partially attributed to the higher holdups used in the present study. In all the above investigations, the viscosities of the dispersed phases used are much less than that of the present study, thereby results in a more beneficial view of the energy utilization in the static mixer investigated.

Similarly as in Figure 4.132, Figure 4.133 shows that the results obtained by Walker and Al Taweel (1983) and Walker (1984) about 8-fold larger than that reported by El-Hamouz et al. (1994) at the same energy expenditure per unit mass of processed liquid. Similarly, this difference may have been caused by the higher holdups used by Walker (1984) and inaccuracies associated with the different techniques used for the measurement of the interfacial area. On the other hand, at dispersed phase concentrations (0.5 to 2%) the results obtained by Al Taweel and Walker (1983), and Walker (1984) were found to be about twice those obtained in the present study, while those obtained by Al Taweel and Chen (1996) using woven screens are 15-fold larger. Part of this discrepancy can be attributed to the larger holdups ($\phi = 1-2\%$ versus 0.5 in the present one) as well as the lower viscosities of the dispersed phases used in the above investigations. As mentioned before, more significant errors may have been introduced by inaccuracies in pressure drop measurement (obtained using a water-on-mercury manometer) and the use of a light attenuation technique to measure the interfacial area. As pointed out earlier, the light attenuation method is known to be particularly sensitive to the presence of ultrafine droplets, which can bias the results because of their extremely high interfacial area yet very small volumetric contribution (Kassireddy and Al Taweel, 1990).

The new liquid-liquid dispersion data reported for Sulzer SMX and SMV mixers (Streiff et al., 1997) could not be included in the comparison because insufficient

information concerning residence time is provided. However, those data are slightly lower than the previously reported data with the difference being attributed to the use of two different methods for drop size measurement. Similarly, it was not possible to compare the present results with those obtained by Middleman (1974) and Sembira et al. (1986) since they did not provide sufficient information from which the mean energy dissipation rates can be calculated.

In addition to the substantial improvement in the magnitude of the generated interfacial area over the other static mixers, screen static mixing elements generate flow patterns and turbulence structure that are radially uniform, a very essential feature for scale-up in multiphase flow systems. Also, screen-elements are easier to design and select due to a better understanding of the hydrodynamics involved. On the other hand, many of the other static mixer designs have complicated geometric configurations that produce non-uniform flow conditions making the scale up relatively a more difficult task. All these factors combined make screen static mixing elements a potential strong competitor with existing static mixers, particularly in the case of multi-phase dispersion.

Chapter 5

CONCLUSIONS AND RECOMMENDATIONS

Several conclusions can be drawn from this work,

1. The total pressure drop in the mixer is mainly a function of screen open area, the superficial velocity and the characteristic Reynolds number.
2. Grid-generated turbulence decays quickly as flow progresses downstream. The decay time is extremely short (i.e., milli-seconds).
3. A 150-fold reduction in energy dissipation rate can be obtained 5 mm downstream of the screen.
4. Generally speaking, the introduction of the dispersed phase to the continuous phase results in drag coefficients which are not significantly different from those of single-phase flow.
5. The reported correlations for predicting drag coefficients of screens can not correlate the coefficients obtained in this work.
6. The average drop size approaches the equilibrium value after the third mixing element.
7. The superficial velocity was found to exert a large influence on the average drop size. The equilibrium average drop size was found to be inversely proportional to the kinetic energy of the flow,

$$d_{32} \propto U^b$$

where b varies from -1.40 to -0.59 depending on the dispersed phase volume fraction used.

8. The equilibrium average drop size was found to be inversely proportional to the energy dissipation rate in the mixer,

$$d_{32} \propto \varepsilon^n$$

where n varies between -0.42 and -0.26 depending on the dispersed phase volume fraction used.

9. Jet velocity and screen geometry were found to be major factors affecting dispersion in flow through screens. The macroscopic jet Weber number, therefore, should be used as a characteristic dimensionless group. The average drop size was found to vary with the jet Weber number as follows,

$$d_{32} \propto We_{jet}^{-0.75}$$

10. The mean drop sizes obtained in presence of surfactant are breakage dominated indicating that the surfactant Triton X100 is effective in promoting drop breakup. Meanwhile, the surfactant Triton X100 is not very effective in suppressing drop coalescence under the conditions investigated as shown from its reduced impact at high dispersed phase holdups.
11. The equilibrium average drop size was found to be proportional to the equilibrium interfacial tension as follows,

$$d_{32} \propto \sigma^n$$

where n is 0.24 and 0.19 for dispersions of 0.5% and 4% dispersed phase holdups respectively. The equilibrium mean drop diameter was also found to decrease linearly with both increasing Marangoni number and surface excess. Meanwhile, the equilibrium average drop size can not be correlated using surfactant diffusivity.

12. The maximum stable drop size was found to be inversely proportional to the energy dissipation rate in the mixer,

$$d_{max} \propto \varepsilon^n$$

where n is -0.53 .

13. The dispersion process in the mixer is breakage dominated with two drop breakage mechanisms coexisting simultaneously. The first mechanism is drop breakup by turbulence, which dominates the dispersion under fully developed turbulent conditions, while the second mechanism is associated with drop cutting action by screen wires. The latter mechanism becomes more significant at higher dispersed phase holdups.
14. Bi-modal distributions that are skewed to the right were obtained for dispersions of 0.5% holdup. These change to unimodal distributions at high superficial velocities. This bi-modality is also lessened as the dispersed phase holdup increases and disappears at sufficiently high dispersed phase concentrations. In the presence of surfactants bi-modality vanishes at high surfactant concentrations.
15. It was found that under fully developed turbulent flow conditions, the variance could be correlated with the jet Weber number as follows,

$$\sigma^2 \propto We_{jet}^{-3.74}$$

16. The normalized variance can not be correlated with the different interfacial characteristics investigated, namely equilibrium interfacial tension, surface excess, surfactant diffusivity and the Marangoni number as well as the surfactant concentration.
17. There is no single theoretical distribution that can fit the number density data obtained. In most cases, the Weibull probability model was found to be the model that provides a fit to the experimental data at a significance level of 95%. Only in three cases, out of 92, was the log-normal distribution capable of fitting the number density data within the 95% significance level, whereas the normal distribution did not fit any even at 75% significance level.
18. The cumulative drop volume density distributions of the all experimental data obtained show reasonable self-similarity and they were fitted by normal distribution with a correlation coefficient of 0.917.
19. Using the analytical population balance solution developed by Rod and Misk (1982), it was possible to predict the temporal variation of the average drop size

reasonably well. It also can also predict the cumulative drop size distributions well.

20. Optimum efficiency of energy utilization can be obtained by using screen static mixing elements at intermediate superficial velocities, high screen open area and high dispersed phase volume fractions.
21. Screen mixing elements were found to be about 5-fold more energy efficient than mechanically agitated tanks equipped with Rushton-type impellers and can generate much higher interfacial areas than other commercially available static mixers for the same rate of energy consumption per unit mass of mixture processed.

It is recommended that:

1. More investigations are needed (using different bar sizes and porosities) in order to develop better correlation for the drag coefficient of screens under single and two phase flow conditions.
2. A new interpretation or modification of the Rod and Misk (1982) model should be considered, since the definition of $p = 0$, which implies that the coalescence rate is independent of drop size contradicts the fundamentals of the breakup/coalescence theory.
3. More investigations are needed using a wider range of screens in order to evaluate further the effect of screen geometry on the dispersion process and efficiency of energy utilization. This will allow for a better understanding of the proposed drop cutting action and the extent of its contribution into the dispersion process at the different experimental conditions. This will also aid in determining the best conditions for achieving optimum efficiency of energy utilization.
4. In order to correlate the experimental data of d_{\max} in a form similar to that correlation developed by Hinze (1955) several liquid-liquid systems need to be investigated. Almost all the previous investigations were limited to verification of Hinze's model through finding the dependence of the average drop size (i.e., d_{32}) on the different parameters in the model individually.

5. Based on the performance (e.g., capability of generating higher interfacial areas and narrower and controllable drop size distributions) of the investigated contacting device, it is suggested that it may be advantageously used to achieve co-current liquid-liquid contacting in a fashion that is more efficient than other available contactors. Counter current may also be achieved through the incorporation of hydrocyclones, which are expected to require low pressure drop in view of the ultra-fine dispersions generated by screen static mixing elements. It is therefore recommended testing of this mixer for determining mass transfer rates and / or the reaction rates between in liquid-liquid dispersions (e.g., caustic treatment).
6. In view of the findings of the present work that the experimental data obtained can not be represented by normal and log-normal models the most frequently reported distributions in the literature, more rigorous statistical fitting procedures should be adopted for analyzing drop size data obtained from liquid-liquid dispersions in future studies.

REFERENCES

- Abrahamson, J., "Collision rates of Small Particles in a Vigorously Turbulent Fluid", *Chem. Eng. Sci.*, **30**, 1371-1379 (1975).
- Ahmed, A. M. and Elghobashi, S., "On the Mechanisms of Modifying the Structure of Turbulent Homogeneous Shear Flows by Dispersed Particles", *Physics of Fluids*, **12**, 2906-2931 (2000).
- Al Taweel, A. and Chen, C."A Novel static Mixer for the Effective Dispersion of Immiscible Liquids", *Trans. Inst. Chem. Eng.*, **74**, 445-450 (1996).
- Al Taweel, A. M., Basu, A., Chen, C., Devavarapu, C., R., Keast, B., Ramadan, A. M., White, D. and Yang, "Gas-Liquid Contacting in Industrially-Relevant Systems", Presentation at ICST Sarinia, Ontario (1995).
- Al Taweel, A. M. and Cheng, Y. H., "Effect of Interfacial Characteristics on Gas/Liquid Contacting in Efficient Mechanically-Agitated Tanks", *Trans. Inst. Chem. Eng.*, **73**, 654-660 (1995).
- Al Taweel, A. and Walker, L. D., "Liquid Dispersion In-Line Mixers", *Can. J.Chem. Eng.*, **61**, 527-533 (1983).
- Al Taweel, A. M., Luo, J. J., Sury, K., Czarnecki, J. and Ng, S."Dynamic Spargers: Means for Improving Gas/Liquid Contacting" AIChE Annual meeting, Miami Nov. (1998).
- Al Taweel, A.M. and J. Landau, "Heat Transfer to Dilute Gas-Solid Suspensions", *J. Eng. Sci.*, **4**, 97-108 (1978).
- Al Taweel, A.M. and Landau, J. "Turbulence modulation in two-phase jets", *Int. J. Multiphase Flow*, **3**, 341-351 (1977).
- Alcaraz, E., Bennani, A. and Mathieu, J., "An experimental set-up for interaction turbulence-chemical reaction research", *Int. J. Heat & Mass Transfer*, **24**, 1549-1553 (1981).
- Angeli, P. and Hewitt, G. F., "Drop Size Distributions in Horizontal Oil-Water Dispersed Flows", *Chem. Eng. Sci.*, **55**, 3133-3143 (2000).
- Araj, K., Chan, K. S. and Chang, C. H., "The Effect of Dispersed Phase Viscosity on the Maximum Stable Drop Size for Breakup in Turbulent Flow," *J. Chem. Eng. Japan*, **10**, 325-330 (1977).

- Bae, J. H. and Tavlarides, L. L., "Laser Capillary Spectrophotometry for Drop-Size Concentration Measurements", *AIChE J.*, **35**, 51-55 (1989).
- Baines, W.D. and Peterson, E.G., "An investigation of flow through screens", *Trans. of ASME July*, 467-480 (1951).
- Baldyga, J. and Bourne, J., "Drop Breakup and Intermittent Turbulence", *J. of Chemical Engineering of Japan*, **26**, 738-741 (1993).
- Baldyga, J. and Podgorska, W., "Drop Breakup in Intermittent Turbulence: Maximum Stable and Transient Sizes of Drops", *Can. J. of Chem. Eng.*, **76**, 456-470 (1998).
- Batchelor, G. K. and Townsend, A. A., "Decay of Vortices in Isotropic Turbulence", *Proc. R. Soc. Lon., A* **193**, 539-558 (1948).
- Batrok, W. and Mason, S. G., "Particle Motion in Sheared Suspensions. VIII Singlets and Doublets of Fluid Spheres", *J. Coll. Sci.*, **14**, 13-26 (1959).
- Bennani, A., Gence, J.N. and Mathieu, S., "The influence of a grid-generated turbulence on the development of chemical reactions", *AIChE J.* **31**, 1157-1166 (1985).
- Bentley, B. J. and Leal, L. G., "An Experimental Investigation of Drop Deformation and Breakup in Steady, Two-Dimensional Linear Flow", *J. Fluid Mech.*, **167**, 241-2283 (1986).
- Berkman, P. D. and Calabrese, R. V., "Dispersion of Viscous Liquids by Turbulent Flow in Static Mixers", *AIChE J.*, **34**, 602-609 (1988).
- Bhardwaj, A. and Hartland, S., "Kinetics of Coalescence of Water Droplets in Water-in-Crude oil Emulsions", *J. Dispersion and Technology*, **15**, 133-146 (1994).
- Bhardwaj, P. D., Emulsions: Theory and Practice, 2nd Edition, Reinhold Publishing Co., New_York (1965).
- Borwankar, R. P., Chung, S. I. And Wasan, D. T., "Drop Sizes in Turbulent Liquid-Liquid Dispersions Containing Polymeric Suspension Stabilizers. I: The Breakage Mechanism", *J. Applied Polymer Sc.*, **32**, 5749-5762 (1986).
- Bourne, J. R. and Lips, M., "Micromixing in Grid Generated Turbulence: Theoretical Analysis and Experimental Study" *Chem. Eng. J.*, **47**, 155-162 (1991).
- Bourne, J. R., Lenzner, J. and Petrozzi, S., "Micromixing in Static Mixers: An Experimental Study", *Ind. Eng. Chem. Res.*, **31**, 1216-1222 (1992).

- Britter, R.E., Hunt, J.C.R., Marsh, G.L. and Snyder, W.H., "The effects of stable stratification on turbulent diffusion and the decay of grid turbulence", *J. Fluid Mech.*, **127**, 27-44 (1983).
- Brodkey, R. S. and Hershey, H., Transport Phenomena a Unified Approach, McGraw-Hill, Inc., New York, pp. 512-526 (1988).
- Brooks, B. W. and Richmond, H. N., "Phase Inversion in Non-Ionic Surfactant-oil-Water Systems –II. Drop Size Studies in Catastrophic Inversion with Turbulent Mixing", *Chem. Eng. Sci.*, **49**, 1065-1075 (1994).
- Brown, D. E. and Pitt, K., "Drop Size Distributions of Stirred Non-Coalescing Liquid-Liquid System", *Chem. Eng. Sc.*, **27**, 577-583 (1972).
- Cabassud, M., Gourdon, C. and Casamatta, G., "Single Drop Break up in a Kuhni Column", *Chem. Eng. J.*, **44**, 27-41 (1990).
- Calabrese, R. V., Chang, T. P. and Dang, P. T., "Drop Break up in Turbulent Stirred-Tank Contactors, Part I: Effect of Dispersed-Phase Viscosity", *AIChE J.*, **32**, 657-666 (1986).
- Calabrese, R. V., Pacek, A. W. and Nienow, A. W., "Coalescence of Viscous Drops in Stirred Dispersions", The Institution of Chemical Engineers Research Event, Birmingham, January; Institution of Chemical Engineers, Rugby, U.K., 642-644 (1993).
- Calabrese, R. V., Wang, C. Y. and Brynet, N. P., "Drop Break up in Turbulent Stirred-Tank Contactors PartIII: Correlation for Mean Size and drop Size Distribution", *AIChE J.*, **32**, No.4, 677-681 (1986).
- Campanelli, J. R. and Cooper, D. G., "Interfacial Viscosity and the Stability of Emulsions", *Can. J. Chem. Eng.*, **67**, 851-855 (1989).
- Campanelli, J. R. and Wang, X., "Comments on Modelling the Diffusion-Controlled Adsorption of Surfactants", *Can. J. Chem. Eng.*, **76**, 51-57 (1998).
- Cauwenberg, V., Degreve, J. and Slater, M. J., "The Interaction of Solute Transfer, Contaminants and Drop Break up in Rotating Disc Contactors: Part I: Correlation of Drop Breakage Probabilities", *Can. J. of Chem. Eng.*, **75**, 1046-1055 (1997).
- Chabra, R.P. and Richardson, J.F., "Flow of liquids through screens: relationship between pressure drop and flow rate", *Chem. Eng. Sci.*, **40**, 313-316 (1985).

- Chatzi, E. and Kiparissides, C., "Steady-State Drop Size Distributions in High Holdup Fraction Dispersion Systems: Effect of the Degree of Hydrolysis of PVA Stabilizer", *Chem. Eng. Sci.*, **49**, 5039-5052 (1994).
- Chatzi, E. and Kiparissides, C., "Steady-State Drop Size Distributions in High Holdup Fraction Dispersion Systems", *AIChE J.*, **41**, No.7, 1640-1651 (1995).
- Chatzi, E., Boutris, C. J. and Kiparissides, C., "On-Line Monitoring of Drop Size Distributions in Agitated Vessels. 1. Effects of Temperature and Impeller Speed", *Ind. Eng. Chem. Res.*, **30**, 536-543 (1991).
- Chen, B.H., Yang, N.S. and McMillan, A.F., "Gas holdup and pressure drop for air-water flow through plate bubble columns", *Can. J. Chem. Eng.*, **64**, 387-392. (1986).
- Chen, C., Breakage and Dispersion in Static Mixer, Ph.D. Thesis, TUNS (1996).
- Chen, H. T. and Middleman, S., "Drop Size Distribution in Agitated Liquid-Liquid Systems", *AIChE J.*, 990-996 (1967).
- Chen, J.D., Hahn, P.S. and Slattery, J.C., "Coalescence Time for a Small Drop or Bubble at a Fluid-Fluid Interface", *AIChE J.*, **30**, No.4, 622-630 (1984).
- Chen, L. and Lee, Y., "The Effects of a Surfactant on the Mass Transfer in Spray-Tower Extraction System", *Chem. Eng. J.*, **73**, 77-81 (1999).
- Chen, S. and Liby, D., "Gas-Liquid and Liquid-Liquid Dispersions in a Kenics Mixer", 71st Annual A.I.Ch.E. Meeting (1978).
- Chen, Z., Pruss, J. and Warnecke, H., "A Population Balance Model for Disperse Systems: Drop Size Distribution in Emulsions", *Chem. Eng. Sci.*, **53**, 1059-1066 (1998).
- Cheng., Y. H., Gas-Liquid Contacting in Mechanically-Agitated Systems, PhD Thesis, TUNS (1994).
- Cheremisinoff, N. P., "Hydrodynamics of Laminar Buoyant Jets", in Encyclopedia of Fluid Mechanics, **2**, 339-348 (1986).
- Chesters, A.K., "The modeling of coalescence processes in fluid-liquid dispersions: A review of current understanding". *Trans. I. Chem. E.*, **69(A)**, 259-270 (1991).
- Choi, C., Kang, K., Kim, M. and Hwang, G., "Convective Instabilities and Transport Properties in Horizontal Fluid Layers", *Korean J. Chem. Eng.*, **15**, 192-198 (1998).

- Church, J. M. and Shinnar, R., "Stabilizing Liquid-Liquid Dispersions by Agitation", *Ind. and Eng. Chemistry*, **53**, 479-483 (1961).
- Clark, M. M., "Drop Breakup in a Turbulent Flow- II Experiments in a Small Mixing Vessel", *Chem. Eng. Sc.*, **43**, No. 3, 671-679 (1988).
- Clift, R., Grace, J. R. and Weber, M. E., Bubbles, Drops and Particles, Academic Press, New York, 321-351 (1978).
- Clay, P. H., "The Mechanism of Emulsion Formation in Turbulent Flow", *Akademie van Wetenschappen proceedings*, **43**, 852-965 (1940).
- Cohen, R. D., "Effect of Turbulence Dampening on the Steady-State Drop Size Distribution in Stirred Liquid-Liquid Dispersion", *Ind. Eng. Chem. Res.*, **30**, 277-279 (1991).
- Collins, S. B. and Knudsen, J. G., "Drop Size Distributions Produced by Turbulent Pipe Flow of Immiscible Liquids", *AIChE J.*, **16**, No.6, 1072-1079 (1970).
- Comte-Bellot, G. and Corrsin, S., "The use of a contraction to improve the isotropy of grid-generated turbulence", *J. Fluid Mech.*, **25**, 657-682 (1966).
- Corrsin, S., Decay of Turbulence Behind Three Similar Grids, PhD Thesis, California Institute of Technology (1944).
- Corrsin, S., Turbulence: Experimental Methods, *Handbuch der Physik*, Vol. 8, Part 2, pp 524-590, Springer (1963).
- Coulaloglou, C. A. and Tavlarides, L. L., "Description of Interface Processes in Agitated Liquid-Liquid Dispersions", *Chem. Eng. Sci.* **32**, 1289-1297 (1977).
- Coulaloglou, C. A. and Tavlarides, L. L., "Drop Size Distribution and Coalescence Frequencies of Liquid-Liquid Dispersions in Flow Vessels", *AIChE J.*, **22**, No.2, 289-298 (1976).
- Coulaloglou, C. A., Dispersed Phase Interaction in an Agitated Flow Vesse, Ph.D. Thesis, Illinois Institute of Technology, Chicago (1975).
- Crowe, C. T., "On Models for Turbulence Modulation in Fluid-Particle Flows", *Int. J. Multiphase Flow*, **26**, 719-727 (2000).
- Cutter, L. A., "Flow and Turbulence in a Stirred Tank", *AIChE J.*, **12**, No.1, 35-45 (1966).

- Das, P. K., Kumar, R. and Ramkrishna, D., "Coalescence of Drops in Stirred Dispersion: a White Noise Model for Coalescence", *Chem. Eng. Sci.*, **42**, 213-220 (1987).
- Davies, G. A., "Mixing and Coalescence Phenomena in Liquid-Liquid Systems", in Science and Practice of Liquid-Liquid Extraction, J.D. Thornton, Ed., Volume 1, Claendon Press, Oxford, pp. 245-342 (1992).
- Davies, J. T., "A Physical Interpretation of Drop Size in Homogenizers and Agitated Tanks, Including the Dispersion of Viscous Oils", *Chem. Eng. Sc.*, **42**, No.7, 1671-1676 (1988).
- Davies, J. T., "Drop Sizes of Emulsions Related to Turbulent Energy Dissipation Rates", *Chem. Eng. Sc.*, **40**, 839-842 (1985).
- Davies, J.T., "Turbulence Phenomena", Academic Press, New York, pp. 57-62 and 348-363 (1972).
- De Bruijn, R. A., Deformation and Break up of Drops in Simple Shear Flow, PhD Thesis, Technische Unversiteit Eindhoven, The Netherlands (1989).
- De Bruijn, R. A., "Tip Streaming in Simple Shear Flows", *Chem. Eng. Sc.*, **48**, No.2, 277-284 (1993).
- Dickey, T. D. and Mellor, G. L., "Decaying Turbulence in Neutral and Stratified Fluids", *J. Fluid Mech.*, **99**, 13-31 (1980).
- Dierendonck, L. L., Zahradnik, J. and Linek, V., "Loop Venturi Reactor-A Feasible Alternative to Stirred Tank Reactors?" *Ind. Eng. Chem. Res.*, **37**, 734-738 (1998).
- Doulah, M. S., "An Effect of Hold-up on Drop Sizes in Liquid-Liquid Dispersions", *Ind. Eng. Chem. Fund.*, **15**, 137-139 (1975).
- Duffy, J. P. and Kadlec, R. H., "The Behaviour of the Dispersed Phase in Liquid-liquid Cocurrent Flow Through a Packed Bed", *Can. J. Chem. Eng.*, **53**, 621-627 (1975).
- Dutta, N. N. and Raghavan, K. V., "Mass Transfer and Hydrodynamic Characteristics of Loop Reactors with Down Flow Liquid Jet Ejector", *Chem. Eng. J.*, **36**, 111-121 (1987).
- Eastoe, J.; Dalton, J. S.; Rogueda, P.G.; Crooks, E. R.; Pitt, A. R.; Simister, E A, "Dynamic Surface Tensions of Nonionic Surfactant Solutions", *J. of Colloid and Interface Science*, **188**, 423-430 (1997).

- Ehrhardt, G., "Flow Measurements for Wire Gauzes", *International Chem. Eng.*, **23**, 455-465 (1983).
- Elghobashi, S., "On Predicting-Laden Turbulent Flows", *Applied Scientific Research*, **52**, 309-329 (1994).
- Elghobashi, S. and Abou-Arab, T. W., "A Two-equation Turbulence Model for Two-phase Flows", *Phys. Fluids*, **26**, No. 4, 931-938 (1983).
- El-Hamouz, A.M., Stewart, A.C. and Davies, G.A. Kerosene/water dispersions produced by a Lightnin "in-line" static mixer. The 8th European Conferences Proceedings of Mixing, Sept. 21-23, 1994, Cambridge, UK (1994).
- Elsayed A. S. and Al Taweel, A. M., "Use of Population Balance to Describe Dispersion Properties in Multi-Phase Contactors", Technical Report, Chemical Engineering Dep., TUNS, Halifax (1994).
- Gad-El-Hak, M. and Corrsin, S., "Measurements of the Nearly Isotropic Turbulence Behind a Uniform Jet Grid", *J. Fluid Mech.*, **62**, 115-143 (1974).
- Gore, R. A. and Crowe, C. T., "Effect of Particle Size on Modulating Turbulent Intensity", *Int. J. Multiphase Flow*, **15**, 279-285 (1989).
- Grace, H. P., "Dispersion Phenomena in High Viscosity Immiscible Fluid Systems and Application of Static Mixers as Dispersion Devices", *Chem. Eng. Commun.*, **14**, 256- (1982).
- Groth, J. and Johansson, A.V. "Turbulence Reduction by Screens", *J. Fluid Mech.*, **197**, 139-155 (1988).
- Haas, P. A., "Turbulent Dispersion of Aqueous Drops in Organic Liquids", *AIChE J.*, **33**, 987-995 (1987).
- Harris, G. V., The Turbulence Generated by an Array of Parallel Rods, M. Sc. Thesis, The Johns Hopkins University, U. S. A. (1965).
- Hinze, J. O., "Fundamentals of the Hydrodynamic Mechanism of Splitting in Dispersion Processes", *AIChE J.*, **1**, 289-295 (1955).
- Hinze, J.O., Turbulence, 2nd ed. McGraw-Hill Book Company, New York, pp. 259-277 (1975).
- Holman, J. P., Experimental Methods for Engineers, McGraw-Hill Book Company, New York, U.S.A. (1978).

- Hong, P. O. and Lee, J. M., "Unsteady-State Liquid-Liquid Dispersions in Agitated Vessels", *Ind. Eng. Chem. Process Des. Dev.*, **22**, 130-135 (1983).
- Hong, P. O. and Lee, J. M., "Changes of the Average Drop Sizes During the Initial Period of Liquid-Liquid Dispersion in Agitated Vessels", *Ind. Eng. Chem. Process Des. Dev.*, **24**, 868-872 (1985).
- Howarth, W.J., "Measurement of Coalescence Frequency in an Agitated Tank", *AIChE J.*, **13**, 1007-1013 (1967).
- Hsia, M.A. and Tavlarides, L.L., "Simulation Analysis of Drop Breakage, Coalescence and Micro-Mixing in Liquid-Liquid Stirred Tanks". *The Chem. Eng. J.*, **26**, No.3, 189-199 (1983).
- Jamialahmadi, M. and Muller-Steinhagen, H., "Effect of Electrolyte Concentration on Bubble Size and Gas Holdup in Bubble Columns", *Trans IChemE*, **68**, 202-204 (1990).
- Janssen, J. J., Boon, A. and Agterof, G. M., "Influence of Dynamic Interfacial Properties on Droplet Breakup in Simple Shear Flow", *AIChE Journal*, **40**, No.12, 1929-1939 (1994).
- Jares, J. and Prochazka, J., "Break up of Droplets in Karr Reciprocating Plate Extraction Column", *Chem. Eng. Sc.*, **42**, No.2, 283-292 (1987).
- Kanel, J. S., Effect of Some Interfacial Phenomena on Mass Transfer in Agitated Liquid-Liquid Dispersions, Ph. D Dissertation, Georgia Institute of Technology, Atlanta, GA (1990).
- Kang, K. H. and Choi, C. K., "Onset of Solutal Marangoni Convection in a Suddenly Desorbing Liquid Layer", *AIChE Journal*, **46**, 15-23 (2000).
- Karabelas, A. J., "Droplet Size Spectra Generated in Turbulent Pipe Flow of Dilute Liquid/Liquid Dispersions", *AIChE J.*, **24**, No.2, 170-179 (1978).
- Karagiannis, C., Papageorgiou, D. and Stamatoudis, M., "Size Distribution of Drops Formed from Nozzles in Liquid-Liquid System at Velocities Below Jetting", *Can. J. Chem. Eng.*, **72**, 13-15 (1994).
- Kassireddy, V. K. and Al Taweel, A. M., "An Improved Light Attenuation Technique for Measuring Large Interfacial Areas", *Can. J. Chem. Eng.*, **68**, 690-693 (1990).

- Karam H. J. and Bellinger, J. C., "Deformation and Breakup of Liquid Droplets in a Simple Shear Flow", *I. & E.C. Fundamentals*, **7**, 576-581 (1968).
- Kato, S., Nakayma, E. and Kawasaki, J., "Types of Dispersion in Agitated Liquid-Liquid Systems", *Can. J. Chem. Eng.*, **69**, 222-227 (1991).
- Kennedy, J. B. and Neville, A. M., Basic Statistical Methods for Engineers and Scientists, Third Ed., Harper & Row Publishers, New York (1986).
- Kenning, V. M. and Crowe, C. T., "Brief Communication on the Effect of Particles on Carrier Phase Turbulence in Gas-Particle Flows", *Int. J. Multiphase Flow*, **23**, 403-408 (1997).
- Kim, Y., Nikolov, A. D., Wasan, D. T., Diaz-Arauzo, H. and Shetty, C. S., "Demulsification of Water-in-Crude Oil Emulsions: Effects of Film Tension, Elasticity, Diffusivity and Interfacial Activity of Demulsifier Individual Components and their Blends", *J. Dispersion Science and technology*, **17**, 33-53 (1996).
- Kistler, A. L. and Vrebalovich, T., "Grid Turbulence at Large Reynolds Numbers", *J. Fluid Mech.*, **26**, 37-47 (1966).
- Kolmogorov, A. N., "On the Disintegration of Drops in Turbulent Flow", *Dokl. Akad. Nauk. USSR*, **66**, 825-832 (1949).
- Konno, M. and Siato, S., "Correlation of Drop Sizes in Liquid-Liquid Agitation at Low Dispersed Phase Volume Fraction", *J. Chem. Japan*, **20**, 533-535 (1987).
- Koshy, A., Das, T. R. and Kumar, R., "Effect of Surfactant on Drop Breakage in Turbulent Liquid Dispersions", *Chem. Eng. Sc.*, **43**, No. 3, 649-654 (1988).
- Kourio, M. J., Gourdon, C. and Casamatta, G., "Study of Drop-Interface Coalescence: Drainage Time Measurement", *Chem. Eng. Tech.*, **17**, 240-254 (1994).
- Krawczyk, M. A., Wasan, D. T. and Shetty, C. S., "Chemical Demulsification of Petroleum Emulsions Using Oil-Soluble Demulsifiers", *Ind. Eng. Chem. Res.*, **30**, 367-375 (1991).
- Kubie, J. and Gardner, G. C., "Drop Sizes and Drop Dispersion in Straight Horizontal Tubes and in Helical Coils", *Chem. Eng. Sci.*, **32**, 195-202 (1977).
- Kuboi, R., Komazawa, I. And Otake, T., "Collisions and Coalescence of Dispersed Drops in Turbulent Liquid Flow", *J. Chem. Engng. Japan*, **5**, 423-424, (1972).

- Kumar, S., Kumar, R. and Gadhi, K. S., "Alternative Mechanisms of Drop Breakage in Stirred Vessels", *Che. Eng. Sc.*, **46**, No.10, 2483-2489 (1991).
- Kurban, A. P., Angeli, P. A., Mendes-Tastis, M. A. and Hewitt, G. F., "Stratified and Dispersed Oil-Water Flows in Horizontal Pipes", *Seventh International Conference on Multiphase Production*, Cannes, France (1995).
- Laats, M. K. and Frishman, F. A., "Development of Techniques and Investigation of Turbulence energy at the Axis of A two-phase turbulent Jet", *Fluid Dyn.*, **8**, 304 (1974).
- Lagisetty, J.S., Das, P.K., Kumar, R. and Gandhi, K.S., "Breakage of Viscous and Non-Newtonian Drops in Stirred Dispersions", *Chem. Eng. Sci.*, **41**, 65-72, (1986).
- Lance, M. and Bataille, J., "Turbulence in the Liquid Phase of a Uniform Bubbly Air-Water Flow", *J. Fluid Mech.*, **222**, 95-118 (1991).
- Laso, M., Steiner L. and Hartland, S., "Dynamic Simulation of Agitated Liquid-Liquid Dispersions-II. Experimental determination of Breakage and Coalescence Rates in a Stirred Tank", *Chem. Eng. Sci.*, **42**, 2437-2445 (1987).
- Laws, E. M. and Livessey, J. L., "Flow Through Screens", *Ann. Review Fluid Mech.*, **10**, 247-266 (1978)
- Lee, Y. H., Tsao, G. T. and Wankat, P. C., "Hydrodynamic Effect of Surfactants on Gas-Liquid Oxygen Transfer", *AIChE J.*, **26**, 1008-1010 (1983).
- Levich, V. G., Physicochemical Hydrodynamics, Prentice Hall, Englewood, Cliffs U.S.A. (1962).
- Liu, S. and Li, D., "Drop Coalescence in Turbulent Dispersions", *Chem. Eng. Sci.*, **54**, 5667-5675 (1999).
- Liu, C. H., Kan, M. and Chen, B. H., "A Correlation of Two-Phase Pressure Drop in Screen-Plate Bubble Column", *Can. J. Chem. Eng.*, **71**, 460-463 (1993).
- Lo, M.Y., Gierczycki, Titchener-Hooker, N. J.A. T. and Shamlou, P. A., "Newtonian Power Curve and Drop Size Distributions for Vibromixers", *Can. J. of Chem. Eng.*, **76**, 471-478 (1998).

- Lucassen-Reynders, E. H. and Kuipers, K. A., "The Role of Interfacial Properties in Emulsification", *Colloids and Surfaces*, **65**, 175-184 (1992).
- Luhning, R. W. and Sawistowski, H., "Phase Inversion in Stirred Liquid-Liquid Systems", I.S.E.C. Session 5A, 873-887 (1974).
- Luxenberg, D. S. and Wiskind, K., "Some Effects of Air Injection on the Turbulence Generated by a Bi-planar Grid", Tech. Rep. FTAS/TR-70-53, Case Western Reserve University, U. S. A. (1969).
- McKenzie, C. P. and Wall, D. B., "Transition from Laminar to Turbulence in Submerged and Bounded Jets", *Fluidics Quart.*, **4**, 38-43 (1968).
- Marrucci, G., "A Theory of Coalescence", *Chem. Eng. Sci.*, **24**, 975-985 (1969).
- Marsters, G. F., "Some Observations on the Transition to Turbulence in Small, Unconfined Free Jets", Rep. No. 1-69, Queens University, Kingston, Ont. (1969).
- Matsumara, K., Y., Morishama, K. and Ikenaga, H., "Some Performance Data of the Hi-Mixer and In-Line Mixer", *Chem. Eng. Tech.*, **53**, 51-58 (1981).
- McDonough, J. A., Tomme, W. J. and Holland, C. D., "Formation of Interfacial Area in Immiscible Liquids by Orifices Mixers", *AIChE Journal*, **6**, 615-618 (1960).
- McManamey, J. W., "Sauter Mean and Maximum Drop Diameters of Liquid-Liquid Dispersions in Turbulent Agitated Vessels at Low Dispersed Phase Holdup", *Chem. Eng. Sci.*, **34**, 432-434 (1979).
- Merchuk, J. C., Shal, R. and Wolf, D., "Experimental Study of Copper Extraction with LIX-64N by Means of Motionless Mixers", *Ind. Eng. Chem. Process Des. Dev.*, **19**, 91-97 (1980).
- Middleman, S., "Drop Size Distributions Produced by Turbulent Pipe Flow of Immiscible Fluids Through a static Mixer", *Ind. Eng. Chem. Process Des. Develop.*, **13**, 78-83 (1974).
- Molag, M., Joosten, G. E. and Drinkenburg, A. H., "Droplet Break up and distribution in Stirred Immiscible Two-Liquid Systems", *Ind. Eng. Chem. Fundam.*, **19**, 275-281 (1980).
- Muralidhar, R. and Ramkrishna, D., "Analysis of Droplet Coalescence in Turbulent Liquid-Liquid dispersions", *Ind. Eng. Chem. Fundam.*, **25**, No.4, 554-556 (1986).

- Muralidhar, R., Drop Coalescence in Turbulent Liquid-Liquid Dispersions, Ph.D. Thesis, Purdue University, (1988).
- Myers, K., Bakker, A. and Ryan, D., "Avoid Agitation by Selecting Static Mixers", Chem. Eng. Prog., 28-38, June (1997).
- Mylnek, Y. and Reshnick, W. "Drop Sizes in an Agitated Liquid-Liquid System", AIChE J., **18**, 122-127 (1972).
- Nakache, E., Longaive, P. and Aiello, S., "Determination of a Coalescence Parameter Related to the Stability of Emulsions with Polymeric Surfactants", Colloids and Surfaces, **96**, 69-76 (1995).
- Nakagawa, T., "Flow behind low open area grids in a pipe at low Reynolds numbers", Int. J. Multiphase Flow, **11**, 109-114 (1985).
- Nakamura, I., Sakai, Y. and Miyata, M., "Diffusion of matter by a non-buoyant plume in grid-generated turbulence", J. Fluid Mech., **178**, 379-403 (1987).
- Ni, X., Zhang, Y. and Mustafa, I., "An Investigation of Droplet Size and Size Distribution in Methylmethacrylate Suspensions in a Batch Oscillatory-Baffled Reactor", Chem. Eng. Sci., **53**, 2903-2919 (1998).
- Nishikawa, M., Moris, F., Fujieda, S., "Scale-up of Liquid-Liquid Phase Mixing Vessel", Journal of chemical Engineering of Japan, **20**, No 5, 454-459 (1987).
- Nsom, B., "Computation of Drag Reduction in Fiber Suspensions", Fluid Dynamics Research, **14**, No. 5, 275-283 (1994).
- Ohtake, T., Hano, T., Takagi, K. and Nakashio, F., "Effects of Viscosity on Drop Diameter of W/O Emulsion Dispersed in a Stirred Tank", J. Chem. Eng. Japan. **20**, No.5, 442-447 (1987).
- Olamoto, T., Nishikawa, M. and Hashimoto, K., "Energy Dissipation Rate Distribution in Mixing Vessel and on Liquid-Liquid Dispersion and Solid-Liquid Mass Transfer", Inter. Chem. Eng., **221**, 88-94 (1981).
- Pacek, A. W., Chamsart, S., Nienow, A. W. and Bakker, A., "The Influence of Impeller Type on Mean Drop Size and Drop Size Distribution in an Agitated Vessel", Chem. Eng. Sci., **54**, 4211-4222 (1999).
- Pacek, A. W., Chamsart, s., Nienow, A. W. and Bakker, "The Influence of Impeller Type on Mean Drop Size and Drop Size Distribution in an Agitated Vessel", Chem. Eng. Sc., **54**, 4211-4222 (1998).

- Pal, R., "Pipeline Flow of Unstable and Surfactant Stabilized Emulsions", *AIChE Journal*, **39**, 1754-1764 (1993).
- Perez De Ortiz, E. S., "Marangoni Phenomena", in Science and Practice of Liquid-Liquid Extraction, Vol. 1, J. D. Thorton ed., Oxford Science Publications, Oxford, U. K. (1992).
- Peru, D. A. and Lorenz, P. B., "The Effect of Equilibration Time and Temperature on Drop-Drop Coalescence of Wilmington Crude Oil in a Weakly Alkaline Brine", *Chem. Eng. Comm.*, **77**, 91-114 (1989).
- Pinker, R.A. and Herbert, M.V., "Pressure loss associated with compressible flow through square-mesh wire gauzes", *J. Mech. Eng. Sci.*, **9**, 11-23 (1967).
- Prince, M.J. and H.W. Blanch "Bubble Coalescence and Break-Up in Air-Sparged Bubble Columns", *AIChE J.*, **36**, 1485-1499 (1990).
- Ramadan, A. M., Physico-Chemical Parameters Affecting Flootation Systems, Ph.D. Thesis, Al-Azhar University, Cairo, Egypt (1996).
- Ramkrishna, D., "The Status of Population Balances", *Rev. Chem. Eng.*, **3**, No.1, 4995-5006 (1985).
- Reynolds, A.J., Turbulent Flows in Engineering, John Wiley & Sons, London, pp. 24-30 & 71-103 (1974).
- Rincon-Rubio, L. M., Kumar, A. and Hartland, S., "Drop-Size Distribution and Average Drop Size in a Wirz Extraction Column", *Trans. I. Chem. E.*, **72**, Part A, 493-502 (1994).
- Rod, V. and Misk, T., "Stochastic Modeling of Dispersion Formation in Agitated Liquid-Liquid Systems", *Trans IChemE*, **60**, 48-53 (1982).
- Ross, S. L., Vergoff, P. H. and Curl, R. L., "Droplet Breakage and Coalescence in Agitated Dispersion. 2: Measurement and Interpretation of Mixing Experiments", *Ind. Eng. Chem. Fund.*, **17**, No.2, 101-108 (1978).
- Rumscheidt, F. D. and Mason, S. G., "Particle Motions in Sheared Suspensions XII Deformation and Burst of Liquid Drops in Shear and Hyperbolic Flow", *J. Cool. Int. Sci.*, **16**, 238-261 (1961).
- Sagert, N. H. and Quinn, M. J., "The Coalescence of Gas Bubbles in Dilute Aqueous Solutions", *Chem. Eng. Sci.*, **33**, 1087-1093 (1978).

- Schott, N. R. and Yuu, D., "Drop Size Distributions for Organic-Water Dispersions in Ross LPD and LLPD motionless Mixers", Paper presented at 71st AIChE Annual Meeting (1978) cf. Chen, C., Breakage and Dispersion in Static Mixers, Ph.D. Thesis, TUNS (1996).
- Scott, L. S., Hayes, W. B. and Holland, C. D., "The Formation of Interfacial Area in Immiscible Liquids by Orifice Mixers", *AICh J.*, **4**, No.3, 346-350 (1958).
- Sears, F. and Zemansky, M., College Physics, Addison-Wesley Publishing Co., Massachusetts, USA (1960).
- Seidshazileh, K., Effect of Interfacial Characteristics on Phase Inversion in Liquid Dispersions, Ph.D. Thesis, Dalhousie University (1999).
- Seidshazileh, K., "Drop Breakage and Coalescence in Turbulent Flow", Technical Report, Dalhousie University, Halifax, N.S., Canada (1998).
- Sembira, J. C., Merchuk, J. C. and Wolf, D., "Characteristics of a Motionless Mixer for Dispersion of Immiscible Fluids – 1. A Modified Electroresistivity Probe Technique", *Chem. Eng. Sc.*, **41**, No.3, 445-455 (1986).
- Shinnar, R., "On the Behavior of Liquid Dispersions in Mixing Vessels", *J. Fluid Mechanics*, **10**, 259-275 (1961).
- Shtilman, L. and Sivashinsky, G., "Negative Viscosity Effect in Three-Dimensional Flows", *J. Phys. France*, **47**, 1137-1140 (1986).
- Simmons, M. J. and Azzopardi, B. J., "Drop Size Distributions in Dispersed Liquid-Liquid Pipe Flow", *Int. Journal of Multiphase Flow*, **27**, 843-859 (2001).
- Skelland, A. H. and Kane, J. S., "Transient Drop Size in Agitated Liquid-Liquid Systems as Influenced by the Direction of Mass Transfer and Surfactant Concentration", *Ind. Eng. Chem. Res.*, **31**, 2556-2563 (1992).
- Sleicher, C.A., "Maximum Stable Drop Size in Turbulent Flow", *AIChE J.*, **8**, No.4, 471-477 (1962).
- Sovova, H., "A Model of Dispersion Hydrodynamics in a Vibrating Plate Extractor", *Chem. Eng. Sc.*, **38**, No.11, 1863-1872 (1983).

- Sovova, H., "Breakage and Coalescence of Drops in a Batch Stirred Vessel – II Comparison of Model and Experiments", *Chem. Eng. Sci.*, **36**, 1567-1573 (1981).
- Sprow, F. B., "Distribution of Drop Sizes Produced in Turbulent Liquid-Liquid Dispersion", *Chem. Eng. Sc.*, **22**, 435-442 (1967b).
- Sprow, F. B., "Drop Size Distributions in Strongly Coalescing Agitated Liquid-Liquid Systems", *AIChE J.*, 996-998 (1967a).
- Sreenivasan, K.R., Tavoularis, S., Henry, R. and Corrsin, S., "Temperature Fluctuations and Scales in Grid-Generated Turbulence", *J. Fluid Mech.*, **100**, 597-621 (1980).
- Sreenivasulu, D., Venkatanarasaiah, D. and Varma, Y., "Drop Size Distributions in Liquid-Liquid Columns", *Bioprocess Engineering*, **17**, 189-195 (1997).
- Stamatoudis, M. and Tavlarides, L.L., "Effect of Continuous-Phase Viscosity on the Drop Sizes of Liquid-Liquid Dispersions in Agitated Vessels", *Ind. Eng. Chem. Process Des. Dev.*, **24**, 1175-1181 (1985).
- Stapountzis, H., Sawford, B.L., Hunt, J.C.R. and Britter, R.E., "Structure of the Temperature Field Downwind of a Line Source in Grid Turbulence", *J. Fluid Mech.*, **165**, 401-424 (1986).
- Stewart, A. C., El-Hammouz, A. M. and Davies, G. A., "Effect of Chemical Additives on the Stability of Kerosene-Water Dispersions", *J. Dispersion and Tech.*, **17**, 675-696 (1996).
- Streiff F., Mathys, P. and Fischer, T., "New Fundamentals for Liquid-Liquid Dispersion Using Static Mixers", *Recents Progres en Genie des Procedes*, **11**, (51), 307-314 (1997).
- Strieff, F., "In-line dispersion and mass transfer using static mixing equipment. Sulzer Tech. Rev", (3):108 (1977).
- Swartz, J. E. and Kessler, D. P., "Single Drop Break up in Developing Turbulent Pipe Flow", *AIChE J.*, **16**, No.2, 254-260 (1970).
- Swartzberg, H. G. and Treybal, R. E., "Fluid and Particle Motion in Turbulent Stirred Tanks", *Ind. Eng. Chem. Fund.*, **7**, 1 (1968).
- Tavlarides, L. L. and Stamatoudis, M., "The Analysis of Interphase Reactions and Mass Transfer in Liquid-Liquid Dispersions. In: Advances in Chemical Engineering", Vol11, Academic Press Inc., 199-273 (1981).

- Tjaberinga, W. J., Boon, A. and Chesters, A. K., "Model Experiments and Numerical on Emulsification Under Turbulent Conditions", *Chem. Eng. Sc.*, **48**, No.2, 285-293 (1993).
- Tobin, T. and Ramkrishna, D., "Coalescence of Charged Droplets in Agitated Liquid-Liquid Dispersions", *AIChE J.*, **38**, 1199-1205 (1992).
- Tobin, T., Muralidhar, R., Wright, W. and Ramkrishna, D., "Determination of Coalescence Frequencies in Liquid-Liquid Dispersions: Effect of Drop Size Dependence", *Chem. Eng. Sci.*, **45**, 3491-3504 (1990).
- Torrez, C. and Andre, C., "Power Consumption of a Rushton Turbine Mixing Viscous Newtonian and Shear-Thinning Fluids: Comparison Between Experimental and Numerical Results", *Chem. Eng. Tech.*, **21**, 7, 599604 (1998).
- Tsouris, C. and Tavlarides, L. L., "Breakage and Coalescence Models for Drops in Turbulent Dispersions", *AIChE Journal*, **40**, 395-406 (1994).
- Tsuji, H. and Hama, F. R., "Experimental on the Decay of Turbulence Behind Two Grids", *J. Aero. Sci.*, **20**, 848-859 (1953).
- Uberoi, M. S., "Energy Transfer in Isotropic Turbulence", *Phys. Fluids*, **6**, 1048-1061 (1963).
- Uberoi, M.S. and Wallis, S., "Effect of grid geometry on turbulence decay. *Phys. Fluids*", **10**, 1216-1224 (1967).
- Uberoi, M.S. and Wallis, S., "Spectra of Grid Turbulence. *Physics of Fluids*", **12**, 1355-1358 (1969).
- Velev, O. D., Danov, K. D. and Ivanov, I. B., "Stability of Emulsions Under Static and Dynamic Conditions", *J. Dispersion Sc. and Tech.*, **18**, 625-645 (1997).
- Verhoff, F. H., Ross, S. L. and Curl, R. L., "Breakage and Coalescence Processes in an Agitated Dispersion", *Ind. Eng. Chem. Fund.*, **16**, 371-379 (1977).
- Villermaux, E., Sommeria, J., Gagne, Y. and Hopfinger, E., "Oscillatory Instability and Genesis of Turbulence Behind a High Solidity Grid", *Eur. J. Mech. B: Fluids*, **10**, No.4, 427-439 (1991).
- Villermaux, J., "The Role of Energy Dissipation in Contacting and Mixing Devices", *Chem. Eng. Tech.*, **11**, 276-287 (1988).
- Von Bohl, J. G., "Das Verhalten Paralleler Luftstrahlen", *Ing. Arch.*, **11**, 295-307 (1940).

- Von Kármán, T. and Howarth, L. (1961), On the statistical theory of isotropic turbulence. (from Proceedings of the Royal Society A164, 192-215 (1938)) In: "Turbulence: Classic papers on statistical theory", S.K. Friedlander and L. Topper eds., Interscience Publishers, Inc., New York, pp. 76-99.
- Wahrhaft, Z. and Lumley, J.L., "An experimental study of the decay of temperature fluctuations in grid-generated turbulence", *J. Fluid Mech.*, **88**, 659-684 (1978).
- Walker, L. D., Liquid-Liquid Dispersion Processes in Static Mixers, M.Sc. Thesis, TUNS (1984).
- Walker, M.D., "Laser Doppler Measurements of Grid Turbulence in a box", Ph D Dissertation, Johns Hopkins University (1986).
- Walstra, P., "Emulsion Stability", in Encyclopedia of Emulsion Technology, **4**, 1-62 (1996).
- Walstra, P., "Prinsiples of Emulsion Formation", *Chem. Eng. Sci.*, **48**, 333-3349 (1993).
- Wang, C. Y. and Calabrese, R. V., "Drop Break up in Turbulent Stirred-Tank Contactors, Part II: Relative Influence of Viscosity and Interfacial Tension", *AIChE J.*, **32**, 667-676 (1986).
- Ward, J. P. and Knudsen, J. G., "Turbulent Flow of Unstable Liquid-Liquid Dispersions: Drop Sizes and Velocity Distributions", *AIChE J.*, **13**, 356-363 (1967).
- Wasan, D. T., Shah, S. M., Aderanjani, N., Chan, M. S. and McNamara, J. J. "Observation on the Coalescence Behavior of Oil Droplets and Emulsion Stability in Enhanced Oil Recovery", *Society of Petroleum Engineer J.*, 409-417 (1978)
- Wasan, D. T., Shah, S. M., Sampath, K., and Aderanjani, N., "The Role of Coalescence Phenomena and Interfacial Rheological Properties in Enhanced Oil Recovery: An Overview", *J. Soc. Rheol.*, **23**, 181-207 (1979).
- White, F.M., Viscous Fluid Flow, McGraw-Hill, New York (1974).
- Wright H. and Ramkrishna D., "Factors Affecting Coalescence Frequency of Droplets on a Stirred Liquid-Liquid Dispersion", *AIChE J.*, **40**, 767-776 (1994).

- Xue, Y., Comparative Evaluation of Techniques for Measuring Dynamic Interfacial Characteristics of Industrial Streams, M.Sc. Thesis, Dalhousie University (1999).
- Yakhot, V. and Pelz, R., "Large-scale Structure Generation by Anisotropic Small-scale Flows", *Phys. Fluids*, **30**, 1272-1277 (1987).
- Yarin, L. P. and Hetsroni, G., "Turbulence Intensity in Dilute Two-Phase Flows — 3 The Particles-Turbulence Interaction in Dilute Two-Phase Flow", *Int. J. Multiphase Flow*, **20**, 27-44 (1994).
- Yeh, T.T. and van Atta, C.W., "Spectral Transfer of Scalar and Velocity Fields in Heated-Grid Turbulence", *J. Fluid Mech.*, **58**, 233-261.Z1 (1973).
- Yuan, Z. and Michaelides, E.E., "Turbulence Modulation in Particulate Flows-A Theoretical Approach", *Int. J. Multiphase Flow*, **18**, 779-785 (1992).
- Zahradnik, J. and Rylek, M., "Design and Scale-up of Venturi-Tube Gas Distributors for Bubble Column Reactors", *Collect. Czech. Che. Commun.*, **56**, 619-635 (1991).
- Zhang, Q. M. and Chen, B. H., "Pressure Drop in Packed Bubble Columns", *Chem. Eng. Comm.*, **140**, 173-181 (1996)
- Zhou, G. and Kresta S., "Evolution of Drop Size Distribution in Liquid-Liquid Dispersions for Various Impellers", *Chem. Eng. Sc.*, **53**, 2099-2113 (1997).
- Zhou, G. and Kresta, S., "Impact of the Maximum Turbulence Energy Dissipation Ratio on the Mean and Minimum Drop Sizes for Various Impellers", Paper presented at the 1996 AIChE National Meeting, Chicago (Nov. 1996).
- Zlokarnik, M., "Tower-Shaped Reactors for Aerobic Biological Waste Water Treatment" in *Biotechnology*, M. Zlokarnik and H. Brauer Ed., 537-569 (1985).

Appendix A: Drop number density distributions.

Effect of Superficial velocity

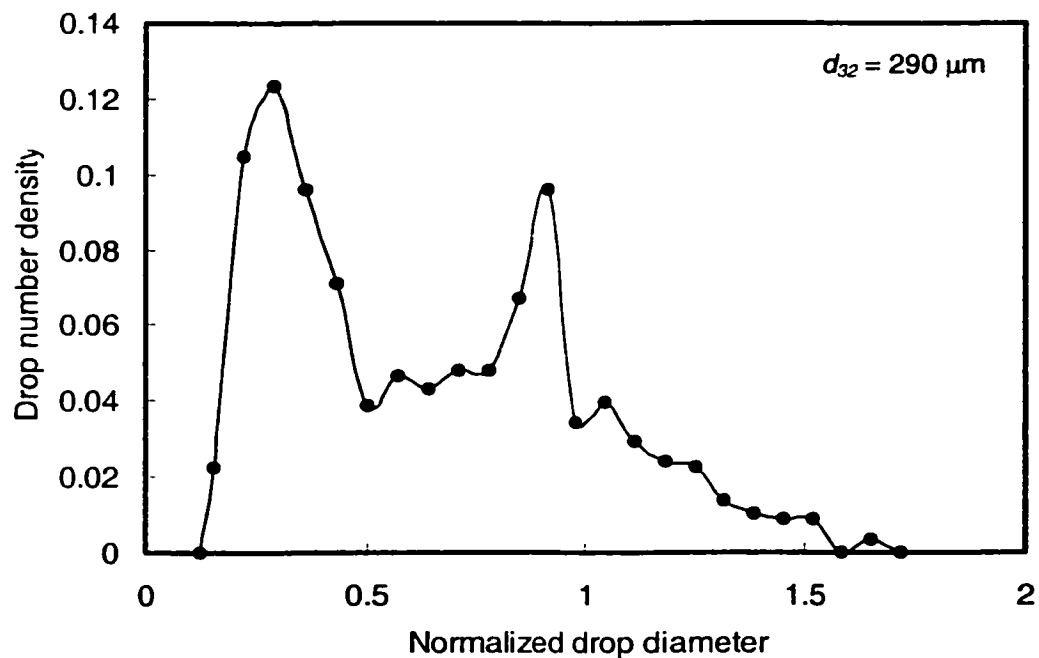


Figure A1. Drop number density distribution
($\alpha = 0.41$, $\phi = 0.5\%$, $U = 0.30$ m/s, 9 screens, $L = 10$ mm).

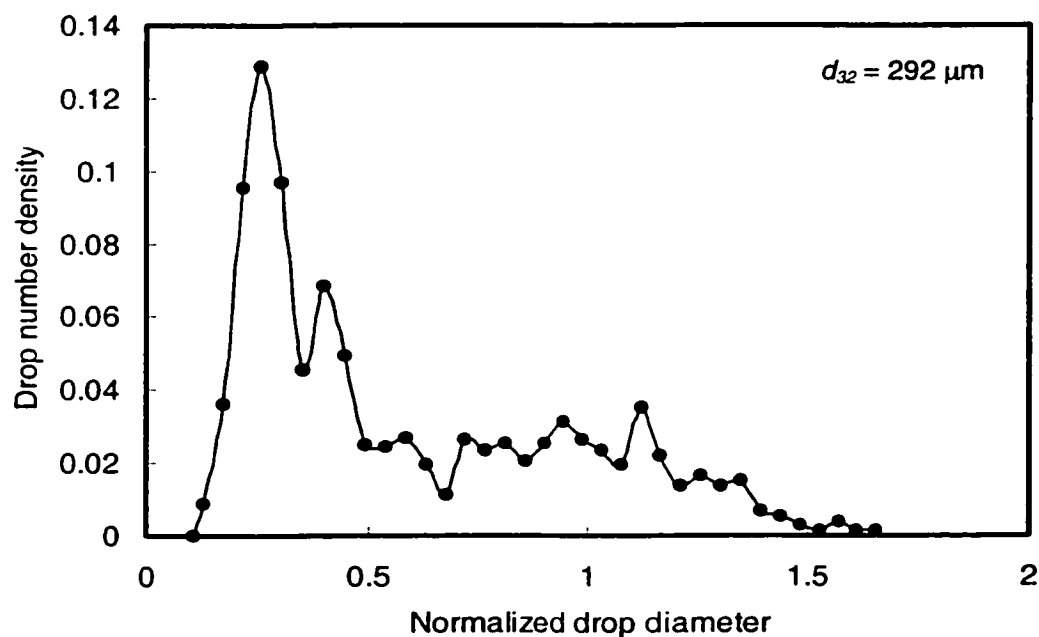


Figure A2. Drop number density distribution
($\alpha = 0.41$, $\phi = 0.5\%$, $U = 0.40$ m/s, 9 screens, $L = 10$ mm).

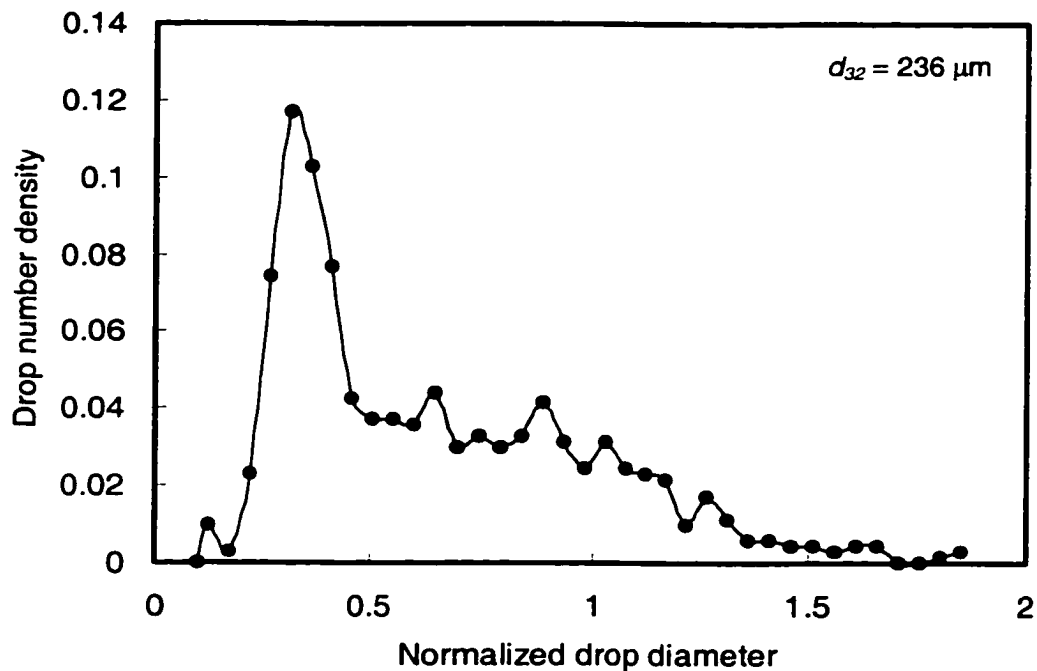


Figure A3. Drop number density distribution
 ($\alpha = 0.41$, $\phi = 0.5\%$, $U = 0.50$ m/s, 9 screens, $L = 10$ mm).

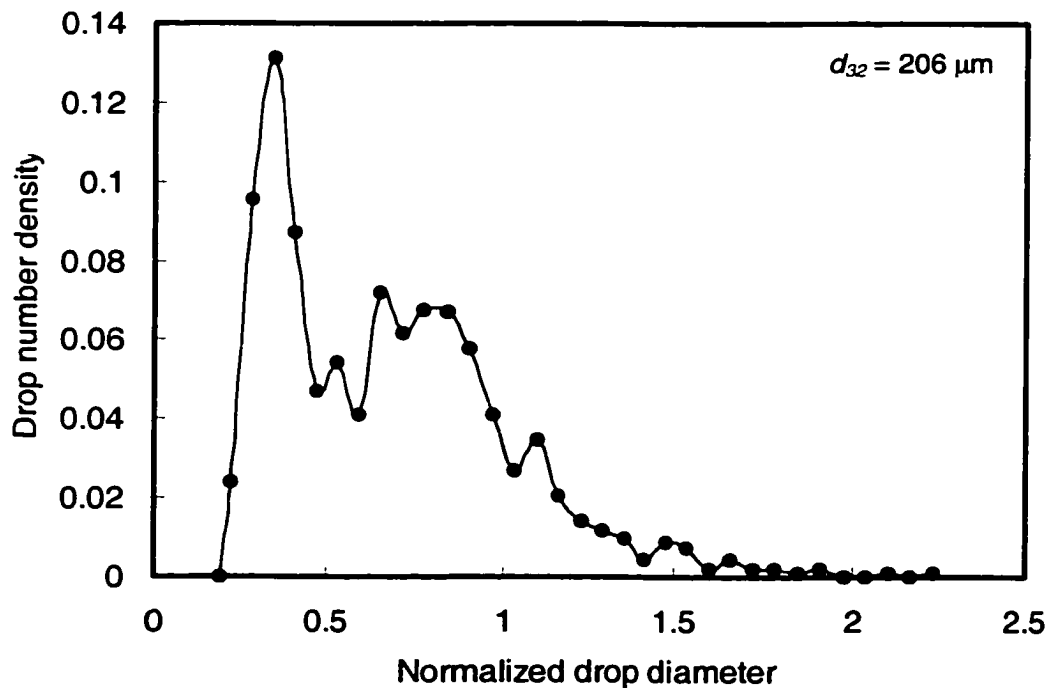


Figure A4. Drop number density distribution
 ($\alpha = 0.41$, $\phi = 0.5\%$, $U = 0.60$ m/s, 9 screens, $L = 10$ mm).

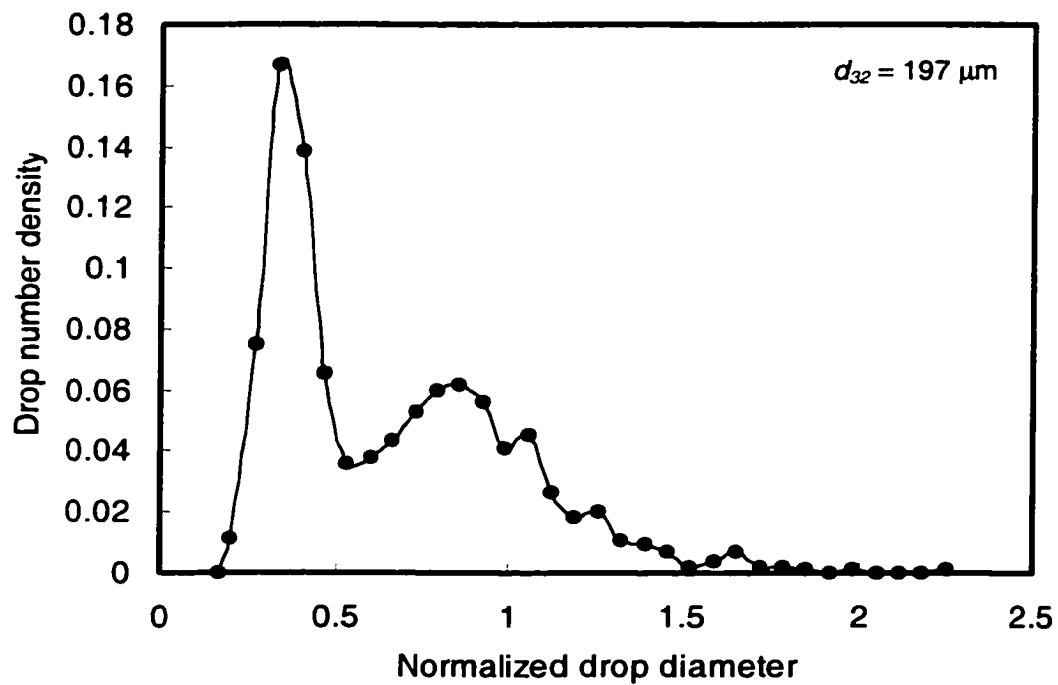


Figure A5. Drop number density distribution
 ($\alpha = 0.41$, $\phi = 0.5\%$, $U = 0.65$ m/s, 9 screens, $L = 10$ mm).

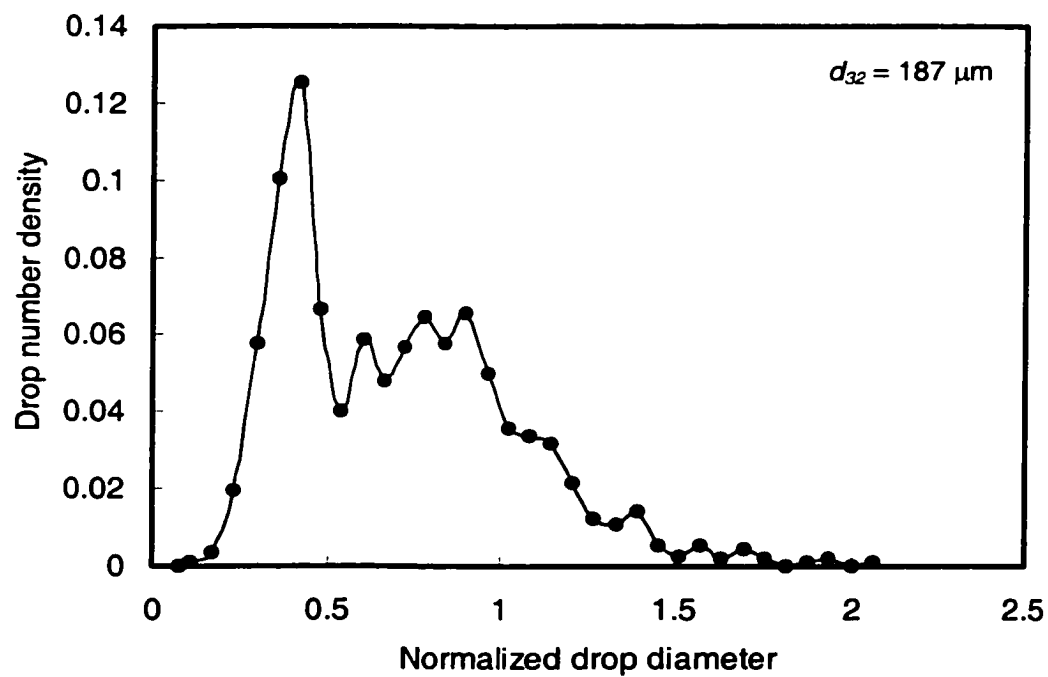


Figure A6. Drop number density distribution
 ($\alpha = 0.41$, $\phi = 0.5\%$, $U = 0.70$ m/s, 9 screens, $L = 10$ mm).

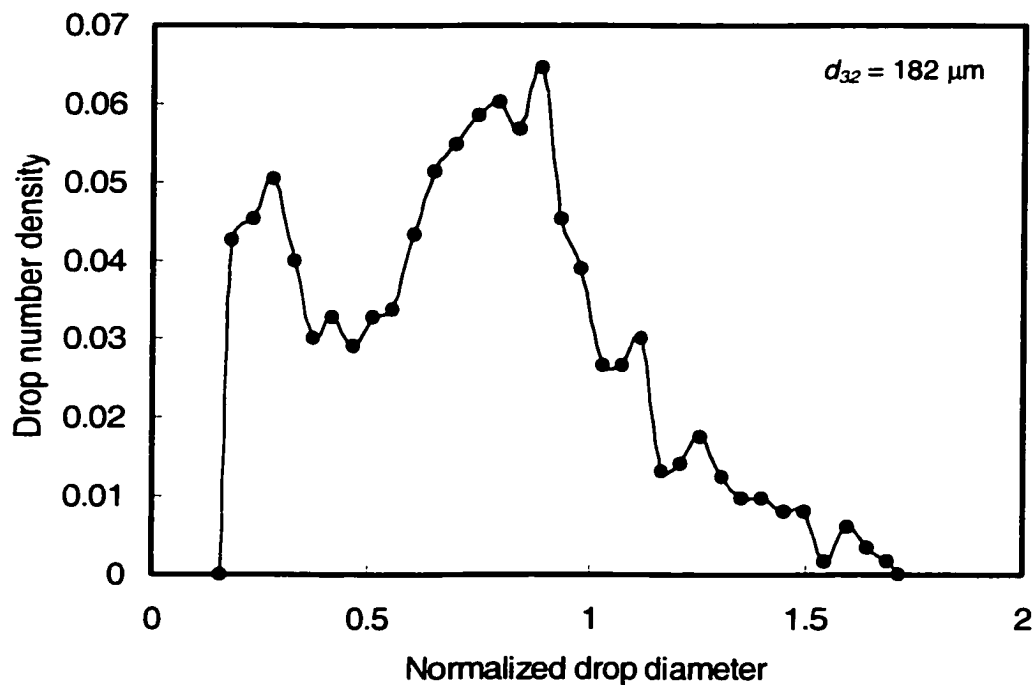


Figure A7. Drop number density distribution
 ($\alpha = 0.41$, $\phi = 0.5\%$, $U = 0.85$ m/s, 9 screens, $L = 10$ mm).

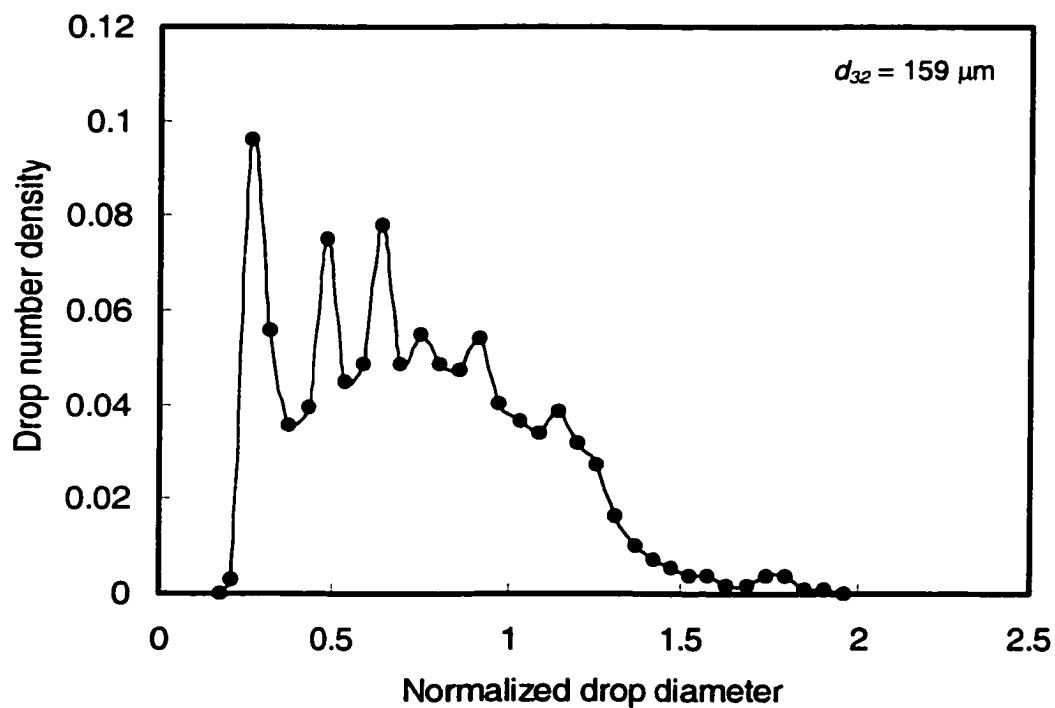


Figure A8. Drop number density distribution
 ($\alpha = 0.41$, $\phi = 0.5\%$, $U = 0.97$ m/s, 9 screens, $L = 10$ mm).

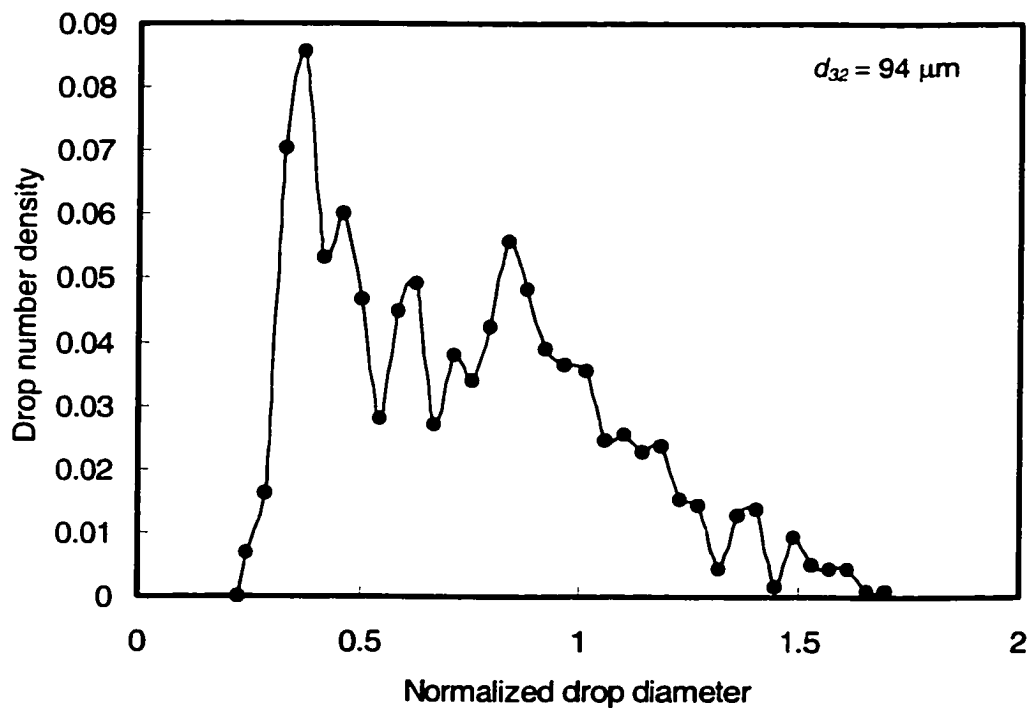


Figure A9. Drop number density distribution
 ($\alpha = 0.41$, $\phi = 0.5\%$, $U = 1.55 \text{ m/s}$, 9 screens, $L = 10 \text{ mm}$).

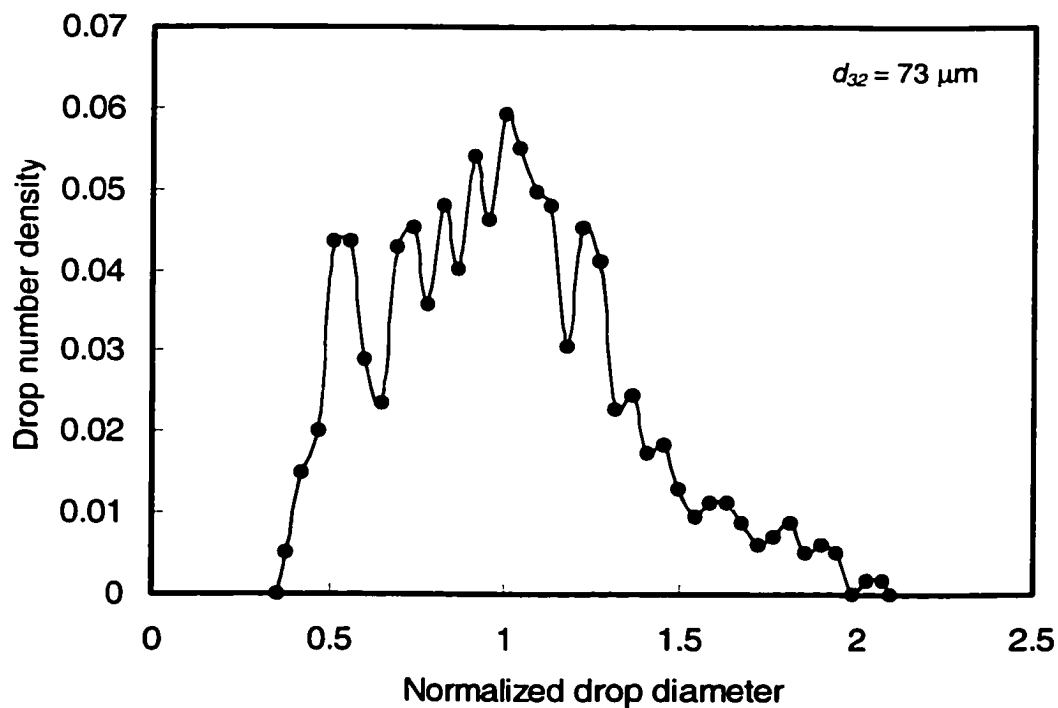


Figure A10. Drop number density distribution
 ($\alpha = 0.41$, $\phi = 0.5\%$, $U = 1.80 \text{ m/s}$, 9 screens, $L = 10 \text{ mm}$).

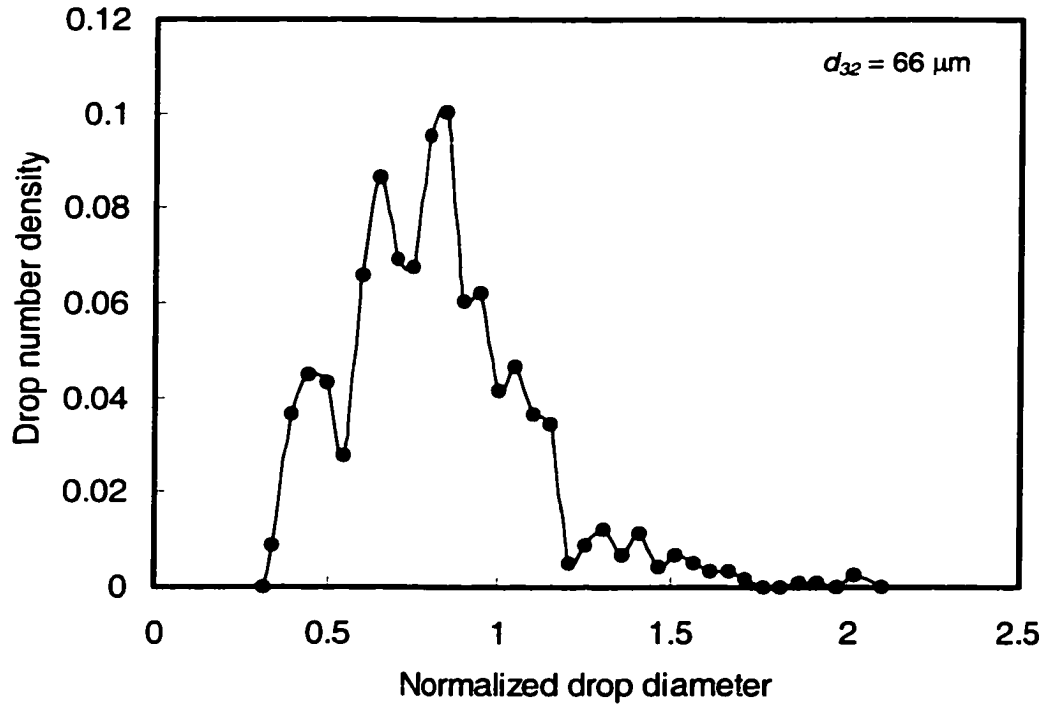


Figure A11. Drop number density distribution
 ($\alpha = 0.41$, $\phi = 0.5\%$, $U = 1.94$ m/s, 9 screens, $L = 10$ mm).

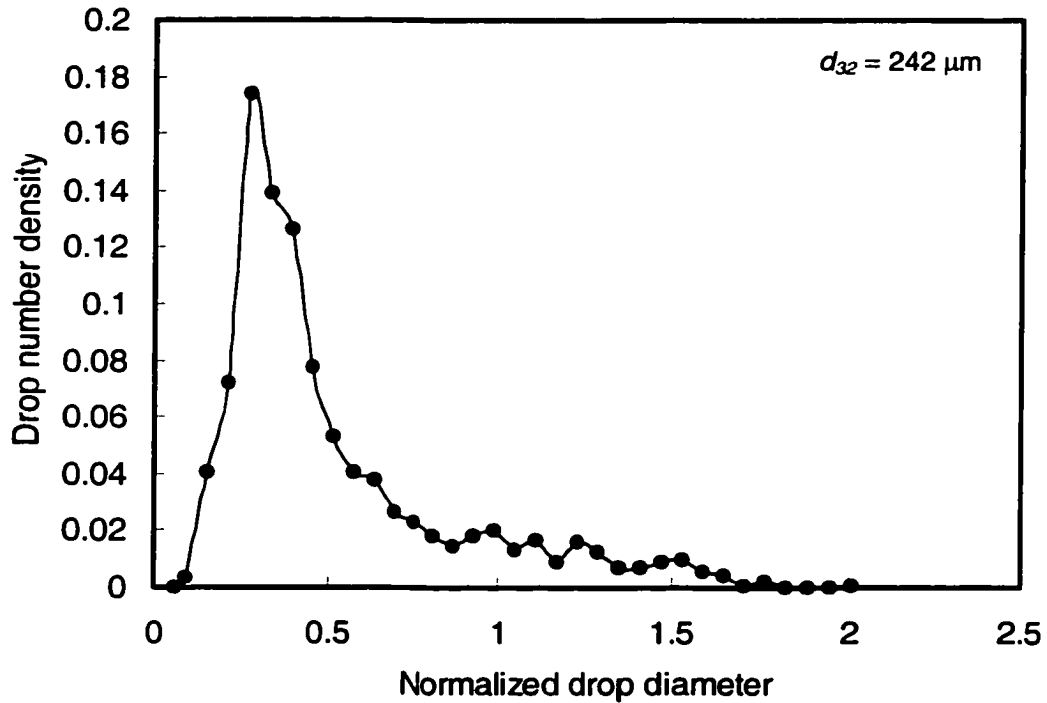


Figure A12. Drop number density distribution
 ($\alpha = 0.41$, $\phi = 4\%$, $U = 0.30$ m/s, 9 screens, $L = 10$ mm).

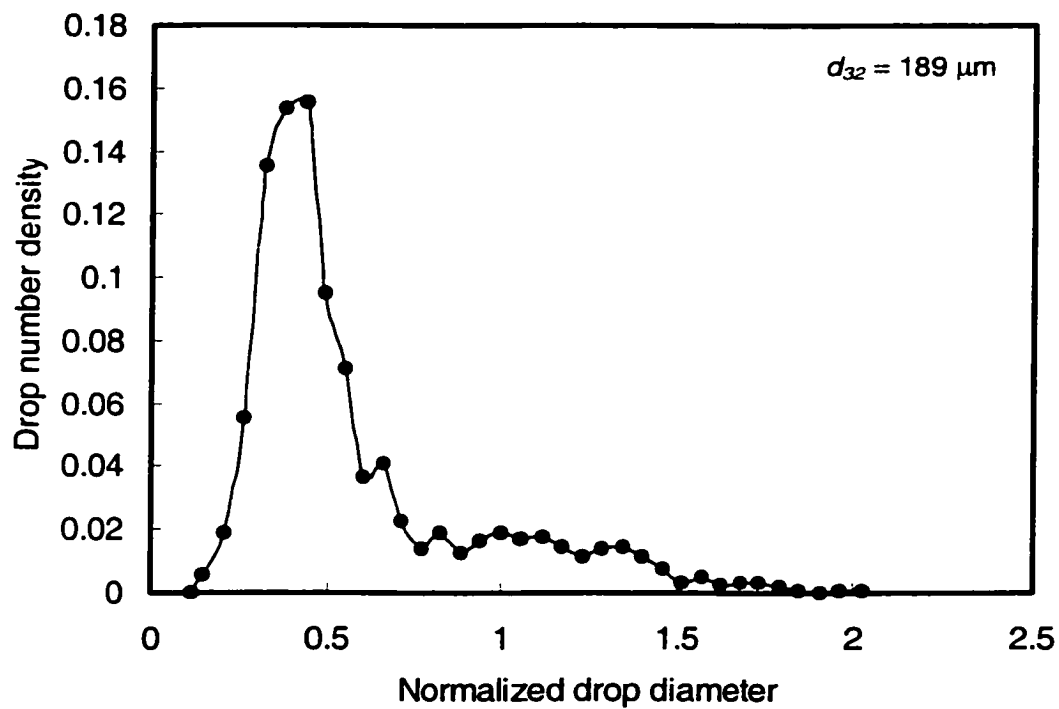


Figure A13. Drop number density distribution
 ($\alpha = 0.41$, $\phi = 4\%$, $U = 0.40$ m/s, 9 screens, $L = 10$ mm).

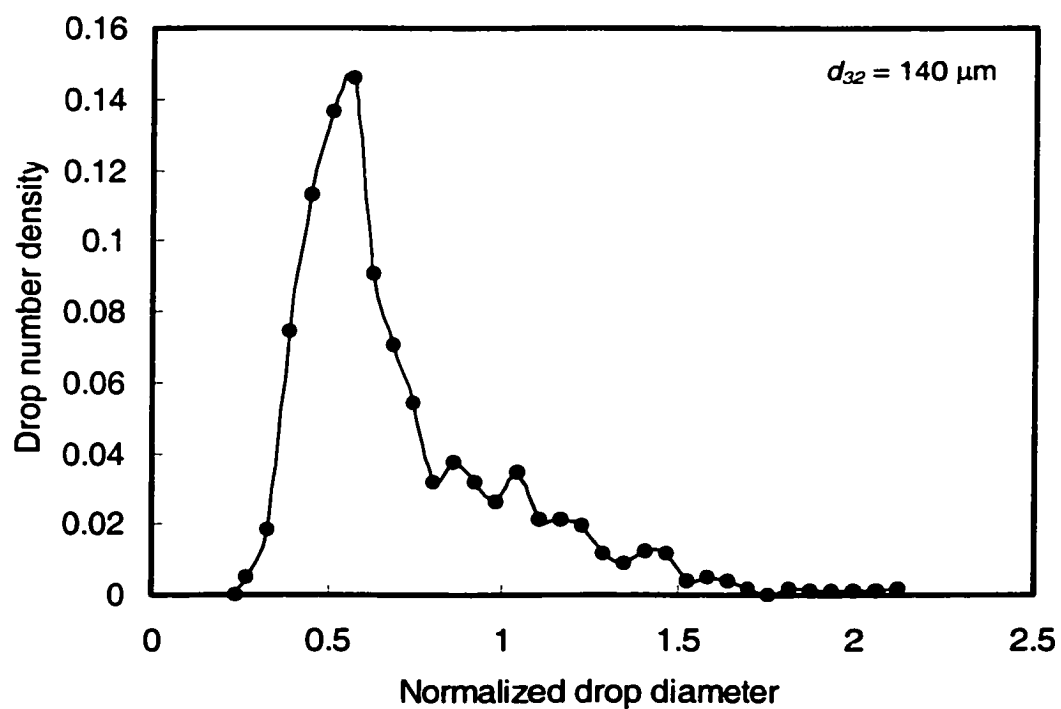


Figure A14. Drop number density distribution
 ($\alpha = 0.41$, $\phi = 4\%$, $U = 0.50$ m/s, 9 screens, $L = 10$ mm).

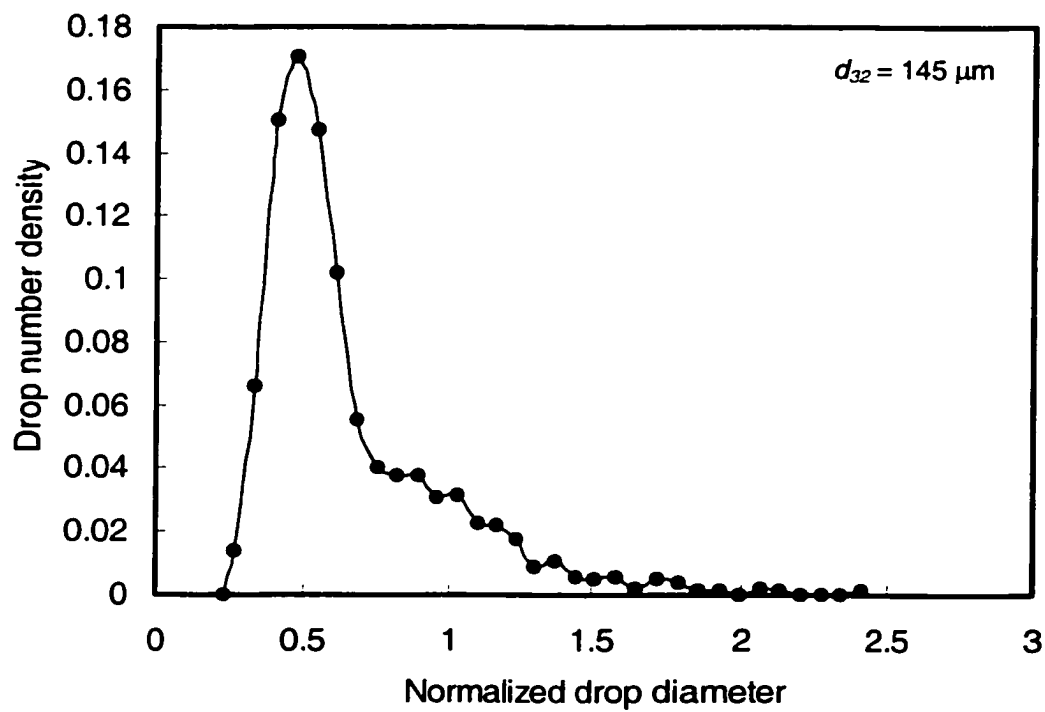


Figure A15. Drop number density distribution
 ($\alpha = 0.41$, $\phi = 4\%$, $U = 0.60$ m/s, 9 screens, $L = 10$ mm).

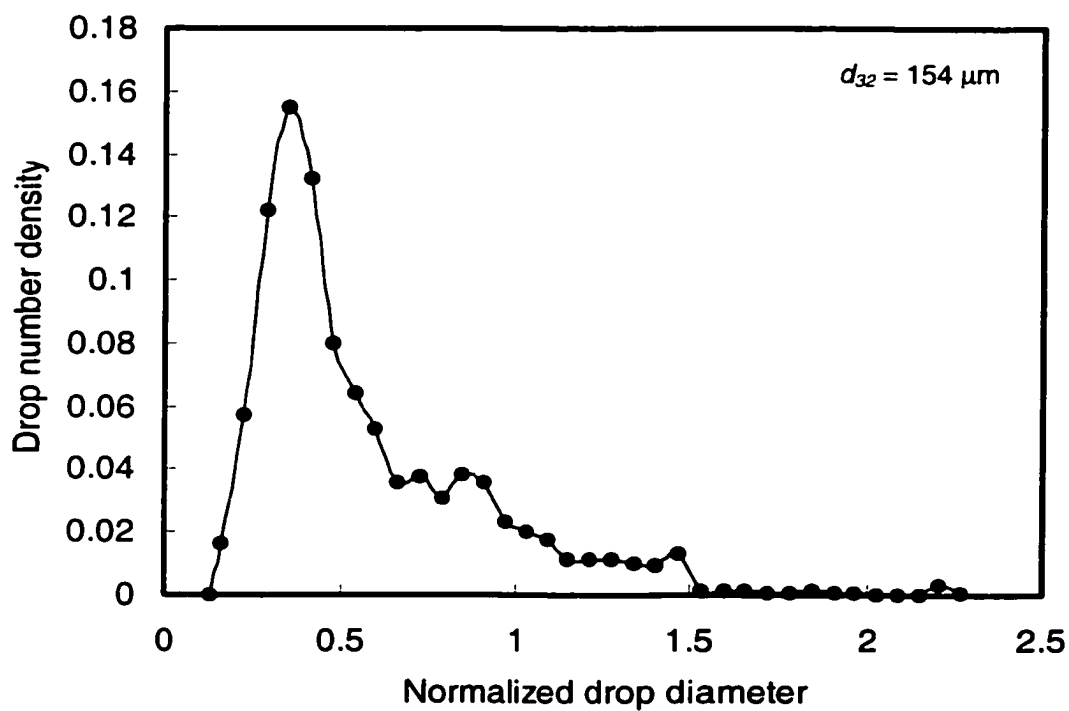


Figure A16. Drop number density distribution
 ($\alpha = 0.41$, $\phi = 4\%$, $U = 0.65$ m/s, 9 screens, $L = 10$ mm).

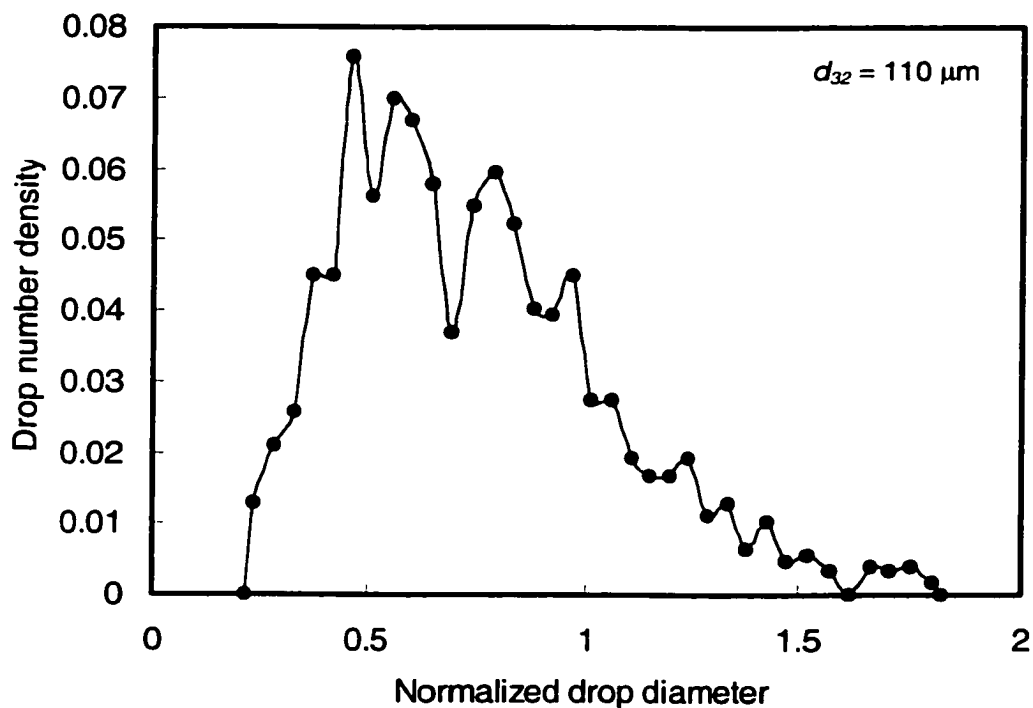


Figure A17. Drop number density distribution
 ($\alpha = 0.41$, $\phi = 4\%$, $U = 0.85$ m/s, 9 screens, 10 mm).

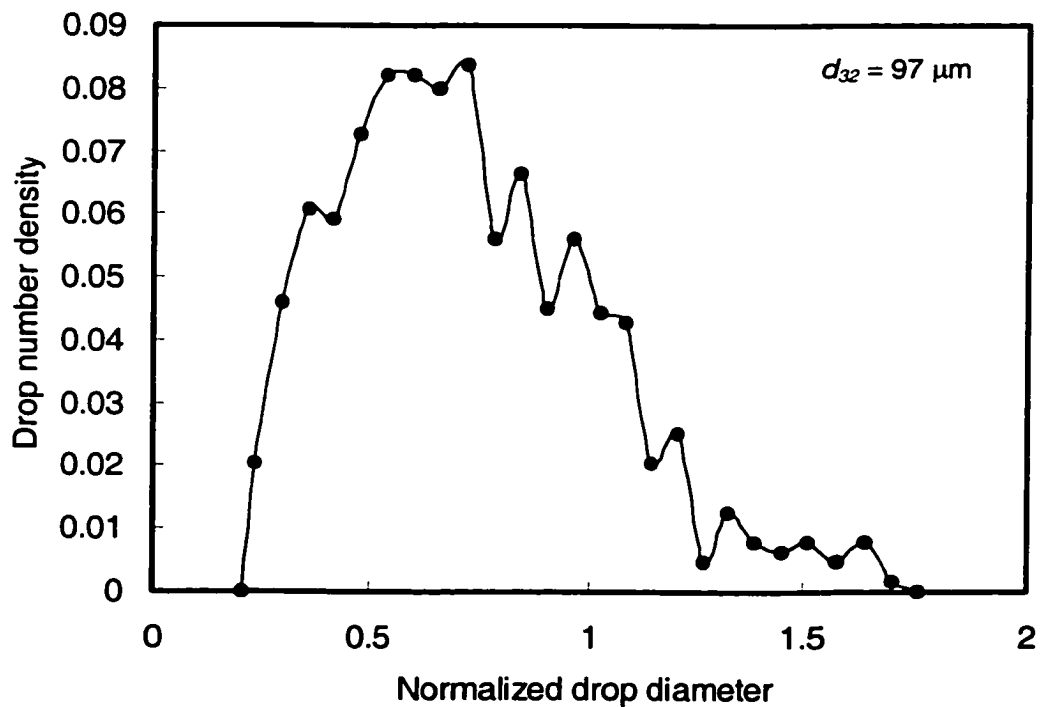


Figure A18. Drop number density distribution
 ($\alpha = 0.41$, $\phi = 4\%$, $U = 0.97$ m/s, 9 screens, $L = 10$ mm).

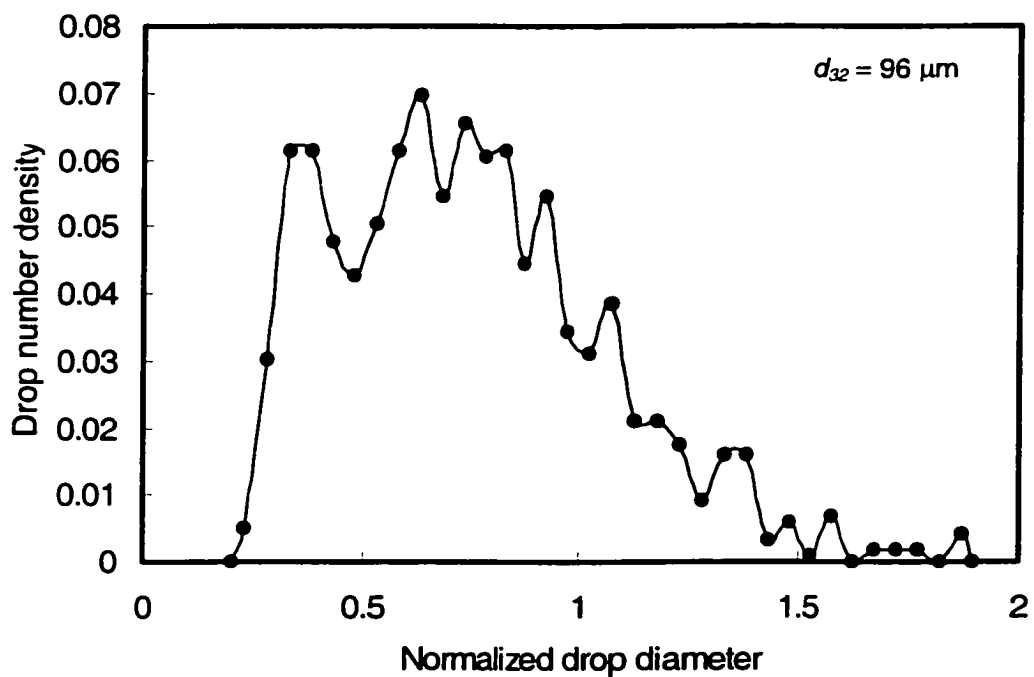


Figure A19. Drop number density distribution
 ($\alpha = 0.41$, $\phi = 4\%$, $U = 1.55 \text{ m/s}$, 9 screens, $L = 10\text{mm}$).

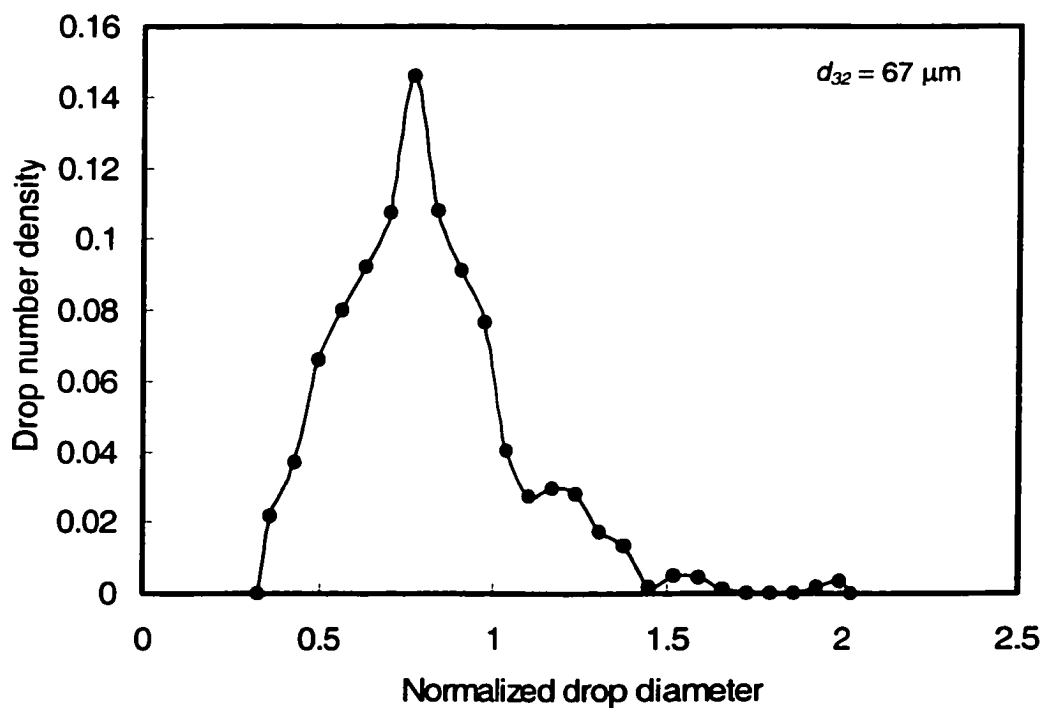


Figure A20. Drop number density distribution
 ($\alpha = 0.41$, $\phi = 4\%$, $U = 1.94 \text{ m/s}$, 9 screens, $L = 10\text{mm}$).

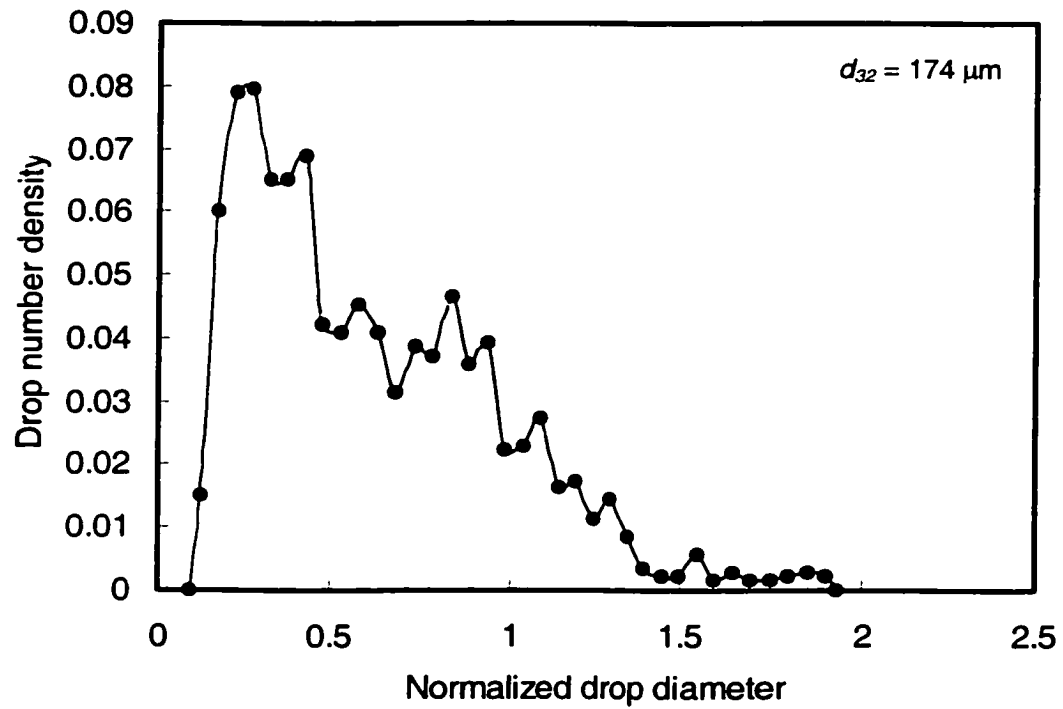


Figure A21. Drop number density distribution
 ($\alpha = 0.33$, $\phi = 0.5\%$, $U = 0.30$ m/s, 9 screens, $L = 10$ mm).

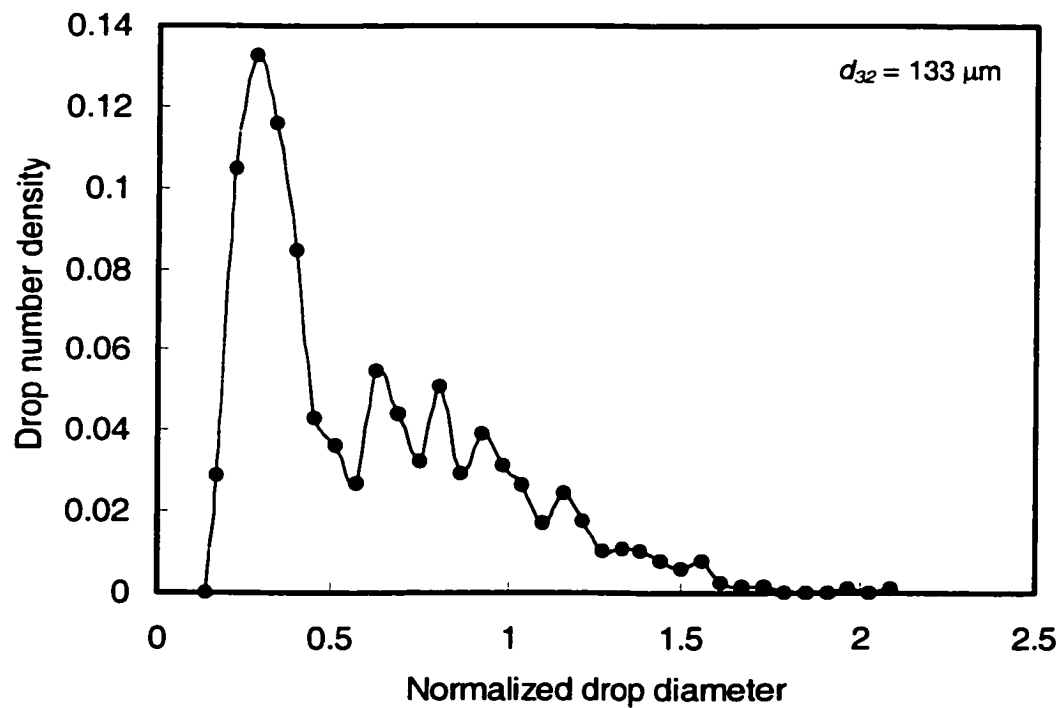


Figure A22. Drop number density distribution
 ($\alpha = 0.33$, $\phi = 0.5\%$, $U = 0.50$ m/s, 9 screens, $L = 10$ mm).

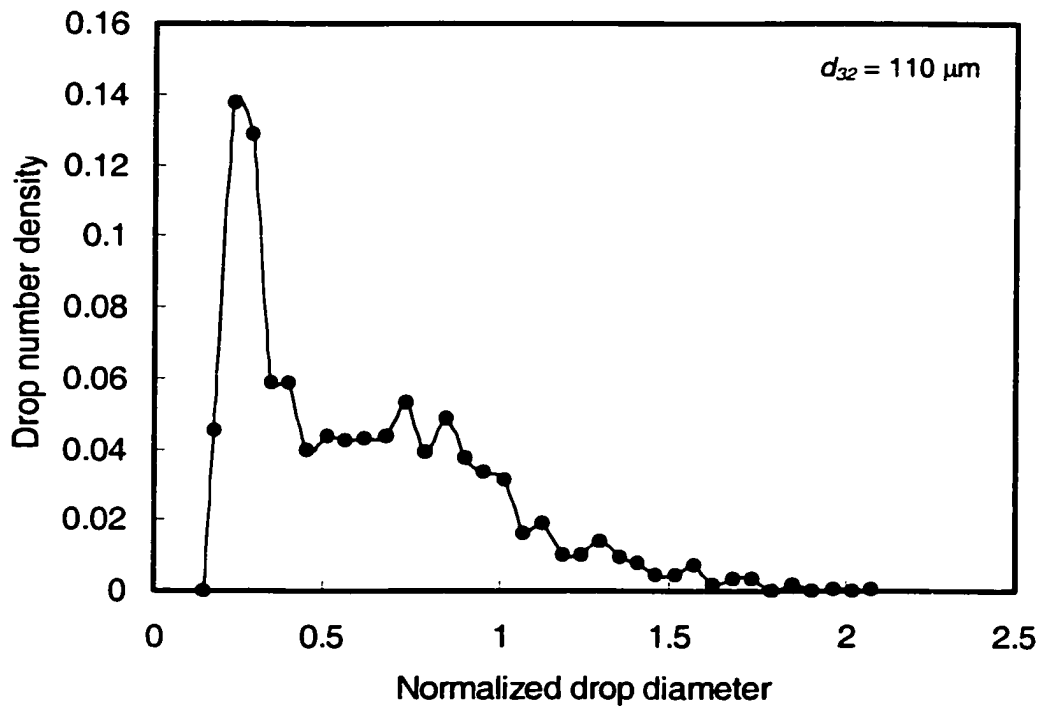


Figure A23. Drop number density distribution
 ($\alpha = 0.33$, $\phi = 0.5\%$, $U = 0.70$ m/s, 9 screens, $L = 10$ mm).

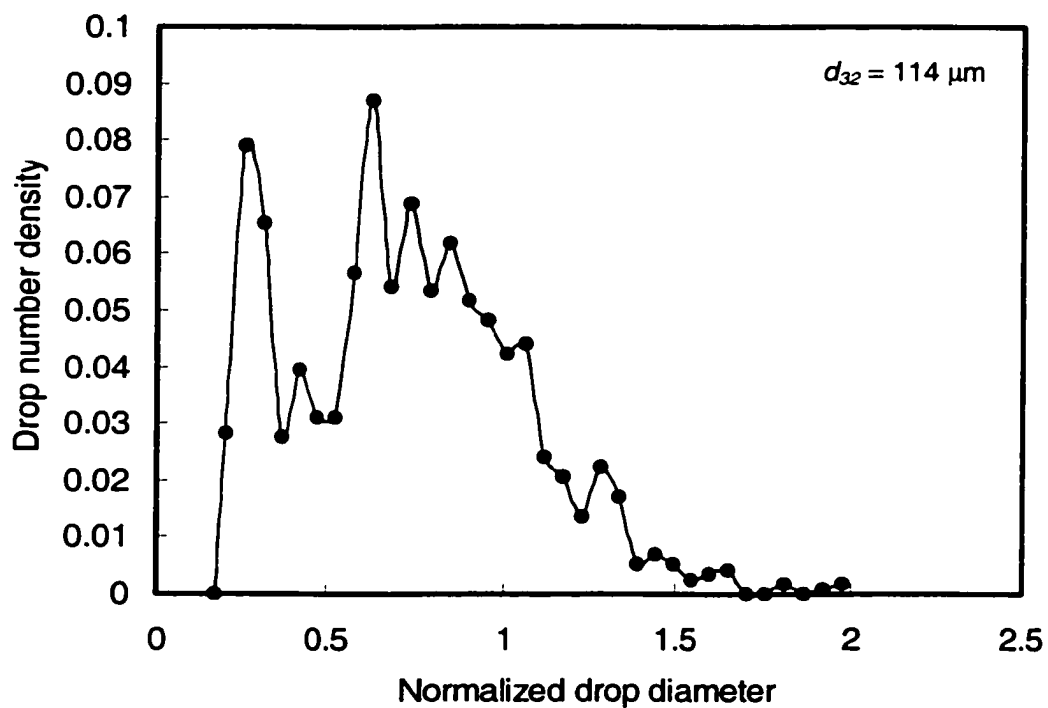


Figure A24. Drop number density distribution
 ($\alpha = 0.33$, $\phi = 0.5\%$, $U = 0.85$ m/s, 9 screens, $L = 10$ mm).

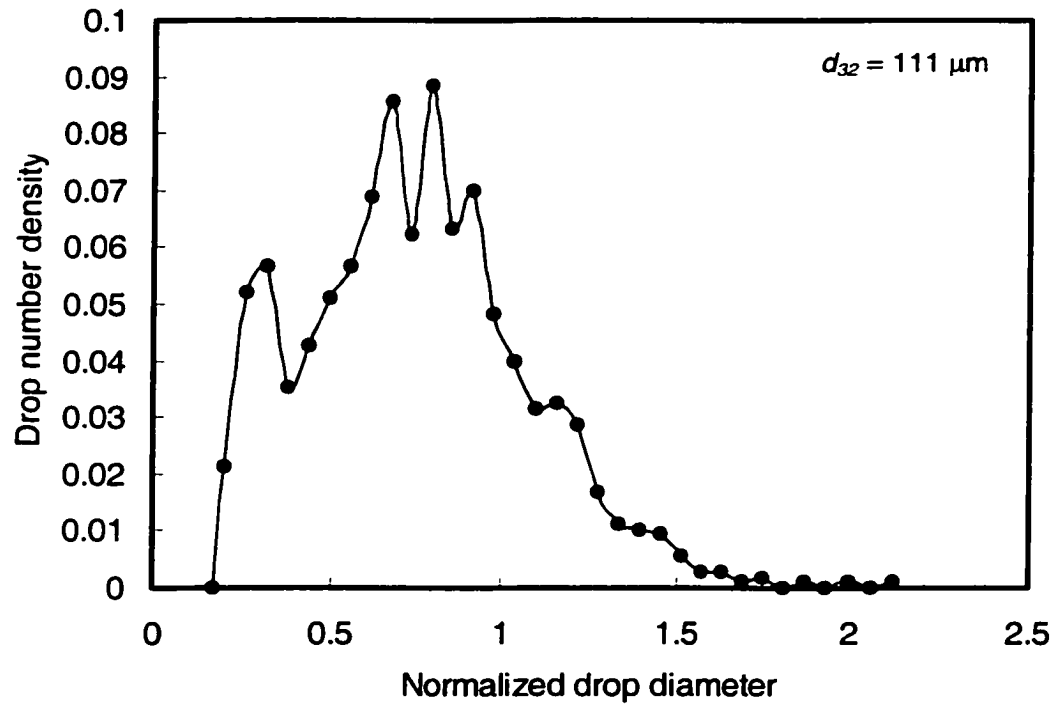


Figure A25. Drop number density distribution
 ($\alpha = 0.33$, $\phi = 0.5\%$, $U = 0.97$ m/s, 9 screens, $L = 10$ mm).

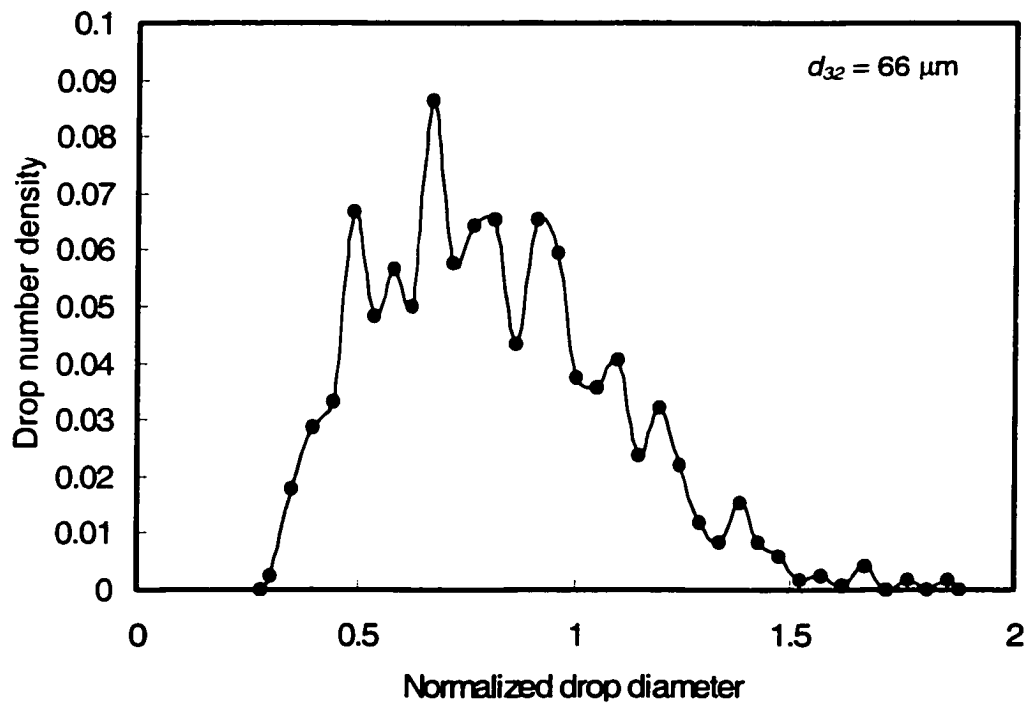


Figure A26. Drop number density distribution
 ($\alpha = 0.33$, $\phi = 0.5\%$, $U = 1.55$ m/s, 9 screens, $L = 10$ mm).

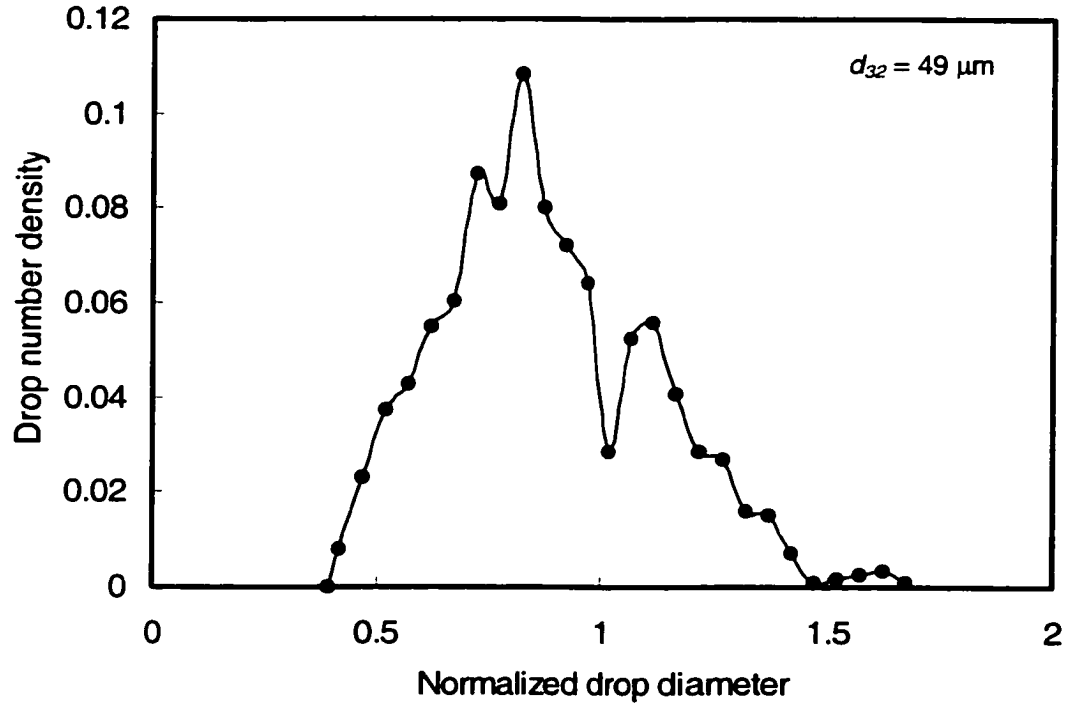


Figure A27. Drop number density distribution
 ($\alpha = 0.33$, $\phi = 0.5\%$, $U = 1.80$ m/s, 9 screens, $L = 10$ mm).

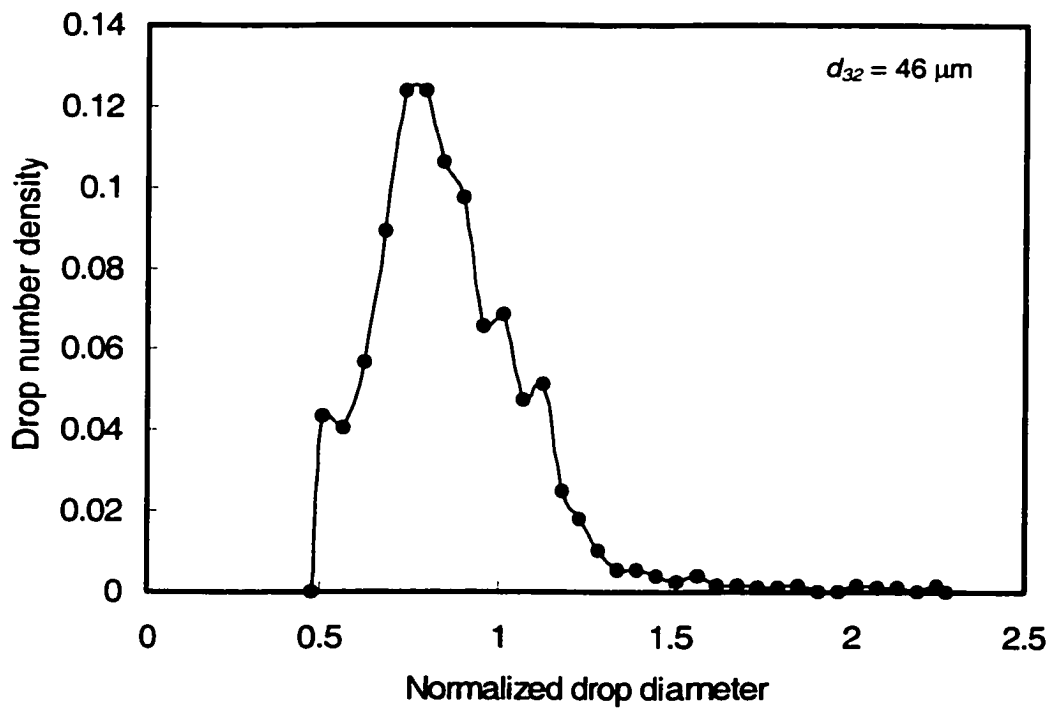


Figure A28. Drop number density distribution
 ($\alpha = 0.33$, $\phi = 0.5\%$, $U = 1.94$ m/s, 9 screens, $L = 10$ mm).

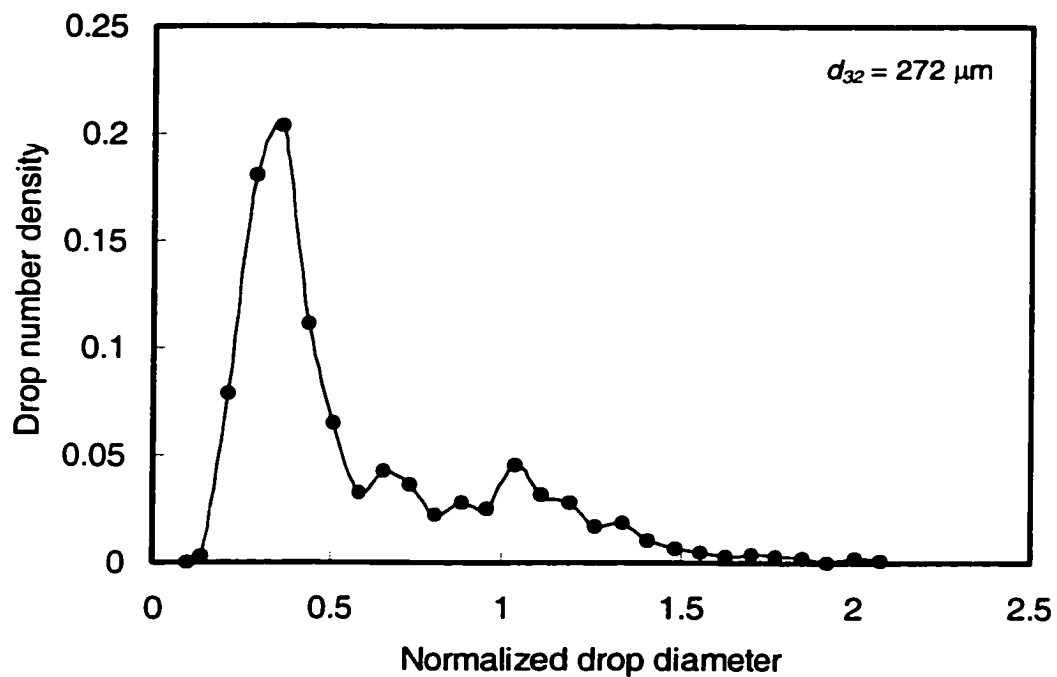


Figure A29. Drop number density distribution
 ($\alpha = 0.27$, $\phi = 0.5\%$, $U = 0.30$ m/s, 9 screens, $L = 10$ mm).

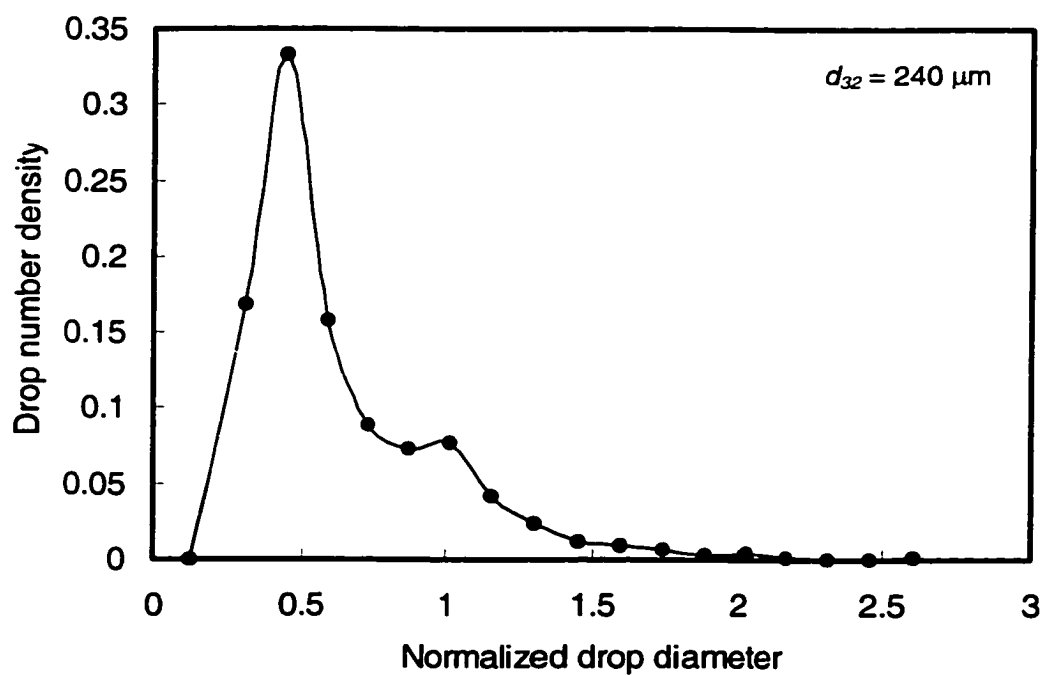


Figure A30. Drop number density distribution
 ($\alpha = 0.27$, $\phi = 0.5\%$, $U = 0.40$ m/s, 9 screens, $L = 10$ mm).

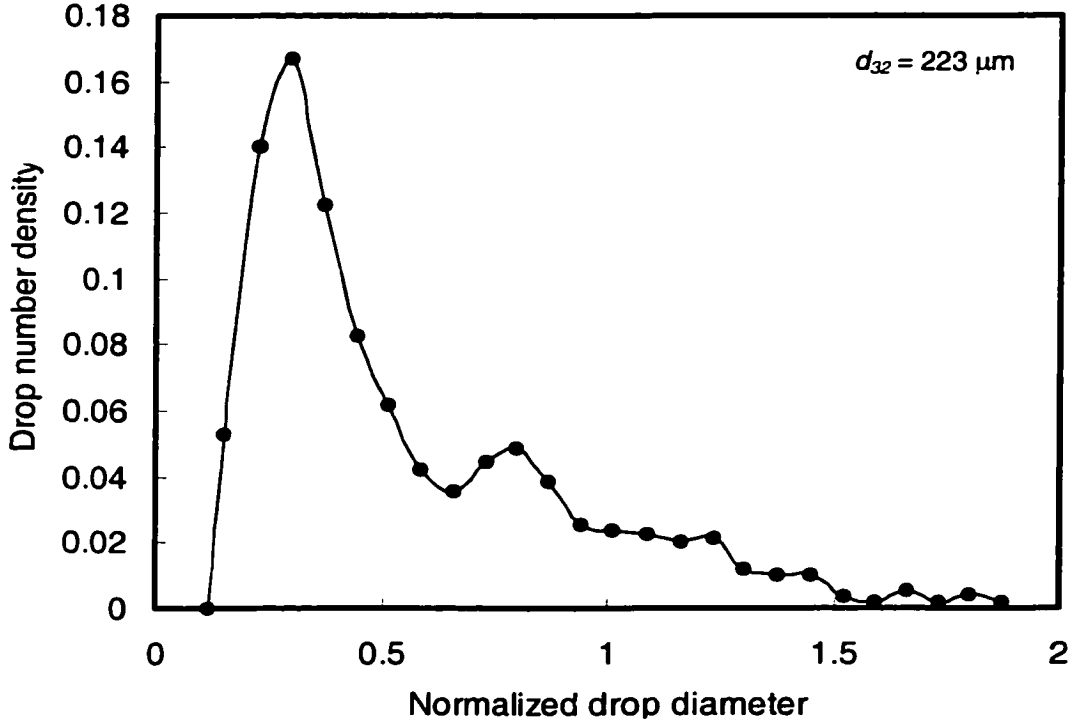


Figure A31. Drop number density distribution ($\alpha = 0.27$, $\phi = 0.5\%$, $U = 0.50$ m/s, 9 screens, $L = 10$ mm).

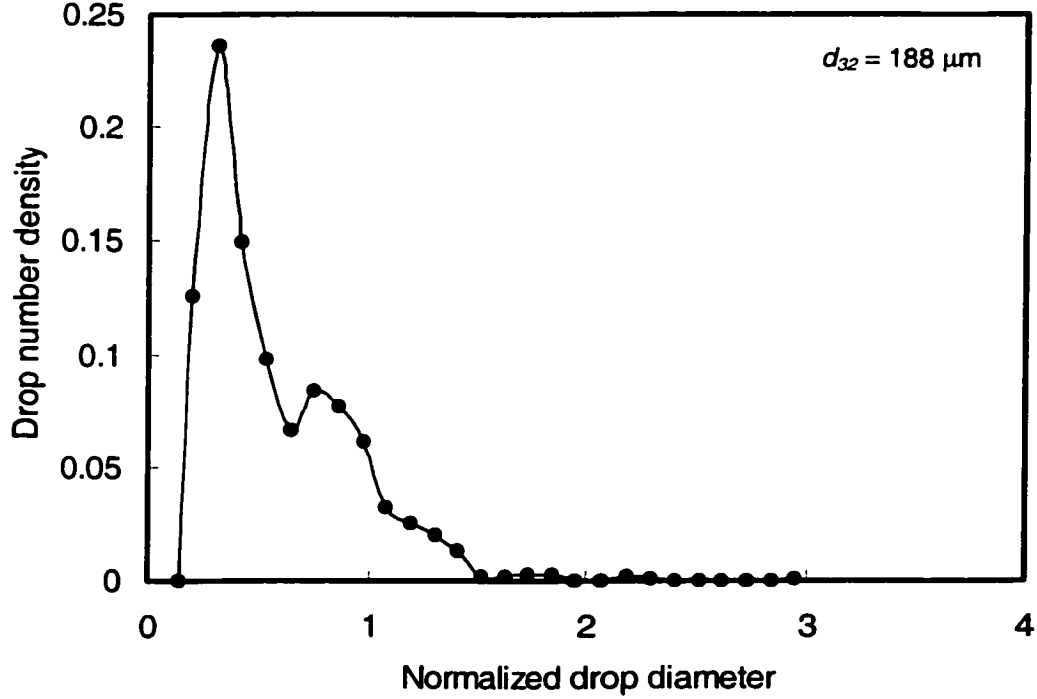


Figure A32. Drop number density distribution ($\alpha = 0.27$, $\phi = 0.5\%$, $U = 0.60$ m/s, 9 screens, $L = 10$ mm).

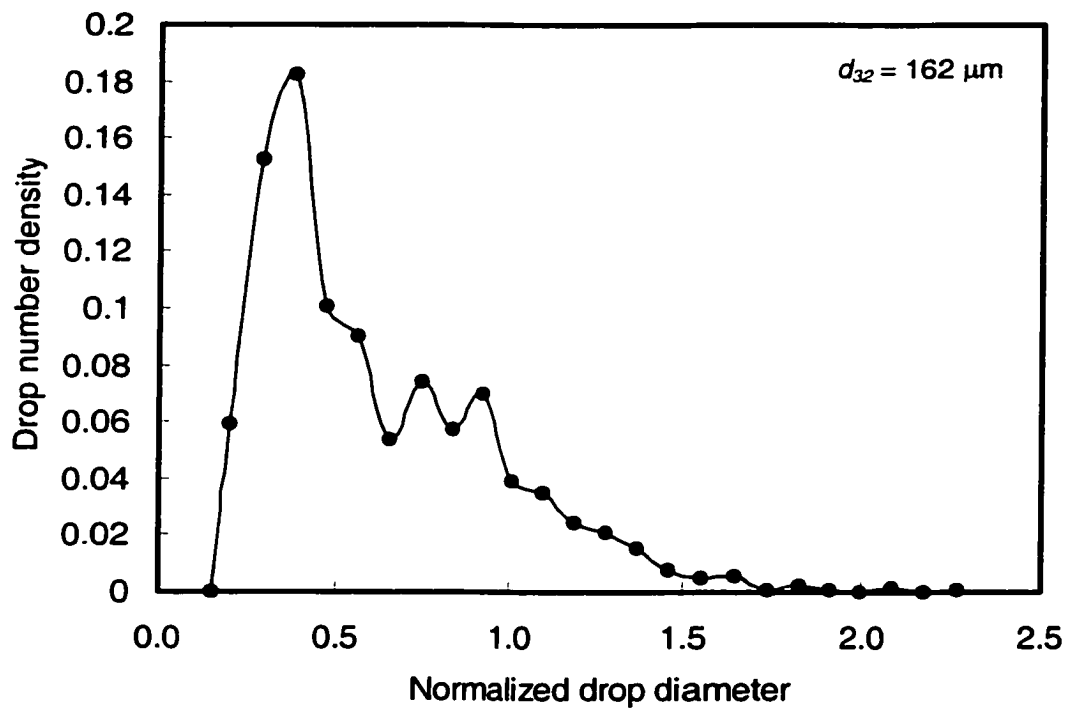


Figure A33. Drop number density distribution
 ($\alpha = 0.27$, $\phi = 0.5\%$, $U = 0.65$ m/s, 9 screens, $L = 10$ mm).

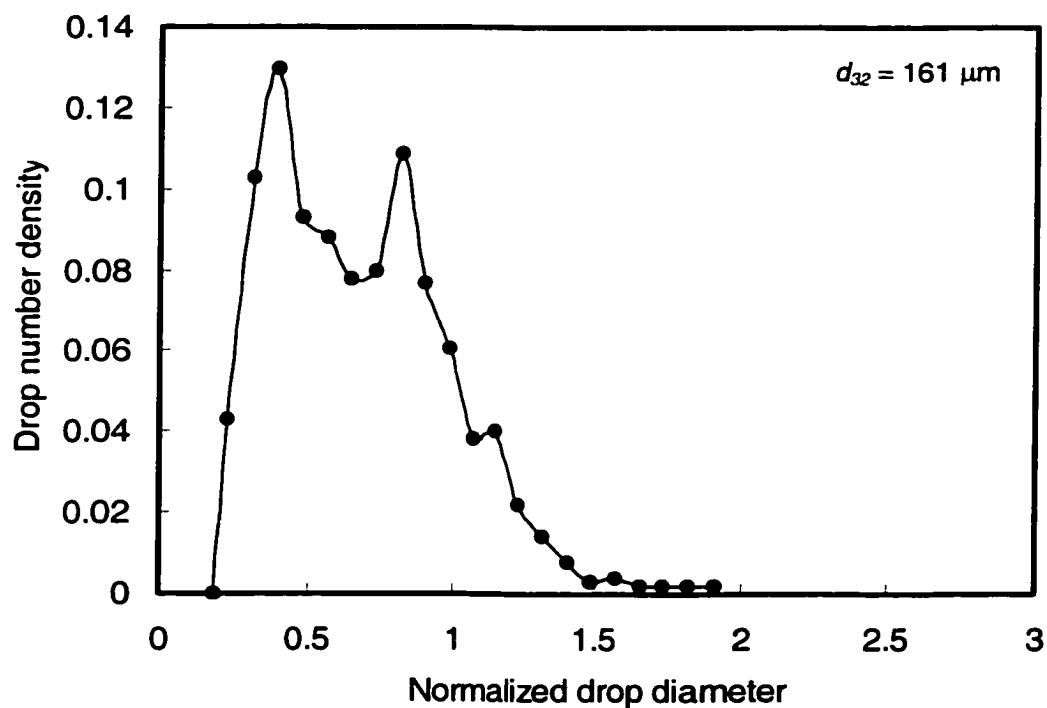


Figure A34. Drop number density distribution
 ($\alpha = 0.27$, $\phi = 0.5\%$, $U = 0.70$ m/s, 9 screens, $L = 10$ mm).

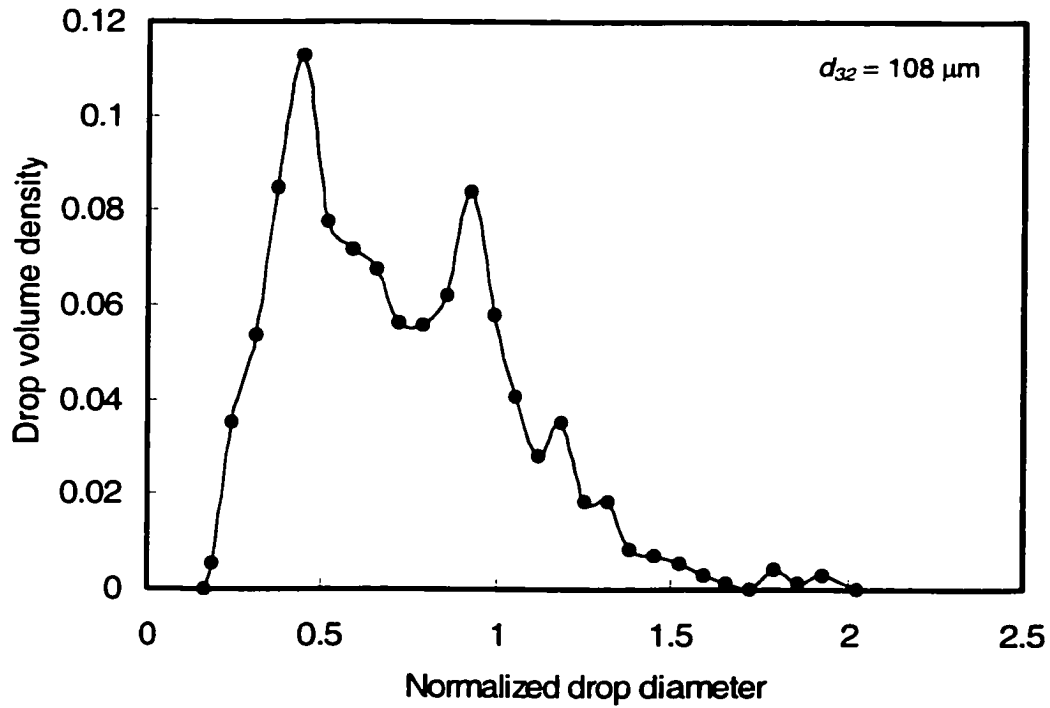


Figure A36. Drop number density distribution
 ($\alpha = 0.27$, $\phi = 0.5\%$, $U = 0.90$ m/s, 9 screens, $L = 10$ mm).

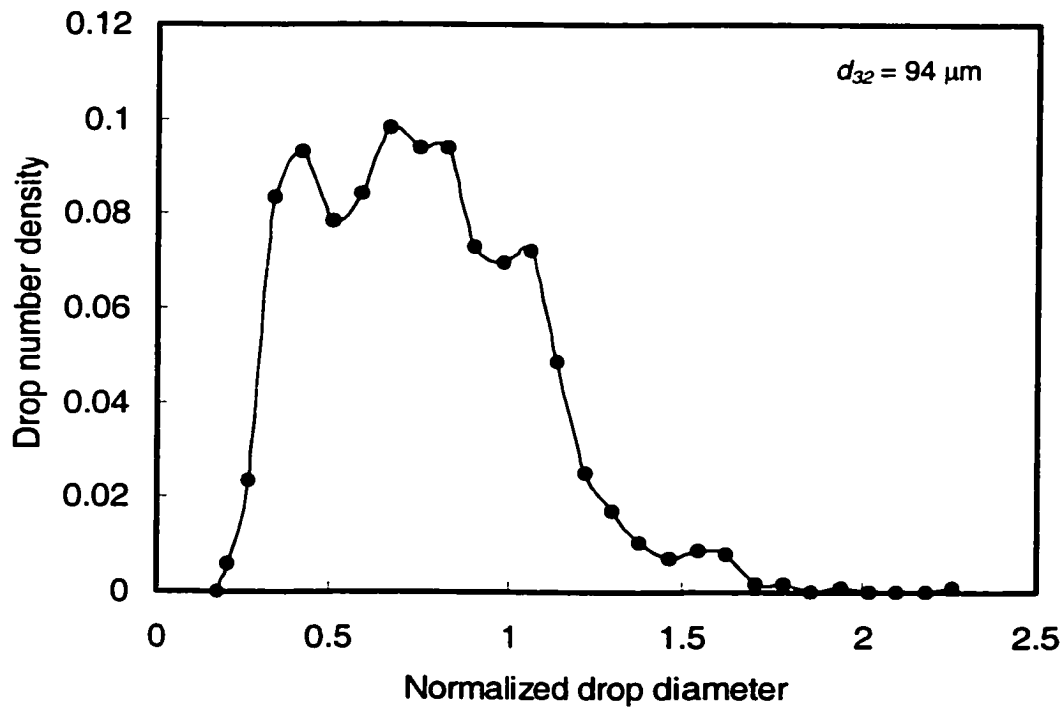


Figure A37. Drop number density distribution
 ($\alpha = 0.27$, $\phi = 0.5\%$, $U = 0.97$ m/s, 9 screens, $L = 10$ mm).

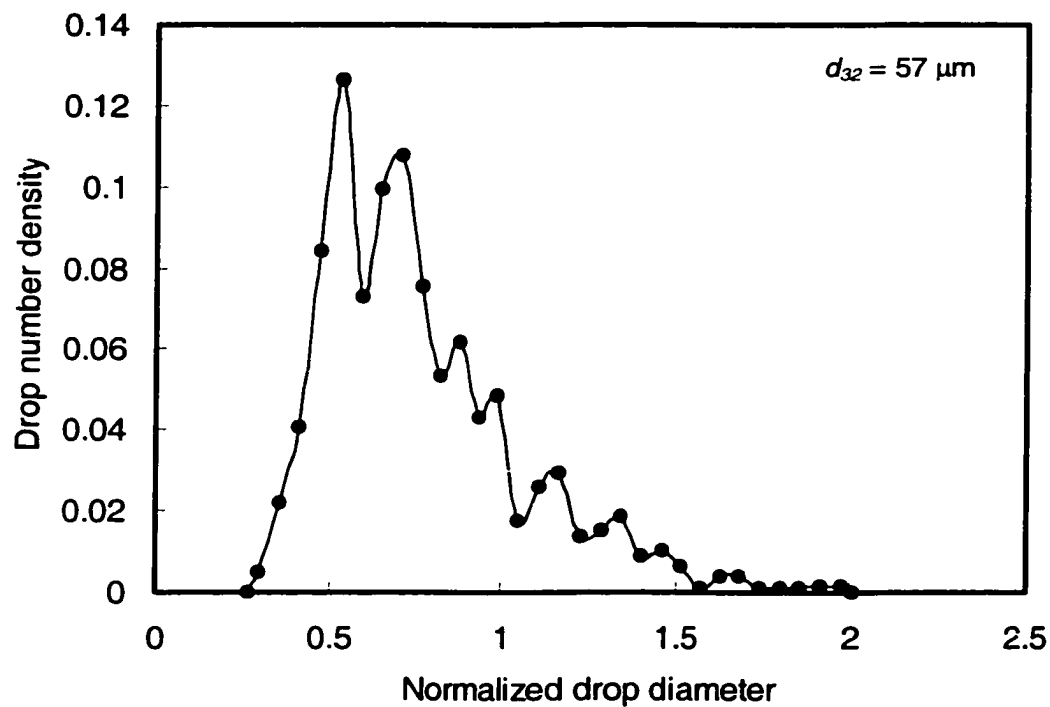


Figure A38. Drop number density distribution
 ($\alpha = 0.27$, $\phi = 0.5\%$, $U = 1.55 \text{ m/s}$, 9 screens, $L = 10\text{mm}$).

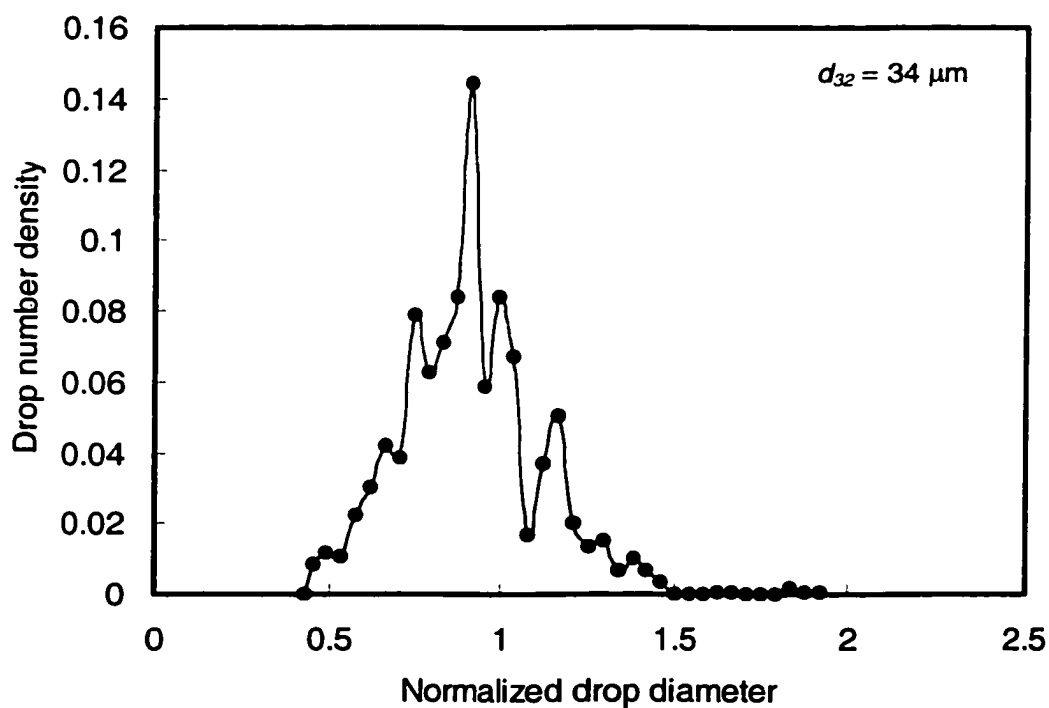


Figure A39. Drop number density distribution
 ($\alpha = 0.27$, $\phi = 0.5\%$, $U = 1.94 \text{ m/s}$, 9 screens, $L = 10\text{mm}$).

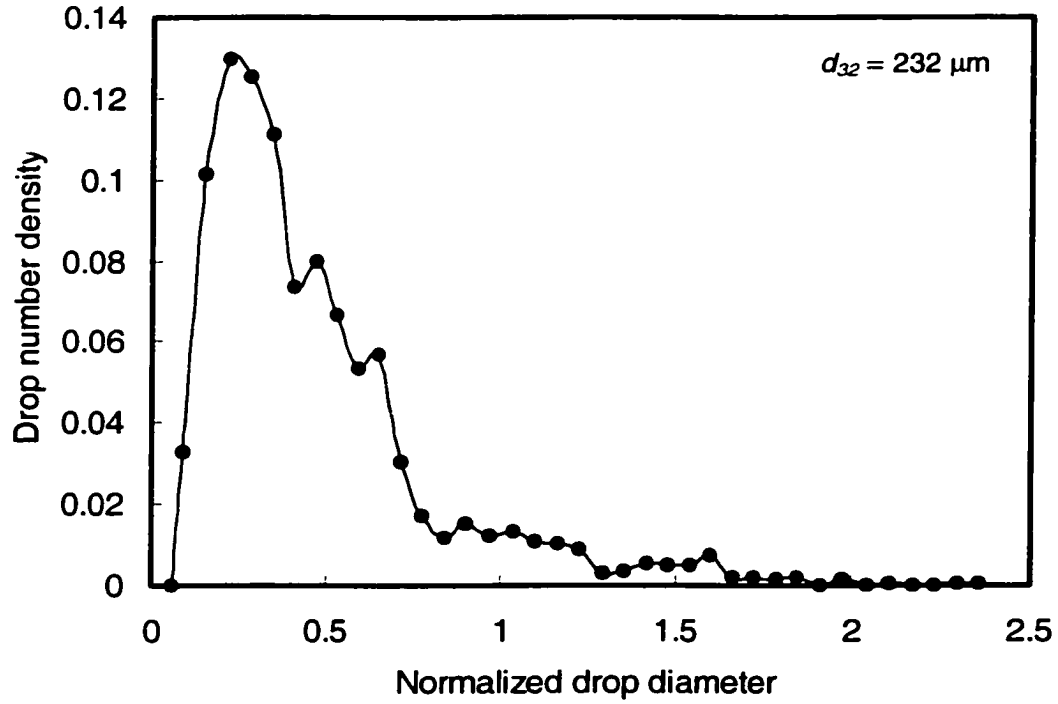


Figure A40. Drop number density distribution
 ($\alpha = 0.27$, $\phi = 4\%$, $U = 0.30 \text{ m/s}$, 9 screens, $L = 10\text{mm}$).

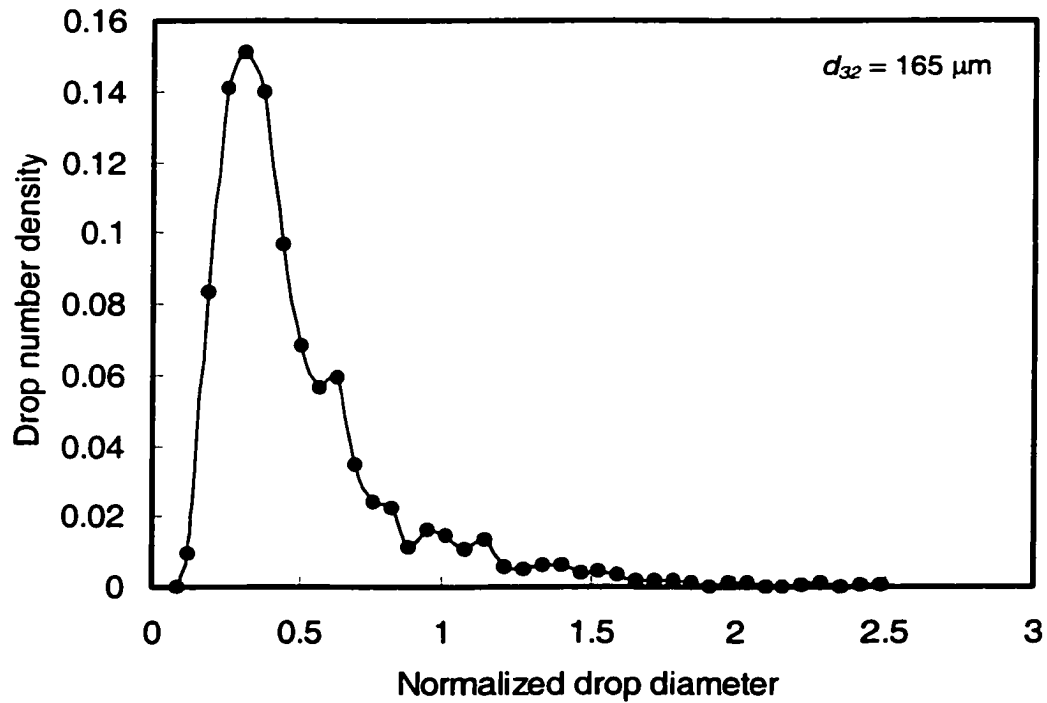


Figure A41. Drop number density distribution
 ($\alpha = 0.27$, $\phi = 4\%$, $U = 0.40 \text{ m/s}$, 9 screens, $L = 10\text{mm}$).

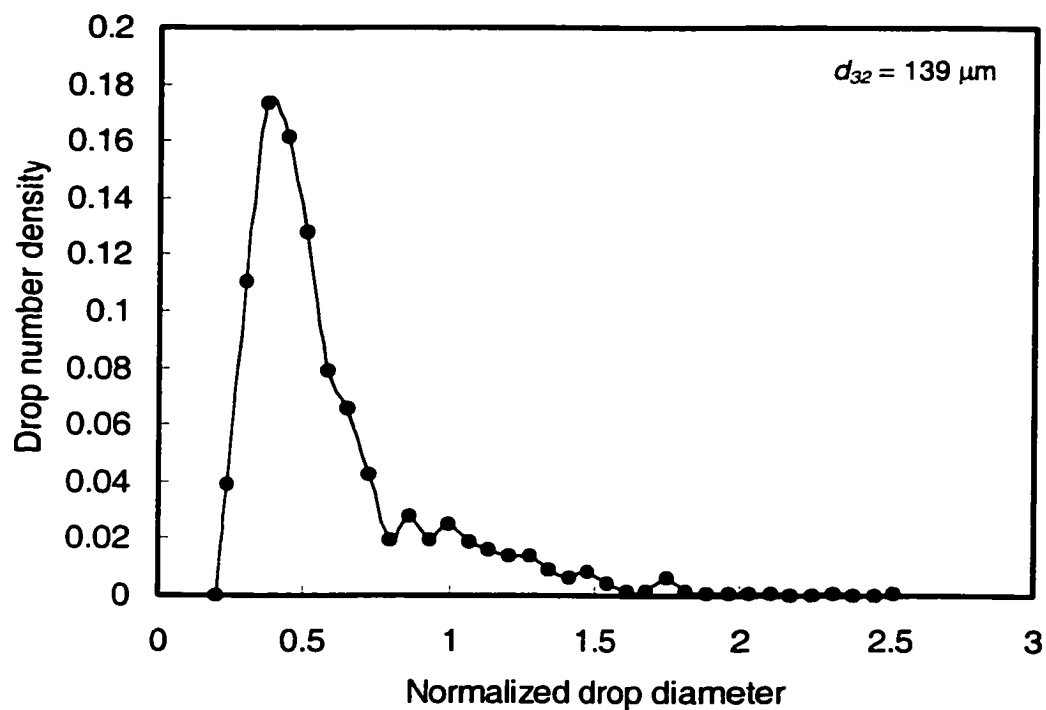


Figure A42. Drop number density distribution
 ($\alpha = 0.27$, $\phi = 4\%$, $U = 0.50$ m/s, 9 screens, $L = 10$ mm).

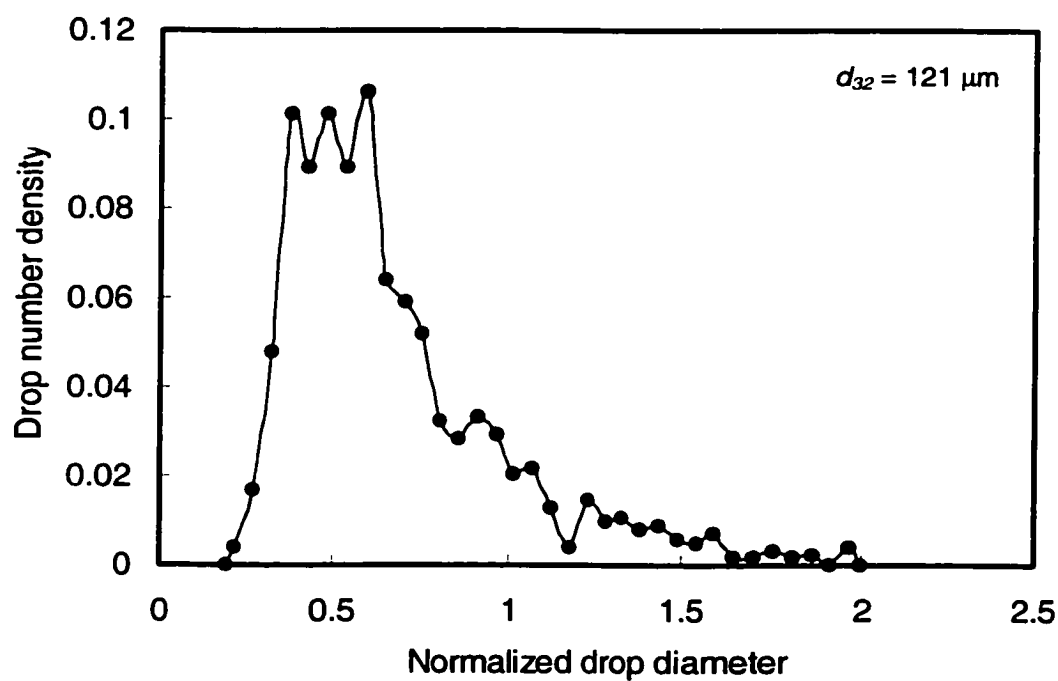


Figure A43. Drop number density distribution
 ($\alpha = 0.27$, $\phi = 4\%$, $U = 0.60$ m/s, 9 screens, $L = 10$ mm).

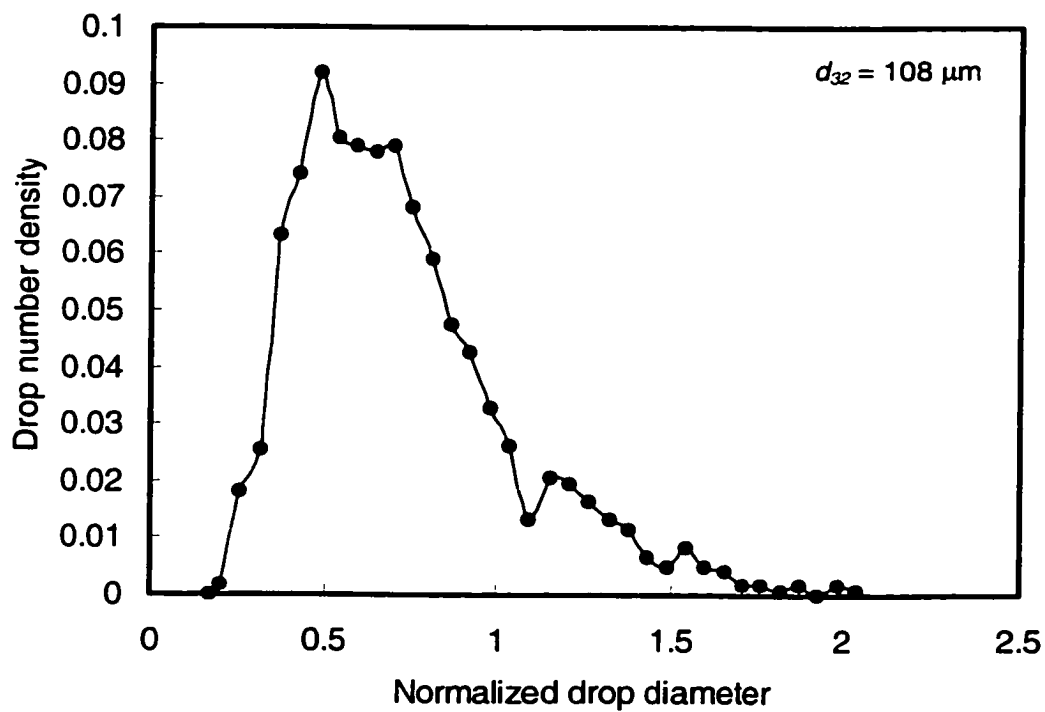


Figure A44. Drop number density distribution
 ($\alpha = 0.27$, $\phi = 4\%$, $U = 0.65 \text{ m/s}$, 9 screens, $L = 10\text{mm}$).

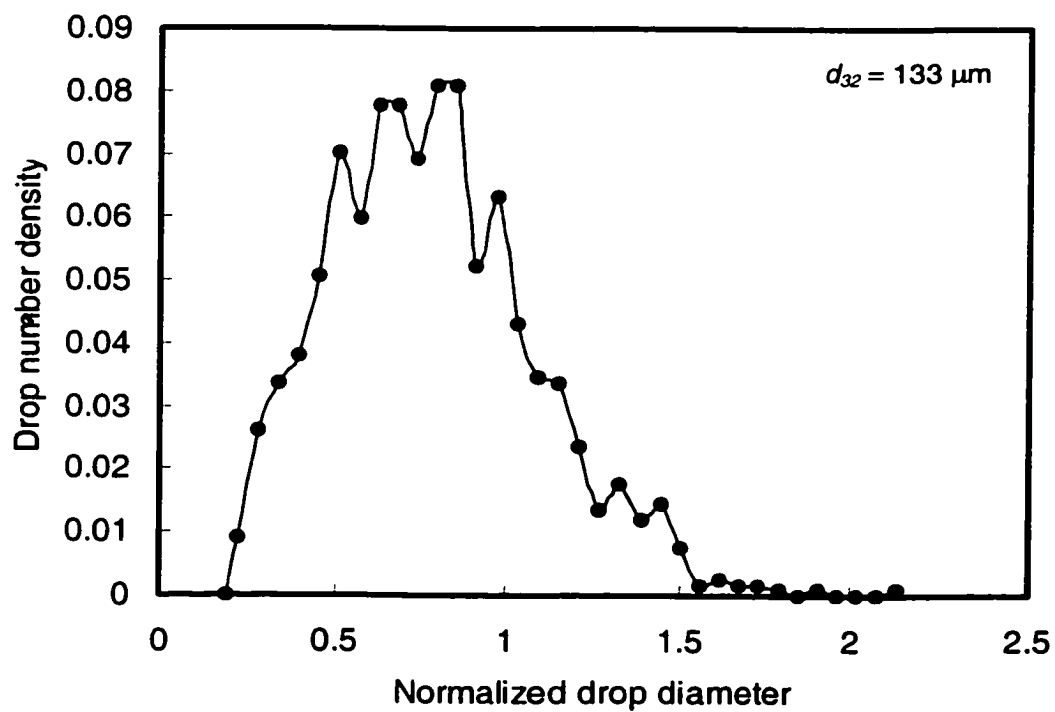


Figure A45. Drop number density distribution
 ($\alpha = 0.27$, $\phi = 4\%$, $U = 0.70 \text{ m/s}$, 9 screens, $L = 10\text{mm}$).

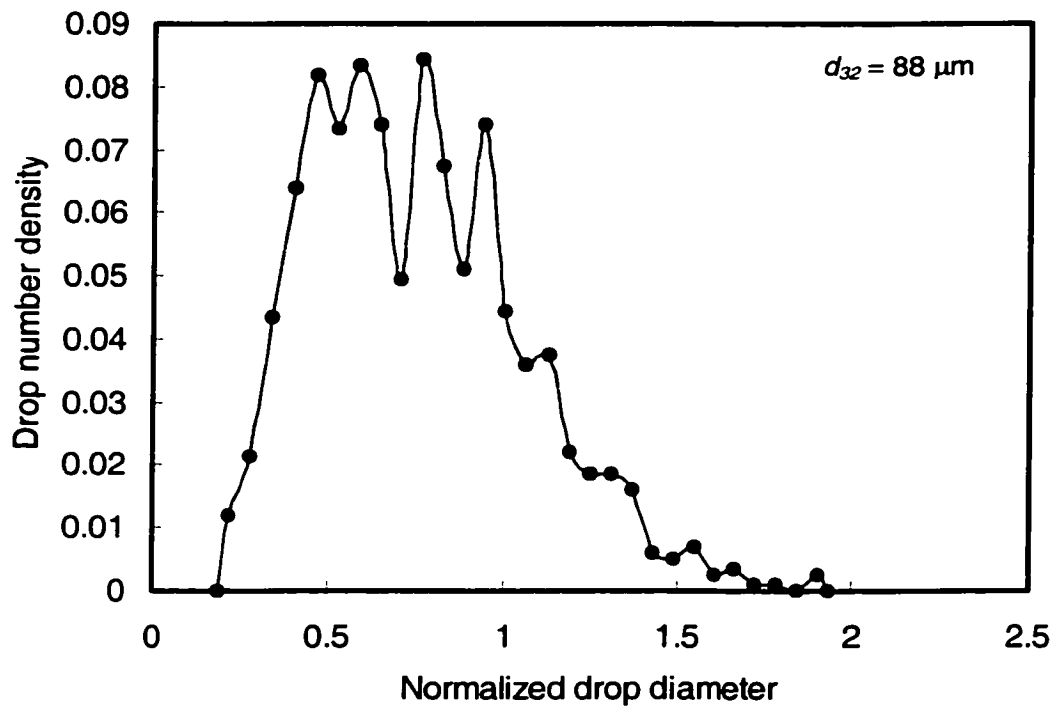


Figure A46. Drop number density distribution
 ($\alpha = 0.27$, $\phi = 4\%$, $U = 0.97 \text{ m/s}$, 9 screens, $L = 10\text{mm}$).

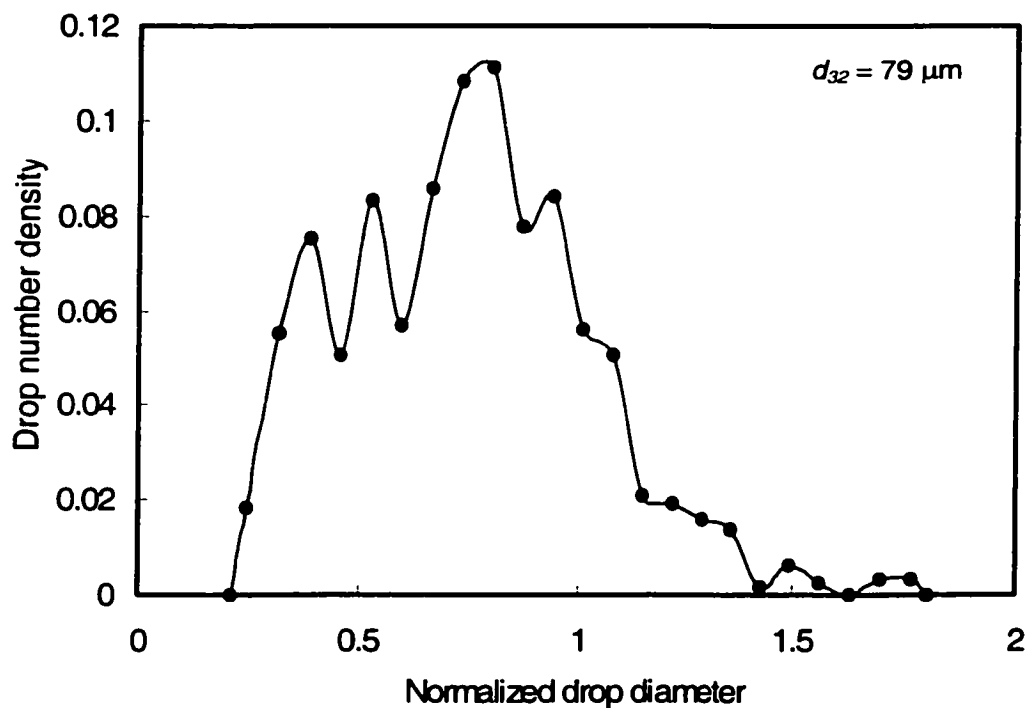


Figure A47. Drop number density distribution
 ($\alpha = 0.27$, $\phi = 4\%$, $U = 1.55 \text{ m/s}$, 9 screens, $L = 10\text{mm}$).

Effect of dispersed phase volume fraction (Holdup)

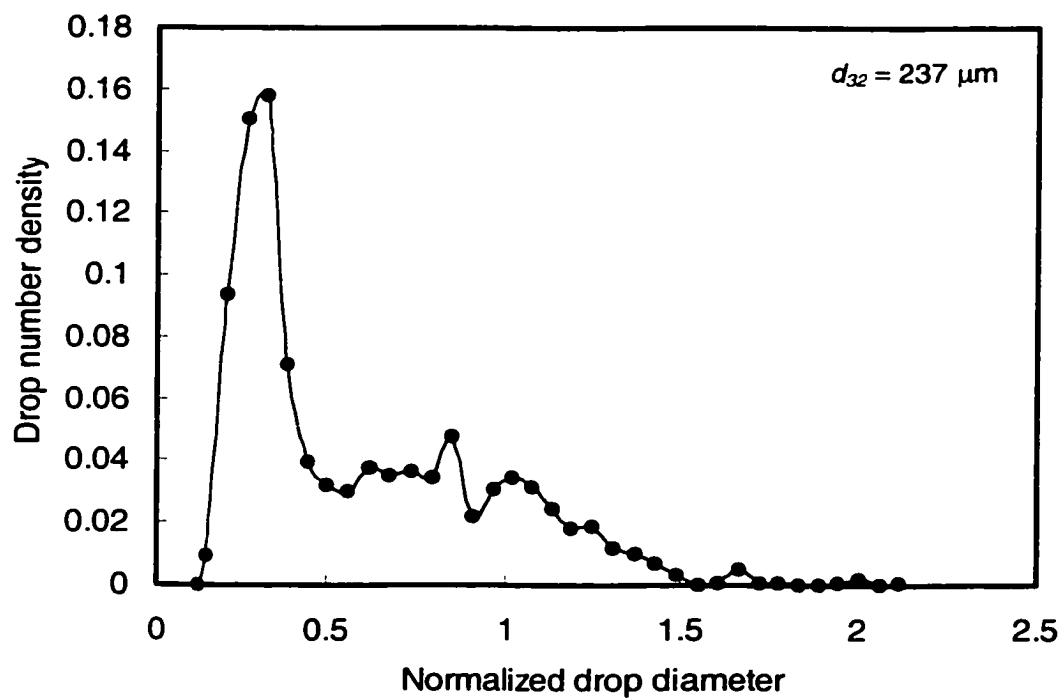


Figure A48. Drop number density distribution
($\alpha = 0.41$, $\phi = 1\%$, $U = 0.40$ m/s, 9 screens, $L = 10$ mm).

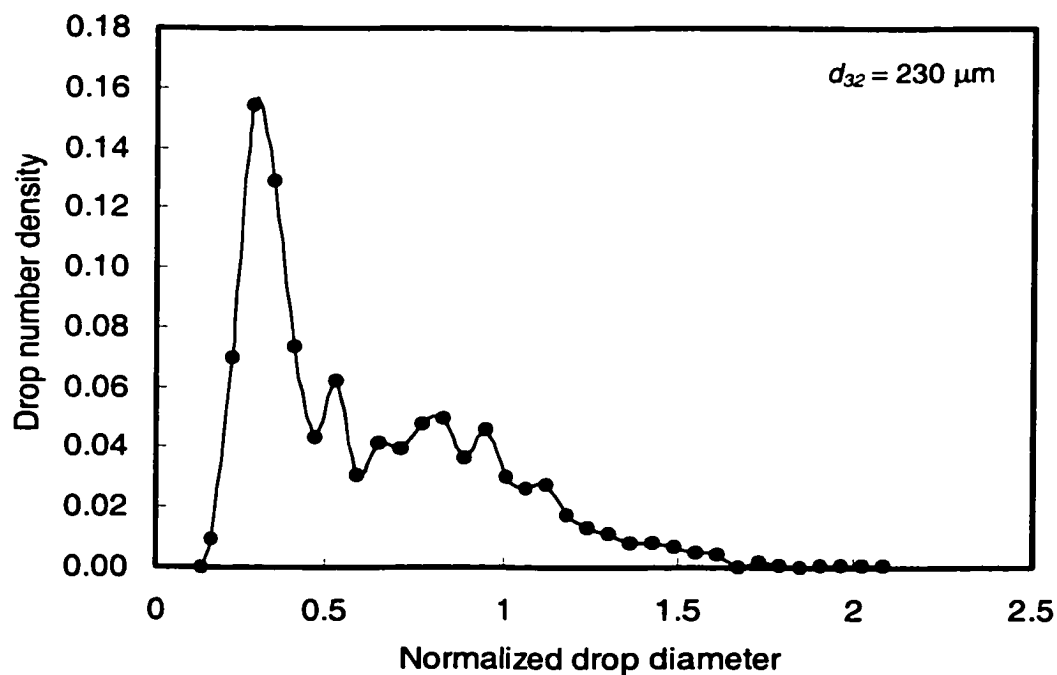


Figure A49. Drop number density distribution
($\alpha = 0.41$, $\phi = 2\%$, $U = 0.40$ m/s, 9 screens, $L = 10$ mm).

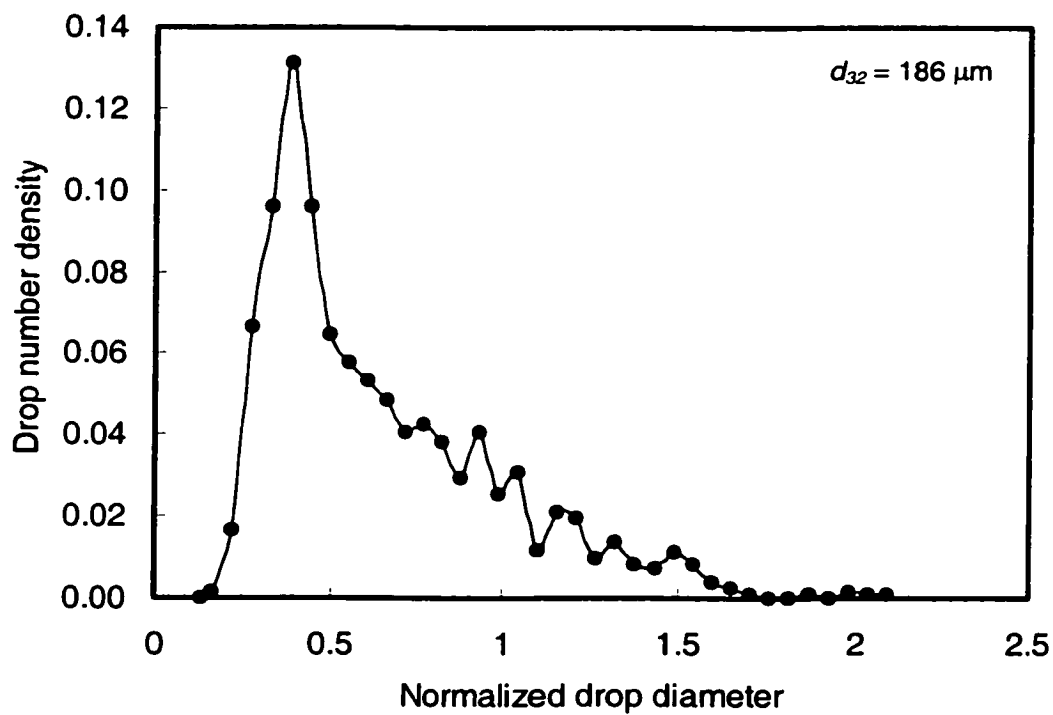


Figure A50. Drop number density distribution
 ($\alpha = 0.41$, $\phi = 3\%$, $U = 0.40$ m/s, 9 screens, $L = 10$ mm).

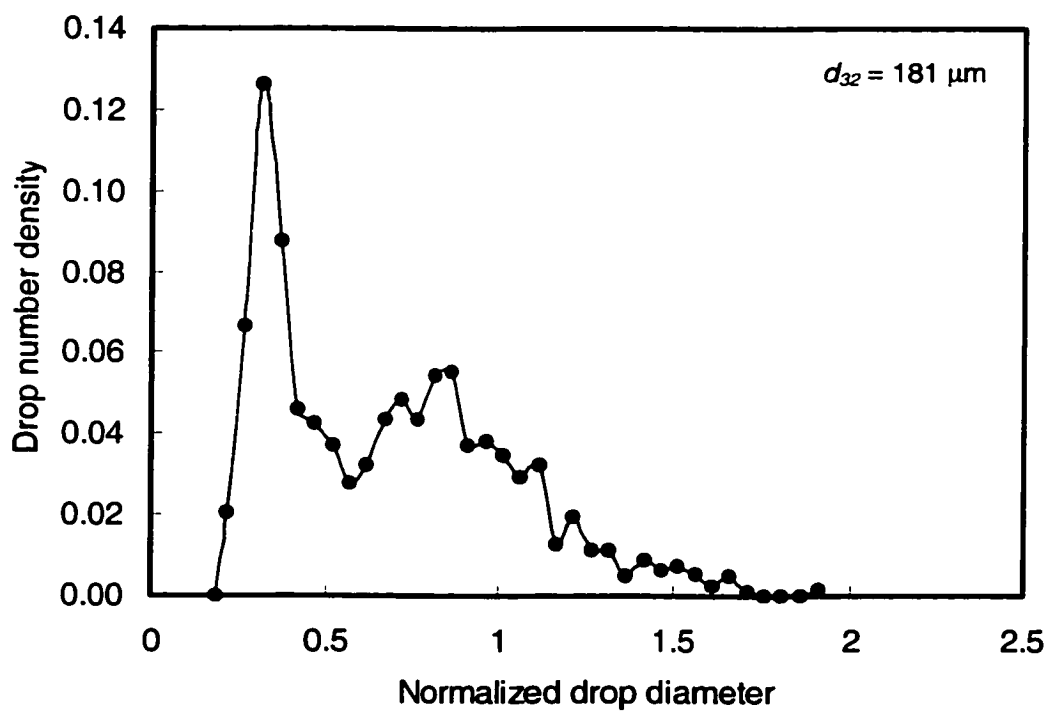


Figure A51. Drop number density distribution
 ($\alpha = 0.41$, $\phi = 1\%$, $U = 0.70$ m/s, 9 screens, $L = 10$ mm).

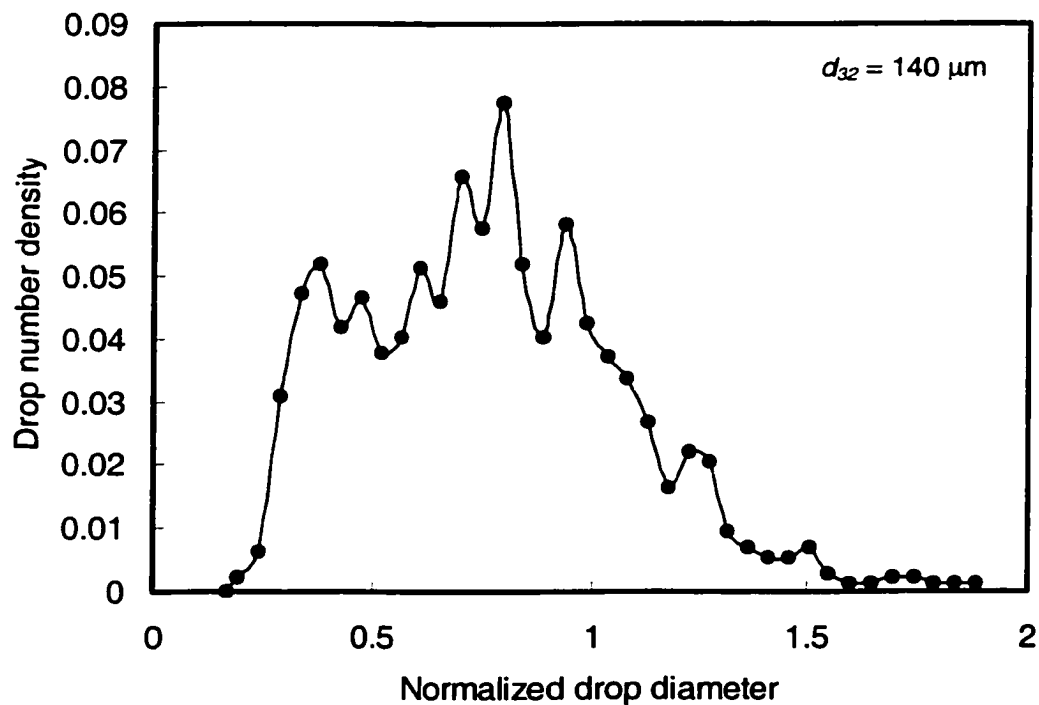


Figure A52. Drop number density distribution
 ($\alpha = 0.41$, $\phi = 2\%$, $U = 0.70$ m/s, 9 screens, $L = 10$ mm).

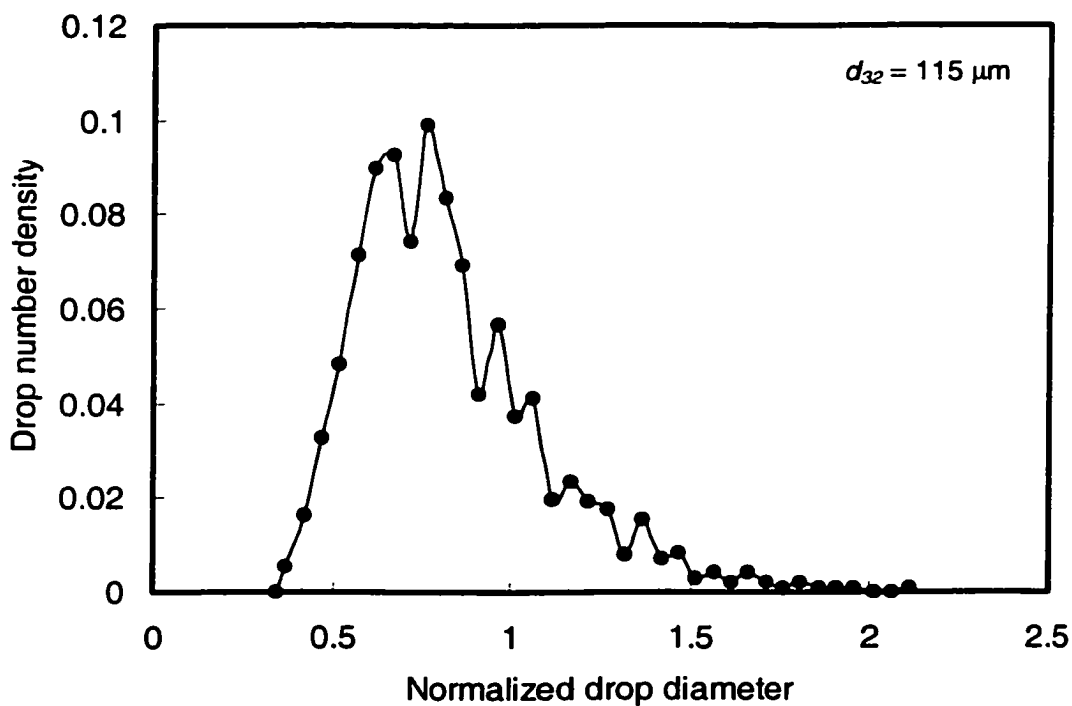


Figure A53. Drop number density distribution
 ($\alpha = 0.41$, $\phi = 3\%$, $U = 0.70$ m/s, 9 screens, $L = 10$ mm).

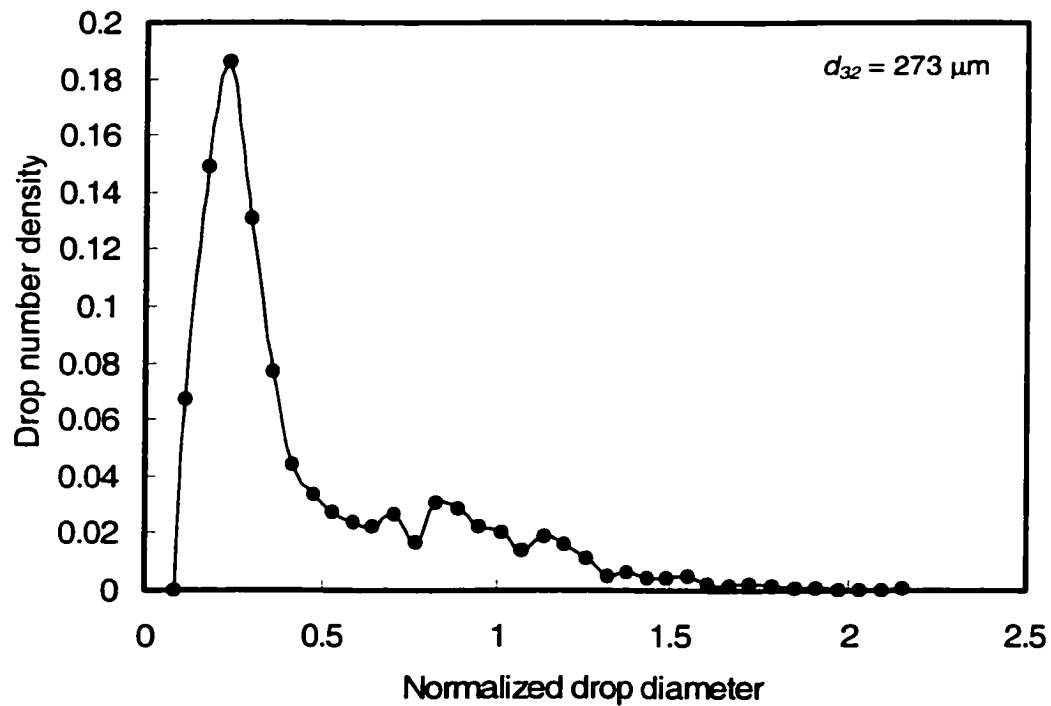


Figure A54. Drop number density distribution
 ($\alpha = 0.27$, $\phi = 1\%$, $U = 0.40$ m/s, 9 screens, $L = 10$ mm).

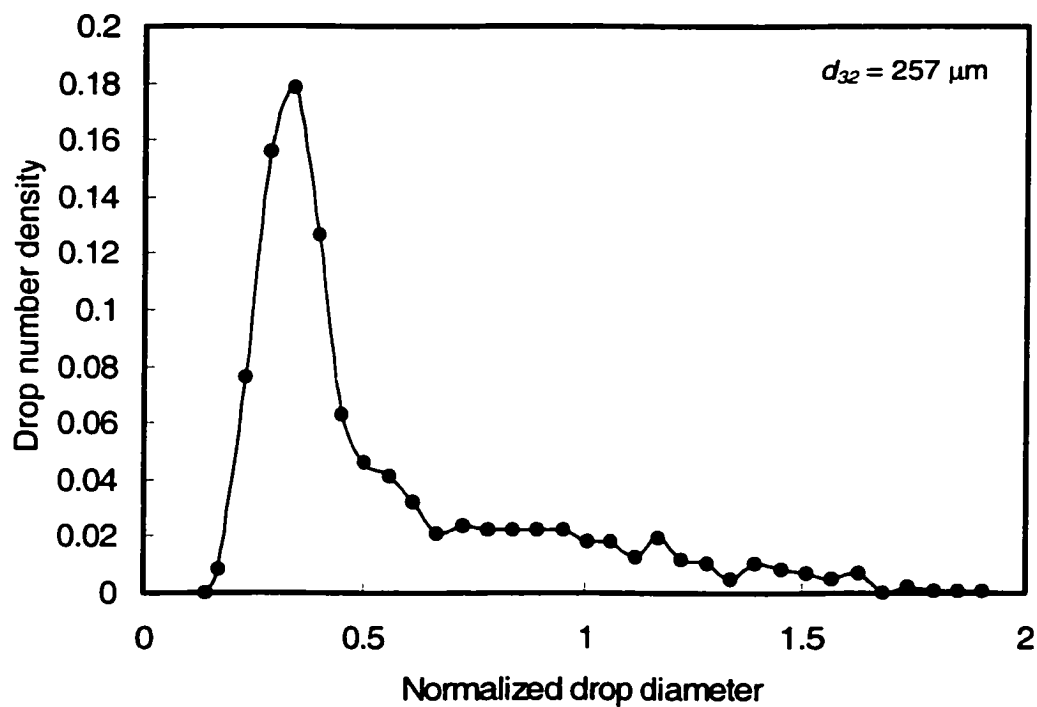


Figure A55. Drop number density distribution
 ($\alpha = 0.27$, $\phi = 2\%$, $U = 0.40$ m/s, 9 screens, $L = 10$ mm).

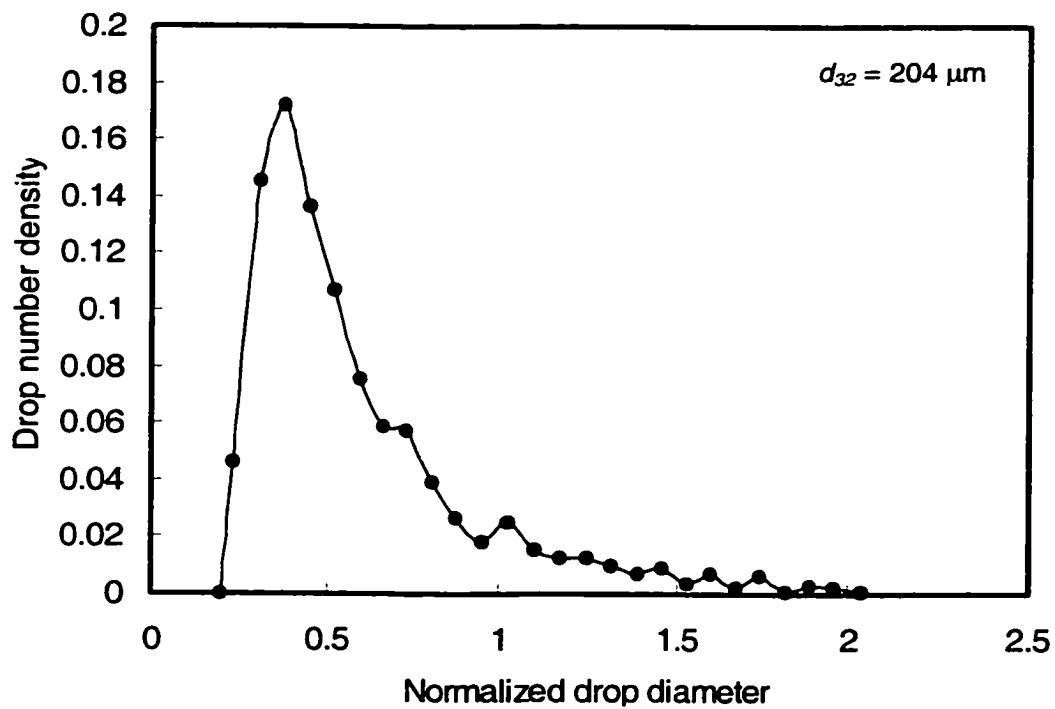


Figure A56. Drop number density distribution
 ($\alpha = 0.27$, $\phi = 3\%$, $U = 0.40$ m/s, 9 screens, $L = 10$ mm).

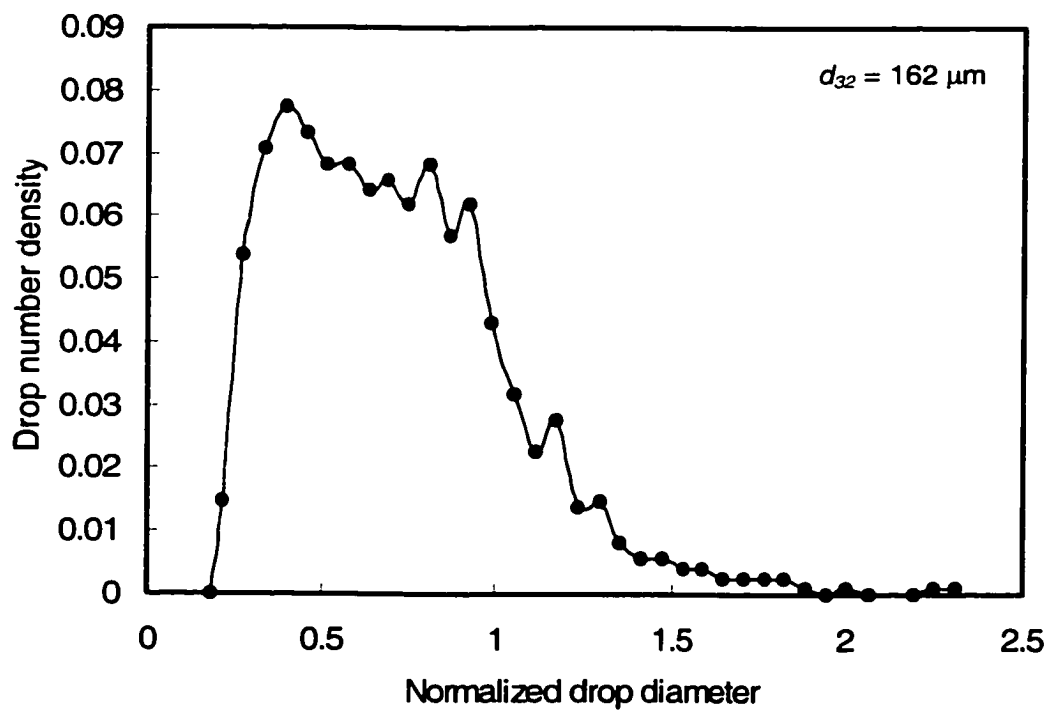


Figure A57. Drop number density distribution
 ($\alpha = 0.27$, $\phi = 1\%$, $U = 0.70$ m/s, 9 screens, $L = 10$ mm).

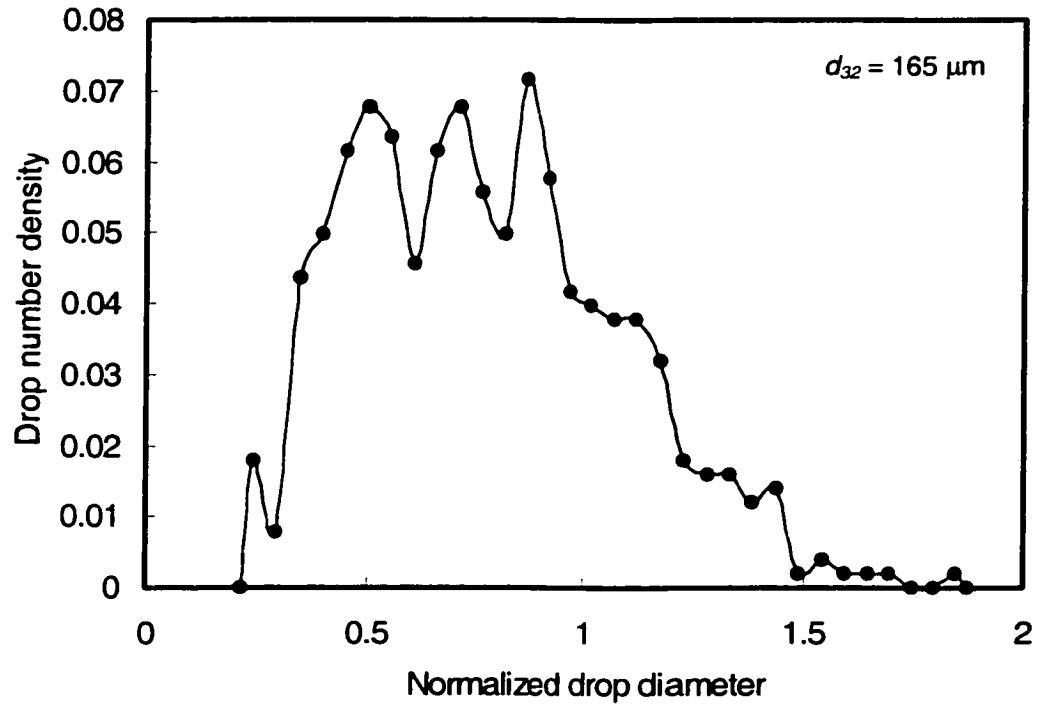


Figure A58. Drop number density distribution
 ($\alpha = 0.27$, $\phi = 2\%$, $U = 0.70$ m/s, 9 screens, $L = 10$ mm).

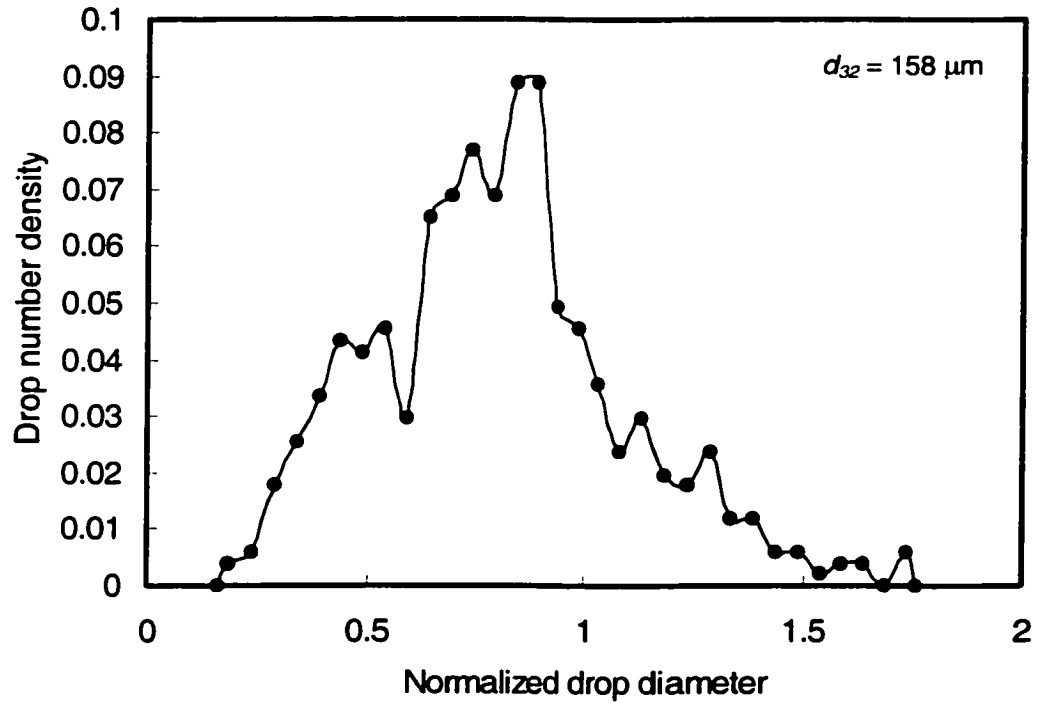


Figure A59. Drop number density distribution
 ($\alpha = 0.27$, $\phi = 3\%$, $U = 0.70$ m/s, 9 screens, $L = 10$ mm).

Effect of number of elements

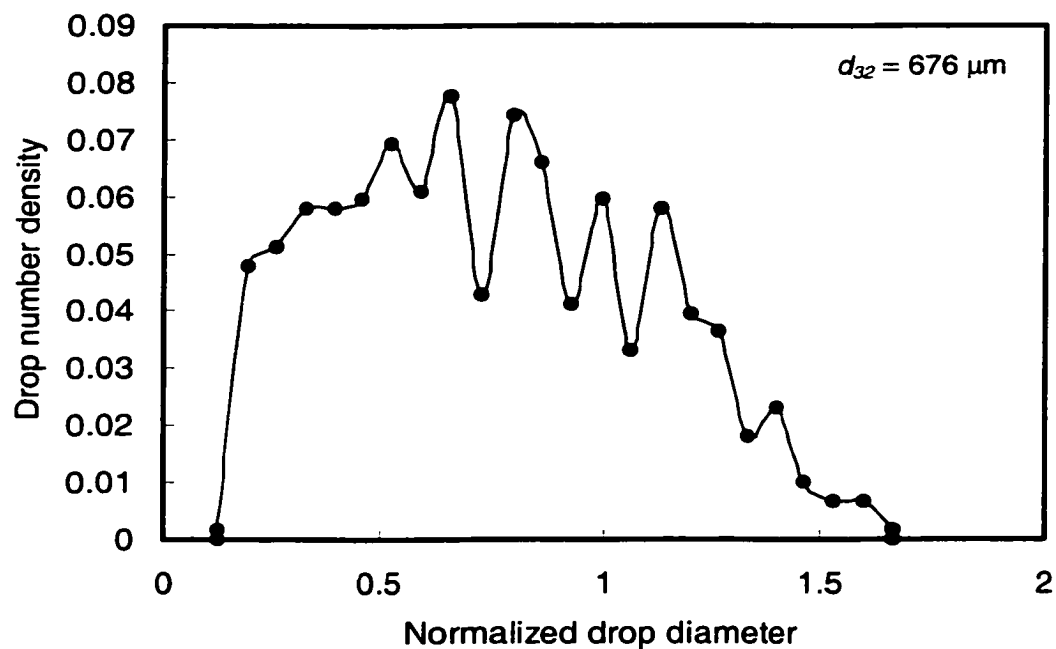


Figure A60. Drop number density distribution
 ($\alpha = 0.27$, $\phi = 2\%$, $U = 0.40$ m/s, 2 elements, $L = 5$ mm).

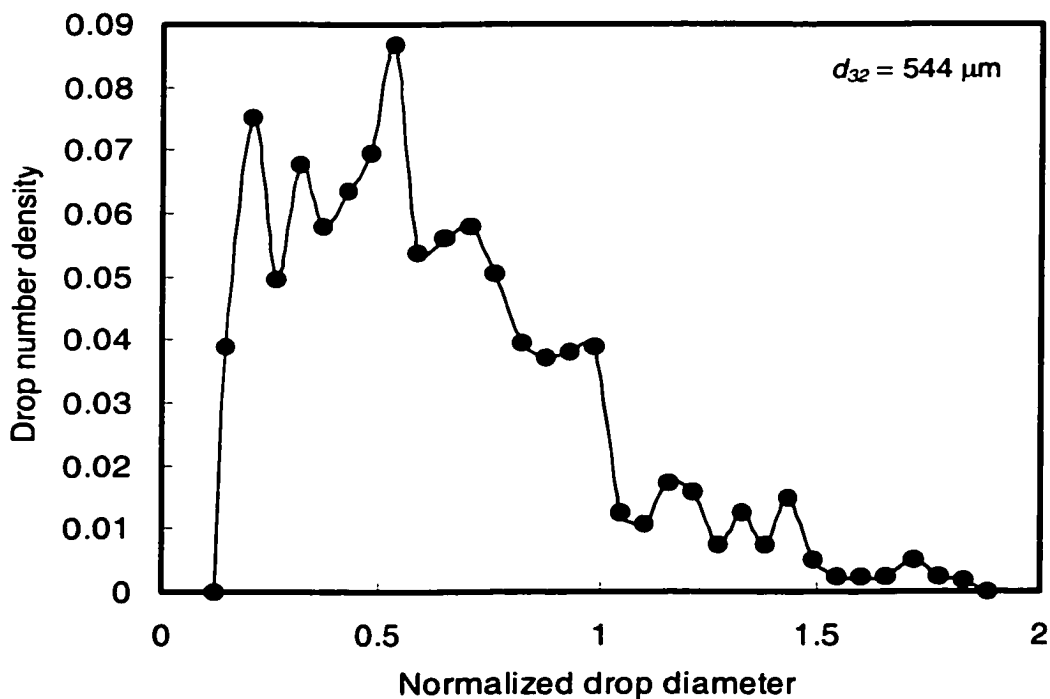


Figure A61. Drop number density distribution
 ($\alpha = 0.27$, $\phi = 2\%$, $U = 0.40$ m/s, 3 elements, $L = 0.5$ cm).

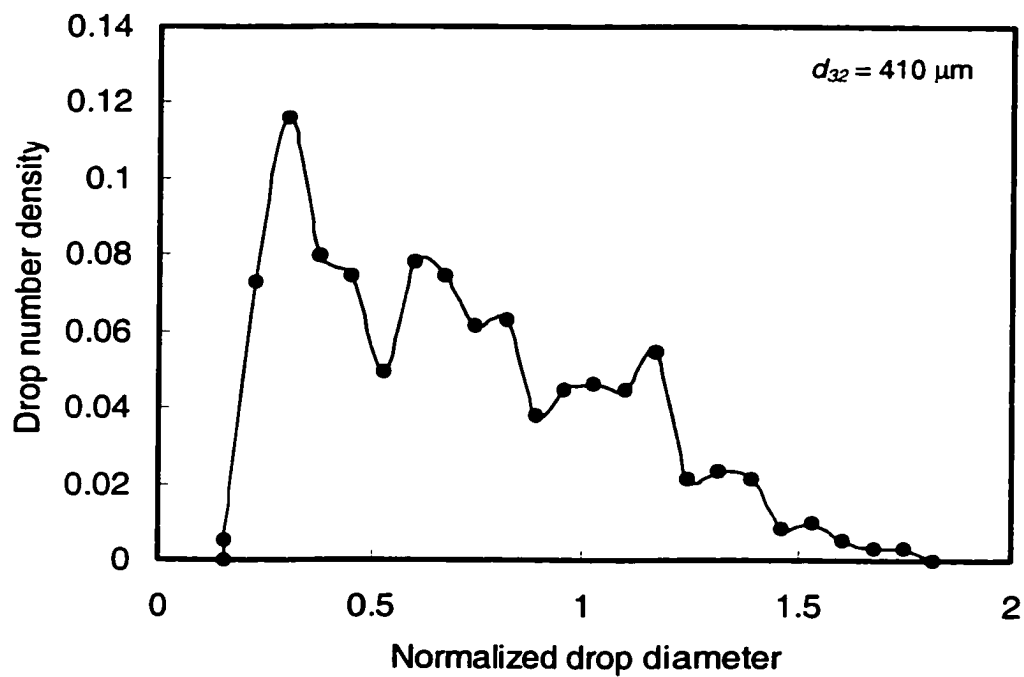


Figure A62. Drop number density distribution
 ($\alpha = 0.27$, $\phi = 2\%$, $U = 0.40$ m/s, 4 elements, $L = 5$ mm).

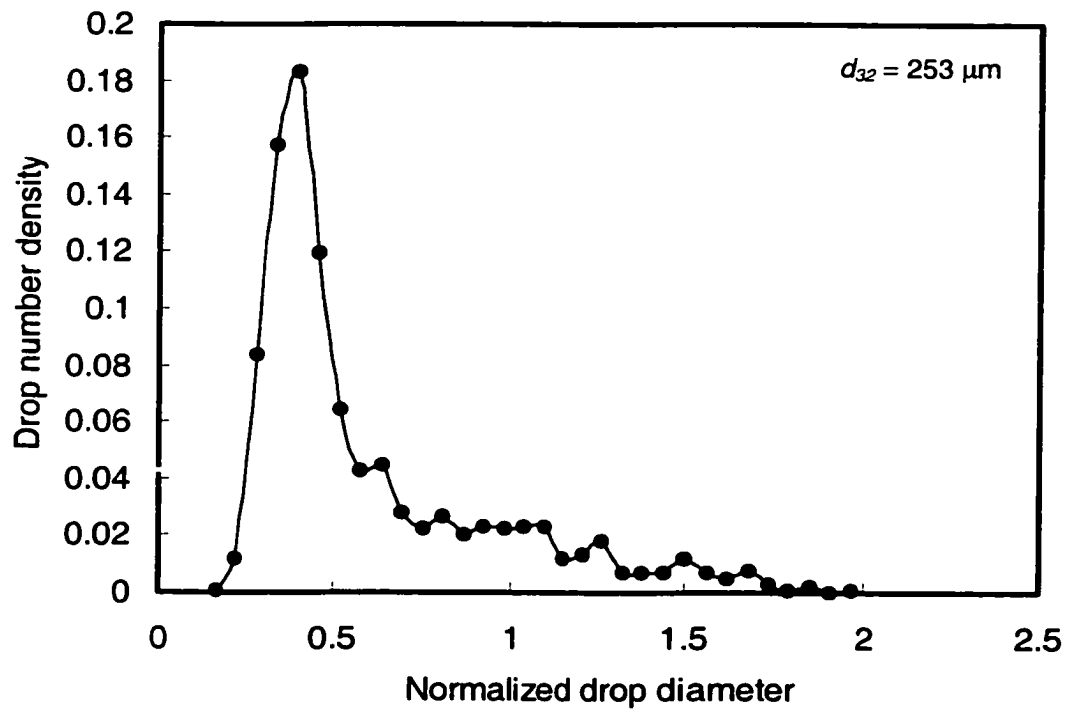


Figure A63. Drop number density distribution
 ($\alpha = 0.27$, $\phi = 2\%$, $U = 0.40$ m/s, 9 screens, $L = 5$ mm).

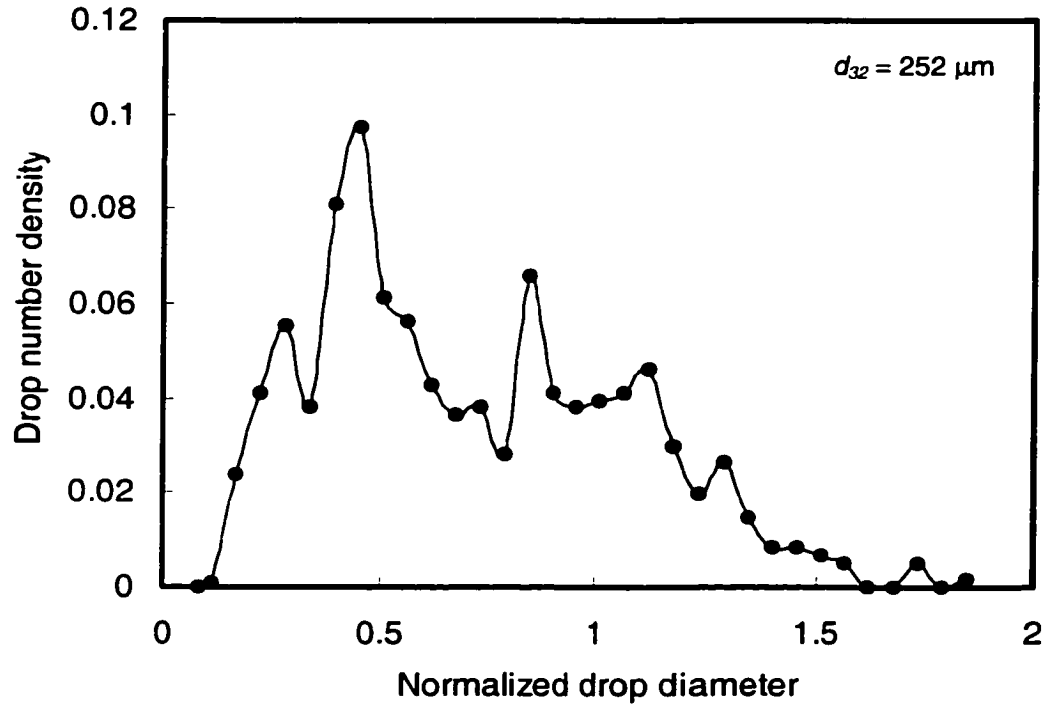


Figure A64. Drop number density distribution
 ($\alpha = 0.27$, $\phi = 2\%$, $U = 0.40$ m/s, 12 screens, $L = 5$ mm).

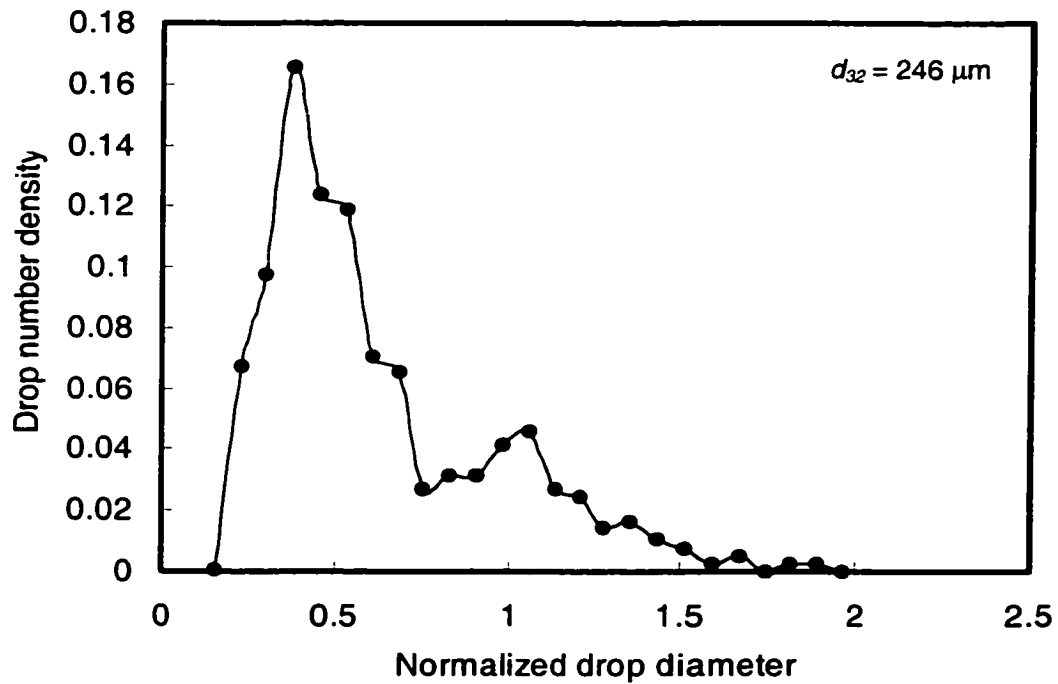


Figure A65. Drop number density distribution
 ($\alpha = 0.27$, $\phi = 2\%$, $U = 0.40$ m/s, 15 screens, $L = 5$ mm).

Effect of the surfactant Triton X100

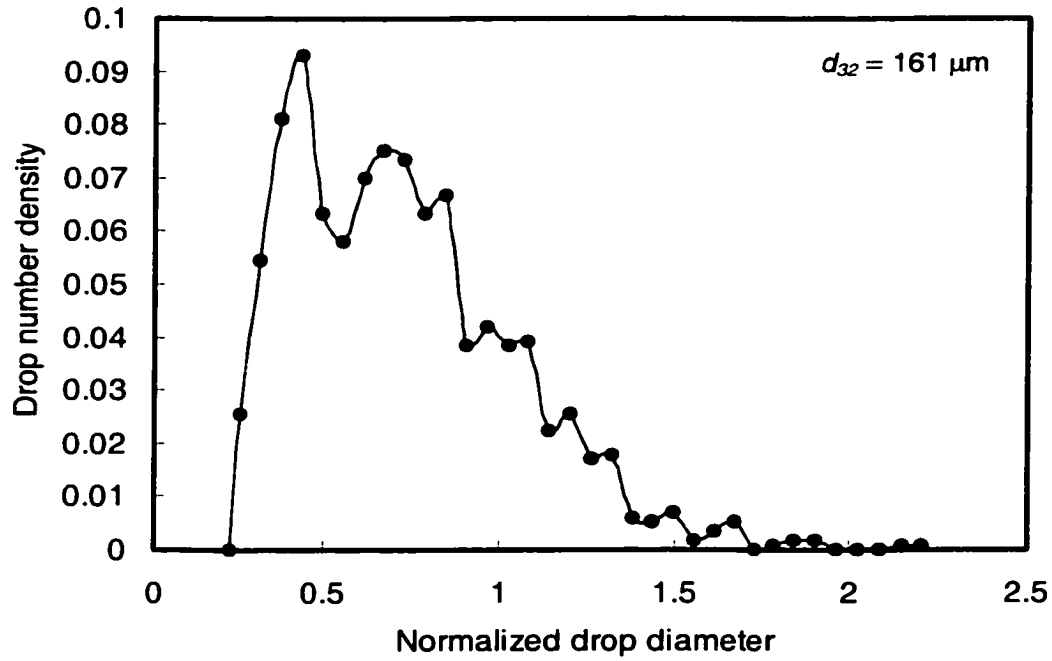


Figure A66. Drop number density distribution with SAA ($\alpha = 0.27$, $\phi = 0.5\%$, $U = 0.70 \text{ m/s}$, $c = 0.01 \text{ mole/m}^3$, 9 screens, $L = 10\text{mm}$).

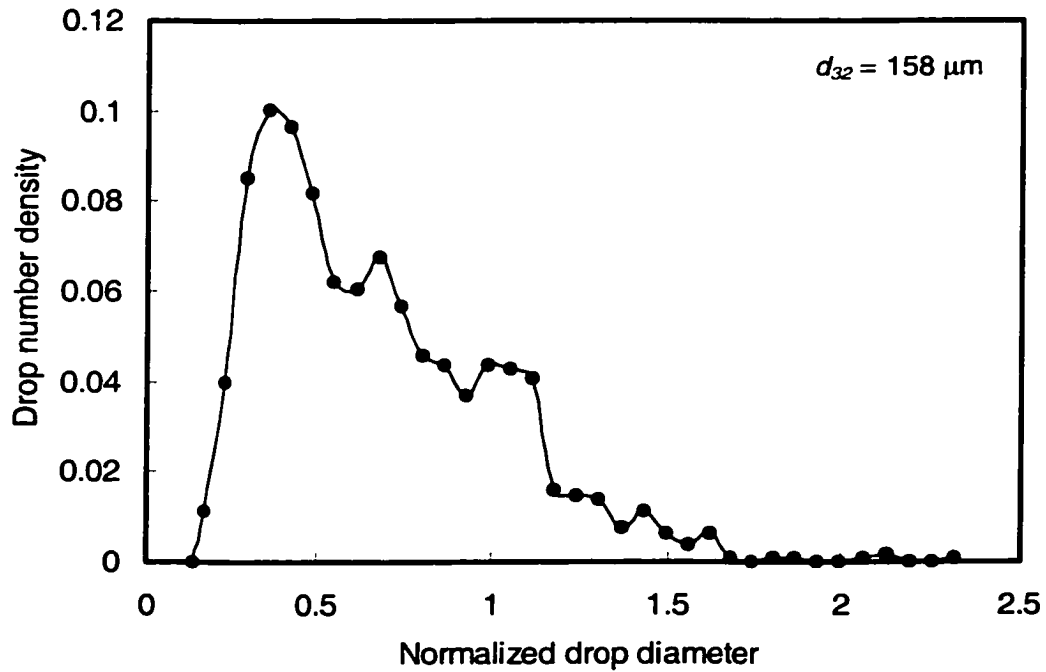


Figure A67. Drop number density distribution with SAA ($\alpha = 0.27$, $\phi = 0.5\%$, $U = 0.70 \text{ m/s}$, $c = 0.05 \text{ mole/m}^3$, 9 screens, $L = 10\text{mm}$).

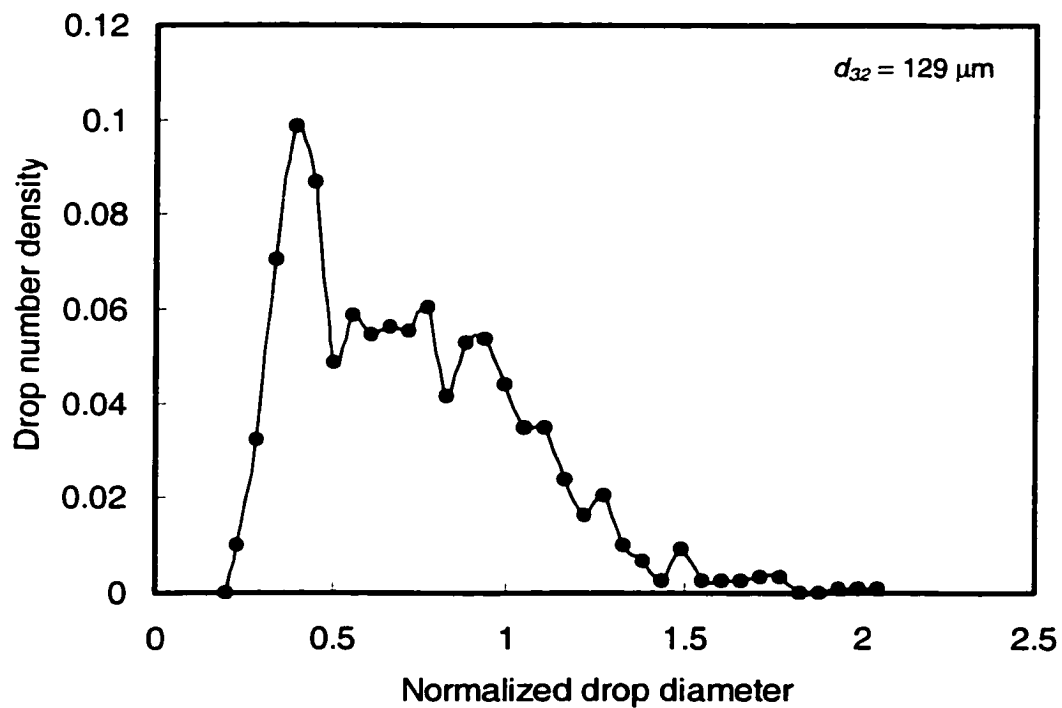


Figure A68. Drop number density distribution with SAA ($\alpha = 0.27$, $\phi = 0.5\%$, $U = 0.70$ m/s, $c = 0.10$ mole/ m^3 , 9 screens, $L = 10$ mm).

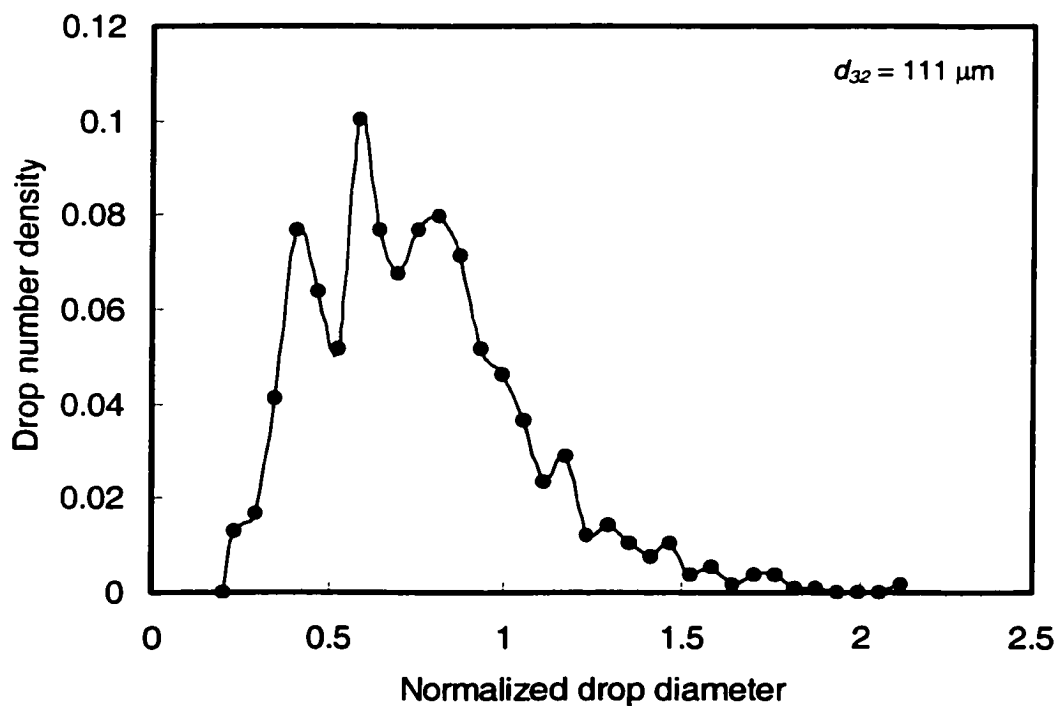


Figure A69. Drop number density distribution with SAA ($\alpha = 0.27$, $\phi = 0.5\%$, $U = 0.70$ m/s, $c = 0.20$ mole/ m^3 , 9 screens, $L = 10$ mm).

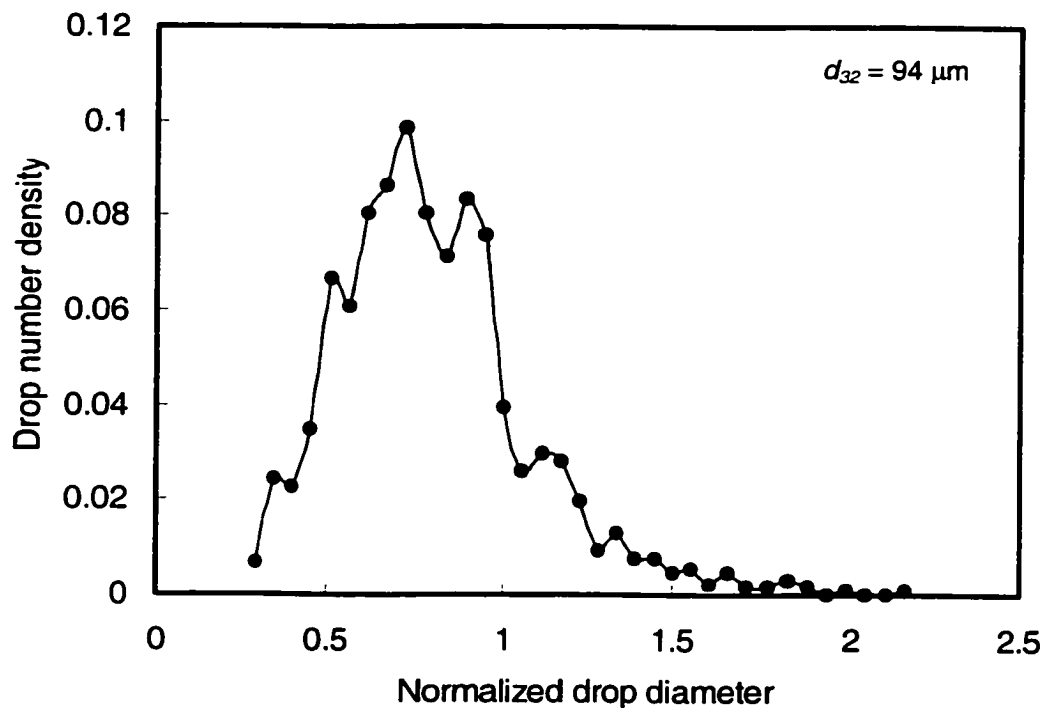


Figure A70. Drop number density distribution with SAA
 ($\alpha = 0.27$, $\phi = 0.5\%$, $U = 0.70$ m/s, $c = 0.30$ mole/m³, 9 screens, 10 mm).

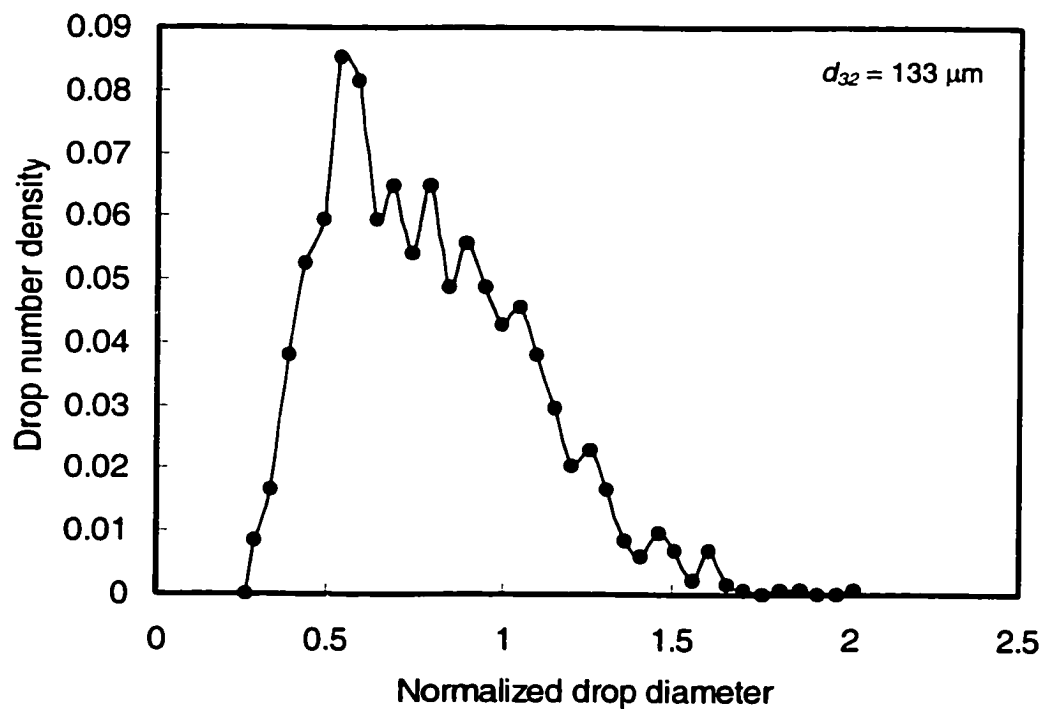


Figure A71. Drop number density distribution with SAA
 ($\alpha = 0.27$, $\phi = 4\%$, $U = 0.70$ m/s, $c = 0.01$ mole/m³, 9 screens, $L = 10$ mm).

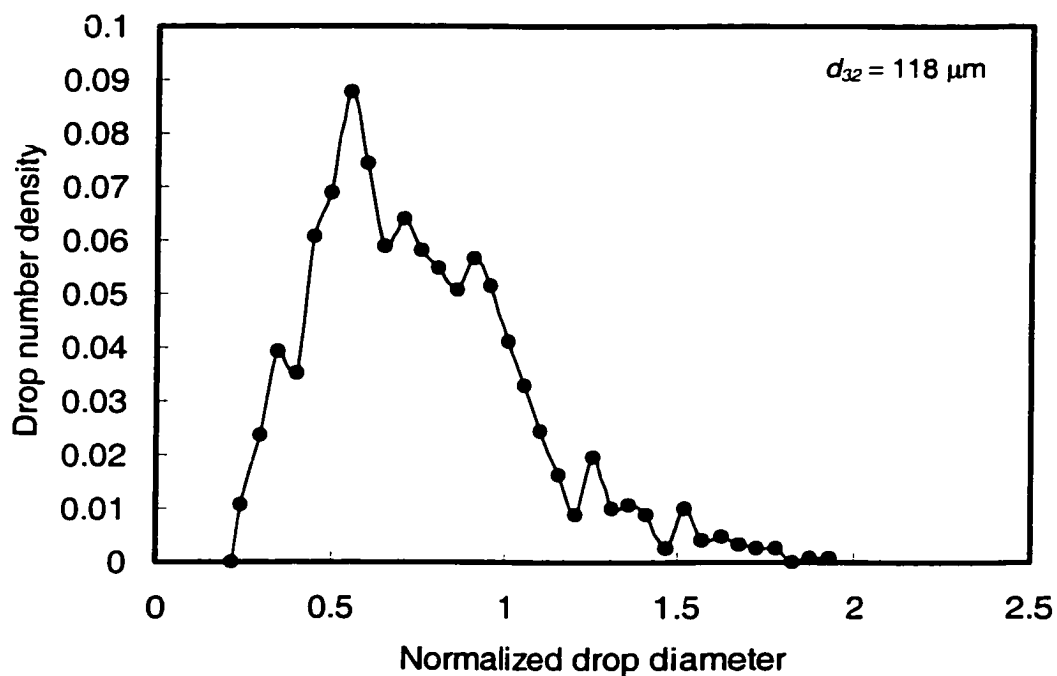


Figure A72. Drop number density distribution with SAA ($\alpha = 0.27$, $\phi = 4\%$, $U = 0.70$ m/s, $c = 0.05$ mole/m³, 9 screens, $L = 10$ mm).

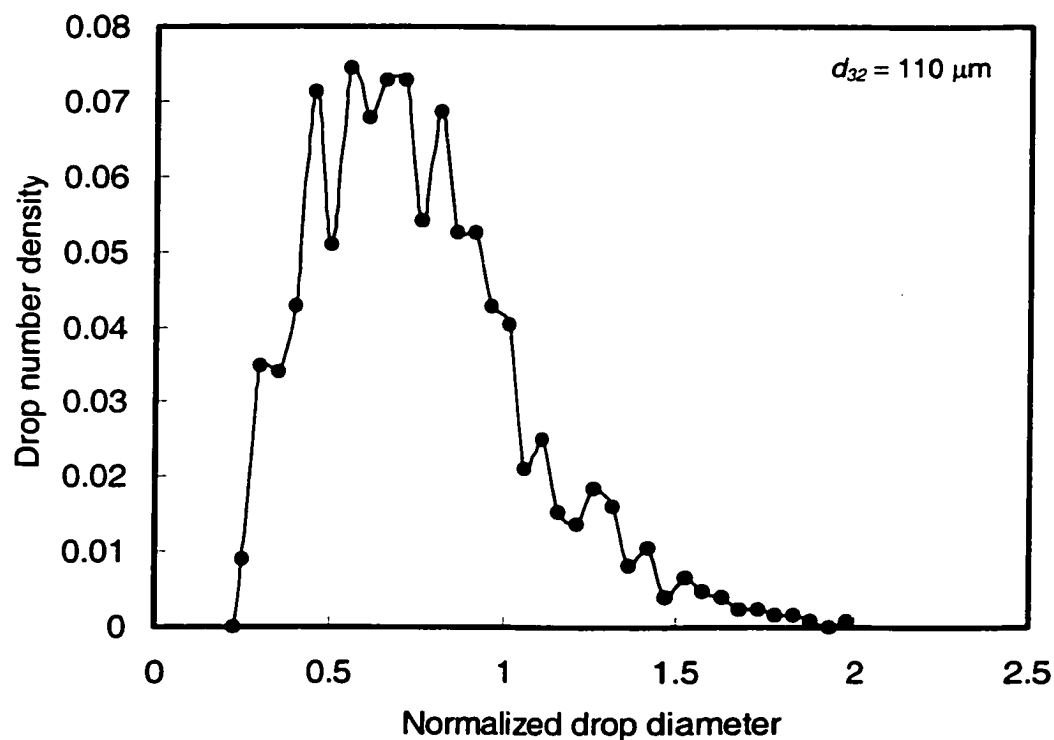


Figure A73. Drop number density distribution with SAA ($\alpha = 0.27$, $\phi = 4\%$, $U = 0.70$ m/s, $c = 0.10$ mole/m³, 9 screens, $L = 10$ mm).

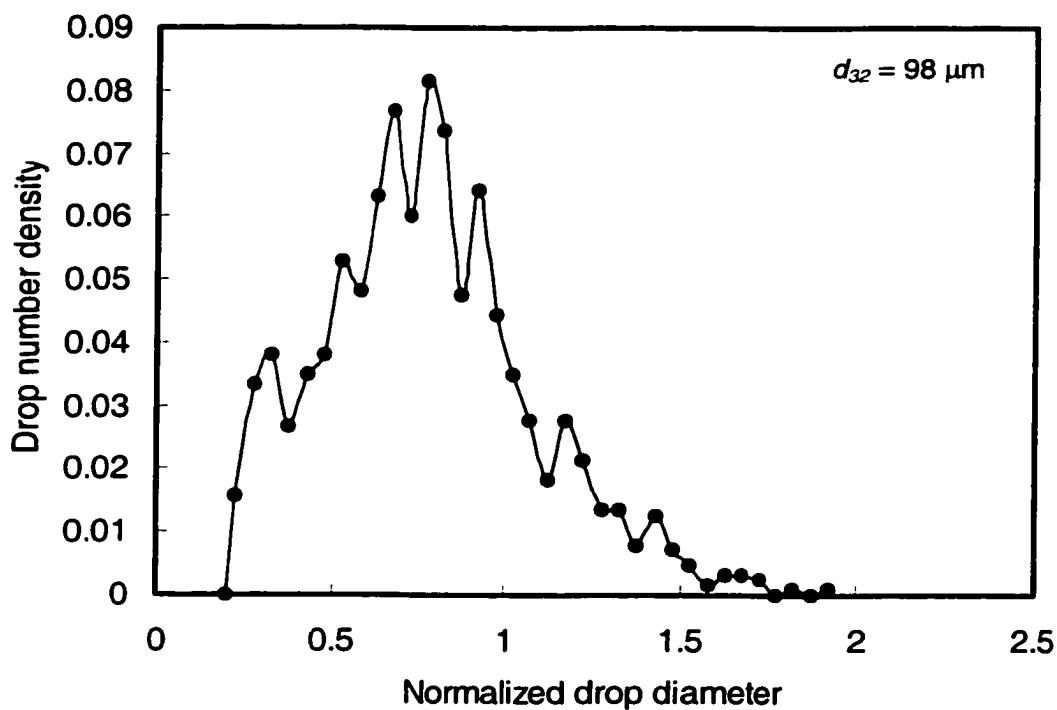


Figure A74. Drop number density distribution with SAA
 ($\alpha = 0.27$, $\phi = 4\%$, $U = 0.70$ m/s, $c = 0.20$ mole/m³, 9 screens, $L = 10$ mm).

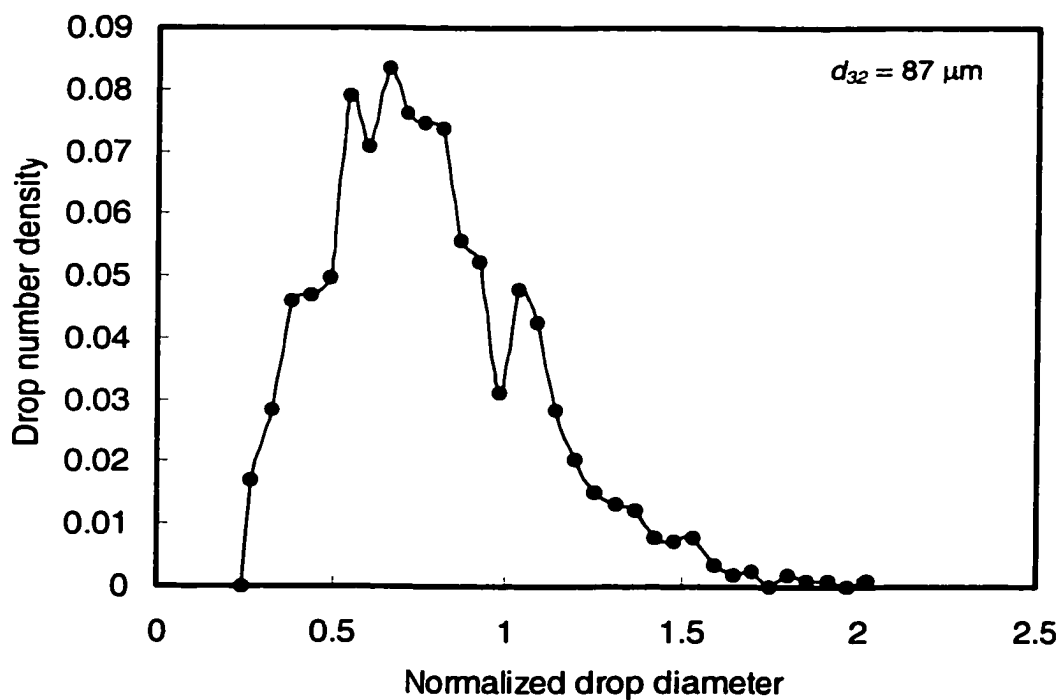


Figure A75. Drop number density distribution with SAA
 ($\alpha = 0.27$, $\phi = 4\%$, $U = 0.70$ m/s, $c = 0.30$ mole/m³, 9 screens, $L = 10$ mm).

Appendix B: Drop volume density distributions,

Effect of Superficial Velocity

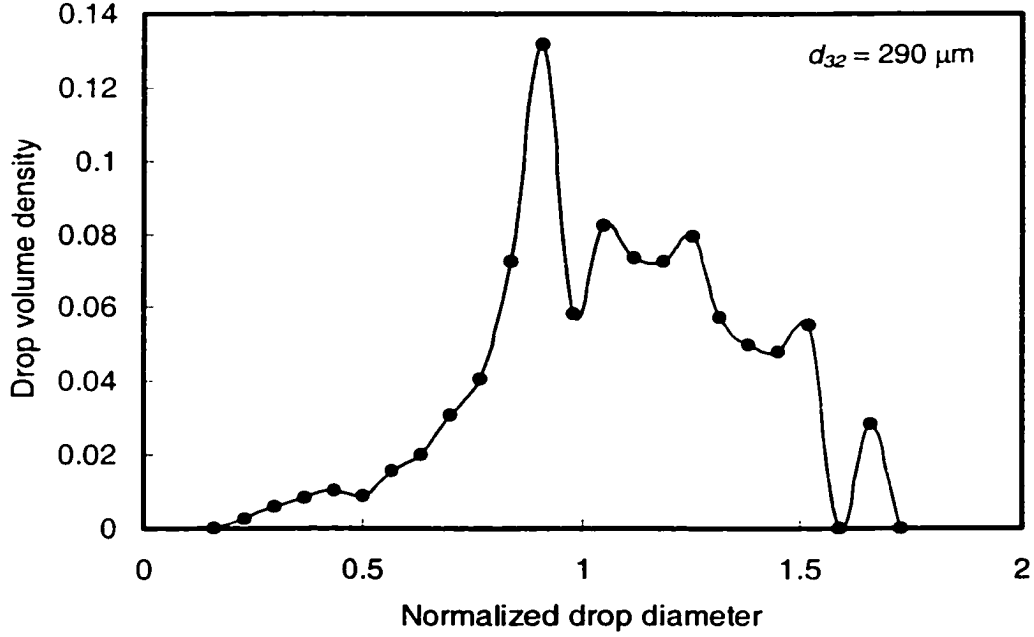


Figure B1. Drop volume density distribution
 ($\alpha = 0.41$, $\phi = 0.5\%$, $U = 0.30$ m/s, 9 screens, $L = 10$ mm).

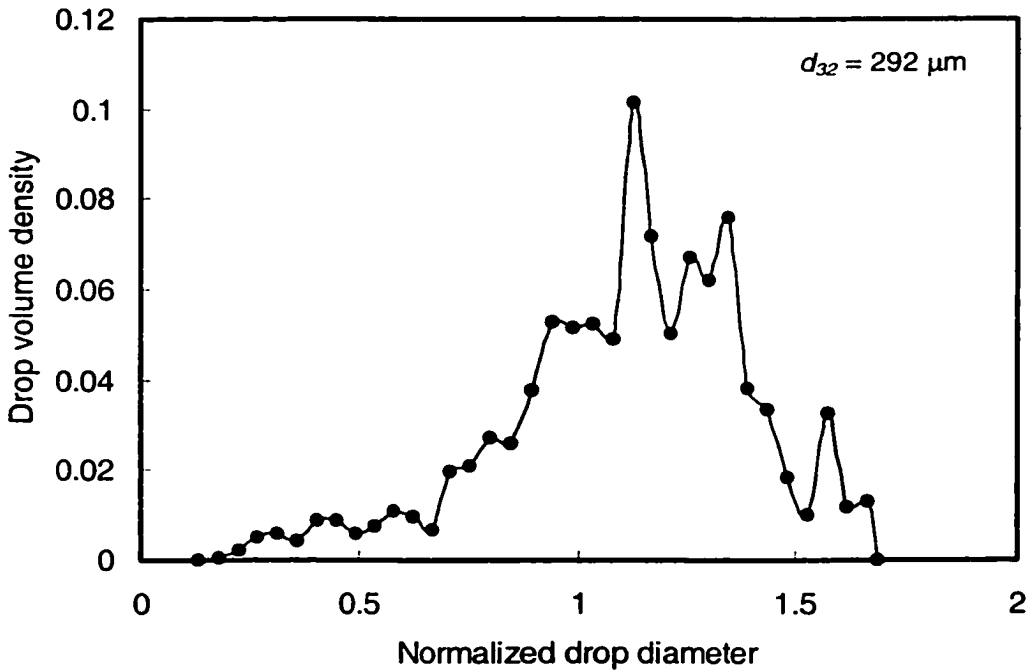


Figure B2. Drop volume density distribution
 ($\alpha = 0.41$, $\phi = 0.5\%$, $U = 0.40$ m/s, 9 screens, $L = 10$ mm).

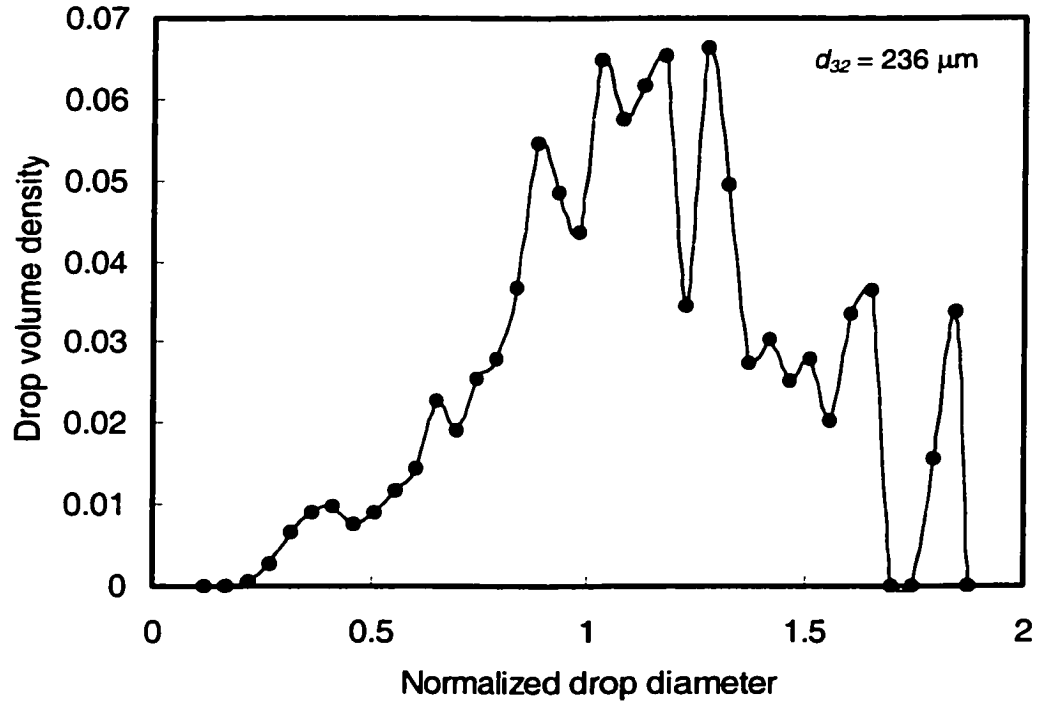


Figure B3. Drop volume density distribution
 ($\alpha = 0.41$, $\phi = 0.5\%$, $U = 0.50 \text{ m/s}$, 9 screens, $L = 10\text{mm}$).

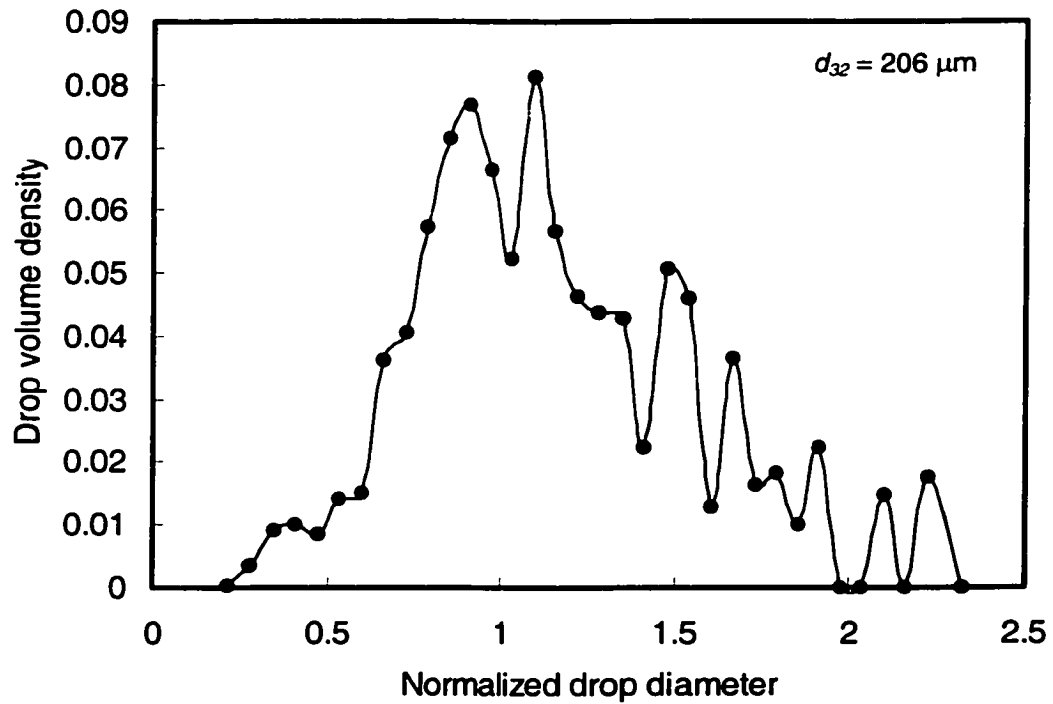


Figure B4. Drop volume density distribution
 ($\alpha = 0.41$, $\phi = 0.5\%$, $U = 0.60 \text{ m/s}$, 9 screens, $L = 10\text{mm}$).

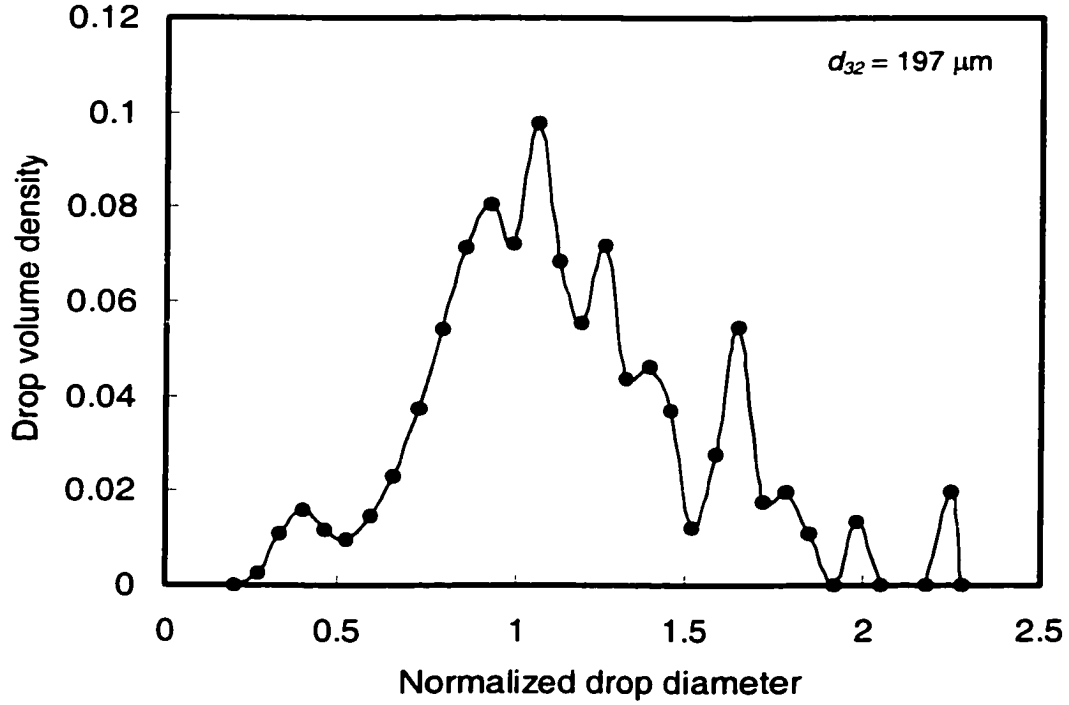


Figure B5. Drop volume density distribution
 ($\alpha = 0.41$, $\phi = 0.5\%$, $U = 0.65 \text{ m/s}$, 9 screens, $L = 10\text{mm}$).

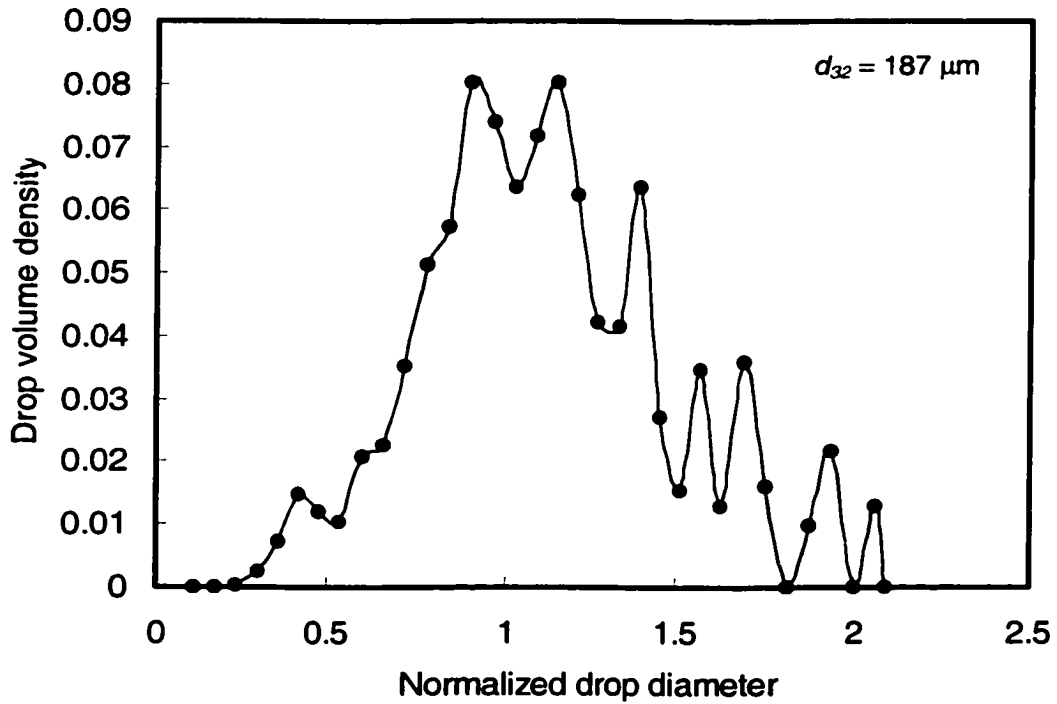


Figure B6. Drop volume density distribution
 ($\alpha = 0.41$, $\phi = 0.5\%$, $U = 0.70 \text{ m/s}$, 9 screens, $L = 10\text{mm}$).

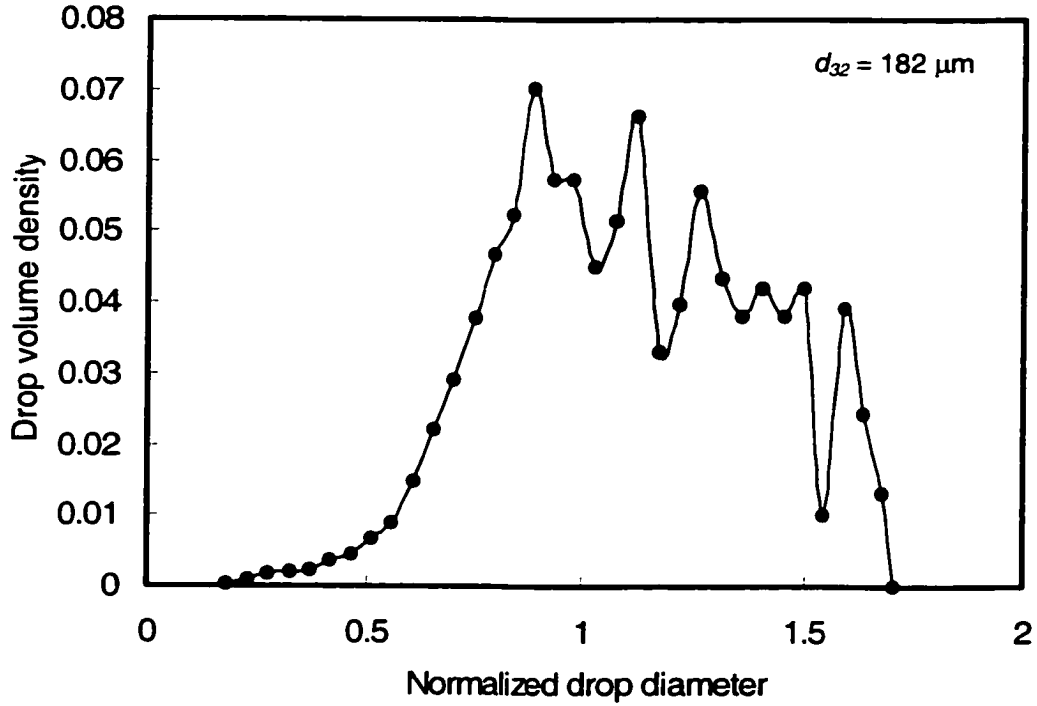


Figure B7. Drop volume density distribution ($\alpha = 0.41$, $\phi = 0.5\%$, $U = 0.85$ m/s, 9 screens, $L = 10$ mm).

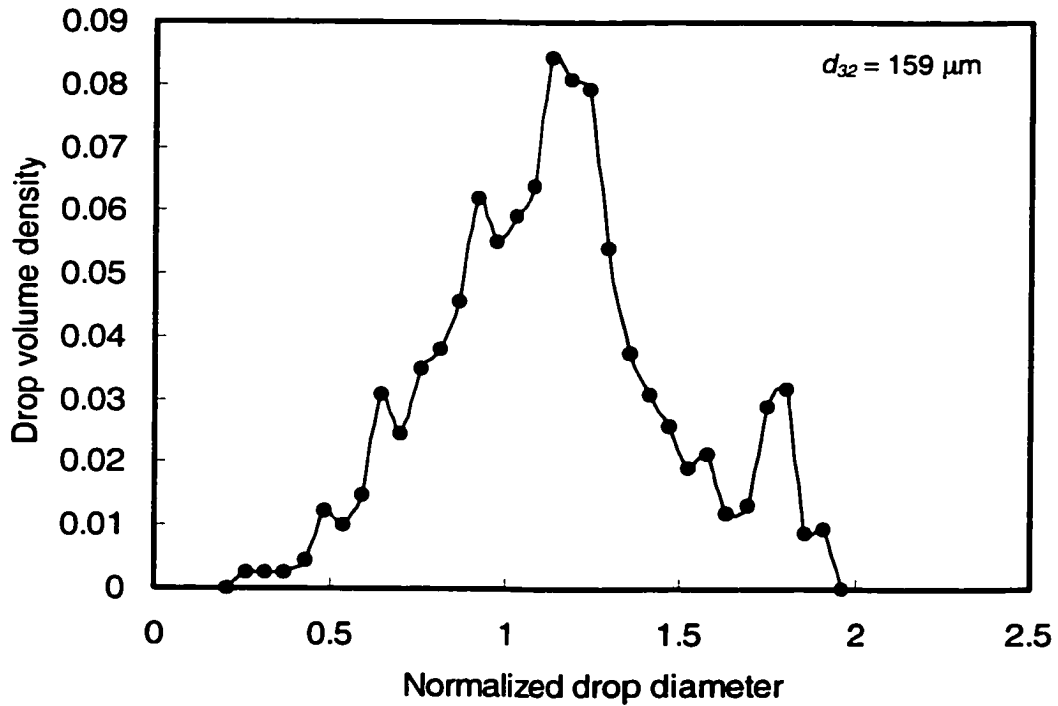


Figure B8. Drop volume density distribution ($\alpha = 0.41$, $\phi = 0.5\%$, $U = 0.97$ m/s, 9 screens, $L = 10$ mm).

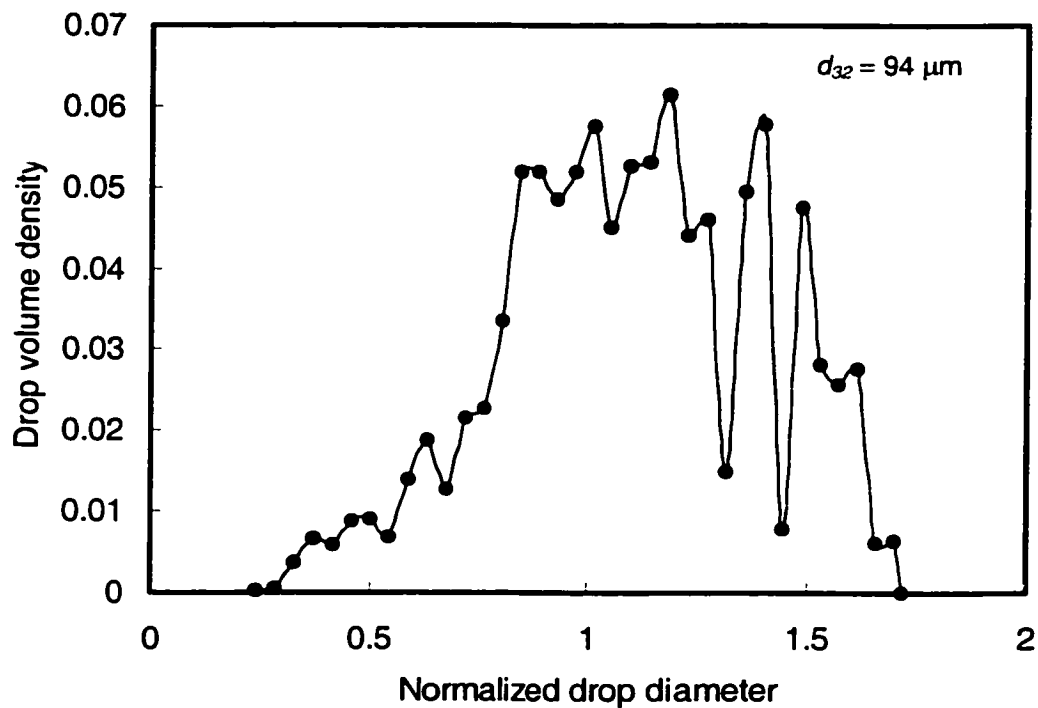


Figure B9. Drop volume density distribution
 ($\alpha = 0.41$, $\phi = 0.5\%$, $U = 1.55$ m/s, 9 screens, $L = 10$ mm).

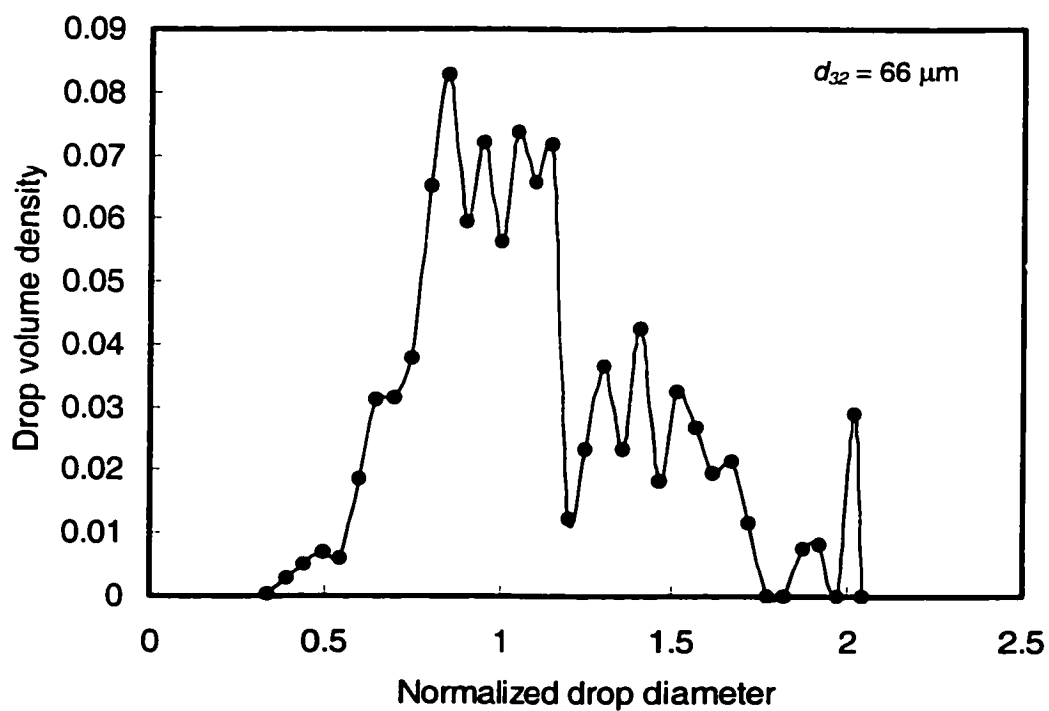


Figure B10. Drop volume density distribution
 ($\alpha = 0.41$, $\phi = 0.5\%$, $U = 1.94$ m/s, 9 screens, $L = 10$ mm).

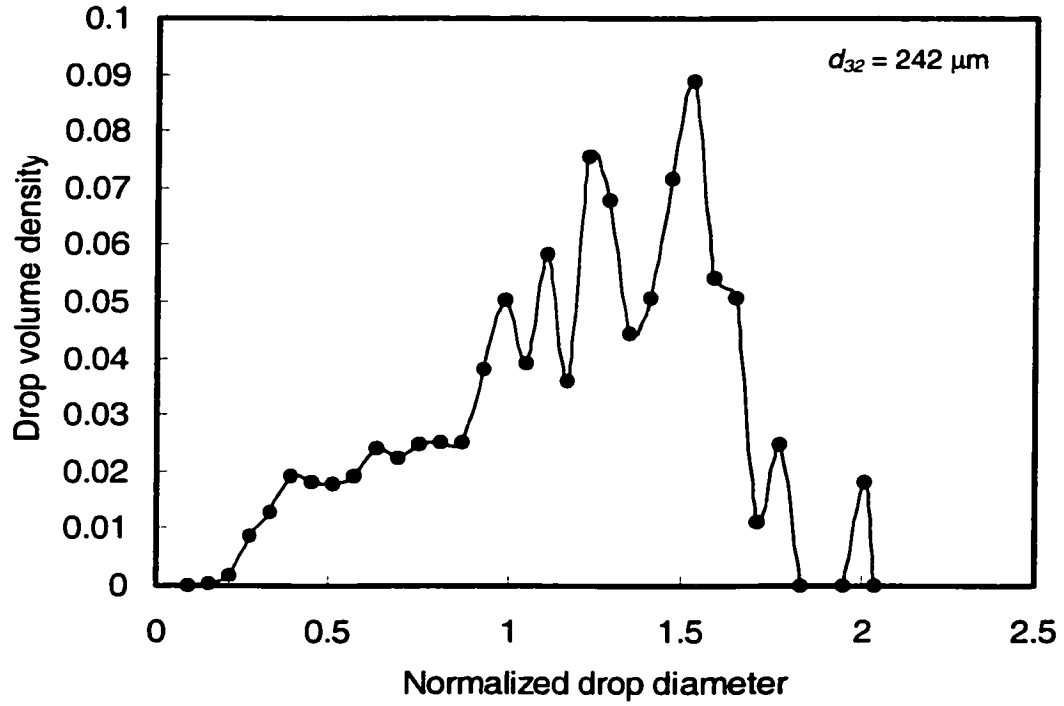


Figure B11. Drop volume density distribution
 ($\alpha = 0.41$, $\phi = 4\%$, $U = 0.30$ m/s, 9 screens, $L = 10\text{mm}$).

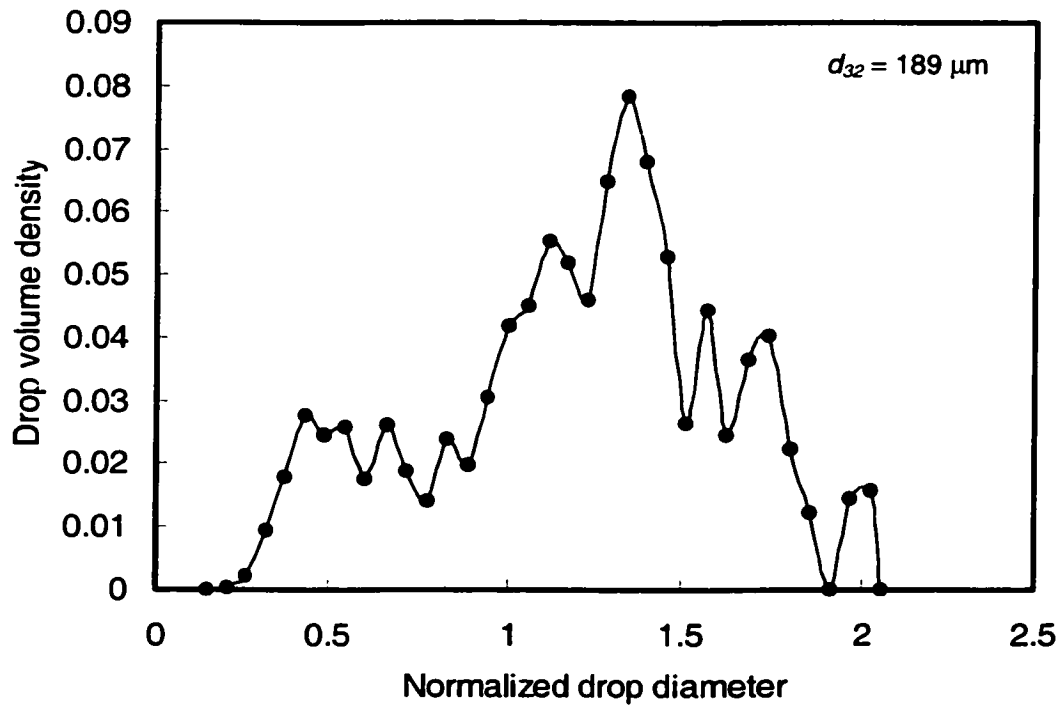


Figure B12. Drop volume density distribution
 ($\alpha = 0.41$, $\phi = 4\%$, $U = 0.40$ m/s, 9 screens, $L = 10\text{mm}$).

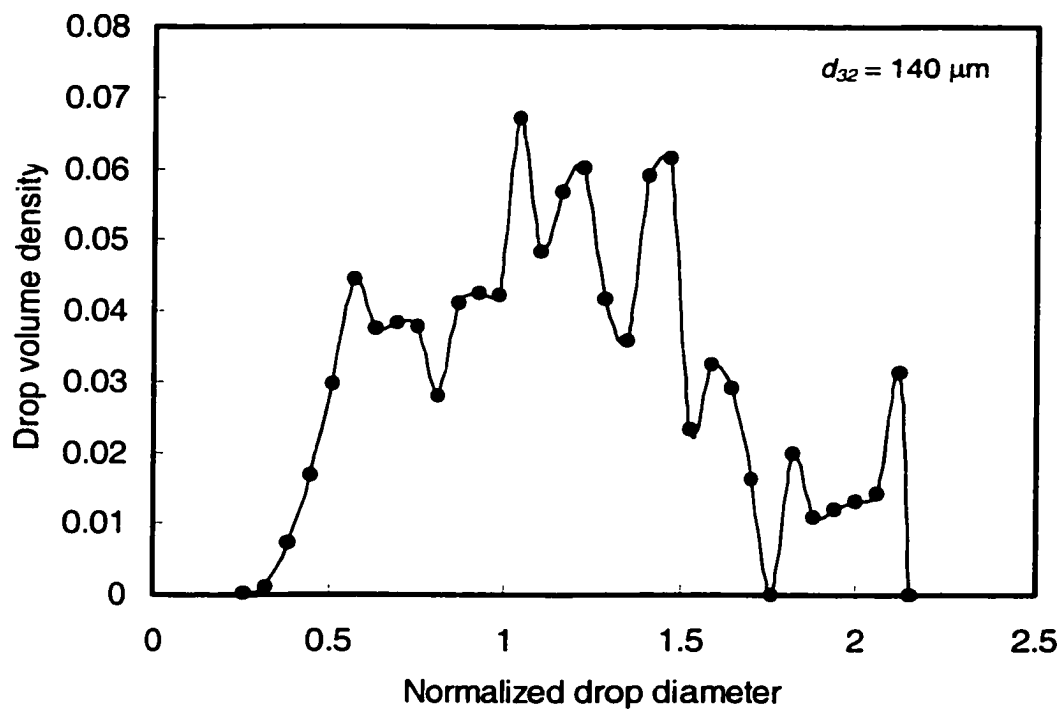


Figure B13. Drop volume density distribution
 $(\alpha = 0.41, \phi = 4\%, U = 0.50 \text{ m/s}, 9 \text{ screens}, L = 10\text{mm})$.

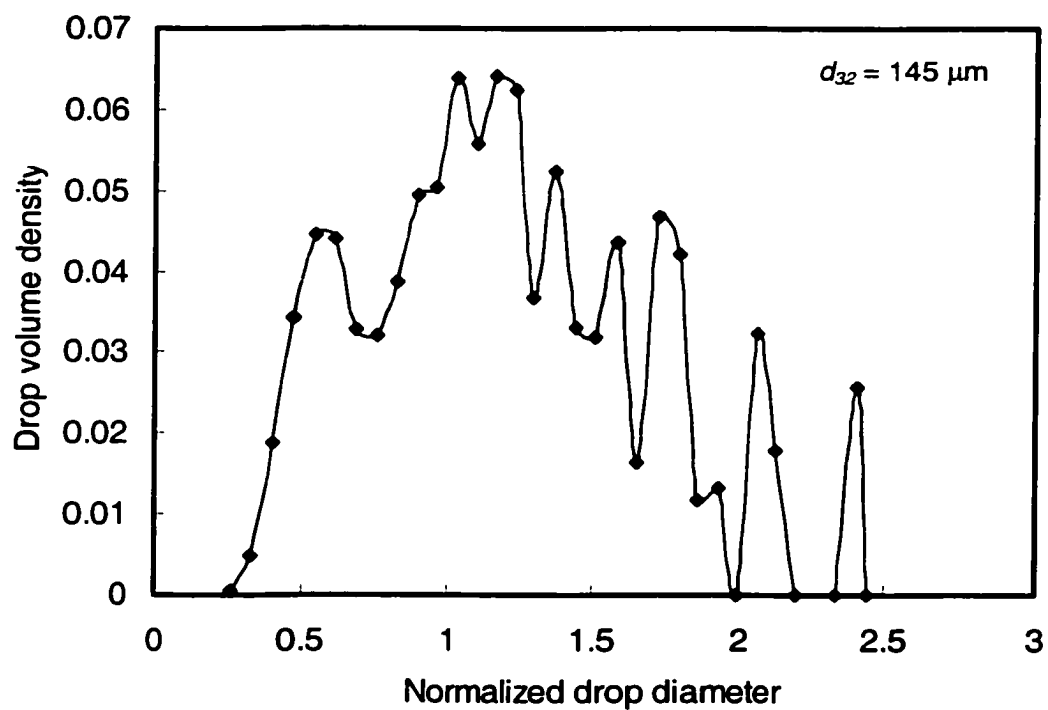


Figure B14. Drop volume density distribution
 $(\alpha = 0.41, \phi = 4\%, U = 0.60 \text{ m/s}, 9 \text{ screens}, L = 10\text{mm})$.

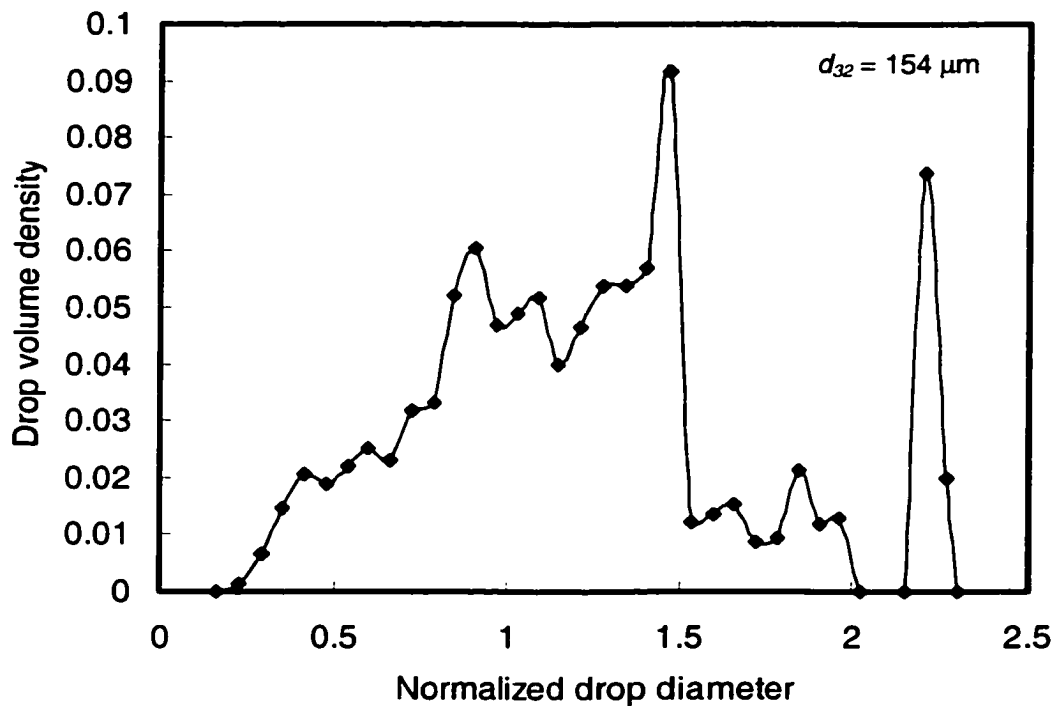


Figure B15. Drop volume density distribution
 $(\alpha = 0.41, \phi = 4\%, U = 0.65 \text{ m/s}, 9 \text{ screens}, L = 10\text{mm})$.

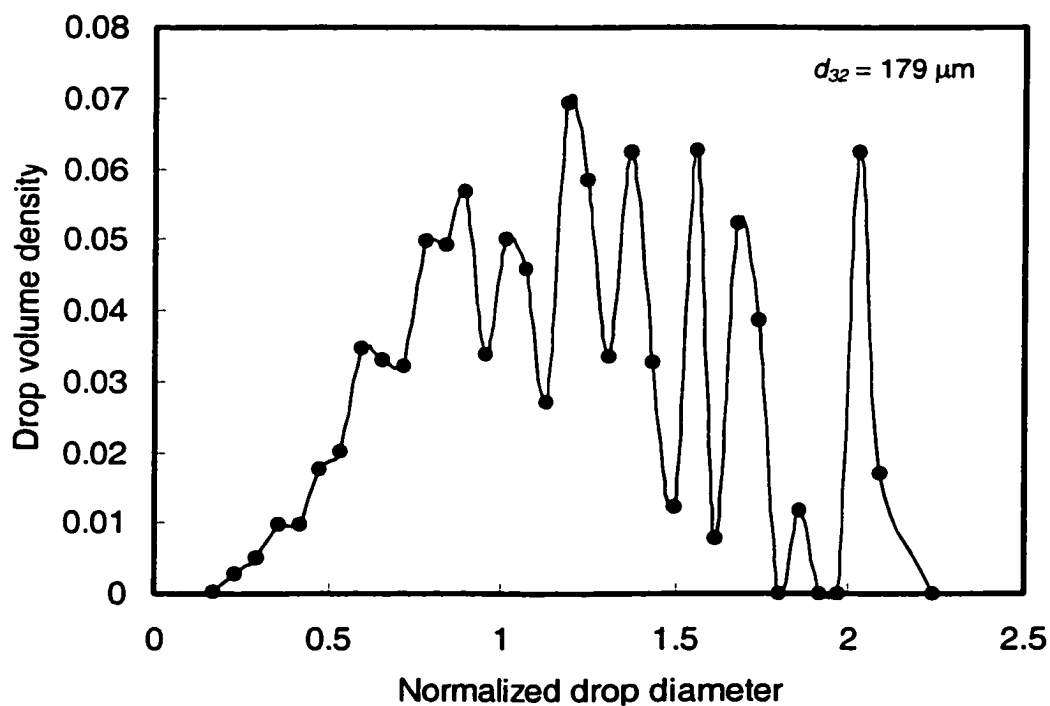


Figure B16. Drop volume density distribution
 $(\alpha = 0.41, \phi = 4\%, U = 0.70 \text{ m/s}, 9 \text{ screens}, L = 10\text{mm})$.

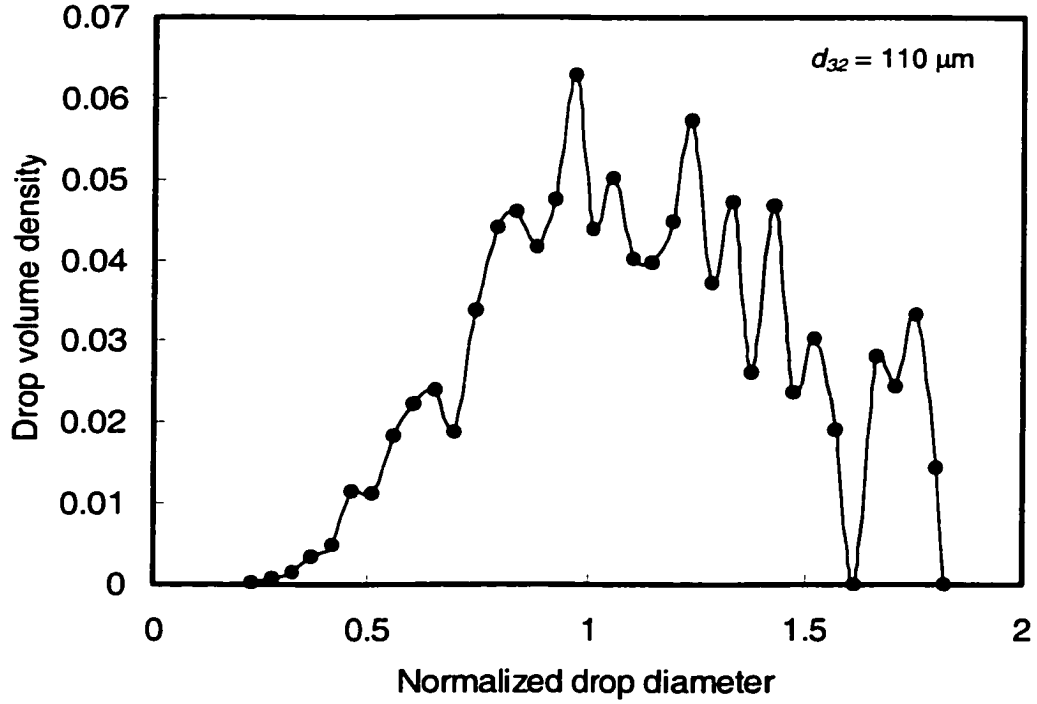


Figure B17. Drop volume density distribution ($\alpha = 0.41$, $\phi = 4\%$, $U = 0.85 \text{ m/s}$, 9 screens, $L = 10\text{mm}$).

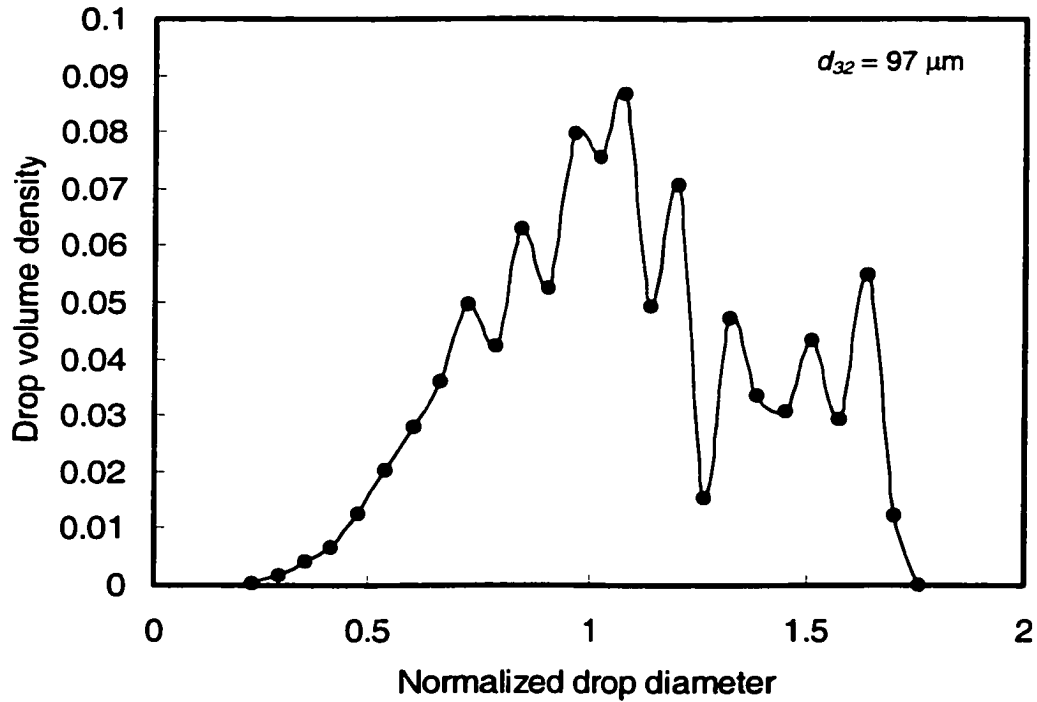


Figure B18. Drop volume density distribution ($\alpha = 0.41$, $\phi = 4\%$, $U = 0.97 \text{ m/s}$, 9 screens, $L = 10\text{mm}$).

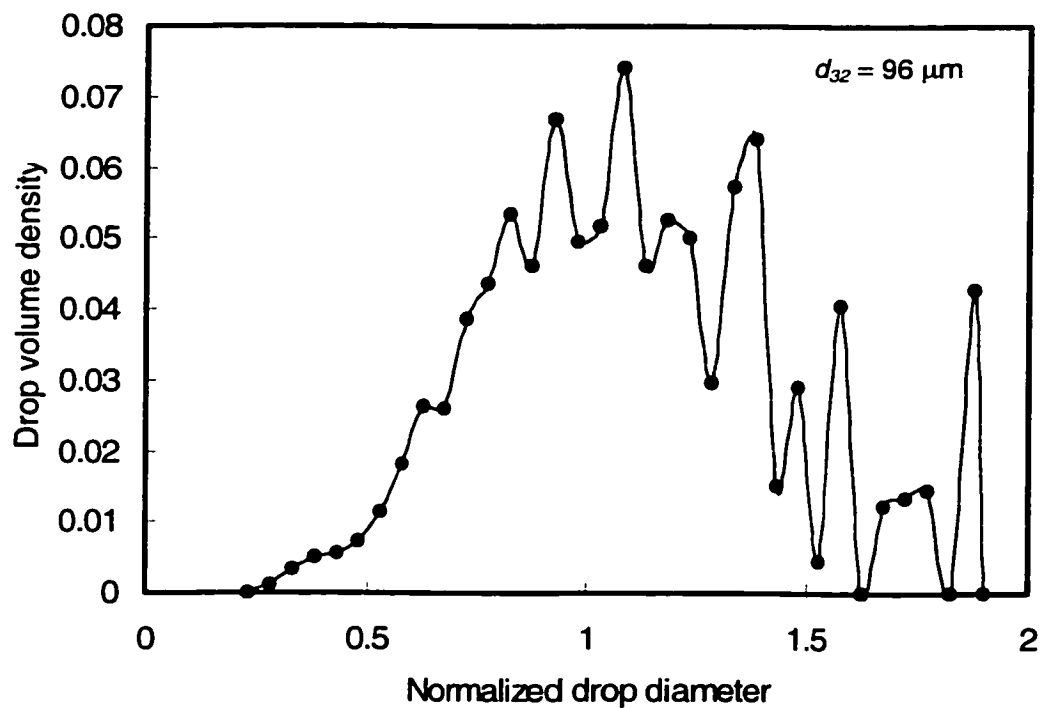


Figure B19. Drop volume density distribution
 $(\alpha = 0.41, \phi = 4\%, U = 1.55 \text{ m/s}, 9 \text{ screens}, L = 10\text{mm})$.

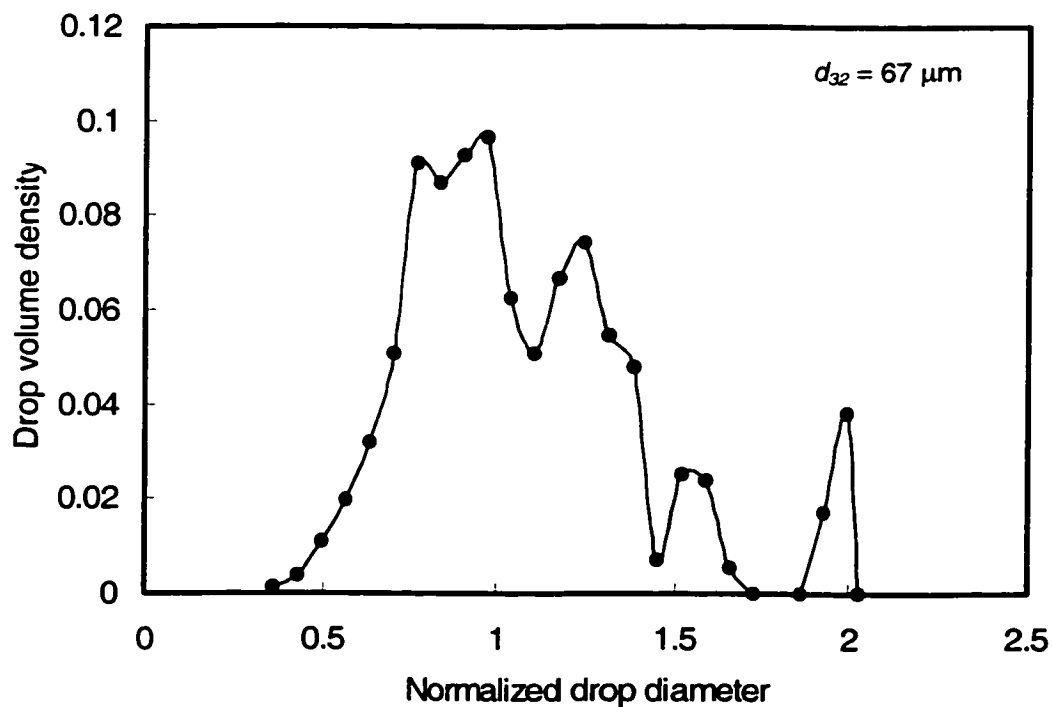


Figure B20. Drop volume density distribution
 $(\alpha = 0.41, \phi = 4\%, U = 1.94 \text{ m/s}, 9 \text{ screens}, L = 10\text{mm})$.

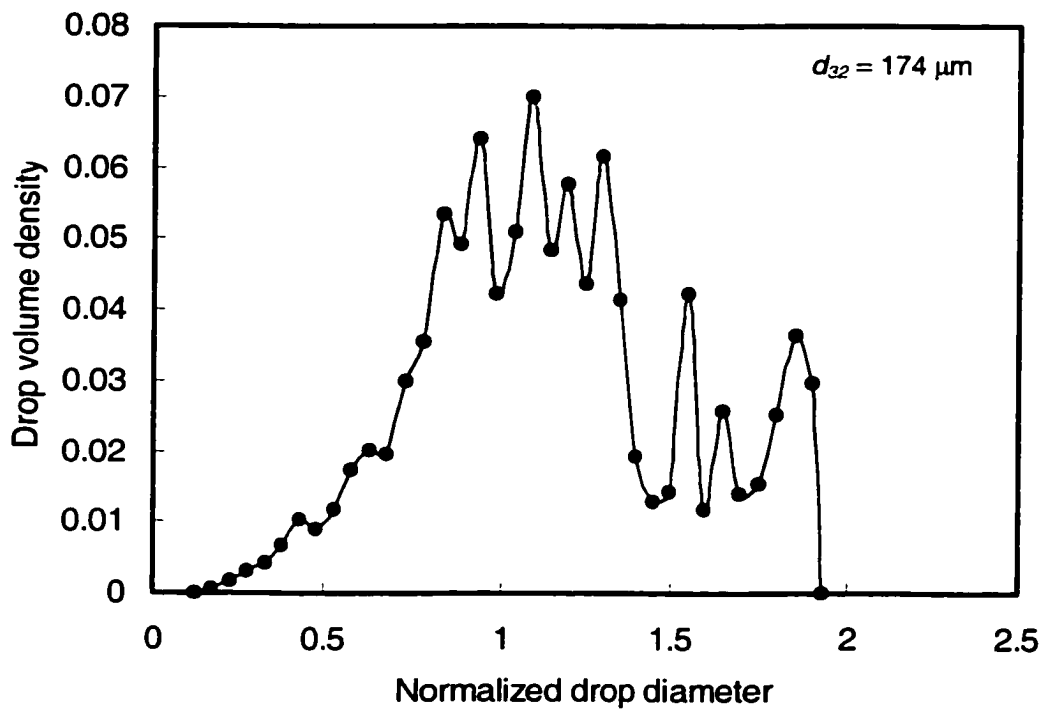


Figure B21. Drop volume density distribution
 ($\alpha = 0.33$, $\phi = 0.5\%$, $U = 0.30$ m/s, 9 screens, $L = 10$ mm).

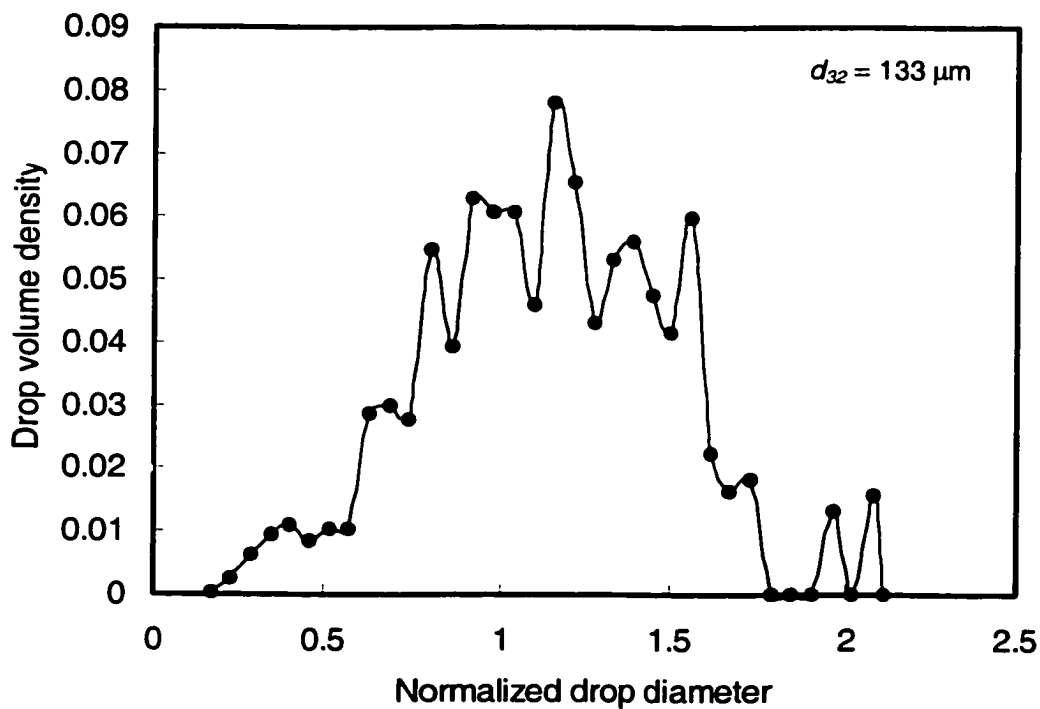


Figure B22. Drop volume density distribution
 ($\alpha = 0.33$, $\phi = 0.5\%$, $U = 0.50$ m/s, 9 screens, $L = 10$ mm).

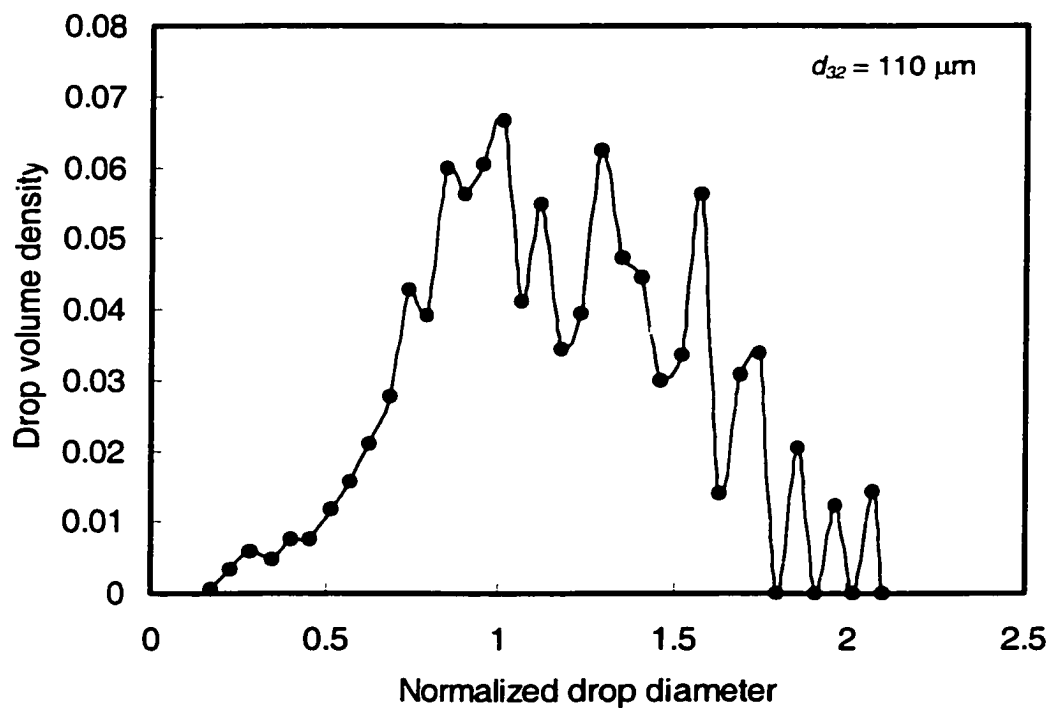


Figure B23. Drop volume density distribution
 ($\alpha = 0.33$, $\phi = 0.5\%$, $U = 0.70$ m/s, 9 screens, $L = 10$ mm).

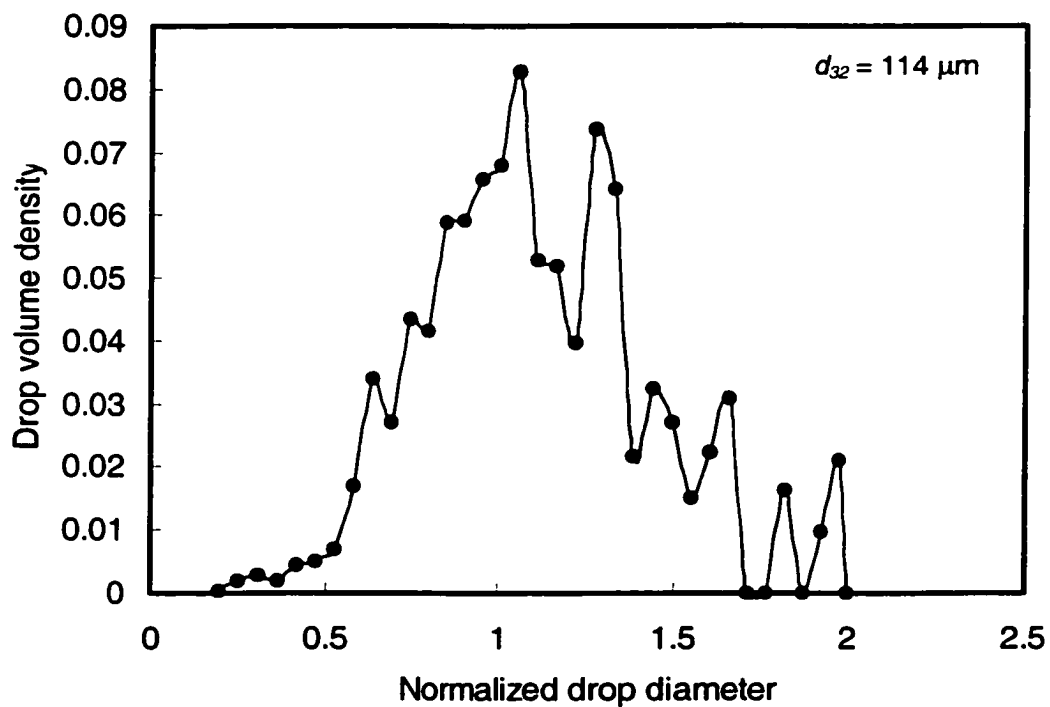


Figure B24. Drop volume density distribution
 ($\alpha = 0.33$, $\phi = 0.5\%$, $U = 0.85$ m/s, 9 screens, $L = 10$ mm).

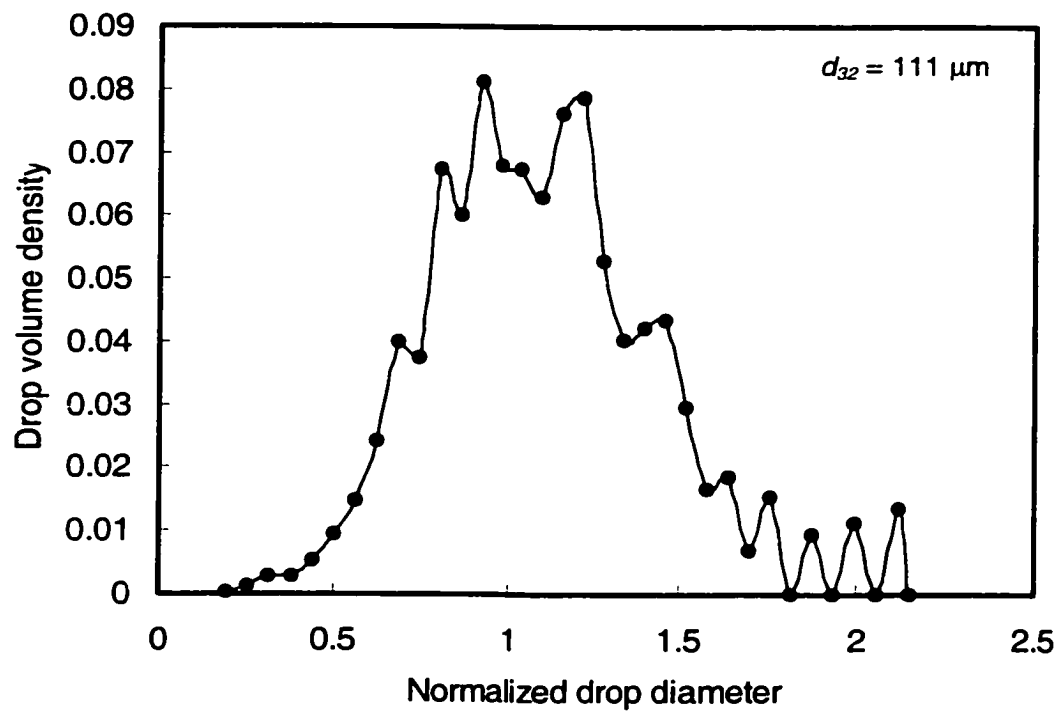


Figure B25. Drop volume density distribution
 ($\alpha = 0.33$, $\phi = 0.5\%$, $U = 0.97$ m/s, 9 screens, $L = 10$ mm).

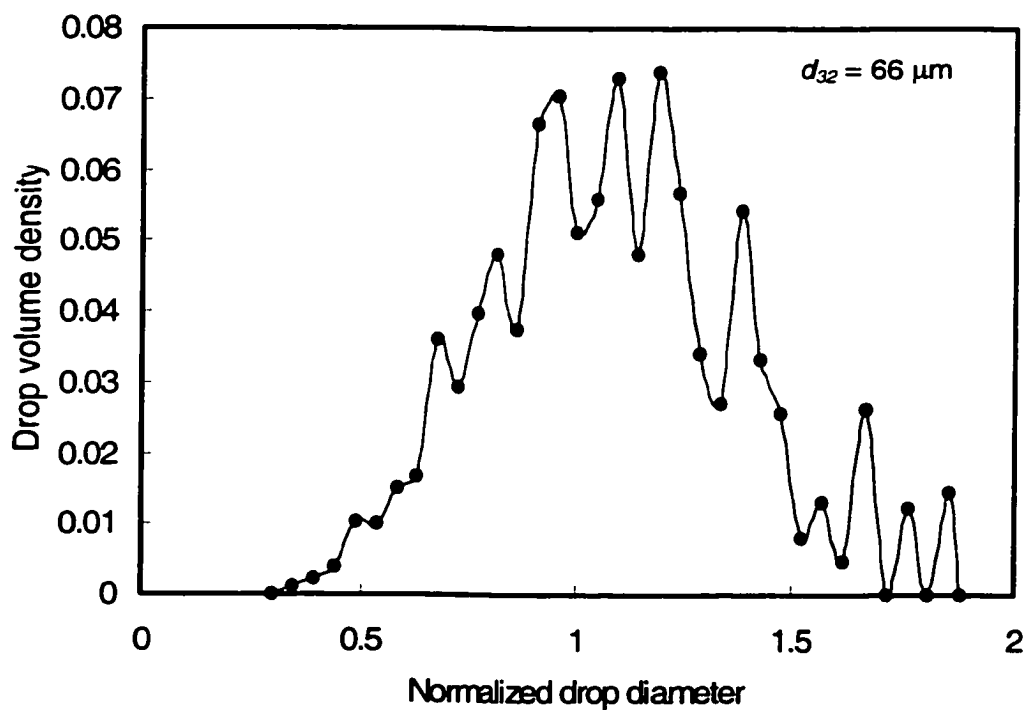


Figure B26. Drop volume density distribution
 ($\alpha = 0.33$, $\phi = 0.5\%$, $U = 1.55$ m/s, 9 screens, $L = 10$ mm).

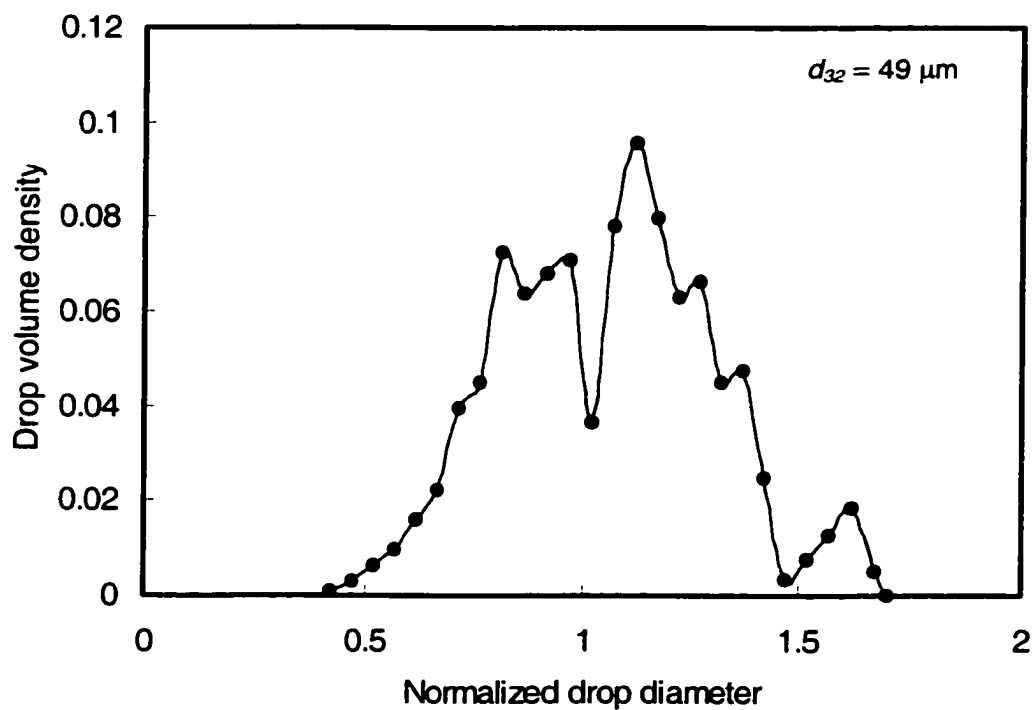


Figure B27. Drop volume density distribution
 $(\alpha = 0.33, \phi = 0.5\%, U = 1.80 \text{ m/s}, 9 \text{ screens}, L = 10\text{mm})$.

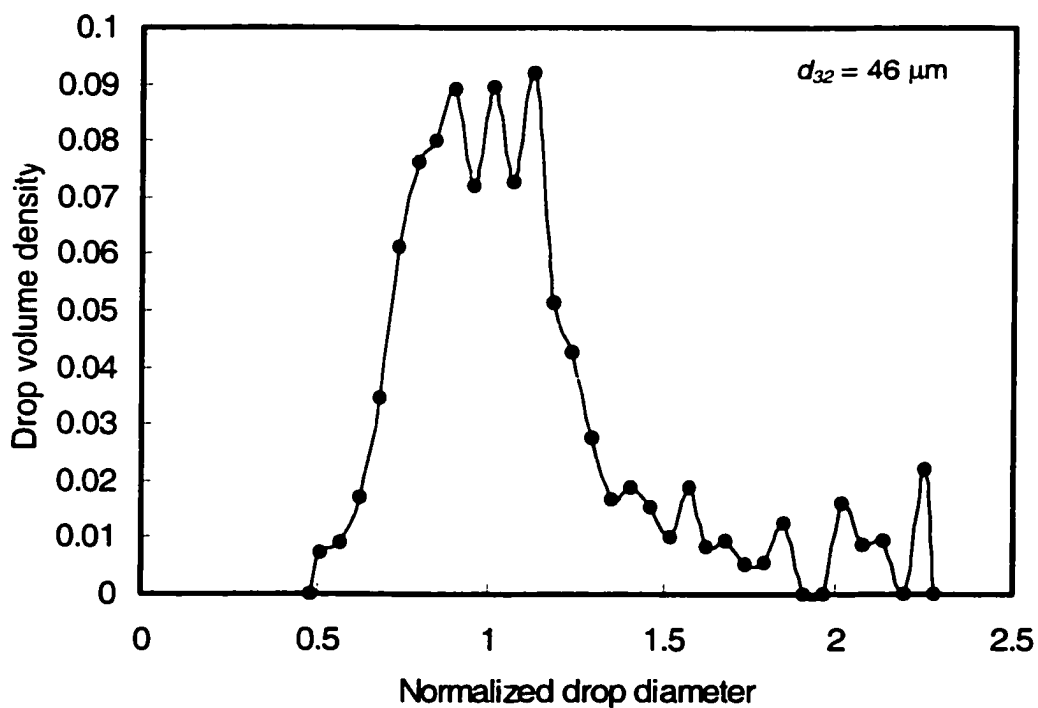


Figure B28. Drop volume density distribution
 $(\alpha = 0.33, \phi = 0.5\%, U = 1.94 \text{ m/s}, 9 \text{ screens}, L = 10\text{mm})$.

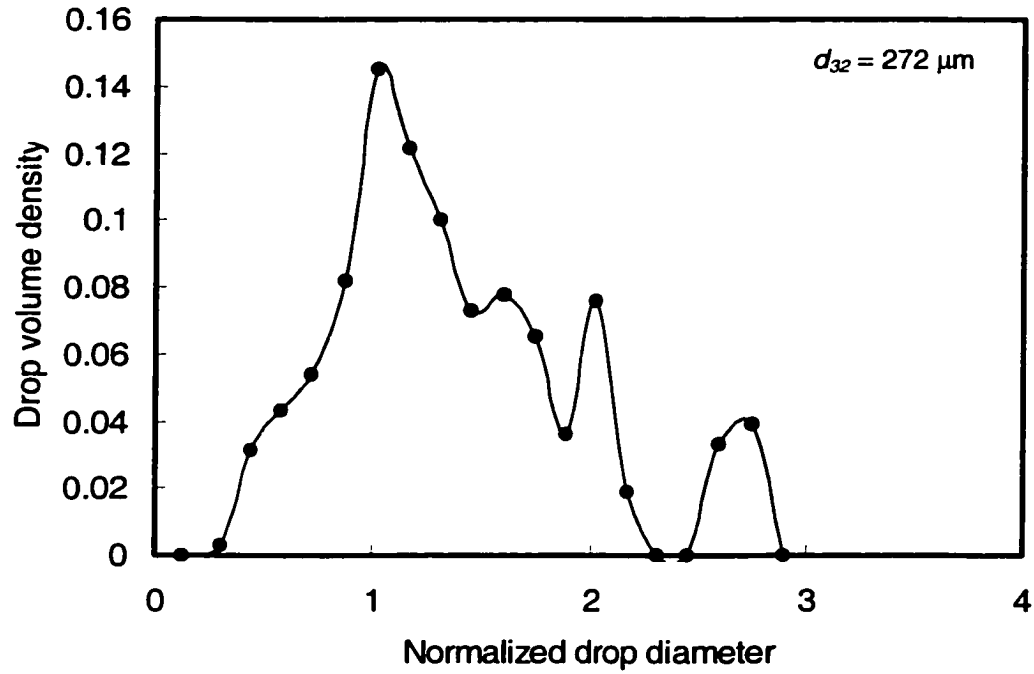


Figure B29. Drop volume density distribution
 $(\alpha = 0.27, \phi = 0.5\%, U = 0.30 \text{ m/s}, 9 \text{ screens}, L = 10\text{mm})$.

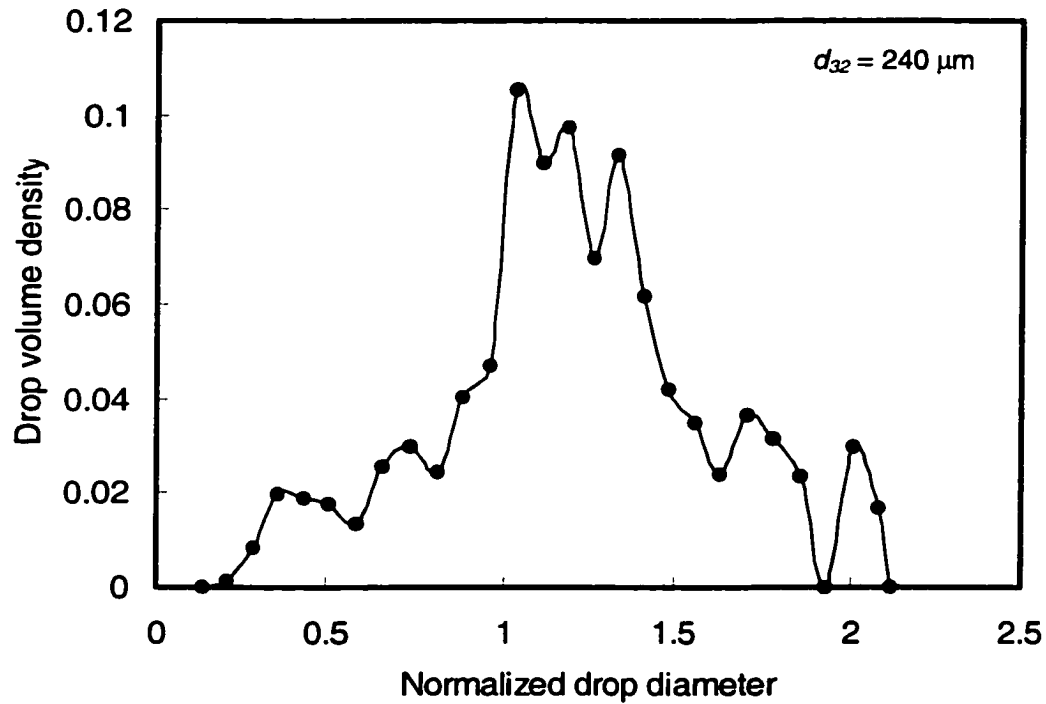


Figure B30. Drop volume density distribution
 $(\alpha = 0.27, \phi = 0.5\%, U = 0.40 \text{ m/s}, 9 \text{ screens}, L = 10\text{mm})$.

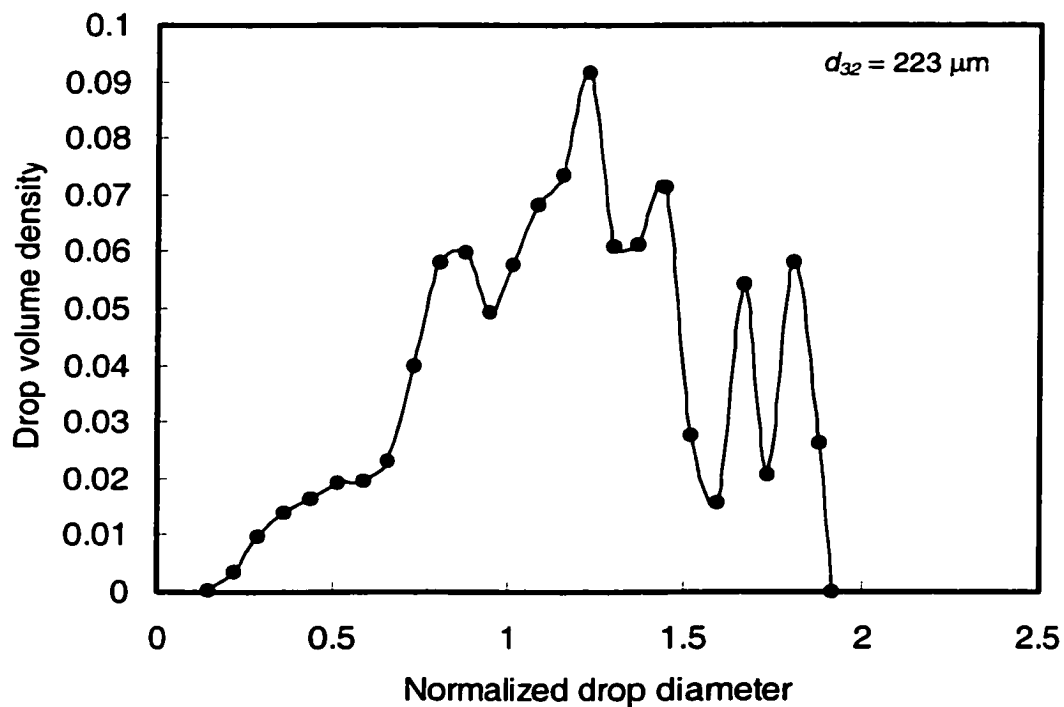


Figure B31. Drop volume density distribution
 ($\alpha = 0.27$, $\phi = 0.5\%$, $U = 0.50$ m/s, 9 screens, $L = 10$ mm).

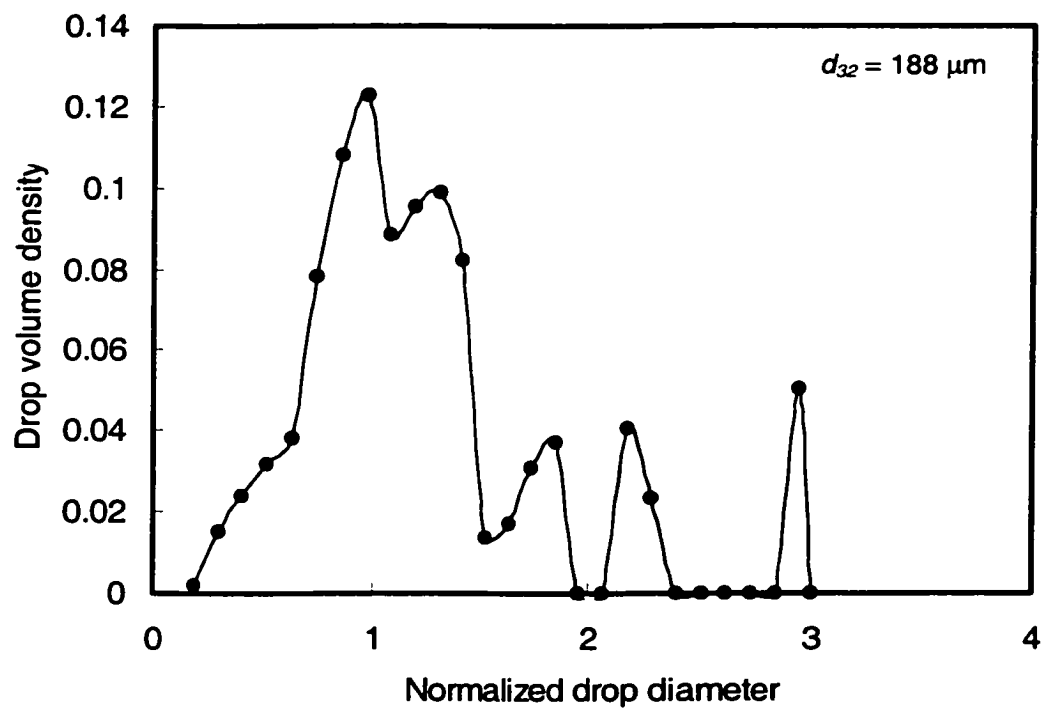


Figure B32. Drop volume density distribution
 ($\alpha = 0.27$, $\phi = 0.5\%$, $U = 0.60$ m/s, 9 screens, $L = 10$ mm).

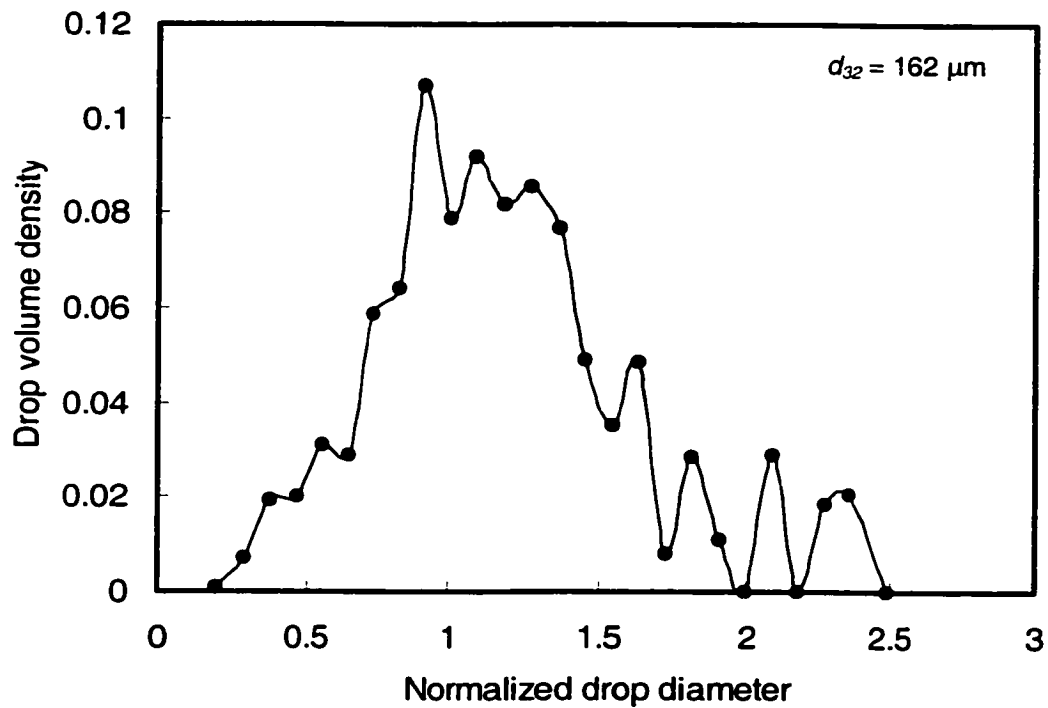


Figure B33. Drop volume density distribution
 ($\alpha = 0.27$, $\phi = 0.5\%$, $U = 0.65$ m/s, 9 screens, $L = 10$ mm).

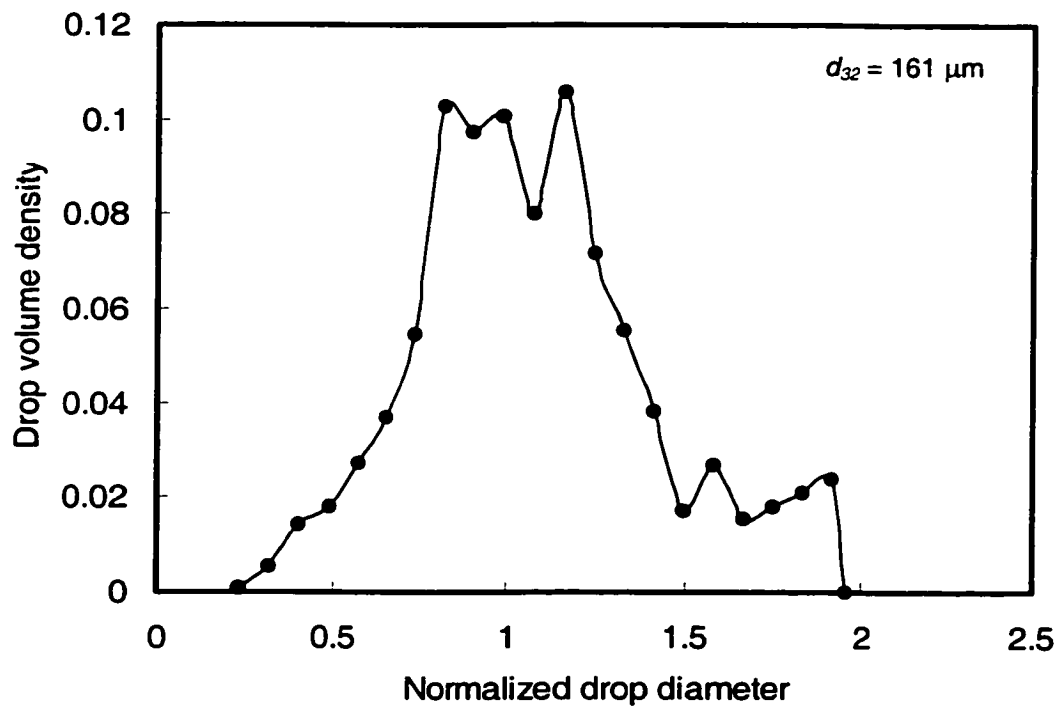


Figure B34. Drop volume density distribution
 ($\alpha = 0.27$, $\phi = 0.5\%$, $U = 0.70$ m/s, 9 screens, $L = 10$ mm).

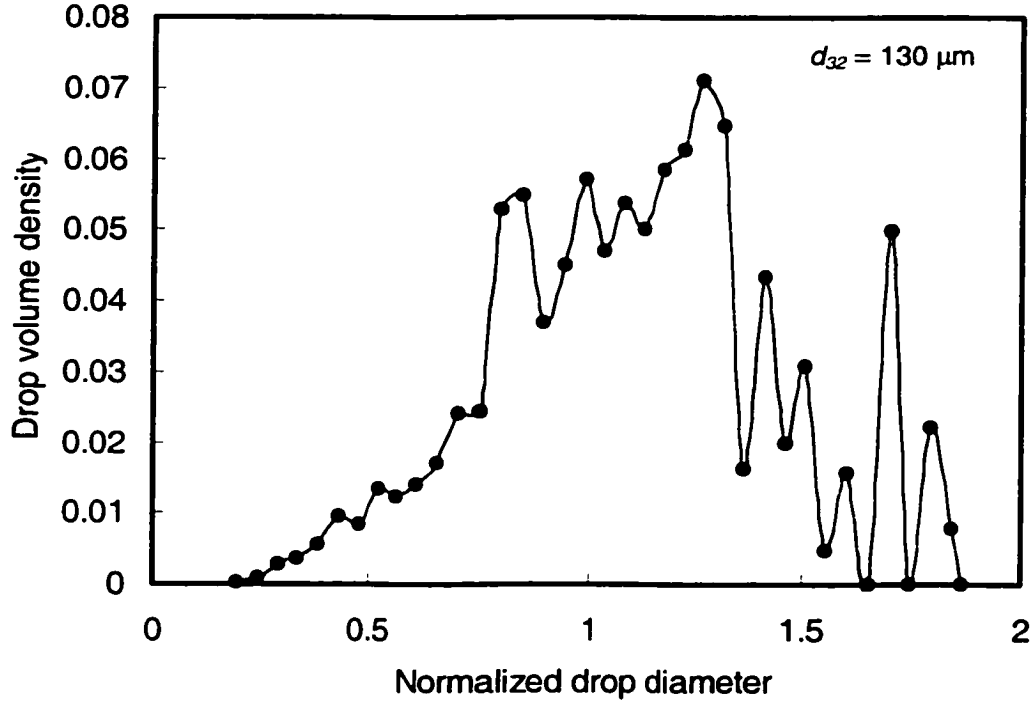


Figure B35. Drop volume density distribution
 ($\alpha = 0.27$, $\phi = 0.5\%$, $U = 0.85 \text{ m/s}$, 9 screens, $L = 10\text{mm}$).

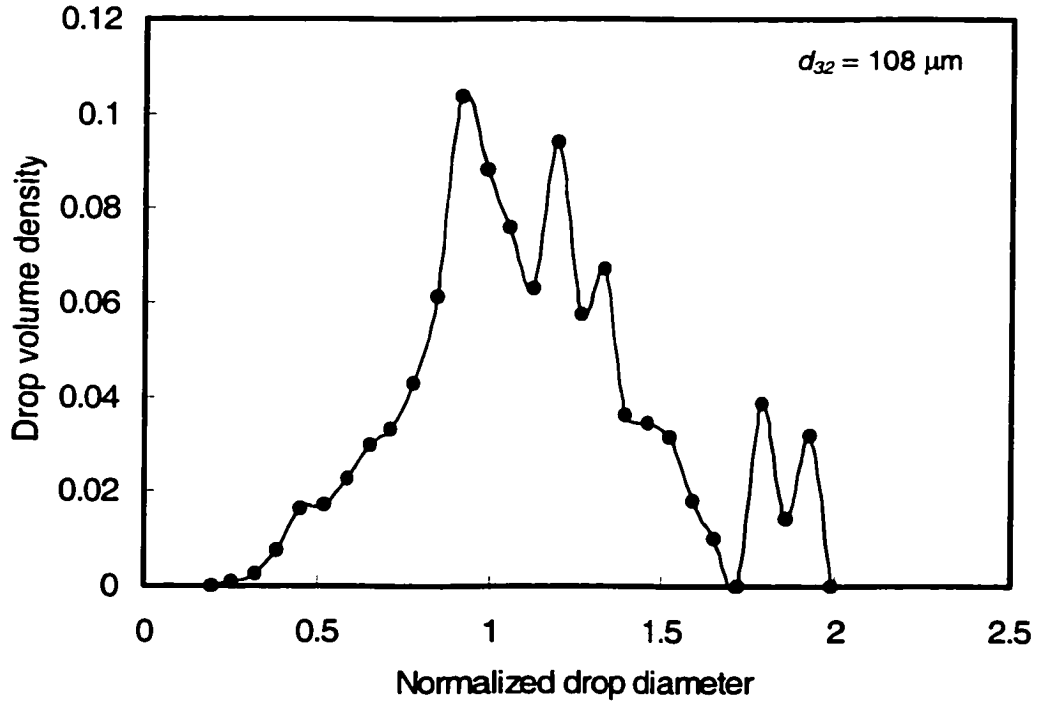


Figure B36. Drop volume density distribution
 ($\alpha = 0.27$, $\phi = 0.5\%$, $U = 0.90 \text{ m/s}$, 9 screens, $L = 10\text{mm}$).

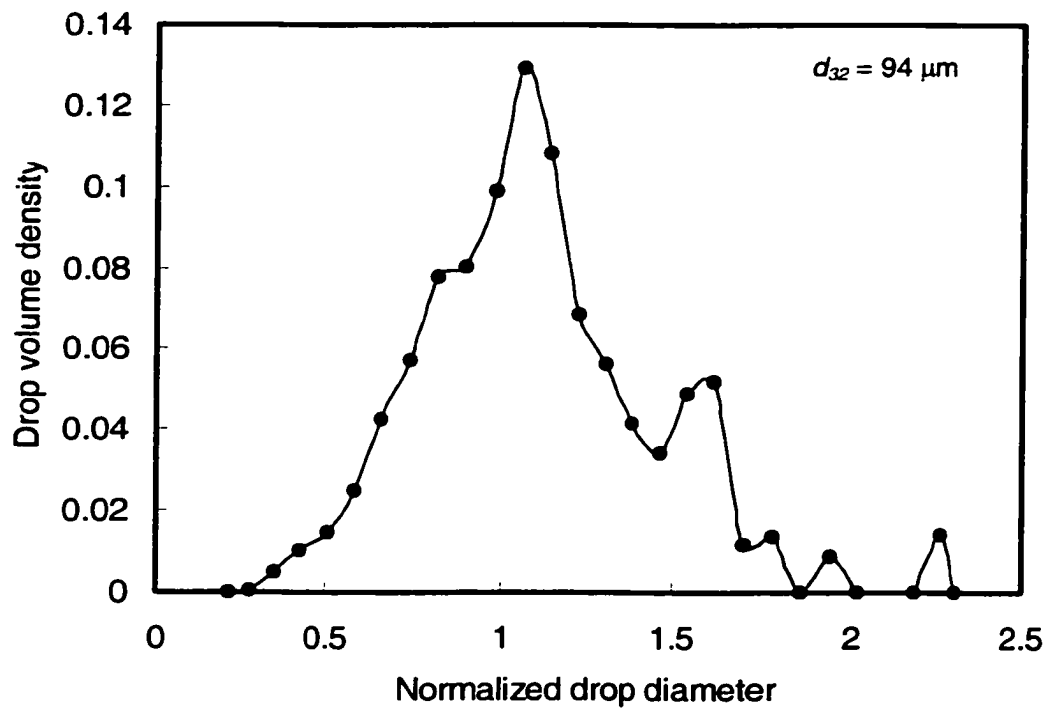


Figure B37. Drop volume density distribution
 ($\alpha = 0.27$, $\phi = 0.5\%$, $U = 0.97$ m/s, 9 screens, $L = 10\text{mm}$).

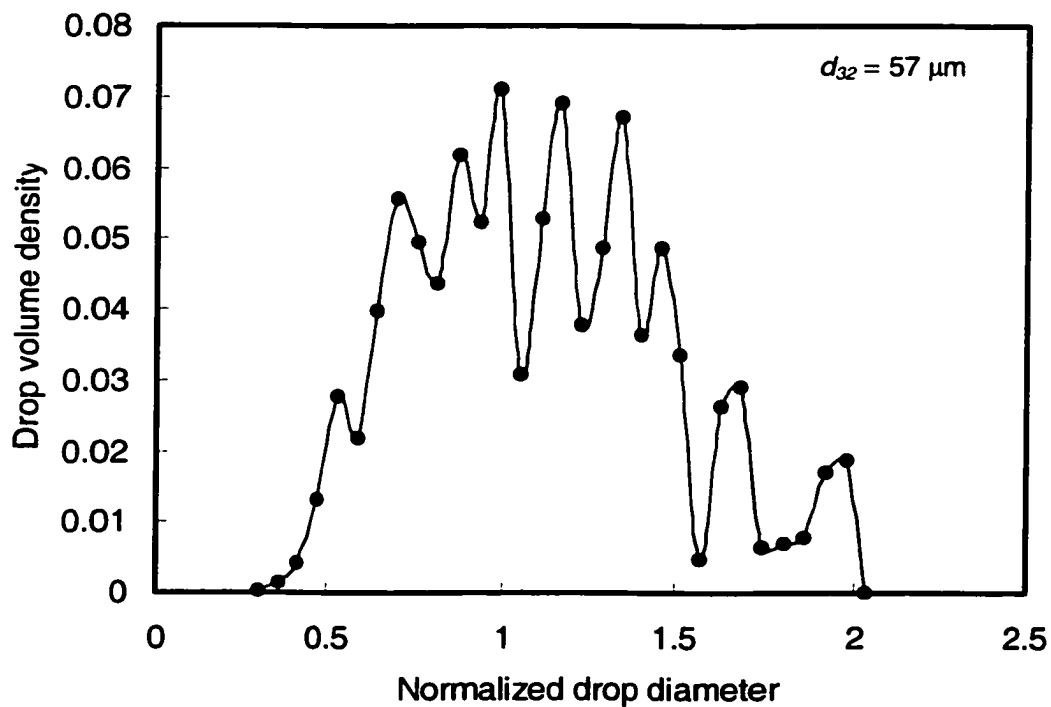


Figure B38. Drop volume density distribution
 ($\alpha = 0.27$, $\phi = 0.5\%$, $U = 1.55$ m/s, 9 screens, $L = 10\text{mm}$).

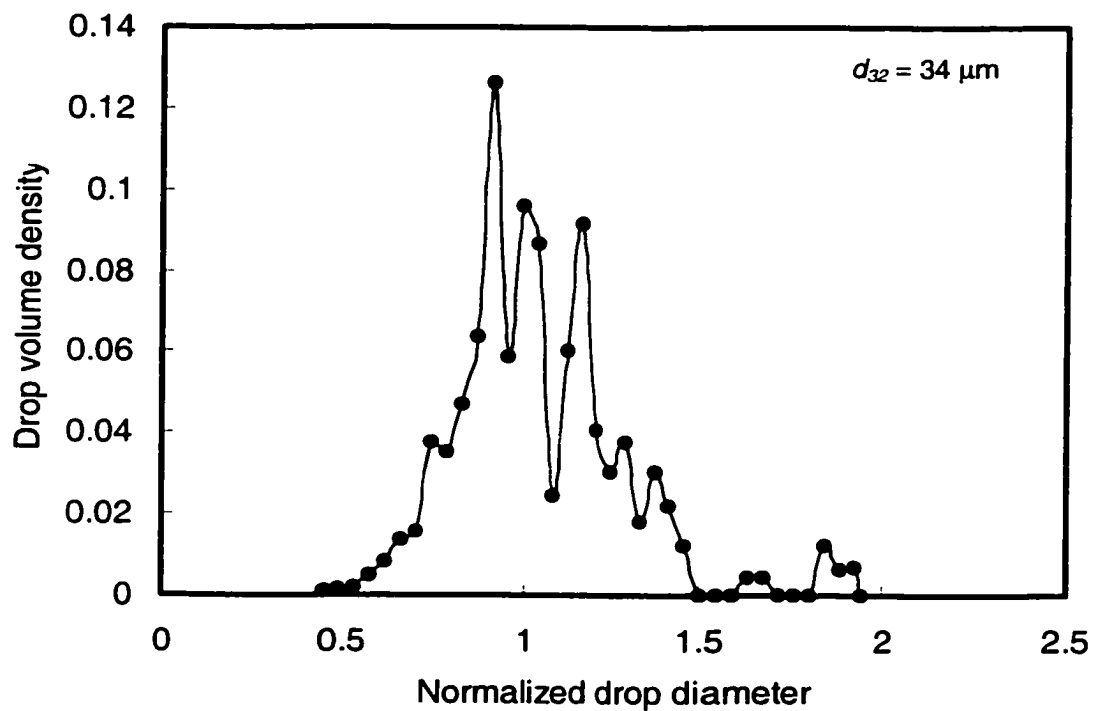


Figure B39. Drop volume density distribution
 ($\alpha = 0.27$, $\phi = 0.5\%$, $U = 1.94$ m/s, 9 screens, $L = 10$ mm).

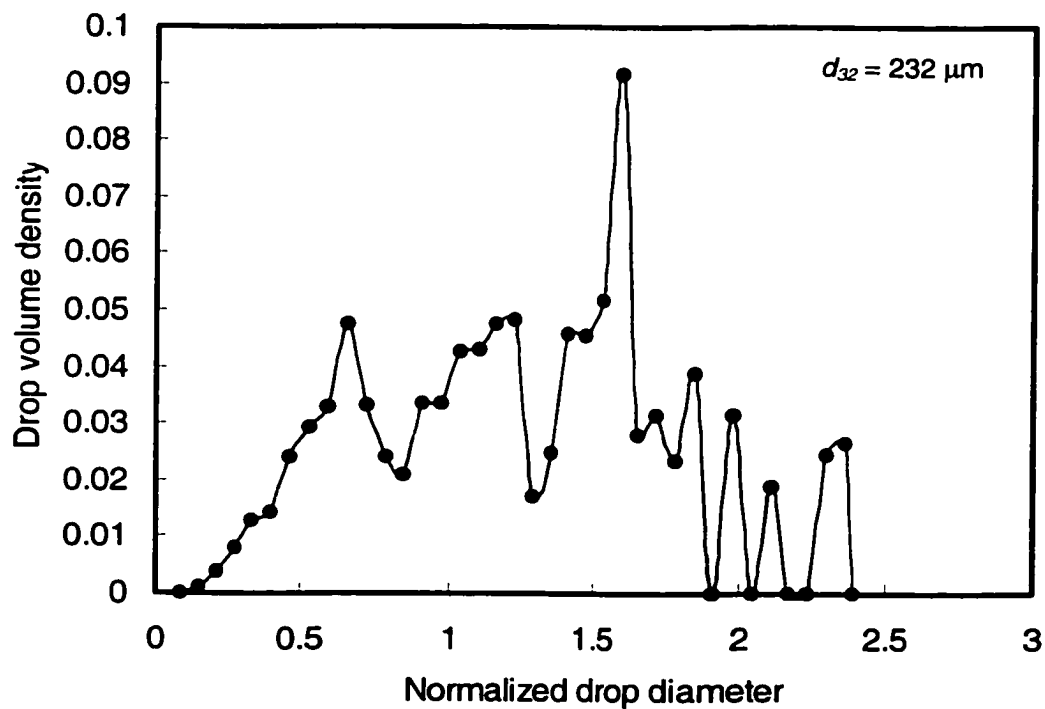


Figure B40. Drop volume density distribution
 ($\alpha = 0.27$, $\phi = 4\%$, $U = 0.30$ m/s, 9 screens, $L = 10$ mm).

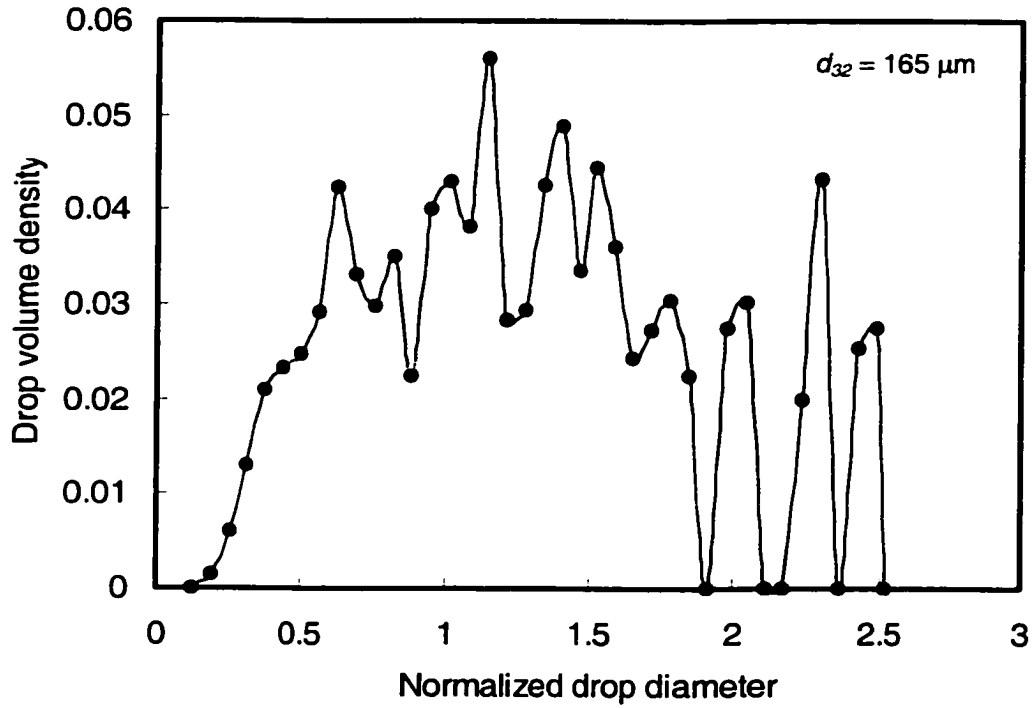


Figure B41. Drop volume density distribution ($\alpha = 0.27$, $\phi = 4\%$, $U = 0.40$ m/s, 9 screens, $L = 10$ mm).

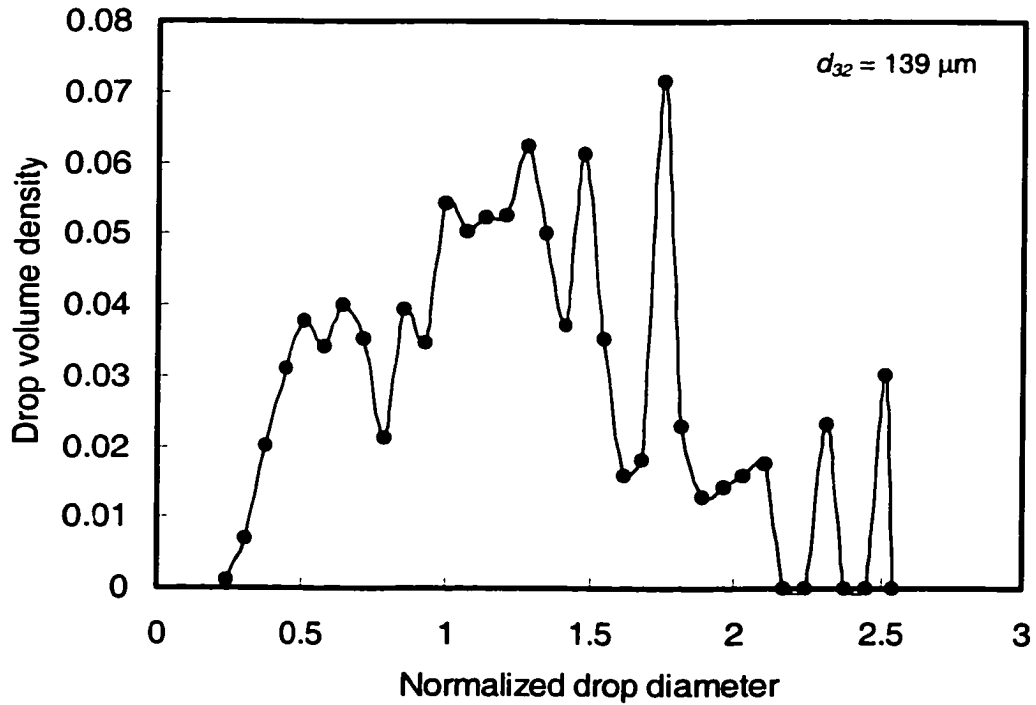


Figure B42. Drop volume density distribution ($\alpha = 0.27$, $\phi = 4\%$, $U = 0.50$ m/s, 9 screens, $L = 10$ mm).

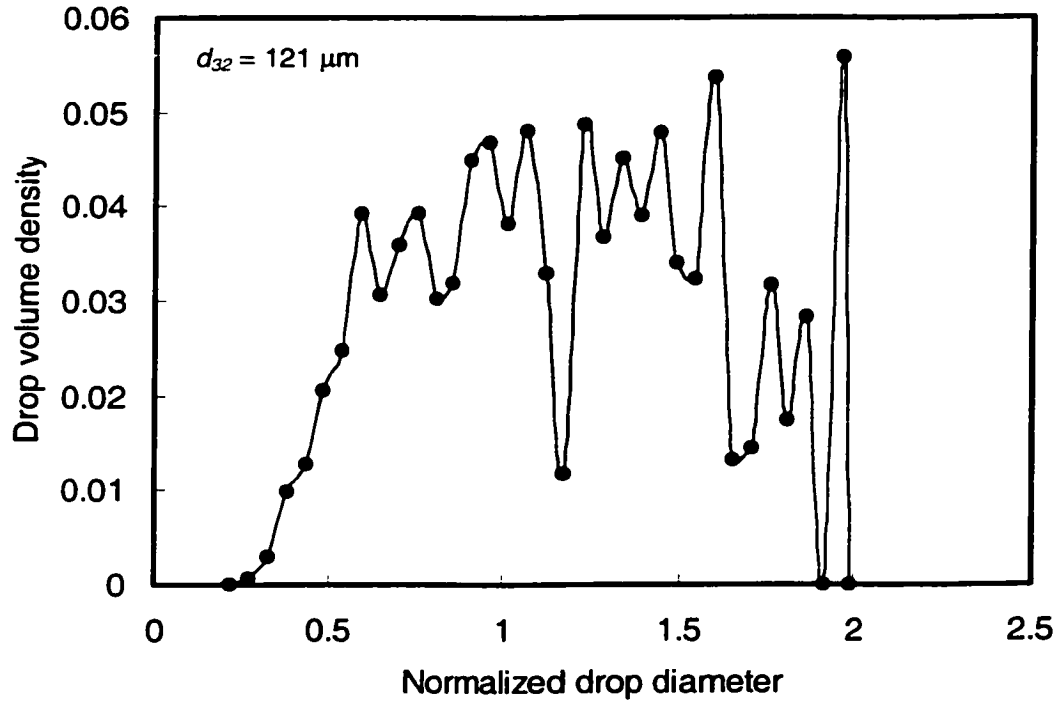


Figure B43. Drop volume density distribution
 ($\alpha = 0.27$, $\phi = 4\%$, $U = 0.60 \text{ m/s}$, 9 screens, $L = 10\text{mm}$).

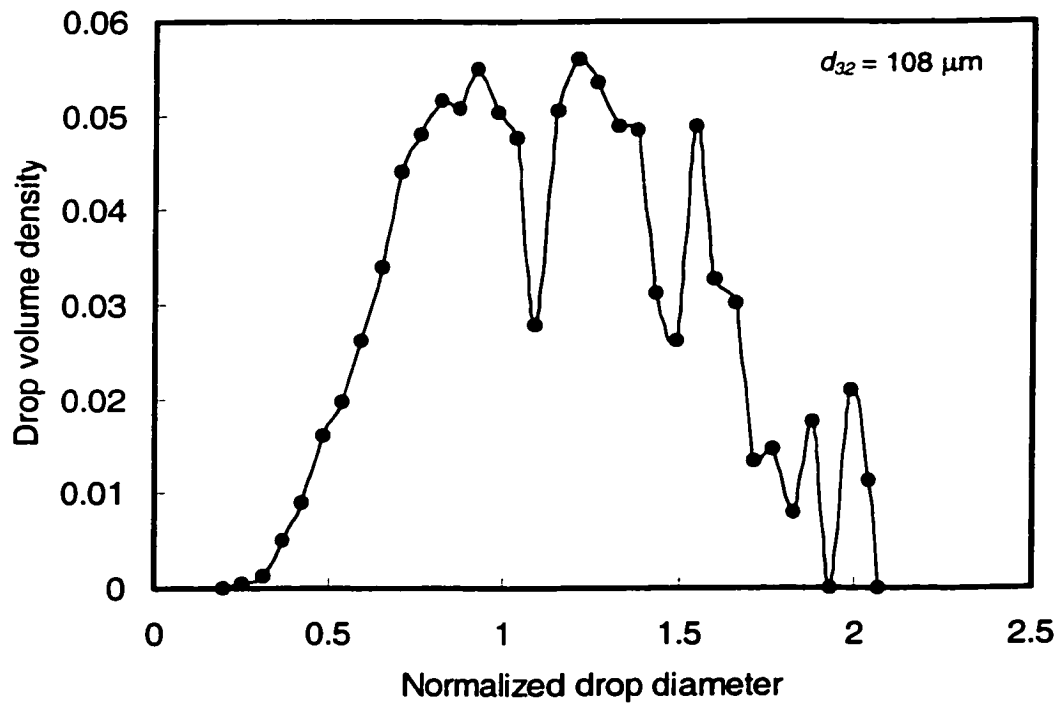


Figure B44. Drop volume density distribution
 ($\alpha = 0.27$, $\phi = 4\%$, $U = 0.65 \text{ m/s}$, 9 screens, $L = 10\text{mm}$).

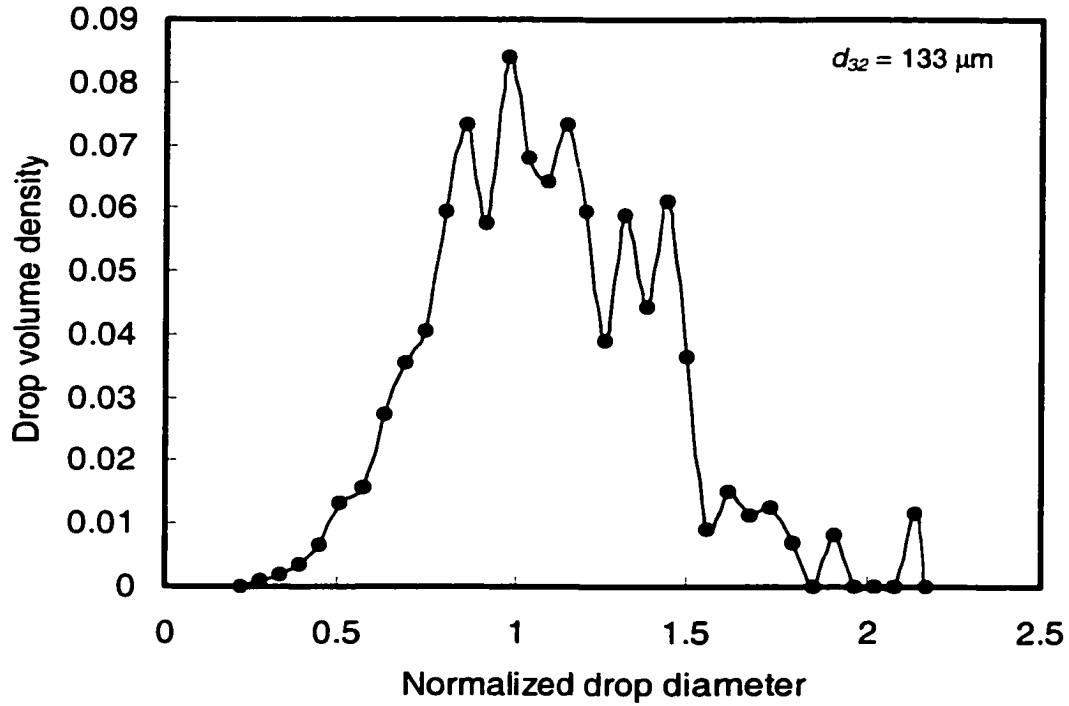


Figure B45. Drop volume density distribution
 ($\alpha = 0.27$, $\phi = 4\%$, $U = 0.70 \text{ m/s}$, 9 screens, $L = 10\text{mm}$).

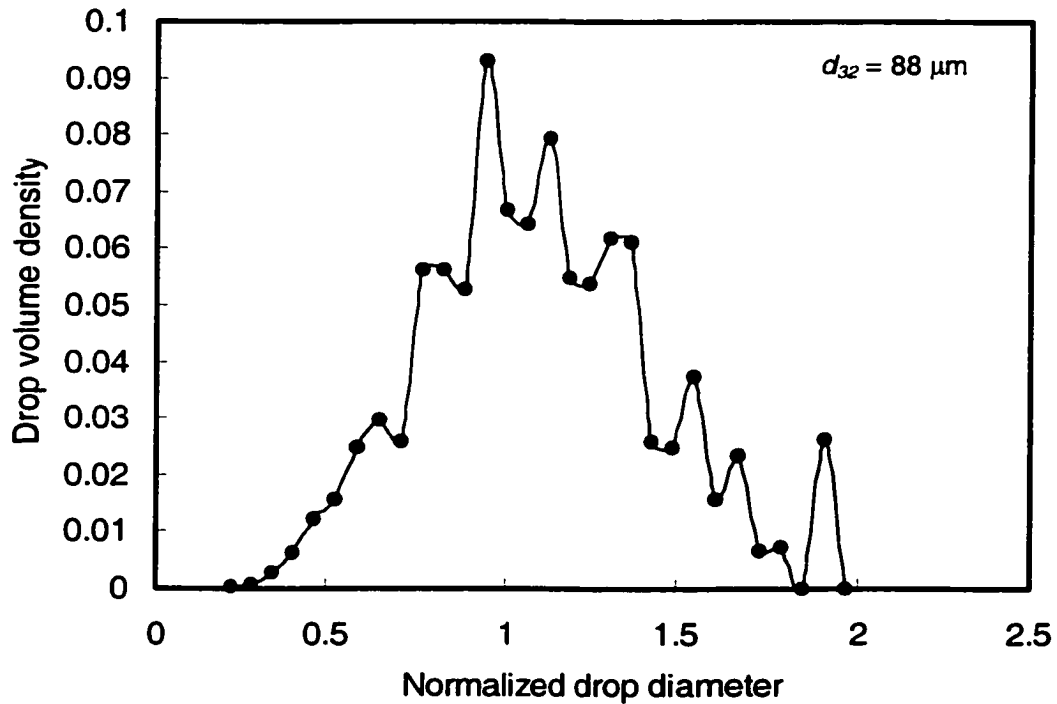


Figure B46. Drop volume density distribution
 ($\alpha = 0.27$, $\phi = 4\%$, $U = 0.97 \text{ m/s}$, 9 screens, $L = 10\text{mm}$).

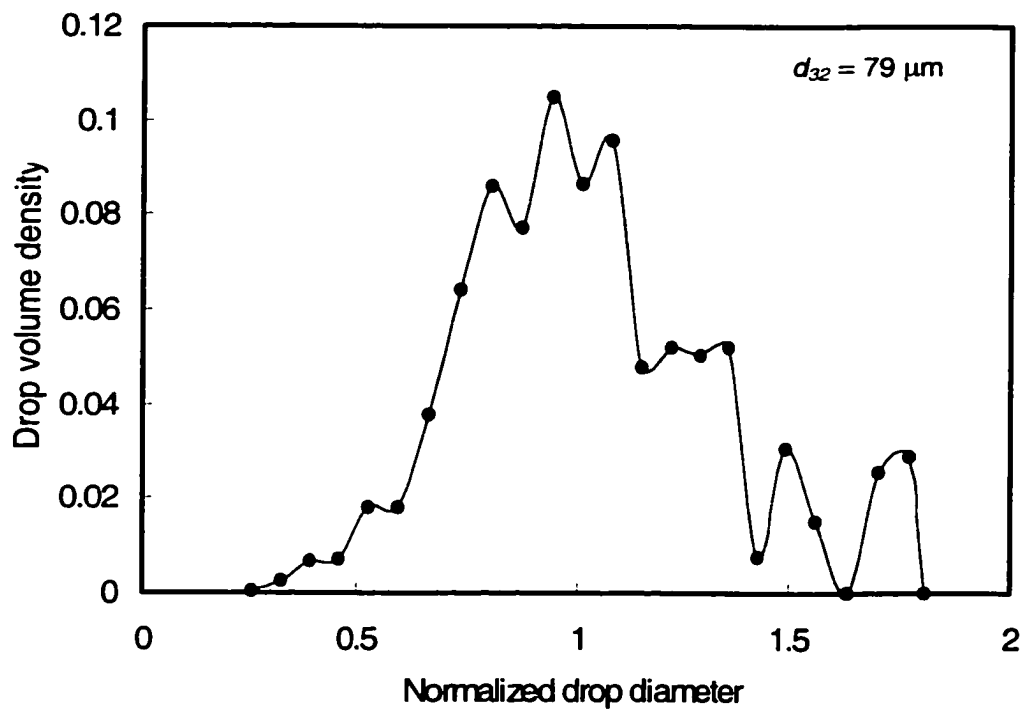


Figure B47. Drop volume density distribution
 ($\alpha = 0.27$, $\phi = 4\%$, $U = 1.55$ m/s, 9 screens, $L = 10$ mm).

Effect of dispersed phase volume fraction

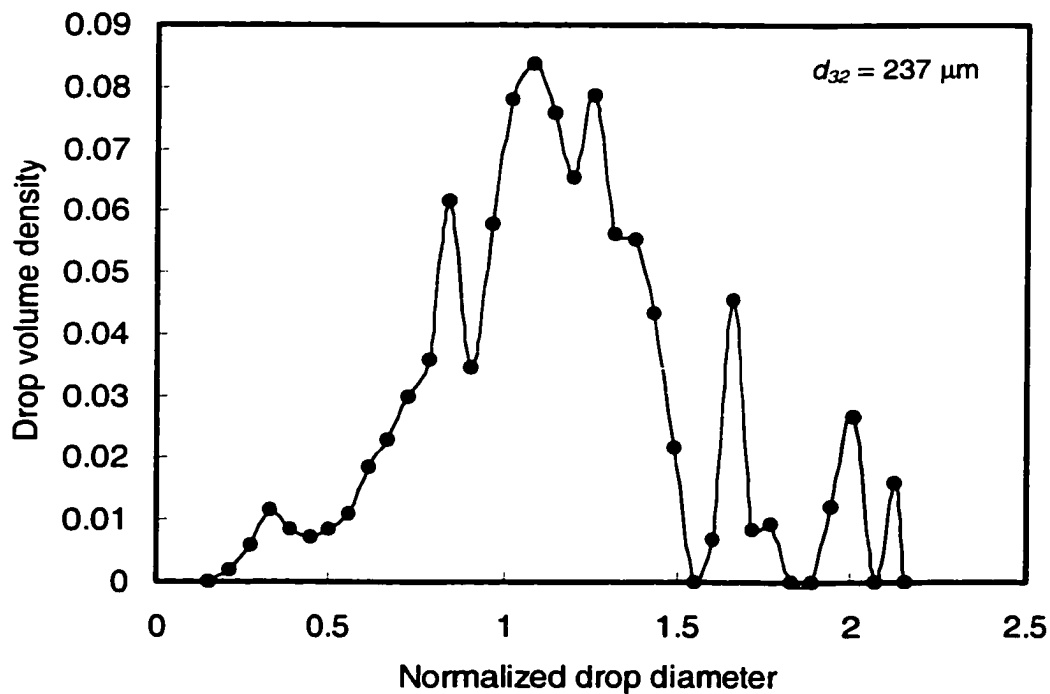


Figure B48. Drop volume density distribution
 ($\alpha = 0.41$, $\phi = 1\%$, $U = 0.40$ m/s, 9 screens, $L = 10$ mm).

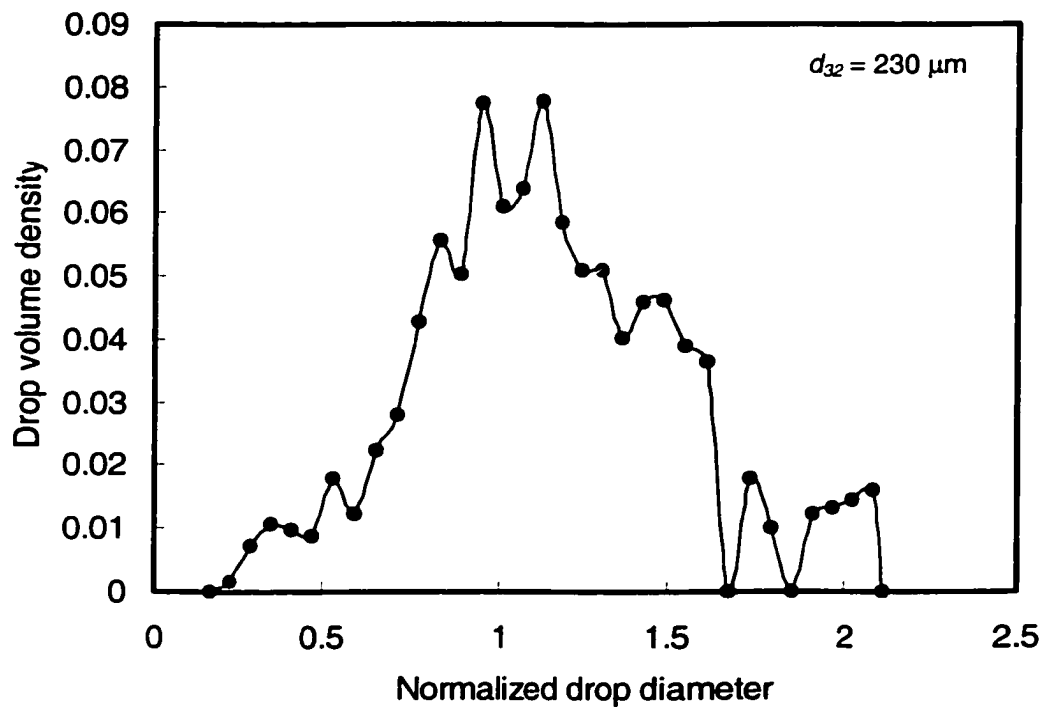


Figure B49. Drop volume density distribution
 $(\alpha = 0.41, \phi = 2\%, U = 0.40 \text{ m/s}, 9 \text{ screens}, L = 10\text{mm})$.

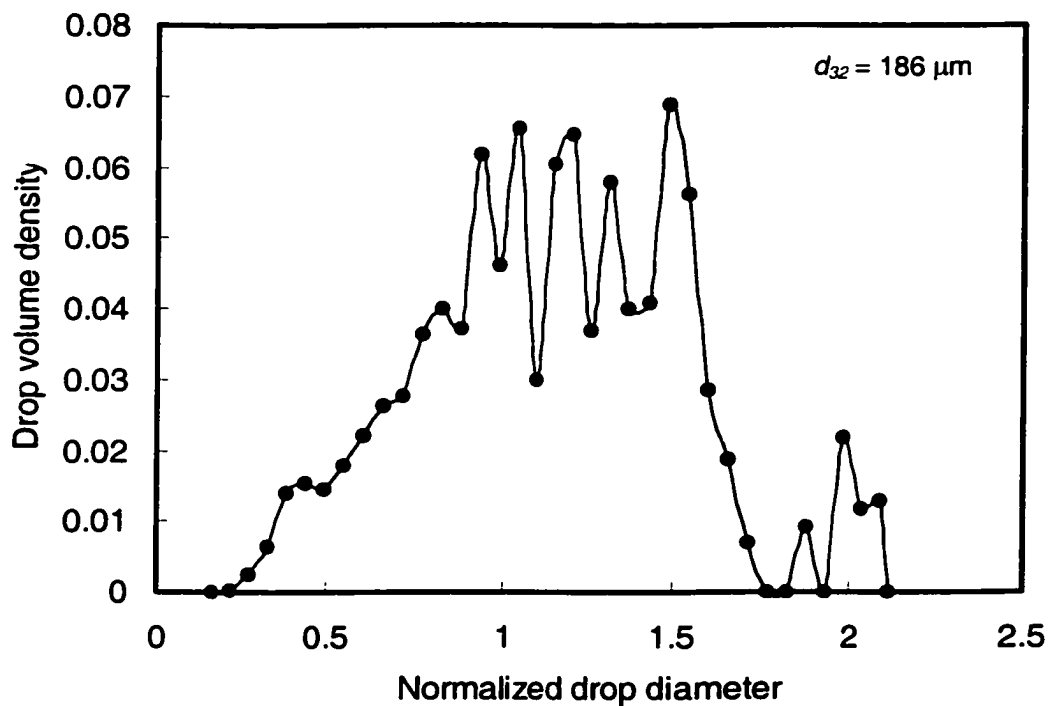


Figure B50. Drop volume density distribution
 $(\alpha = 0.41, \phi = 3\%, U = 0.40 \text{ m/s}, 9 \text{ screens}, L = 10\text{mm})$.

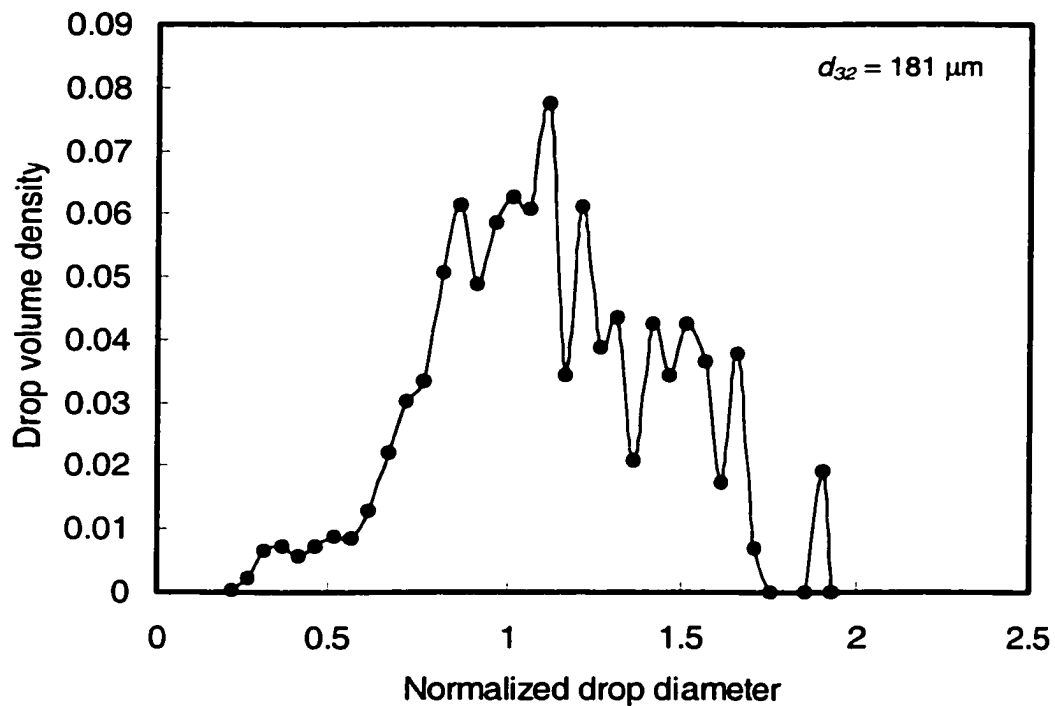


Figure B51. Drop volume density distribution
($\alpha = 0.41$, $\phi = 1\%$, $U = 0.70$ m/s, 9 screens, $L = 10$ mm).

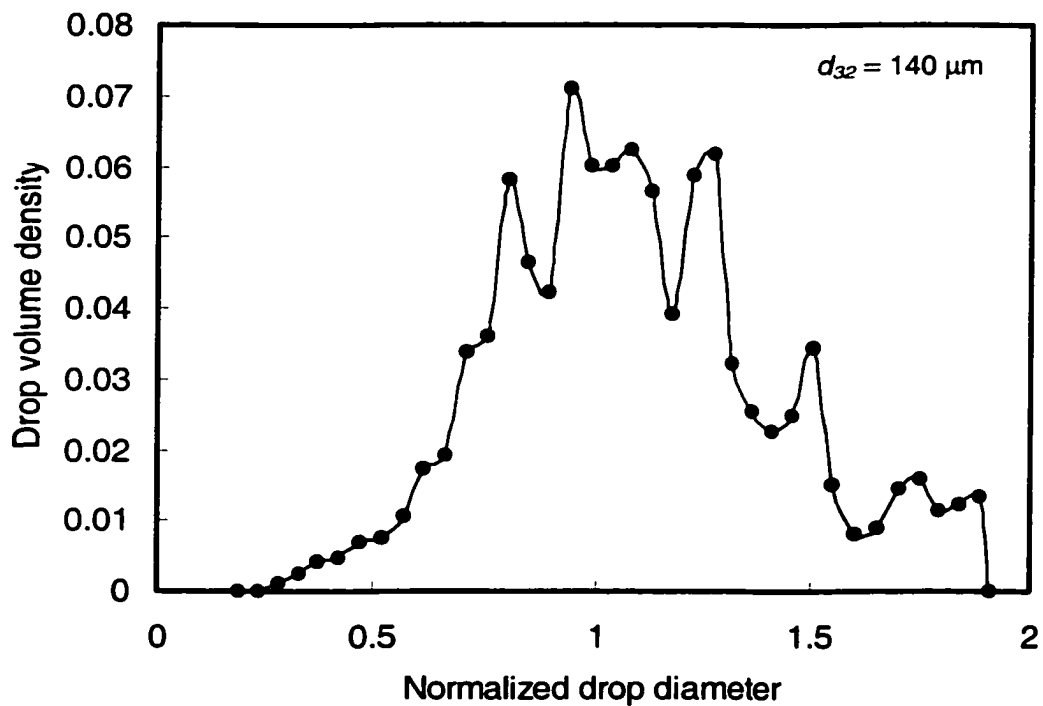


Figure B52. Drop volume density distribution
($\alpha = 0.41$, $\phi = 2\%$, $U = 0.70$ m/s, 9 screens, $L = 10$ mm).

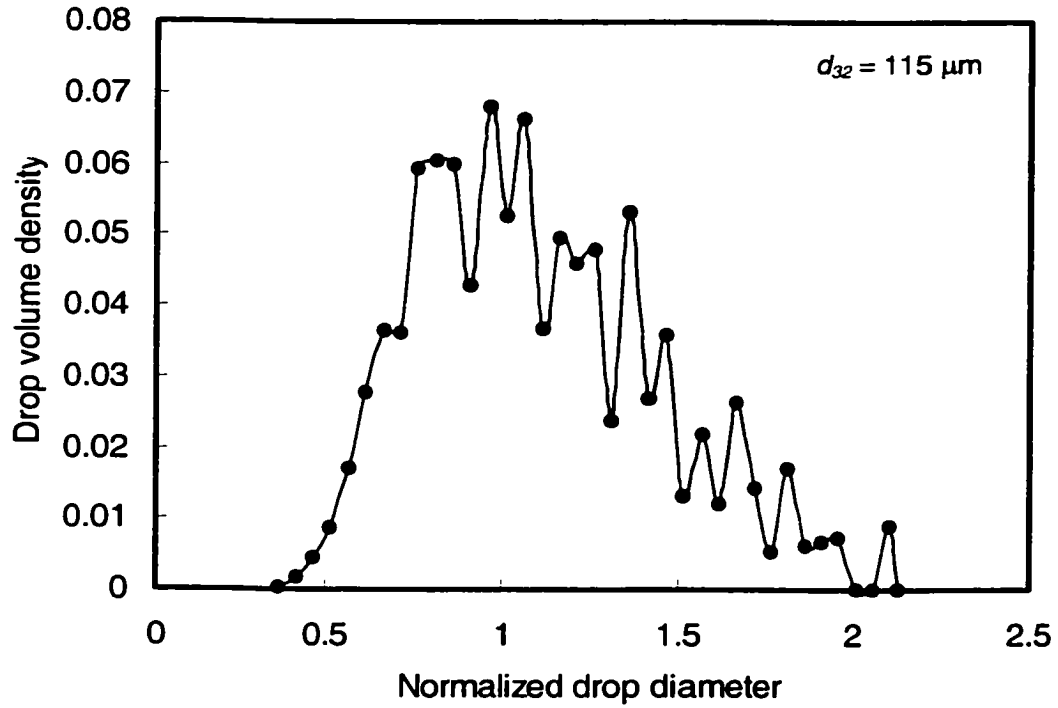


Figure B53. Drop volume density distribution
 $(\alpha = 0.41, \phi = 3\%, U = 0.70 \text{ m/s}, 9 \text{ screens}, L = 10\text{mm})$.

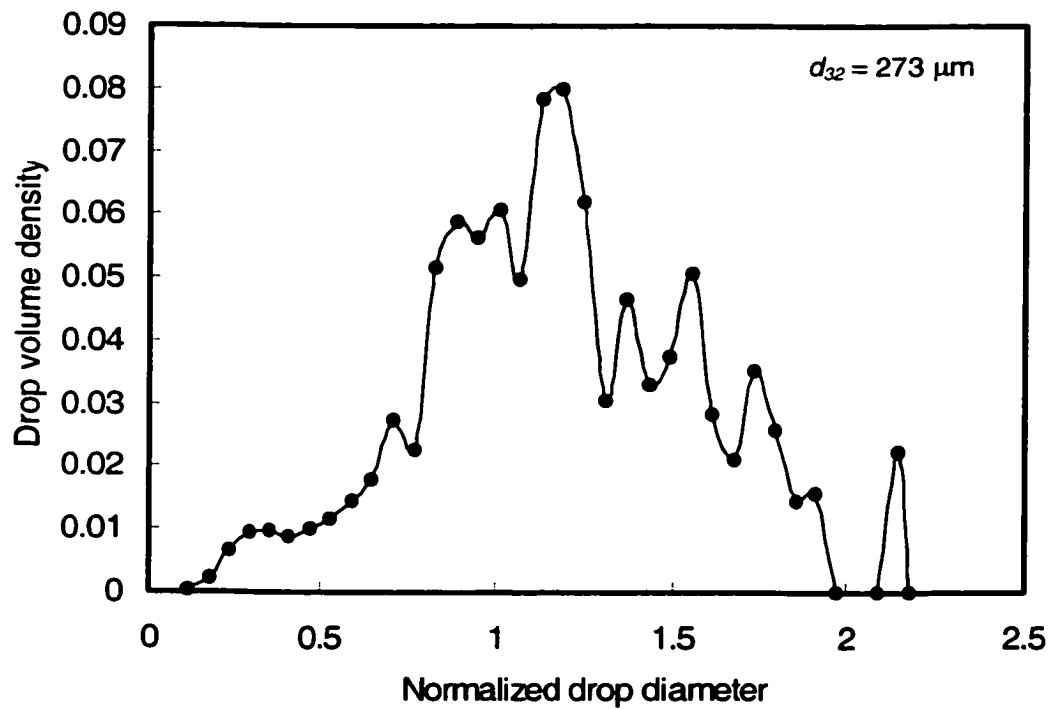


Figure B54. Drop volume density distribution
 $(\alpha = 0.27, \phi = 1\%, U = 0.40 \text{ m/s}, 9 \text{ screens}, L = 10\text{mm})$.

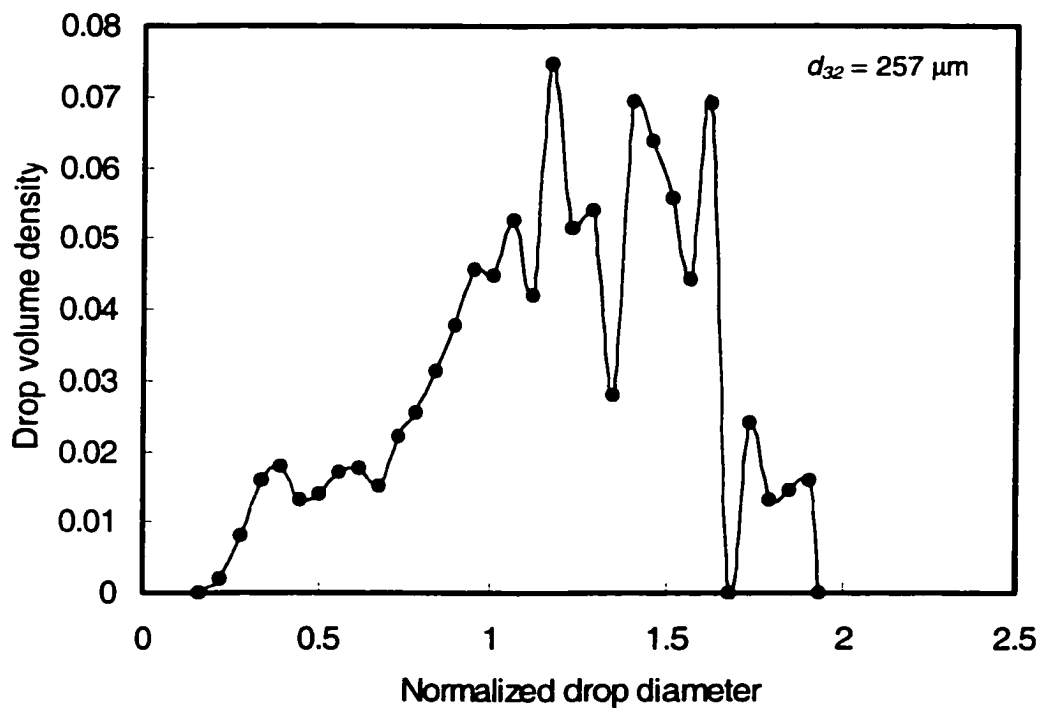


Figure B55. Drop volume density distribution
 ($\alpha = 0.27$, $\phi = 2\%$, $U = 0.40$ m/s, 9 screens, $L = 10$ mm).

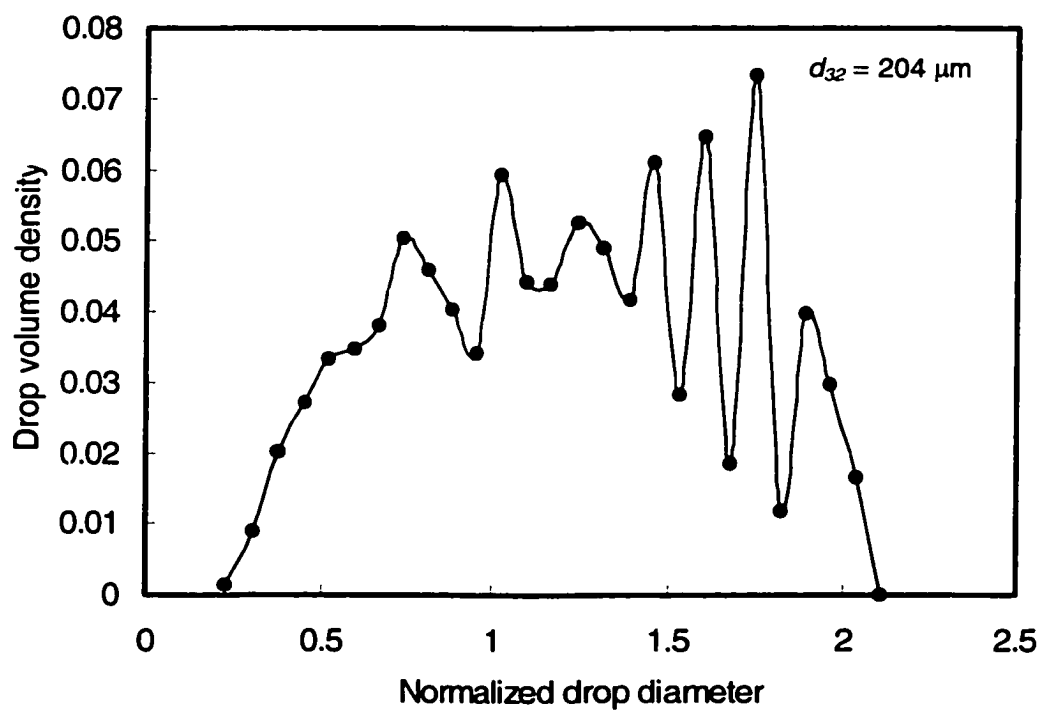


Figure B56. Drop volume density distribution
 ($\alpha = 0.27$, $\phi = 3\%$, $U = 0.40$ m/s, 9 screens, $L = 10$ mm).

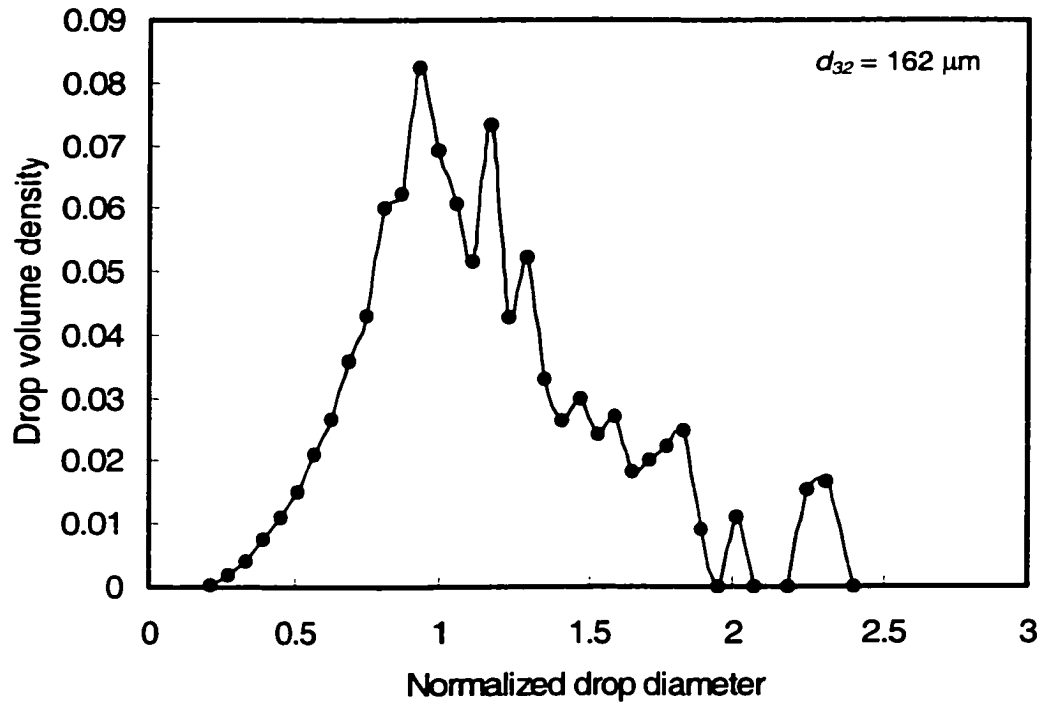


Figure B57. Drop volume density distribution
 ($\alpha = 0.27$, $\phi = 1\%$, $U = 0.70$ m/s, 9 screens, $L = 10$ mm).

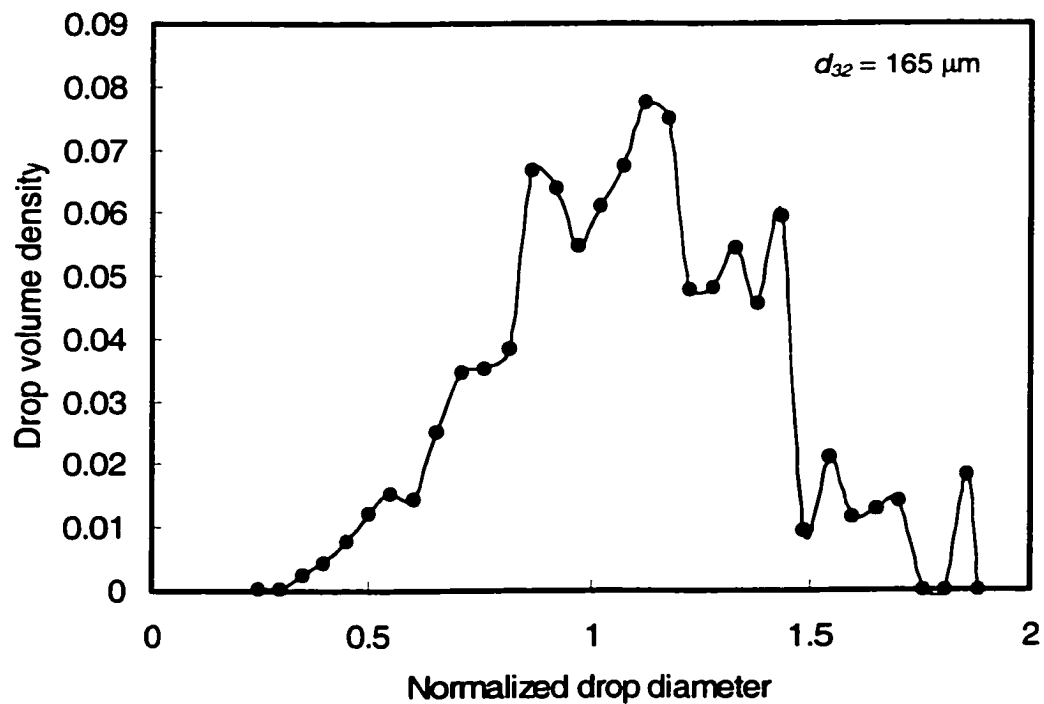


Figure B58. Drop volume density distribution
 ($\alpha = 0.27$, $\phi = 2\%$, $U = 0.70$ m/s, 9 screens, $L = 10$ mm).

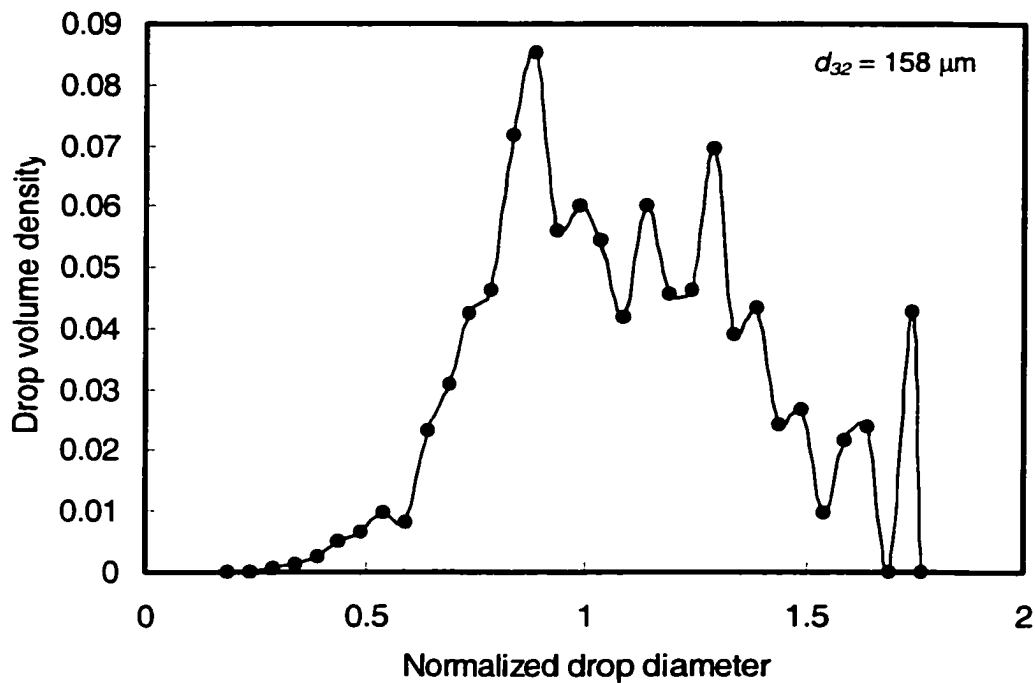


Figure B59. Drop volume density distribution
 ($\alpha = 0.27$, $\phi = 3\%$, $U = 0.70$ m/s, 9 screens, $L = 10$ mm).

Effect of Number of Elements

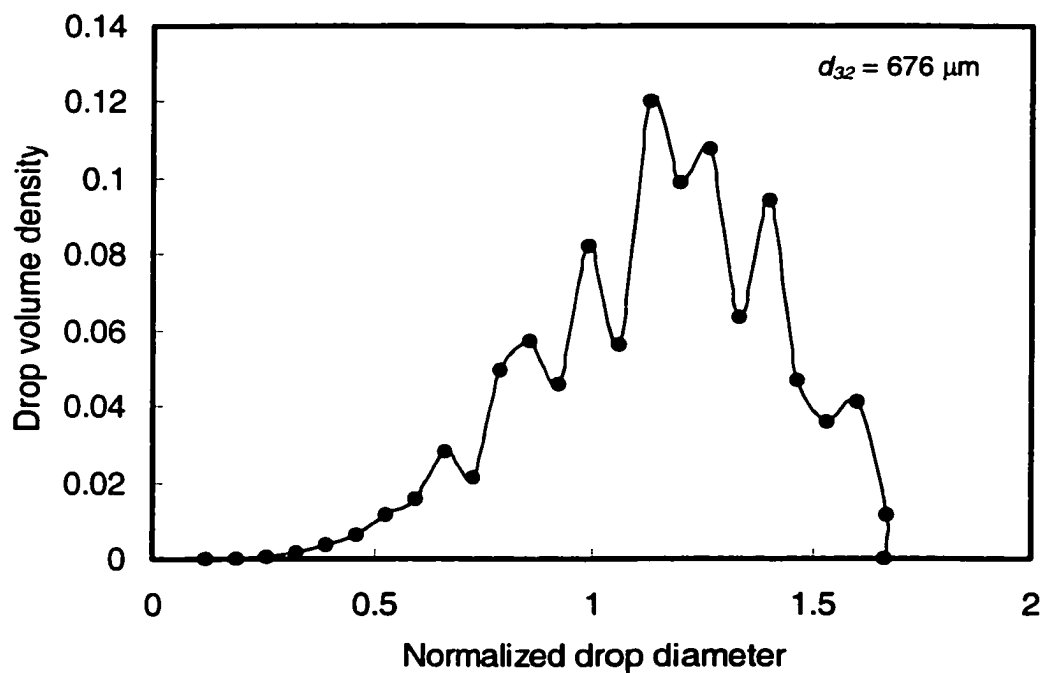


Figure B60. Drop volume density distribution
 ($\alpha = 0.27$, $\phi = 2\%$, $U = 0.40$ m/s, 2 screens, $L = 5$ mm).

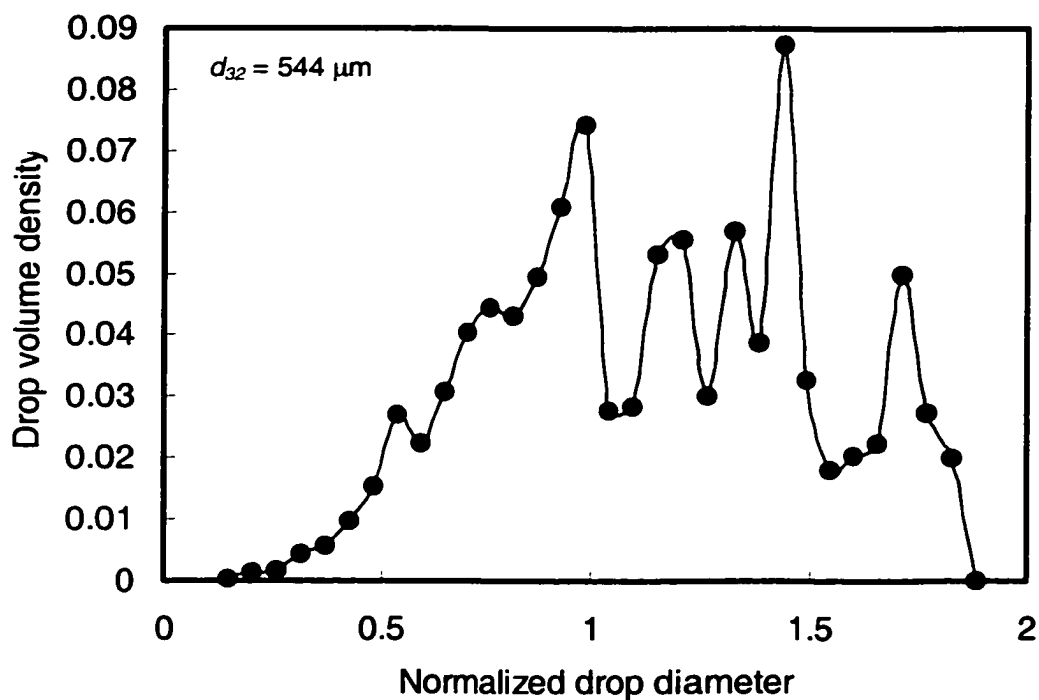


Figure B61. Drop volume density distribution
 ($\alpha = 0.27$, $\phi = 2\%$, $U = 0.40$ m/s, 3 screens, $L = 5$ mm).

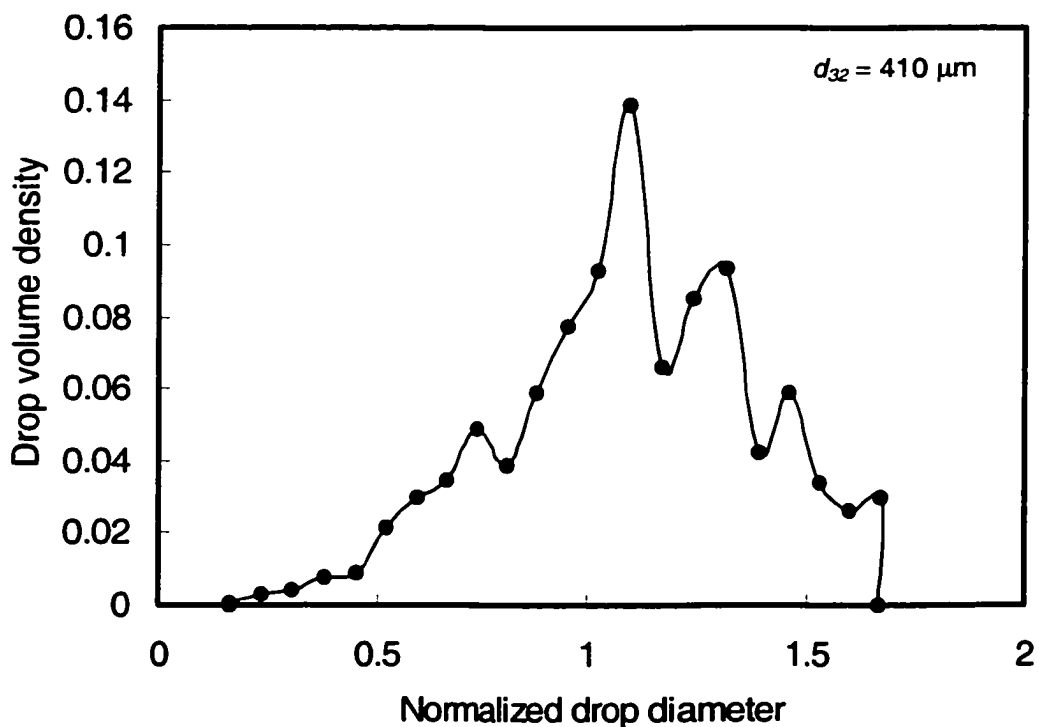


Figure B62. Drop volume density distribution
 ($\alpha = 0.27$, $\phi = 2\%$, $U = 0.40$ m/s, 4 screens, $L = 5$ mm).

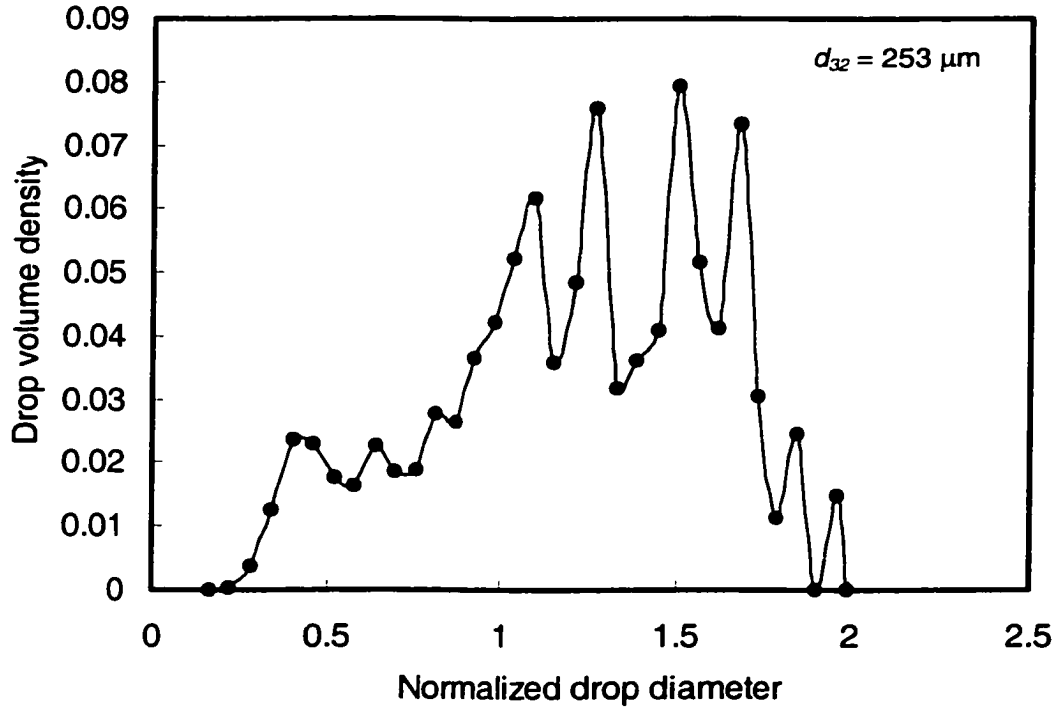


Figure B63. Drop volume density distribution
 ($\alpha = 0.27$, $\phi = 2\%$, $U = 0.40 \text{ m/s}$, 9 screens, $L = 5 \text{ mm}$).

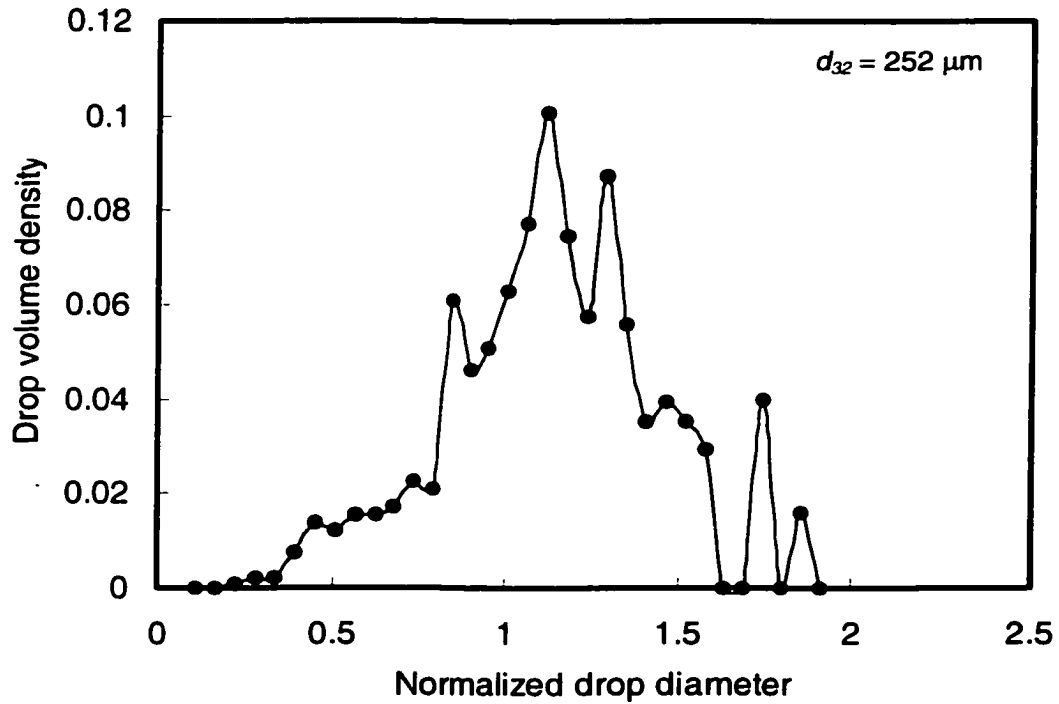


Figure B64. Drop volume density distribution
 ($\alpha = 0.27$, $\phi = 2\%$, $U = 0.40 \text{ m/s}$, 12 screens, $L = 5 \text{ mm}$).

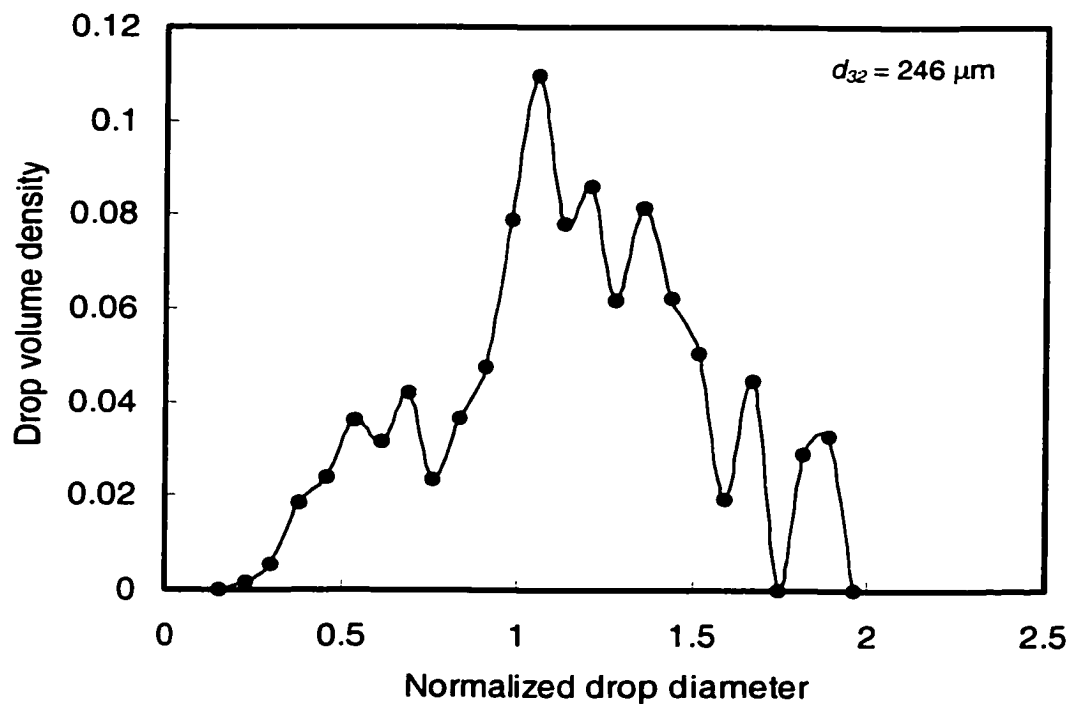


Figure B65. Drop volume density distribution
 $(\alpha = 0.27, \phi = 2\%, U = 0.40 \text{ m/s}, 15 \text{ screens}, L = 5 \text{ mm})$.

Effect of Surfactant Triton X100

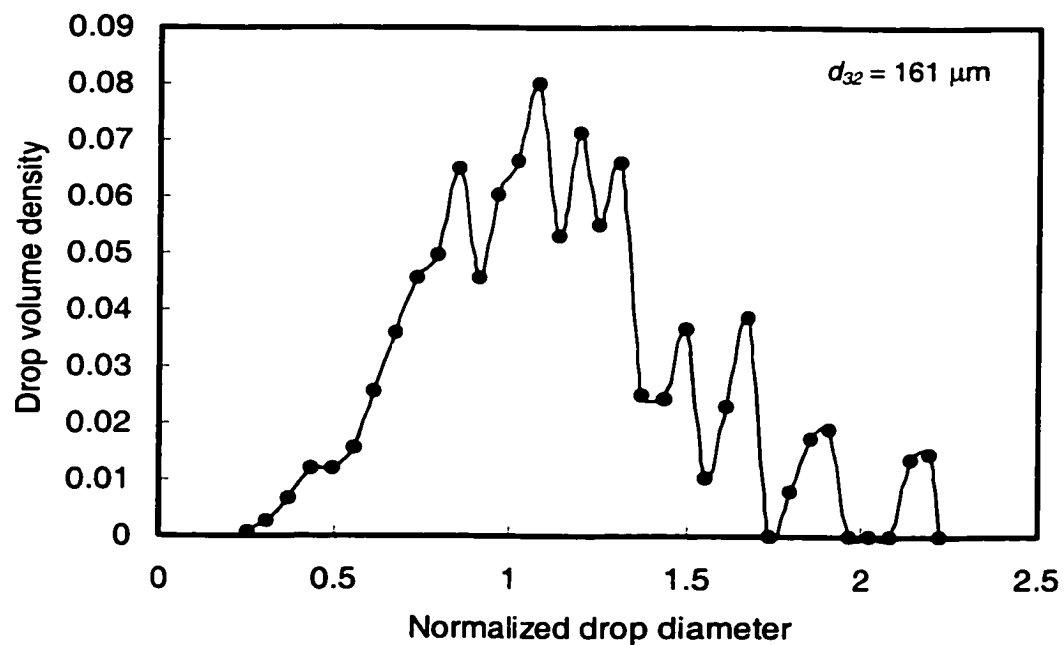


Figure B66. Drop number density distribution with SAA
 $(\alpha = 0.27, \phi = 0.5\%, U = 0.70 \text{ m/s}, c = 0.01 \text{ mole/m}^3, 9 \text{ screens}, L = 10\text{mm})$.

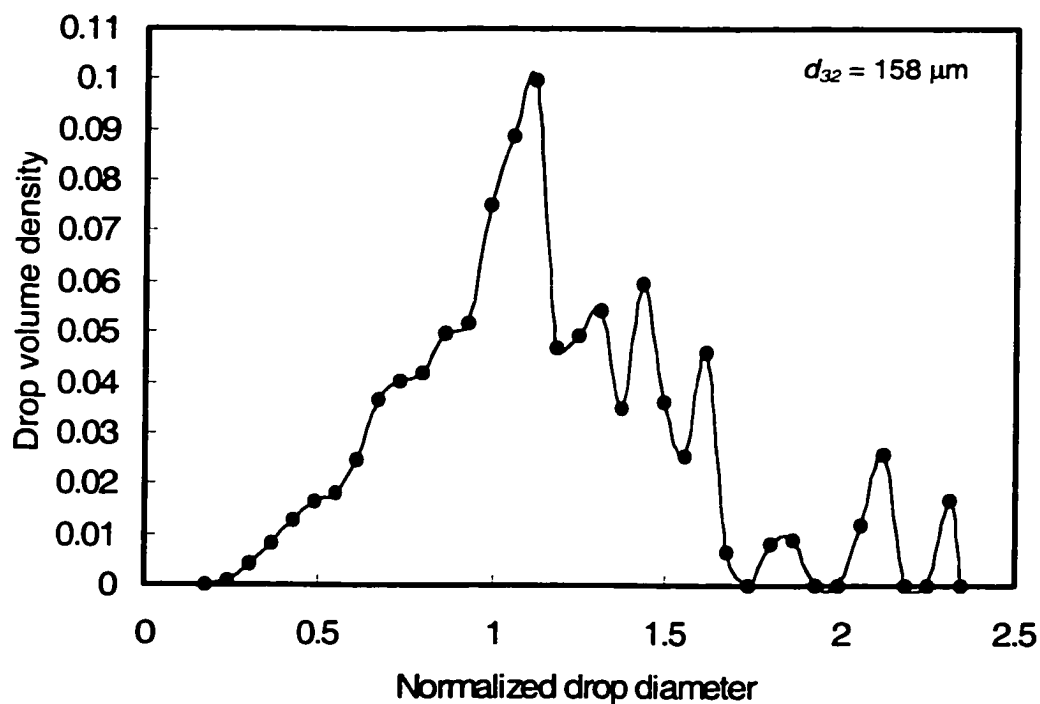


Figure B67. Drop number density distribution with SAA
 ($\alpha = 0.27$, $\phi = 0.5\%$, $U = 0.70 \text{ m/s}$, $c = 0.05 \text{ mole/m}^3$, 9 screens, $L = 10\text{mm}$).

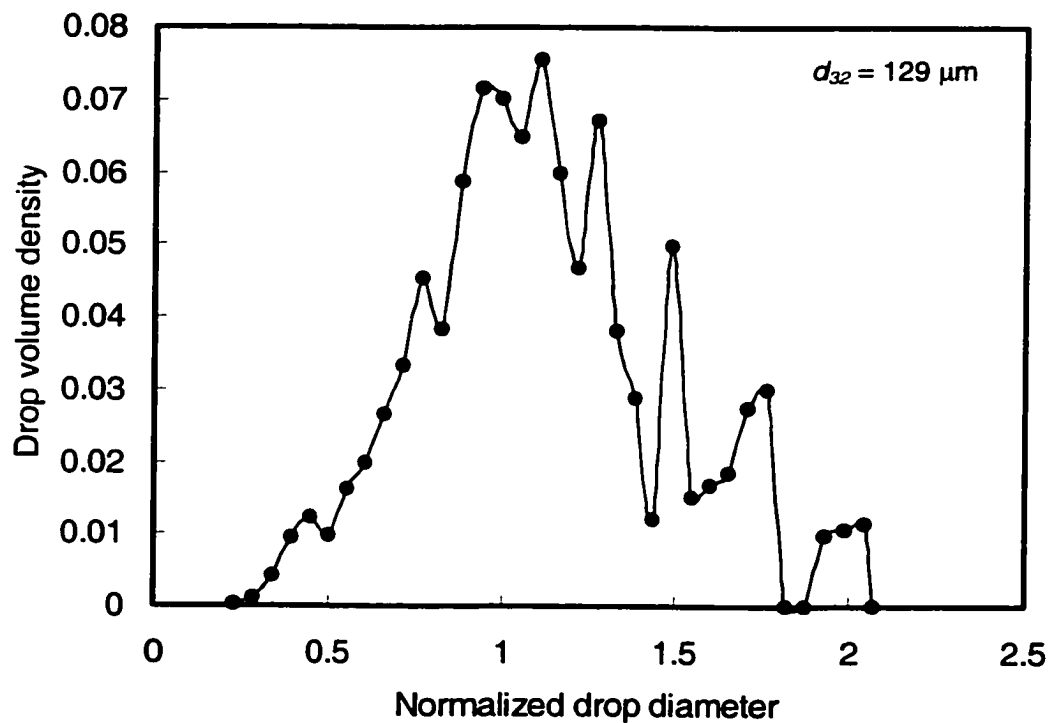


Figure B68. Drop number density distribution with SAA
 ($\alpha = 0.27$, $\phi = 0.5\%$, $U = 0.70 \text{ m/s}$, $c = 0.10 \text{ mole/m}^3$, 9 screens, $L = 10\text{mm}$).

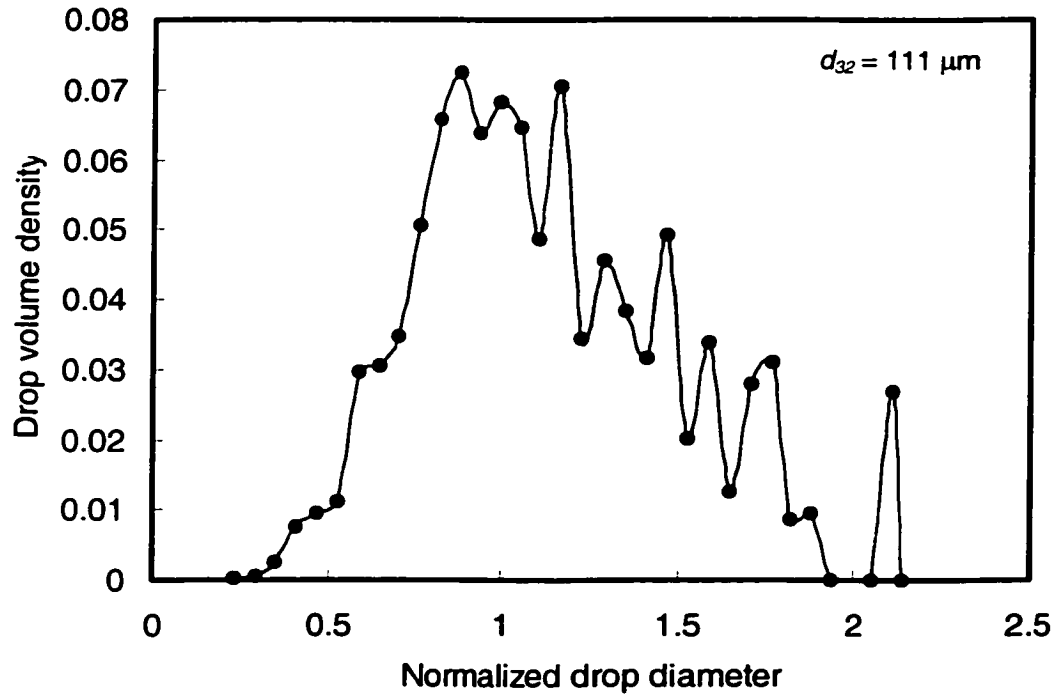


Figure B69. Drop number density distribution with SAA
 ($\alpha = 0.27$, $\phi = 0.5\%$, $U = 0.70$ m/s, $c = 0.20$ mole/m³, 9 screens, $L = 10$ mm).

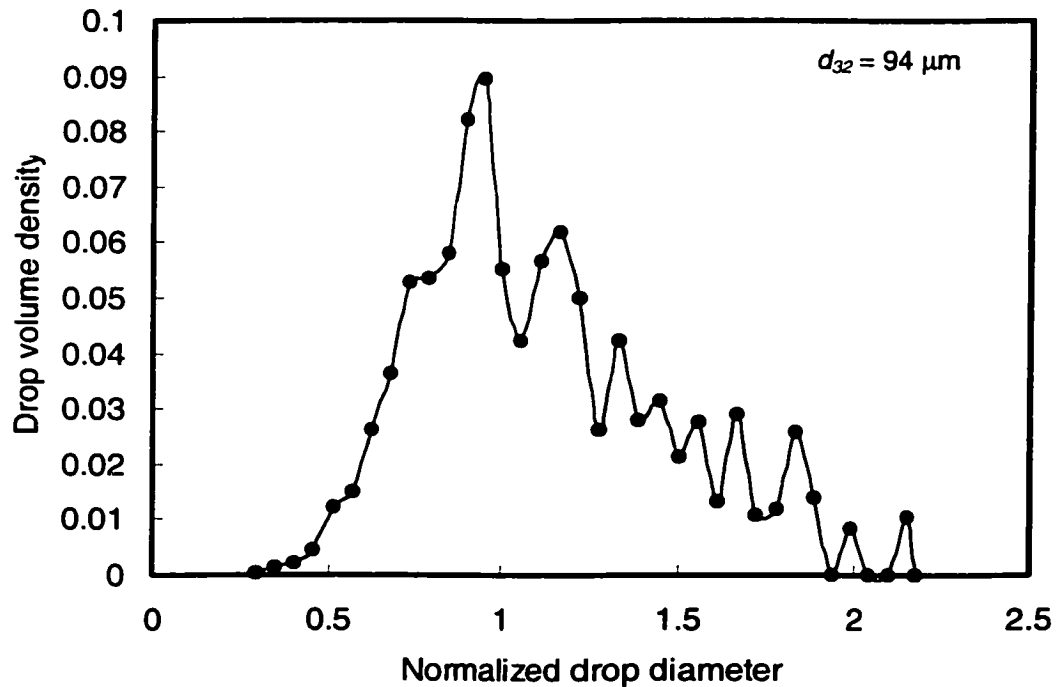


Figure B70. Drop number density distribution with SAA
 ($\alpha = 0.27$, $\phi = 0.5\%$, $U = 0.70$ m/s, $c = 0.30$ mole/m³, 9 screens, $L = 10$ mm).

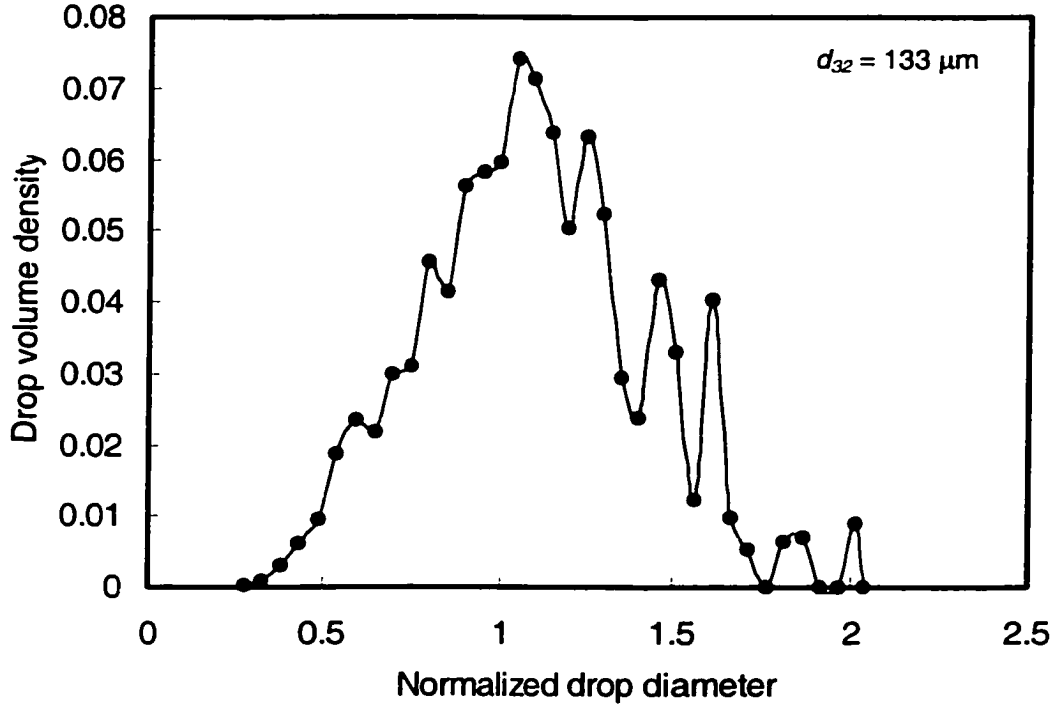


Figure B71. Drop number density distribution with SAA ($\alpha = 0.27$, $\phi = 4\%$, $U = 0.70 \text{ m/s}$, $c = 0.01 \text{ mole/m}^3$, 9 screens, $L = 10\text{mm}$).

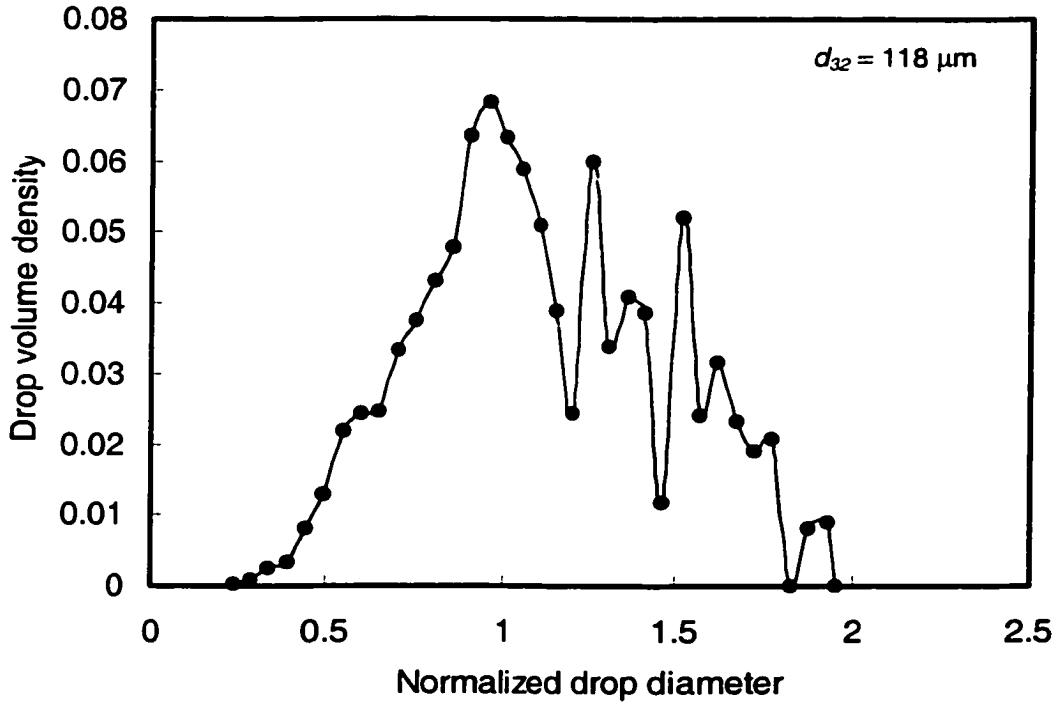


Figure B72. Drop number density distribution with SAA ($\alpha = 0.27$, $\phi = 4\%$, $U = 0.70 \text{ m/s}$, $c = 0.05 \text{ mole/m}^3$, 9 screens, $L = 10\text{mm}$).

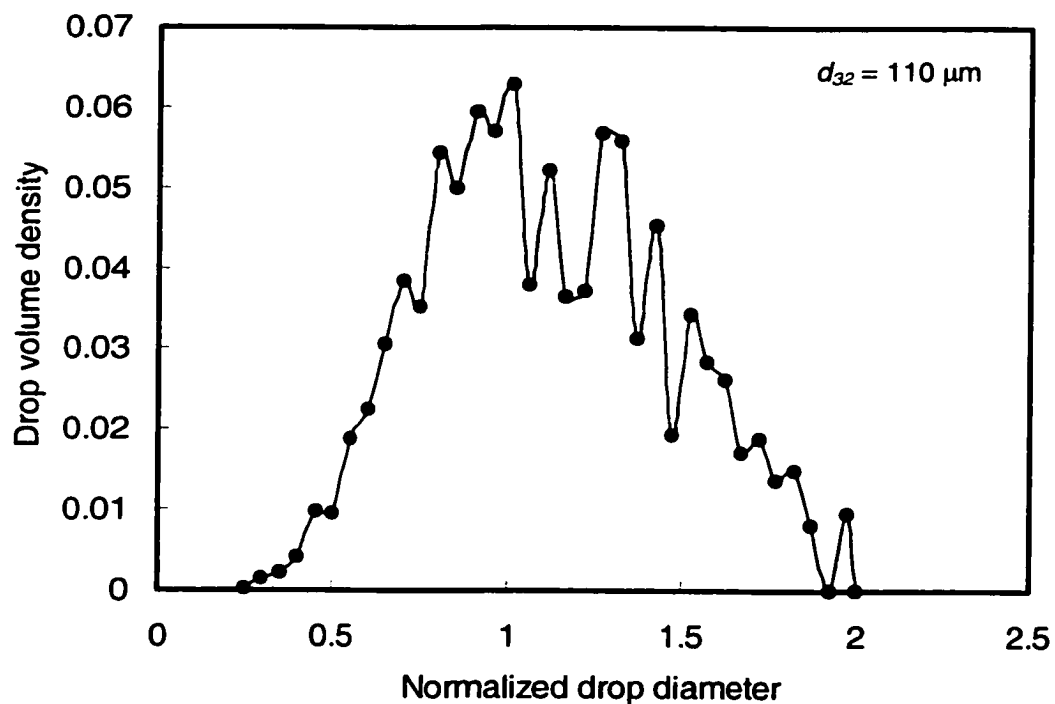


Figure B73. Drop number density distribution with SAA
 ($\alpha = 0.27$, $\phi = 4\%$, $U = 0.70$ m/s, $c = 0.10$ mole/m³, 9 screens, $L = 10$ mm).

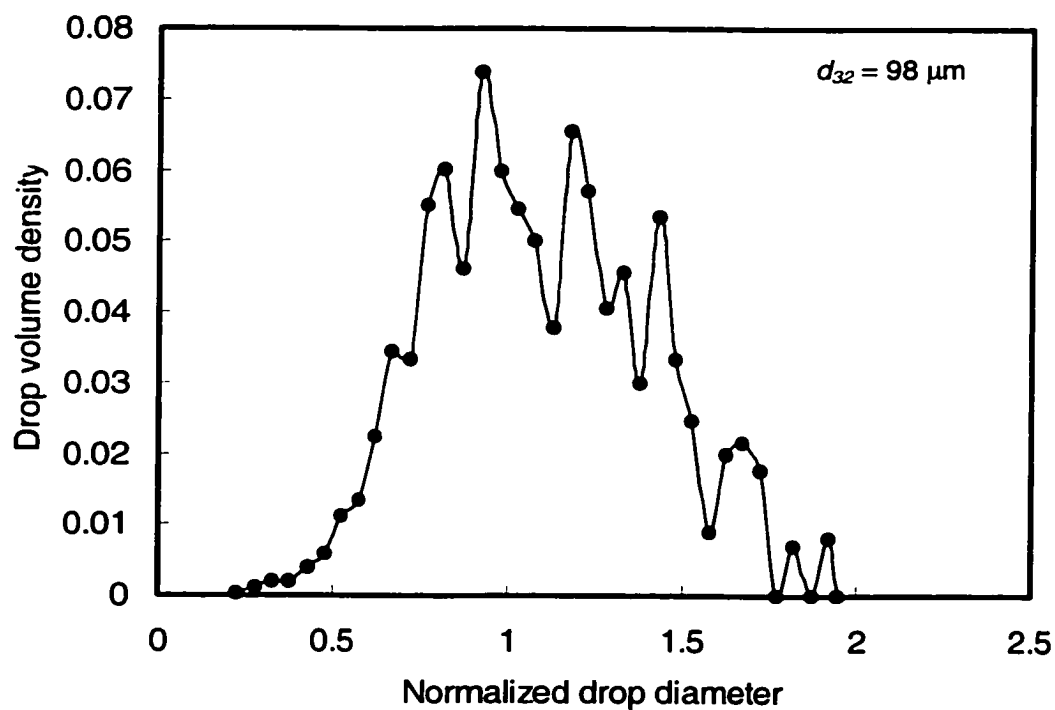


Figure B74. Drop number density distribution
 ($\alpha = 0.27$, $\phi = 4\%$, $U = 0.70$ m/s, $c = 0.20$ mole/m³, 9 screens, $L = 10$ mm).

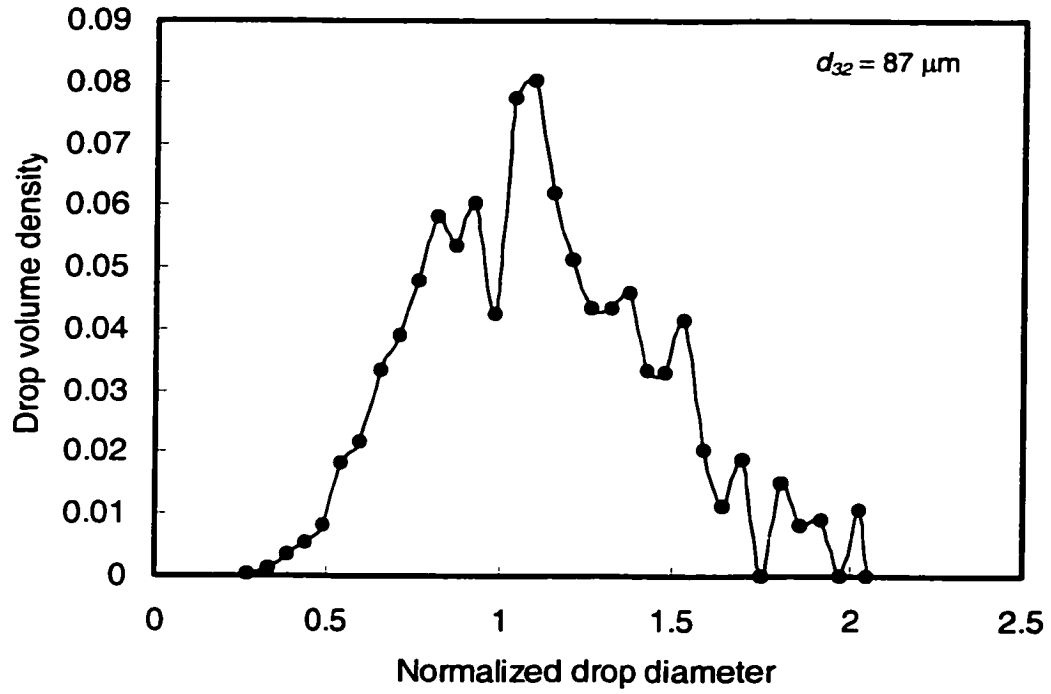


Figure B75. Drop number density distribution with SAA ($\alpha = 0.27$, $\phi = 4\%$, $U = 0.70$ m/s, $c = 0.30$ mole/m³, 9 screens, $L = 10$ mm).

Appendix C: Analytical Solution of Population Balance Equation Presented by Rod and Misk

Rod and Misk presented the following differential equation:

$$\frac{\partial d_{32}}{\partial t} = \frac{\Gamma(p+2)}{3} K_d d_{32}^{3p-2} (d_{32\infty}^6 - d_{32}^6) \quad (\text{C-1})$$

with an initial condition

$$d_{32}(t)|_{t=0} = d_{320} \quad (\text{C-2})$$

For $p = 0$ Equation (C-1) becomes,

$$\frac{\partial d_{32}}{\partial t} = \frac{1}{3} K_d d_{32}^{-2} (d_{32\infty}^6 - d_{32}^6) \quad (\text{C-3})$$

Integrate Equation (C-3)

$$\int \frac{d_{32}^2 d(d_{32})}{d_{32}^6 - d_{32\infty}^6} = -\frac{1}{3} K_d t + c \quad (\text{C-4})$$

Let $u = d_{32}^3$ and $b = d_{32\infty}^3$ so Equation (C-4) becomes

$$\frac{1}{3} \int \frac{du}{u^2 - b^2} = -\frac{1}{3} K_d t \quad (\text{C-5})$$

Integrate L.H.S. of Equation (C-5)

$$\frac{1}{3} \int \frac{du}{u^2 - b^2} = \frac{1}{6b} \ln \frac{u-b}{u+b} \quad (\text{C-6})$$

Substitute the values of u and b in Equation (C-6)

$$\frac{1}{3} \int \frac{du}{u^2 - b^2} = \frac{1}{6d_{32\infty}^3} \ln \frac{d_{32}^3 - d_{32\infty}^3}{d_{32}^3 + d_{32\infty}^3} \quad (\text{C-7})$$

Applying the initial condition and combining Equations (C-7) and (C-5) gives

$$\frac{d_{32}^3 - d_{32\infty}^3}{d_{32}^3 + d_{32\infty}^3} = A \exp(-2K_d d_{32\infty}^3 t) \quad (\text{C-8})$$

Rearrange

$$d_{32}(t) = d_{32\infty} \left[\frac{1 + A \exp(-2K_d d_{32\infty}^3 t)}{1 - A \exp(-2K_d d_{32\infty}^3 t)} \right]^{1/3} \quad (\text{C-9})$$

where

$$A = \frac{d_{320}^3 - d_{32\infty}^3}{d_{320}^3 + d_{32\infty}^3} \quad (\text{C-10})$$

For $p = 1$ the original differential equation becomes

$$\frac{\partial d_{32}}{\partial t} = \frac{2}{3} K_d d_{32} (d_{32\infty}^6 - d_{32}^6) \quad (\text{C-11})$$

In a similar fashion as before, the integral of Equation (C-11) is as follows

$$\int \frac{d(d_{32})}{d_{32} (d_{32}^6 - d_{32\infty}^6)} = -\frac{2}{3} K_d t + c \quad (\text{C-12})$$

Integrating Equation (C-12)

$$\frac{1}{6d_{32\infty}^6} \ln \frac{d_{32}^6}{d_{32}^6 - d_{32\infty}^6} = -\frac{2}{3} K_d t + c \quad (\text{C-13})$$

Applying the initial condition gives

$$\frac{d_{32}^6}{d_{32}^6 - d_{32\infty}^6} = \frac{d_{320}^6}{d_{320}^6 - d_{32\infty}^6} \exp(-4K_d d_{32\infty}^6 t) \quad (\text{C-14})$$

Rearranging Equation (C-14), then

$$d_{32}(t) = d_{32\infty} \left[\frac{\exp(-4K_d d_{32\infty}^6 t)}{\exp(-4K_d d_{32\infty}^6 t) - 1 + \left(\frac{d_{32\infty}}{d_{320}}\right)^6} \right]^{1/6} \quad (\text{C-15})$$

For $p = -1$, the original differential equation becomes

$$\frac{\partial d_{32}}{\partial t} = \frac{1}{3} K_d d_{32}^{-5} (d_{32\infty}^6 - d_{32}^6) \quad (\text{C-16})$$

Similarly

$$\int \frac{d_{32}^5 d(d_{32})}{d_{32}^6 - d_{32\infty}^6} = -\frac{1}{3} K_d t + c \quad (\text{C-17})$$

Integrating Equation (C-17) gives

$$\ln(d_{32}^6 - d_{32\infty}^6) = -2K_d t + c \quad (\text{C-18})$$

Applying the initial condition and rearranging gives

$$d_{32}(t) = \left[(d_{320}^6 - d_{32\infty}^6) \exp(-2K_d t) + d_{32\infty}^6 \right]^{1/6} \quad (\text{C-19})$$

Appendix D: Comparison of cumulative density distributions with Rod and Misk Model.

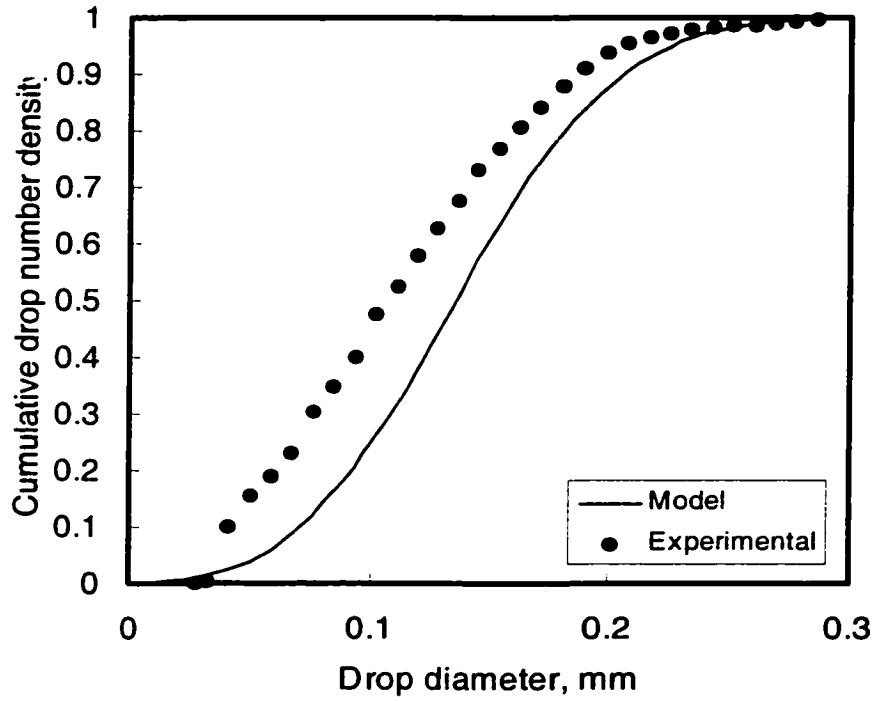


Figure D1. Cumulative drop number density distribution ($\alpha = 41\%$, $\phi = 0.5\%$, $U = 0.97$ m/s, 9 screens, $L = 10$ mm)

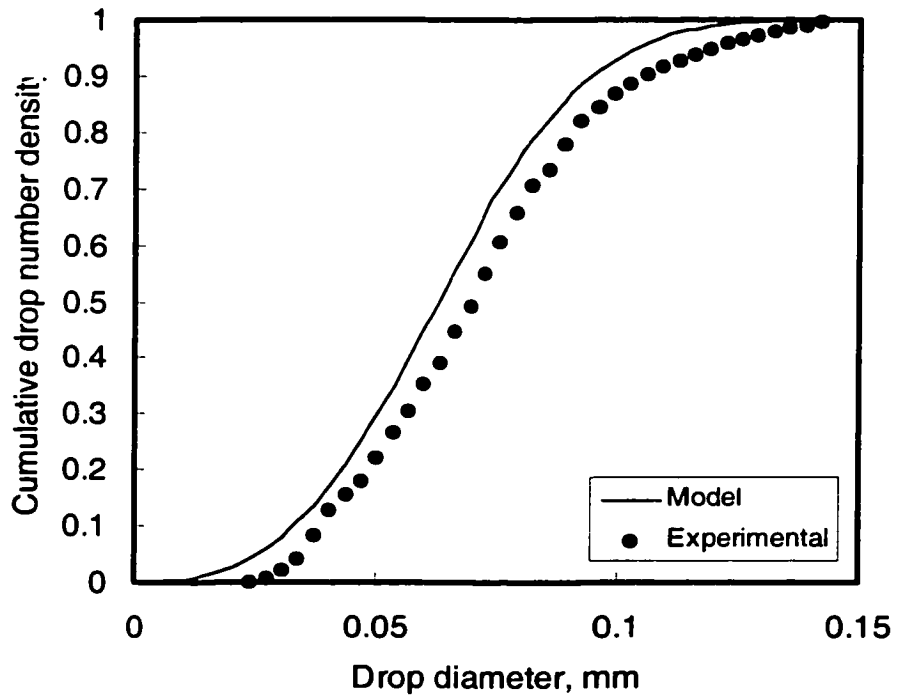


Figure D2. Cumulative drop number density distribution ($\alpha = 41\%$, $\phi = 0.5\%$, $U = 1.80$ m/s, 9 screens, $L = 10$ mm)

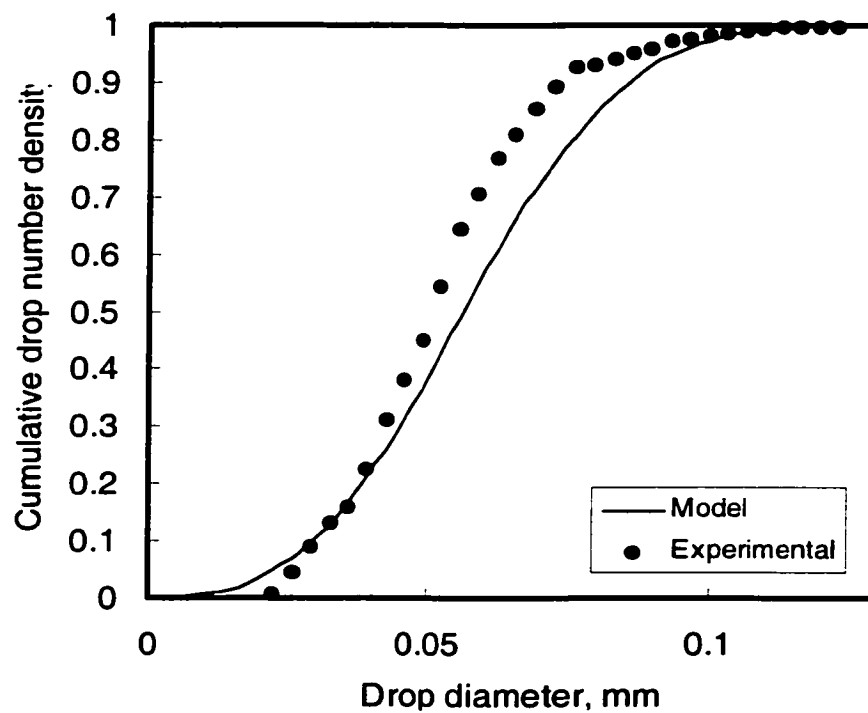


Figure D3. Cumulative drop number density distribution ($\alpha = 41\%$, $\phi = 0.5\%$, $U = 1.94$ m/s, 9 screens, $L = 10$ mm)

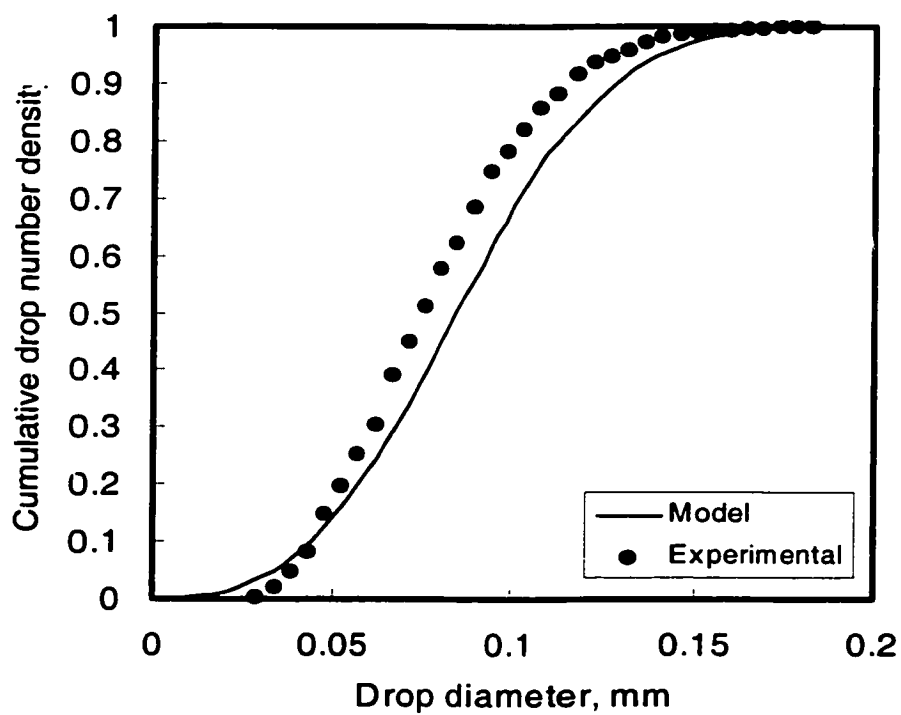


Figure D4. Cumulative drop number density distribution ($\alpha = 33\%$, $\phi = 0.5\%$, $U = 1.55$ m/s, 9 screens, $L = 10$ mm)

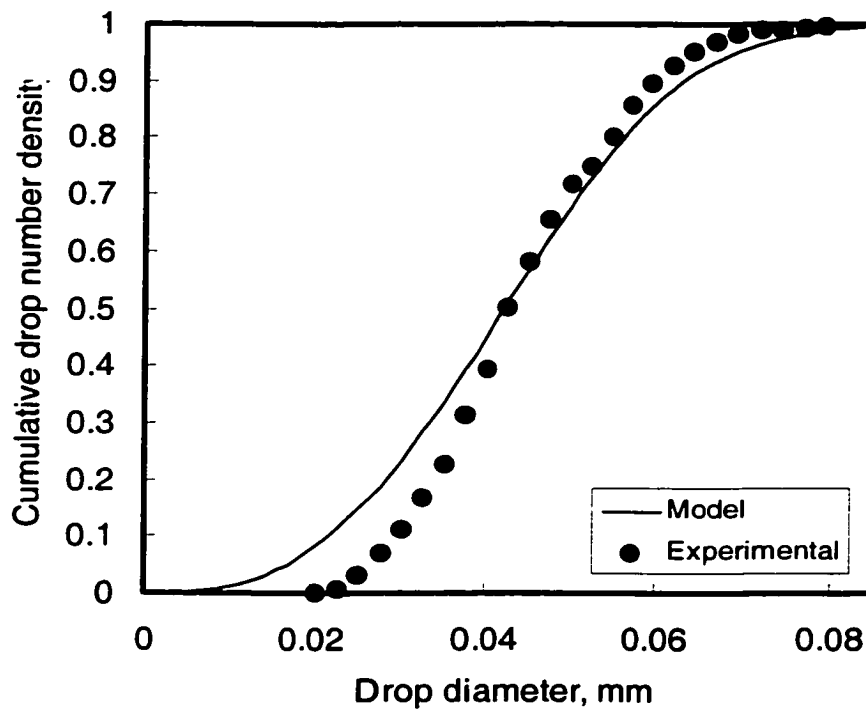


Figure D5. Cumulative drop number density distribution ($\alpha = 33\%$, $\phi = 0.5\%$, $U = 1.80$ m/s, 9 screens, $L = 10$ mm)

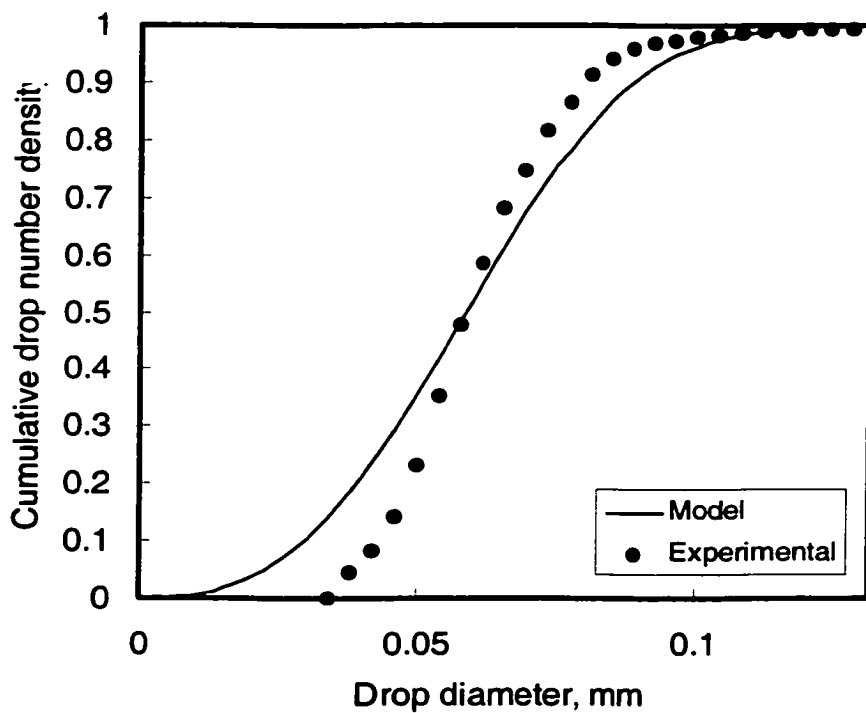


Figure D6. Cumulative drop number density distribution ($\alpha = 33\%$, $\phi = 0.5\%$, $U = 1.94$ m/s, 9 screens, $L = 10$ mm)

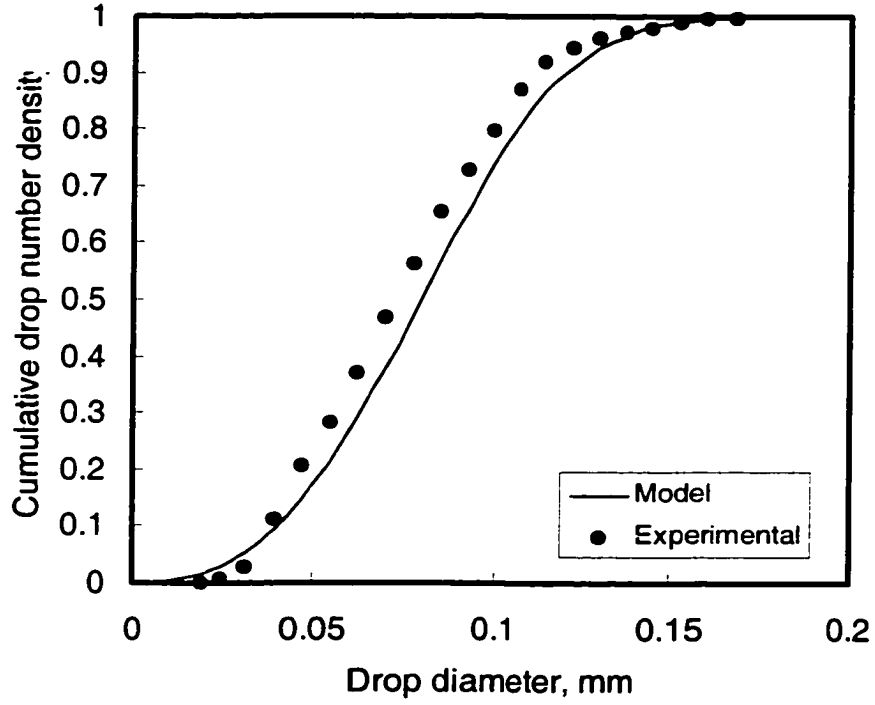


Figure D7. Cumulative drop number density distribution ($\alpha = 27\%$, $\phi = 0.5\%$, $U = 0.97$ m/s, 9 screens, $L = 10$ mm)

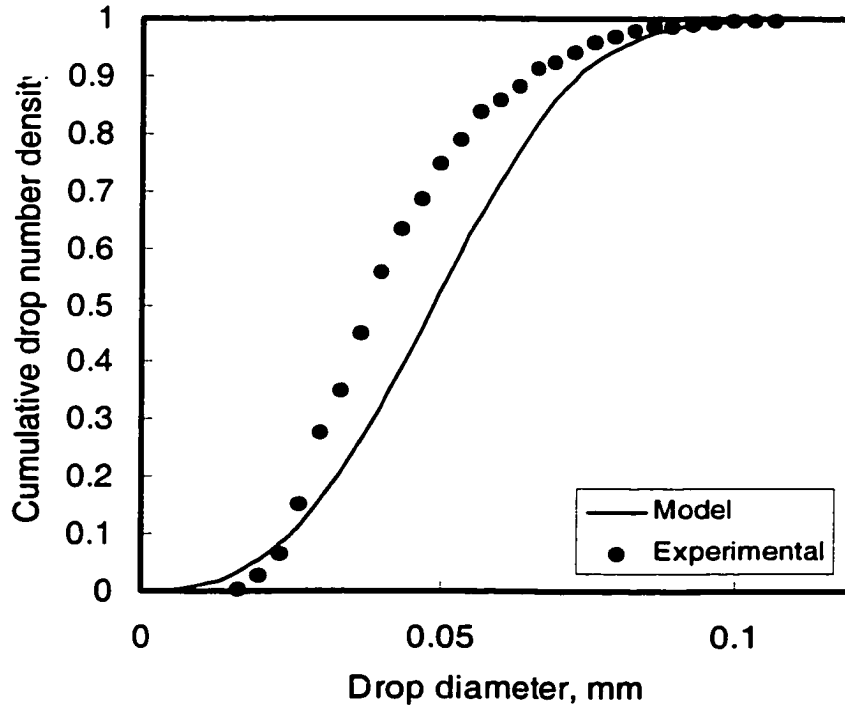


Figure D8. Cumulative drop number density distribution ($\alpha = 27\%$, $\phi = 0.5\%$, $U = 1.55$ m/s, 9 screens, $L = 10$ mm)

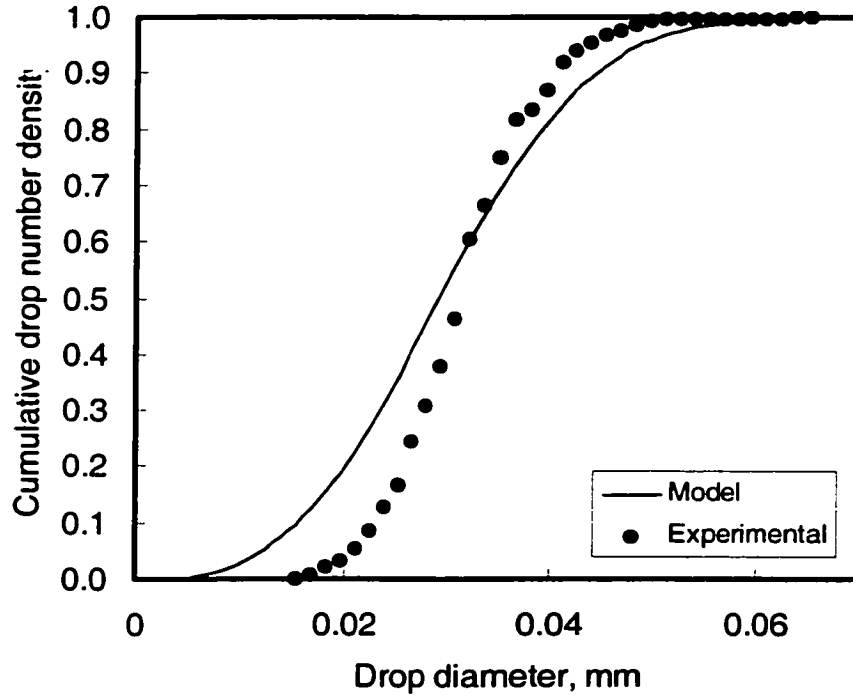


Figure D9. Cumulative drop number density distribution ($\alpha = 27\%$, $\phi = 0.5\%$, $U = 1.94$ m/s, 9 screens, $L = 10$ mm)

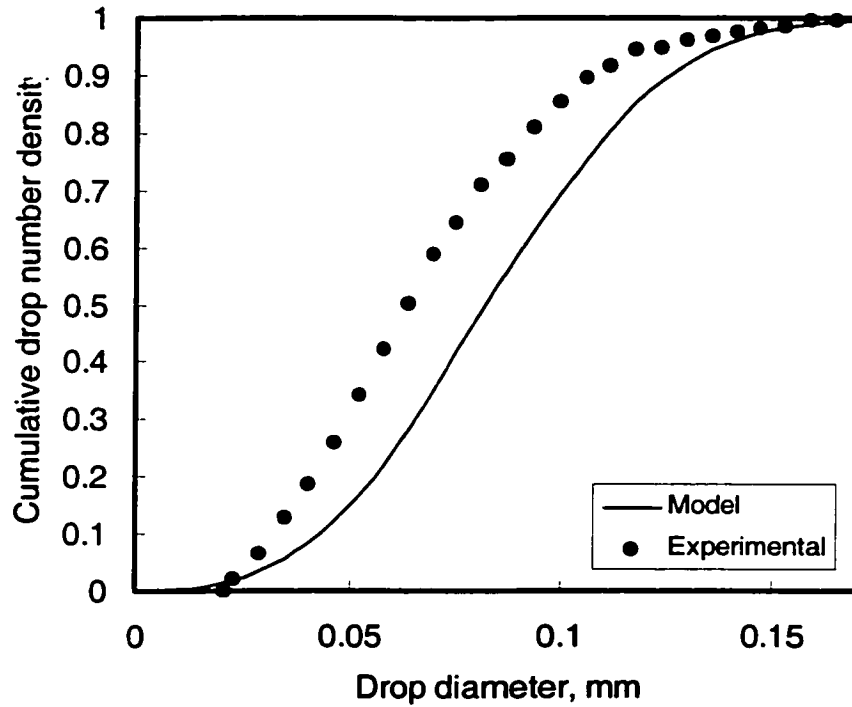


Figure D10. Cumulative drop number density distribution ($\alpha = 41\%$, $\phi = 4\%$, $U = 0.97$ m/s, 9 screens, $L = 10$ mm)

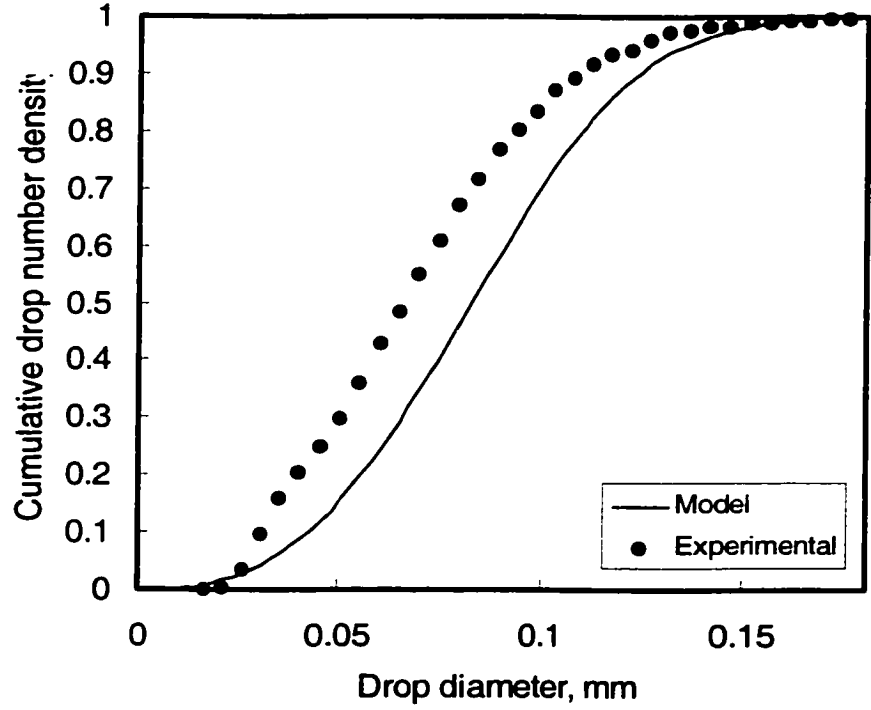


Figure D11. Cumulative drop number density distribution ($\alpha = 41\%$, $\phi = 4\%$, $U = 1.55$ m/s, 9 screens, $L = 10$ mm)

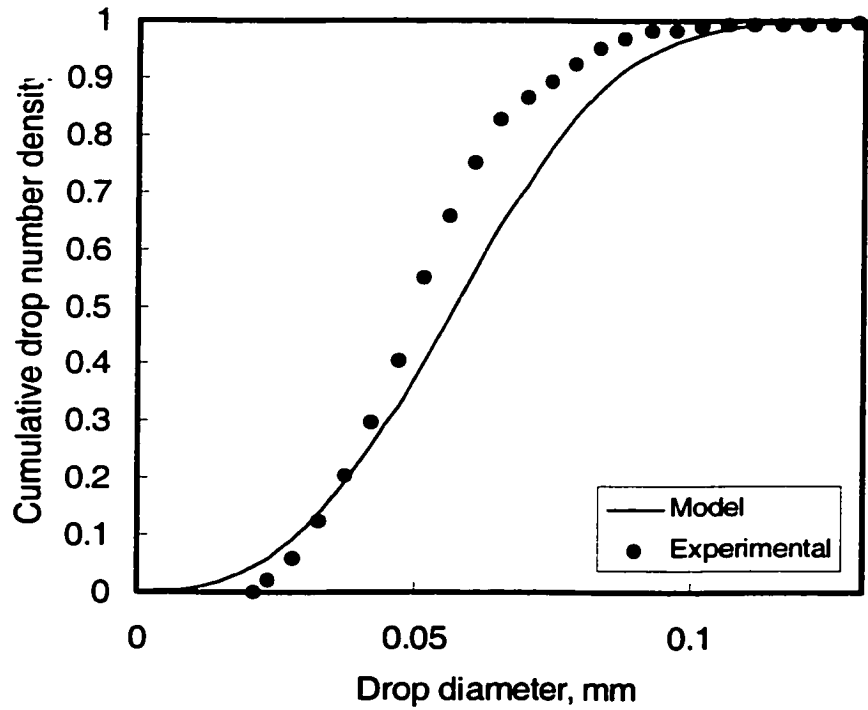


Figure D12. Cumulative drop number density distribution ($\alpha = 41\%$, $\phi = 4\%$, $U = 1.94$ m/s, 9 screens, $L = 10$ mm)

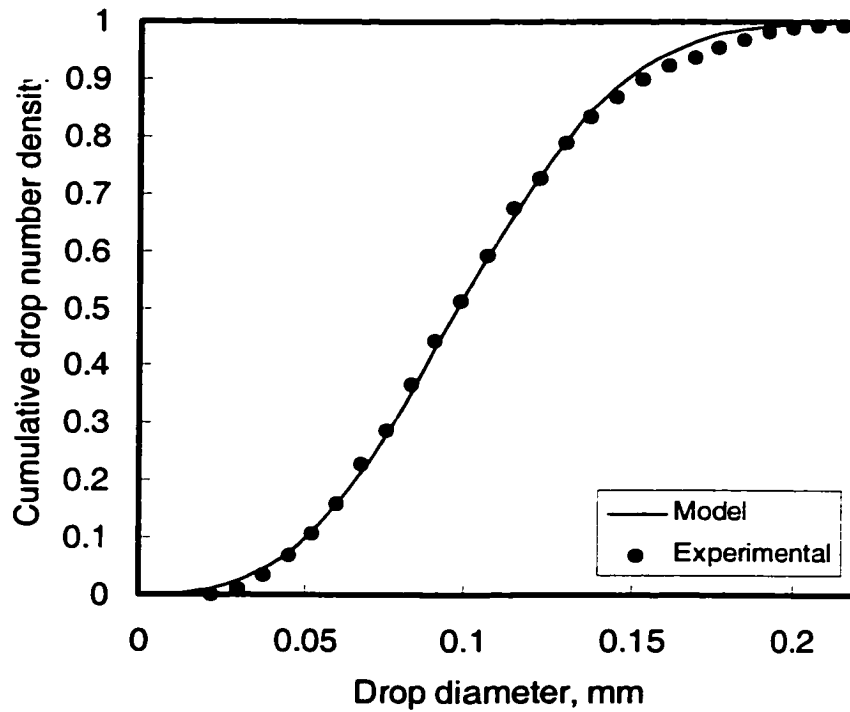


Figure D13. Cumulative drop number density distribution ($\alpha = 27\%$, $\phi = 4\%$, $U = 0.70$ m/s, 9 screens, $L = 10$ mm)

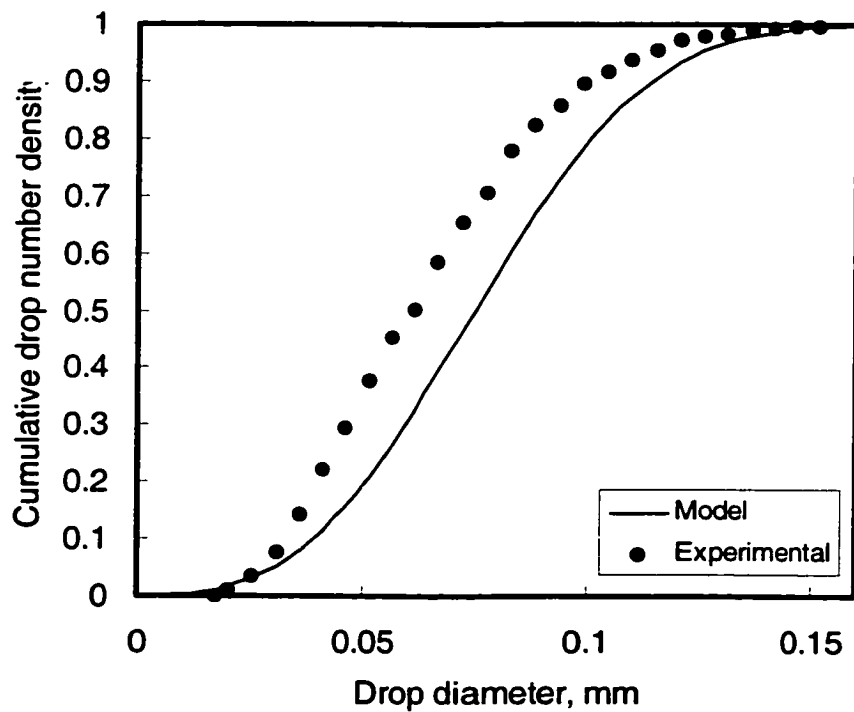


Figure D14. Cumulative drop number density distribution ($\alpha = 27\%$, $\phi = 4\%$, $U = 0.97$ m/s, 9 screens, $L = 10$ mm)

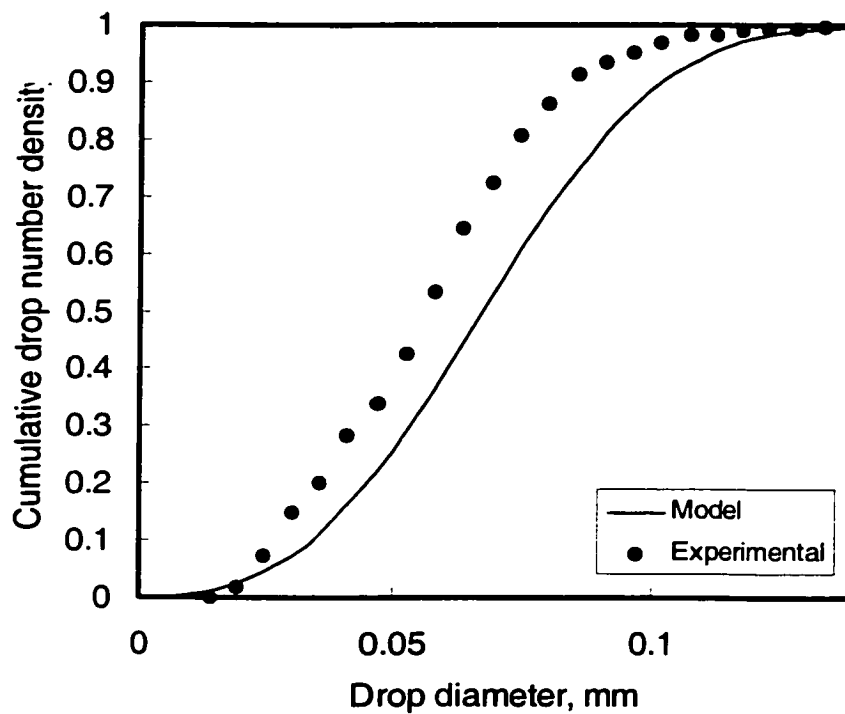


Figure D15. Cumulative drop number density distribution ($\alpha = 27\%$, $\phi = 4\%$, $U = 1.55$ m/s, 9 screens, $L = 10$ mm)

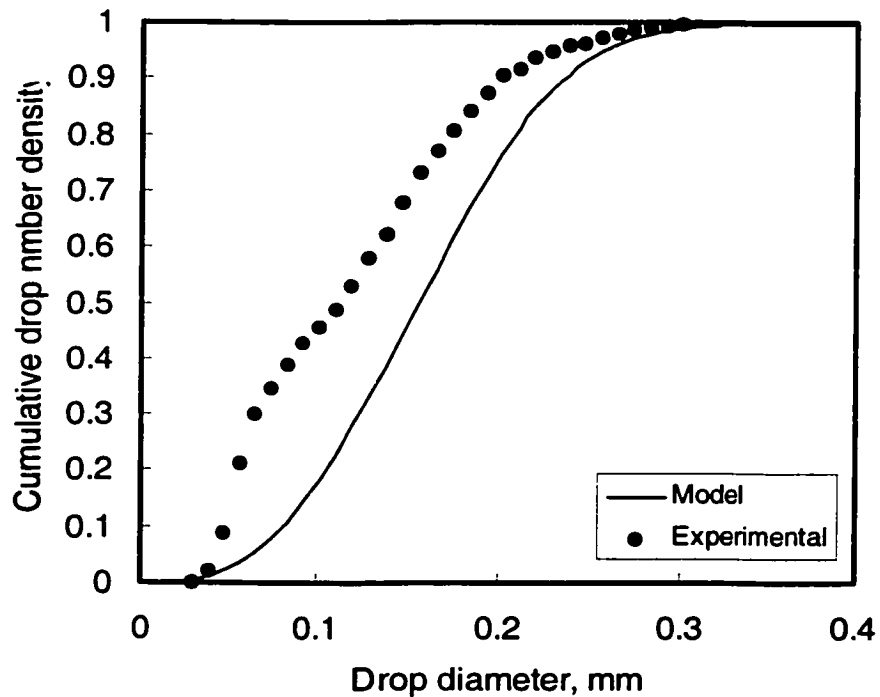


Figure D16. Cumulative drop number density distribution ($\alpha = 41\%$, $\phi = 1\%$, $U = 0.70$ m/s, 9 screens, $L = 10$ mm)

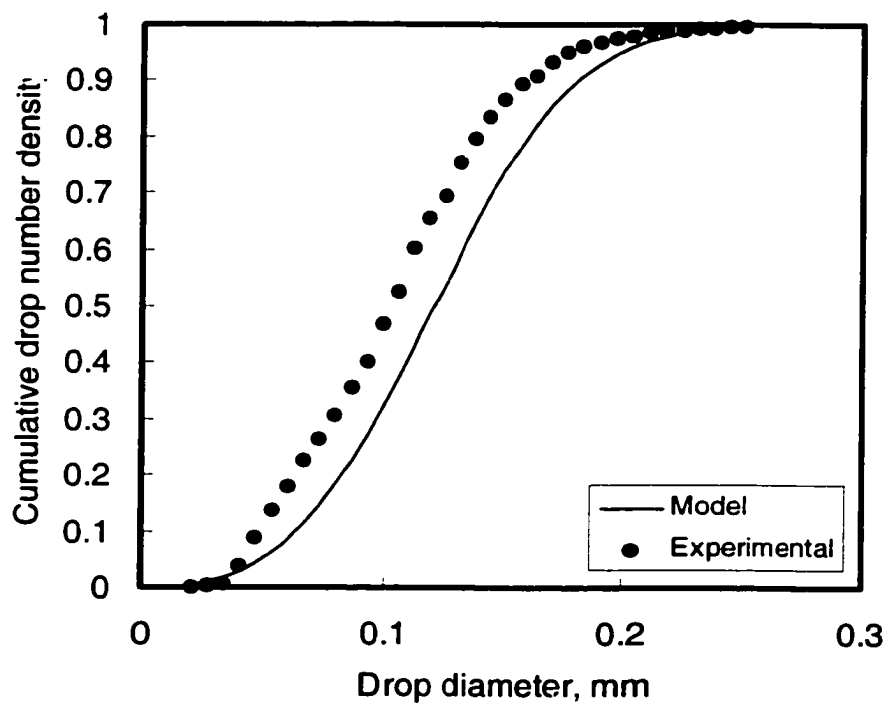


Figure D17. Cumulative drop number density distribution
 ($\alpha = 41\%$, $\phi = 2\%$, $U = 0.70$ m/s, 9 screens, $L = 10$ mm)

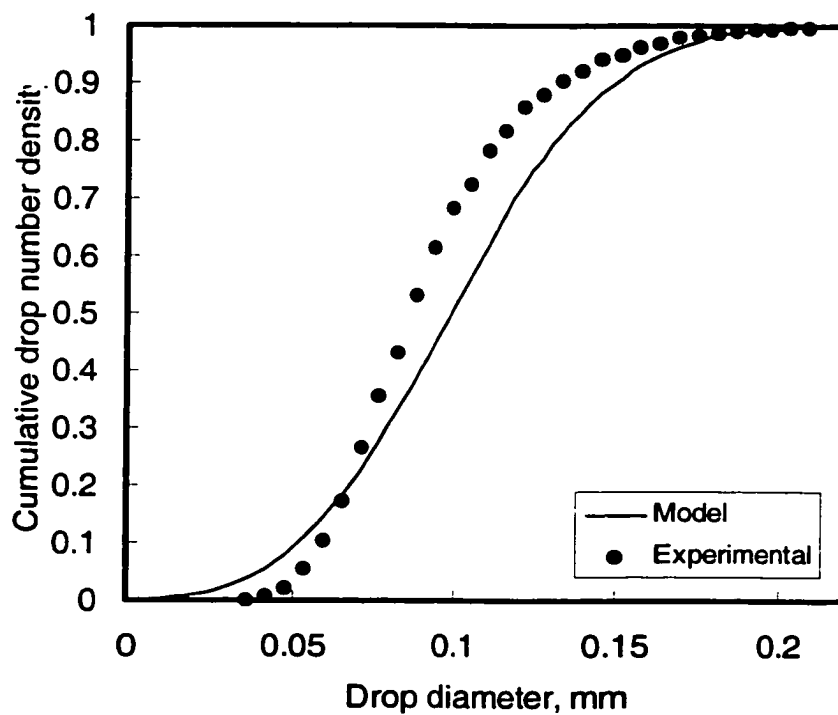


Figure D18. Cumulative drop number density distribution
 ($\alpha = 41\%$, $\phi = 3\%$, $U = 0.70$ m/s, 9 screens, $L = 10$ mm)

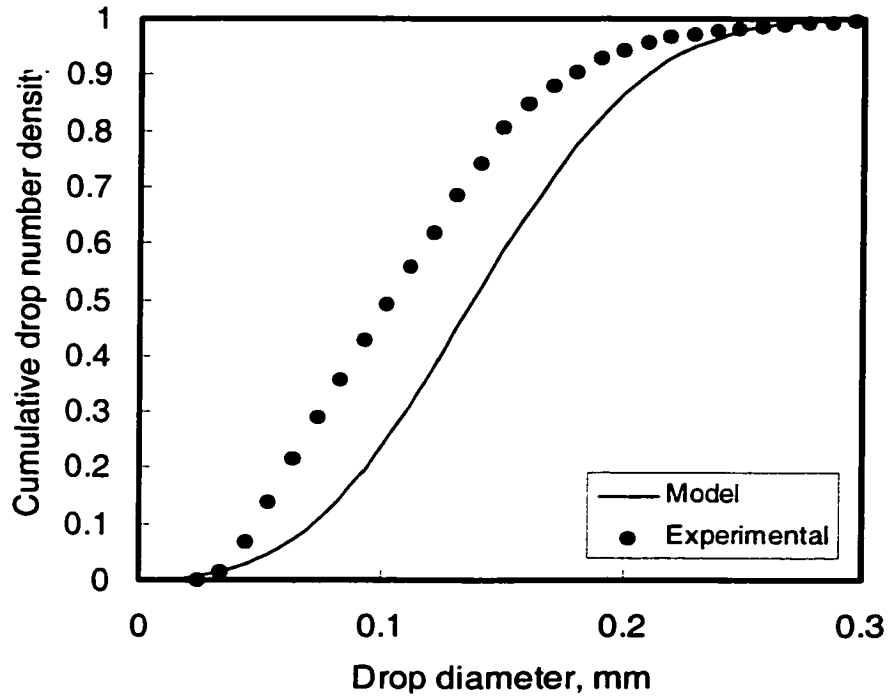


Figure D19. Cumulative drop number density distribution
 ($\alpha = 27\%$, $\phi = 1\%$, $U = 0.70$ m/s, 9 screens, $L = 10$ mm)

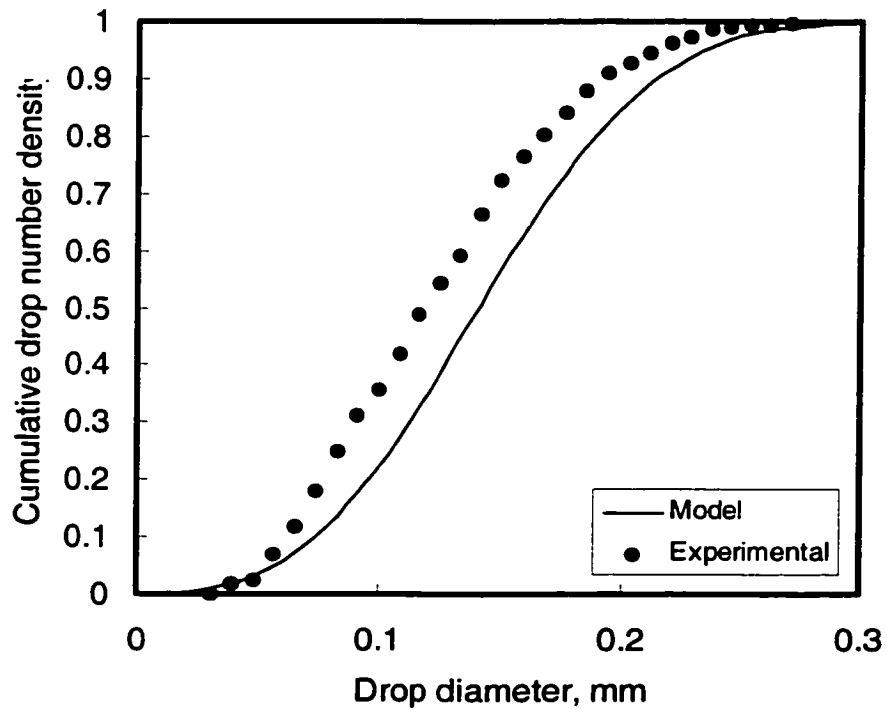


Figure D20. Cumulative drop number density distribution
 ($\alpha = 27\%$, $\phi = 2\%$, $U = 0.70$ m/s, 9 screens, $L = 10$ mm)

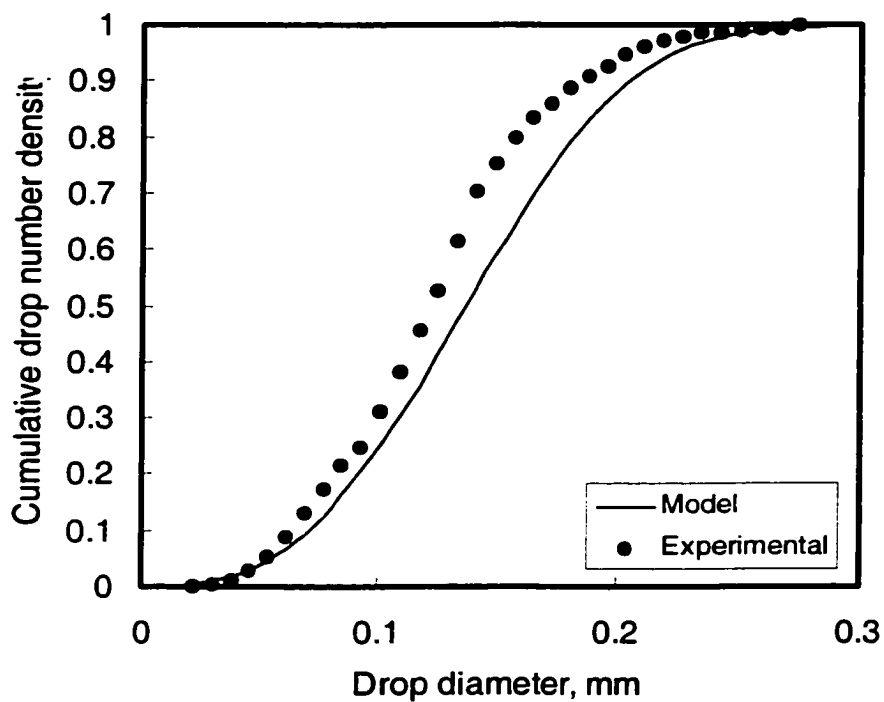


Figure D21. Cumulative drop number density distribution
 ($\alpha = 27\%$, $\phi = 3\%$, $U = 0.70$ m/s, 9 screens, $L = 10$ mm)

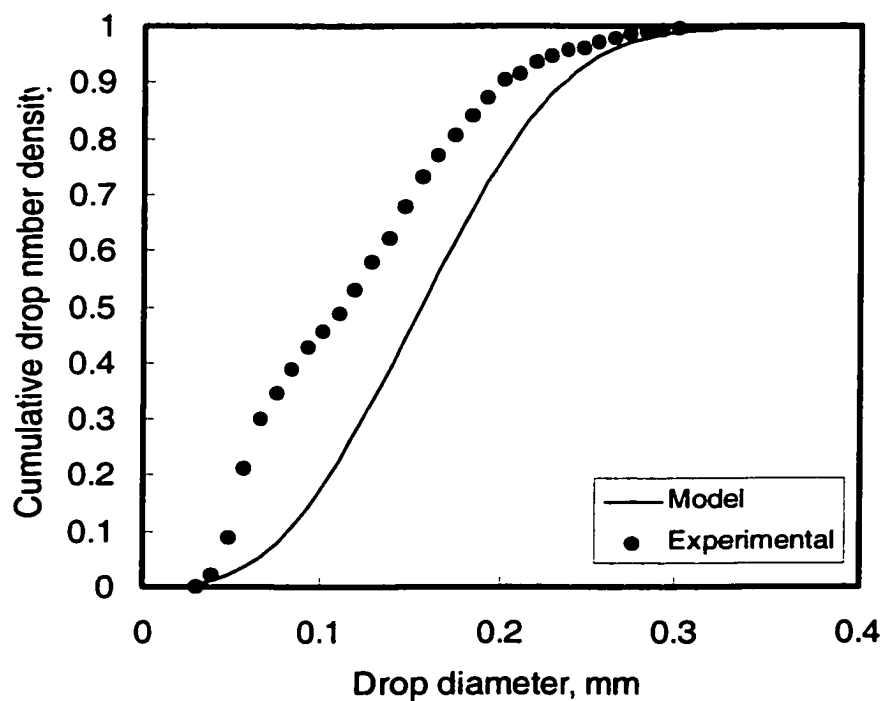


Figure D22. Cumulative drop number density distribution
 ($\alpha = 41\%$, $\phi = 1\%$, $U = 0.70$ m/s, 9 screens, $L = 10$ mm)

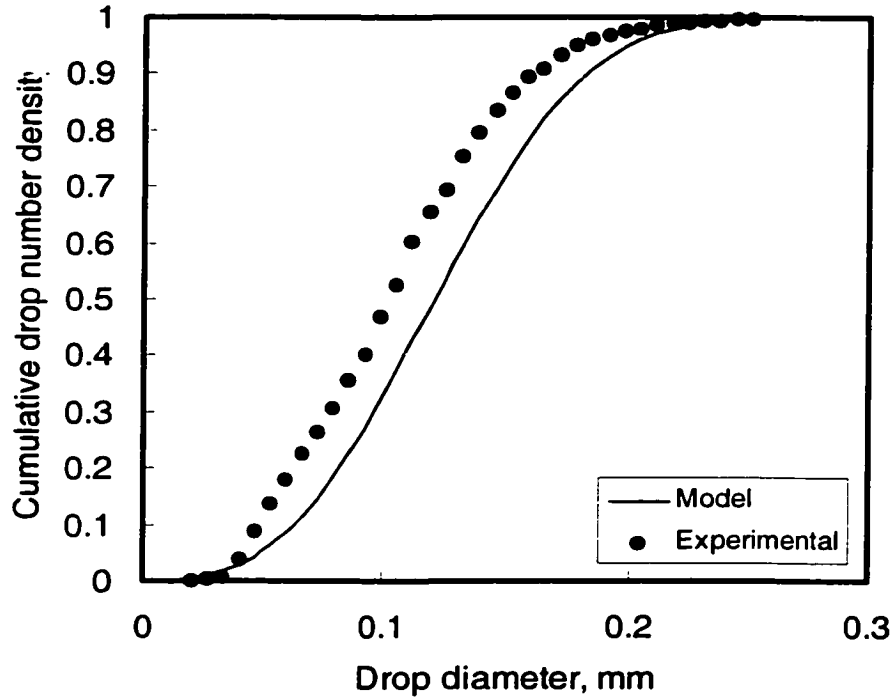


Figure D23. Cumulative drop number density distribution
 ($\alpha = 41\%$, $\phi = 2\%$, $U = 0.70$ m/s, 9 screens, $L = 10$ mm)

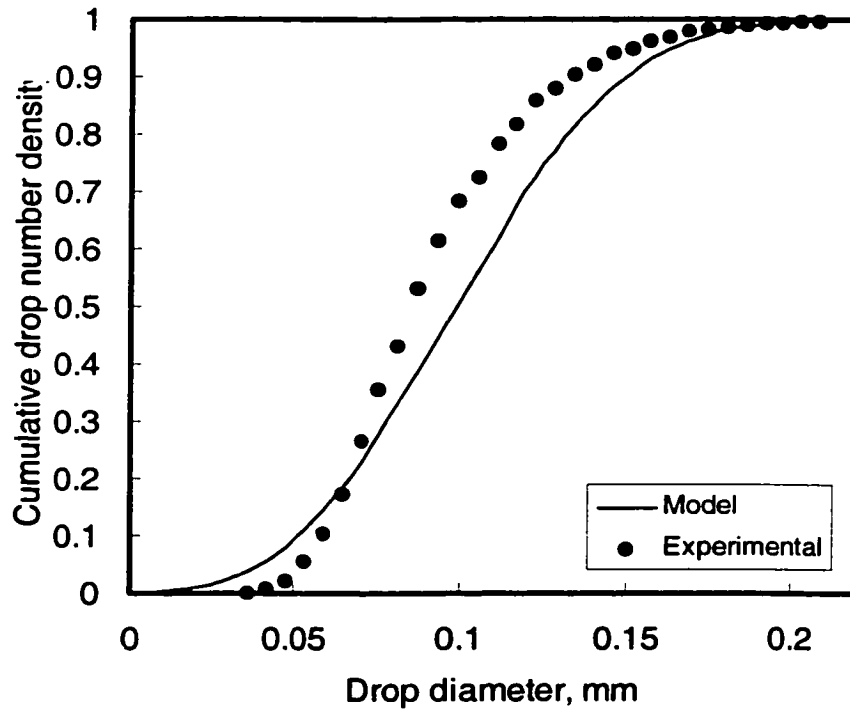


Figure D24. Cumulative drop number density distribution
 ($\alpha = 41\%$, $\phi = 3\%$, $U = 0.70$ m/s, 9 screens, $L = 10$ mm)

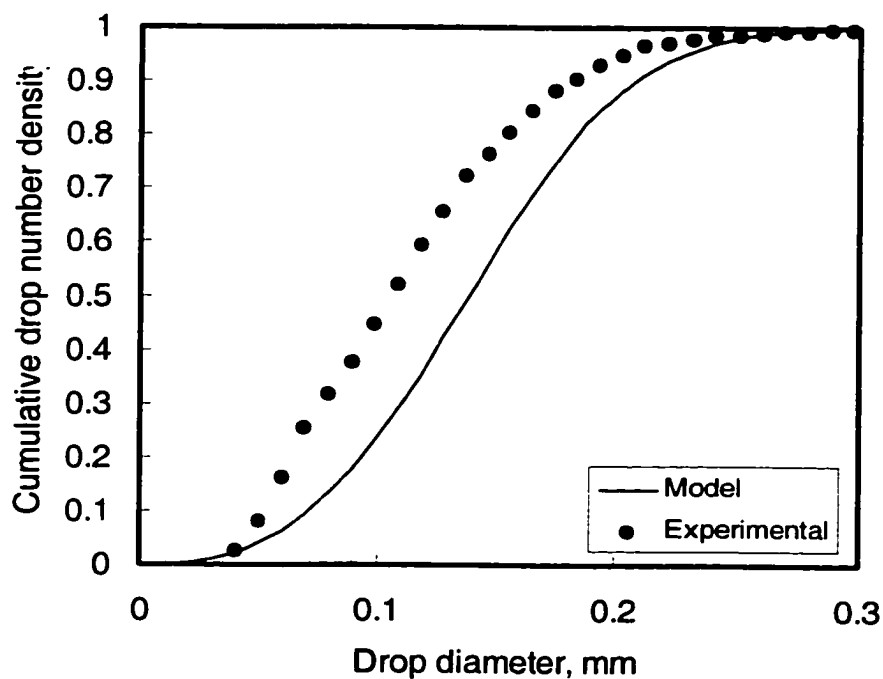


Figure D25. Cumulative drop number density distribution
 ($\alpha = 27\%$, $\phi = 0.5\%$, $U = 0.70$ m/s, Triton X100= 0.01 mole/m³, 9 screens, $L = 10$ mm)

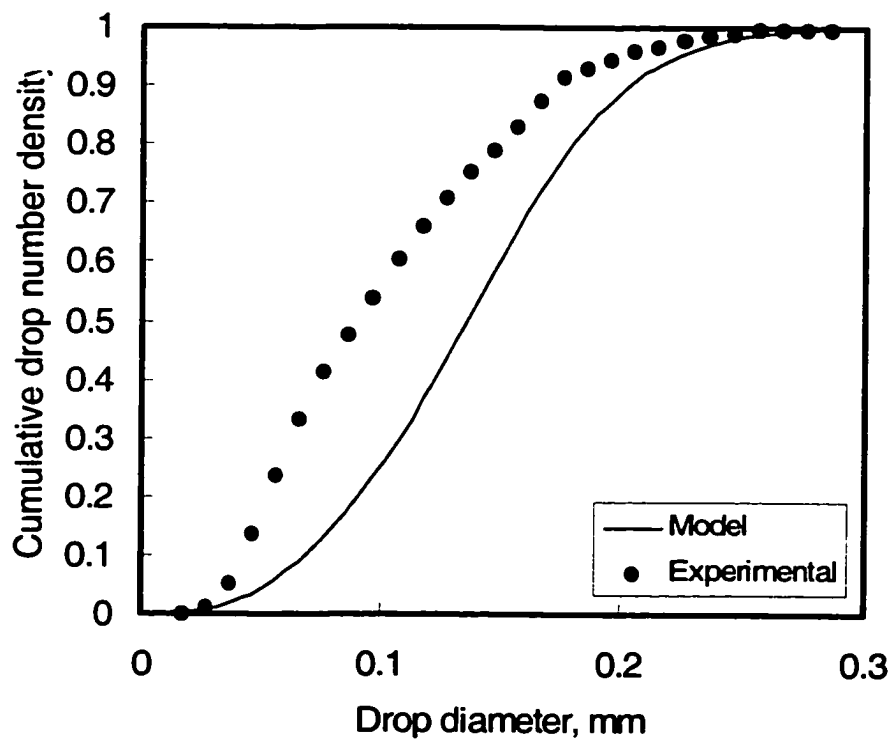


Figure D26. Cumulative drop number density distribution
 ($\alpha = 27\%$, $\phi = 0.5\%$, $U = 0.70$ m/s, Triton X100= 0.05 mole/m³, 9 screens, $L = 10$ mm)

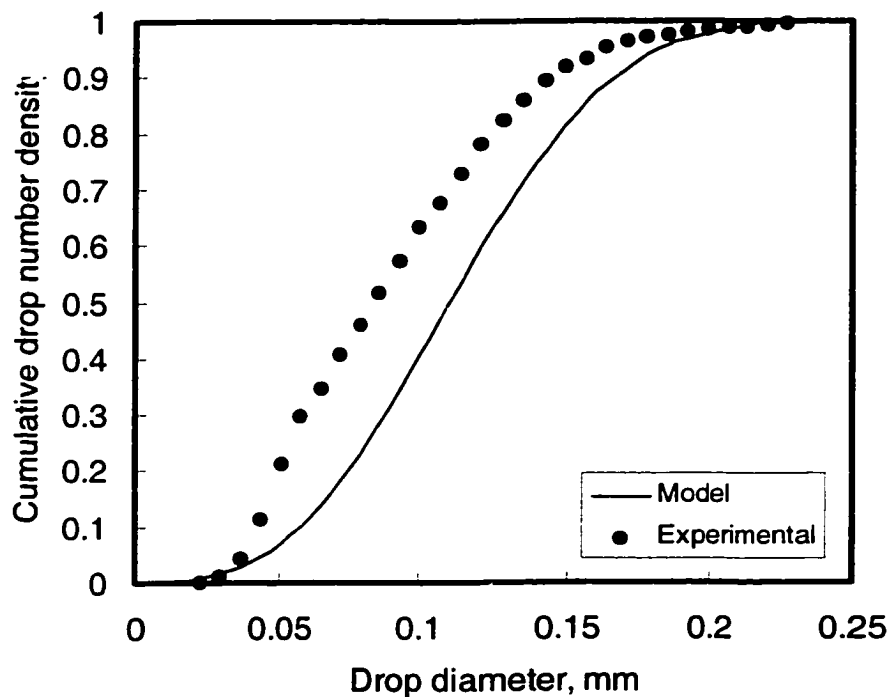


Figure D27. Cumulative drop number density distribution
 ($\alpha = 27\%$, $\phi = 0.5\%$, $U = 0.70$ m/s, Triton X100 = 0.1 mole/m³, 9 screens, $L = 10$ mm)

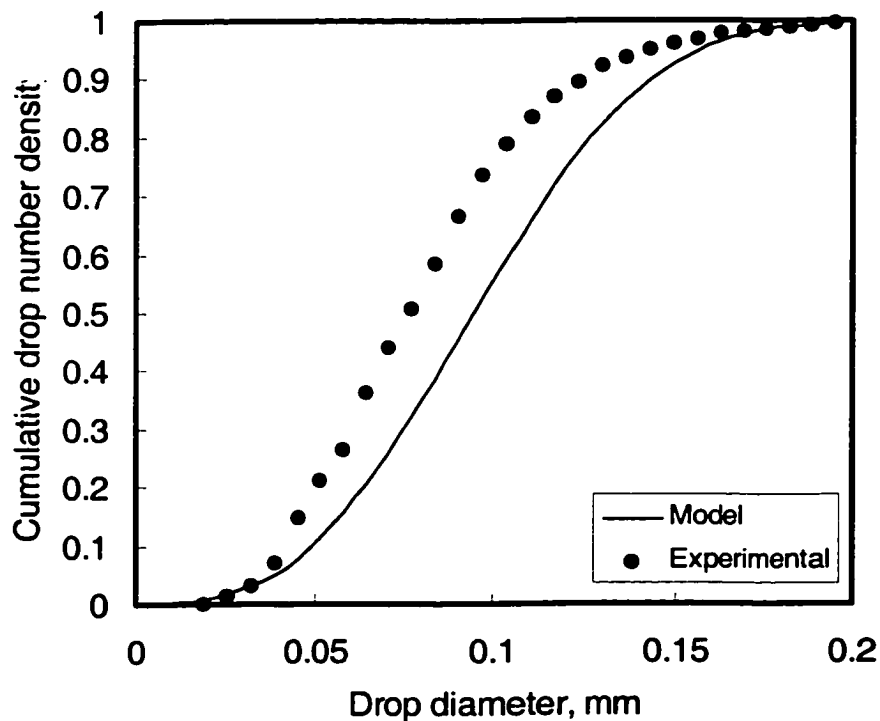


Figure D28. Cumulative drop number density distribution
 ($\alpha = 27\%$, $\phi = 0.5\%$, $U = 0.70$ m/s, Triton X100 = 0.2 mole/m³, 9 screens, $L = 10$ mm)

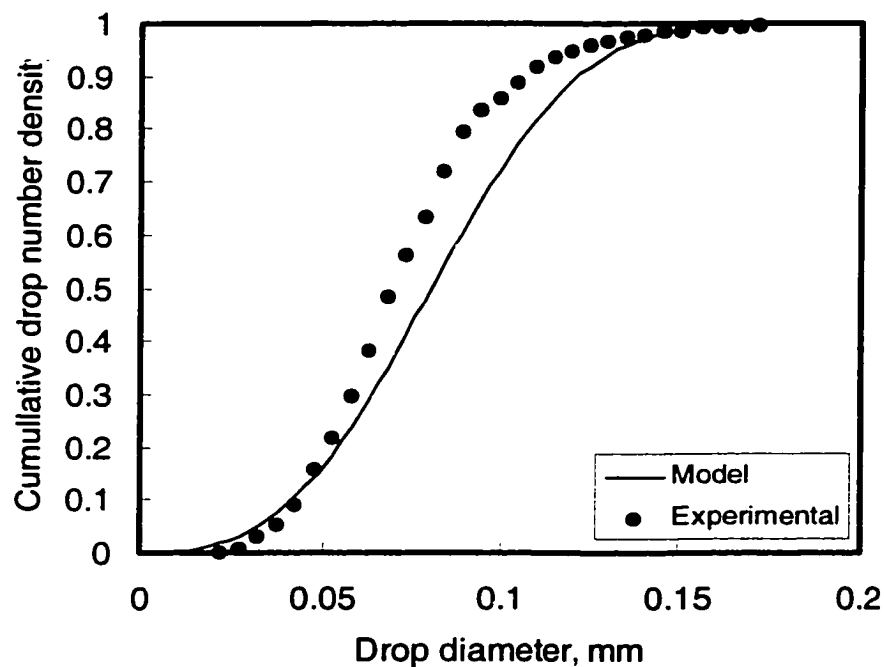


Figure D29. Cumulative drop number density distribution
 ($\alpha = 27\%$, $\phi = 0.5\%$, $U = 0.70$ m/s, Triton X100 = 0.3 mole/m³, 9 screens, $L = 10$ mm)

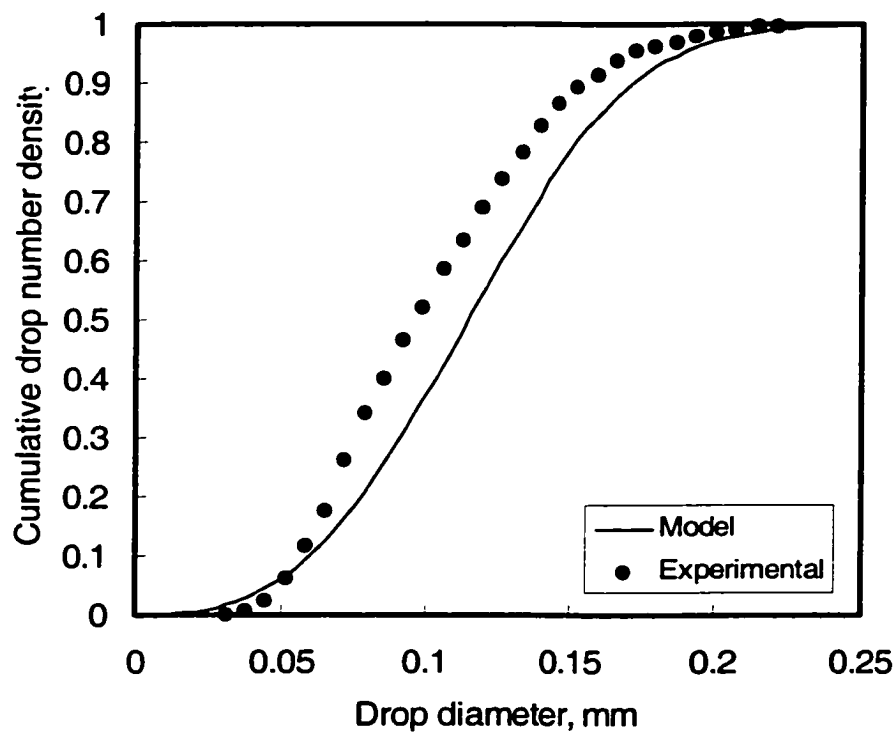


Figure D30. Cumulative drop number density distribution
 ($\alpha = 27\%$, $\phi = 4\%$, $U = 0.70$ m/s, Triton X100 = 0.01 mole/m³, 9 screens, $L = 10$ mm)

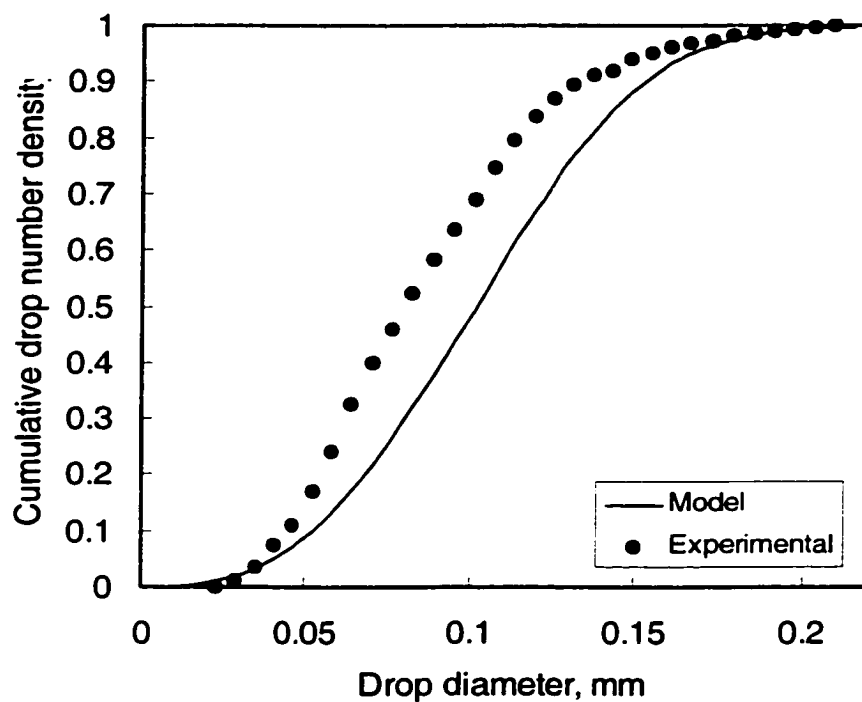


Figure D31. Cumulative drop number density distribution
 ($\alpha = 27\%$, $\phi = 4\%$, $U = 0.70$ m/s, Triton X100 = 0.05 mole/m³, 9 screens, $L = 10$ mm)

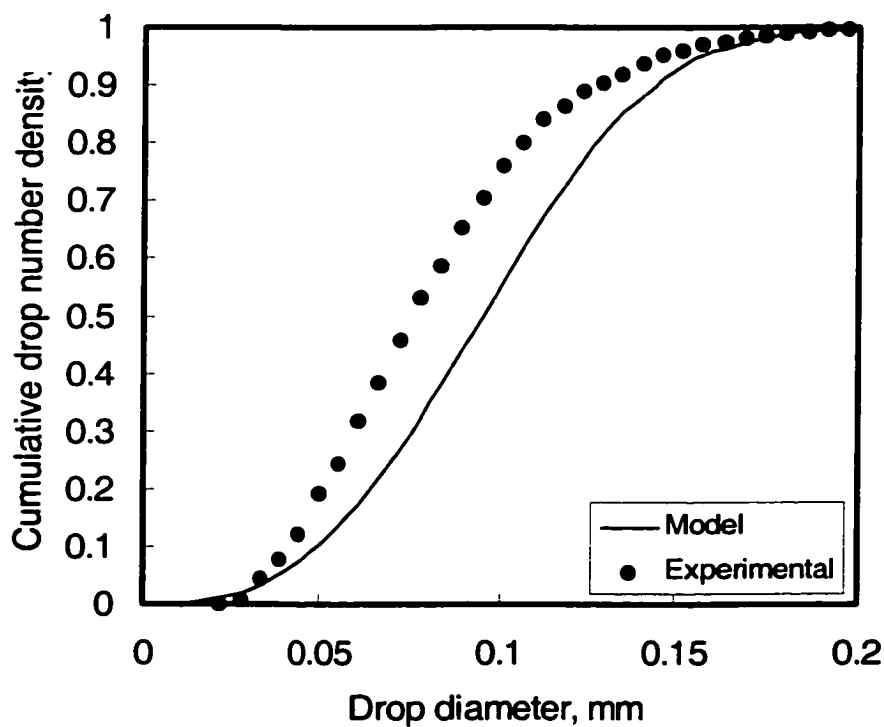


Figure D32. Cumulative drop number density distribution
 ($\alpha = 27\%$, $\phi = 4\%$, $U = 0.70$ m/s, Triton X100 = 0.1 mole/m³, 9 screens, $L = 10$ mm)

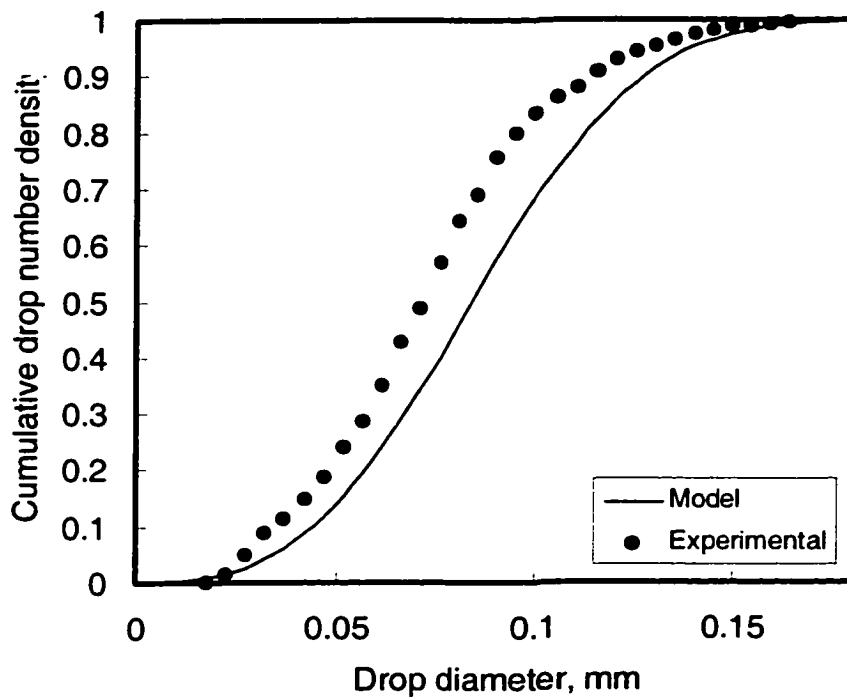


Figure D33. Cumulative drop number density distribution
 ($\alpha = 27\%$, $\phi = 4\%$, $U = 0.70$ m/s, Triton X100 = 0.2 mole/m³, 9 screens, $L = 10$ mm)

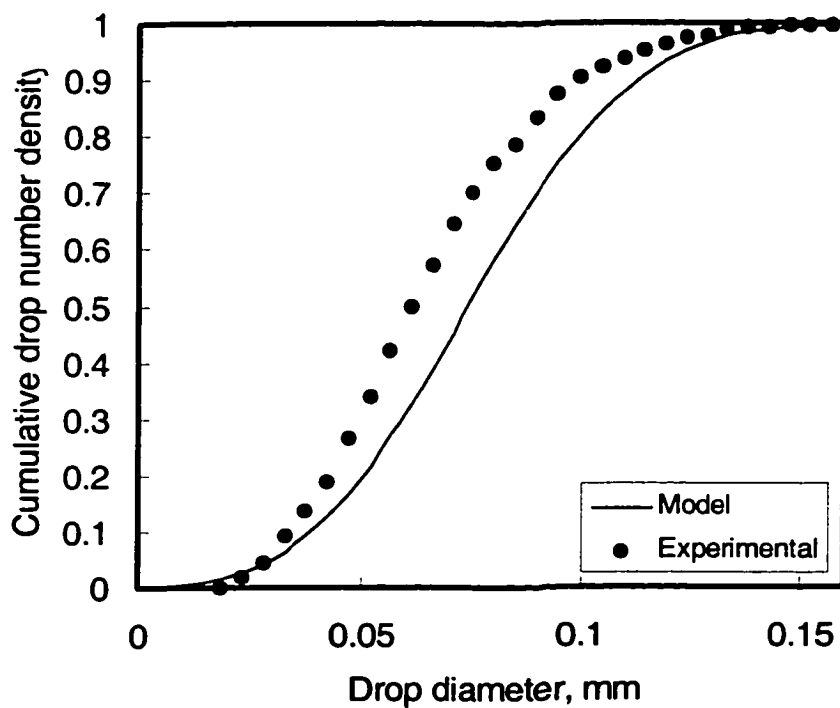


Figure D34. Cumulative drop number density distribution
 ($\alpha = 27\%$, $\phi = 4\%$, $U = 0.70$ m/s, Triton X100 = 0.3 mole/m³, 9 screens, $L = 10$ mm)

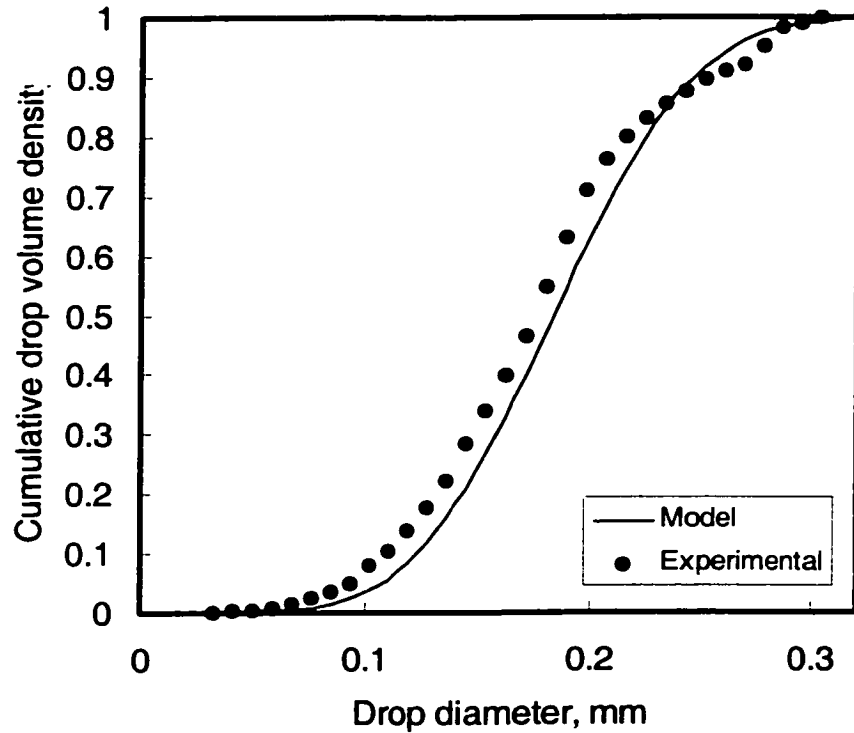


Figure D35. Cumulative drop volume density distribution ($\alpha = 41\%$, $\phi = 0.5\%$, $U = 0.97$ m/s, 9 screens, $L = 10$ mm)

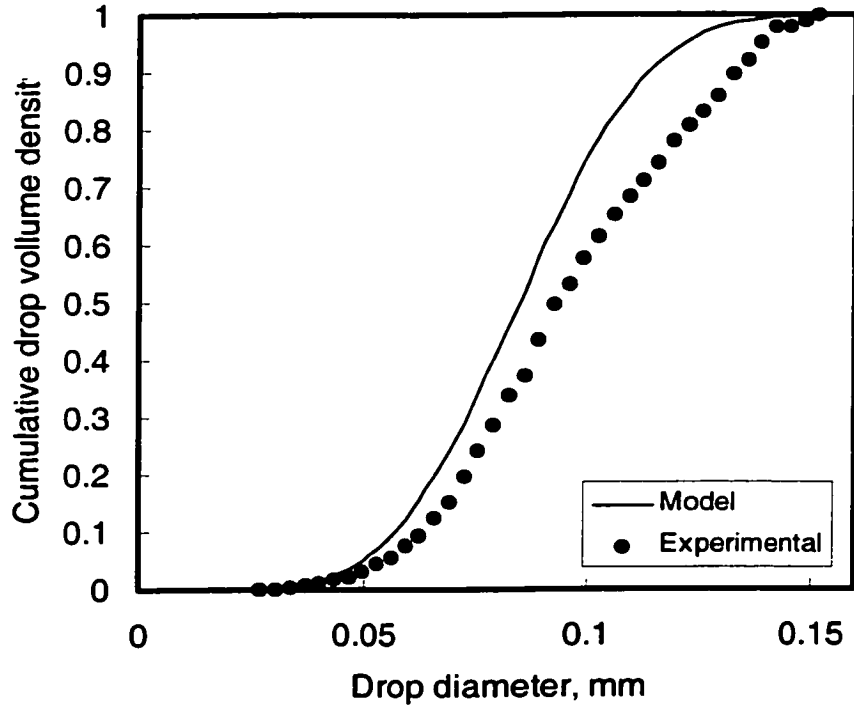


Figure D36. Cumulative drop volume density distribution ($\alpha = 41\%$, $\phi = 0.5\%$, $U = 1.80$ m/s, 9 screens, $L = 10$ mm)

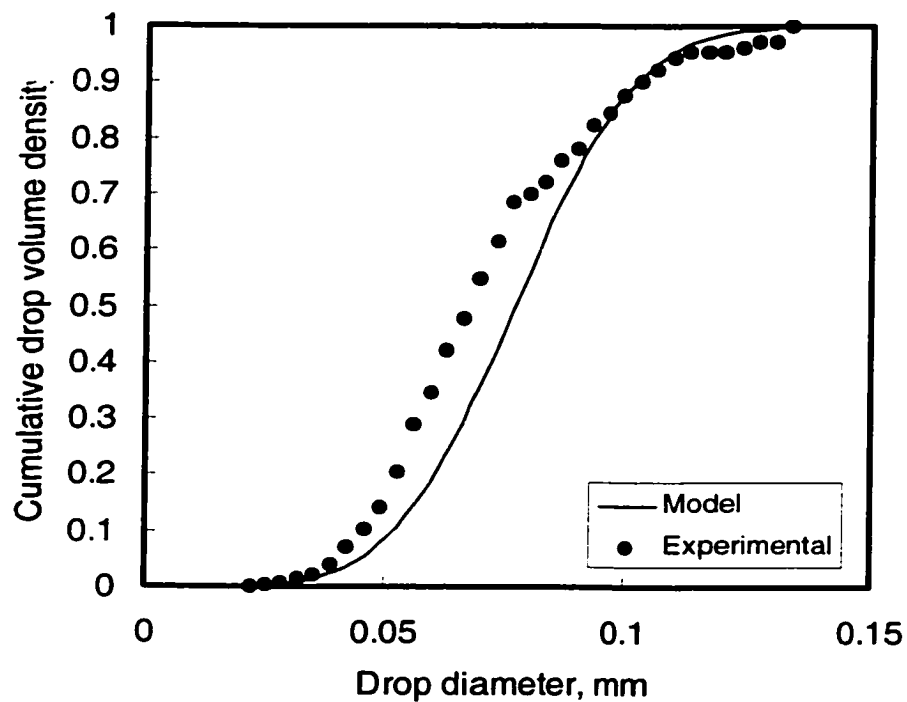


Figure D37. Cumulative drop volume density distribution ($\alpha = 41\%$, $\phi = 0.5\%$, $U = 1.94$ m/s, 9 screens, $L = 10$ mm)

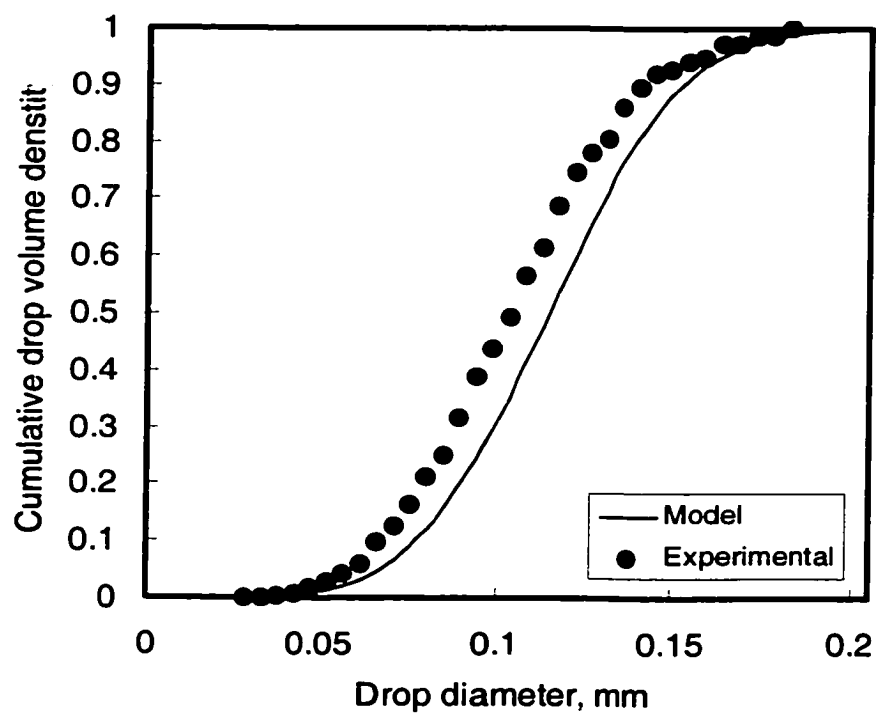


Figure D38. Cumulative drop volume density distribution ($\alpha = 33\%$, $\phi = 0.5\%$, $U = 1.55$ m/s, 9 screens, $L = 10$ mm)

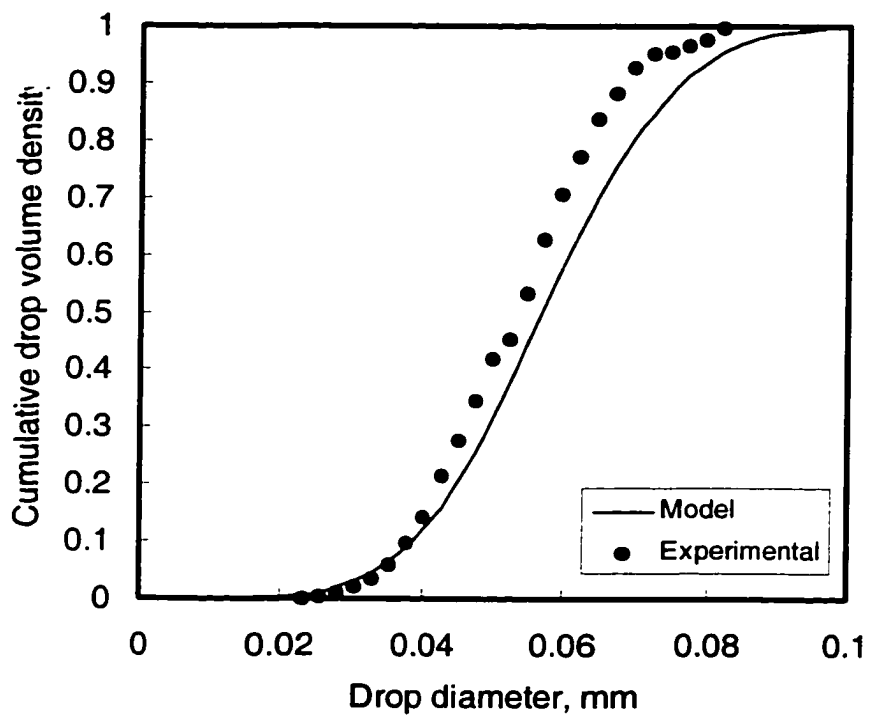


Figure D39. Cumulative drop volume density distribution ($\alpha = 33\%$, $\phi = 0.5\%$, $U = 1.80$ m/s, 9 screens, $L = 10$ mm)

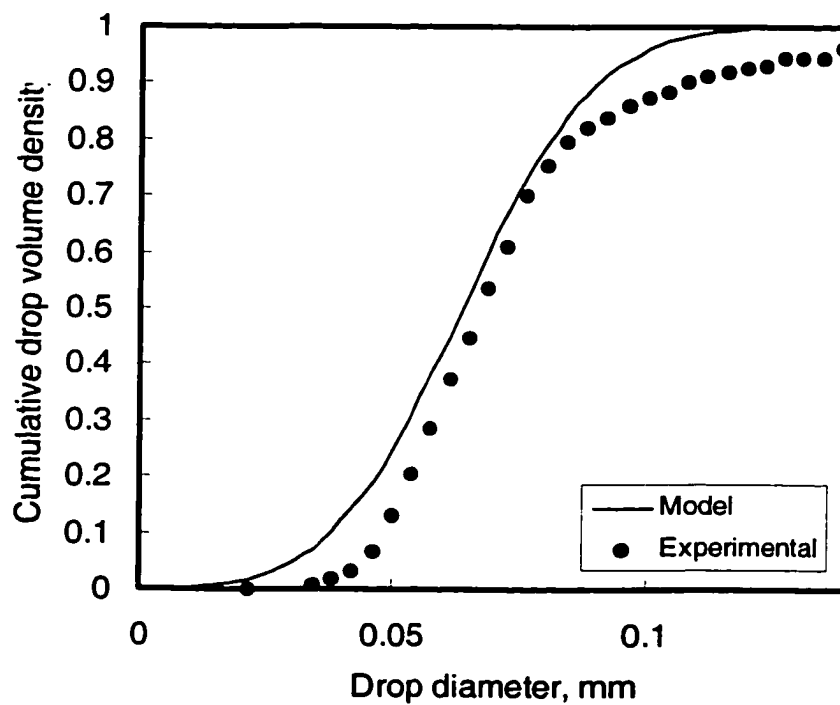


Figure D40. Cumulative drop volume density distribution ($\alpha = 33\%$, $\phi = 0.5\%$, $U = 1.94$ m/s, 9 screens, $L = 10$ mm)

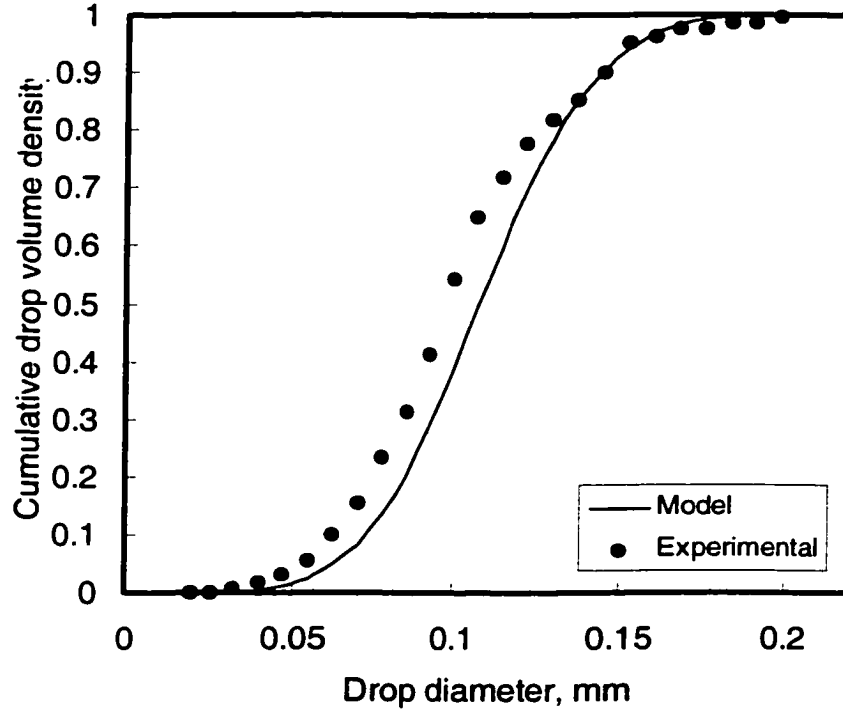


Figure D41. Cumulative drop volume density distribution ($\alpha = 27\%$, $\phi = 0.5\%$, $U = 0.97$ m/s, 9 screens, $L = 10$ mm)

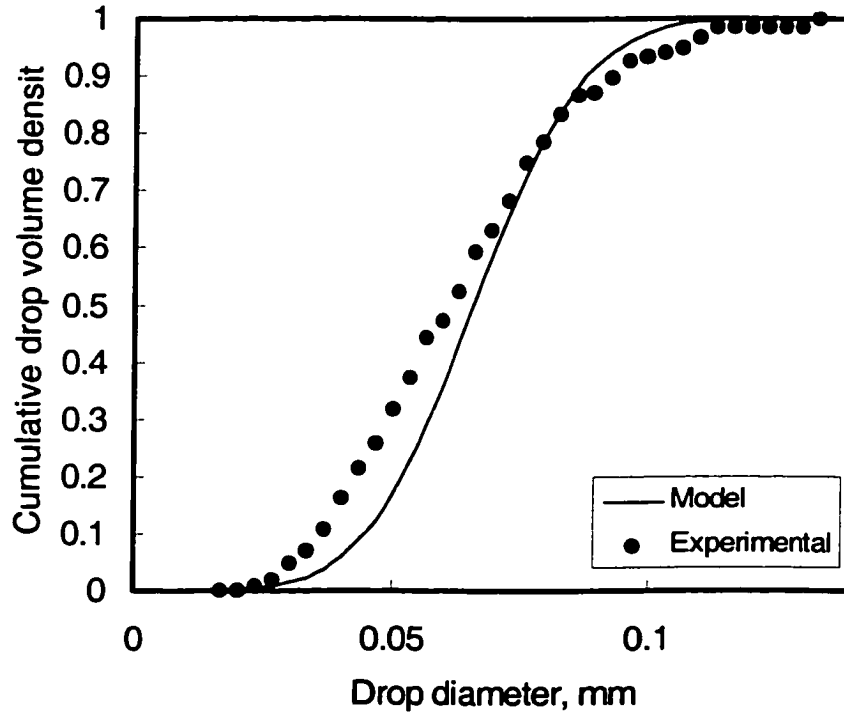


Figure D42. Cumulative drop volume density distribution ($\alpha = 27\%$, $\phi = 0.5\%$, $U = 1.55$ m/s, 9 screens, $L = 10$ mm)

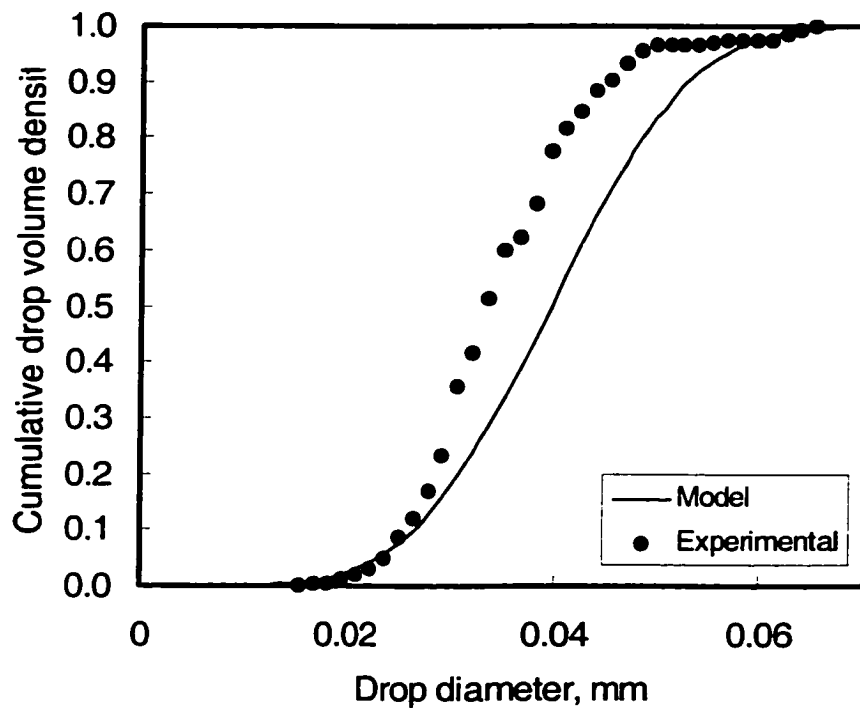


Figure D43. Cumulative drop volume density distribution
 ($\alpha = 27\%$, $\phi = 0.5\%$, $U = 1.94$ m/s, 9 screens, $L = 10$ mm)

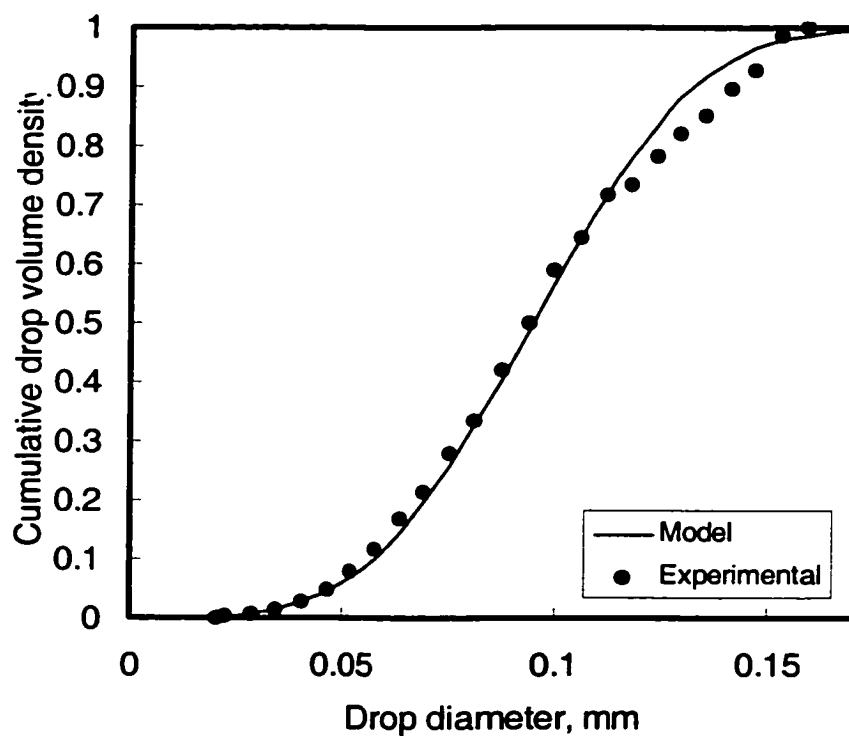


Figure D44. Cumulative drop volume density distribution
 ($\alpha = 41\%$, $\phi = 4\%$, $U = 0.97$ m/s, 9 screens, $L = 10$ mm)

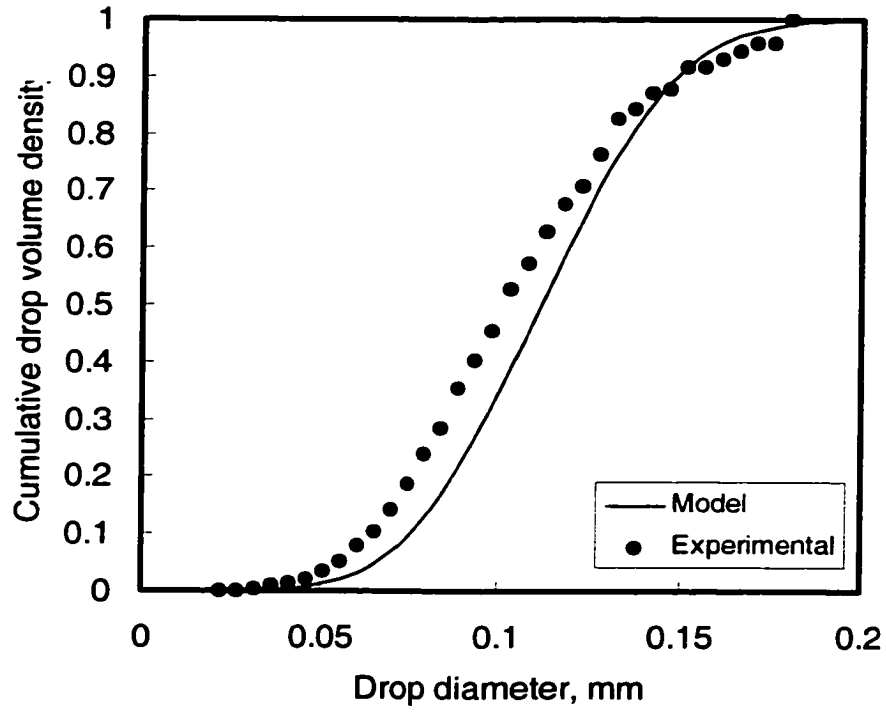


Figure D45. Cumulative drop volume density distribution ($\alpha = 41\%$, $\phi = 4\%$, $U = 1.55$ m/s, 9 screens, $L = 10$ mm)

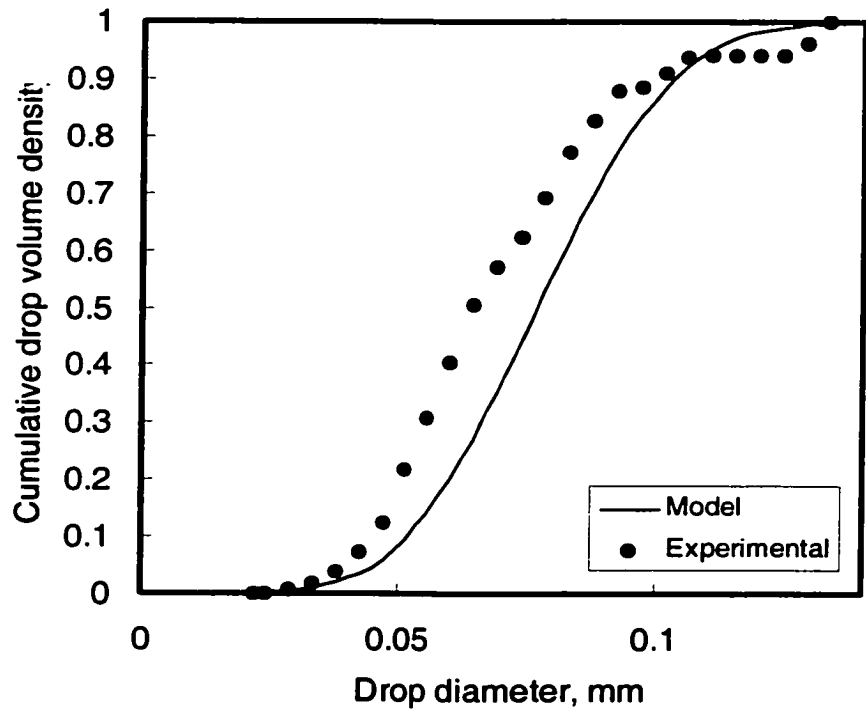


Figure D46. Cumulative drop volume density distribution ($\alpha = 41\%$, $\phi = 4\%$, $U = 1.94$ m/s, 9 screens, $L = 10$ mm)

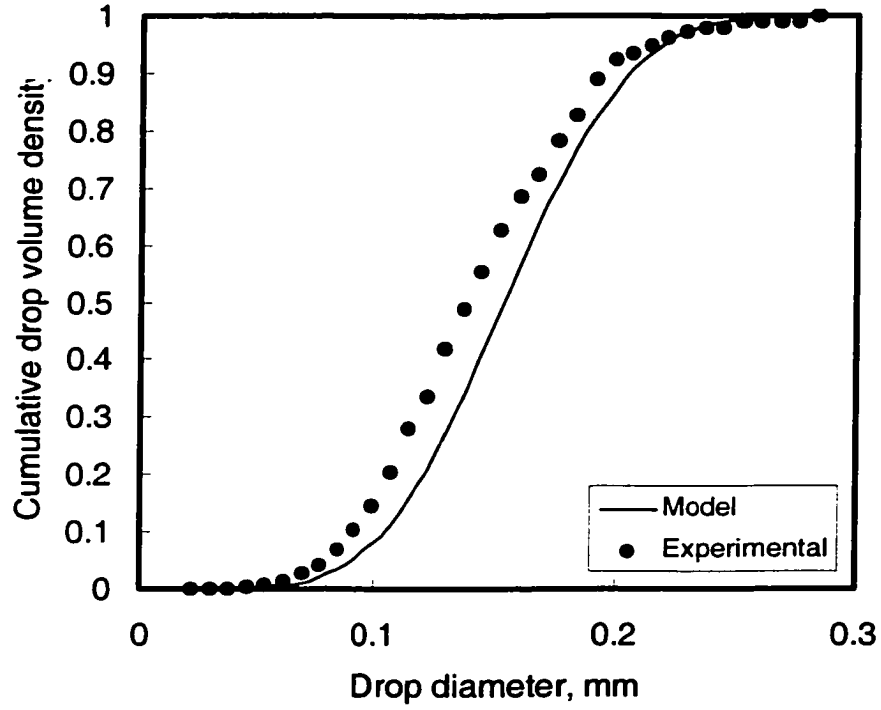


Figure D47. Cumulative drop volume density distribution ($\alpha = 27\%$, $\phi = 4\%$, $U = 0.70$ m/s, 9 screens, $L = 10$ mm)

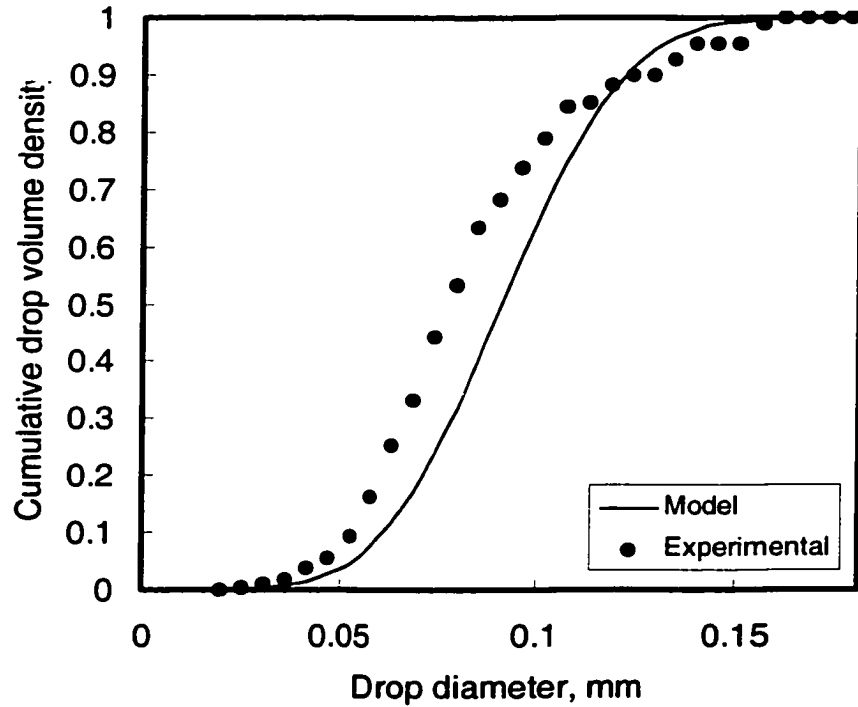


Figure D48. Cumulative drop volume density distribution ($\alpha = 27\%$, $\phi = 4\%$, $U = 1.55$ m/s, 9 screens, $L = 10$ mm)

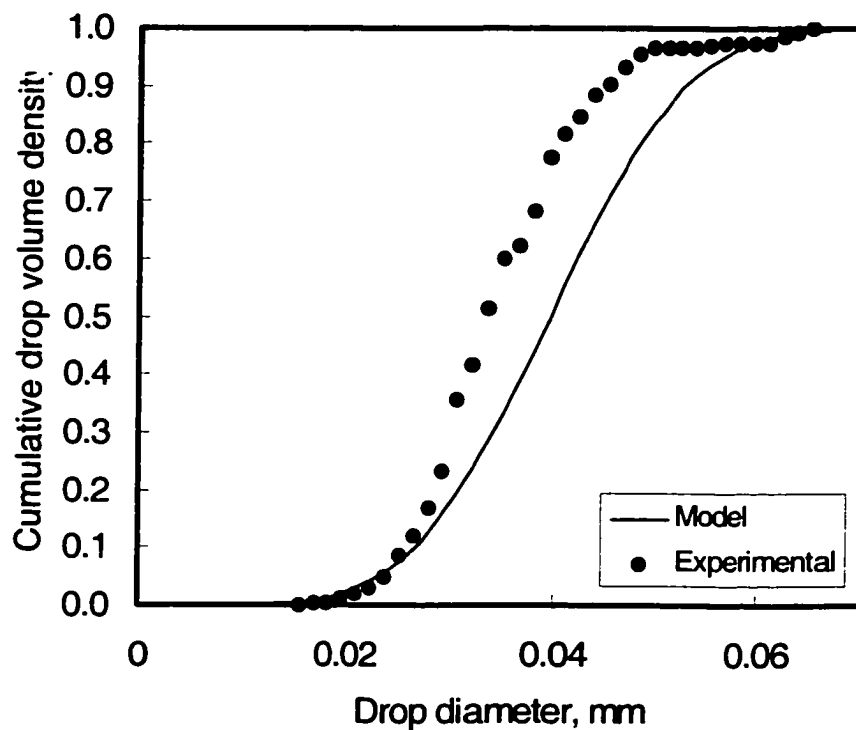


Figure D49. Cumulative drop volume density distribution ($\alpha = 27\%$, $\phi = 4\%$, $U = 1.94$ m/s, 9 screens, $L = 10$ mm)

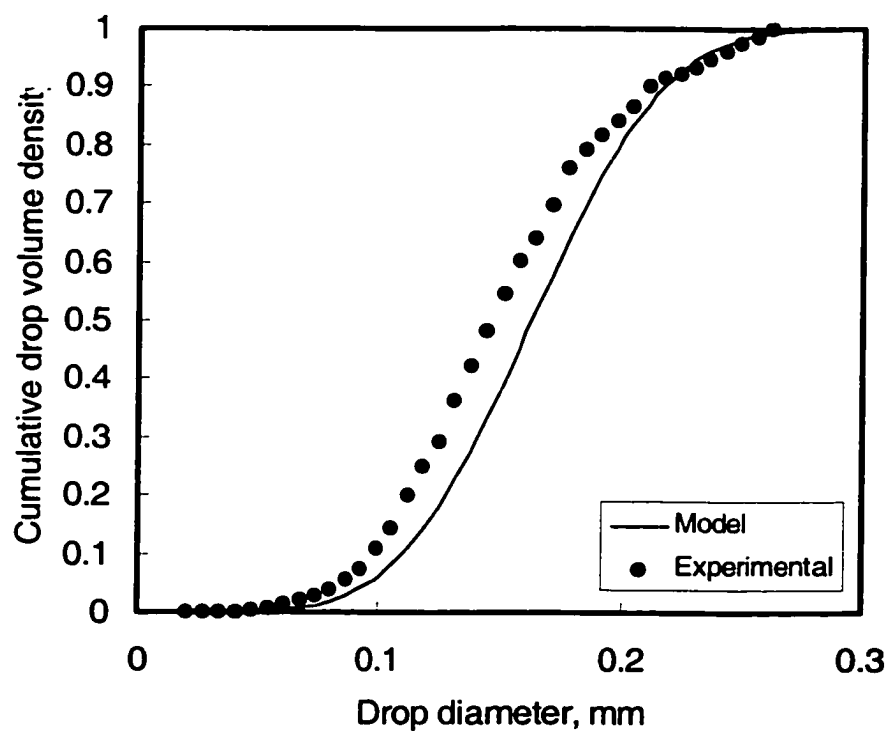


Figure D50. Cumulative drop volume density distribution ($\alpha = 41\%$, $\phi = 1\%$, $U = 0.70$ m/s, 9 screens, $L = 10$ mm)

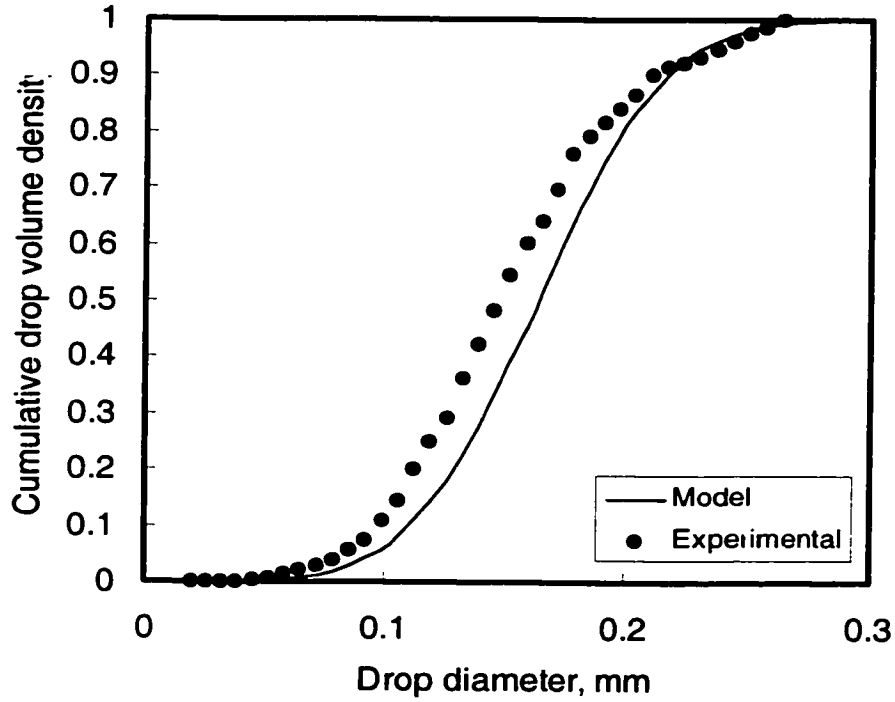


Figure D51. Cumulative drop volume density distribution ($\alpha = 41\%$, $\phi = 2\%$, $U = 0.70$ m/s, 9 screens, $L = 10$ mm)

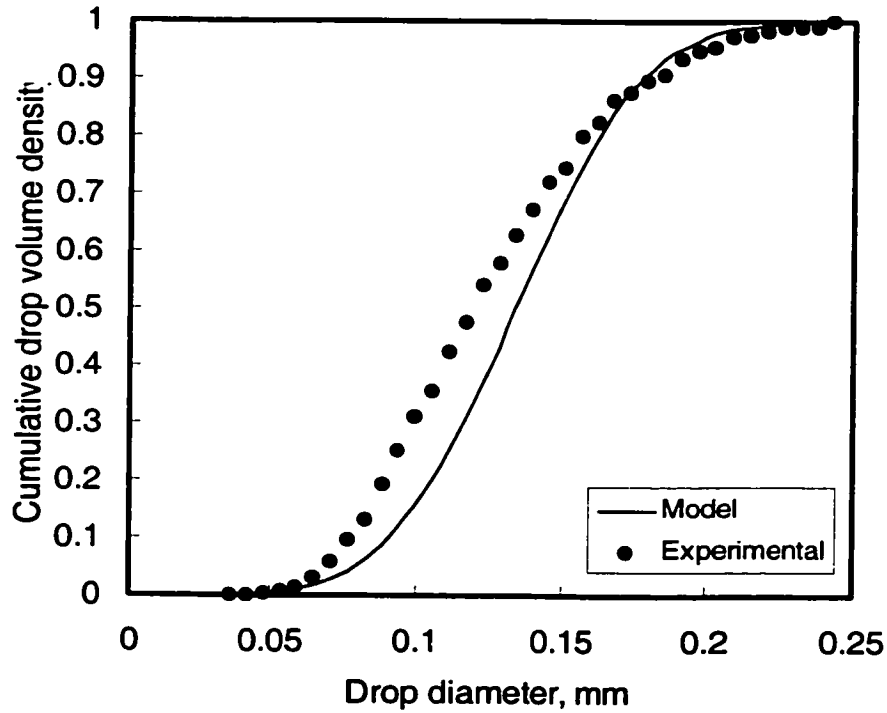


Figure D52. Cumulative drop volume density distribution ($\alpha = 41\%$, $\phi = 3\%$, $U = 0.70$ m/s, 9 screens, $L = 10$ mm)

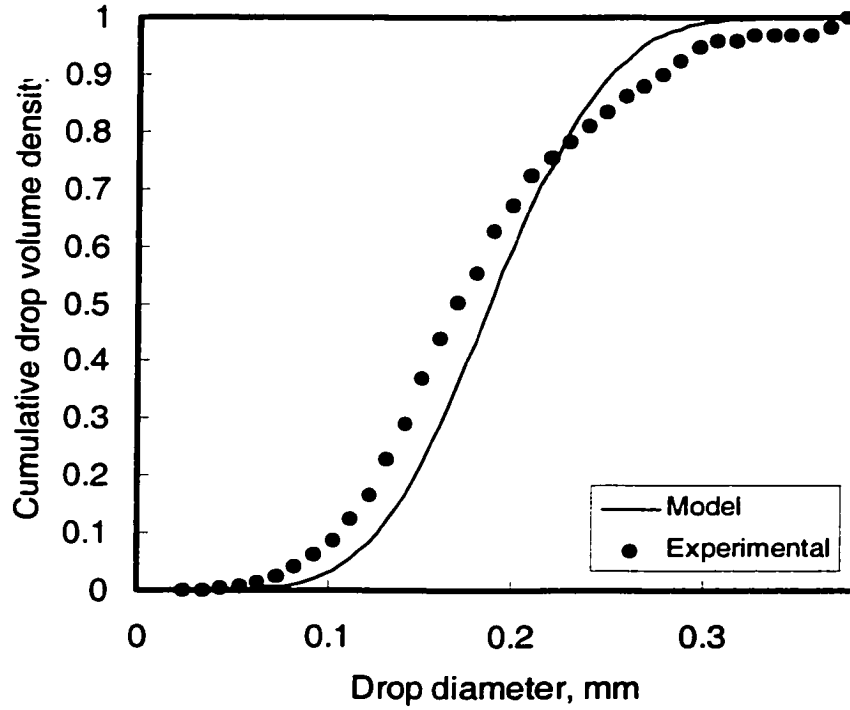


Figure D53. Cumulative drop volume density distribution
($\alpha = 27\%$, $\phi = 1\%$, $U = 0.70$ m/s, 9 screens, $L = 10$ mm)

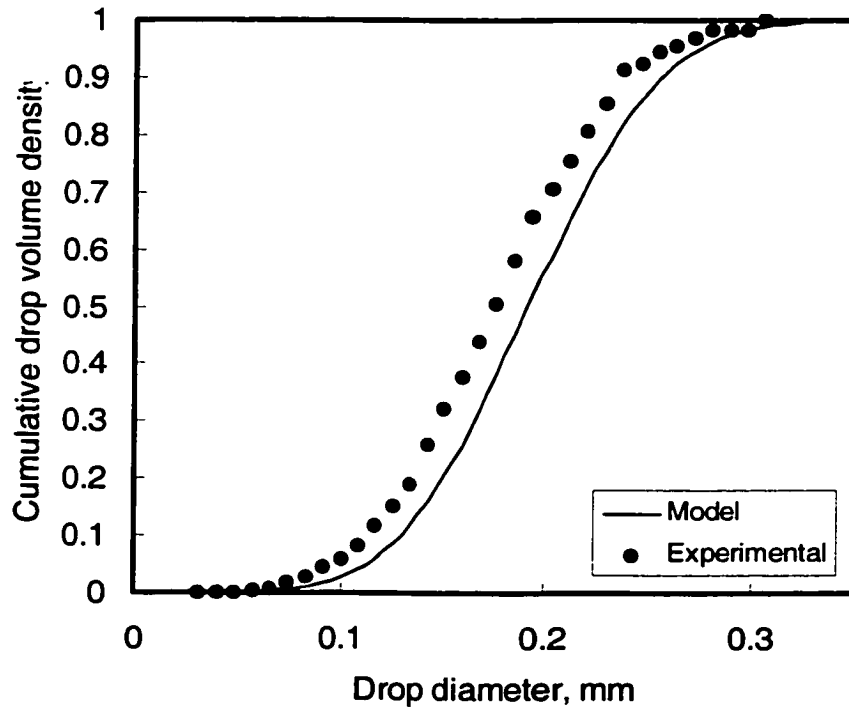


Figure D54. Cumulative drop volume density distribution
($\alpha = 27\%$, $\phi = 2\%$, $U = 0.70$ m/s, 9 screens, $L = 10$ mm)

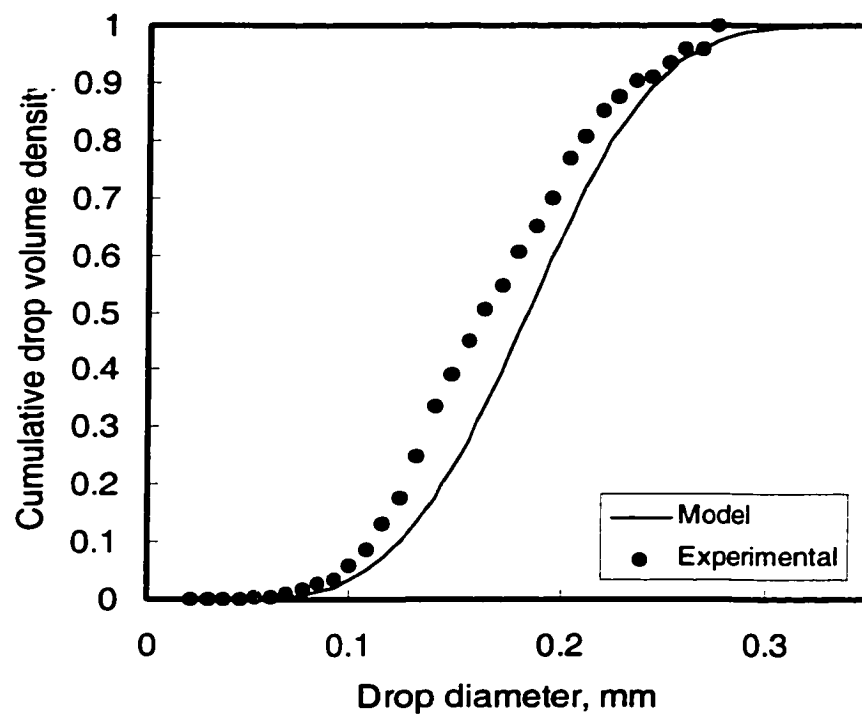


Figure D55. Cumulative drop volume density distribution
 ($\alpha = 27\%$, $\phi = 3\%$, $U = 0.70$ m/s, 9 screens, $L = 10$ mm)

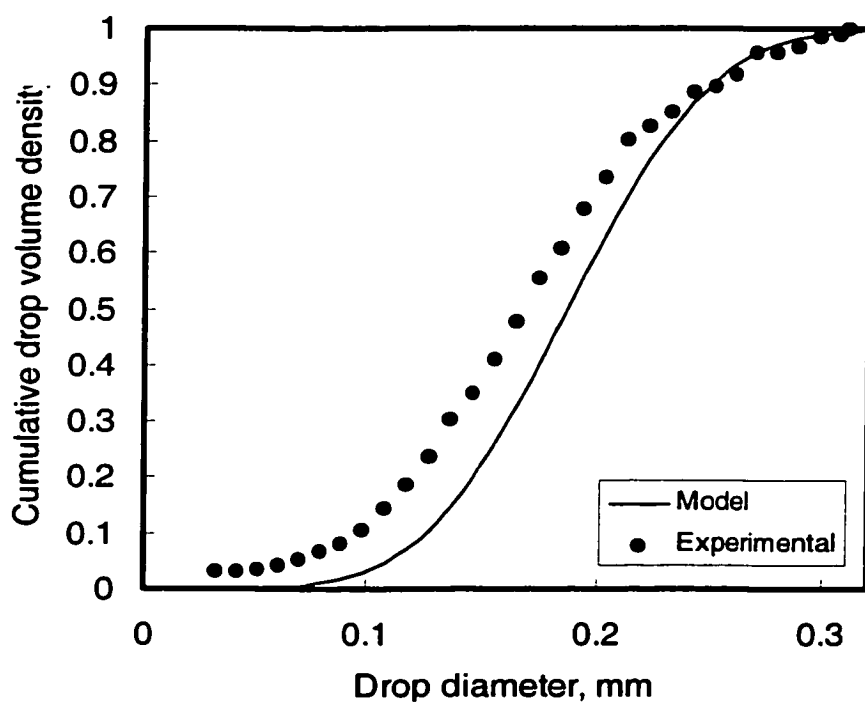


Figure D56. Cumulative drop number density distribution
 ($\alpha = 27\%$, $\phi = 0.5\%$, $U = 0.70$ m/s, Triton X100= 0.01 mole/m³, 9 screens, $L = 10$ mm)

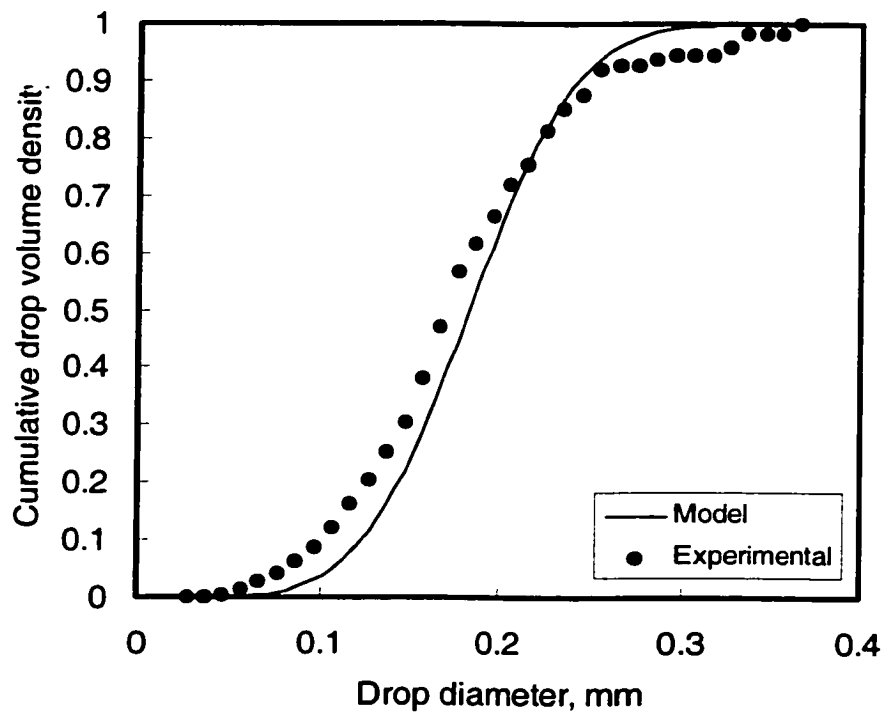


Figure D57. Cumulative drop number density distribution
 ($\alpha = 27\%$, $\phi = 0.5\%$, $U = 0.70$ m/s, Triton X100= 0.05 mole/m³, 9 screens, $L = 10$ mm)

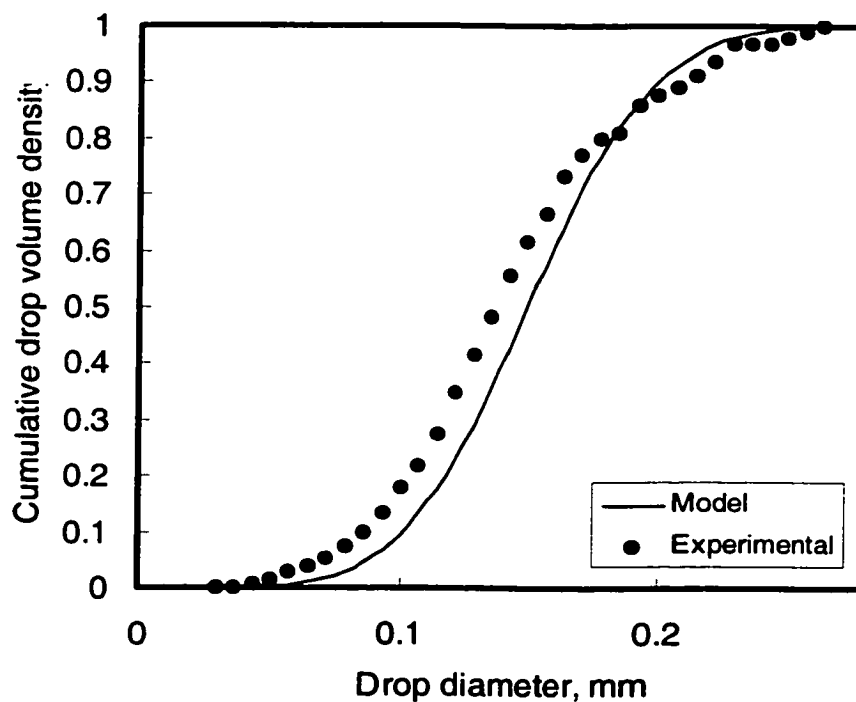


Figure D58. Cumulative drop number density distribution
 ($\alpha = 27\%$, $\phi = 0.5\%$, $U = 0.70$ m/s, Triton X100= 0.1 mole/m³, 9 screens, $L = 10$ mm)

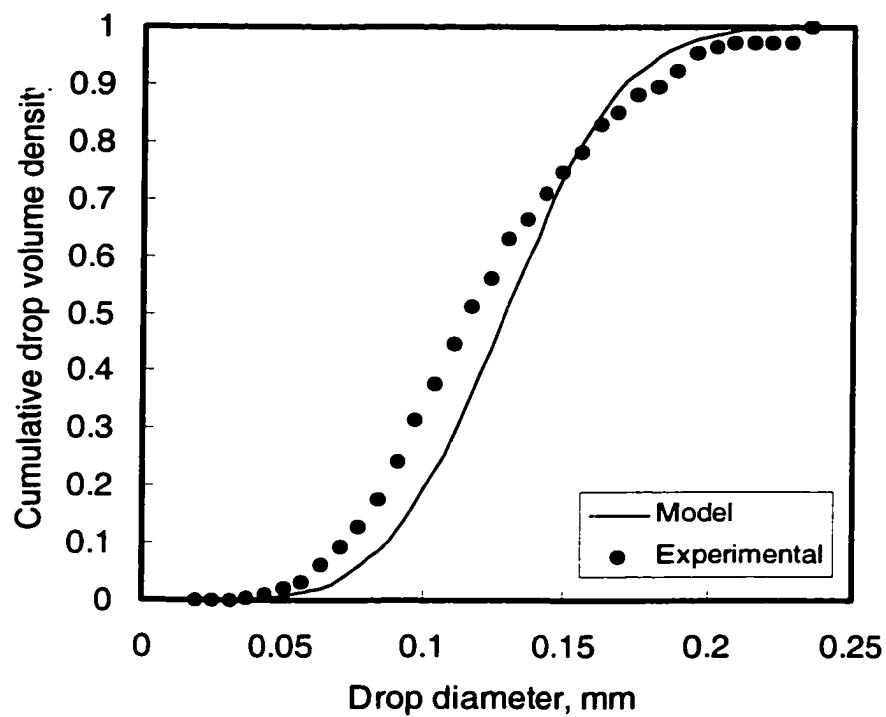


Figure D59. Cumulative drop number density distribution
 ($\alpha = 27\%$, $\phi = 0.5\%$, $U = 0.70$ m/s, Triton X100 = 0.2 mole/m³, 9 screens, $L = 10$ mm)

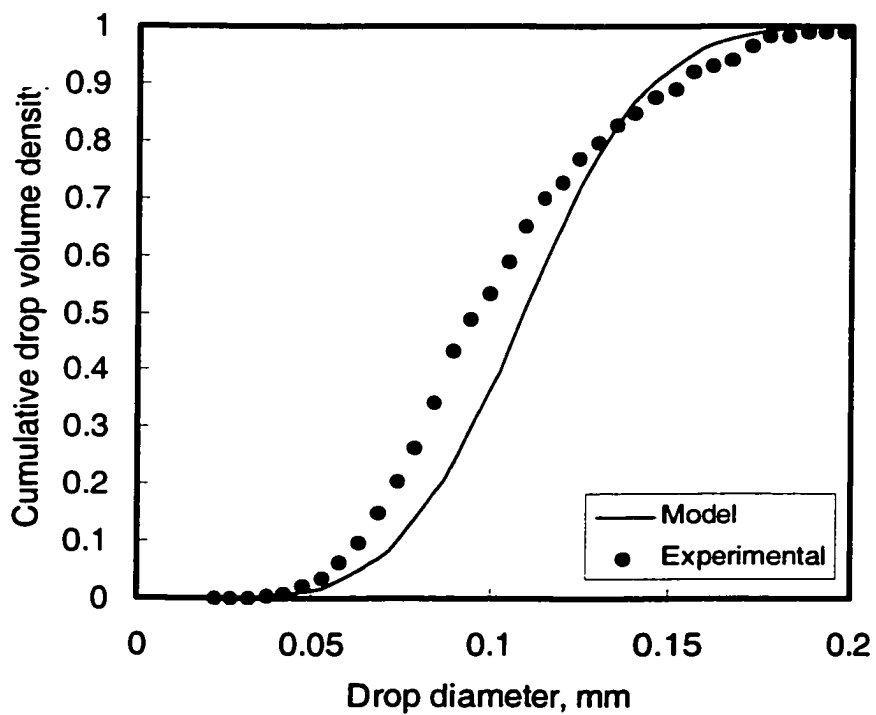


Figure D60. Cumulative drop number density distribution
 ($\alpha = 27\%$, $\phi = 0.5\%$, $U = 0.70$ m/s, Triton X100 = 0.3 mole/m³, 9 screens, $L = 10$ mm)

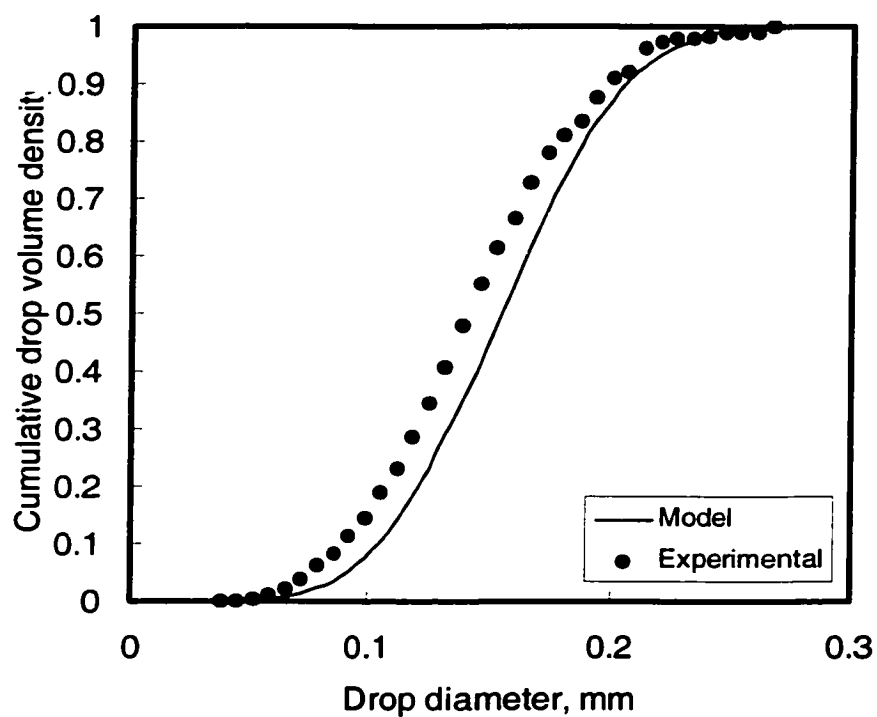


Figure D61. Cumulative drop number density distribution
 ($\alpha = 27\%$, $\phi = 4\%$, $U = 0.70$ m/s, Triton X100 = 0.01 mole/m³, 9 screens, $L = 10$ mm)

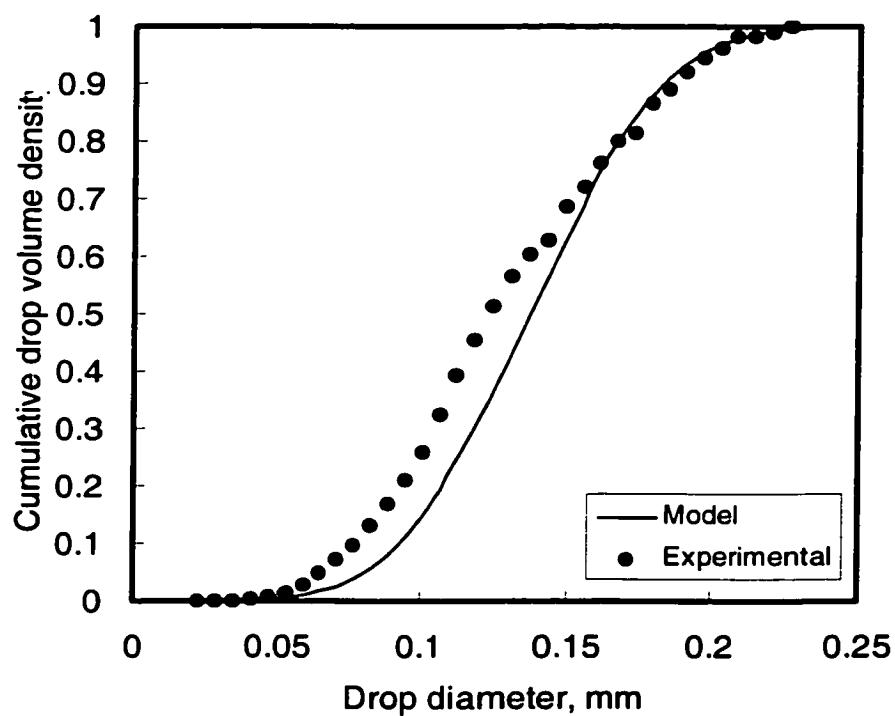


Figure D62. Cumulative drop number density distribution
 ($\alpha = 27\%$, $\phi = 4\%$, $U = 0.70$ m/s, Triton X100 = 0.05 mole/m³, 9 screens, $L = 10$ mm)

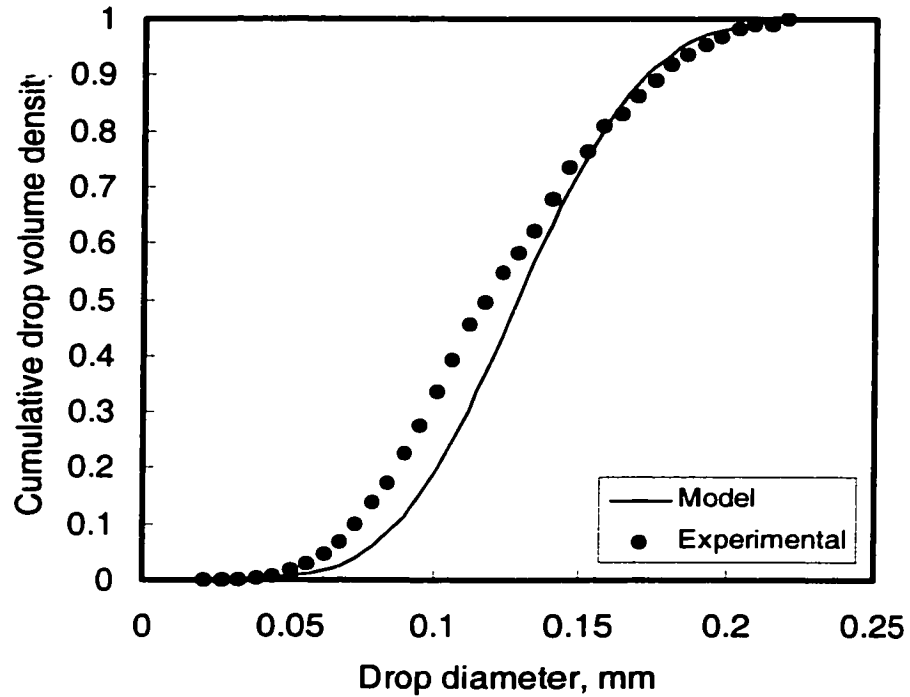


Figure D63. Cumulative drop number density distribution
 ($\alpha = 27\%$, $\phi = 4\%$, $U = 0.70$ m/s, Triton X100 = 0.1 mole/m³, 9 screens, $L = 10$ mm)

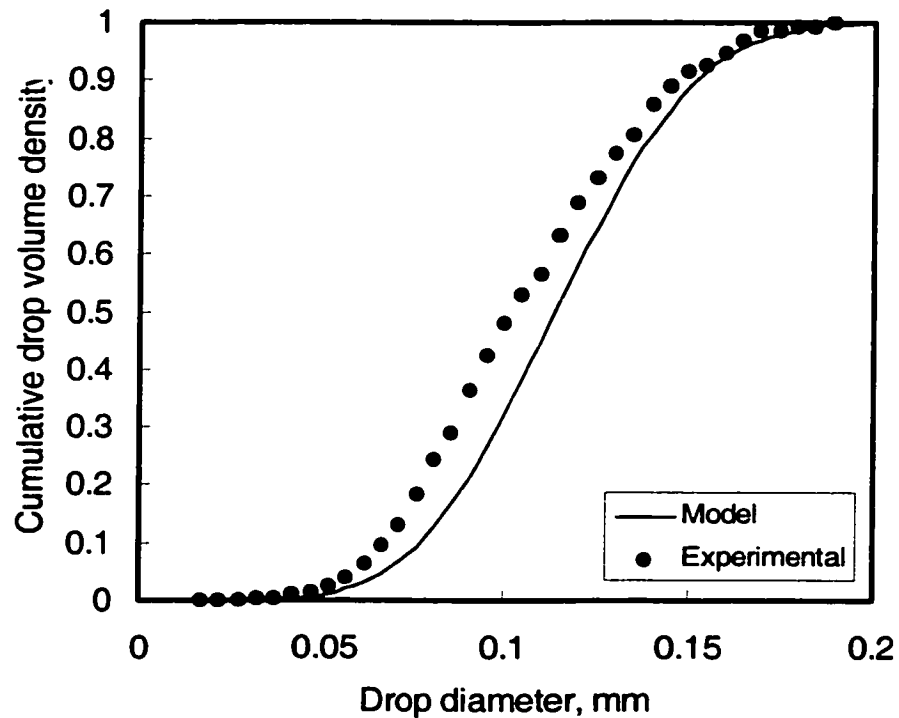


Figure D64. Cumulative drop number density distribution
 ($\alpha = 27\%$, $\phi = 4\%$, $U = 0.70$ m/s, Triton X100 = 0.2 mole/m³, 9 screens, $L = 10$ mm)

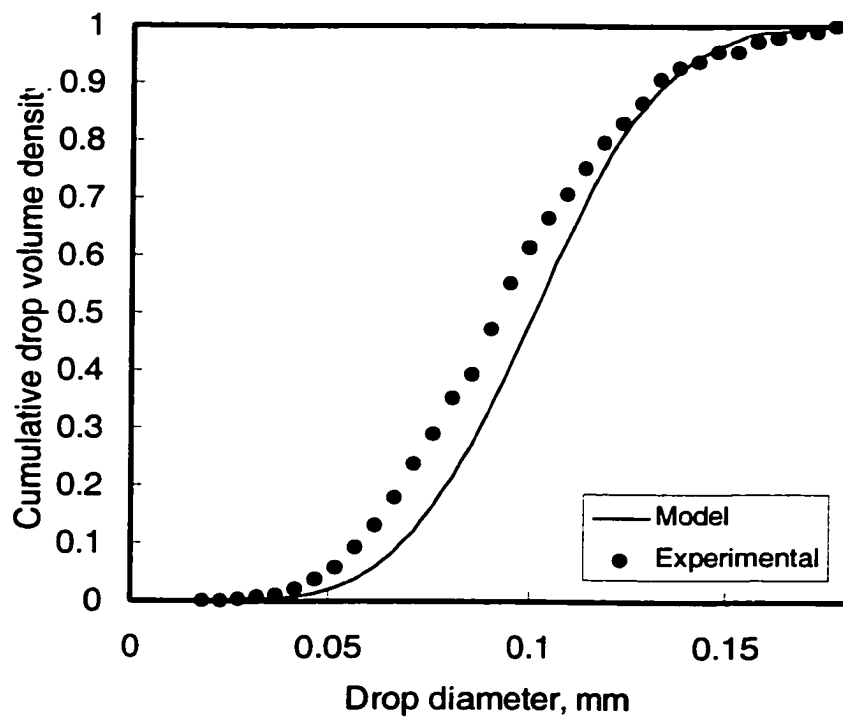


Figure D65. Cumulative drop number density distribution
($\alpha = 27\%$, $\phi = 4\%$, $U = 0.70$ m/s, Triton X100 = 0.3 mole/m³, 9 screens, $L = 10$ mm)